frontiers | Research Topics

Interactions between filamentous plant pathogens with their host plants and biocontrol agents

Edited by
Maofeng Jing, Qunqing Wang, Xiaodan Wang, Yurong Li and Ryan Kessens

Published in
Frontiers in Microbiology

ISSN 1664-8714
ISBN 978-2-83251-980-6
DOI 10.3389/978-2-83251-980-6

About Frontiers

Frontiers is more than just an open access publisher of scholarly articles: it is a pioneering approach to the world of academia, radically improving the way scholarly research is managed. The grand vision of Frontiers is a world where all people have an equal opportunity to seek, share and generate knowledge. Frontiers provides immediate and permanent online open access to all its publications, but this alone is not enough to realize our grand goals.

Frontiers journal series

The Frontiers journal series is a multi-tier and interdisciplinary set of open-access, online journals, promising a paradigm shift from the current review, selection and dissemination processes in academic publishing. All Frontiers journals are driven by researchers for researchers; therefore, they constitute a service to the scholarly community. At the same time, the *Frontiers journal series* operates on a revolutionary invention, the tiered publishing system, initially addressing specific communities of scholars, and gradually climbing up to broader public understanding, thus serving the interests of the lay society, too.

Dedication to quality

Each Frontiers article is a landmark of the highest quality, thanks to genuinely collaborative interactions between authors and review editors, who include some of the world's best academicians. Research must be certified by peers before entering a stream of knowledge that may eventually reach the public - and shape society; therefore, Frontiers only applies the most rigorous and unbiased reviews. Frontiers revolutionizes research publishing by freely delivering the most outstanding research, evaluated with no bias from both the academic and social point of view. By applying the most advanced information technologies, Frontiers is catapulting scholarly publishing into a new generation.

What are Frontiers Research Topics?

Frontiers Research Topics are very popular trademarks of the *Frontiers journals series*: they are collections of at least ten articles, all centered on a particular subject. With their unique mix of varied contributions from Original Research to Review Articles, Frontiers Research Topics unify the most influential researchers, the latest key findings and historical advances in a hot research area.

Find out more on how to host your own Frontiers Research Topic or contribute to one as an author by contacting the Frontiers editorial office: frontiersin.org/about/contact

Interactions between filamentous plant pathogens with their host plants and biocontrol agents

Topic editors

Maofeng Jing — Nanjing Agricultural University, China
Qunqing Wang — Shandong Agricultural University, China
Xiaodan Wang — China Agricultural University, China
Yurong Li — Corteva Agriscience™, United States
Ryan Kessens — Corteva Agriscience™, United States

Citation

Jing, M., Wang, Q., Wang, X., Li, Y., Kessens, R., eds. (2023). *Interactions between filamentous plant pathogens with their host plants and biocontrol agents*. Lausanne: Frontiers Media SA. doi: 10.3389/978-2-83251-980-6

Table of contents

frontiers | Frontiers in Microbiology

ORIGINAL RESEARCH
published: 16 June 2022
doi: 10.3389/fmicb.2022.923281

Transgenic Soybeans Expressing Phosphatidylinositol-3 -Phosphate-Binding Proteins Show Enhanced Resistance Against the Oomycete Pathogen *Phytophthora sojae*

Emily E. Helliwell[1,2], Peter Lafayette[3], Brent N. Kronmiller[1], Felipe Arredondo[1], Madeleine Duquette[1], Anna Co[1], Julio Vega-Arreguin[4], Stephanie S. Porter[2], Eli J. Borrego[5,6], Michael V. Kolomiets[5], Wayne A. Parrott[3] and Brett M. Tyler[1]*

[1]Department of Botany and Plant Pathology, Oregon State University, Corvallis, OR, United States, [2]School of Biological Sciences, Washington State University, Vancouver, WA, United States, [3]Department of Crop and Soil Sciences, University of Georgia, Athens, GA, United States, [4]Escuela Nacional de Estudios Superiores – León, Universidad Nacional Autónoma de México, León, Mexico, [5]Department of Plant Pathology and Microbiology, Texas A&M University, College Station, TX, United States, [6]Thomas H. Gosnell School of Life Sciences, Rochester Institute of Technology, Rochester, NY, United States

OPEN ACCESS

Edited by:
Maofeng Jing,
Nanjing Agricultural University, China

Reviewed by:
Lisong Ma,
Australian National University, Australia
Tingli Liu,
Jiangsu Academy of Agricultural Sciences (JAAS), China

***Correspondence:**
Emily E. Helliwell
emily.helliwell@gmail.com

Specialty section:
This article was submitted to Microbe and Virus Interactions With Plants, a section of the journal Frontiers in Microbiology

Received: 19 April 2022
Accepted: 06 May 2022
Published: 16 June 2022

Citation:
Helliwell EE, Lafayette P, Kronmiller BN, Arredondo F, Duquette M, Co A, Vega-Arreguin J, Porter SS, Borrego EJ, Kolomiets MV, Parrott WA and Tyler BM (2022) Transgenic Soybeans Expressing Phosphatidylinositol-3-Phosphate-Binding Proteins Show Enhanced Resistance Against the Oomycete Pathogen Phytophthora sojae. Front. Microbiol. 13:923281. doi: 10.3389/fmicb.2022.923281

Oomycete and fungal pathogens cause billions of dollars of damage to crops worldwide annually. Therefore, there remains a need for broad-spectrum resistance genes, especially ones that target pathogens but do not interfere with colonization by beneficial microbes. Motivated by evidence suggesting that phosphatidylinositol-3-phosphate (PI3P) may be involved in the delivery of some oomycete and fungal virulence effector proteins, we created stable transgenic soybean plants that express and secrete two different PI3P-binding proteins, GmPH1 and VAM7, in an effort to interfere with effector delivery and confer resistance. Soybean plants expressing the two PI3P-binding proteins exhibited reduced infection by the oomycete pathogen *Phytophthora sojae* compared to control lines. Measurements of nodulation by nitrogen-fixing mutualistic bacterium *Bradyrhizobium japonicum*, which does not produce PI3P, revealed that the two lines with the highest levels of *GmPH1* transcripts exhibited reductions in nodulation and in benefits from nodulation. Transcriptome and plant hormone measurements were made of soybean lines with the highest transcript levels of *GmPH1* and *VAM7*, as well as controls, following *P. sojae*- or mock-inoculation. The results revealed increased levels of infection-associated transcripts in the transgenic lines, compared to controls, even prior to *P. sojae* infection, suggesting that the plants were primed for increased defense. The lines with reduced nodulation exhibited elevated levels of jasmonate-isoleucine and of transcripts of a *JAR1* ortholog encoding jasmonate-isoleucine synthetase. However, lines expressing *VAM7* transgenes exhibited normal nodulation and no increases in jasmonate-isoleucine. Overall, together with previously published data from cacao

and from *P. sojae* transformants, the data suggest that secretion of PI3P-binding proteins may confer disease resistance through a variety of mechanisms.

Keywords: soybean, oomycetes, resistance gene, phosphatidylinositol-3-phosphate, *Phytophthora sojae*

INTRODUCTION

Like all eukaryotic organisms, plants have evolved to perceive and respond to a wide spectrum of microbes. These include pathogens, which invade and colonize to the overall detriment of host plants, as well as mutualists that provide benefits such as increased nutrition or protection against biotic or abiotic stress. Plants detect and respond to this wide range of microbes through complex networks of response pathways that integrate information about microbial signals, endogenous signals, and abiotic conditions (Wang et al., 2019). One class of microbial signals includes microbe-associated molecular patterns (also called pathogen-associated molecular patterns, PAMPs) that are widespread across diverse taxa. Well-characterized PAMPs include bacterial flagellin, and chitin from fungal cell walls. These PAMPs are perceived through binding to host plant pattern recognition receptors (PRRs) on the plasma membrane surface, which may trigger a cascade of responses including but not limited to production of defense-related hormones such as salicylic acid, jasmonic acid, and ethylene (Aerts et al., 2021), production of phytoalexins, and pathogenesis-related proteins (Wang et al., 2019). Collectively these responses have been termed PAMP-triggered immunity (PTI) or basal resistance (Jones and Dangl, 2006; Wang et al., 2019; Naveed et al., 2020). These responses are often sufficient to inhibit potential pathogens from colonizing plant tissue to a detrimental degree.

Successful pathogens can overcome PAMP-triggered defense responses to enter and colonize host cells through production of toxins or specialized effector proteins that can inhibit basal defense, as well as initiate metabolic, physiological, or morphological changes within host cells to facilitate colonization (Torto-Alalibo et al., 2010). Effector proteins may be targeted to the apoplast or to the host cell cytoplasm. These proteins are often specific to particular pathogen species or strains. An additional, highly effective layer of plant defense, called effector-triggered immunity (ETI), is initiated by the detection of pathogen effectors by cytoplasmic receptors (Wang et al., 2019). Detection of apoplastic effectors by cell surface receptors can also trigger an effective defense response (Wang et al., 2019). Many plant disease resistance genes identified by plant breeders encode these cell surface or cytoplasmic receptors. However, those resistance proteins typically recognize only specific effectors, rendering otherwise resistant plants vulnerable against pathogen strains that do not produce the recognized effector. For this reason, an important goal has been the search for conserved pathogen processes that could be inhibited to produce broad-spectrum immunity.

Oomycete pathogens produce a superfamily of cytoplasm-targeted effectors characterized by a highly conserved Arg-X-Leu-Arg (RXLR) motif located near the N-terminus (Jiang et al., 2008), which is required for movement into plant cells (Whisson et al., 2007; Dou et al., 2008; Kale et al., 2010; Song et al., 2013). Analysis of fungal effectors has suggested that some may utilize related motifs (Kale et al., 2010; Rafiqi et al., 2010; Plett et al., 2011). Furthermore, some research has suggested that RXLR and RXLR-like motifs may bind to the lipid phosphatidylinositol 3-phosphates (PI3P), as part of the process of delivering effectors inside the plant cell (Kale et al., 2010). That observation has motivated attempts to interfere with the interaction of effectors with PI3P by secretion of PI3P-binding proteins. Helliwell et al. (2016) showed that constitutive expression of a transgene composed of a PI3P-binding domain fused to a soybean PR1a secretory leader conferred increased resistance against both oomycetes (*Phytophthora tropicalis* and *Promecotheca palmivora*) and fungi (*Colletotrichum theobromicola*) in *Theobroma cacao* using both transient and stable transformation methods. Lu et al. (2013) showed that secretion of PI3P-binding proteins by *P. sojae* interfered with infection of soybean and that PI3P-binding proteins targeted the surface of *P. sojae* hyphae. Zhou et al. (2021) also showed that PI3P-binding proteins could target the surface of *Phytophthora* hyphae to confer improved disease resistance in transgenic soybean and potato plants.

In this study, we constructed stable transgenic soybean (*Glycine max*) plants expressing several lipid-binding proteins and control proteins. We observed that soybean plants expressing functional PI3P-binding proteins fused to a soybean PR1a secretory leader exhibited substantially increased resistance to *Phytophthora sojae* infection, though some, but not all, lines also exhibited reduced colonization by the mutualistic nitrogen-fixing bacterium *B. japonicum*, which is not known to produce PI3P. In the transgenic soybean plants expressing PI3P-binding proteins, measurements of the transcriptomes and of plant hormones suggested that the plants may be primed for elevated defense.

MATERIALS AND METHODS

Generation and Validation of Soybean Transgenic Lines

The PI-P-binding domains fused to EGFP were amplified from pGH126gfp (Helliwell et al., 2016) with primers PR1a-F-Asc ATTAGGCGCGCCATGGGGTACATGTGCATTAAGA and eGFP-R-Avr, ATATCCTAGGTTACTTGTACAGCTCGTCCATGC and cloned into pGmUbiP between the soybean GmUbi3 promoter (Hernandez-Garcia et al., 2009) and the pea rbcS terminator (Coruzzi et al., 1984). The expression cassette was then moved into pSPH2 (Jacobs et al., 2015), which contains a hygromycin phosphotransferase gene under the control of the potato Ubi3 promoter and terminator for transgenic event

selection. Transgenic soybeans were derived as described by Hancock et al. (2011). Events homozygous for the hph gene and null segregants were identified using Invader (Third Wave AgBio, Madison, WI) and verified with primers PR1a-F-Asc and eGFP-R-Avr.

Inoculation With *Phytophthora sojae* and Quantification of Disease

For all inoculation conditions, six soybean seeds were sown in potting soil in 6-inch pots and maintained in growth chambers at 28°C light/24°C dark. For inoculation of detached soybean trifoliate leaves with zoospores, *P. sojae* strain P6497 (race 2) was inoculated on sterile 10% V8 agar and then incubated for 10 days at 23°C in the dark. Zoospores were produced by washing the resulting mycelia on the plates with sterile deionized water, every 30 min for 4 h, until zoospore release began. Plates were then flooded with 7 ml deionized water and incubated for 12–16 h at 14°C in the dark. The second trifoliate leaves were cut from 14-day-old soybean plants and placed in petri dishes containing a Kimwipe (Kimberly–Clark) wetted with 1 ml of sterile deionized water. Each leaflet of a trifoliate leaf was inoculated with a single drop of deionized water containing 200 zoospores (2×10^3 zoospores per ml). Plates were sealed with parafilm and incubated for 4 days at room temperature, with 12-h dark and light. Disease severity was assessed by photographing each leaflet and measuring the area of each lesion using ImageJ (Schneider et al., 2012). To measure the relative amount of *P. sojae* biomass, inoculated leaflets were frozen in liquid nitrogen, and genomic DNA was extracted using a CTAB method (Helliwell et al., 2016). For quantitative real-time PCR (qRT-PCR), Takara SYBR green was used according to the manufacturer's instructions, with 50 ng of genomic DNA per reaction with primers measuring housekeeping genes *G. max Cyclophilin 2* (*CYP2*) and *Phytophthora sojae Actin* (Wang et al., 2011). The $\Delta\Delta C_t$ method was used to calculate the relative quantity to *P. sojae* gDNA to *G. max* gDNA (Wang et al., 2011).

For hypocotyl inoculation, *P. sojae* P6497 was inoculated onto sterile 10% V8 agar and incubated in the conditions described above for 7 days. On the day of inoculation, soybean hypocotyls (on 10-day-old soybeans, six per pot) were wounded by gently scraping 0.5 cm between the soil line and the cotyledons, and a 2.5-mm^2 square of *P. sojae* mycelia was placed, mycelial side down over the wounded area. Inoculated plants were maintained in a growth chamber at 28°C light/24°C dark for 3 days; then, plants were scored by measuring the lesion length and the percentage of collapsed plants per pot.

Inoculation With *Bradyrhziobium japonicum* and Quantification of Nodulation

Soybean seeds were sterilized by exposure to chlorine gas for 6 h and then sown individually into 130-ml cone-shaped containers containing a sterile mix of 2:1 sand and SunGrow Sunshine #1 potting medium (Sun Gro Horticulture). *Bradyrhziobium japonicum* USDA 110 was maintained on plates containing modified arabinose gluconate (MAG) agar and inoculated into a 1-ml culture of MAG media and incubated at 28°C, 270 rpm for 48 h. The 1-ml cultures were added into a 24-ml volume of MAG media in a 50-ml Falcon tube and incubated at 29°C, 270 rpm for 72 h (modified from Sachs et al., 2011). *Bradyrhziobium japonicum* cells were harvested and resuspended in sterile 1/2X Jensen's media at a concentration of 10^7 cells/ml. Nine-day-old plants were inoculated by pipetting 1 ml of either the *B. japonicum* suspension or negative (1/2X Jensen's buffer) at the base of the shoot. Plants were maintained in 28°C/24°C day/night greenhouse conditions for 4 weeks before harvest and data collection.

Just prior to harvest, a Soil Plant Analysis Development (SPAD) chlorophyll meter (Spectrum Technologies) was used to quantify leaf chlorophyll content by taking a reading from the center of the middle leaf in the 1st, 2nd, and 3rd trifoliate. The shoots were clipped off at the soil line, then placed into an envelope, and dried in a 60°C oven for 3 days before collecting shoot weight. Roots were washed to remove all planting substrate; then, the total number of nodules was counted per root. The size (diameter) was recorded for the largest three nodules on each root using a set of calipers.

Assay of Soybean Transcript Levels by Quantitative Real-Time PCR

RNA was extracted from primary leaves of 10-day-old soybean seedlings using RNeasy (Qiagen) RNA extraction reagent according to the manufacturer's instructions. cDNA synthesis was performed by pre-treating 1 μg RNA with DNAse I (Promega) at room temperature for 30 min. cDNA synthesis from RNA was performed using 50 ng oligo(dT) and New England Biolabs (NEB) M-MLV according to the manufacturer's instructions. qRT-PCR was performed on an Applied Biosystems PRISM® 7500 FAST Sequence Detection System using Takara SYBR green according to the manufacturers' instructions.

RNA Sequencing and Transcriptomic Analysis

Six soybean seeds were sown per pot, seven pots per line per replicate. Pots were arranged in a randomized block design and maintained in a growth chamber under the conditions described above. Soybean hypocotyls were inoculated as described above, with four pots per line inoculated with *P. sojae* P6497 (*P. sojae*-inoculated), and three pots per line inoculated with a sterile 2.5-mm^2 square of 10% clarified V8 agar (mock-inoculated). Hypocotyl segments, 1 cm long, centered on the inoculated areas were harvested 12 h later, pooling 18 plants each for mock- and *P. sojae*-inoculated lines, then snap-frozen in liquid nitrogen and stored in −80°C. One *P. sojae*-inoculated pot per line was maintained for an additional 3 days in the growth chamber to verify successful inoculation. The experiment was repeated independently three more times (for a total of four replicates), and the three most successful (determined by verification of disease development) replicates were used for RNA sequencing. RNA was extracted from each sample (pool of 18 hypocotyl segments per treatment per line) by the method

described above, and 1 μg of total RNA sequenced on an Illumina HiSeq 3000, using a 150-base pair, paired-end module at the Oregon State University Center for Genome Research and Biocomputing. **Supplementary Table 2** shows the detailed FASTQ report, including the numbers of passed filter reads, the yield, and the quality score for each demultiplexed RNA sample.

The *G. max* genome v1.1 (Schmutz et al., 2010) or the *P. sojae* genome v3.0 (Tyler et al., 2006) was indexed using TopHat (Trapnell et al., 2009), and the fastq files were aligned to the genome with Bowtie2 (Langmead et al., 2009). Count tables to quantify the number of reads per gene were generated with the SAMtools function htseq-count (Li et al., 2009). Normalization of the number of counts was run using EstimateSizeDisperson function, and PCA plots were conducted using the R package DESeq (Anders and Huber, 2010). A mixed model analysis, using replicate as a random effect, was run to determine differential expression with a significance cutoff of Benjamini–Hochberg-adjusted $p < 0.1$. The transcriptome data have been deposited in the NCBI Gene Expression Omnibus database accession GSE201739.

Gene Ontology Annotations and Enrichment Analysis

Annotations of soybean genes of interest, including the identity of Arabidopsis orthologs, were obtained initially using AgriGO (Du et al., 2010). Then, each annotation was reviewed manually using information about the Arabidopsis ortholog obtained from The Arabidopsis Information resources (TAIR)[1] version December 2021. Gene Ontology (GO) biological process annotations were transferred to the soybean genes from their Arabidopsis orthologs, and higher level parent terms such as "GO:0098542 Defense response to other organism" and "GO:0009725 Response to hormone" were added where appropriate in order to aggregate annotations. To calculate the enrichment of specific GO terms among particular soybean gene sets, the fraction of the soybean gene set carrying the annotation was compared to the fraction of the Arabidopsis genome containing the annotation, using Fisher's exact test. The false discovery rate was controlled (adjusted $p < 0.1$) using the method of Benjamini and Hochberg (1995) based on the total number of GO terms represented in the soybean gene set of interest.

Soybean Hormone Assays

Experimental design and soybean inoculation were carried out identically to that of the RNA sequencing experiment, except that only control and GmPH lines were included. In addition to harvesting and pooling soybean hypocotyls, primary leaves were collected and snap-frozen in liquid nitrogen and then stored at −80°C. Tissue was ground in liquid nitrogen, and 100 mg of frozen powder was placed in 2-ml screw-top microcentrifuge tubes. Phytohormone measurement and quantification were performed at Texas A&M University, with three independent biological replicates, two technical repeats per biological replicate. Phytohormone extractions followed Christensen et al. (2013), with the following modifications: 500 μl of phytohormone extraction buffer [1-propanol/water/HCl (2:1:0.002 v/v/v)] and 10 μl of 5 μM solution of deuterated internal standards: d-IAA [(2 H5) indole-3-acetic acid, Olchem], d-ABA [(2 H6) (+)-cis,trans-ABA; (Olchem)], and d-JA (2,4,4-d3, acetyl-2,2-d2 JA; CDN Isotopes), and d-SA (d6-SA, Sigma) was added to ~100 mg of ground mesocotyl tissue. Samples were agitated for 30 min at 4°C in dark conditions, and then, 500 μl of dichloromethane was added to the samples. The samples were agitated again for 30 min at 4°C and centrifuged at 13,000 × *g* for 5 min. To prevent autoxidation of reactive fatty acid derivatives, the lower layer collected into a glass vial was evaporated under a nitrogen gas stream to concentrate the extracted metabolites. The concentrated samples were resuspended in 150 μl of methanol and were centrifuged at 14,000 × *g* for 2 min to pellet any debris. One hundred microliters of supernatant was collected into an autosampler vial for direct injection into LC-ESI-MS/MS. The quantification of multiple hormones, oxylipins, and other defense-related metabolites utilized methods described in Wang et al. (2020). In particular, the quantification utilized an Ascentis Express C-18 Column (3 cm × 2.1 mm, 2.7 μm) connected to an API 3200 LC-electrospray ionization-tandem mass spectrometry (MS/MS) with multiple reaction monitoring (MRM). The injection volume was 2 μl and had a 600 μl/min mobile phase consisting of Solution A (0.05% acetic acid in water) and Solution B (0.05% acetic acid in acetonitrile) with a gradient consisting of (time–%B): 0.3%–1%, 2%–45%, 5%–100%, 8%–100%, 9%–1%, 11–stop. The metabolite and phytohormone m/z values and retention times are as listed in Wang et al. (2020). Statistical analysis was done using a one-way ANOVA with Duncan's multiple range test, and letters represent significance groups at $p < 0.05$.

RESULTS

Creation and Validation of Soybean Transgenic Lines

Transgene design and verification followed Helliwell et al. (2016). Three different phosphoinositide binding domains were chosen based on their differing specificities for PI3P and phosphatidylinositol-4-phosphate (PI4P). The pleckstrin homology (PH) domain from soybean GmPH1 (ortholog of AtPH1; Dowler et al., 2000), and the Phox homology (PX) domain from yeast VAM7 (Lee et al., 2006) were chosen for their specificity for PI3P. As a control, the PI4P-binding PH domain from human FAPP1 was chosen (Dowler et al., 2000; DiNitto and Lambright, 2006; Lemmon, 2008). All genes were fused to an enhanced GFP reporter gene at the 3'end and the secretory leader from the soybean PR1a protein (Cutt et al., 1988; Honée et al., 1998; van Esse et al., 2007) at the 5′ end to deliver the encoded protein to the apoplastic space. The gene fusions were placed under the control of the strong, constitutive soybean *Ubiquitin 3* promoter. An illustration of the transgene construct and comparative amino acid sequences of VAM7 and its non-binding mutant control (Vmut) are shown in **Figures 1A,B**. All recovered soybean transgenic lines exhibited normal growth, development and seed set.

[1]https://www.arabidopsis.org/

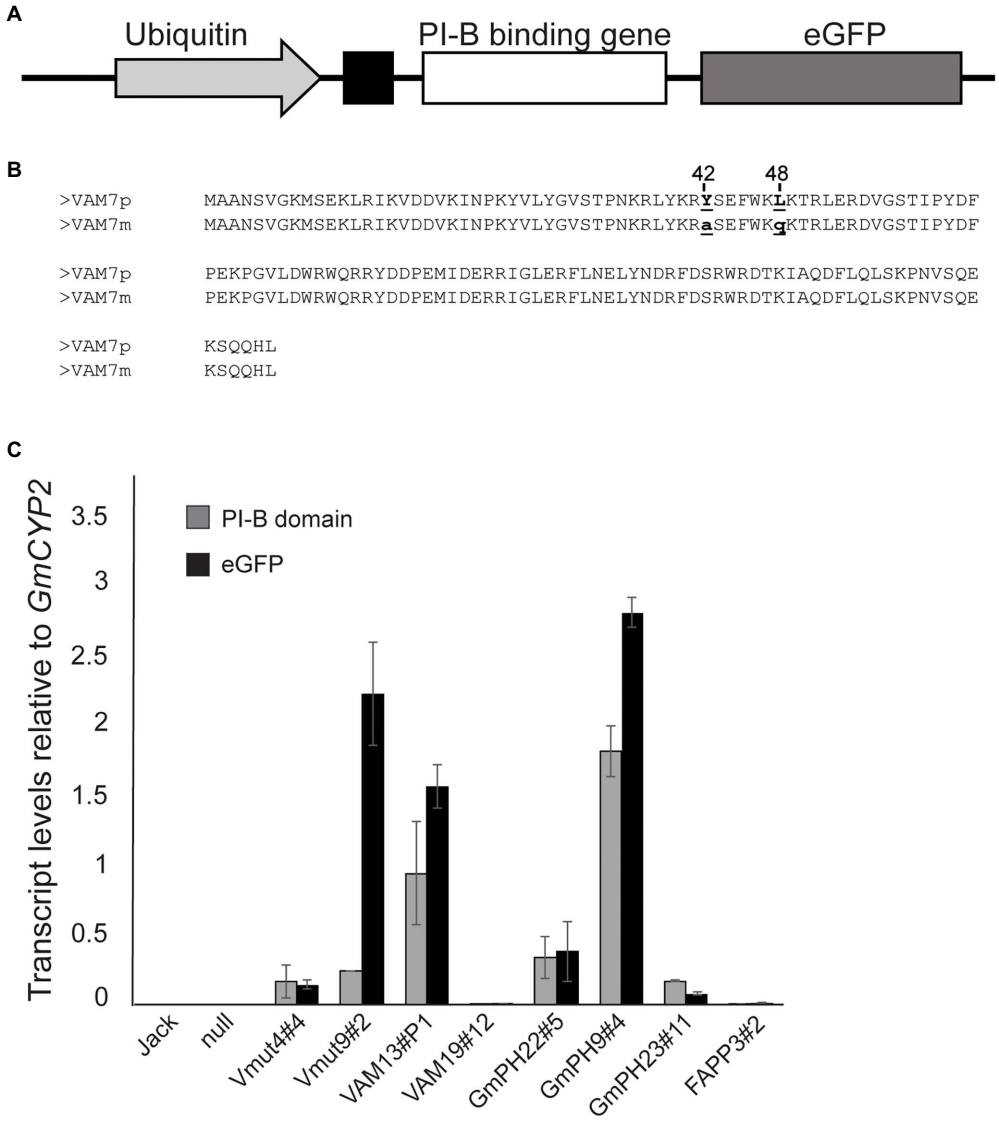

FIGURE 1 | Structure and expression of transgenes encoding phosphoinositide-binding proteins. **(A)** Illustration of transgene showing the phosphoinositide-binding protein gene fused to the eGFP reporter gene, downstream of a PR1a secretory leader. The transgene is placed under control of the soybean *Ubiquitin 3* promoter. **(B)** Amino acid sequence alignment of the VAM7 PX domain compared to the non-PI3P-binding VAM7 mutant (Vmut). Amino acid substitutions from VAM7 to Vmut include tyrosine to alanine at position 42, and leucine to glutamine at position 48. **(C)** Transcript levels of transgenes across independent soybean lines, measured by quantitative reverse transcriptase PCR. Primer pairs specific for each PI-binding (PI-B) domain (e.g., VAM7, GmPH) and for the eGFP reporter domain were used in each case (**Supplementary Table 6**). Transcript levels are relative to the internal control gene *GmCYP2*. Bars are average of values from the trifoliates of three different plants, each trifoliate run in duplicate. Error bars show the SEM.

Quantitative reverse transcriptase PCR (qRT-PCR) was used to determine transcript levels of each transgene in each of the homozygous T2 soybean lines. Using the *GmCYP2* housekeeping gene as an internal control (Jian et al., 2008), transcript levels of the specific PI-binding domain, along with the *GFP* reporter gene, were measured in each line. The results are shown in **Figure 1C**. As expected, there was no expression of any PI-binding protein gene, nor *GFP* reporter gene in the non-transgenic cv. Jack and null segregant line. Independent transgenic soybean lines expressing non-binding mutant *VAM* (Vmut4#4 and Vmut9#2) showed similar *VAM* transcript levels as each other (0.16 ± 0.01 and 0.25 ± 0.01, respectively), relative to *GmCYP2*. However, they exhibited vastly different *GFP* transcript levels (0.14 and 2.24), respectively, relative to *GmCYP2*, suggesting an aberrant transgene in Vmut9#2. Independent soybean lines expressing functional PI3P-binding *VAM* (VAM13#P1, VAM19#12) showed concordant *VAM* and *GFP* transcript levels, but the two differed greatly in the relative transcript levels of their *VAM-GFP* transgenes, with VAM13#P1 (*VAM* 0.94, *GFP* 1.57) much greater than VAM19#12 (*VAM* 0.0003, *GFP* 0.01). Similarly, the three independent soybean lines expressing functional PI3P-binding *GmPH* domain

(GmPH22#5, GmPH9#4, and GmPH23#11) represented a range of *GmPH* and *GFP* expression. GmPH9#4 showed the highest relative transcript levels (*GmPH* 1.82, *GFP* 2.82) compared to GmPH22#8 (*GmPH* 0.33, *GFP* 0.38) and GmPH23#11 (*GmPH* 0.17, *GFP* 0.08). Lastly, the single line expressing functional PI4P-binding *FAPP* domain (FAPP3#2) showed low transcript levels of both *FAPP* (0.007) and *GFP* (0.016), relative to *GmCYP2*.

Transgenic Soybeans Expressing Functional PI3P-Binding Proteins Showed Enhanced Resistance to a Virulent Isolate of *Phytophthora sojae*

To establish the susceptibility of transgenic soybeans expressing PI3P-binding proteins to a pathogenic oomycete, inoculation tests were conducted using both zoospores and mycelia of *P. sojae* strain, P6497. First, detached first trifoliate leaves were inoculated with *P. sojae* zoospores (**Figures 2A,C**). Independent lines expressing functional VAM7-GFP showed a significant partial reduction in lesion areas compared to the non-transformed control Jack (~35% and 50% for lines VAM19#12 and VAM13#P1, respectively; $p < 0.05$) 4 days after inoculation, with no significant difference between the two lines. Independent lines expressing GmPH-GFP showed a more substantial reduction in lesion area 4 days after inoculation (~65% and 71%, for lines GmPH9#4 and GmPH23#1, respectively; $p < 0.05$), with no significant difference between the two lines. Furthermore, statistical tests showed that there were no significant differences between non-transformed cv. Jack and a null segregant from the VAM7-19#12 transgenic population ("null"), one VAM7-non-binding

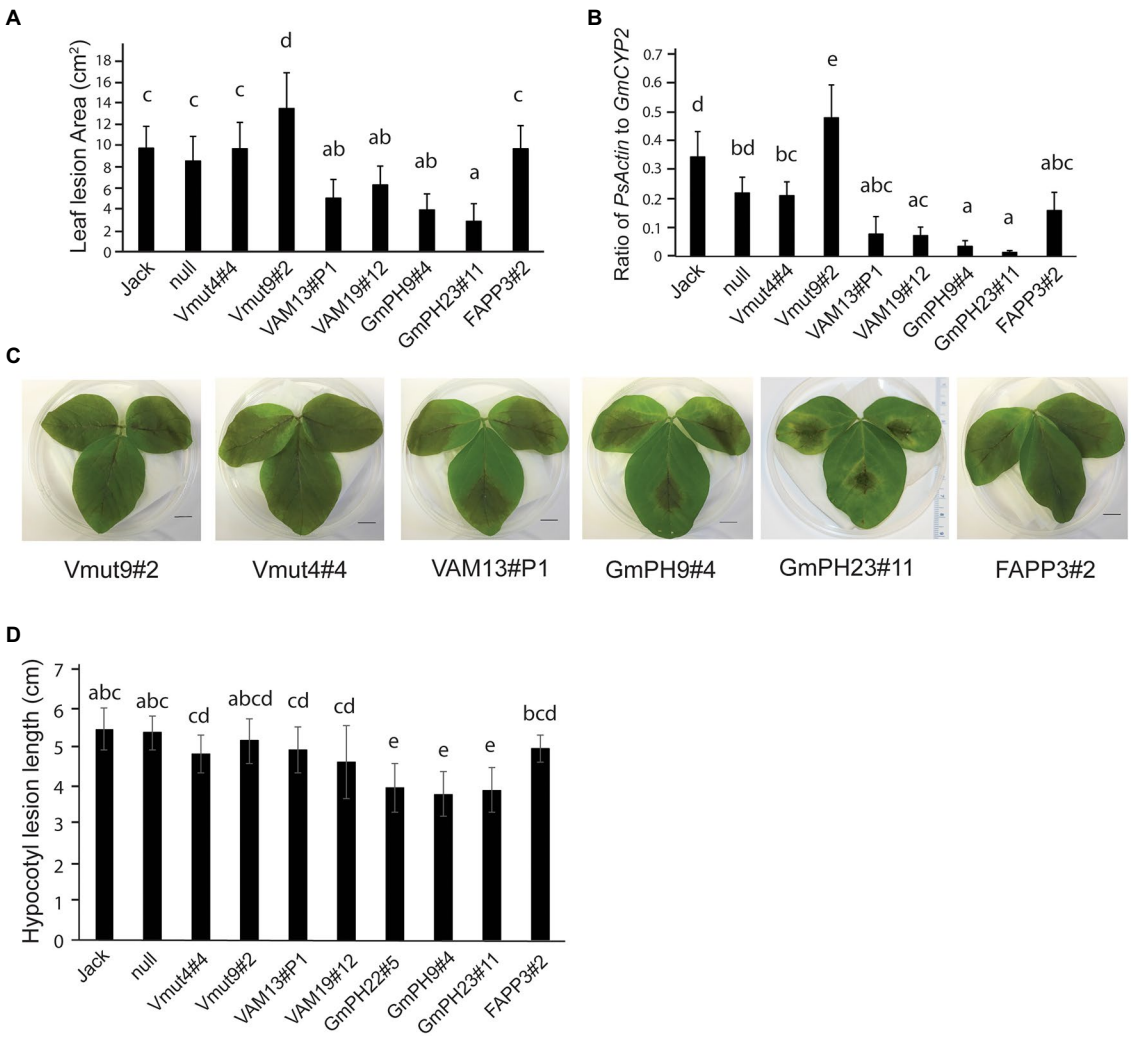

FIGURE 2 | Inoculation of transgenic lines with *Phytophthora sojae*. **(A)** Lesion area measured 4 days after inoculation by zoospores of *P. sojae* strain P6497. Jack is the non-transformed cultivar and null is the null segregant originating from the VAM7-19 transgenic population **(B)** Ratio of *P. sojae* Actin genomic DNA to *Glycine max CYP2* genomic DNA in leaves, 4 days after inoculation by *P. sojae* zoospores. **(C)** Representative photographs of 2nd trifoliate leaves, 4 days after inoculation by *P. sojae* zoospores. **(D)** Length of *P. sojae* lesions 3 days after inoculation of soybean hypocotyls by mycelia. In **(A,B,D)**, letters represent different significance groups as measured by one-way ANOVA ($p < 0.05$). Letters represent different significance groups. Averages of 12 plants from each of three independent biological replicates are shown for all graphs; bars indicate SE.

mutant line (Vmut4#4), and the soybean line expressing a functional PI4P-binding FAPP protein. It is noteworthy to add that the second soybean line expressing a non-binding mutant (Vmut9#2) showed a hyper-susceptible response, with the resulting lesion area significantly larger ($p < 0.05$) than all other lines tested.

To confirm the lesion area measurements, qRT-PCR was used to determine the relative amount of *P. sojae* genomic DNA to soybean genomic DNA as a measure of pathogen proliferation (**Figure 2B**). Independent lines expressing functional VAM7-GFP showed a significant reduction in *P. sojae* biomass (77% for VAM13#P1, and 79% for VAM19#12; $p < 0.05$) as compared to non-transformed control cv. Jack. Independent lines expressing GmPH-GFP showed a very substantial reduction in *P. sojae* biomass (83% for line B, 96% for line C; $p < 0.05$) compared to non-transformed control cv. Jack. There were no significant differences among the FAPP3#2 line, null segregant, and non-binding VAM7 line Vmut4#4 ($p > 0.05$). Similarly to the lesion area measurements, non-binding VAM7 mutant line Vmut9#2 showed a significantly higher *P. sojae* biomass as compared to all of the other lines.

To test the effects of the transgenes on *P. sojae* stem infection, we performed hypocotyl inoculation tests (**Figure 2D**). As with the leaf assays, the soybean lines expressing GmPH PI3P-binding domains showed the smallest lesions with a significant 27%–30% reduction in lesion length. For the remainder of the transgenic lines, we saw more intermediate phenotypes. The soybean lines expressing functional VAM domains did not show significant differences from the soybeans expressing non-functional VAM mutants, or from soybeans expressing a functional PI4P-binding FAPP domain. However, this intermediate phenotype seen in the VAM, VAM mutant, and FAPP lines had a slight, yet significant reduction of 10%–15% in lesion length compared to the non-transgenic cv. Jack and null segregant lines.

Overall, the results of the infection assays indicated that the two transgenes encoding functional PI3P-binding proteins, *GmPH* and *VAM7*, could confer resistance to *P. sojae* compared to control lines, with the *GmPH-GFP* transgenes substantially more effective than the *VAM7*-GFP transgenes.

Some Transgenic PI3P-Binding Soybean Lines Exhibit Reduced Colonization by Mutualistic *Bradyrhizobium japonicum*

Since in cacao, PI3P-binding domains conferred broad-spectrum resistance against oomycetes and fungi (Helliwell et al., 2016), and since colonization by mutualistic nitrogen-fixing bacteria is important for soybean growth and production, we conducted experiments in which the transgenic and control soybean lines were inoculated with mutualistic nitrogen-fixing *Bradyrhizobium japonicm*. The two GmPH-expressing lines with the highest transgene transcript levels (GmPH22#5 and GmPH9#4) exhibited significantly fewer nodules per plant than the control lines (non-transformed Jack, null segregant, transgenic non-binding mutant Vmut, PI4P-binding FAPP line; **Figures 3A,E**). These same PI3P-binding transgenic lines GmPH22#5 and GmPH9#4 showed a modest reduction in nodule size (21% compared to average of Jack and null; 15% relative to average of VAMmut and FAPP), but the only the difference with Jack and the null segregant line was statistically significant. GmPH23#11 showed no significant differences compared to the controls (**Figures 3B,E**). Data were also collected on the physiological responses of the soybean lines after inoculation by *B. japonicum* to gauge the benefits that the plant might be receiving from the mutualist. Dried shoot mass measurements were taken for sterile-inoculated and *B. japonium*-inoculated plants, and pairwise t-tests for each line showed that lines GmPh22#8 and GmPh9#4 failed to show a significant increase in shoot mass in *B. japonicum*-inoculated plants, in contrast to all other lines except the null segregant, and the strong transgenic GmPH22#8 and GmPH9#4 lines (**Figure 3C**). Chlorophyll content data collected with a SPAD meter from sterile-inoculated and *B. japonicum*-inoculated plants showed that lines GmPH22#5 and GmPH9#4 exhibited a significantly lower chlorophyll content response compared to the non-transformed cv. Jack (45 and 55% reduction, respectively; $p < 0.05$), but the differences with the other control lines (24 and 36% reduction, respectively) were not significant (**Figure 3D**). The remainder of the lines (non-binding Vmut, PI4P-binding FAPP, weak-expressing GmPH23#11) showed no significant differences (**Figure 3D**).

Taken together, these results revealed that expression of some PI3P-binding domains that confer *P. sojae* resistance also could increase resistance to colonization by a nitrogen-fixing symbiont, *B. japonicum*, despite the fact that *B. japonicum* does not produce PI3P.

RNA Sequencing Analysis

Since the lines expressing PI3P-binding proteins appeared to exhibit resistance to *B. japonicum* as well as *P. sojae*, we conducted transcriptome measurements to assess the physiological states of the resistant lines compared to the control lines. In particular, we aimed to identify genes that might be elevated in both the GmPH and VAM lines compared to the controls, either in healthy or *P. sojae*-infected tissues. We also aimed to determine whether there were gene expression differences between the GmPH and VAM lines that might account for their differences in resistance levels and nodulation phenotypes. To identify an optimal early timepoint after inoculation of *P. sojae* to sample for RNA sequencing, we aimed to find a time point when there was abundant colonized tissue, but the host tissue was still largely intact.

Seedlings of susceptible cultivar Williams were inoculated with *P. sojae* P6497 mycelia on the hypocotyl and then sampled 0, 6, 12, 18, 24, and 48 h after inoculation. The earliest visible signs of infection appeared 18 h after inoculation, as evidenced by discoloration of the host tissue. Real-time quantitative PCR of genomic DNA was used to measure the ratio of *P. sojae* to soybean biomass in each sample (**Supplemental Figure 1**). The relative level of *P. sojae Actin* showed a 28-fold increase between 6 and 12 h after inoculation, followed by continued rapid proliferation of the pathogen. Therefore, we selected 12 h post-inoculation to sample the tissues for RNA sequencing.

The design of the RNA sequencing experiment included two GmPH lines, two functional VAM lines, and the Vmut

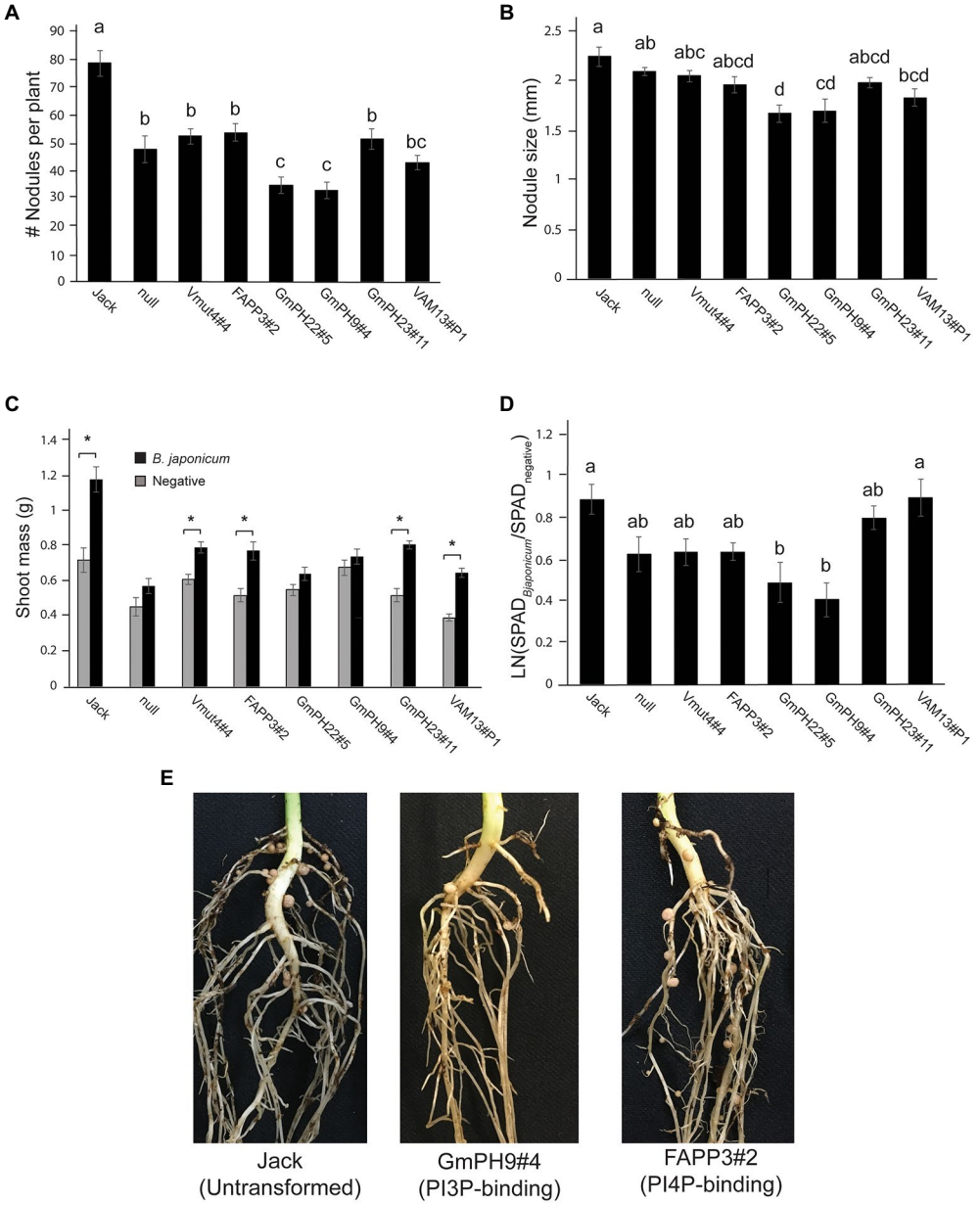

FIGURE 3 | Effect of mutualistic nitrogen-fixing *Bradyrhizobium japonicum* USDA 110 on transgenic soybean lines. **(A)** Nodule count per plant. **(B)** Average size of the three largest nodules per plant. Data from **A** and **B** were analyzed using a one-way ANOVA with significance groups assigned by a Tukey HSD *post hoc* test, with significance threshold at $p < 0.05$. Each bar represents the average of 13 plants from a randomized block design. Error bars indicate the SD of the mean. **(C)** The average shoot mass for plants inoculated with sterile buffer (gray bars) or 10^6 cells *B. japonicum* (black bars). Asterisks show the soybean lines where the shoot masses of the sterile-inoculated plants are significantly different than the *B. japonicum*-inoculated plants at a threshold of $p < 0.05$. **(D)** Response ratio of chlorophyll content of *B. japonicum*-inoculated plants relative to mock-inoculated plants. Measurements represent the log of the Soil Plant Analysis Development (SPAD) chlorophyll scores of inoculated plants over SPAD scores of mock-inoculated plants. Letters indicate significance groups as determined by a mixed model regression analysis followed by a Tukey HSD *post hoc* test. **(E)** Photographs show representative plants, 3 weeks post-inoculation.

and null as controls (**Supplementary Table 1**). The sequences (150 bp paired ends) were aligned to *G. max* genome V1.1 (Phytozome id360 V9.0; **Supplementary Figure 2**). Principal components analysis (**Figure 4**) was used to identify the major sources of variation among the transcriptomes. As expected, *P. sojae* infection accounted for most variation (PC1, 86.7% of variation). PC2 (2.8% of variation) accounted for much of the differences associated with the type of transgene. In particular, the highest-expressing GmPH line (GmPH9#4) clearly separated from the other lines, both with and without *P.sojae* infection. The lower-expressing GmPH line (GmPH23#11) and the higher expression VAM line (VAM13#P1) also consistently separated

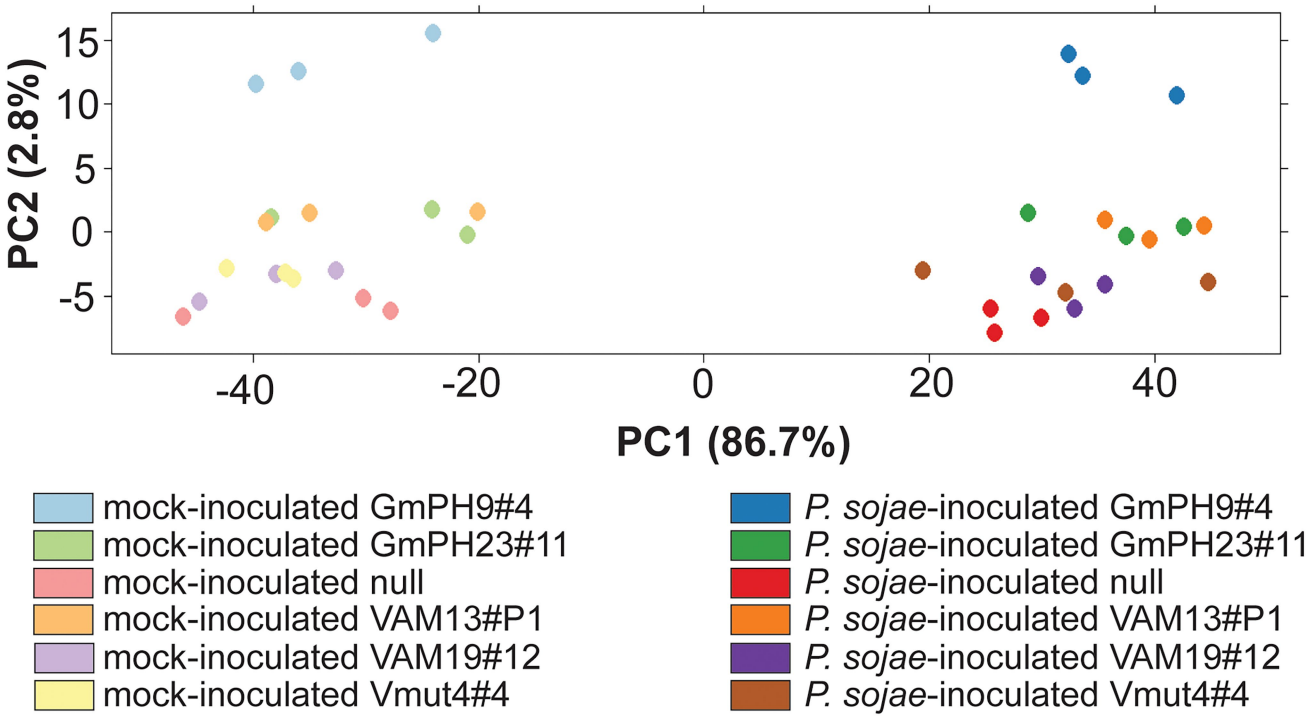

FIGURE 4 | Principal component analysis of RNA sequencing count data generated by DEseq. Each dot represents one RNA library; there were three libraries per genotype-treatment replicate.

from the controls under both treatments. The non-transformed null segregant, and the VAM mutant line, but also the lower-expressing VAM line (VAM19#12) were indistinguishable within each treatment. For subsequent analyses, data from the non-transformed null segregant line and transgenic non-binding VAM (Vmut) lines were combined as the "Control," the two independent VAM lines (VAM13#P1 and VAM19#12) were combined into genotype "VAM," and the two independent GmPH lines (GmPH9#4, GmPH23#11) were combined into genotype "GmPH."

To calculate differential expression, we used a mixed model analysis to compare Genotype (VAM or GmPH compared to Control), Treatment (*P. sojae* compared to Mock), and Genotype X Treatment interaction as fixed effects, with Replicate as a random effect. Effects were estimated for 34,527 out of 73,320 genes (47.1%) in the *G. max* v1.1 transcriptome. Of the genes not analyzed, 93% exhibited 0 counts for all conditions. The false discovery rate threshold was set at $p < 0.1$ using the method of Benjamini and Hochberg (1995). We added an additional threshold of a 2-fold difference based on likely biological relevance. The numbers of genes exhibiting significant differences and at least 2-fold differences are summarized in **Figure 5**.

To validate the results of the differential expression analysis of the RNA sequencing data, quantitative reverse-transcriptase PCR was used to measure a small sample of genes that tested as significantly different in the mock-treated GmPH control group, relative to the internal control gene *GmCYP2* (Glyma12g02790), which consistently showed a negligible change across genotypes and treatments. Four genes with different expression patterns were tested, namely Glyma04g02230, Glyma10g26320, Glyma02g14630, and Glyma18g07396. The results revealed good agreement between the estimates of transcript level changes from the RNAseq and qRT-PCR measurements (**Supplementary Figure 3**).

Transcript Levels Altered by GmPH and VAM Transgenes in the Absence of Infection

In mock-inoculated tissues, 67 genes were significantly changed by 2-fold or more in the GmPH lines compared to the controls, whereas 54 were changed in the VAM lines (**Figure 5A**; **Supplementary Table 3**). However, only 25 genes were changed in both GmPH and VAM lines. Of these 25, only three were significantly elevated more than 2-fold in both sets of lines, while 21 were decreased in both sets of lines (**Table 1**). One of the genes elevated in both lines (155-fold in the GmPH lines and 6.4-fold on the VAM lines) was *Glyma17g19845*, which encodes a dihydroflavonol 4-reductase involved in anthocyanin biosynthesis. One of the genes decreased in both sets of lines was Glyma06g21480 which encodes an ortholog of the *Arabidopsis* ENHANCED DISEASE RESISTANCE 2 (EDR2), which is a negative regulator of cell death elicited by pathogen attack. Of note, a single gene was significantly elevated in the GmPH lines but decreased in the VAM lines (5.3-fold and 3.2-fold, respectively, resulting in a 17-fold difference

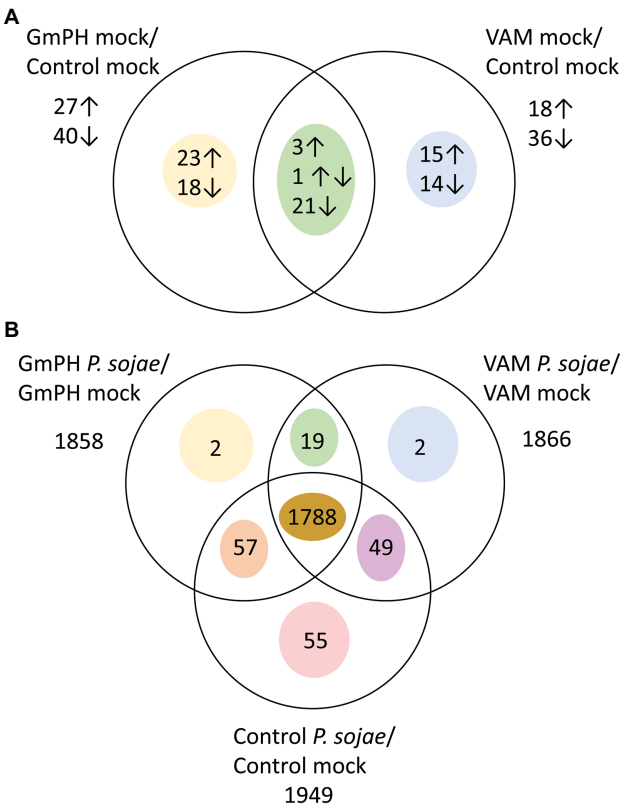

FIGURE 5 | Genes differentially expressed among transgenic lines following mock or *P. sojae* inoculation. **(A)** Numbers of genes with transcript levels differing significantly (FDR $p < 0.1$) and by at least 2-fold comparing GmPH or VAM lines with control lines. Arrows indicate whether transcript levels were higher or lower than the control lines. One gene had higher levels in GmPH lines but lower in the VAM lines. **(B)** Numbers of genes with transcript levels differing significantly (FDR $p < 0.1$) and by at least 2-fold comparing *P. sojae*-with mock-inoculated tissue.

TABLE 1 | Transcript-level differences in the absence of *Phytophthora sojae*.

Transcript-level differences in the absence of *P. sojae*	Number of genes
Mean (GmPH,VAM)/control >2x	3
Mean (GmPH,VAM)/control <0.5x	21
Total	24
GmPH/VAM >2x	26
GmPH more increased than VAM	15
GmPH less decreased than VAM	11
VAM/GmPH >2x	23
VAM more increased than GmPH	8
VAM less decreased than GmPH	15
Total	49

between the two sets of lines). This gene, Glyma06g37401, encoded an ortholog of the *Arabidopsis* protein JAR1, which is responsible for the synthesis of the key defense signal jasmonate-isoleucine.

There were 41 genes significantly changed more than 2-fold in the GmPH lines but not the VAM lines (**Figure 5A**), including three glycosyl hydrolases that were elevated 3.2- to 4.3-fold. Among 29 genes significantly changed more than 2-fold in the VAM lines but not the GmPH lines, there were three transcription factors including *Glyma02g00870* (elevated 2.1-fold) which encodes an ortholog of the Arabidopsis ETHYLENE-RESPONSE FACTOR 1 (AtERF1). Also included was *Glyma14g12210* (elevated 4.6-fold) which encodes an ortholog of the *Arabidopisis* CULLIN 1, subunit of an SCF ubiquitin ligase complex involved in mediating responses to auxin and jasmonic acid. A third gene was *Glyma19g38740* (elevated 18-fold), which encodes an ortholog of *Arabidopisis* PUB22, an E3 ubiquitin ligase that negatively regulates plant immunity.

Transcript Levels Altered in Both GmPH and VAM Lines in the Presence of *Phytophthora sojae*

In *P. sojae*-inoculated tissues, a total of 1972 gene transcript levels were significantly altered (FDR-adjusted $p < 0.1$) compared to mock inoculation by 2-fold or more in at least one of the GmPH, VAM, or control tissues (**Figure 5B**; **Supplementary Table 4**). Of those genes, 1788 were altered in all three genotypes. Only 19 genes exhibited transcript levels changed in both GmPH and VAM lines but not in the controls, whereas transcript levels of 55 genes were changed in the controls but not in either of the GmPH and VAM lines. To better explore the similarities in the GmPH and VAM lines' responses to *P. sojae* infection, we selected all genes significantly altered by infection in both the GmPH and VAM lines, or only in the controls, and calculated those in which the geometric mean response to infection in the GmPH and VAM lines was at least 2-fold different than in the control lines. There were 43 genes in which the mean of the two lines was at least 2-fold greater than in the control lines and 14 in which the mean was at least 2-fold less (**Table 2**).

Transcript Levels Differentially Altered in GmPH and VAM Lines in the Presence of *Phytophthora sojae*

In order to explore differences in the transcript profiles of GmPH lines compared to VAM lines that might be associated with the differences in resistance of the lines to *P. sojae* infection, we identified genes in which transcript levels during *P. sojae*

TABLE 2 | Common transcript-level changes in the presence of *Phytophthora sojae*.

Transcript-level changes in the presence of *P. sojae*	Number of genes
Mean (GmPH,VAM)/control >2x	43
GmPH, VAM more increased	22
GmPH, VAM less decreased	9
GmPH, VAM unchanged; control decreased	12
Mean (GmPH,VAM)/control <0.5x	14
GmPH, VAM less increased	4
GmPH, VAM more decreased	4
GmPH, VAM unchanged; control increased	6
Total	57

infection were more than 2-fold different between the two sets of lines, as well as significantly elevated (FDR-adjusted value of $p < 0.1$) during *P. sojae* infection in at least one of the two sets of lines. There were 22 genes with transcripts more strongly elevated during *P. sojae* infection of GmPH lines than of VAM lines, and 30 genes for which the reverse was true (**Table 3**). The 22 genes included *Glyma13g17340* (elevated 161-fold by infection in the GmPH lines, but only 73-fold in the VAM lines), which is an ortholog of the Arabidopsis *FMO1* gene involved in biosynthesis of L-pipecolic acid, a long-distance signal of systemic acquired resistance. The 30 genes more strongly elevated in the VAM lines included eight transcription factors, four in the myb class, three basic helix–loop–helix factors, and one C_2H_2 domain factor.

TABLE 3 | Differential transcript-level changes in the presence of *Phytophthora sojae*.

Transcript-level changes in the presence of *P. sojae*	Number of genes
GmPH/VAM >2x	22
GmPH more increased than VAM	16
GmPH less decreased than VAM	6
VAM/GmPH >2x	30
VAM more increased than GmPH	25
VAM less decreased than GmPH	5
Total	52

Gene Ontology Annotations of Genes Affected by Transgene Expression in the Absence of *Phytophthora sojae*

In order to explore the biological significance of the transcript-level changes noted above, we performed Gene Ontology (GO) annotation enrichment analysis. We compared the fraction of significantly changed transcripts annotated with each GO term with the overall frequency of genes annotated with that GO term within the Arabidopsis database used to annotate the soybean genes. We used Fisher's exact test with false discovery rate control of 0.1 to identify annotation terms significantly enriched among each soybean gene set of interest.

Among 96 transcript levels significantly altered (FDR $p < 0.1$) by at least 2-fold in the GmPH or VAM lines compared to the control lines, in the absence of *P. sojae*, there were 10 in which the *Arabidopsis* ortholog was annotated with the GO term "GO:0098542 Defense response to other organism" (3.5-fold enrichment; FDR $p < 0.1$), 11 annotated with "GO:0009725 Response to hormone" (3.0-fold enrichment; FDR $p < 0.1$), and four genes annotated with "GO:0009753 Response to Jasmonic Acid" (7.3-fold enrichment; FDR $p < 0.1$). However, neither of these terms were significantly enriched among the 24 genes altered in both the GmPH and VAM lines (**Table 4**).

Among 49 transcripts differing in level by more than 2-fold between the GmPH and VAM lines (**Table 1**), there were nine in which the *Arabidopsis* ortholog was annotated with the GO

TABLE 4 | Enrichment of Gene Ontology (GO) terms among genes significantly altered in transcript levels in GmPH and VAM lines in the absence of *Phytophthora sojae*.

Gene transcript changes	Altered in VAM or GmPH lines[b]		Altered in both VAM and GmPH lines[c]		Differing between VAM and GmPH lines[d]	
Significant genes[a]	(96 Genes)		(24 Genes)		(49 Genes)	
GO term or other treatment	Genes[e]	Enrichment[f]	Genes	Enrichment	Genes	Enrichment
GO:0098542 Defense response to other organism	10	3.5*	1	1.4	9	6.1**
GO:0050832 Defense response to fungus	4	2.5	1	2.5	2	2.5
GO:0042742 Defense response to bacterium	2	1.8	0	0	2	3.4
GO:0009725 Response to hormone	11	3.0*	2	2.2	7	3.8*
GO:0009753 Response to jasmonic acid	4	7.3*	0	0	3	10.7*
GO:0009737 Response to abscisic acid	2	1.4	0	0	2	2.7
GO:0009723 Response to ethylene	3	6.9	1	9.1	0	0.0
GO:0009735 Response to cytokinin	2	3.2	1	0	1	3.0
GO:0009733 Response to auxin	1	1.0	0	0	1	1.9
GO:0009751 Response to salicylic acid	1	1.8	1	7.0	0	0.0
GO:0009416 Response to light stimulus	4	5.7	3	17.1*	0	0.0
GO:0006979 Response to oxidative stress	3	3.1	0	0	3	6.0
GO:0009611 Response to wounding	2	3.0	0	0	1	0.0
Changed during *P. sojae* infection of control lines[g]	21	3.9***	4	3.0*	8	2.9**

[a]*Detailed list of genes, annotations, and transcript levels are provided in* ***Supplementary Table 2****.*

[b]*Significantly (FDR-adjusted value of $p < 0.1$) elevated or decreased at least 2-fold in the mock-inoculated GmPH lines or VAM lines compared to the control lines.*

[c]*Genes that showed significant (FDR-adjusted value of $p < 0.1$) transcript changes of at least 2-fold in the same direction in both the GmPH and VAM lines compared to the control lines.*

[d]*Genes in which transcript levels differed between the GmPH and VAM lines by at least 2-fold and in which at least one set of lines (GmPH or VAM) differed significantly from the control lines.*

[e]*Number of genes meeting the criterion that were annotated with each GO term.*

[f]*The fraction of all significantly altered genes with the GO annotation, divided by the fraction of all genes with the GO annotation; asterisks indicate whether the enrichment is statistically significant based on a Fisher's exact test with a false discovery rate correction, * FDR-adjusted $p < 0.1$; ** FDR-adjusted $p < 0.001$; *** FDR-adjusted $p < 0.001$.*

[g]*Transcript levels changed significantly (FDR-adjusted value of $p < 0.1$) by at least 2-fold in P. sojae-inoculated control lines compared to mock-inoculated control lines.*

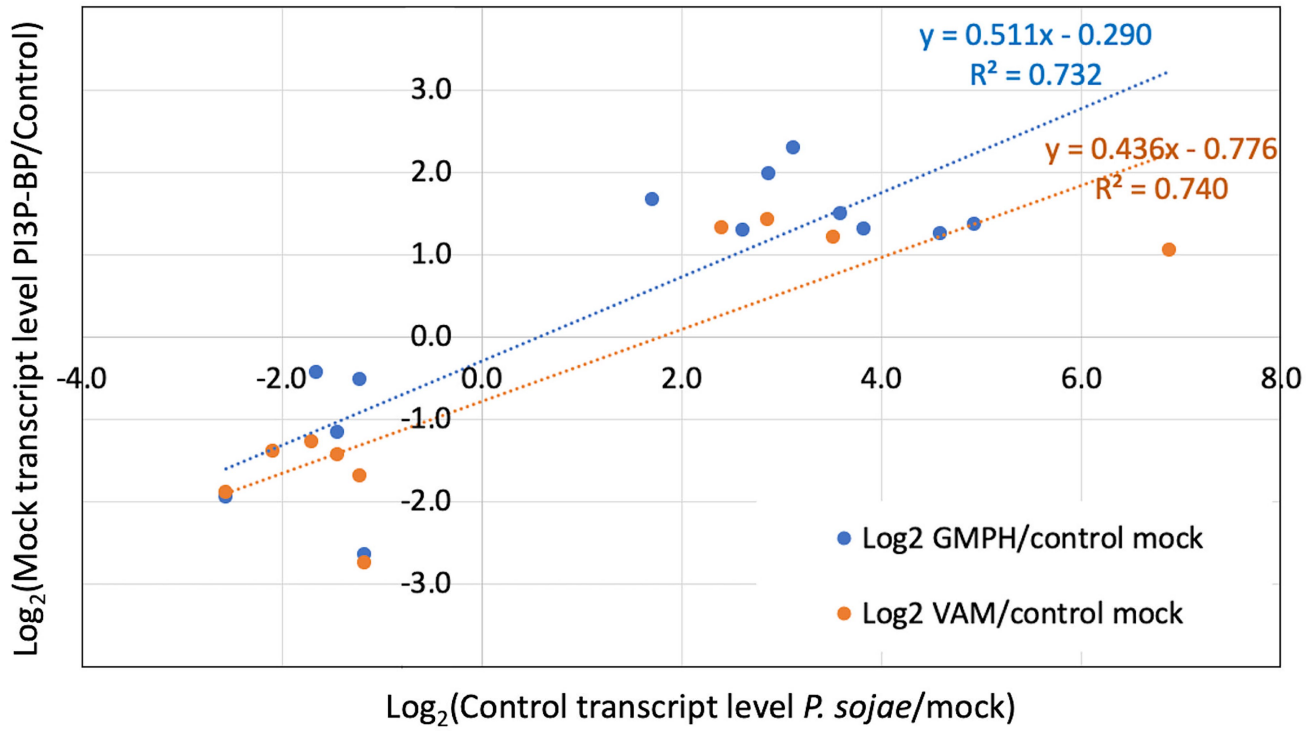

FIGURE 6 | Correlation of relative transcript levels in mock inoculated GmPH and VAM lines with relative transcript levels in *P. sojae*-inoculated control lines. Only genes exhibiting significant changes in both Mock GmPH/Control and *P. sojae*/Mock Control or both Mock VAM/Control and *P. sojae*/Mock Control are included.

term "GO:0098542 Defense response to other organism" (6.1-fold enrichment; FDR $p < 0.01$), 7 annotated with "GO:0009725 Response to hormone" (3.8-fold enrichment; FDR $p < 0.1$), and 3 genes annotated with "GO:0009753 Response to Jasmonic Acid" (10.7-fold enrichment; FDR $p < 0.1$; **Table 4**).

We also performed enrichment analysis on each gene set to determine the overlap with genes significantly altered by *P. sojae* infection of the control lines, to determine whether the expression of the GmPH and/or VAM transgenes was causing infection-associated genes to be altered. All three gene sets noted above exhibited significant enrichment for genes also altered by *P. sojae* infection of the control lines (2.9- to 3.9-fold, FDR $p < 0.1$; **Table 4**). Furthermore, as shown in **Figure 6**, there was a strong correlation ($R^2 > 0.7$) between the changes induced by transgene expression in the absence of *P. sojae* with the changes induced by *P. sojae* infection of the control lines.

Gene Ontology Annotations of Genes Affected by Transgene Expression in the Presence of *Phytophthora sojae*

As expected, infection-related GO terms were significantly enriched among the 57 genes in which the mean response of the GmPH and VAM lines to *P. sojae* infection was >2-fold different than the control lines. Those terms included "GO:0098542 Defense response to other organism," "GO:0050832 Defense response to fungus," and "GO:0006979 Response to oxidative stress" (**Table 5**). Also significantly enriched were genes annotated with "GO:0009725 Response to hormone" (8.4-fold, FDR $p < 0.001$) including genes annotated with "GO:0009753 Response to jasmonic acid" (18.4-fold, FDR $p < 0.001$) and "GO:0009737 Response to abscisic acid" (7.1-fold, FDR $p < 0.01$; **Table 5**).

Similarly, among the 52 genes in which the response to infection differed between the GmPH and VAM lines, "GO:0098542 Defense response to other organism" (6.4-fold, FDR $p < 0.001$) and "GO:0009725 Response to hormone" (4.6-fold, $p < 0.01$) were significantly enriched (**Table 5**). However, "GO:0009753 Response to jasmonic acid" (3.4-fold, FDR $p > 0.1$) was not significantly enriched (**Table 5**).

Transgenic Soybeans Expressing GmPH Domains Show Changes in Levels of Phytohormones Involved in Defense Signaling

Given the significant enrichment of genes annotated with "GO:0009725 Response to hormone" among the transcriptome data, we assessed differences in phytohormone production in the mock-and *P. sojae*-inoculated GmPH and control soybean lines, using a similar experimental design as for the RNA sequencing experiment. After inoculation of hypocotyls, both infected hypocotyl tissue and uninfected primary leaves were harvested 12 h later and hormones measured with LC-electrospray ionization-tandem mass spectrometry (LC-ESI-MS/MS). The full set of phytohormone measurements is listed in **Supplementary Table 5**.

TABLE 5 | Enrichment of GO terms among genes significantly altered in transcript levels in GmPH and VAM lines in the presence of *Phytophthora sojae*.

Gene transcript changes	Mean response of VAM and GmPH lines different than controls[a]		Differing response between VAM and GmPH lines[b]	
Significant genes	**(57 Genes)**		**(52 Genes)**	
GO term	**Genes[c]**	**Enrichment[d]**	**Genes**	**Enrichment**
GO:0098542 Defense response to other organism	12	7.0***	11	7.1***
GO:0050832 Defense response to fungus	7	7.5***	6	7.0**
GO:0042742 Defense response to bacterium	6	8.9**	5	8.1**
GO:0009725 Response to hormone	18	8.4***	8	4.1*
GO:0009753 Response to jasmonic acid	6	18.4***	1	3.4
GO:0009739 Response to gibberellin	0	0.0	2	9.7
GO:0009737 Response to abscisic acid	6	7.1**	1	1.3
GO:0009723 Response to ethylene	2	7.7	0	0.0
GO:0009735 Response to cytokinin	1	2.6	0	0.0
GO:0009733 Response to auxin	2	3.3	1	1.8
GO:0009751 Response to salicylic acid	2	5.9	1	3.2
GO:0009416 Response to light stimulus	4	9.6**	3	7.9*
GO:0006979 Response to oxidative stress	4	6.9*	3	5.7
GO:0009611 Response to wounding	3	7.4*	0	0.0

Gene transcript criteria were as follows:

[a]Genes which showed significant (FDR-adjusted value of $p < 0.1$) transcript changes of at least 2-fold in the same direction in both the GmPH and VAM lines in response to P. sojae and in which the mean change of the GmPH and VAM lines was at least 2-fold different compared to the control lines, also includes genes in which the response in the control lines was at least 2-fold and significant (FDR-adjusted value of $p < 0.1$), but the GmPH and VAM lines both did not respond significantly.

[b]Genes in which changes in transcript levels in response to P. sojae infection differed between the GmPH and VAM lines by at least 2-fold and in which at least one set of lines (GmPH or VAM) differed significantly (FDR-adjusted value of $p < 0.1$) by at least 2-fold from the control lines.

[c]Number of genes meeting the criterion that were annotated with each GO term.

*[d]The fraction of all significantly altered genes with the GO annotation, divided by the fraction of all genes with the GO annotation; asterisks indicated whether the enrichment is statistically significant based on a Fisher's exact test with a false discovery rate correction: * FDR-adjusted $p < 0.1$; ** FDR-adjusted $p < 0.01$; *** FDR-adjusted $p < 0.001$.*

Analysis of mock-inoculated hypocotyl tissue showed that transgenic GmPH soybeans had a significantly higher level of JA-isoleucine, the bioactive form of jasmonic acid (33.2% increase). However, with *P. sojae* infection, the elevation was only 26.3% and not statistically significant (**Figure 7A**). Levels of jasmonic acid were elevated slightly in GmPH hypocotyl tissue for both treatments, but this was not significant (13.3% difference in mock, 11.1% difference in *P. sojae*-treated tissue, **Figure 7C**). Altered levels of JA-isoleucine were also seen in the uninfected primary leaf tissue distal to the site of inoculation on the hypocotyl. Levels of JA-isoleucine in control leaves showed a 44.2% decrease in *P. sojae*-inoculated tissue compared to mock (**Figure 7B**). This pattern was not seen in GmPH leaf tissue, where there was no change JA-Ile levels between mock- and *P. sojae*-inoculated tissue (**Figure 7B**). Likewise, there were no significant differences in JA levels among the leaf samples (**Figure 7D**). In addition to JA-Ile, there were also altered patterns of 12-hydroxyjasmonic acid and its isoleucine conjugate between control and GmPH leaf tissue (**Supplementary Table 5**).

The wound-induced hormone, traumatin [(10E)-12-Oxododec-10-enoic acid] (English et al., 1939; Zimmerman and Coudron, 1979; Nakashima et al., 2013), showed significantly altered patterns in both hypocotyl and leaf tissue that suggested an increased induction following *P. sojae* inoculation of GmPH plants. The increase in hypocotyl tissue was slight (13.6% between mock- and *P. sojae*-inoculated control tissue; 21.2% between mock- and *P. sojae*-inoculated GmPH tissue, **Figure 7E**). However in leaf tissue, the difference in levels of traumatin in both mock- and *P. sojae*-inoculated control tissues was negligible, but there was a 43.8% increase in the *P. sojae*-inoculated tissue compared to mock-inoculated GmPH tissue ($p < 0,05$; **Figure 7F**).

DISCUSSION

The objective of this study was to test whether secretion of phosphoinositide-3-phosphate (PI3P)-binding proteins could confer disease resistance on stable transgenic soybean plants. The motivation for this strategy was evidence suggesting that binding to PI3P was involved in entry of oomycete RXLR effectors and some fungal effectors into host cells (Kale et al., 2010). Although the involvement of PI3P in effector entry remains controversial (Kale et al., 2010; Petre and Kamoun, 2014; Wawra et al., 2017), Helliwell et al. (2016) showed that secretion of phosphoinositide-3-phosphate (PI3P)-binding proteins could confer resistance against oomycete and fungal pathogens on stable transgenic cacao (*T. cacao*) plants. In that study, the transgenic PI3P-binding cacao leaves were shown to have enhanced resistance to two different species of oomycete pathogens: *Phytophthora tropicalis* and *P. palmivora*, which are both causal agents of Black pod rot, along with two isolates of fungal pathogen *Colletotrichum theobromicola*, which causes a leaf and pod spot disease. Resistance could be observed when any of four different phosphoinositide-3-phosphate (PI3P)-binding proteins were expressed in the cacao leaves. Furthermore, resistance required a functional PI3P-binding site and also required secretion of the proteins to the apoplast. Those results demonstrated that the strategy was effective against diverse pathogens (Helliwell et al., 2016).

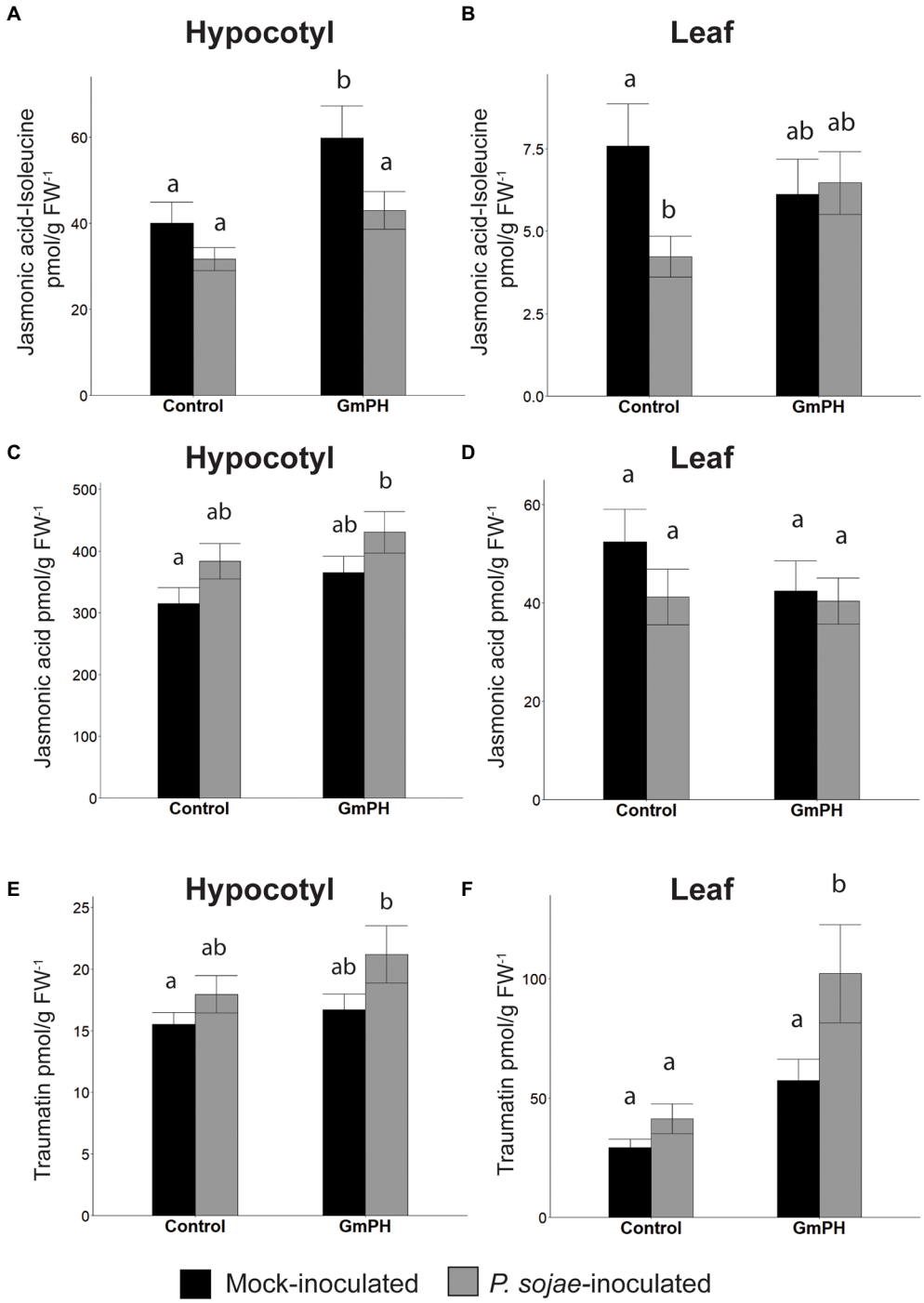

FIGURE 7 | Phytohormone levels in GmPH and Control soybean lines. **(A,B)** Levels of Jasmonic acid-Isoleucine conjugate in hypocotyls **(A)** or primary leaves **(B)** of control (null and Vmut) and GmPH (GmPH9#4 and GmPH23#11) lines after mock- or *P. sojae* inoculation. **(C,D)** Levels of jasmonic acid, in hypocotyls **(C)** or primary leaves **(D)** of control and GmPH lines after mock- or *P. sojae* inoculation. **(E,F)** Levels of traumatin in hypocotyls **(E)** or primary leaves **(F)** of control and GmPH lines after mock- or *P. sojae* inoculation. All measurements represent the average of three independent biological replicates, 12 plants pooled per replicate. Letters represent significance groups at $p < 0.05$.

In this study, we selected two PI3P-binding proteins that would be considered acceptable in a transgenic food plant, namely the soybean PH domain protein GmPH1 and the yeast PX domain protein VAM7. As controls, we selected a VAM7 mutant that had been validated as a negative control by Helliwell et al. (2016) as well as a PI4P-binding protein FAPP1, which

had also been shown to be ineffective in conferring resistance in cacao. Our results confirmed that stable expression of the two PI3P-binding proteins in soybean could increase resistance against *P. sojae*. Plants expressing GmPH protein showed resistance in both detached leaf and hypocotyl inoculation assays, while plants expressing VAM7 protein showed statistically significant resistance only in the leaf assays. Plants expressing the two proteins displayed a wide range of transcript levels for the relevant transgenes, but the level of resistance was not correlated with transcript levels. In cacao, the VAM7 constructs conferred a slightly higher level of resistance than the GmPH constructs (Helliwell et al., 2016). Differences in the level of resistance conferred might result from the level and stability of the secreted proteins in the apoplast of each species.

Here, we also examined the effect of transgene expression on nodulation by the mutualist, *B. japonicum*, which is important to soybean production and hence to the phenotype conferred by the transgenes. The results showed that two of the GmPH lines, GmPH9#4 and GmPH22#5, exhibited fewer and smaller nodules, as well as reduced physiological benefits from nodulation. Since *B. japonicum*, like other prokaryotes, does not produce PI3P, these results suggested that the physiology of the plants themselves might be responsible for the resistance to both *P. sojae* and *B. japonicum*.

To assess the physiology of the plants, we conducted transcriptome and hormone analyses. In particular, we aimed to investigate the physiological basis for the enhanced resistance against *P. sojae* and also to investigate why two of the GmPH lines, but not the VAM lines, showed increased resistance to *B. japonicum*.

Although 96 genes exhibited altered transcript levels in either the GmPH or VAM lines in the absence of *P. sojae*, only 24 exhibited altered transcript levels in both the GmPH and VAM lines. Changes shared by the two sets of lines might be associated with the PI3P-binding activities of the GmPH and VAM domain proteins produced by the lines. The GO terms "GO:0098542 Defense response to other organism" and "GO:0009753 Response to jasmonic acid" were elevated among the larger set of 96 genes, but not among the shared set of 24 genes. On the other hand, genes that responded to *P. sojae* infection in the control lines were significantly enriched in the shared set of 24 genes as well as the larger set of 96 genes. Furthermore, there was a significant correlation between the magnitude of the change during infection of the control lines and the magnitude of the change in the GmPH and VAM lines in the absence of infection. These observations suggest that expression of either of the PI3P-binding domains, but not the control constructs, may produce a physiological state related to a defense response, which perhaps better prepares the plants to resist infection. Decreased expression of an ortholog of *Arabidopsis* EDR2 in both sets of lines is consistent with this hypothesis. *Arabidopsis edr2* mutants exhibit enhanced resistance against biotrophic fungi (Tang et al., 2005; Vorwerk et al., 2007). Defense-related genes are elevated more strongly in *edr2* mutants following infection compared to wild-type plants (Tang et al., 2005; Vorwerk et al., 2007).

In the presence of *P. sojae*, a wider set of genes (56) showed greater than a 2-fold difference in both the GmPH and VAM lines than in the controls. These genes included the GO annotations "GO:0009753 Response to jasmonic acid" (12.5-fold, FDR $p < 0.01$) and "GO:0009737 Response to abscisic acid." These observations are consistent with a stronger defense response in the GmPH and VAM lines, possibly involving altered jasmonate and abscisic acid signaling. Consistent with this observation, jasmonyl-isoleucine levels were 49.9% higher ($p < 0.05$) in mock-inoculated GmPH hypocotyls compared to the control lines. Jasmonate is well documented as being required for *Phytophthora* resistance in several plant species (Li et al., 2020; Long et al., 2021). Abscisic acid has been documented as a negative regular of plant defense against hemi-biotrophic pathogen, but can contribute positively to defense through the regulation of callose deposition (Mauch-Mani and Mauch, 2005) and also positively regulates defense against necrotrophs (García-Andrade et al., 2020). Leaf tissue distal to the site of infection exhibited elevated levels of the wounding signal traumatin and decreased levels of IAA, which can inhibit defense responses (**Figure 7**). Therefore, these signal compounds could also possibly contribute to elevated resistance. On the other hand, the transcriptome data did not reveal enrichment of genes annotated with "GO:0009611 Response to wounding" or "GO:0009733 Response to auxin" in any lines in the presence or absence of *P. sojae*. Fatty acid oxylipins and epoxides with anti-microbial activity (Prost et al., 2005) that were elevated in the distal leaf tissues (**Supplementary Table 5**) may also contribute to increased resistance.

Genes that differ in expression between the GmPH and VAM lines might account for the different levels of *P. sojae* resistance conferred by the transgenes and also the negative effects on nodulation observed in some GmPH lines but not in the VAM lines. A substantial number of genes differed more than 2-fold in transcript levels between the GmPH and VAM lines, 52 in the presence of *P. sojae* and 49 in its absence. The GO term, "GO:0098542 Defense response to other organism" was significantly enriched among both gene sets. Furthermore, genes altered during *P. sojae* infection of the control lines were significantly enriched among the 49 genes differentially altered by transgene expression in the absence of *P. sojae*. One example was an ortholog of the Arabidopsis *FMO1* gene involved in biosynthesis of L-pipecolic acid, a long-distance signal of systemic acquired resistance (elevated 161-fold by infection in the GmPH lines, but only 73-fold in the VAM lines). Although the GO term "GO:0009753 Response to jasmonic acid" was not enriched within either gene set, a key jasmonate metabolic gene, JAR1, encoding jasmonyl-isoleucine synthetase, was 5.3-fold elevated in GmPH hypocotyls in the absence of *P. sojae* compared to control lines but 3.2-fold decreased in VAM hypocotyls. Consistent with this observation, jasmonyl-isoleucine levels were 49.9% higher ($p < 0.05$) in mock-inoculated GmPH hypocotyls compared to the control lines. These observations suggest that the different levels of resistance of the GmPH lines compared to the VAM lines may derive from elevated levels of signaling compounds such as L-pipecolic acid and jasmonyl-isoleucine.

Negative effects on nodulation were observed in the two lines with the highest expression levels of the GmPH domain protein (GmPh9#4 and GmPh22#5) but not in the line (GmPH23#11) with the lowest *GmPH* gene expression, nor in the lines expressing VAM domain proteins. Jasmonate has been implicated as negative regulator of nodulation in *Lotus japonicus* and *Medicago truncatula* (Nakagawa and Kawaguchi, 2006; Sun et al., 2006), so it is possible that elevated synthesis of jasmonyl-isoleucine observed in the two lines expressing the highest levels of the GmPH domain proteins may be responsible for this negative effect. However, the fact that the VAM lines and the lowest-expressing GmPH line all exhibited elevated *P. sojae* resistance in the absence of negative effects on nodulation indicates that the two phenotypes are not inevitably connected.

Overall, the results from this study confirm the observation by Helliwell et al. (2016) that transgenic expression of PI3P-binding proteins is an effective strategy for increasing *Phytophthora* resistance in crop plants. In particular, our results show that the soybean GmPH and yeast VAM domain proteins, both from species regularly consumed by humans, are effective in this role. Our results also show that potential negative effects on interactions with beneficial microbes such as rhizobia are not an inevitable consequence of increased oomycete resistance and can be avoided. Ultimately though, additional factors may play a role in resistance when the plants are grown outside of a controlled environment. As a case in point, two small field tests conducted to date did not reveal statistically significant differences between lines expressing PI3P-binding proteins and non-transgenic soybeans for seedling establishment or yield in the presence of *P. sojae*.

The mechanisms by which secretion of PI3P-binding proteins increases resistance to *Phytophthora* infection remain to be fully resolved. Since multiple PI3P-binding proteins, but not mutant proteins, confer resistance in both soybean (this study) and cacao (Helliwell et al., 2016), the PI3P-binding activities of the proteins appear essential for producing resistance. The original rationale for employing these proteins, namely interfering with PI3P-mediated effector entry, was not directly addressed by this study, though the increased expression of many host defense genes during *P. sojae* infection could plausibly result from decreased entry of defense-suppressing effector proteins. This study does, however, demonstrate that the expression of the PI3P-binding proteins induces elevated expression of many infection-associated genes, consistent with the triggering of some kind of primed state in the plants (Mauch-Mani et al., 2017) possibly involving jasmonate (Arévalo-Marín et al., 2021). The mechanisms by which this state is produced remain to be investigated, in particular whether the PI3P molecules involved are located externally or internally. Helliwell et al. (2016) showed that PI3P-binding protein must be secreted in order to confer resistance to *Phytophthora* species. However, our experiments did not test whether PI3P-binding proteins without a secretory leader could trigger transcriptional changes associated with a possible primed state. Lu et al. (2013) also showed that secreted PI3P-binding proteins could target the mycelial surface of *P. sojae*, and Zhou et al. (2021) showed that this action could be used to target anti-microbial peptides to the surface of several *Phytophthora* species. So it is possible that secreted PI3P-binding proteins could negatively impact the pathogen directly, as a third mechanism of action.

DATA AVAILABILITY STATEMENT

The datasets presented in this study can be found in online repositories. The names of the repository/repositories and accession number(s) can be found at: NCBI GEO—GSE201739.

AUTHOR CONTRIBUTIONS

BT and WP conceived the project. EH, PL, JV-A, SP, EB, MK, WP, and BT planned the experiments. EH, PL, FA, MD, AC, JV-A, BK, and EB conducted the experiments. EH, BK, EB, and BT analyzed the data. EH and BT wrote the paper with input from all authors. All authors contributed to the article and approved the submitted version.

FUNDING

This work was supported by NSF grant IOS-0965353 (to BT), USDA NIFA AFRI grant 2011-68004-30104 (to BT and WP), and by Oregon State University. The metabolite analyses were in part supported by USDA NIFA grant 2017-67013-26524 to MK, and the *B. japonicum* assays were in part supported by NSF-DEB-193239 to SP.

ACKNOWLEDGMENTS

We thank Mark Dasenko and Shawn O'Neil of the Center for Genome Research and Biocomputing, and Yuan Jiang at Oregon State University for generation, processing, and help with statistical analysis of transcriptome data, Zoie Lopez at Washington State University Vancouver for help with statistical analysis of *B. japonicum* data, and Thomas Jacobs at University of Georgia for technical assistance. We also thank Sarah Johnson and April Lang for generation and characterization of the transgenic soybean plants, and Alison Roberts at Iowa State University and Martin Chilvers at Michigan State University for work on the field trials.

SUPPLEMENTARY MATERIAL

The Supplementary Material for this article can be found online at: https://www.frontiersin.org/articles/10.3389/fmicb.2022.923281/full#supplementary-material

Supplementary Figure 1 | Quantitative real-time PCR (qRT-PCR) measurements of the quantity of *P. sojae* genomic DNA relative to soybean genomic DNA (*PsActin* vs. *GmCYP2*) in non-transformed cv. Williams within 48 h after inoculation. Bars represent the average of three biological replicates (six pooled plants per replicate). Errors represent the SEM.

Supplementary Figure 2 | Alignment summary of RNA sequencing output to *Glycine max* genome. Left refers to the average percentage of left reads across all RNA samples that aligned to the *G. max* genome, right refers to the average percentage of right reads across all samples that aligned to the *G. max* genome, and concordant refers to the average percentage of paired reads across all genomes that aligned with the respective mate orientation to the *G. max* genome.

Supplementary Figure 3 | Quantitative reverse transcriptase PCR verification of transcript levels measured by RNA sequencing analysis from mock-inoculated soybean. Transcripts measured were Glyma04g02230 (Ornithine decarboxylase-like), Glyma10g26320 (Asparagine synthase-like), Glyma18g07396 (Glutamate synthase), and Glyma02g14630 (Phosphoenolpyruvate carboxykinase). Transcripts were normalized to the internal control gene *GmCYP2* then levels in GmPH lines (GmPh9#4 and GmPh23#11) or VAM lines (VAM13 and VAM19) were compared to the Control lines (null and Vmut). RNAseq differences were derived by linear mixed model analysis. Each qRT-PCR sample assay was run in duplicate. **(A)** GmPH lines and **(B)** VAM lines.

Supplementary Table 1 | Design of RNA sequencing experiment, showing the genotype, category, treatment, and number of replicates for each RNA library sequenced.

Supplemental Table 2 | FASTQ run reports and summary of RNA sequencing.

Supplemental Table 3 | Genes with transcript levels differing among mock-inoculated genotypes.

Supplemental Table 5 | Hormone measurements in soybean lines. Letter groups denote a significant difference between Control and GmPH soybean.

Supplemental Table 6 | List of primers and sequences used in this study.

REFERENCES

Aerts, N., Pereira Mendes, M., and Van Wees, S. C. (2021). Multiple levels of crosstalk in hormone networks regulating plant defense. *Plant J.* 105, 489–504. doi: 10.1111/tpj.15124

Anders, S., and Huber, W. (2010). Differential expression analysis for sequence count data. *Genome Biol.* 11:R106. doi: 10.1038/npre.2010.4282.1

Arévalo-Marín, D. F., Briceño-Robles, D. M., Mosquera, T., Melgarejo, L. M., and Sarmiento, F. (2021). Jasmonic acid priming of potato uses hypersensitive response-dependent defense and delays necrotrophic phase change against *Phytophthora infestans*. *Physiol. Mol. Plant Pathol.* 115:101680. doi: 10.1016/j.pmpp.2021.101680

Benjamini, Y., and Hochberg, Y. (1995). Controlling the false discovery rate: a practical and powerful approach to multiple testing. *J. R. Stat. Soc. Series B Stat. Methodol.* 57, 289–300.

Christensen, S. A., Nemchenko, A., Borrego, E., Murray, I., Sobhy, I. S., Bosak, L., et al. (2013). The maize lipoxygenase, *ZmLox10*, mediates green leaf volatile, jasmonate and herbivore-induced plant volatile production for defense against insect attack. *Plant J.* 74, 59–73. doi: 10.1111/tpj.12101

Coruzzi, G., Broglie, R., Edwards, C., and Chua, N.-H. (1984). Tissue-specific and light-regulated expression of a pea nuclear gene encoding the small subunit of ribulose-1, 5-bisphosphate carboxylase. *EMBO J.* 3, 1671–1679. doi: 10.1002/j.1460-2075.1984.tb02031.x

Cutt, J. R., Dixon, D. C., Carr, J. P., and Klessig, D. F. (1988). Isolation and nucleotide sequence of cDNA clones for the pathogenesis-related proteins PR1a, PR1b and PR1c of Nicotiana tabacum cv. Xanthi nc induced by TMV infection. *Nucleic Acids Res.* 16:9861.

DiNitto, J. P., and Lambright, D. G. (2006). Membrane and juxtamembrane targeting by PH and PTB domains. *Biochim. Biophys. Acta Mol. Cell Biol. Lipids* 1761, 850–867.

Dou, D., Kale, S. D., Wang, X., Jiang, R. H., Bruce, N. A., Arredondo, F. D., et al. (2008). RXLR-mediated entry of Phytophthora sojae effector Avr1b into soybean cells does not require pathogen-encoded machinery. *The Plant Cell* 20, 1930–1947.

Dowler, S., Currie, R. A., Campbell, D. G., Deak, M., Kular, G., Downes, C. P., et al. (2000). Identification of pleckstrin-homology-domain-containing proteins with novel phosphoinositide-binding specificities. *Biochem. J.* 351, 19–31.

Du, Z., Zhou, X., Ling, Y., Zhang, Z., and Su, Z. (2010). agriGO: a GO analysis toolkit for the agricultural community. *Nucleic Acids Res.* 38(Suppl. 2), W64–W70. doi: 10.1093/nar/gkq310

English, J., Bonner, J., and Haagen-Smit, A. J. (1939). The wound hormones of plants. IV. Structure and synthesis of a traumatin. *J. Am. Chem. Soc.* 61, 3434–3436. doi: 10.1021/ja01267a059

García-Andrade, J., González, B., Gonzalez-Guzman, M., Rodriguez, P. L., and Vera, P. (2020). The role of ABA in plant immunity is mediated through the PYR1 receptor. *Int. J. Mol. Sci.* 21:5852. doi: 10.3390/ijms21165852

Hancock, C. N., Zhang, F., Floyd, K., Richardson, A. O., LaFayette, P., Tucker, D., et al. (2011). The rice miniature inverted repeat transposable element mping is an effective insertional mutagen in soybean. *Plant Physiol.* 157, 552–562. doi: 10.1104/pp.111.181206

Helliwell, E. E., Vega-Arreguin, J., Shi, Z., Bailey, B., Xiao, S., Maximova, S. N., et al. (2016). Enhanced resistance in *Theobroma cacao* against oomycete and fungal pathogens by secretion of phosphatidylinositol-3-phosphate-binding proteins. *Plant Biotechnol. J.* 14, 875–886. doi: 10.1111/pbi.12436

Hernandez-Garcia, C. M., Martinelli, A. P., Bouchard, R. A., and Finer, J. J. (2009). A soybean (*Glycine max*) polyubiquitin promoter gives strong constitutive expression in transgenic soybean. *Plant Cell Rep.* 28, 837–849. doi: 10.1007/s00299-009-0681-7

Honée, G., Buitink, J., Jabs, T., De Kloe, J., Sijbolts, F., Apotheker, M., et al. (1998). Induction of defense-related responses in Cf9 tomato cells by the AVR9 elicitor peptide of Cladosporium fulvum is developmentally regulated. *Plant Physiol.* 1178, 809–820.

Jacobs, T. B., LaFayette, P. R., Schmitz, R. J., and Parrott, W. A. (2015). Targeted genome modifications in soybean with crispr/cas9. *BMC Biotechnol.* 15, 1–10. doi: 10.1186/s12896-015-0131-2

Jian, B., Liu, B., Bi, Y., Hou, W., Wu, C., and Han, T. (2008). Validation of internal control for gene expression study in soybean by quantitative real-time PCR. *BMC Mol. Biol.* 9, 1–14.

Jiang, R. H., Tripathy, S., Govers, F., and Tyler, B. M. (2008). RXLR effector reservoir in two Phytophthora species is dominated by a single rapidly evolving superfamily with more than 700 members. *PNAS* 105, 4874–4879. doi: 10.1073/pnas.0709303105

Jones, J. D., and Dangl, J. L. (2006). The plant immune system. *Nature* 444, 323–329. doi: 10.1038/nature05286

Kale, S. D., Gu, B., Capelluto, D. G. S., Dou, D.-L., Feldman, E., Rumore, A., et al. (2010). External lipid PI-3-P mediates entry of eukaryotic pathogen effectors into plant and animal host cells. *Cell* 142, 284–295. doi: 10.1016/j.cell.2010.06.008

Langmead, B., Trapnell, C., Pop, M., and Salzberg, S. L. (2009). Ultrafast and memory-efficient alignment of short DNA sequences to the human genome. *Genome Biol.* 10, 1–10.

Lee, C. S., Kim, I. S., Park, J. B., Lee, M. N., Lee, H. Y., Suh, P. G., et al. (2006). The phox homology domain of phospholipase D activates dynamin GTPase activity and accelerates EGFR endocytosis. *Nat. Cell Biol.* 8, 477–484.

Lemmon, M. A. (2008). Membrane recognition by phospholipid-binding domains. *Nat. Rev. Mol. Cell Biol.* 9, 99–111.

Li, H., Handsaker, B., Wysoker, A., Fennell, T., Ruan, J., Homer, N., et al. (2009). The sequence alignment/map format and SAMtools. *Bioinformatics* 25, 2078–2079. doi: 10.1093/bioinformatics/btp352

Li, W., Zhao, D., Dong, J., Kong, X., Zhang, Q., Li, T., et al. (2020). AtRTP5 negatively regulates plant resistance to *Phytophthora* pathogens by modulating the biosynthesis of endogenous jasmonic acid and salicylic acid. *Mol. Plant Pathol.* 21, 95–108. doi: 10.1111/mpp.12883

Long, J., Yang, M., Zuo, C., Song, N., He, J. M., Zeng, J., et al. (2021). Requirement of jasmonate signaling for defense responses against *Alternaria alternata* and *Phytophthora nicotiane* in tobacco. *Crop Sci.* 61, 4273–4283. doi: 10.1002/csc2.20625

Lu, S., Chen, L., Tao, K., Sun, N., Wu, Y., Lu, X., et al. (2013). Intracellular and extracellular phosphatidylinositol 3-phosphate produced by phytophthora

species are important for infection. *Mol. Plant* 6, 1592–1604. doi: 10.1093/mp/sst047

Mauch-Mani, B., Baccelli, I., Luna, E., and Flors, V. (2017). Defense priming: an adaptive part of induced resistance. *Annu. Rev. Plant Biol.* 68, 485–512. doi: 10.1146/annurev-arplant-042916-041132

Mauch-Mani, B., and Mauch, F. (2005). The role of abscisic acid in plant–pathogen interactions. *Curr. Opin. Plant Biol.* 8, 409–414. doi: 10.1016/j.pbi.2005.05.015

Nakagawa, T., and Kawaguchi, M. (2006). Shoot-applied MeJA suppresses root nodulation in *Lotus japonicus*. *Plant Cell Physiol.* 47, 176–180. doi: 10.1093/pcp/pci222

Nakashima, A., von Reuss, S. H., Tasaka, H., Nomura, M., Mochizuki, S., Iijima, Y., et al. (2013). Traumatin- and dinortraumatin-containing galactolipids in *Arabidopsis*: their formation in tissue-disrupted leaves as counterparts of green leaf volatiles. *J. Biol. Chem.* 288, 26078–26088. doi: 10.1074/jbc.M113.487959

Naveed, Z. A., Wei, X., Chen, J., Mubeen, H., and Ali, G. S. (2020). The PTI to ETI continuum in *Phytophthora*-plant interactions. *Front. Plant Sci.* 11:593905. doi: 10.3389/fpls.2020.593905

Petre, B., and Kamoun, S. (2014). How do filamentous pathogens deliver effector proteins into plant cells. *PLoS Biol.* 12:e1001801. doi: 10.1371/journal.pbio.1001801

Plett, J. M., Kemppainen, M., Kale, S. D., Kohler, A., Legué, V., Brun, A., et al. (2011). A secreted effector protein of Laccaria bicolor is required for symbiosis development. *Curr. Biol.* 21, 1197–1203.

Prost, I., Dhondt, S., Rothe, G., Vicente, J., Rodriguez, M. J., Kift, N., et al. (2005). Evaluation of the antimicrobial activities of plant oxylipins supports their involvement in defense against pathogens. *Plant Physiol.* 139, 1902–1913. doi: 10.1104/pp.105.066274

Rafiqi, M., Gan, P. H., Ravensdale, M., Lawrence, G. J., Ellis, J. G., Jones, D. A., et al. (2010). Internalization of flax rust avirulence proteins into flax and tobacco cells can occur in the absence of the pathogen. *The Plant Cell* 22, 2017–2032.

Sachs, J. L., Russell, J. E., and Hollowell, A. C. (2011). Evolutionary instability of symbiotic function in Bradyrhizobium japonicum. *PloS One* 6:e26370.

Schmutz, J., Cannon, S. B., Schlueter, J., Ma, J., Mitros, T., Nelson, W., et al. (2010). Genome sequence of the palaeopolyploid soybean. *Nature* 463, 178–183. doi: 10.1038/nature08670

Schneider, C. A., Rasband, W. S., and Eliceiri, K. W. (2012). NIH image to ImageJ: 25 years of image analysis. *Nat. Methods* 9, 671–675. doi: 10.1038/nmeth.2089

Song, T., Kale, S. D., Arredondo, F. D., Shen, D., Su, L., Liu, L., et al. (2013). Two RxLR avirulence genes in Phytophthora sojae determine soybean Rps 1k-mediated disease resistance. *Molecular Plant- Microbe Interactions* 26, 711–720.

Sun, J., Cardoza, V., Mitchell, D. M., Bright, L., Oldroyd, G., and Harris, J. M. (2006). Crosstalk between jasmonic acid, ethylene and nod factor signaling allows integration of diverse inputs for regulation of nodulation. *Plant J.* 46, 961–970. doi: 10.1111/j.1365-313X.2006.02751.x

Tang, D., Ade, J., Frye, C. A., and Innes, R. W. (2005). Regulation of plant defense responses in *Arabidopsis* by EDR2, a PH and START domain-containing protein. *Plant J.* 44, 245–257. doi: 10.1111/j.1365-313X.2005.02523.x

Torto-Alalibo, T., Collmer, C. W., Gwinn-Giglio, M., Lindeberg, M., Meng, S.-W., Chibucos, M. C., et al. (2010). Unifying themes in microbial associations with animal and plant hosts described using the gene ontology. *Microbiol. Mol. Biol. Rev.* 74, 479–503. doi: 10.1128/MMBR.00017-10

Trapnell, C., Pachter, L., and Salzberg, S. L. (2009). TopHat: discovering splice junctions with RNA-Seq. *Bioinformatics* 25, 1105–1111. doi: 10.1093/bioinformatics/btp120

Tyler, B. M., Tripathy, S., Zhang, X., Dehal, P., Jiang, R. H., Aerts, A., et al. (2006). Phytophthora genome sequences uncover evolutionary origins and mechanisms of pathogenesis. *Science* 313, 1261–1266.

van Esse, H. P., Bolton, M. D., Stergiopoulos, I., de Wit, P. J., and Thomma, B. P. (2007). The chitin-binding Cladosporium fulvum effector protein Avr4 is a virulence factor. *Mol. Plant Microbe Interact.* 20, 1092–1011.

Vorwerk, S., Schiff, C., Santamaria, M., Koh, S., Nishimura, M., Vogel, J., et al. (2007). Edr2 negatively regulates salicylic acid-based defenses and cell death during powdery mildew infections of *Arabidopsis thaliana*. *BMC Plant Biol.* 7, 1–14. doi: 10.1186/1471-2229-7-35

Wang, K.-D., Borrego, E. J., Kenerley, C. M., and Kolomiets, M. V. (2020). Oxylipins other than jasmonic acid are xylem-resident signals regulating systemic resistance induced by *Trichoderma virens* in maize. *Plant Cell* 32, 166–185. doi: 10.1105/tpc.19.00487

Wang, Q., Han, C., Ferreira, A. O., Yu, X., Ye, W., Tripathy, S., et al. (2011). Transcriptional programming and functional interactions within the *Phytophthora sojae* RXLR effector repertoire. *Plant Cell* 23, 2064–2086. doi: 10.1105/tpc.111.086082

Wang, Y., Tyler, B. M., and Wang, Y. (2019). Defense and counterdefense during plant-pathogenic oomycete infection. *Annu. Rev. Microbiol.* 73, 667–696. doi: 10.1146/annurev-micro-020518-120022

Wawra, S., Trusch, F., Matena, A., Apostolakis, K., Linne, U., Zhukov, I., et al. (2017). The RXLR motif of the host targeting effector Avr3a of *Phytophthora infestans* is cleaved before secretion. *Plant Cell* 29, 1184–1195. doi: 10.1105/tpc.16.00552

Whisson, S. C., Boevink, P. C., Moleleki, L., Avrova, A. O., Morales, J. G., Gilroy, E. M., et al. (2007). A translocation signal for delivery of oomycete effector proteins into host plant cells. *Nature* 450, 115–118.

Zhou, Y., Yang, K., Yan, Q., Wang, X., Cheng, M., Si, J., et al. (2021). Targeting of anti-microbial proteins to the hyphal surface amplifies protection of crop plants against *Phytophthora* pathogens. *Mol. Plant* 14, 1391–1403. doi: 10.1016/j.molp.2021.05.007

Zimmerman, D. C., and Coudron, C. A. (1979). Identification of Traumatin, a wound hormone, as 12-Oxo-trans-10-dodecenoic acid. *Plant Physiol.* 63, 536–541. doi: 10.1104/pp.63.3.536

Conflict of Interest: The authors declare that the research was conducted in the absence of any commercial or financial relationships that could be construed as a potential conflict of interest.

Publisher's Note: All claims expressed in this article are solely those of the authors and do not necessarily represent those of their affiliated organizations, or those of the publisher, the editors and the reviewers. Any product that may be evaluated in this article, or claim that may be made by its manufacturer, is not guaranteed or endorsed by the publisher.

frontiers | Frontiers in Microbiology

ORIGINAL RESEARCH
published: 28 June 2022
doi: 10.3389/fmicb.2022.928464

Mitochondrial Genome Contributes to the Thermal Adaptation of the Oomycete *Phytophthora infestans*

Lin-Lin Shen[1†], *Abdul Waheed*[1†], *Yan-Ping Wang*[2], *Oswald Nkurikiyimfura*[3], *Zong-Hua Wang*[1], *Li-Na Yang*[1*] *and Jiasui Zhan*[4]

[1] *Institute of Oceanography, Minjiang University, Fuzhou, China,* [2] *Sichuan Provincial Key Laboratory for Development and Utilization of Characteristic Horticultural Biological Resources, Chengdu Normal University, Chengdu, China,* [3] *Institute of Plant Virology, Fujian Agriculture and Forestry University, Fuzhou, China,* [4] *Department of Forest Mycology and Plant Pathology, Swedish University of Agricultural Sciences, Uppsala, Sweden*

OPEN ACCESS

Edited by:
Maofeng Jing,
Nanjing Agricultural University, China

Reviewed by:
Marina Cvetkovska,
University of Ottawa, Canada
Nuria Montes,
Hospital Universitario de La Princesa, Spain

***Correspondence:**
Li-Na Yang
yikeshu1114@126.com

[†] *These authors have contributed equally to this work*

Specialty section:
This article was submitted to Microbe and Virus Interactions With Plants, a section of the journal Frontiers in Microbiology

Received: *25 April 2022*
Accepted: *23 May 2022*
Published: *28 June 2022*

Citation:
Shen L-L, Waheed A, Wang Y-P, Nkurikiyimfura O, Wang Z-H, Yang L-N and Zhan J (2022) Mitochondrial Genome Contributes to the Thermal Adaptation of the Oomycete Phytophthora infestans. Front. Microbiol. 13:928464. doi: 10.3389/fmicb.2022.928464

As a vital element of climate change, elevated temperatures resulting from global warming present new challenges to natural and agricultural sustainability, such as ecological disease management. Mitochondria regulate the energy production of cells in responding to environmental fluctuation, but studying their contribution to the thermal adaptation of species is limited. This knowledge is needed to predict future disease epidemiology for ecology conservation and food security. Spatial distributions of the mitochondrial genome (mtDNA) in 405 *Phytophthora infestans* isolates originating from 15 locations were characterized. The contribution of MtDNA to thermal adaptation was evaluated by comparative analysis of mtDNA frequency and intrinsic growth rate, relative population differentiation in nuclear and mtDNA, and associations of mtDNA distribution with local geography climate conditions. Significant variation in frequency, intrinsic growth rate, and spatial distribution was detected in mtDNA. Population differentiation in mtDNA was significantly higher than that in the nuclear genome, and spatial distribution of mtDNA was strongly associated with local climatic conditions and geographic parameters, particularly air temperature, suggesting natural selection caused by a local temperature is the main driver of the adaptation. Dominant mtDNA grew faster than the less frequent mtDNA. Our results provide useful insights into the evolution of pathogens under global warming. Given its important role in biological functions and adaptation to local air temperature, mtDNA intervention has become an increasing necessity for future disease management. To secure ecological integrity and food production under global warming, a synergistic study on the interactive effect of changing temperature on various components of biological and ecological functions of mitochondria in an evolutionary frame is urgently needed.

Keywords: mitochondria, evolutionary ecology, population genetic, local adaptation, agricultural pathogen, climate change

INTRODUCTION

Local adaptation is a phenomenon whereby a member of species demonstrate a higher fitness, here defined as the competitive ability of survival, development, reproduction, and transmission (Kaltz and Shykoff, 1998; Giraud et al., 2017), in its native environment than other members of the same species that domicile elsewhere (Hoeksema and Forde, 2008). Phenotypic and genetic differentiation of species along defined ecological gradients, such as a continuous variation in thermal niches and altitudes (Roy et al., 2015), can also be used to infer local adaptation. This pattern of adaptation results from a complex interaction among members of a species as well as between species and the environment or is regulated by eco-evolutionary processes involving in genetic and phenotypic modification of genome structure and expression (Consuegra et al., 2015). Although local adaptation has been a paradigm of evolutionary study (Giraud et al., 2017), knowledge related to the topic is still fragmented. For example, local adaptation involves trades-offs and synergies among various ecological traits in a species, and it is unclear how different parts of a genome (e.g., nuclear vs. organelle) function together to shape the adaptation.

Natural selection and migration are two key evolutionary processes determining the pattern of species' adaptation to ecological gradients due to their counter-effect on the accumulation of the genetic variation required for phenotypic clines (Santangelo et al., 2018). Depending on their relative contribution to population genetic structure, interactions between these processes may increase, retain, or even decrease the performance of species members in their native ecosystems (Kaltz and Shykoff, 1998), leading to local adaptation, no adaptation, and mal-adaptation, respectively. Other evolutionary processes regulating genetic variation also contribute to the pattern and rate of local adaptation. For example, population extinctions or re-colonization associated with frequent bottlenecks or founder effects can prevent the development of local adaptation (Weaver et al., 2021). Phenotypic plasticity generated by gene expression and biochemical network regulation can also hamper local adaptation.

As an important component of ecosystems, temperature is expected to play an important role in local adaptation. By regulating genomic resilience and cellular activity, such as replication of proofreading (Barshis et al., 2013), transcription and translation profiles (Morgan et al., 2018), enzyme stability (Arcus et al., 2020), respiration, signal transduction (Xiang et al., 2021) etc., temperature exerts a critical influence on genetic, biological, ecological, and evolutionary processes of species such as mutation rate, survival, reproduction, competition, and dispersal. For example, an increased extinction rate associated with elevated temperatures was documented from a 30-year interaction between *Triphragmium ulmariae* and *Filipendula ulmaria* in Sweden (Zhan et al., 2018). An elevation of selection intensity and mutation rate that resulted from increasing temperature was observed in a genome-wide analysis of seed beetle (Berger et al., 2021). Adaptive evolution mediated by local temperature was also documented at an organismal level in many other species (Zhan and McDonald, 2011; Roy et al., 2015; He et al., 2018), including plant pathogens *Zymoseptoria tritici* (Zhan and McDonald, 2011) and *Rhynchosporium commune* (Stefansson et al., 2013).

Mitochondria are the organelles in which chemical energy required for cellular processes is generated (Roger et al., 2017). They can be found in the cytoplasm of eukaryotic organisms. The organelles have their own genome that is independent of the nucleus, but substantially like prokaryotic bacteria (Roger et al., 2017). Mitochondrial genomes (MtDNA) usually demonstrate a faster evolutionary rate than their nuclear counterparts, particularly in many species of mammal and plant species, and exhibit uniparental inheritance or reduced recombination (Popadin et al., 2012) even for species involving a biparental inheritance. These genetic and biological characteristics make mtDNA a ubiquitous material to address many evolutionary questions (Zhan et al., 2004), such as experimental tests for species adaptation. The feature of fast evolution enables the detection of genomic changes in a reasonable time (Zhan and McDonald, 2011; Yang et al., 2016). With uniparental inheritance, allelic polymorphisms are exclusively generated by mutation, removing potential genetic noise caused by recombination events (Popadin et al., 2012).

In addition to supplying energy for cellular activities, mtDNA is involved in many other biological and biochemical processes, such as calcium storage (Deline et al., 2021), cellular proliferation, signal conduction, etc. Interestingly, mtDNA has long been assumed to be exempted from natural selection (Galtier et al., 2009) and used to address evolutionary questions that require neutral markers, such as phylogenetic analysis of species relationships (Mao et al., 2020). Experimental evaluation of mitochondrial contribution to ecological adaptation such as thermal adaptation is limited, especially in plant pathogens. Therefore, the overall aim of the current study is to investigate the role of mtDNA in species adaptation to thermal conditions using *P. infestans*, a pathogenic microbe that originated from potato plants in agricultural ecosystems.

Phytophthora infestans is an infamous plant pathogen, which can greatly reduce the fitness of potatoes and tomatoes by damaging leaves, stems, and other parts of host tissues (Leesutthiphonchai et al., 2018). The pathogen has a worldwide distribution but thrives best under high humidity and temperate conditions (Leesutthiphonchai et al., 2018). Although it is mainly reproduced asexually, *P. infestans* is observed with a high capacity (Li et al., 2012) for acquiring resistance to host immunity (Yang et al., 2020) and tolerance to fungicide (Chen et al., 2018) and environmental stresses genetically or physiologically (Wu et al., 2019, 2020; Lurwanu et al., 2020; Wang et al., 2020), possibly attributed to its large genome enriched with transposable elements (Haas et al., 2009), short epidemic cycle (Leesutthiphonchai et al., 2018), and continuous gene flow (Dey et al., 2018). Indeed, *P. infestans* can complete its reproduction cycles and destroy entire plants in a few days when environmental conditions are conducive (Harrison, 1992). It has rendered the effectiveness of naïve host resistance within a few years

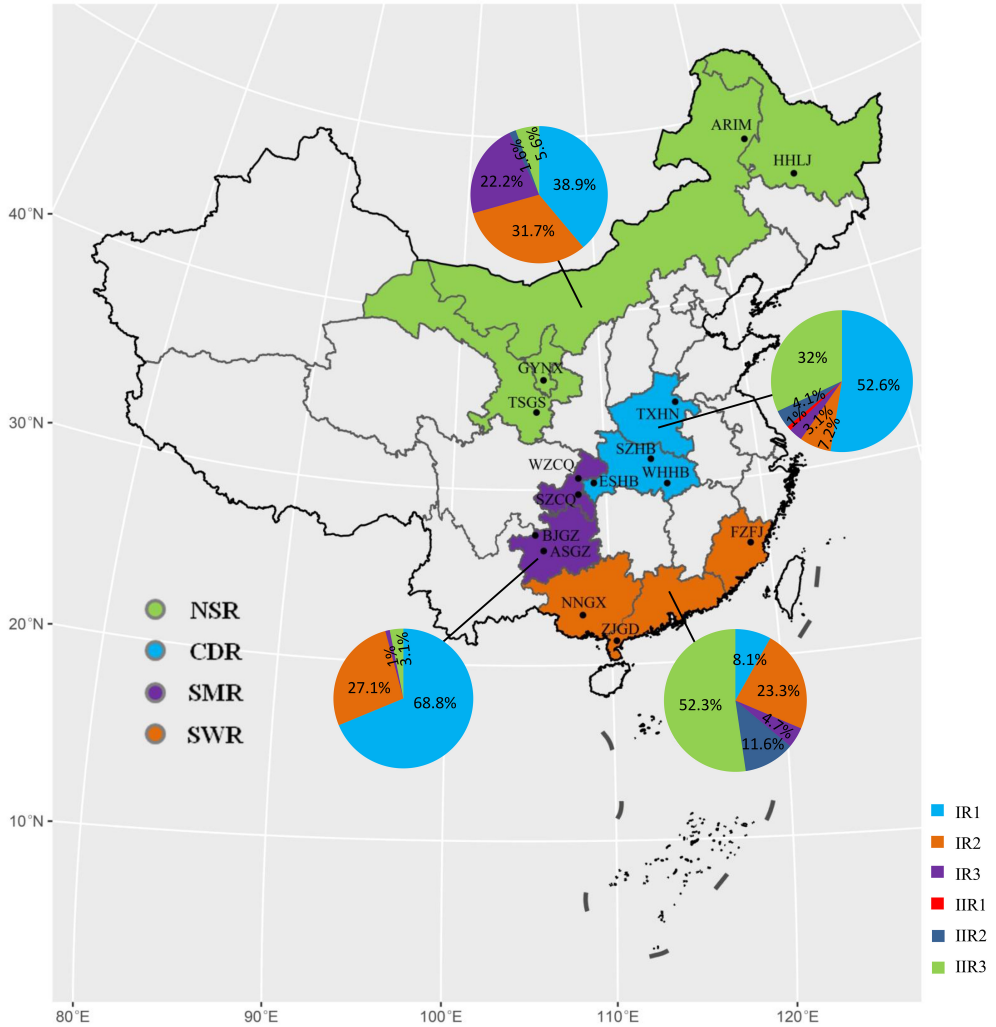

FIGURE 1 | Map showing the geographic origins and frequency distribution of mitochondrial haplotypes in the *Phytophthora infestans* populations sampled from four potato cultivation areas in China.

of being encountered (Forbes, 2012) and quickly increased fitness after a short period of training under thermal stresses (Wu et al., 2020).

The mtDNA *of P. infestans* is ∼40 kb in size with 53 predicted protein-coding genes (Avila-Adame et al., 2006; Patil et al., 2017), much smaller compared to its nuclear counterpart. In addition to the common features of uniparental inheritance (probably maternal inheritance), rapid mutation, and non-recombination (Avila-Adame et al., 2006), *P. infestans* mtDNA is easy to work with and has shown spatial heterogeneity of genetic polymorphism (Yang et al., 2013), making it a useful material to study the thermal adaptation of species.

To reach the overarching aim, we molecularly assayed the mitochondrial profile of more than 400 *P. infestans* isolates originating from geographic locations along environmental gradients across a major potato production country in the world. The spatial population genetic structure of the mitochondrial genome was contrasted to climatic conditions (temperature, rainfall, and solar radiation) in the collection sites. Phenotypic values of mitochondrial types were quantified using intrinsic growth rate and linked to their competitive ability. The specific objectives of the research were to: (1) understand the spatial distribution of mitochondrial haplotypes in *P. infestans;* (2) reveal the relative importance of genetic drift and natural selection on the spatial distribution of mtDNA; (3) evaluate how meteorological factors and geographic positions affect the spatial distribution of *P. infestans* haplotypes; and (4) explore the link between the intrinsic growth rate of *P. infestans* mtDNA and its frequency in nature.

MATERIALS AND METHODS

Spatial Origin of Pathogen Collections

Pathogen isolates were collected from 15 sites across the four potato production regions of China during the 2010–2013

TABLE 1 | Climatic conditions and their associated geographic coordinates of the collection sites for the 15 *Phytophthora infestans* populations used in the study.

PCA	Regions	Years	Sample size	AMT (°C)	Altitude (m)	Longitude	Latitude	AR (mm)	AID (h)
NSR	HHLJ	2013	22	3.68	126	126.64°E	45.76°N	633.5	2,023.5
	ARIM	2013	36	2.75	219	123.46°E	48.13°N	758.1	2,632.1
	TSGS	2010	40	11.7	1,169	105.72°E	34.58°N	401.9	1,968.7
	GYNX	2010	28	7	1,778	106.29°E	36.00°N	458.3	2,563
CDR	TXHN	2012	21	16.17	67	114.47°E	34.48°N	467.1	1,803.7
	ESHB	2012	25	13.08	490	109.49°E	30.28°N	1,258	1,066.5
	SZHB	2012	21	16.25	71	113.37°E	31.72°N	714.9	1,558.8
	WHHB	2010	30	16.33	16	114.30°E	30.58°N	1,338	1,544
SMR	ASGZ	2011	44	14.7	1,378	105.93°E	26.25°N	851.1	1,276.4
	BJGZ	2012	24	13.08	1,490	105.29°E	27.30°N	828.5	873.2
	WZCQ	2012	14	18.08	328	108.38°E	30.81°N	1,016	1,072.9
	SZCQ	2010	14	16.75	553	108.11°E	30.00°N	1,170	1,195.4
SWR	FZFJ	2010	32	20.5	10	119.31°E	26.08°N	1,605	1,485.6
	ZJGD	2011	15	24.42	17	110.36°E	21.27°N	1,409	1,822.3
	NNGX	2011	39	22.6	79	108.32°E	22.82°N	1,253	1,663.3

PCA, Potato cultivation areas; AMT, Annual means temperature (°C); AR, Annual rainfall (mm); AID, Annual insolation duration (h).

growing seasons (**Figure 1**, **Table 1**). Among these sites, Harbin Heilongjiang (HHLJ), Arong Inner Mongolia (ARIM), Tianshui Gansu (TSGS), and Guyua Ningxia (GYNX) are located in the Northern single-cropping region (NSR); Tongxu Henan (TXHN), Enshi Hubei (ESHB), Suizhou Hubei (SZHB), and Wuhan Hubei (WHHB) are located in Central double-cropping region (CDR); Anshun Guizhou (ASGZ), Bijie Guizhou (BJGZ), Wanzhou Chongqing (WZCQ), and Shizhu Chongqing (SZCQ) are located in Southwestern multiple-cropping region (SMR); and Fuzhou Fujian (FZFJ), Zhanjiang Guangdong (ZJGD), and Nanning Guangxi (NNGX) are located in the Southern Winter-cropping region (SWR). These collection sites vary dramatically in climatic conditions due to their geographic positions (Zhu et al., 2016). SWR belongs to a tropical or subtropical monsoon climate which is characterized by hot summers and mild winters (https://www.fmprc.gov.cn/ce/cggb/eng/gyzg/jbgq/t216954.htm). NSR usually has severe cold winters and experiences little annual rainfall. However, summers in some areas can be very hot. Many areas in CDR have a long and humid summer with medium to high temperatures. Temperatures in the winters can drop well-below freezing and the airs can be wet. SMR has a mild temperature with a very wet summer, where potatoes can be grown in all seasons. In general, altitude gradually increases from East to West. Most potatoes in NSR and SMR are grown in high altitude areas while those in CDR and SWR are grown in low altitude areas.

In all collections, infected leaves were sampled from potato plants separated by >100 cm. Only one infected leaf was collected from a plant and only one single-spore strain was isolated from a leaf. The isolates were genotyped by SSR assay of nuclear genomes as described (Knapova and Gisi, 2002). The details for pathogen isolation and the biological and molecular characterizations of the pathogen can be found in previous publications (Qin et al., 2016; Wu et al., 2016; Zhu et al., 2016).

PCR Detection of Mitochondrial Haplotypes

P. infestans isolates retrieved from long-term storage were cultured on rye B media supplemented with 10 mg/L rifampicin and 100 mg/L ampicillin at 18°C in the dark for 2 weeks. A total of 200–300 mg of mycelia were harvested for DNA extraction using Easy Pure Plant Genomic DNA Kit (Transgen, Beijing). The genomic DNA was amplified with the two sets of primers specified to the mitochondria of *P. infestans* (Yang et al., 2013). One set of the primers (i.e., Insertion-F and Insertion-R) amplifies the HVRi region of the mtDNA while another set (i.e., VNTR-F and VNTR-R) amplifies the HVRii region. The reaction volume of PCR amplification was 25 μL, including 2.5 μL 10 × Trans TaqHiFi Buffer, 2 μL dNTPs (2.5 mmol·L^{-1}), 1 μL of each primer (10μmol·L^{-1}), 0.20 μL Trans Taq HiFi Polymerase (5 U·μL^{-1}), 1 μL DNA template, and 17.7 μL ddH_2O. The thermal reaction for the implication of HVRi region was started by an initial denaturation at 95°C for 2 min, followed by 27 cycles of denaturation at 95°C for 45 s, annealing at 64°C for 3 min, and elongation at 72°C for 3 min. The reaction was terminated by a final extension of 72°C for 10 min. The PCR amplification of HVRii region consisted of an initial denaturation at 95°C for 4 min, followed by 30 cycles of denaturation at 95°C for 45 s, annealing at 45°C for 45 s, and elongation at 72°C for 45 s, and ended with an elongation cycle at 72°C for 7 min. The HVRi and HVRii PCR products were separated by electrophoresis in 1.0 and 2.0 % (wt/vol) TBE buffer agarose gels at 110 V for 30 min and 100 V for 45 min, respectively. DNA markers MD5000 and MD500 (Transgen, Beijing, China) were used as molecular size standards for the HVRi and HVRii amplicons, respectively.

Meteorological and Geographical Data of the Collection Sites

Monthly temperature data presented as an average over 15–30 years for each collection site was downloaded from the World Climate (http://www.worldclimate.com/) as described previously (Zhan and McDonald, 2011; Yang et al., 2016; Wu et al., 2020). Annual mean temperature at each site was estimated from the mean temperature over 12 months. Altitude, longitude, latitude, annual rainfall, and annual insolation duration data for each site were downloaded from the National Greenhouse Data System (http://data.sheshiyuanyi.com/WeatherData/). The annual rainfall and annual insolation duration data were presented as the accumulation of a year.

Data Analysis

Mitochondrial haplotypes were assigned based on their PCR profiles amplified by the primers. Haplotype frequency was tabulated according to individual collections, and also their combination and heterogeneity within and among cropping regions were evaluated by a contingency χ^2 test (Everitt, 1992). Haplotype diversity (HD) was estimated by Nei's index (Nei, 1978) for each individual collection. The overall population differentiation in mtDNA was estimated by G_{ST} (Nei, 1973) using mitochondrial haplotype frequency detected in each population, while the overall population differentiation in the nuclear genome was estimated by F_{ST} (Wright, 1943) using SSR data taken from previous publications (Qin et al., 2016; Yang et al., 2016). The standard deviation of $G_{ST}$was generated by 100 resamples of original data with replacement, as described previously (Zhan et al., 2003), and used for a t-test to infer the evolutionary history of mtDNA (Yang et al., 2016). A higher G_{ST}than F_{ST}indicates that population genetic differentiation in the mitochondrial genome was caused by the natural selection for local adaptation while the lower G_{ST} than F_{ST}indicates that mtDNA in *P. infestans* was generated by constraining selection for the same mitochondrial traits across regions. The hypothesis of neutral evolution in the mitochondria of *P. infestans will* not be rejected if G_{ST} does not differ from F_{ST}.

The association of mitochondrial haplotype (frequency and diversity) with climatic (annual mean temperature, annual insolation duration, and annual rainfall) or geographic data (altitude; longitude, latitude, and longitude) in the collection sites were evaluated by linear and quadratic models. Climatic or geographic effect on haplotype frequency and diversity was evaluated by a multiple regression analysis using an analytical tool embedded in Microsoft Excel 2017.

The intrinsic growth rates of the isolates in a subset of populations were estimated by a logistic model (Aguayo et al., 2014) using the colony data taken from a previous publication (Yang et al., 2016). The colony sizes were measured during a10-day culture for each of the isolates at five experimental temperatures (13, 15, 19, 22, and 25 °C). The thermal reaction norm of the isolates was generated by fitting the *in-vitro* growth rates into a quadratic model. The expected maximum growth rates (MGR) of the isolates were calculated by taking the first derivative of the thermal reaction norm equation with the online derivative calculator (https://www.derivative-calculator.net/) and then solving the derivative after setting it to zero. MGRs were subjected to analysis of variance (ANOVA) by a General Linear Model (GLM) incorporated in SAS 9 and compared among haplotypes by the least-significant difference (LSD) test (Ott and Longnecker, 2015). In the GLM partition, "mitochondrial haplotype" was treated as a fixed variable, while isolates were treated as random variables. Haplotypes IR3 and IIR1 were absent in most of the isolated with the *in-vitro* growth rate data and were excluded from the GLM and LSD analysis.

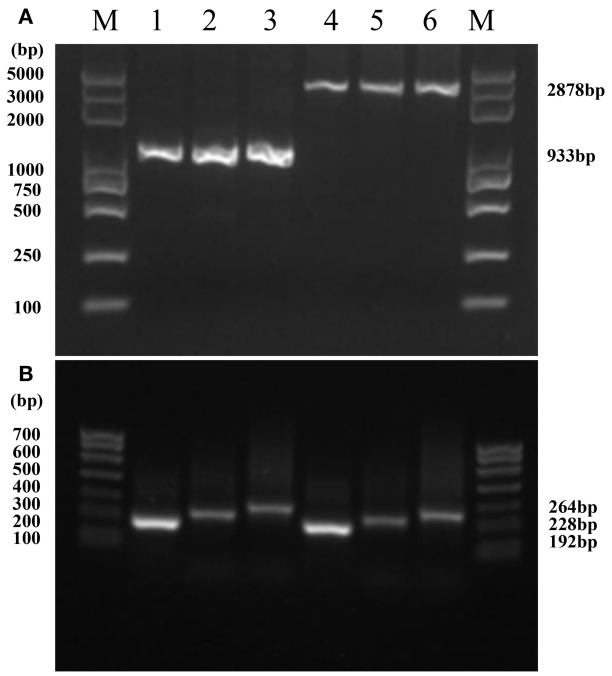

FIGURE 2 | Amplicon profiles of *P. infestans* mitochondrial regions: **(A)** Band patterns of the mitochondrial region I (HVRI) amplified by the primers Insertion-F and Insertion-R. Lanes 1–3 represent mtDNA type I and lanes 4–6 represent mtDNA type II; M lanes are MD5000 DNA marker; **(B)**: Band patterns of the mitochondrial region II (HVRII) amplified by the primers VNTR-F and VNTR-R. Lanes 1 and 4 represent R1; lanes 2 and 3 represent R2; and lanes 5 and 6 represent R3. M lanes are MD700 DNA marker.

RESULTS

Mitochondrial Type Detection

Only a single, clear, and reproducible band was generated by PCR amplification of the mtDNA of *P. infestans* from each isolate by each of the two pairs of primers (**Figure 2**). The HVRii primers generated two bands with a fragment size of 993 bp (type I, **Figure 2A**, lanes 1-3) and 2,878 bp (type II, **Figure 2A**, lanes 4-6) while HVRi primers yielded three bands with a size of 192 bp (Type R1, **Figure 2B**, lanes 1 and 4), 228 bp (Type R2, **Figure 2B**, lanes 2 and 3), and 264 bp (Type R3, **Figure 2B**, lanes 5 and 6), respectively. Therefore, the combination of the two primers can generate six mitochondrial types, and all of them were detected in the 405 isolates of *P. infestans* amplified in the study.

TABLE 2 | Mitochondrial diversity and homogeneity test for haplotype frequency in the 15 *Phytophthora infestans* populations sampled from China.

PCA	Regions	HD	Haplotype frequency						(χ^2-test)
			IR1	IR2	IR3	IIR1	IIR2	IIR3	
NSR	HHLJ	0.51	0.00	0.82	0.18	0.00	0.00	0	118.595 (12)*
	ARIM	0.33	0.06	0.19	0.67	0.00	0.06	0.03	
	TSGS	0.49	0.68	0.18	0.00	0.00	0.00	0.15	
	GYNX	0.41	0.71	0.29	0.00	0.00	0.00	0.00	
CDR	TXHN	0.43	0.24	0.00	0.00	0.05	0.00	0	42.335 (15)*
	ESHB	0.28	0.84	0.12	0.04	0.00	0.00	0.00	
	SZHB	0.66	0.52	0.10	0.05	0.00	0.14	0.19	
	WHHB	0.62	0.47	0.07	0.03	0.00	0.03	0.40	
SMR	ASGZ	0.45	0.70	0.23	0.00	0.00	0.00	0	16.67 (9)
	BJGZ	0.33	0.79	0.21	0.00	0.00	0.00	0.00	
	WZCQ	0.44	0.71	0.21	0.07	0.00	0.00	0.00	
	SZCQ	0.49	0.43	0.57	0.00	0.00	0.00	0.00	
SWR	FZFJ	0.58	0.03	0.44	0.00	0.00	0.06	0.	35.669 (8)*
	ZJGD	0.62	0.00	0.13	0.27	0.00	0.07	0.53	
	NNGX	0.62	0.15	0.10	0.00	0.00	0.18	0.56	

PCA, Major potato cultivation areas; HD, Haplotype diversity.
**: Significant at P < 0.0001.*

Genetic Variation and Spatial Distribution of Mitochondrial DNA

The amplification assessment revealed a highly skewed band frequency in the *P. infestans* population from China (**Table 2**). Among the 405 isolates tested, 302 (74.57%) were classified as Type I and 103 (25.43%) as Type II. On the other hand, 174 (42.96%), 109 (26.91%), and 122 (30.10%) were designated as Type R1, R2, and R3, respectively. When the applications from the two sets of primers were considered together, IR1 was the most dominant mitochondrial haplotype, accounting for nearly half (42.72%) of the isolates assayed (**Table 2**), followed sequentially by IR2 (22.96%), IIR3 (21.23%), IR3 (8.89%), IIR2 (3.95%), and IIR1 (0.25%).

The spatial distribution in the mitochondrial haplotypes was also highly skewed (**Figure 1**). The three dominant haplotypes, IR1, IR2, and IIR3 were underrepresented in the south, central, and south-western parts of China, representatively. IR3 was mainly restricted to the North part of the country, while IIR1 was only detected once at TXHN in CDR. Further analysis by homogeneity test showed a significant difference in haplotype frequency among field locations ($\chi^2 = 477.07$, $p < 0.0001$). Significant differences were also detected among field locations within three cropping regions (NSR, CDR, and SWR) (**Table 2**).

The haplotype diversity in the 15 locations ranged from 0.28 to 0.66 (**Table 2**) with an average of 0.48 (95% CI: ±0.06). Both the highest and the lowest diversity were found in the populations sampled from Hubei in CDR (SZHE and ESHB) on a regional scale. The pathogen population sampled from SWR had the highest haplotype diversity (0.61 ± 0.06) followed by those from CDR (0.50 ± 0.17) and NSR (0.44± 0.08). The population sampled from SMR had the lowest diversity (0.43 ± 0.07). However, the difference in haplotype diversity among the regions was insignificant by the LSD test ($p = 0.1836$). The population differentiation (G_{ST}) in the mtDNA was 0.15, which was significantly higher than 0.08, the population differentiation (F_{ST}) in SSR neutral markers by *t*-test (T = 5.67, $p = 0.0024$).

Geographic Pattern of Spatial Distribution in Mitochondrial Haplotypes and Associations of the Distribution With Climatic Conditions

The annual mean temperature in the 15 collection sites was negatively correlated to the frequency of mitochondrial Type I ($R^2 = 0.4150$, $p = 0.0090$, **Figure 3A**) but positively correlated to haplotype diversity ($R^2 = 0.3160$, $p = 0.0234$, **Figure 4A**). Annual insolation duration in the collection sites was significantly and quadratically associated with haplotype diversity ($R^2 = 0.2140$, $p = 0.0458$, **Figure 4F**) but only marginally associated with haplotype frequency ($R^2 = 0.2330$, $p = 0.0804$, **Figure 3F**). On the other hand, altitude in the collection sites was significantly and linearly associated with haplotype frequency ($R^2 = 0.3440$, $p = 0.0210$; **Figure 3B**) but only marginally associated with haplotype diversity ($R^2 = 0.1750$, $p = 0.1069$, **Figure 4B**). Latitude was marginally associated with both haplotype frequency and diversity (**Figures 3D**, **4D**). No associations were detected between other climatic conditions or geographic positions in the collection sites with haplotype (frequency and diversity). Multiple regression analysis also revealed that annual mean temperature and altitude in the collection sites contributed significantly to the spatial distribution of haplotype frequency and diversity (**Table 4**). On the other hand, annual insulation duration and latitude in the collection sites only significantly contributed to the spatial distribution of mitochondrial haplotype in term of frequency but not diversity.

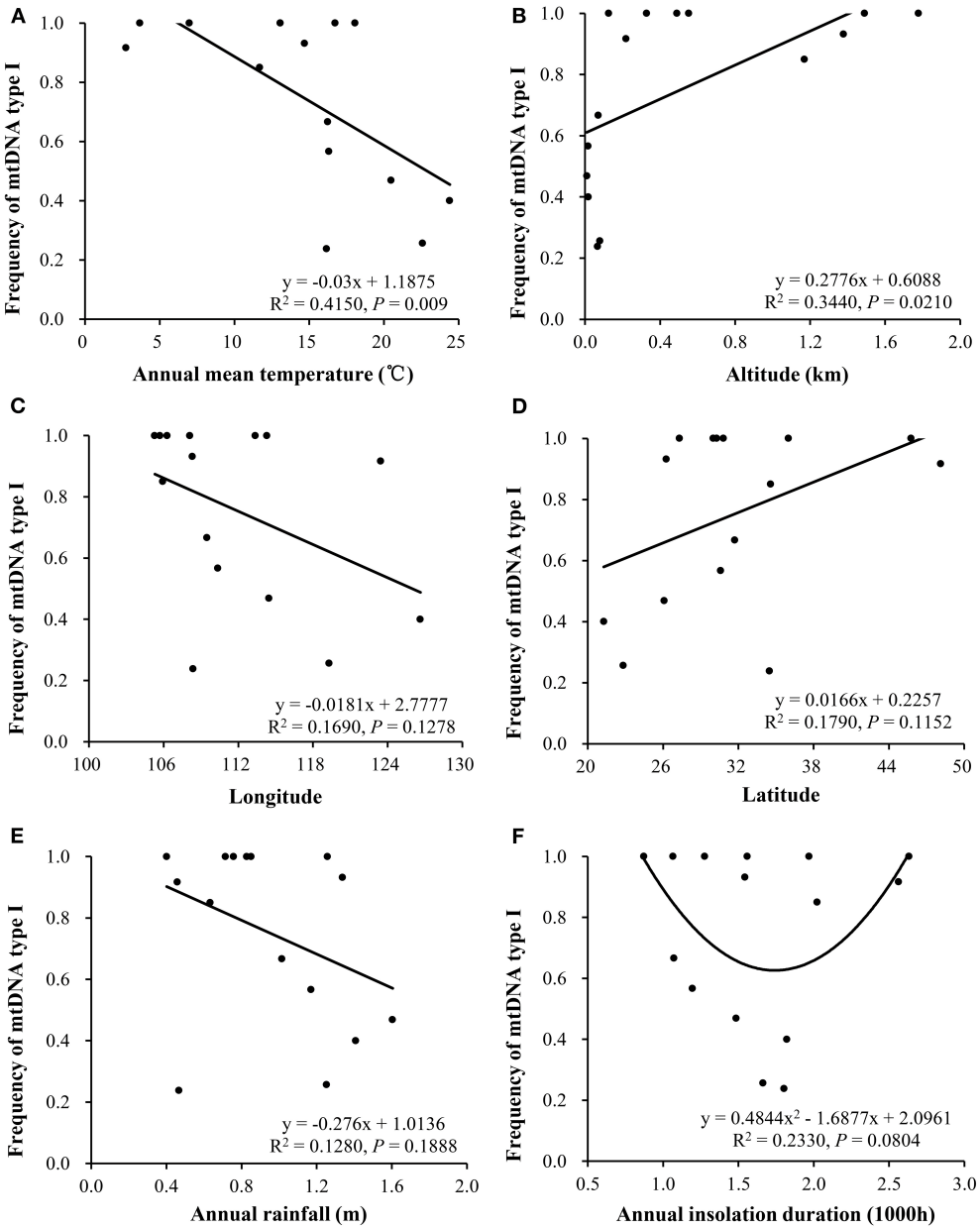

FIGURE 3 | Associations of mitochondrial haplotype I with climatic conditions and tick in the *P. infestans* populations collected from China: **(A)** Annual means temperature, **(B)** altitude, **(C)** longitude, **(D)** latitude, **(E)** annual rainfall, and **(F)** insolation.

Differences in Temperature Response Among Mitochondrial Haplotypes

Exploratory analysis showed that MGR in the pathogen was normally distributed, therefore, original data were not transformed. Significant differences in the expected maximum intrinsic growth rate (MGR) were detected among the haplotypes by ANOVA ($p = 0.001$). The average MGR of Type I (0.5044 ± 0.0286) was significantly higher that of Type II (0.4774 ± 0.0248). Further analysis showed that MGR of IR1 and IR2 haplotypes was significantly higher than that of IIR3. No differences in MGR were detected among IR1, IR2, and IIR2, and IIR2 and IIR3 (**Table 3**). MGR of the haplotype was positively associated with its frequency ($r = 0.9523$, $p = 0.0477$).

DISCUSSION

High population differentiation in the mitochondrial genome of *P infestans* was revealed by spatial analysis of haplotype frequency and diversity. Both deterministic and stochastic events can generate the observed spatial distribution. Natural selection for genetic variation ensuring a better chance of survival, reproduction, and transmission for a species in the

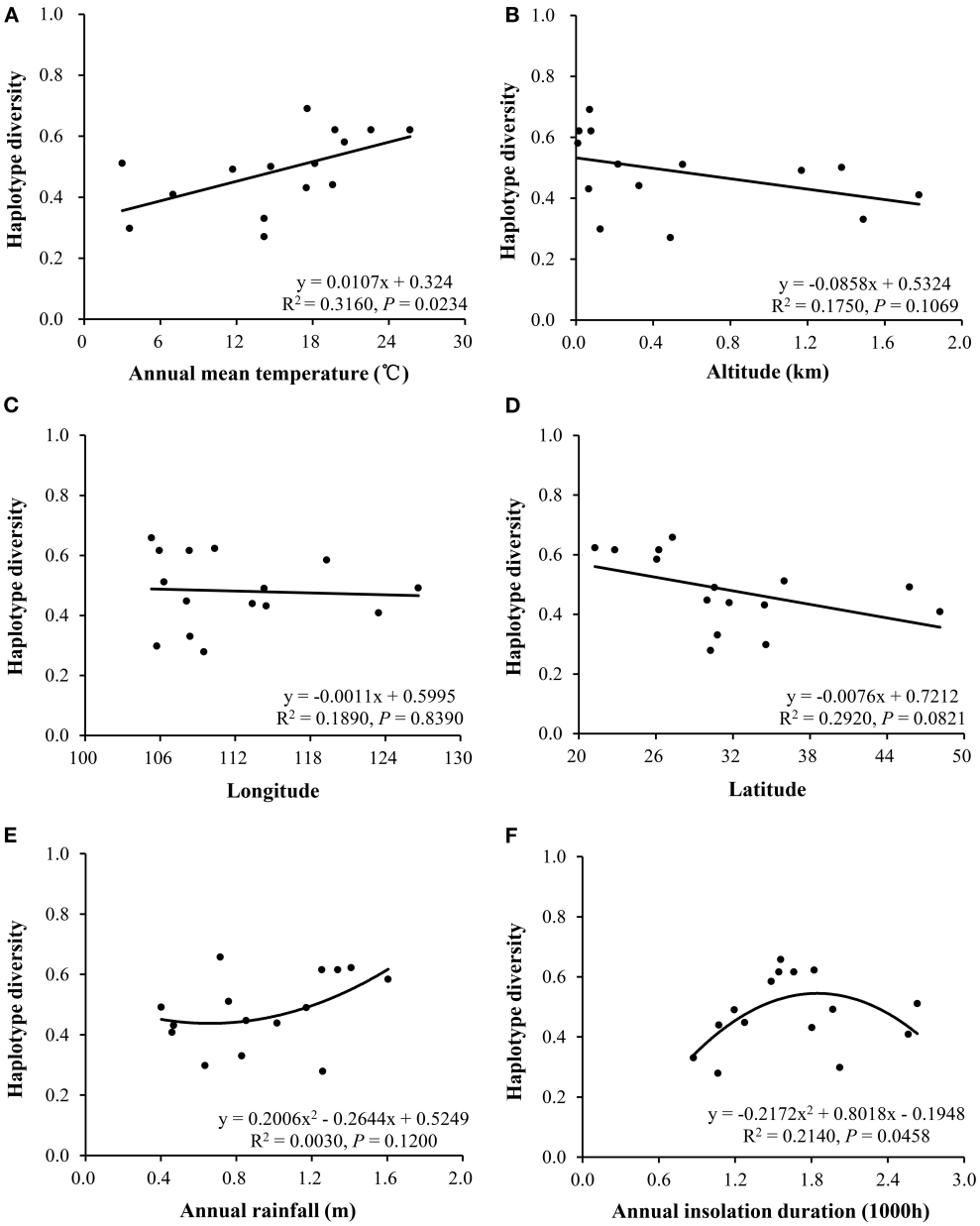

FIGURE 4 | Correlation of annual mean temperature, altitude, latitude, and annual insolation duration of the collection sites with haplotype diversity in the *P. infestans* populations collected from China: **(A)** annual mean temperature, **(B)** altitude, **(C)** longitude, **(D)** latitude, **(E)** annual rainfall, and **(F)** insolation.

specified ecological ecotypes such as community structure and climate conditions of a geographic location may lead to adaptive differentiation (Dumartinet et al., 2020). When gene flow is limited, stochastic changes of genetic variation in the mitochondrial genome domiciling in different geographic areas associated with genetic drift can lead to non-adaptive genetic differentiation (Zhan et al., 2003).

MtDNAs have historically been assumed to be selectively neutral (Galtier et al., 2009; Immonen et al., 2020). However, accumulating information shows that this molecule may be under strong selection for ecological adaptation (Zhan et al., 2004; Immonen et al., 2020), consistent with its involvement in the differentiation, information transmission and apoptosis of cells (Scheckhuber et al., 2007), regulation of body biomass (Illescas et al., 2021), response to environmental stresses such as pathogen resistance to host immunity (Bartelli et al., 2018) and pesticides, and we believe that natural selection for local adaptation also contributes to the spatial distribution of mtDNA observed in *P. infestans*. Our argument is supported by several lines of evidence as listed below.

As a proxy of ecotypes, many biotic and abiotic elements of an ecosystem, such as temperature, UV irradiation, oxygen

TABLE 3 | Least-significant difference (LSD) tests for difference in the estimated maximum growth rate (MGR) of different mitochondrial haplotypes.

mtDNA	MGR
IR1	0.508^{A}
IR2	0.499^{A}
IIR2	0.480^{AB}
IIR3	0.477^{B}

Values followed by different letters in a column are significantly different from each other at P = 0.05.

TABLE 4 | Multiple regression analysis of the contribution of local climatic conditions or geographic positions to the mitochondrial genome in the *P. infestans* populations from China.

Factor	Parameter	Type I frequency		Mitochondrial diversity	
		Coefficients	*P*-values	Coefficients	*P*-values
Climates	AMT	0.0450 ± 0.0192	0.0003	0.0158 ± 0.0103	0.0058
	AID	0.0003 ± 0.0002	0.0077	0.0001 ± 0.0001	0.099
Coordinates	Altitude	0.0003 ± 0.0002	0.0107	0.0001 ± 0.0001	0.0483
	Latitude	0.0171 ± 0.0168	0.0470	0.0068 ± 0.0079	0.0841

AMT, Annual mean temperature (°C); AID, Annual insolation duration (h).

level and species richness, density, and morphology are changed directionally in response to increase or decrease in altitude (Tanaka et al., 2019; Wang et al., 2020). For example, plants adapting to low altitudes tend to have long, thinner, and less hairy leaves than those adapting to high altitudes (Liu et al., 2020). The finding of linear association between haplotype diversity and altitude (**Figure 4**) indicates the spatial distribution of mitochondrial haplotypes is not random across ecosystems in China.

Differentiation caused by genetic drift is expected to have no impact on fitness (Orr, 2009). In this study, we find significant difference in intrinsic growth rate among the mitochondrial haplotypes (**Table 3**) and the difference can be successfully transferred to competitive ability as indicated by the positive association between haplotype frequency observed in nature and its intrinsic growth rate. Apparently, mitochondrial Type I is a more successful than Type II in *P. infestans*. It is the dominant haplotype, possibly attributed to its higher fitness, and the result is similar to other reports. For example, Type I dominated in the surveys conducted in India (Sharma et al., 2016), Turkey (Gunacti et al., 2019), as well as other parts of China (Yang et al., 2013) and adapts to wider ecological niches (Sharma et al., 2016).

A higher degree of population differentiation in mtDNA than neutral genome represented by SSR provides further evidence supporting an adaptive evolution (Wu et al., 2016; Yang et al., 2018; Shen et al., 2021; Waheed et al., 2021) in the *P. infestans* molecules. Gene flow is the main evolutionary mechanism determining the population differentiation of species (Gao et al., 2020). Low population differentiation (0.08) in neutral genome achieved by natural and/or human-mediated dispersal (Gao et al., 2020) is consistent with a high gene flow of the pathogen. The propagules of *P. infestans* can be transmitted to a long distance by air current (Firester et al., 2018), and intensive cultivation of its potato and tomato hosts year-round in the country (Guha Roy et al., 2021) creates a unique opportunity for transmission. In agriculture, anthropogenic activities such as commercial trading of plant materials by human activities are the main channels of plant pathogens dispersal (Meng et al., 2018). In China, a remarkably large amount of potato products is transported around the country annually either as seed tubers or foods (Gao et al., 2020).

Among the three most important climatic elements in agricultural ecosystems available in the historical weather records, the temperature is found to have a consistent association with the spatial distribution of mitochondrial haplotypes (**Figures 3**, **4**, **Table 4**), suggesting that the thermal condition in the collection sites contributes greatly to the local adaptation of mtDNA in the pathogen, while other climatic elements might play no (e.g., rainfall) or less role (e.g., insolation). The mirrored associations of mitochondrial distribution with temperature and altitude may also reflect the importance of temperature in the adaptation because temperature always decreases as altitude increases. This argument is aligned with documented results in other species (Luo et al., 2013).

Indeed, it has been shown that the spatial distribution of mtDNAs in many species in nature corresponds with their ability to adapt to thermal conditions. Over 10% of the mitochondrial haplotypes in fresh water gastropod sampled from a volcanic lake in northern Iceland were specified to a particular thermal habitat (Quintela et al., 2014) and mitochondrial haplotypes experienced stronger selection at high altitudes, where cold and hypoxic conditions are a major challenge for aerobic organisms (Camus et al., 2017). The ability of *Drosophila melanogaster* to tolerate thermal stresses in Australia was regulated by genomic variation of mitochondrial haplotypes, with the subtropical population displaying a greater resilience to heat stress but lower resilience to cold stress relative to temperate populations and vice versa (Camus et al., 2017). In *Saccharomyces cerevisiae,* mtDNA is an evolutionary hotspot for thermal adaptation where a large part of the genome is dedicated to develop heat and cold tolerance (Li et al., 2019). Similarly, low temperatures are selected for increasing metabolic efficiency in Atlantic salmon mtDNA (Consuegra et al., 2015).

CONCLUSION

Global climates are undergoing an unprecedented change. It is projected that the air temperature of the planet would increase several degrees in the next 50 years, accompanied by more frequent heat and chilly waves (Masson-Delmotte et al., 2021). Given the critical role of temperature on the biological and evolutionary processes of species, these changes in global thermal profile greatly challenge ecological sustainability in terms of structure, function, or regulating disease

epidemics. Consequently, understanding the mechanisms of thermal adaptation in species is necessary for the prediction and mitigation of the impacts. As the major manufacturer where cells carry out aerobic respiration, mitochondria are popularly known as the "powerhouse" of living organisms. They are involved in oxidative phosphorylation processes in which chemical energy from food and other resources are converted into adenosine triphosphate (ATP), the energy which is used for all metabolic processes (Sandor et al., 2018). The respiratory activities, and consequently the production of ATPs in cells, are environment-, particularly temperature-dependent. Low temperatures generally decrease the rate of cellular respiration due to the reduced kinetic energy required, leading to the differential suppression of relative genes and vice versa (Salomon and Buchholz, 2000). Therefore, it is expected that mtDNA plays a pivotal role in the thermal adaptation of species. However, research on the evolutionary mechanisms of thermal adaptation has mainly focused on the nuclear genome while the contribution of mtDNA to the adaptation is largely overlooked (Consuegra et al., 2015; Camus et al., 2017; Immonen et al., 2020). We believe that our research will draw more attention to narrow the gap.

DATA AVAILABILITY STATEMENT

The original contributions presented in the study are included in the article/supplementary material, further inquiries can be directed to the corresponding author.

AUTHOR CONTRIBUTIONS

L-LS and AW performed the experiments, analyzed data, and wrote the manuscript. Y-PW and ON collected pathogen isolates and genotyped pathogen isolates. Z-HW revised the manuscript. L-NY supervised the project and wrote the manuscript. JZ conceived, designed and supervised the experiments, analyzed the data, and wrote the manuscript. All authors reviewed the manuscript, contributed to the article, and approved the submitted version.

FUNDING

This research was funded by the National Natural Science Foundation of China (31761143010, 31901861, and U1405213 grant to JZ and L-NY).

REFERENCES

Aguayo, J., Elegbede, F., Husson, C., Saintonge, F. X., and Marçais, B. (2014). Modeling climate impact on an emerging disease, the *Phytophthora alni* induced alder decline. *Global Change Biol.* 20, 3209–3221. doi: 10.1111/gcb.12601

Arcus, V. L., Van Der Kamp, M. W., Pudney, C. R., and Mulholland, A. J. (2020). Enzyme evolution and the temperature dependence of enzyme catalysis. *Curr. Opin. Struct. Biol.* 65, 96–101. doi: 10.1016/j.sbi.2020.06.001

Avila-Adame, C., Gomez-Alpizar, L., Zismann, V., Jones, K. M., Buell, C. R., and Ristaino, J. B. (2006). Mitochondrial genome sequences and molecular evolution of the Irish potato famine pathogen, *Phytophthora infestans*. *Curr. Genet.* 49, 39–46. doi: 10.1007/s00294-005-0016-3

Barshis, D. J., Ladner, J. T., Oliver, T. A., Seneca, F. O., Traylor-Knowles, N., and Palumbi, S. R. (2013). Genomic basis for coral resilience to climate change. *Proc. Natl. Acad. Sci.* 110, 1387–1392. doi: 10.1073/pnas.1210224110

Bartelli, T. F., Bruno, D. C., and Briones, M. R. (2018). Evidence for mitochondrial genome methylation in the yeast *Candida albicans*: a potential novel epigenetic mechanism affecting adaptation and pathogenicity? *Front. Genet.* 9, 166. doi: 10.3389/fgene.2018.00166

Berger, D., Stångberg, J., Baur, J., and Walters, R. J. (2021). Elevated temperature increases genome-wide selection on de novo mutations. *Proc. R. Soc. B.* 288, 20203094. doi: 10.1098/rspb.2020.3094

Camus, M. F., Wolff, J. N., Sgr,ò, C. M., and Dowling, D. K. (2017). Experimental support that natural selection has shaped the latitudinal distribution of mitochondrial haplotypes in Australian *Drosophila melanogaster*. *Mol. Biol. Evol.* 34, 2600–2612. doi: 10.1093/molbev/msx184

Chen, F., Zhou, Q., Qin, C., Li, Y., and Zhan, J. (2018). Low evolutionary risk of iprovalicarb resistance in *Phytophthora infestans*. *Pestic. Biochem. Physiol.* 152, 76–83. doi: 10.1016/j.pestbp.2018.09.003

Consuegra, S., John, E., Verspoor, E., and de Leaniz, C. G. (2015). Patterns of natural selection acting on the mitochondrial genome of a locally adapted fish species. *Genet. Sel. Evol.* 47, 1–10. doi: 10.1186/s12711-015-0138-0

Deline, M. L., Grashei, M., van Heijster, F. H., Schilling, F., Straub, J., and Fromme, T. (2021). Adenylate kinase derived ATP shapes respiration and calcium storage of isolated mitochondria. *BBA-Bioenergetics.* 1862, 148409. doi: 10.1016/j.bbabio.2021.148409

Dey, T., Saville, A., Myers, K., Tewari, S., Cooke, D. E., Tripathy, S., et al. (2018). Large sub-clonal variation in *Phytophthora infestans* from recent severe late blight epidemics in India. *Sci. Rep.* 8, 4429. doi: 10.1038/s41598-018-22192-1

Dumartinet, T., Abadie, C., Bonnot, F., Carreel, F., Roussel, V., Habas, R., et al. (2020). Pattern of local adaptation to quantitative host resistance in a major pathogen of a perennial crop. *Evol. Appl.* 13, 824–836. doi: 10.1111/eva.12904

Everitt, B. S. (1992). *The Analysis of Contingency Tables.* N.W. Corporate Blvd., Boca Raton, FL: Chapman and Hall/CRC.

Firester, B., Shtienberg, D., and Blank, L. (2018). Modelling the spatiotemporal dynamics of *Phytophthora infestans* at a regional scale. *Plant Pathol.* 67, 1552–1561. doi: 10.1111/ppa.12860

Forbes, G. (2012). Using host resistance to manage potato late blight with particular reference to developing countries. *Potato Res.* 55, 205–216. doi: 10.1007/s11540-012-9222-9

Galtier, N., Nabholz, B., Glémin, S., and Hurst, G. (2009). Mitochondrial DNA as a marker of molecular diversity: a reappraisal. *Mol. Ecol.* 18, 4541–4550. doi: 10.1111/j.1365-294X.2009.04380.x

Gao, F., Chen, C., Li, B., Weng, Q., and Chen, Q. (2020). The gene flow direction of geographically distinct *Phytophthora infestans* populations in China corresponds with the route of seed potato exchange. *Front. Microbiol.* 11, 1077. doi: 10.3389/fmicb.2020.01077

Giraud, T., Koskella, B., and Laine, A. L. (2017). Introduction: microbial local adaptation: insights from natural populations, genomics and experimental evolution. *Mol. Ecol.* 26, 1703–1710. doi: 10.1111/mec.14091

Guha Roy, S., Dey, T., Cooke, D. E., and Cooke, L. R. (2021). The dynamics of *Phytophthora infestans* populations in the major potato-growing regions of Asia–a review. *Plant Pathol.* 70, 1015–1031. doi: 10.1111/ppa.13360

Gunacti, H., Ay, T., and Can, C. (2019). Genotypic and phenotypic characterization of *Phytophthora infestans* populations from potato in Turkey. *Phytoparasitica.* 47, 429–439. doi: 10.1007/s12600-019-00737-y

Haas, B. J., Kamoun, S., Zody, M. C., Jiang, R. H., Handsaker, R. E., Cano, L. M., et al. (2009). Genome sequence and analysis of the Irish potato famine pathogen *Phytophthora infestans*. *Nature.* 461, 393–398. doi: 10.1038/nature 08358

Harrison, J. (1992). Effects of the aerial environment on late blight of potato foliage–a review. *Plant Pathol.* 41, 384–416. doi: 10.1111/j.1365-3059.1992.tb02435.x

He, M. H., Li, D. L., Zhu, W., Wu, E. J., Yang, L. N., Wang, Y. P., et al. (2018). Slow and temperature-mediated pathogen adaptation to a nonspecific fungicide in agricultural ecosystem. *Evol. Appl.* 11, 182–192. doi: 10.1111/eva.12526

Hoeksema, J. D., and Forde, S. E. (2008). A meta-analysis of factors affecting local adaptation between interacting species. *Am. Nat.* 171, 275–290. doi: 10.1086/527496

Illescas, M., Peñas, A., Arenas, J., Martín, M. A., and Ugalde, C. (2021). Regulation of mitochondrial function by the actin cytoskeleton. *Front. Cell Dev. Biol.* 9, 795838. doi: 10.3389/fcell.2021.795838

Immonen, E., Berger, D., Sayadi, A., Liljestrand-Rönn, J., and Arnqvist, G. (2020). An experimental test of temperature-dependent selection on mitochondrial haplotypes in *Callosobruchus maculatus* seed beetles. *Ecol. Evol.* 10, 11387–11398. doi: 10.1002/ece3.6775

Kaltz, O., and Shykoff, J. A. (1998). Local adaptation in host–parasite systems. *Heredity*. 81, 361–370. doi: 10.1046/j.1365-2540.1998.00435.x

Knapova, G., and Gisi, U. (2002). Phenotypic and genotypic structure of *Phytophthora infestans* populations on potato and tomato in France and Switzerland. *Plant Pathol.* 51, 641–653. doi: 10.1046/j.1365-3059.2002.00750.x

Leesutthiphonchai, W., Vu, A. L., Ah-Fong, A. M., and Judelson, H. S. (2018). How does *Phytophthora infestans* evade control efforts? modern insight into the late blight disease. *Phytopathol.* 108, 916–924. doi: 10.1094/PHYTO-04-18-0130-IA

Li, X. C., Peris, D., Hittinger, C. T., Sia, E. A., and Fay, J. C. (2019). Mitochondria-encoded genes contribute to evolution of heat and cold tolerance in yeast. *Sci. Adv.* 5, eaav1848. doi: 10.1126/sciadv.aav1848

Li, Y., Van Der Lee, T., Evenhuis, A., van Den Bosch, G., Van Bekkum, P., Förch, M., et al. (2012). Population dynamics of *Phytophthora infestans* in the Netherlands reveals expansion and spread of dominant clonal lineages and virulence in sexual offspring. *G3-Genes Genom. Genet.* 2, 1529–1540. doi: 10.1534/g3.112.004150

Liu, W., Zheng, L., and Qi, D. (2020). Variation in leaf traits at different altitudes reflects the adaptive strategy of plants to environmental changes. *Ecol. Evol.* 10, 8166–8175. doi: 10.1002/ece3.6519

Luo, Y., Yang, X., and Gao, Y. (2013). Mitochondrial DNA response to high altitude: a new perspective on high-altitude adaptation. *Mitochondrial DNA.* 24, 313–319. doi: 10.3109/19401736.2012.760558

Lurwanu, Y., Wang, Y. P., Abdul, W., Zhan, J., and Yang, L. N. (2020). Temperature-mediated plasticity regulates the adaptation of *Phytophthora infestans* to azoxystrobin fungicide. *Sustainability.* 12, 1188. doi: 10.3390/su12031188

Mao, S., Yan, C., Bai, J., Ye, Y., Li, J., Guo, Y., et al. (2020). The complete mitochondrial genome and phylogenetic analysis of *Omphalius rusticus* (Gastropoda, Tegulidae). *Mitochondrial DNA Part B.* 5, 2282–2283. doi: 10.1080/23802359.2020.1772146

Masson-Delmotte, V., Zhai, P., Pirani, A., Connors, S., Péan, C., Berger, S., et al. (2021). *Climate change 2021: the Physical Science Basis. Working Group I contribution to the Sixth Assessment Report of the Intergovernmental Panel on Climate Change*. Cambridge: Cambridge University Press.

Meng, J. W., He, D. C., Zhu, W., Yang, L. N., Wu, E., Xie, J. H., et al. (2018). Human-mediated gene flow contributes to metapopulation genetic structure of the pathogenic fungus *Alternaria alternata* from potato. *Front. Plant Sci.* 9, 198. doi: 10.3389/fpls.2018.00198

Morgan, G. J., Burkhardt, D. H., Kelly, J. W., and Powers, E. T. (2018). Translation efficiency is maintained at elevated temperature in *Escherichia coli*. *J. Biol. Chem.* 293, 777–793. doi: 10.1074/jbc.RA117.000284

Nei, M. (1973). Analysis of gene diversity in subdivided populations. *Proc. Natl. Acad. Sci.* 70, 3321–3323. doi: 10.1073/pnas.70.12.3321

Nei, M. (1978). Estimation of average heterozygosity and genetic distance from a small number of individuals. *Genetics.* 89, 583–590. doi: 10.1093/genetics/89.3.583

Orr, H. A. (2009). Fitness and its role in evolutionary genetics. *Nat. Rev. Genet.* 10, 531–539. doi: 10.1038/nrg2603

Ott, R. L., and Longnecker, M. T. (2015). *An Introduction to Statistical Methods and Data analysis*. Singapore: Cengage Learning.

Patil, V. U., Vanishree, G., Pattanayak, D., Sharma, S., Bhardwaj, V., Singh, B. P., et al. (2017). Complete mitogenome mapping of potato late blight pathogen, *Phytophthora infestans* A2 mating type. *Mitochondrial DNA Part B* 2, 90–91. doi: 10.1080/23802359.2017.1280699

Popadin, K. Y., Nikolaev, S. I., Junier, T., Baranova, M., and Antonarakis, S. E. (2012). Purifying selection in mammalian mitochondrial protein-coding genes is highly effective and congruent with evolution of nuclear genes. *Mol. Biol. Evol.* 30, 347–355. doi: 10.1093/molbev/mss219

Qin, C. F., He, M. H., Chen, F. P., Zhu, W., Yang, L. N., Wu, E., et al. (2016). Comparative analyses of fungicide sensitivity and SSR marker variations indicate a low risk of developing azoxystrobin resistance in *Phytophthora infestans*. *Sci. Rep.* 6, 1–10. doi: 10.1038/srep20483

Quintela, M., Johansson, M. P., Kristjansson, B. K., Barreiro, R., and Laurila, A. (2014). AFLPs and mitochondrial haplotypes reveal local adaptation to extreme thermal environments in a freshwater gastropod. *PLoS ONE.* 9, e101821. doi: 10.1371/journal.pone.0101821

Roger, A. J., Muñoz-Gómez, S. A., and Kamikawa, R. (2017). The origin and diversification of mitochondria. *Curr. Biol.* 27, R1177–R1192. doi: 10.1016/j.cub.2017.09.015

Roy, D. B., Oliver, T. H., Botham, M. S., Beckmann, B., Brereton, T., Dennis, R. L., et al. (2015). Similarities in butterfly emergence dates among populations suggest local adaptation to climate. *Global Change Biol.* 21, 3313–3322. doi: 10.1111/gcb.12920

Salomon, M., and Buchholz, F. (2000). Effects of temperature on the respiration rates and the kinetics of citrate synthase in two species of Idotea (*Isopoda, Crustacea*). *COMP Biochem. Phys. B.* 125, 71–81. doi: 10.1016/S0305-0491(99)00158-3

Sandor, S., Zhang, Y., and Xu, J. (2018). Fungal mitochondrial genomes and genetic polymorphisms. *Appl. Microbiol. Biotechnol.* 102, 9433–9448. doi: 10.1007/s00253-018-9350-5

Santangelo, J. S., Johnson, M. T., and Ness, R. W. (2018). Modern spandrels: the roles of genetic drift, gene flow and natural selection in the evolution of parallel clines. *Proc. R. Soc. B.* 285, 20180230. doi: 10.1098/rspb.2018.0230

Scheckhuber, C., Erjavec, N., Tinazli, A., Hamann, A., Nyström, T., and Osiewacz, H. (2007). Reducing mitochondrial fission results in increased life span and fitness of two fungal ageing models. *Nat. Cell Biol.* 9, 99–105. doi: 10.1038/ncb1524

Sharma, S., Singh, B., Sharma, S., and Patil, V. (2016). Phenotypic and genotypic characterization of *Phytophthora infestans* population of Himachal Pradesh. *Indian Phytopathol.* 69, 391–395.

Shen, L. L., Waheed, A., Wang, Y. P., Nkurikiyimfura, O., Wang, Z. H., Yang, L. N., et al. (2021). Multiple mechanisms drive the evolutionary adaptation of *Phytophthora infestans* effector *Avr1* to host resistance. *J. Fungi.* 7, 789. doi: 10.3390/jof7100789

Stefansson, T. S., McDonald, B. A., and Willi, Y. (2013). Local adaptation and evolutionary potential along a temperature gradient in the fungal pathogen *Rhynchosporium commune*. *Evol. Appl.* 6, 524–534. doi: 10.1111/eva.12039

Tanaka, D., Sato, K., Goto, M., Fujiyoshi, S., Maruyama, F., Takato, S., et al. (2019). Airborne microbial communities at high-altitude and suburban sites in Toyama, Japan suggest a new perspective for bioprospecting. *Front. Bioeng. Biotech.* 7, 12. doi: 10.3389/fbioe.2019.00012

Waheed, A., Wang, Y. P., Nkurikiyimfura, O., Li, W. Y., Liu, S. T., Lurwanu, Y., et al. (2021). Effector *Avr4* in *Phytophthora infestans* escapes host immunity mainly through early termination. *Front. Microbiol.* 12, 646062. doi: 10.3389/fmicb.2021.646062

Wang, Y. P., Xie, J. H., Wu, E. J., Yahuza, L., Duan, G. H., Shen, L. L., et al. (2020). Lack of gene flow between *Phytophthora infestans* populations of two neighboring countries with the largest potato production. *Evol. Appl.* 13, 318–329. doi: 10.1111/eva.12870

Weaver, S. C., Forrester, N. L., Liu, J., and Vasilakis, N. (2021). Population bottlenecks and founder effects: implications for mosquito-borne arboviral emergence. *Nat. Rev. Microbiol.* 19, 184–195. doi: 10.1038/s41579-020-00482-8

Wright, S. (1943). Isolation by distance. *Genetics.* 28, 114. doi: 10.1093/genetics/28.2.114

Wu, E. J., Wang, Y. P., Shen, L. L., Yahuza, L., Tian, J. C., Yang, L. N., et al. (2019). Strategies of *Phytophthora infestans* adaptation to local UV radiation conditions. *Evol. Appl.* 12, 415–424. doi: 10.1111/eva.12722

Wu, E. J., Wang, Y. P., Yahuza, L., He, M. H., Sun, D. L., Huang, Y. M., et al. (2020). Rapid adaptation of the Irish potato famine pathogen *Phytophthora infestans* to changing temperature. *Evol. Appl.* 13, 768–780. doi: 10.1111/eva.12899

Wu, E. J., Yang, L. N., Zhu, W., Chen, X. M., Shang, L. P., and Zhan, J. (2016). Diverse mechanisms shape the evolution of virulence factors in the potato late

blight pathogen *Phytophthora infestans* sampled from China. *Sci. Rep.* 6, 26182. doi: 10.1038/srep26182

Xiang, N., Hu, J. G., Yan, S., and Guo, X. (2021). Plant hormones and volatiles response to temperature stress in sweet corn (*Zea mays* L.) seedlings. *J. Agric. Food Chem.* 69, 6779–6790. doi: 10.1021/acs.jafc.1c02275

Yang, L. N., Liu, H., Duan, G. H., Huang, Y. M., Liu, S. T., Fang, Z. G., et al. (2020). *Phytophtora infestans AVR2* effector escapes R2 recognition through effector disordering. *Mol. Plant Microbe Interact.* 33, 921–931. doi: 10.1094/MPMI-07-19-0179-R

Yang, L. N., Ouyang, H. B., Fang, Z. G., Zhu, W., Wu, E. J., Luo, G. H., et al. (2018). Evidence for intragenic recombination and selective sweep in an effector gene of *Phytophthora infestans*. *Evol. Appl.* 11, 1342–1353. doi: 10.1111/eva.12629

Yang, L. N., Zhu, W., Wu, E. J., Yang, C., Thrall, P. H., Burdon, J. J., et al. (2016). Trade-offs and evolution of thermal adaptation in the Irish potato famine pathogen *Phytophthora infestans*. *Mol. Ecol.* 25, 4047–4058. doi: 10.1111/mec.13727

Yang, Z. H., Qi, M. X., Qin, Y. X., Zhu, J. H., Gui, X. M., Tao, B., et al. (2013). Mitochondrial DNA polymorphisms in *Phytophthora infestans*: new haplotypes are identified and re-defined by PCR. *J. Microbiol. Methods.* 95, 117–121. doi: 10.1016/j.mimet.2013.08.001

Zhan, J., Ericson, L., and Burdon, J. J. (2018). Climate change accelerates local disease extinction rates in a long-term wild host–pathogen association. *Global. Change Biol.* 24, 3526–3536. doi: 10.1111/gcb.14111

Zhan, J., Kema, G. H., and McDonald, B. A. (2004). Evidence for natural selection in the mitochondrial genome of *Mycosphaerella graminicola*. *Phytopathol.* 94, 261–267. doi: 10.1094/PHYTO.2004.94.3.261

Zhan, J., and McDonald, B. A. (2011). Thermal adaptation in the fungal pathogen *Mycosphaerella graminicola*. *Mol. Ecol.* 20, 1689–1701. doi: 10.1111/j.1365-294X.2011.05023.x

Zhan, J., Pettway, R. E., and McDonald, B. A. (2003). The global genetic structure of the wheat pathogen *Mycosphaerella graminicola* is characterized by high nuclear diversity, low mitochondrial diversity, regular recombination, and gene flow. *Fungal Genet. Biol.* 38, 286–297. doi: 10.1016/S1087-1845(02)00538-8

Zhu, W., Shen, L. L., Fang, Z. G., Yang, L. N., Zhang, J. F., Sun, D. L., et al. (2016). Increased frequency of self-fertile isolates in *Phytophthora infestans* may attribute to their higher fitness relative to the A1 isolates. *Sci. Rep.* 6, 1–10. doi: 10.1038/srep29428

Conflict of Interest: The authors declare that the research was conducted in the absence of any commercial or financial relationships that could be construed as a potential conflict of interest.

Publisher's Note: All claims expressed in this article are solely those of the authors and do not necessarily represent those of their affiliated organizations, or those of the publisher, the editors and the reviewers. Any product that may be evaluated in this article, or claim that may be made by its manufacturer, is not guaranteed or endorsed by the publisher.

frontiers | Frontiers in Microbiology

TYPE Correction
PUBLISHED 11 August 2022
DOI 10.3389/fmicb.2022.1002575

OPEN ACCESS

APPROVED BY
Frontiers Editorial Office,
Frontiers Media SA, Switzerland

*CORRESPONDENCE
Li-Na Yang
yikeshu1114@126.com

†These authors have contributed equally to this work and share first authorship

SPECIALTY SECTION
This article was submitted to Microbe and Virus Interactions with Plants, a section of the journal Frontiers in Microbiology

RECEIVED 25 July 2022
ACCEPTED 26 July 2022
PUBLISHED 11 August 2022

CITATION
Shen L-L, Waheed A, Wang Y-P, Nkurikiyimfura O, Wang Z-H, Yang L-N and Zhan J (2022) Corrigendum: Mitochondrial genome contributes to the thermal adaptation of the oomycete *Phytophthora infestans*. *Front. Microbiol.* 13:1002575. doi: 10.3389/fmicb.2022.1002575

Corrigendum: Mitochondrial genome contributes to the thermal adaptation of the oomycete *Phytophthora infestans*

Lin-Lin Shen[1†], Abdul Waheed[1†], Yan-Ping Wang[2], Oswald Nkurikiyimfura[3], Zong-Hua Wang[1], Li-Na Yang[1*] and Jiasui Zhan[4]

[1]Institute of Oceanography, Minjiang University, Fuzhou, China, [2]Sichuan Provincial Key Laboratory for Development and Utilization of Characteristic Horticultural Biological Resources, Chengdu Normal University, Chengdu, China, [3]Institute of Plant Virology, Fujian Agriculture and Forestry University, Fuzhou, China, [4]Department of Forest Mycology and Plant Pathology, Swedish University of Agricultural Sciences, Uppsala, Sweden

KEYWORDS

mitochondria, evolutionary ecology, population genetic, local adaptation, agricultural pathogen, climate change

A corrigendum on
Mitochondrial genome contributes to the thermal adaptation of the oomycete *Phytophthora infestans*

by Shen, L.-L., Waheed, A., Wang, Y.-P., Nkurikiyimfura, O., Wang, Z.-H., Yang, L.-N., and Zhan, J. (2022). *Front. Microbiol.* 13:928464. doi: 10.3389/fmicb.2022.928464

In the published article, there was an error made during production in the manuscript text that should be written Table 4 instead of Table 3.

A correction has been made to **[Results]**, [**Geographic pattern of spatial distribution in mitochondrial haplotypes and associations of the distribution with climatic conditions**], [Paragraph Number 5]. This sentence previously stated: "The annual mean temperature in the 15 collection sites was negatively correlated to the frequency of mitochondrial Type I ($R^2 = 0.4150$, $p = 0.0090$, Figure 3A) but positively correlated to haplotype diversity ($R^2 = 0.3160$, $p = 0.0234$, Figure 4A). Annual insolation duration in the collection sites was significantly and quadratically associated with haplotype diversity ($R^2 = 0.2140$, $p = 0.0458$, Figure 4F) but only marginally associated with haplotype frequency ($R^2 = 0.2330$, $p = 0.0804$, Figure 3F). On the other hand, altitude in the collection sites was significantly and linearly associated with haplotype frequency ($R^2 = 0.3440$, $p = 0.0210$; Figure 3B) but only marginally associated with haplotype diversity ($R^2 = 0.1750$, $p = 0.1069$, Figure 4B). Latitude was marginally associated with both haplotype frequency and diversity (Figures 3D, 4D). No associations were detected between other climatic conditions or geographic positions

in the collection sites with the haplotype frequency and diversity. Multiple regression analysis also revealed that annual mean temperature and altitude in the collection sites contributed significantly to the spatial distribution of haplotype frequency and diversity (Table 3). On the other hand, annual insolation duration and latitude in the collection sites only significantly contributed to the spatial distribution of mitochondrial haplotype in terms of frequency but not diversity."

The corrected sentence appears below:

"The annual mean temperature in the 15 collection sites was negatively correlated to the frequency of mitochondrial Type I ($R^2 = 0.4150$, $p = 0.0090$, Figure 3A) but positively correlated to haplotype diversity ($R^2 = 0.3160$, $p = 0.0234$, Figure 4A). Annual insolation duration in the collection sites was significantly and quadratically associated with haplotype diversity ($R^2 = 0.2140$, $p = 0.0458$, Figure 4F) but only marginally associated with haplotype frequency ($R^2 = 0.2330$, $p = 0.0804$, Figure 3F). On the other hand, altitude in the collection sites was significantly and linearly associated with haplotype frequency ($R^2 = 0.3440$, $p = 0.0210$; Figure 3B) but only marginally associated with haplotype diversity ($R^2 = 0.1750$, $p = 0.1069$, Figure 4B). Latitude was marginally associated with both haplotype frequency and diversity (Figures 3D, 4D). No associations were detected between other climatic conditions or geographic positions in the collection sites with haplotype (frequency and diversity). Multiple regression analysis also revealed that annual mean temperature and altitude in the collection sites contributed significantly to the spatial distribution of haplotype frequency and diversity (Table 4). On the other hand, annual insulation duration and latitude in the collection sites only significantly contributed to the spatial distribution of mitochondrial haplotype in term of frequency but not diversity."

In the published article, there was an error made during production in the manuscript text that should be written Table 3 instead of Table 4.

A correction has been made to Discussion, Paragraph Number 4. This sentence previously stated: "Differentiation caused by genetic drift is expected to have no impact on fitness (Orr, 2009). In this study, we find a significant difference in intrinsic growth rate among the mitochondrial haplotypes (Table 4) and the difference can be successfully transferred to competitive ability as indicated by the positive association between haplotype frequency observed in nature and its intrinsic growth rate. Apparently, mitochondrial Type I is more successful than Type II in *P. infestans*. It is the dominant haplotype, possibly attributed to its higher fitness, and the result is similar to other reports. For example, Type I dominated in the surveys conducted in India (Sharma et al., 2016), Turkey (Gunacti et al., 2019), as well as other parts of China (Yang et al., 2013) and adapts to wider ecological niches (Sharma et al., 2016)."

The corrected sentence appears below:

"Differentiation caused by genetic drift is expected to have no impact on fitness (Orr, 2009). In this study, we find significant difference in intrinsic growth rate among the mitochondrial haplotypes (Table 3) and the difference can be successfully transferred to competitive ability as indicated by the positive association between haplotype frequency observed in nature and its intrinsic growth rate. Apparently, mitochondrial Type I is a more successful than Type II in *P. infestans*. It is the dominant haplotype, possibly attributed to its higher fitness, and the result is similar to other reports. For example, Type I dominated in the surveys conducted in India (Sharma et al., 2016), Turkey (Gunacti et al., 2019) as well as other parts of China (Yang et al., 2013) and adapts to wider ecological niches (Sharma et al., 2016)."

The authors apologize for this error and state that this does not change the scientific conclusions of the article in any way. The original article has been updated.

Publisher's note

References

Gunacti, H., Ay, T., and Can, C. (2019). Genotypic and phenotypic characterization of *Phytophthora infestans* populations from potato in Turkey. *Phytoparasitica*. 47, 429–439. doi: 10.1007/s12600-019-00737-y

Orr, H. A. (2009). Fitness and its role in evolutionary genetics. *Nat. Rev. Genet.* 10, 531–539. doi: 10.1038/nrg2603

Sharma, S., Singh, B., Sharma, S., and Patil, V. (2016). Phenotypic and genotypic characterization of *Phytophthora infestans* population of Himachal Pradesh. *Indian Phytopathol.* 69, 391–395.

Yang, Z. H., Qi, M. X., Qin, Y. X., Zhu, J. H., Gui, X. M., Tao, B., et al. (2013). Mitochondrial DNA polymorphisms in *Phytophthora infestans*: new haplotypes are identified and re-defined by PCR. *J. Microbiol. Methods.* 95, 117–121. doi: 10.1016/j.mimet.2013.08.001

frontiers | Frontiers in Microbiology

ORIGINAL RESEARCH
published: 30 June 2022
doi: 10.3389/fmicb.2022.925868

BcMettl4-Mediated DNA Adenine N^6-Methylation Is Critical for Virulence of *Botrytis cinerea*

Zhengang Miao[1†], Guangyuan Wang[2†], Heng Shen[1], Xue Wang[3], Dean W. Gabriel[4] and Wenxing Liang[1]*

[1] College of Plant Health and Medicine, Engineering Research Center for Precision Pest Management for Fruits and Vegetables of Qingdao, Shandong Engineering Research Center for Environment-Friendly Agricultural Pest Management, Shandong Province Key Laboratory of Applied Mycology, Qingdao Agricultural University, Qingdao, China, [2] College of Life Sciences, Shandong Province Key Laboratory of Applied Mycology, Qingdao Agricultural University, Qingdao, China, [3] Yantai Agricultural Technology Extension Center, Yantai, China, [4] Department of Plant Pathology, University of Florida, Gainesville, FL, United States

OPEN ACCESS

Edited by:
Qunqing Wang,
Shandong Agricultural University, China

Reviewed by:
Qiya Yang,
Jiangsu University, China
Xiaowei Han,
Huazhong Agricultural University, China

***Correspondence:**
Wenxing Liang
wliang1@qau.edu.cn

[†] These authors have contributed equally to this work and share first authorship

Specialty section:
This article was submitted to Microbe and Virus Interactions with Plants, a section of the journal Frontiers in Microbiology

Received: 22 April 2022
Accepted: 23 May 2022
Published: 30 June 2022

Citation:
Miao Z, Wang G, Shen H, Wang X, Gabriel DW and Liang W (2022) BcMettl4-Mediated DNA Adenine N^6-Methylation Is Critical for Virulence of Botrytis cinerea. Front. Microbiol. 13:925868. doi: 10.3389/fmicb.2022.925868

DNA adenine N^6-methylation (6mA) plays a critical role in various biological functions, but its occurrence and functions in filamentous plant pathogens are largely unexplored. *Botrytis cinerea* is an important pathogenic fungus worldwide. A systematic analysis of 6mA in *B. cinerea* was performed in this study, revealing that 6mA is widely distributed in the genome of this fungus. The 2 kb regions flanking many genes, particularly the upstream promoter regions, were susceptible to methylation. The role of BcMettl4, a 6mA methyltransferase, in the virulence of *B. cinerea* was investigated. *BcMETTL4* disruption and point mutations of its catalytic motif "DPPW" both resulted in significant 6mA reduction in the genomic DNA and in reduced virulence of *B. cinerea*. RNA-Seq analysis revealed a total of 13 downregulated genes in the disruption mutant ΔBcMettl4 in which methylation occurred at the promoter sites. These were involved in oxidoreduction, secretory pathways, autophagy and carbohydrate metabolism. Two of these genes, *BcFDH* and *BcMFS2,* were independently disrupted. Knockout of *BcFDH* led to reduced sclerotium formation, while disruption of *BcMFS2* resulted in dramatically decreased conidium formation and pathogenicity. These observations indicated that 6mA provides potential epigenetic markers in *B. cinerea* and that BcMettl4 regulates virulence in this important plant pathogen.

Keywords: *Botrytis cinerea*, 6mA, methyltransferase, MeDIP-Seq, virulence

INTRODUCTION

DNA methylation is one of the basic epigenetic markers involved in regulation of various biological functions in both prokaryotes and eukaryotes (Bird, 2007; Vasu and Nagaraja, 2013). Among the methylation modifications, DNA adenine N^6-methylation (6mA) and 5-methylcytosine (5mC) are two of the most important. The 5mC modification has been well studied as an epigenomic marker in eukaryotes (Zemach et al., 2010), while adenine N^6-methylation has been found to be predominantly distributed in prokaryotic genomes (Blow et al., 2016) and eukaryotic RNA (Fu et al., 2014). In recent years, 6mA has also been found to be widespread in the genomic

DNA of many eukaryotes, including fungi (Mondo et al., 2017), *Chlamydomonas* (Fu et al., 2015), *Caenorhabditis elegans* (Greer et al., 2015), *Arabidopsis thaliana* (Liang et al., 2018), rice (Zhou et al., 2018) and humans (Xiao et al., 2018). However, compared with those in prokaryotes, the characteristics of 6mA methylation in eukaryotes are still largely unknown.

Previous studies have shown that 6mA is dynamically controlled by methyltransferase and demethylase (Greer et al., 2015; Zhang et al., 2015). In prokaryotes, M.*Mun*I is a classic 6mA methyltransferase (Iyer et al., 2016). It has been well documented that the orthologs of MT-A70 that evolved from M.*Mun*I (Iyer et al., 2011) in eukaryotes are important 6mA methyltransferases (Bujnicki et al., 2002). Three MT-A70 methyltransferases, namely, Mettl4 in *Bombyx mori* (Wang et al., 2018) and Mettl3 and Mettl14 in humans (Wang et al., 2016), have been shown to play important roles in regulating the levels of 6mA. Mta1, an MT-A70 ortholog in *Oxytricha*, can form a dimer with Mta9 and has the function of a DNA methyltransferase (Woodcock et al., 2020). We found an MT-A70 homologous protein, BcMettl4, in *Botrytis cinerea*, but the function of this protein in DNA methylation was unclear.

Botrytis cinerea is an important necrotrophic fungal pathogen that infects over 1,000 plants and causes gray mold disease. Many economically important vegetables and fruits, including strawberry, tomato, cucumber and grape, are susceptible to *B. cinerea*. *B. cinerea* is ranked as the second most common plant pathogenic fungus in the world (Dean et al., 2012) and causes severe preharvest and postharvest economic losses worldwide (Mousavi-Derazmahalleh et al., 2019). However, the biological role of the 6mA DNA modification in *B. cinerea* is still unclear.

In this study, the 6mA DNA modification in *B. cinerea* was investigated and 6mA was found to be widely distributed in *B. cinerea*. The gene *BcMETTL4* was disrupted in the wild-type strain B05.10. Methylated DNA immunoprecipitation sequencing (MeDIP-Seq) was further employed to analyze the methylome characteristics of the wild-type strain B05.10 and the gene disruption mutant ΔBcMettl4. Deletion of *BcMETTL4* caused a global reduction in DNA 6mA. RNA-Seq analysis was subsequently used to investigate global gene expression patterns in the disruption mutant ΔBcMettl4 and its wild-type strain B05.10. Finally, the relationships between 6mA, gene expression and virulence were investigated. Expression of key genes involved in virulence and conidiation was strongly affected by 6mA modification in *B. cinerea*.

MATERIALS AND METHODS

Strains and Growth Assays

Strain B05.10 of *B. cinerea* used in this study was isolated from *Vitis vinifera* (Yang et al., 2018). The wild-type strain, gene deletion derivatives and complemented strains were grown on PDA plates (20% potato, 2% dextrose, and 1.5% agar). The growth ratios, conidial development, and sclerotium formation of different strains of *B. cinerea* were measured according to previously described methods (Yang et al., 2019). For mycelial growth assays, the different strains were cultured at 25°C for 3 day on PDA plates supplemented with 0.5 mM CR, 0.73 mM SDS, 20 mM H_2O_2, 1 M sorbitol, 1 M KCl, 1 M NaCl, and 1 M glycerine.

Construction of Gene Deletions, Complementation, Subcellular Localization and Point Mutations

To construct the gene mutant cassette for targeted deletions, two flanking sequences of each gene were obtained from genomic DNA of strain B05.10 by PCR. The hygromycin B phosphotransferase (*HPH*) gene was derived from the plasmid pBS-HPH1 (Yang et al., 2018). The two flanking fragments and the *HPH* gene were fused by splice overlap PCR. The resulting deletion cassettes (*Promoter:HPH:Terminator*) were connected to the pMD19-T vector for sequencing. The gene deletion cassette was transformed into strain B05.10.

For complementation, full-length genes, including promoters and terminators, were amplified from the B05.10 genome. The resulting PCR products were cloned into plasmid pBS-neo (Yang et al., 2018). The resulting vectors were subsequently transformed into the deletion mutants.

To construct BcMettl4-GFP, BcDamt-GFP, and BcMettl4$^{\Delta NLS}$-GFP fusion cassettes, the open reading frames (ORFs) of *BcMETTL4* and *BcDAMT* without the stop codons were amplified by PCR from strain B05.10. The NLS of BcMettl4 was deleted using overlap PCR (Heckman and Pease, 2007). The PCR products were ligated into plasmid pNAH-OGG-G418 that was derived by replacing the hygromycin B resistance gene of pNAH-OGG (Schumacher, 2012) with a geneticin G418 resistance gene from plasmid pBS-neo (Yang et al., 2018).

For generation of the BcMettl4 point mutant, we first designed primers that contained the mutated site. The sites upstream and downstream of the mutated site were obtained by PCR and the products were joined by overlap PCR. The resulting PCR products were cloned into the plasmid pBS-neo and transformed into the ΔBcMettl4 strain using standard protoplast formation procedures as previously described (Gronover et al., 2001; Yang et al., 2018).

All primers and their descriptions are shown in **Supplementary Table 1**. Positive transformants were selected on PDA plates with 0.01% hygromycin B or 0.01% geneticin G418 sulfate. PCR was used to confirm the positive transformants.

Dot Blot Assay

Genomic DNA from various strains was extracted using a Fungi Genomic DNA Purification Kit (Sangon Biotech, China). After denaturation at 98°C for 5 min, the extracted DNA was chilled on ice for 10 min and then transferred to a HybondTM-N + membrane. After drying at room temperature, the DNA was fixed to the membrane by UV cross-linking. The HybondTM-N + membrane was blocked in 5% skim milk powder for 1.5 h at room temperature, followed by incubation with 6mA antibody (1:2,000 dilution, Abcam, ab151230) for 10 h at 4°C. The membrane was then washed four times for 8 min using TBST [25 mM Tris–HCl (pH 7.4), 140 mM NaCl and 0.1% Tween-20]. After incubation with secondary antibody (1:5,000

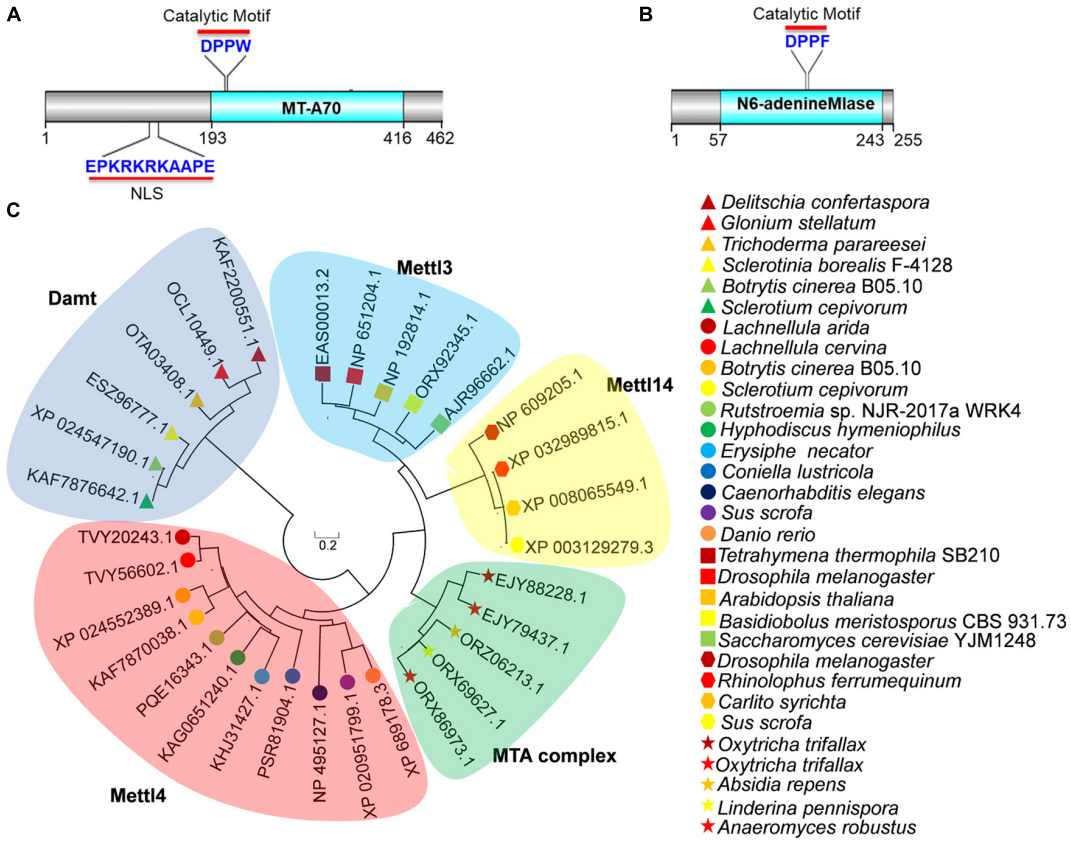

FIGURE 1 | Bioinformatics analysis of BcMettl4 and BcDamt. **(A)** The structural domains encoded by BCIN_12g06440. **(B)** The structural domain encoded by BCIN_02g05970. **(C)** Phylogenetic tree of methyltransferase orthologs based on a neighbor-joining analysis.

dilution, Sigma A0545) at room temperature for 2 h, the membrane was washed 4 times for 8 min using TBST. Finally, an ECL Immunoblotting Detection Kit (Thermo Fisher) was used for signal visualization. The input DNA was normalized by using methylene blue.

MeDIP-Seq

MeDIP-Seq was performed according to previously described protocols (Fu et al., 2015; Chen et al., 2018; Zhou et al., 2018). In brief, the genomic DNAs of different strains were extracted from conidia grown in YEPD medium for 24 h at 25°C, followed by incubation with RNase A overnight. After sonication, the DNA fragments (200–400 bp) were repaired, followed by adaptor ligation. The resulting DNA was purified using a TIANquick Midi Purification Kit (DP204, TIANGEN BIOTECH, China). The purified DNA fragments were denatured at 94°C for 15 min and chilled on ice for 10 min. An aliquot of denatured DNA was used as input. The remaining DNA was incubated with anti-6mA antibody at 4°C for 12 h. After elution by 6mA salt competition, a 6mA-IP-Seq library was constructed by PCR amplification. The resulting DNA fragments were sequenced with a HiSeq 2500 (Illumina) (Zhou et al., 2018). Raw reads were trimmed to remove adaptors and low-quality bases, and the reads with 6mA-rich regions were called with MASC2 (Liu, 2014).

RNA-Seq Analysis

After conidial germination in YEPD medium at 25°C for 24 h, the mycelia of different strains were collected by centrifugation for RNA extraction. Total RNA was extracted using TRIzol Reagent (Invitrogen). A NanoDrop spectrophotometer (Thermo Scientific) was employed to determine the RNA concentration, quality and integrity. Poly-T oligo-attached magnetic beads were purified to enrich mRNA. First-strand cDNA was obtained using random oligonucleotides and SuperScript II. Second-strand cDNA synthesis was subsequently performed using DNA polymerase I and RNase H. The resulting cDNA fragments were further adenylated at the 3' ends and ligated with Illumina PE adaptor oligonucleotides. PCR was performed to enrich the DNA fragments with ligated adaptors on both ends. After purification using an AMPure XP system and quantification using an Agilent high-sensitivity DNA assay, the obtained sequencing library was sequenced on a NovaSeq 6000 platform (Illumina).

Bioinformatics Analysis

TopHat (v2.0.12) was employed to map the obtained sequences against the database of *B. cinerea* (Trapnell et al., 2009). The mapped genes were calculated using HTSeq (v0.6.1) (Anders et al., 2015). Gene expression was quantitatively estimated by using the reads per kilobase per million mapped reads (RPKM)

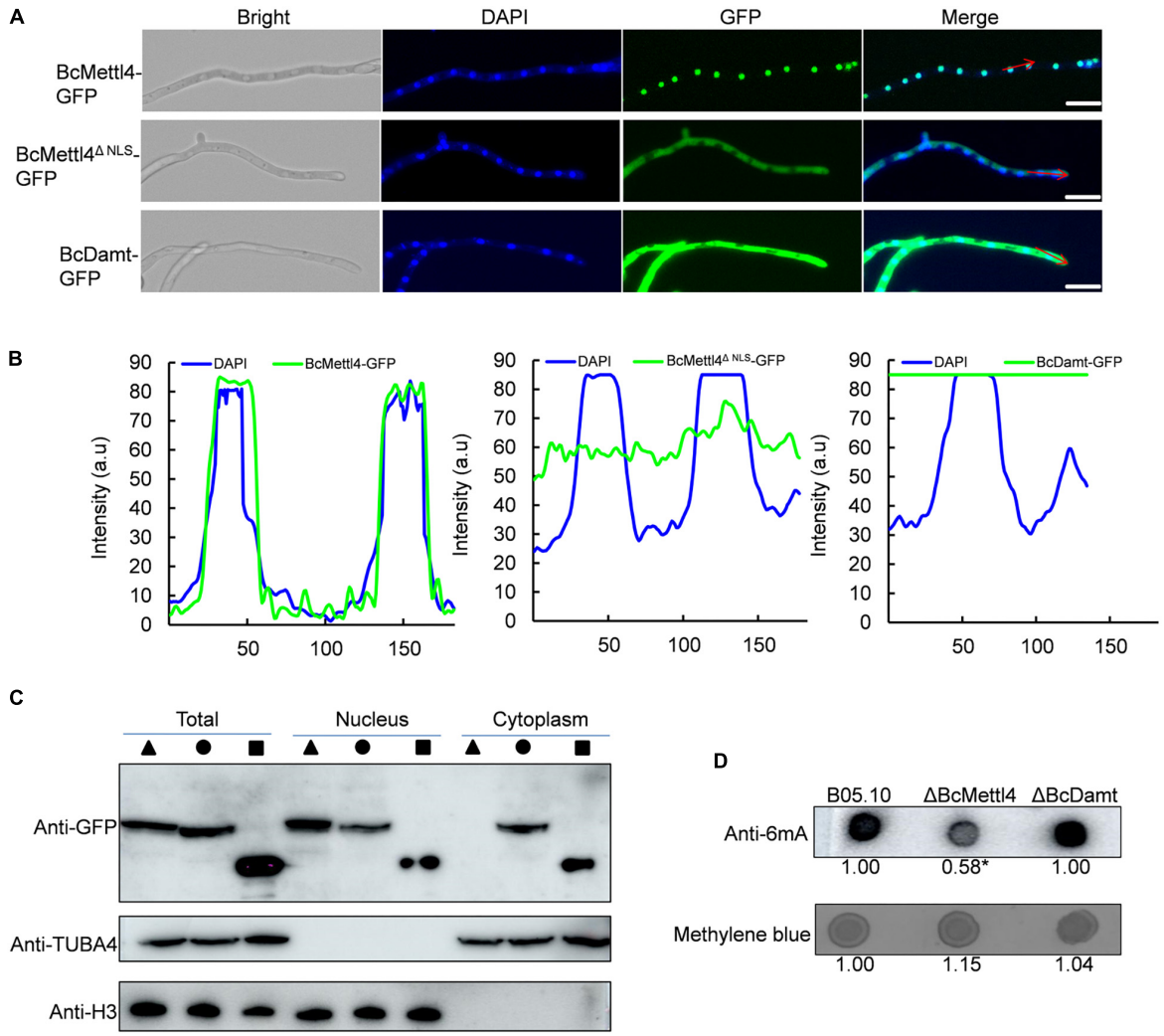

FIGURE 2 | Subcellular localization of BcMettl4 and BcDamt, and effects of *BcMETTL4* and *BcDAMT* deletion on genome methylation. **(A)** Mycelia images for subcellular localization of the BcMettl4-GFP, BcMettl4$^{\Delta\ NLS}$-GFP, and BcDamt-GFP. Scale bar = 20 μm. **(B)** Fluorescence intensity of BcMettl4-GFP, BcMettl4$^{\Delta\ NLS}$-GFP, and BcDamt-GFP. The blue line represents DAPI while the green line shows GFP. The signal areas were marked by red lines in **Figure 2A** and the signal quantification were calculated by ImageJ. **(C)** Western blot analysis of BcMettl4-GFP (triangle), BcMettl4$^{\Delta\ NLS}$-GFP (circle), and BcDamt-GFP (square). Histone H3 served as a reference for proteins in the nucleus. Alpha tubulin 4a was used as a control for cytoplasmic proteins. **(D)** Dot blot assay for verification the presence of 6mA in the genome DNA of *B. cinerea*. A total of 200 ng DNA was investigated by dot blot assay. Relative 6mA abundance in different strains was calculated by ImageJ. The relative ratio after normalization is to reflect the difference among various treatments. The asterisk means significant difference in values at $p < 0.05$.

value (Trapnell et al., 2010). DESeq was used to analyze the differentially expressed genes between the wild-type and the gene deletion mutants (Wang et al., 2010).

Pathogenicity Experiments on Tomato Leaves and Onion Epidermis

After growth on PDA plates at 25°C for 7 days, the conidia produced by different strains of *B. cinerea* were harvested and resuspended in buffer (6.7 mm K_2HPO_4 and 10 mm glucose). A total of 5 μl of conidia suspension (5.0×10^5 conidia/ml) was transferred to 8-week-old tomato (*Solanum lycopersicum*) leaves, incubated at 25°C for 72 h, and developing disease lesions caused by different strains were measured.

Additionally, infection-related morphogenesis was observed on onion epidermis. The conidial suspensions (3.0×10^3 conidia/ml) were inoculated onto the epidermis. After culturing for 12 h at 25°C in the dark, the onion skin was stained with aniline blue and observed.

Induced Expression of *BcMETTL4* and *BcDAMT* in Interactions Between *Botrytis cinerea* and Tomato Leaves

The expression levels of *BcMETTL4* and *BcDAMT* in wild-type B05.10 in interaction between *B. cinerea* and tomato leaves were investigated by real-time PCR. In brief, 45 ml of conidia suspension (5.0×10^6 conidia/ml) and 5 ml of YEPD

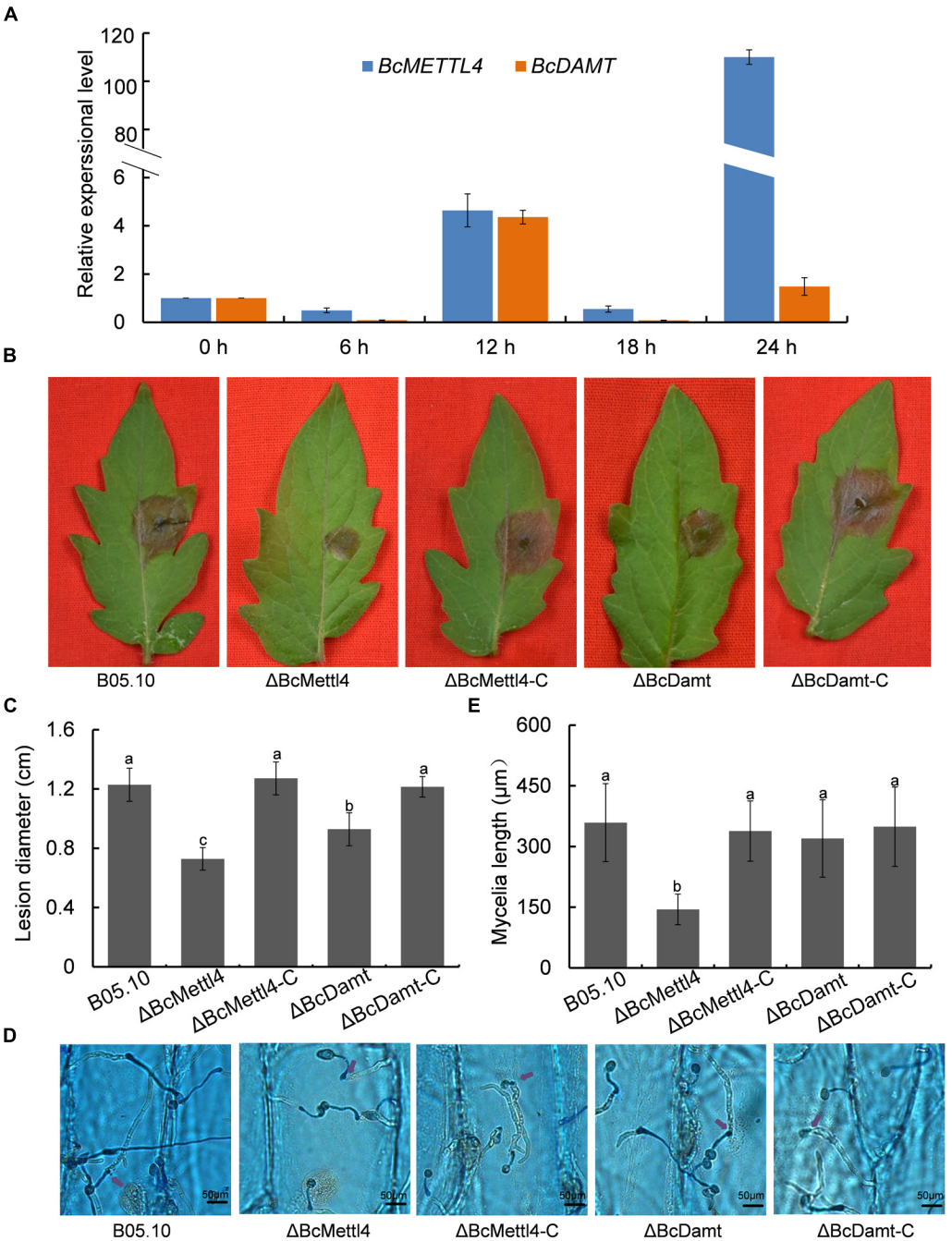

FIGURE 3 | Effects of *BcMETTL4* and *BcDAMT* disruption on virulence and conidia infection. **(A)** The expression levels of *BcMETTL4* and *BcDAMT* at early infection stages evaluated by qRT-PCR. **(B)** Lesions on tomato leaves caused by different strains 72 h after inoculation. **(C)** Lesion diameter of the strains inoculated on tomato leaves. Three experiments were carried out and nine leaves were measured in one biological experiment. Statistical tests were carried out using Tukey's test. The same letters marked on the bars indicate no significant difference in values at $p < 0.05$. **(D)** Infection of conidia from different strains after 12 h of incubation on onion epidermis. Mycelia growing outside onion cells were colored blue, while mycelia growing inside onion cells are not stained. Penetrated positions are marked by purple arrows. **(E)** Mycelia length of different strains at 12 h after conidia infection on onion epidermis. Data are given as the mean ± SD, $n = 10$. The different letters showed on the columns were significantly different at $p < 0.05$.

medium were mixed and 3 g of sterile fresh intact tomato leaves (3 weeks old) was added, and then gently agitated in a shaker at 25°C. Samples were collected at 6 h intervals for 24 h. RNA was extracted according to a previously described protocol (Yang et al., 2018). cDNA was biosynthesized by reverse transcription using a PrimeScript RT Kit (Takara, Japan). The

primers used are shown in **Supplementary Table 1**. Relative expression levels were calculated using the $2^{-\Delta\Delta Ct}$ method (Livak and Schmittgen, 2001).

Western Blot

The mycelia grown in YEPD medium at 25°C for 24 h were collected. A nuclear protein extraction kit (R0050, Solarbio) was used to separate nuclear and cytoplasmic proteins. The proteins were separated by SDS-PAGE and immunoblotted using anti-GFP antibody (ab290, Abcam), anti-H3 antibody (ab1791, Abcam), and anti-TUBA4A antibody (D110022, BBI Life Sciences).

RESULTS

Analysis of the Methyltransferases in *Botrytis cinerea*

To investigate the presence of 6mA in *B. cinerea*, we searched the genome of *B. cinerea* B05.10 using BLAST and found two potential candidates for 6mA methyltransferase. One candidate was BCIN_12g06440 (also known as BC1G_13837), encoding a hypothetical protein (NCBI id: XP_024552389.1) which is a 462-amino-acid ortholog of MT-A70 in *B. cinerea* (**Figure 1A**). The other was BCIN_02g05970 (also known as BC1G_16157), encoding a hypothetical protein (255 amino acids) containing a N6-adenineMlase (probable N6-adenine methyltransferase) catalytic domain (NCBI id: XP_024547190.1) (**Figure 1B**). As shown in **Figure 1A**, the protein encoded by BCIN_12g06440 contained a conserved catalytic motif ("DPPW") and a nuclear localization signal (NLS). However, the protein encoded by BCIN_02g05970 contained only one catalytic motif, "DPPF" (**Figure 1B**).

A variety of methyltransferases, including Mta1, Mta9, Mettl3, Mettl4, Mettl14, and Damt, have previously been reported (Wang et al., 2016, 2018; Chen et al., 2018; Beh et al., 2019; Woodcock et al., 2020). A phylogenetic tree of methyltransferase orthologs was constructed using MEGA 7.0 software, revealed that the protein encoded by BCIN_12g06440 in *B. cinerea* was closely related to a branch representing the MT-A70 ortholog Mettl4, while the protein encoded by BCIN_02g05970 belonged to a clade of Damt (**Figure 1C**). The hypothetical proteins encoded by BCIN_12g06440 and BCIN_02g05970 were thus named BcMettl4 and BcDamt, respectively. The roles of BcMettl4 and BcDamt in the virulence of *B. cinerea* were subsequently studied in some detail.

Effects of *BcMETTL4* and *BcDAMT* Disruption on Genome Methylation in *Botrytis cinerea*

Since BcMettl4 contains a predicted NLS signal (**Figure 1A**), this protein might localize in the nucleus. To test this hypothesis, two fusion proteins, BcMettl4-GFP and BcMettl4$^{\Delta\ NLS}$-GFP (without a NLS), were expressed in strain B05.10 of *B. cinerea*. After growth on PDA plates for 3 days, the transformants containing the fusion protein BcMettl4-GFP or BcMettl4$^{\Delta\ NLS}$-GFP were observed by fluorescence microscopy. The results showed that the GFP signal of BcMettl4-GFP overlapped with nuclei stained with DAPI fluorescent dye, while BcMettl4$^{\Delta\ NLS}$-GFP was present in both the cytoplasm and the nucleus (**Figures 2A,B**). A western blot analysis was performed using extracted total proteins, nuclear proteins and cytoplasmic proteins and revealed that BcMettl4-GFP was significantly enriched in the nucleus compared with BcMettl4$^{\Delta\ NLS}$-GFP (**Figure 2C**). These findings confirmed that BcMettl4 was located in the nucleus and that the NLS of BcMettl4 played an important role in controlling the subcellular localization of BcMettl4. By contrast, the fusion protein BcDamt-GFP was mainly located in the cytoplasm (**Figures 2A–C**).

The genes *BcMETTL4* and *BcDAMT* were disrupted in the wild-type strain B05.10. PCR amplification revealed that one transformant, ΔBcMettl4, exhibited *BcMETTL4* gene disruption (**Supplementary Figure 1**), and another transformant, ΔBcDamt, exhibited *BcDAMT* gene deletion (**Supplementary Figure 2**). To investigate the presence of 6mA DNA modification in *B. cinerea*, the genomic DNAs (gDNAs) of B05.10, ΔBcMettl4, and ΔBcDamt were extracted and a dot blot assay performed using a specific 6mA antibody. As shown in **Figure 2D**, a strong immune blot signal was detected in the gDNA of B05.10. Compared with those of B05.10 and ΔBcDamt, the signal in the gene deletion mutant ΔBcMettl4 was significantly weaker, based on ImageJ analysis ($p < 0.05$) (**Figure 2D**).

Taken together, these observations suggested that 6mA was a widespread DNA modification in the genome of *B. cinerea* and that BcMettl4 may play a role in modifying nuclear DNA.

Impacts of *BcMETTL4* and *BcDAMT* Disruption on Virulence of *Botrytis cinerea*

The transcript levels of *BcMETTL4* and *BcDAMT* at the point of germination in culture in the presence of tomato leaf tissue to 24 h later were assessed as a proxy for the early interaction stage between *B. cinerea* and tomato leaves. As shown in **Figure 3A**, the expression levels of *BcMETTL4* and *BcDAMT* remained stable until 12 h and then increased approximately four-fold compared to those at 0 h. However, after 24 h of growth, the expression of *BcMETTL4* increased approximately 110-fold, compared with a twofold increase in *BcDAMT* gene expression (**Figure 3A**). Highly induced expression of *BcMETTL4* by presence of tomato leaf tissue indicated that BcMettl4 might be involved in the virulence of *B. cinerea*.

The impacts of *BcMETTL4* and *BcDAMT* disruption on the virulence of *B. cinerea* were therefore investigated. First, the mutants ΔBcMettl4 and ΔBcDamt were complemented with the genes *BcMETTL4* and *BcDAMT*, respectively. These two genes including their native promoters and terminators were amplified from wild-type strain B05.10 genomic DNA using the primers listed in **Supplementary Table 1**. The obtained fragments were inserted into the plasmid pBS-neo and subsequently transformed into the mutants according to the method described above. Finally, two complemented strains, ΔBcMettl4-C and ΔBcDamt-C, were obtained. Deletion of any of the genes, that is, *BcMETTL4* or *BcDAMT*, reduced the pathogenicity of *B. cinerea* on tomato,

especially deletion of *BcMETTL4* (**Figure 3B**). As shown in **Figure 3C**, the spreading of the lesion induced by the disruption mutant ΔBcMettl4 was significantly reduced compared with that induced by the wild-type strain B05.10 or the disruption mutant ΔBcDamt.

We further examined the ability of these strains to penetrate onion epidermal cells. As shown in **Figure 3D**, deletion of *BcMETTL4* weakened the infection of mycelia in onion epidermal cells. Mycelia length of different strains of *B. cinerea* at 12 h after conidia infection on onion epidermis were further investigated. It was found that the mycelia length of ΔBcMettl4 invaded onion cells were 144 μm, while those of other strains, B05.10, ΔBcMettl4-C, ΔBcDamt, and ΔBcDamt-C, were 359, 338, 320, and 349 μm (**Figure 3E**), respectively, revealing that *BcMETTL4* interruption decreased virulence of *B. cinerea* on onion by reducing the conidia infectivity.

Effects of *BcMETTL4* and *BcDAMT* Disruption on Mycelial Growth, Conidial, Sclerotial Formation and Stress Tolerance

The reduction in genome-wide 6mA (**Figure 2D**) in the disruption mutant ΔBcMettl4 led to investigations of the biological phenotypes of the different mutations affecting 6mA. After 3 days of cultivation on PDA plates, there were no obvious differences in mycelial growth of B05.10, ΔBcMettl4, ΔBcDamt, ΔBcMettl4-C, and ΔBcDamt-C (**Figure 4A**). Disruption of *BcMETTL4* or *BcDAMT* also did not affect conidial formation (**Figure 4A**). However, after growth on PDA plates for 30 days in darkness, ΔBcMettl4 exhibited significantly decreased sclerotial formation compared with B05.10, ΔBcMettl4-C, ΔBcDamt, and ΔBcDamt-C (**Figure 4B**). Our previous studies have shown that the reduction of sclerotia in *B. cinerea* is often accompanied by a decrease in pathogenicity (Yang et al., 2015; Wang et al., 2020). These observations suggested that the reduction in sclerotia in the *BcMETTL4* mutant might also be correlated with a decrease in the pathogenicity of *B. cinerea*.

The sensitivity of different strains to stress tolerance was also measured. Disruption of *BcMETTL4* or *BcDAMT* did not cause significant sensitivity to cell wall stress, osmotic stabilization, or oxidative stress (**Figures 4C,D**), indicating that *BcMETTL4* and *BcDAMT* were not involved in the regulation of cell stress tolerance.

The Point Mutant BcMettl4-APPA Exhibited Phenotypes Similar to Those of ΔBcMettl4

Methyltransferases contain a conserved catalytic motif, "DPPW." A 3-dimensional structure of BcMettl4 was constructed, and the signature motif "DPPW" was found to be located in the catalytic domain (**Figure 5A**). Multiple sequence alignments of the catalytic motifs in 6mA methyltransferases were performed. The results showed that the conserved catalytic motif "DPPW" in BcMettl4 exhibited high similarity with Mettl4 orthologs (**Figure 5B**). To study the catalytic function of BcMettl4, the catalytic domain "DPPW" was mutated to "APPA" in BcMettl4. After the mutation to "APPA," the methylation level of DNA in *B. cinerea* decreased (**Figure 5C**) and both virulence and sclerotium formation decreased (**Figures 5D,E**), which was consistent with the phenotype of the ΔBcMettl4 mutant. These data suggested that the catalytic motif "DPPW" plays a key role in the enzymatic function of BcMettl4 and that BcMettl4 is involved in the regulation of DNA methylation levels and virulence.

Genomic Profiling of 6mA in *Botrytis cinerea*

To detect naturally occurring methylated genes globally regulated by *BcMETTL4* in *B. cinerea*, we performed a MeDIP-Seq analysis of the 6mA methylomes of the disruption mutant ΔBcMettl4 and its wild-type strain B05.10. The expression of *BcMETTL4* increased significantly after 24 h infection (**Figure 3A**). We therefore collected the samples of conidial germination at 24 h for MeDIP-seq. Three biological replicates for each strain of ΔBcMettl4 and B05.10 were investigated in MeDIP-Seq experiments. A total of 30,320 6mA-enriched regions (peaks) were captured from the three B05.10 biological replicates, while a total of 28,385 methylation peaks were obtained from the three ΔBcMettl4 biological replicates (**Supplementary Table 2**). These observations further confirmed that disruption of *BcMETTL4* reduced the methylation level of *B. cinerea*. After assembling the attained sequences, it was found that most of the 6mA peaks (57%) were distributed in the upstream regions of genes, followed by 24% in the exon, and 15% in the downstream regions in wild-type B05.10 and the mutant ΔBcMettl4 (**Figures 6A,B**). The 6mA peaks were further investigated and wild-type B05.10 exhibited 1,297 unique 6mA peaks while 689 unique 6mA peaks were identified in the mutant ΔBcMettl4 (**Figure 6C**). There were 8,357 6mA peaks that were found in both the wild-type B05.10 and the mutant ΔBcMettl4 (**Figure 6C**). Among the unique 6mA peaks of wild-type B05.10, 2,396 genes were detected (**Figure 6D** and **Supplementary Table 3**). However, only 1,330 genes were detected in the unique 6mA peaks of the mutant ΔBcMettl4 (**Figure 6D** and **Supplementary Table 4**).

BcMETTL4 Inactivation Downregulated the Expression of 13 Methylated Genes in Which Methylation Occurred in the Promoter Region

Since the majority of the 6mA peaks were identified in the regions upstream of the affected genes (**Figures 6A,B**), involvement of the promoter regions and regulation of gene expression was indicated. To identify all genes that might exhibit differential expression due to the disruption of *BcMETTL4* in *B. cinerea*, we performed an RNA-Seq analysis of the full transcriptomic profiles of the wild-type strain B05.10 and the disruption mutantΔBcMettl4. The differentially expressed genes were further analyzed using DESeq software (Wang et al., 2010). A total of 792 genes, including 601 upregulated genes (**Supplementary Table 5**) and 191 downregulated genes (**Supplementary Table 6**), were found to be differentially

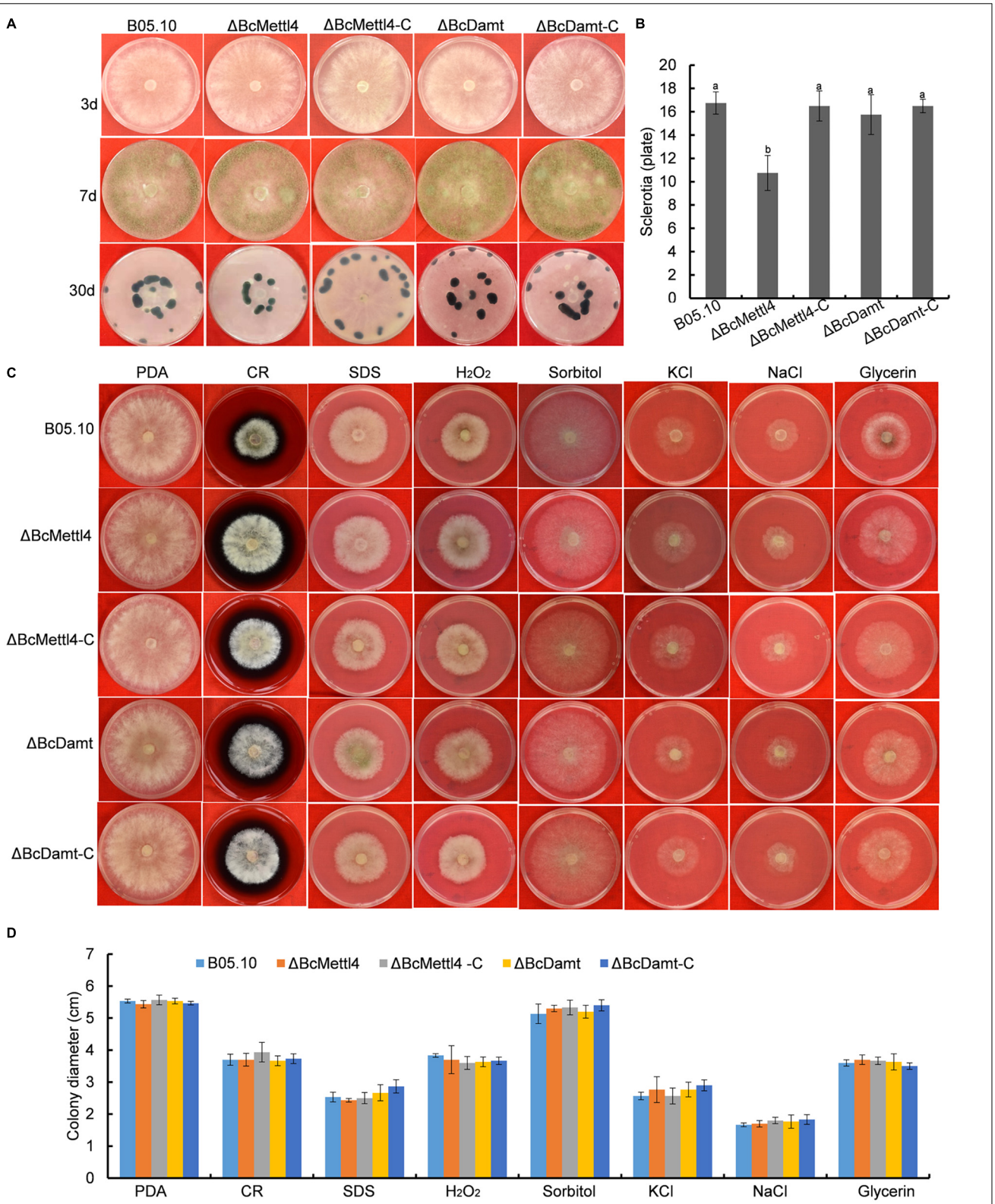

FIGURE 4 | Mycelial growth, conidial and sclerotial formation and stress tolerance of the indicated strains. **(A)** Mycelial growth, conidial and sclerotial development of various strains grown on PDA plates. **(B)** Number of sclerotia produced by various strains grown on PDA plates for 30 days in darkness. Bars denote standard errors from three plates. Tukey's test was employed to calculate significance. The same letters indicated on the bars mean no significant difference in values at $p < 0.05$. **(C)** The sensitivity of various strains on stress tolerance. **(D)** Colony diameter of the indicated strains grown on various stress conditions. Bars represent standard errors from three plates.

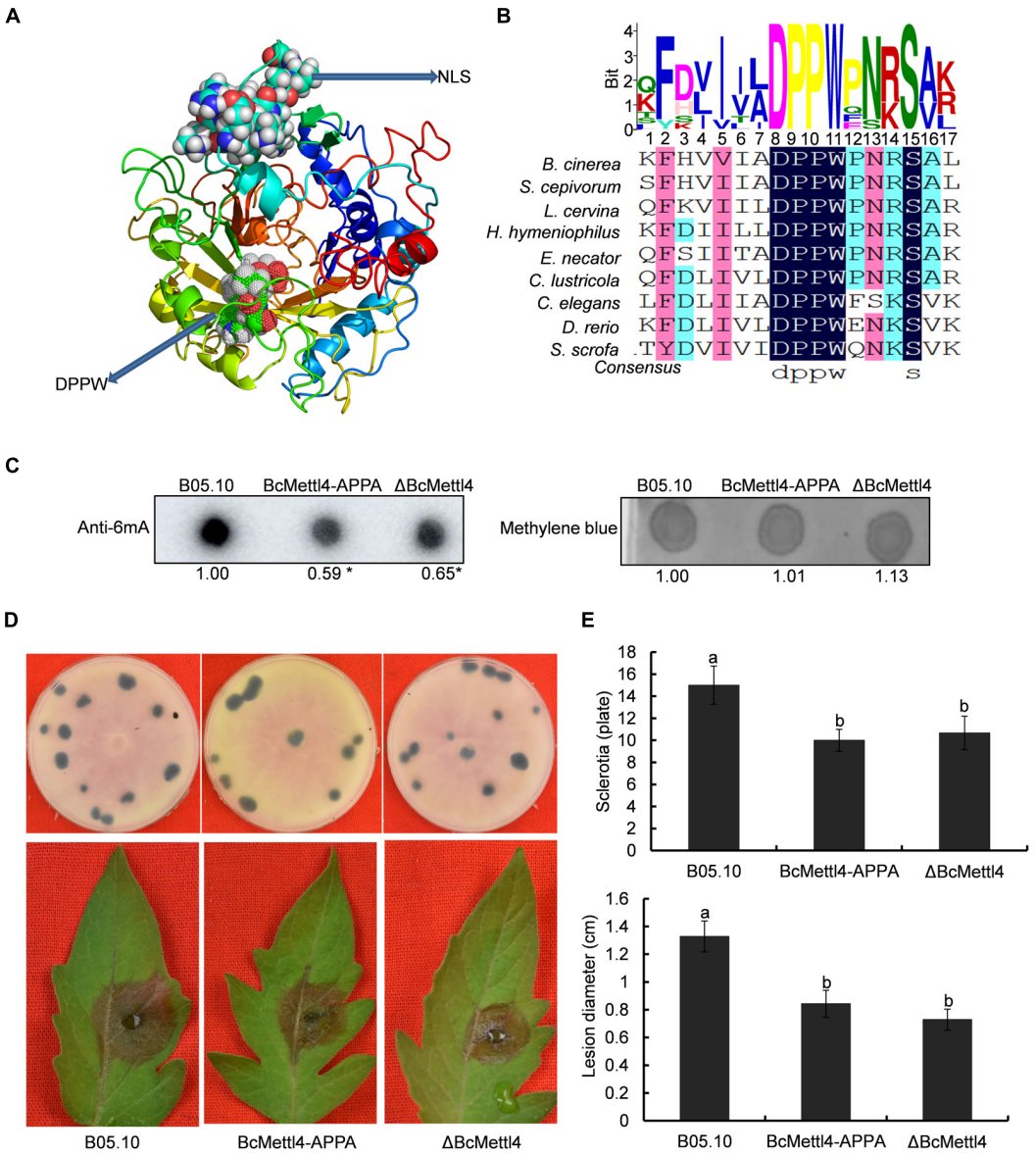

FIGURE 5 | Impact of BcMettl4 loss-of-function on DNA modification, pathogenicity, and sclerotia formation of *B. cinerea*. **(A)** Three-dimensional structure of BcMettl4 modeled were predicted by I-TASSER. **(B)** Sequence alignment of motifs in methyltransferase form *B. cinerea*, *Sclerotium cepivorum*, *Lachnellula cervine*, *Hyphodiscus hymeniophilus*, *Erysiphe necator*, *Coniella lustricola*, *Caenorhabditis elegans*, *Danio rerio,* and *Sus scrofa*. **(C)** Dot blot assay of 6mA in the indicated strains. A total of 200 ng DNA was investigated on each dot. The relative ratio of 6mA in wild-type strain B05.10 and point mutant BcMettl4-APPA was calculated by ImageJ. The asterisk represents significant difference at $p < 0.05$. **(D)** The disease lesions caused by various strains following inoculation on tomato leaves for 3 days and the sclerotia formation of various strains after grown in darkness for 30 days. **(E)** Lesion diameter of the strains inoculated on tomato leaves and the number of sclerotia in various stains. Error-bars were from three experiments. For lesion diameter, nine leaves were investigated in one biological experiment. Three plates were used to count sclerotia. Tukey's test was used to calculate significance. The same letters marked on the columns were not significantly different at $p < 0.05$.

expressed in the *BcMETTL4* mutant compared with the wild-type strain B05.10, which accounted for 4.82% (792/16,448) of the annotated genes in *B. cinerea*.

To test the hypothesis that the unique genes modified at promoter sites might be directly regulated by BcMettl4, the transcription levels of the unique genes were further analyzed in the mutant ΔBcMettl4. After disruption of *BcMETTL4*, among the unique methylated genes modified at promoter sites in the wild-type strain B05.10, 32 genes were upregulated (**Supplementary Table 7**) and 13 genes were downregulated (**Figures 7A,B**). Since the virulence of the *BcMETTL4* mutant was significantly reduced, we hypothesized that the 13 methylated genes modified in the promoter region with downregulated expression might be associated with

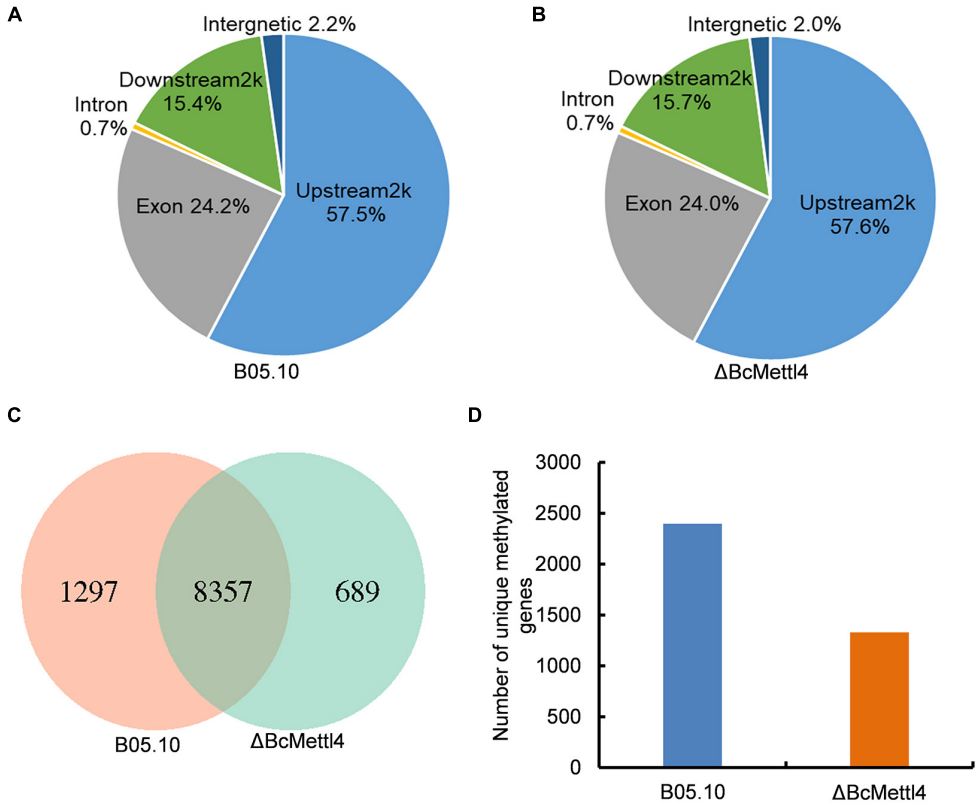

FIGURE 6 | The 6mA methylated genes in *B. cinerea*. **(A)** Peak distribution in genomic elements of the wild-type strain B05.10. **(B)** Peak distribution in genomic elements of the disruption mutant ΔBcMettl4. **(C)** Venn diagram comparing unique 6mA peaks between the wild-type B05.10 and the mutant ΔBcMettl4. **(D)** The number of unique methylated genes in wild-type strain B05.10 and the disruption mutant ΔBcMettl4.

pathogenicity. The genes shown in **Figure 7A** were therefore subsequently further analyzed.

The reduced transcript levels of the 13 genes shown in **Figure 7B** were further validated by fluorescent real-time qRT-PCR (**Figure 7C**). As shown in **Figure 7A**, these methylated genes were divided into five categories, including oxidoreduction, secretory pathways, autophagy and carbohydrate metabolism, according to their biological functions. It has been well documented that proteins related to oxidative stress sensitivity (Yang et al., 2015), autophagy (Ren et al., 2018), and secretion (Zhang et al., 2016) are important factors affecting the virulence of *B. cinerea*. These observations indicated that the downregulated methylated genes related to oxidoreduction, secretory pathways and autophagy may cause a decrease in the pathogenicity of *B. cinerea*.

The Roles of BcMfs2 and BcFdh in the Virulence of *Botrytis cinerea*

Deletion of *BcMETTL4* both reduced the methylation and expression levels of 13 genes (**Figure 7**). We speculated that these genes might be involved in virulence of *B. cinerea*. Two of them were randomly selected for targeted disruption. *BcMFS2* encoding a major facilitator superfamily (MFS) transporter and *BcFDH* encoding a FAD/FMN-containing dehydrogenase were independently deleted in the wild-type strain B05.10. Two mutants, ΔBcMfs2 and ΔBcFdh, were subsequently obtained. The genes *BcMFS2* and *BcFDH* were also cloned and complemented both mutants, resulting in transformants, ΔBcMfs2-C and ΔBcFdh-C, respectively. Deletion of *BcMFS2* reduced sclerotium formation (**Figures 8A,B**). Further infection assays of tomato leaves were performed, and the results showed that deletion of *BcMFS2* did not reduce the virulence of *B. cinerea* (**Figures 8A,B**). These findings indicated that *BcMFS2* was involved in sclerotium formation but not in the virulence of *B. cinerea*. Another interesting finding was that deletion of *BcFDH* severely hindered conidium formation in *B. cinerea* (**Figure 8B**). Infection of tomato leaves by ΔBcFdh was further performed, and the results showed that deletion of the *BcFDH* gene reduced the pathogenicity of *B. cinerea* by 20% (**Figure 8B**). These observations demonstrated that *BcFDH* was involved in both conidium formation and the pathogenicity of *B. cinerea*.

DISCUSSION

As a basic epigenetic marker, DNA methylation has been widely documented in both eukaryotes and prokaryotes (Bird, 2007; Vasu and Nagaraja, 2013). However, its characteristics in *B. cinerea* are still elusive. In this study, we found that 6mA

A

Category	Name	Gene tag	Description
Oxidoreduction	BcFdh	BC1G_15423	FAD/FMN-containing dehydrogenase
	BcThi	BC1G_12830	Thioredoxin
Secretory pathway	BcMfs1	BC1G_14772	Major Facilitator Superfamily
	BcMfs2	BC1G_11072	Major Facilitator Superfamily
Autophagy	BcApg6	BC1G_03102	Autophagy protein Apg6
Carbohydrate metabolism	BcGlu	BC1G_02333	Glucoamylase
	BcAlg	BC1G_00709	Alginate O-acetyl transferase
	BcTpk	BC1G_06503	Tagatose 6 phosphate kinase
Other	BcCup	BC1G_12147	Cupin superfamily
	BcDp	BC1G_02278	DNA primase
		BC1G_12192	unknown function
		BC1G_05616	unknown function
		BC1G_03851	unknown function

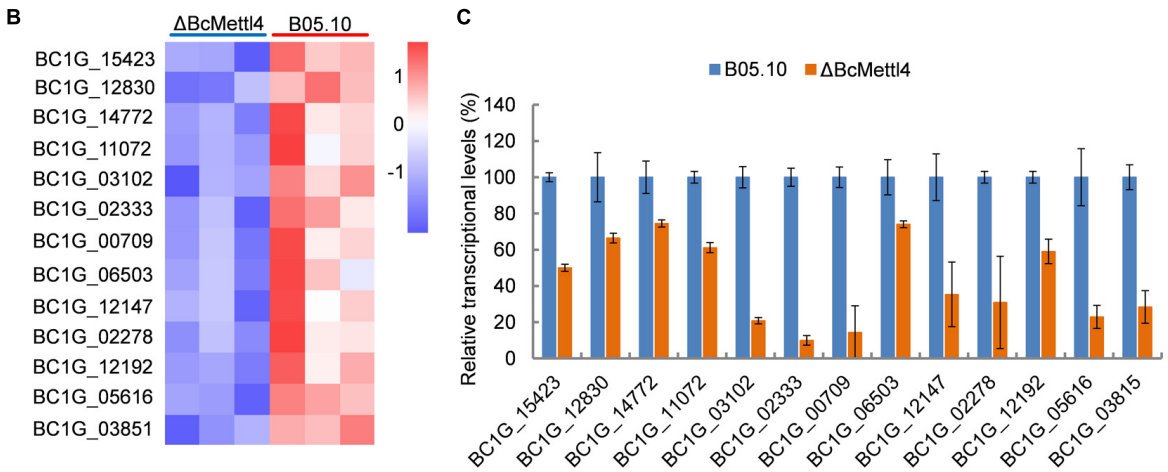

FIGURE 7 | The downregulated methylated genes in which modification occurs in the promoter region. **(A)** Categories of the screened genes. **(B)** RNA-Seq analysis of 13 methylated genes. The colored squares show the level of gene expression referred to log2 FPKM value in each of the three replicas. **(C)** Validation of RNA-Seq data of selected genes by fluorescent real-time qRT-PCR. The reference gene used in this study was Beta-tubulin. Data are given as the mean ± SD, $n = 3$.

is a widespread DNA modification in the *B. cinerea* genome. Previous studies have shown that DNA methylation levels are dynamic and controlled by two enzymes, methyltransferase and demethylase (Greer et al., 2015; Zhang et al., 2015). MT-A70 is an important 6mA methyltransferase (Bujnicki et al., 2002). Gray mold contains two homologous methyltransferases, BcMettl4 (**Figure 1A**) and BcDamt (**Figure 1B**). As shown in **Figure 2D**, disruption of *BcMETTL4* but not *BcDAMT* resulted in a decrease in the DNA methylation level of *B. cinerea*, suggesting that BcMettl4 is related to 6mA modification. Previous reports have shown that the signature motif "DNSH/PP/YFW" of 6mA methyltransferase is responsible for substrate binding and catalytic activity (Iyer et al., 2016; Wang et al., 2019). After the mutation of "DPPW" to "APPA," the methylation level in *B. cinerea* decreased (**Figure 5C**), demonstrating a catalytic role of "DPPW" in BcMettl4. Consistent with these results, the *AMT1* APPA mutant of *Tetrahymena thermophila* had a reduced 6mA level (Wang et al., 2019). Unlike the genome of *B. cinerea*, the genome of *Phytophthora sojae* contains three 6mA methyltransferase genes (*DAMT1*, *DAMT2*, and *DAMT3*), and single knockouts of any of these genes in the *P. sojae* strain P6497 resulted in a significant decrease in DNA methylation (Chen et al., 2018).

Using MeDIP-Seq analysis, we identified a large number of 6mA peaks that were distributed in the genome of *B. cinerea*. As shown in **Figures 6A,B**, 6mA was significantly enriched in upstream and downstream gene regions in both the wild-type strain B05.10 and the disruption mutant ΔBcMettl4. Consistent with our observations, almost all of the 6mA were found in the promoter regions, either at or slightly downstream of the transcription start sites in early-diverging fungi, *Hesseltinella vesiculosa*, *Absidia repens*, *Lobosporangium transversale*, and *Syncephalastrum racemosum* (Mondo et al., 2017). Several other studies also revealed that the transcription initiation sites of *Chlamydomonas* (Fu et al., 2015) and *Phytophthora* (Chen et al., 2018) were readily modified by 6mA. In *Arabidopsis*, the 6mA modification level in gene bodies was higher than that of intergenic regions (Liang et al., 2018).

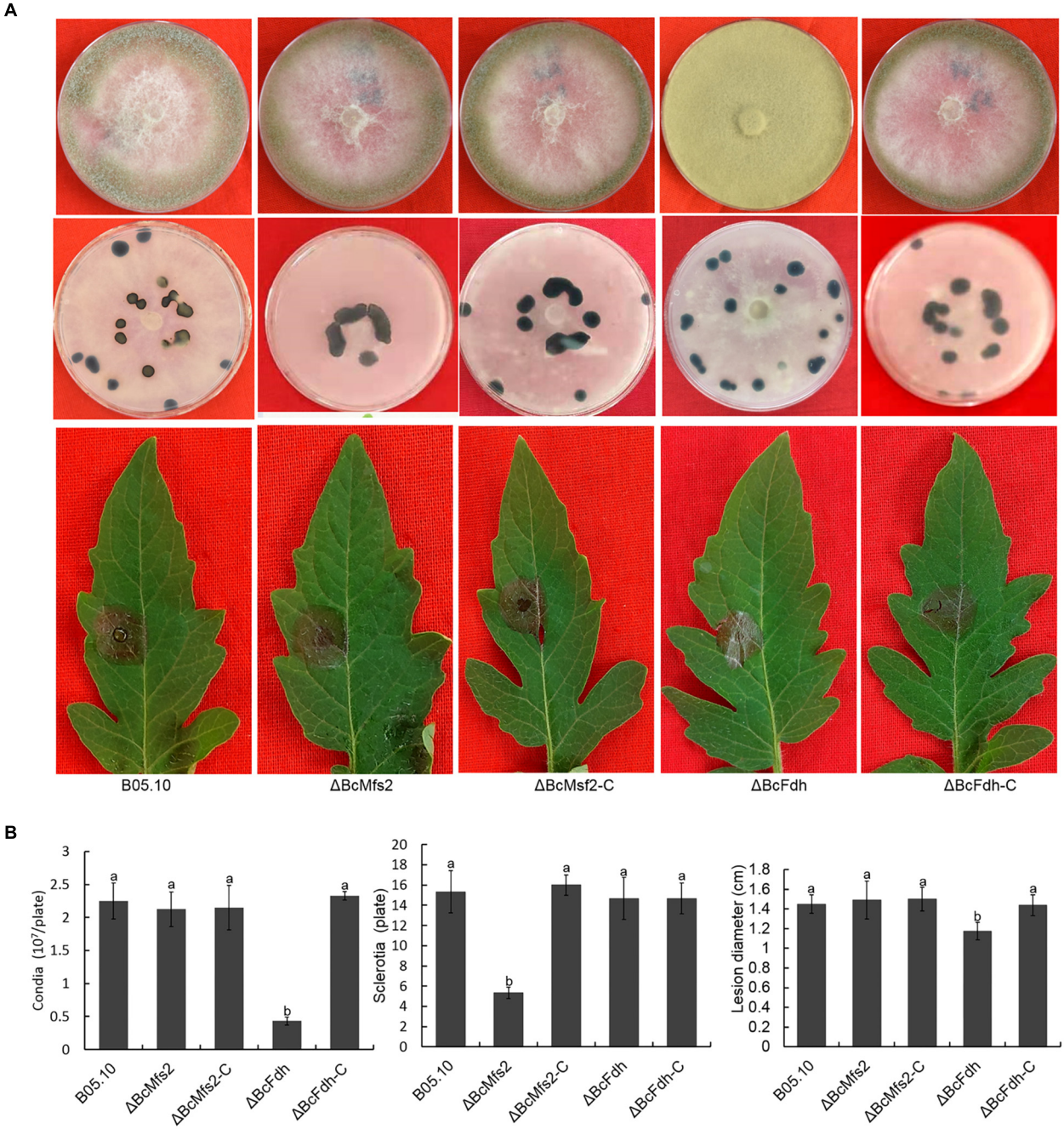

FIGURE 8 | Impact of *BcMFS2* and *BcFDH* deletion on pathogenicity of *B. cinerea*. **(A)** Effect of deletions *BcMFS2* or *BcFDH* on conidia biosynthesis, sclerotia formation and virulence. **(B)** Quantification of conidia, sclerotia and pathogenicity of different strains. Bars represent standard errors from three experiments. In each biological experiment, lesion diameters of nine leaves were investigated. Three plates were used to count sclerotia and conidia. Statistical tests were carried out using Tukey's test. The different letters marked on the columns indicate statistical significance $p < 0.05$.

Similar to the result for *Arabidopsis*, DNA 6mA modification was preferentially distributed in the gene bodies rather than the intergenomic regions in *Tetrahymena* (Wang et al., 2017). However, 6mA was evenly distributed on chromosomes and correlated with 5mC distribution in rice (Zhou et al., 2018). Inconsistent with the above findings, DNA 6mA modification was significantly enriched in exon regions in the human genome (Xiao et al., 2018). Taken together, the results suggested that the genomic localization pattern of DNA 6mA modification in different species varies greatly, indicating that these modifications are hitherto unknown epigenetic markers.

Botrytis cinerea is an important necrotizing pathogen. It has been well documented that cellular accumulation of reactive oxygen species (ROS) is one of the immune responses of plants after infection by pathogens (Kaku et al., 2006; Cheval et al., 2013; Wada et al., 2019). Previous studies have documented that the virulence of pathogens is often related to resistance to oxidative stress (Yan et al., 2011; Yang et al., 2015, 2018). In a previous study, we found that knocking out the catalase *BcCAT* (*BC1G_12146*) reduced the toxicity of gray mold (Wang et al., 2020). In this study, *BcCAT* was downregulated in the disruption mutant ΔBcMettl4 (**Supplementary Table 6**). We also found that three oxidative stress-related genes, *BcCATA* (*BC1G_01095*), *BcCAT3* (*BC1G_02407*), and *BcCAT4* (*BC1G_09386*), were upregulated in ΔBcMettl4 (**Supplementary Table 5**), which might compensate for the effect of downregulation of BcCAT. After *BcMETTL4* was inactivated, two methylated genes, *BcFDH* and *BcTHI*, which are related to oxidoreduction, were also downregulated (**Figure 7A**). Further experiments confirmed that knockout of *BcFDH* reduced the pathogenicity of *B. cinerea* (**Figure 8B**). The disruption of *BcFDH* severely hindered conidia formation (**Figure 8B**). The genome of *B. cinerea* contains 16 genes involved in conidiation (Amselem et al., 2011). We found that only one of them, *BcPPOA80* (*BC1G_14780*), were downregulated when *BcMETTL4* was deleted (**Supplementary Table 6**), indicating that the downregulation of only *BcPPOA80* might have little effect on conidia formation. However, it is still completely unknown why the conidia formation was severely hindered when the *BcFDH* gene was deleted.

Two methylated genes, *BcMFS1* and *BcMFS2,* which are associated with MFS transporters, were downregulated in the mutant ΔBcMettl4 (**Figure 7A**). After *BcMFS2* was deleted, the mutant's ability to form sclerotia was reduced (**Figure 8A**). BcSec14 and BcSec31 are involved in vesicle transport, and deletion of BcSec14 and BcSec31 resulted in a reduction in pathogenicity and protein secretion in gray mold (Zhang et al., 2016). It has been well documented that MFS is the largest group of membrane transporters (Law et al., 2008). MFS transporters are also involved in cell secretion and can transport some secondary metabolites and compounds (Vela-Corcía et al., 2019). The polysaccharide components of the cell wall are mainly hydrolyzed into monosaccharides and oligosaccharides by degrading enzymes, thereby reducing the protection of the cell wall against pathogens and increasing the ability of pathogens to infect plants (Cantarel et al., 2009; Kubicek et al., 2014). A cell polysaccharide-degrading enzyme-encoding gene, *BcGLU,* was found among the downregulated methylated genes (**Figure 7A**); this gene may be involved in the pathogenicity of *B. cinerea*. Taken together, these findings suggest that BcMettl4 may regulate pathogenicity via its effect on multiple pathways.

CONCLUSION

DNA adenine N^6-methylation sites are widely distributed in the genome of *B. cinerea*. BcMettl4 is nuclear-localized and contains the conserved motif "DPPW," which is likely related to its interaction with DNA for methylation modification. MeDIP-Seq showed that the regions 2,000 bp upstream and downstream of the genes were preferentially modified by methylation in *B. cinerea*. *BcMETTL4* disruption and mutation of "DPPW" to "APPA" both resulted in a significant reduction in the genomic methylation and pathogenicity of *B. cinerea*. These observations indicate that 6mA provides potential epigenetic markers in *B. cinerea* and that BcMettl4 regulates the level of DNA methylation in this important plant pathogen. Our results extend the current understanding of the global regulatory role of 6mA in filamentous plant pathogens.

DATA AVAILABILITY STATEMENT

The data has been made available at NCBI with accession numbers PRJNA817858 and PRJNA817835.

AUTHOR CONTRIBUTIONS

ZM, GW, and WL contributed to the conception and design of the study. ZM, GW, and XW performed the experiments. ZM, GW, HS, and XW organized the database. ZM, HS, and XW performed the statistical analysis. ZM, GW, and WL wrote the first draft of the manuscript. GW, WL, and DG reviewed and edited the manuscripts. All authors provided comments on the manuscript and approved the submitted version.

FUNDING

This work was supported by the National Natural Science Foundation of China (31972213), the Shandong Provincial Natural Science Foundation (ZR2020KC003 and ZR2019MC052), the Key Research and Development Program of Shandong Province (2019YQ017), Taishan Scholar Construction Foundation of Shandong Province (tshw20130963), and Shandong Province "Double-Hundred Talent Plan" (WST2018008).

SUPPLEMENTARY MATERIAL

The Supplementary Material for this article can be found online at: https://www.frontiersin.org/articles/10.3389/fmicb.2022.925868/full#supplementary-material

Supplementary Figure 1 | Disruption of *BcMETTL4* and validation of three different mutants by PCR. **(A)** Marker exchange technique used for disruption of *BcMETTL4*. **(B)** PCR products with Mettl4-in-F/R (the first four lanes except Marker) or Mettl4-out-F/R (the last four lanes) from the genomic DNAs of wild-type (lanes 1 and 5) and ΔBcMettl4 (three different mutants).

Supplementary Figure 2 | Work procedure for *BcDAMT* deletion. **(A)** Marker exchange technique used for disruption of *BcDAMT*. **(B)** PCR products with DAMT-in-F/R (the first four lanes except Marker) or DAMT-out-F/R (the last four lanes) from the genomic DNAs of wild-type (lanes 1 and 5) and ΔBcDamt (three different mutants).

REFERENCES

Amselem, J., Cuomo, C. A., van Kan, J. A., Viaud, M., Benito, E. P., Couloux, A., et al. (2011). Genomic analysis of the necrotrophic fungal pathogens *Sclerotinia sclerotiorum* and *Botrytis cinerea*. *PLoS Genet.* 7:e1002230. doi: 10.1371/journal.pgen.1002230

Anders, S., Pyl, P. T., and Huber, W. (2015). HTSeq–a Python framework to work with high-throughput sequencing data. *Bioinformatics* 31, 166–169. doi: 10.1093/bioinformatics/btu638

Beh, L. Y., Debelouchina, G. T., Clay, D. M., Thompson, R. E., Lindblad, K. A., Hutton, E. R., et al. (2019). Identification of a DNA N6-adenine methyltransferase complex and its impact on chromatin organization. *Cell* 177, 1781–1796.e25. doi: 10.1016/j.cell.2019.04.028

Bird, A. (2007). Perceptions of epigenetics. *Nature* 447, 396–398. doi: 10.1038/nature05913

Blow, M. J., Clark, T. A., Daum, C. G., Deutschbauer, A. M., Fomenkov, A., Fries, R., et al. (2016). The epigenomic landscape of prokaryotes. *PLoS Genet.* 12:e1005854. doi: 10.1371/journal.pgen.1005854

Bujnicki, J. M., Feder, M., Radlinska, M., and Blumenthal, R. M. (2002). Structure prediction and phylogenetic analysis of a functionally diverse family of proteins homologous to the MT-A70 subunit of the human mRNA:m(6)A methyltransferase. *J. Mol. Evol.* 55, 431–444. doi: 10.1007/s00239-002-2339-8

Cantarel, B. L., Coutinho, P. M., Rancurel, C., Bernard, T., Lombard, V., and Henrissat, B. (2009). The carbohydrate-active enzymes database (CAZy): an expert resource for glycogenomics. *Nucleic Acids Res.* 37, D233–D238. doi: 10.1093/nar/gkn663

Chen, H., Shu, H., Wang, L., Zhang, F., Li, X., Ochola, S. O., et al. (2018). Phytophthora methylomes are modulated by 6mA methyltransferases and associated with adaptive genome regions. *Genome Biol.* 19:181. doi: 10.1186/s13059-018-1564-4

Cheval, C., Aldon, D., Galaud, J. P., and Ranty, B. (2013). Calcium/calmodulin-mediated regulation of plant immunity. *Biochim. Biophys. Acta* 1833, 1766–1771. doi: 10.1016/j.bbamcr.2013.01.031

Dean, R., Van Kan, J. A., Pretorius, Z. A., Hammond-Kosack, K. E., Di Pietro, A., Spanu, P. D., et al. (2012). The Top 10 fungal pathogens in molecular plant pathology. *Mol. Plant Pathol.* 13, 414–430. doi: 10.1111/j.1364-3703.2011.00783.x

Fu, Y., Dominissini, D., Rechavi, G., and He, C. (2014). Gene expression regulation mediated through reversible m6A RNA methylation. *Nat. Rev. Genet.* 15, 293–306. doi: 10.1038/nrg3724

Fu, Y., Luo, G. Z., Chen, K., Deng, X., Yu, M., Han, D., et al. (2015). N6-methyldeoxyadenosine marks active transcription start sites in *Chlamydomonas*. *Cell* 161, 879–892. doi: 10.1016/j.cell.2015.04.010

Greer, E. L., Blanco, M. A., Gu, L., Sendinc, E., Liu, J., Aristizabal-Corrales, D., et al. (2015). DNA methylation on N6-adenine in *C. elegans*. *Cell* 161, 868–878. doi: 10.1016/j.cell.2015.04.005

Gronover, C. S., Kasulke, D., Tudzynski, P., and Tudzynski, B. (2001). The role of G protein alpha subunits in the infection process of the gray mold fungus *Botrytis cinerea*. *Mol. Plant Microbe Interact.* 14, 1293–1302. doi: 10.1094/mpmi.2001.14.11.1293

Heckman, K. L., and Pease, L. R. (2007). Gene splicing and mutagenesis by PCR-driven overlap extension. *Nat. Protoc.* 2, 924–932. doi: 10.1038/nprot.2007.132

Iyer, L. M., Abhiman, S., and Aravind, L. (2011). Natural history of eukaryotic DNA methylation systems. *Prog. Mol. Biol. Transl. Sci.* 101, 25–104. doi: 10.1016/b978-0-12-387685-0.00002-0

Iyer, L. M., Zhang, D., and Aravind, L. (2016). Adenine methylation in eukaryotes: apprehending the complex evolutionary history and functional potential of an epigenetic modification. *BioEssays* 38, 27–40. doi: 10.1002/bies.201500104

Kaku, H., Nishizawa, Y., Ishii-Minami, N., Akimoto-Tomiyama, C., Dohmae, N., Takio, K., et al. (2006). Plant cells recognize chitin fragments for defense signaling through a plasma membrane receptor. *Proc. Natl. Acad. Sci. U. S. A.* 103, 11086–11091. doi: 10.1073/pnas.0508882103

Kubicek, C. P., Starr, T. L., and Glass, N. L. (2014). Plant cell wall-degrading enzymes and their secretion in plant-pathogenic fungi. *Annu. Rev. Phytopathol.* 52, 427–451. doi: 10.1146/annurev-phyto-102313-045831

Law, C. J., Maloney, P. C., and Wang, D. N. (2008). Ins and outs of major facilitator superfamily antiporters. *Annu. Rev. Microbiol.* 62, 289–305. doi: 10.1146/annurev.micro.61.080706.093329

Liang, Z., Shen, L., Cui, X., Bao, S., Geng, Y., Yu, G., et al. (2018). DNA N(6)-adenine methylation in *Arabidopsis thaliana*. *Dev. cell* 45, 406–416.e3. doi: 10.1016/j.devcel.2018.03.012

Liu, T. (2014). Use model-based analysis of ChIP-Seq (MACS) to analyze short reads generated by sequencing protein-DNA interactions in embryonic stem cells. *Methods Mol. Biol.* 1150, 81–95. doi: 10.1007/978-1-4939-0512-6_4

Livak, K. J., and Schmittgen, T. D. (2001). Analysis of relative gene expression data using real-time quantitative PCR and the 2(-Delta Delta C(T)) Method. *Methods* 25, 402–408. doi: 10.1006/meth.2001.1262

Mondo, S. J., Dannebaum, R. O., Kuo, R. C., Louie, K. B., Bewick, A. J., LaButti, K., et al. (2017). Widespread adenine N6-methylation of active genes in fungi. *Nat. Genet.* 49, 964–968. doi: 10.1038/ng.3859

Mousavi-Derazmahalleh, M., Chang, S., Thomas, G., Derbyshire, M., Bayer, P. E., Edwards, D., et al. (2019). Prediction of pathogenicity genes involved in adaptation to a lupin host in the fungal pathogens *Botrytis cinerea* and *Sclerotinia sclerotiorum* via comparative genomics. *BMC Genom.* 20:385. doi: 10.1186/s12864-019-5774-2

Ren, W., Liu, N., Sang, C., Shi, D., Zhou, M., Chen, C., et al. (2018). The autophagy gene BcATG8 regulates the vegetative differentiation and pathogenicity of *Botrytis cinerea*. *Appl. Environ. Microbiol.* 84, e2455–e2417. doi: 10.1128/aem.02455-17

Schumacher, J. (2012). Tools for *Botrytis cinerea*: new expression vectors make the gray mold fungus more accessible to cell biology approaches. *Fungal Genet. Biol.* 49, 483–497. doi: 10.1016/j.fgb.2012.03.005

Trapnell, C., Pachter, L., and Salzberg, S. L. (2009). TopHat: discovering splice junctions with RNA-Seq. *Bioinformatics* 25, 1105–1111. doi: 10.1093/bioinformatics/btp120

Trapnell, C., Williams, B. A., Pertea, G., Mortazavi, A., Kwan, G., van Baren, M. J., et al. (2010). Transcript assembly and quantification by RNA-Seq reveals unannotated transcripts and isoform switching during cell differentiation. *Nat. Biotechnol.* 28, 511–515. doi: 10.1038/nbt.1621

Vasu, K., and Nagaraja, V. (2013). Diverse functions of restriction-modification systems in addition to cellular defense. *Microbiol. Mol. Biol. Rew.* 77, 53–72. doi: 10.1128/mmbr.00044-12

Vela-Corcía, D., Aditya Srivastava, D., Dafa-Berger, A., Rotem, N., Barda, O., and Levy, M. (2019). MFS transporter from *Botrytis cinerea* provides tolerance to glucosinolate-breakdown products and is required for pathogenicity. *Nat. Commun.* 10:2886. doi: 10.1038/s41467-019-10860-3

Wada, S., Cui, S., and Yoshida, S. (2019). Reactive Oxygen Species (ROS) Generation Is Indispensable for Haustorium Formation of the Root Parasitic Plant Striga hermonthica. *Front. Plant Sci.* 10:328. doi: 10.3389/fpls.2019.00328

Wang, G., Song, L., Bai, T., and Liang, W. (2020). BcSas2-Mediated Histone H4K16 Acetylation Is Critical for Virulence and Oxidative Stress Response of *Botrytis cinerea*. *Mol. Plant Microbe Interact.* 33, 1242–1251. doi: 10.1094/mpmi-06-20-0149-r

Wang, L., Feng, Z., Wang, X., Wang, X., and Zhang, X. (2010). DEGseq: an R package for identifying differentially expressed genes from RNA-seq data. *Bioinformatics* 26, 136–138. doi: 10.1093/bioinformatics/btp612

Wang, P., Doxtader, K. A., and Nam, Y. (2016). Structural Basis for Cooperative Function of Mettl3 and Mettl14 Methyltransferases. *Mol. Cell* 63, 306–317. doi: 10.1016/j.molcel.2016.05.041

Wang, X., Li, Z., Zhang, Q., Li, B., Lu, C., Li, W., et al. (2018). DNA methylation on N6-adenine in lepidopteran *Bombyx mori*. *Biochim. Biophys. Acta Gene Regul. Mech.* [Epub ahead of print]. doi: 10.1016/j.bbagrm.2018.07.013

Wang, Y., Chen, X., Sheng, Y., Liu, Y., and Gao, S. (2017). N6-adenine DNA methylation is associated with the linker DNA of H2A.Z-containing well-positioned nucleosomes in Pol II-transcribed genes in *Tetrahymena*. *Nucleic Acids Res.* 45, 11594–11606. doi: 10.1093/nar/gkx883

Wang, Y., Sheng, Y., Liu, Y., Zhang, W., Cheng, T., Duan, L., et al. (2019). A distinct class of eukaryotic MT-A70 methyltransferases maintain symmetric DNA N6-adenine methylation at the ApT dinucleotides as an epigenetic mark associated with transcription. *Nucleic Acids Res.* 47, 11771–11789. doi: 10.1093/nar/gkz1053

Woodcock, C. B., Horton, J. R., Zhang, X., Blumenthal, R. M., and Cheng, X. (2020). Beta class amino methyltransferases from bacteria to humans: evolution and structural consequences. *Nucleic Acids Res.* 48, 10034–10044. doi: 10.1093/nar/gkaa446

Xiao, C. L., Zhu, S., He, M., Chen, D., Zhang, Q., Chen, Y., et al. (2018). N(6)-methyladenine DNA modification in the human genome. *Mol. Cell* 71, 306–318.e7. doi: 10.1016/j.molcel.2018.06.015

Yan, L., Yang, Q., Jiang, J., Michailides, T. J., and Ma, Z. (2011). Involvement of a putative response regulator Brrg-1 in the regulation of sporulation, sensitivity to fungicides, and osmotic stress in *Botrytis cinerea*. *Appl. Microbiol. Biotechnol.* 90, 215–226. doi: 10.1007/s00253-010-3027-z

Yang, Q., Song, L., Miao, Z., Su, M., Liang, W., and He, Y. (2019). Acetylation of BcHpt lysine 161 regulates *Botrytis cinerea* sensitivity to fungicides, multistress adaptation and virulence. *Front. Microbiol.* 10:2965. doi: 10.3389/fmicb.2019.02965

Yang, Q., Yin, D., Yin, Y., Cao, Y., and Ma, Z. (2015). The response regulator BcSkn7 is required for vegetative differentiation and adaptation to oxidative and osmotic stresses in *Botrytis cinerea*. *Mol. Plant Pathol.* 16, 276–287. doi: 10.1111/mpp.12181

Yang, Q., Zhang, J., Hu, J., Wang, X., Lv, B., and Liang, W. (2018). Involvement of BcYak1 in the regulation of vegetative differentiation and adaptation to oxidative stress of *Botrytis cinerea*. *Front. Microbiol.* 9:281. doi: 10.3389/fmicb.2018.00281

Zemach, A., McDaniel, I. E., Silva, P., and Zilberman, D. (2010). Genome-wide evolutionary analysis of eukaryotic DNA methylation. *Science* 328, 916–919. doi: 10.1126/science.1186366

Zhang, G., Huang, H., Liu, D., Cheng, Y., Liu, X., Zhang, W., et al. (2015). N6-methyladenine DNA modification in Drosophila. *Cell* 161, 893–906. doi: 10.1016/j.cell.2015.04.018

Zhang, Z., Li, H., Qin, G., He, C., Li, B., and Tian, S. (2016). The MADS-Box transcription factor Bcmads1 is required for growth, sclerotia production and pathogenicity of *Botrytis cinerea*. *Sci. Rep.* 6:33901. doi: 10.1038/srep33901

Zhou, C., Wang, C., Liu, H., Zhou, Q., Liu, Q., Guo, Y., et al. (2018). Identification and analysis of adenine N(6)-methylation sites in the rice genome. *Nat. Plants* 4, 554–563. doi: 10.1038/s41477-018-0214-x

Conflict of Interest: The authors declare that the research was conducted in the absence of any commercial or financial relationships that could be construed as a potential conflict of interest.

Publisher's Note: All claims expressed in this article are solely those of the authors and do not necessarily represent those of their affiliated organizations, or those of the publisher, the editors and the reviewers. Any product that may be evaluated in this article, or claim that may be made by its manufacturer, is not guaranteed or endorsed by the publisher.

frontiers | Frontiers in Microbiology

TYPE Original Research
PUBLISHED 22 July 2022
DOI 10.3389/fmicb.2022.950742

OPEN ACCESS

EDITED BY
Maofeng Jing,
Nanjing Agricultural University,
China

REVIEWED BY
Wenxing Liang,
Qingdao Agricultural University,
China
Xinchi Shi,
Nantong University,
China

*CORRESPONDENCE
Hongtao Tu
tuhongtao@caas.cn

SPECIALTY SECTION
This article was submitted to Microbe and Virus Interactions With Plants, a section of the journal Frontiers in Microbiology

RECEIVED 23 May 2022
ACCEPTED 27 June 2022
PUBLISHED 22 July 2022

CITATION
Yuan H, Yuan M, Shi B, Wang Z, Huang T, Qin G, Hou H, Wang L and Tu H (2022) Biocontrol activity and action mechanism of *Paenibacillus polymyxa* strain Nl4 against pear Valsa canker caused by *Valsa pyri*. *Front. Microbiol.* 13:950742. doi: 10.3389/fmicb.2022.950742

Biocontrol activity and action mechanism of *Paenibacillus polymyxa* strain Nl4 against pear Valsa canker caused by *Valsa pyri*

Hongbo Yuan, Mengjia Yuan, Bingke Shi, Zhuoni Wang, Tianxiang Huang, Genhong Qin, Hui Hou, Li Wang and Hongtao Tu*

Zhengzhou Fruit Research Institute, Chinese Academy of Agricultural Sciences, Zhengzhou, China

Pear Valsa canker caused by *Valsa pyri* is among the most destructive diseases of pear, which causes significant economic loss. The present study was developed to explore the biocontrol efficiency and underlying antagonistic mechanism of *Paenibacillus polymyxa* strain Nl4 against *V. pyri*. *P. polymyxa* strain Nl4, one of the 120 different endophytic bacterial strains from pear branches, exhibited strong inhibitory effects against the mycelial growth of *V. pyri* and caused hyphal malformation. Culture filtrate derived from strain Nl4 was able to effectively suppress mycelial growth of *V. pyri*, and was found to exhibit strong protease, cellulase and β-1, 3-glucanase activity. Through re-isolation assay, strain Nl4 was confirmed to be capable of colonizing and surviving in pear branch. Treatment with strain Nl4 effectively protected against pear Valsa canker symptoms on detached pear twigs inoculated with *V. pyri*. Moreover, strain Nl4 promoted enhanced plant growth probably through the solubilization of phosphorus. Comparative transcriptomic analyses revealed that strain Nl4 was able to suppress *V. pyri* growth in large part through the regulation of the expression of membrane- and energy metabolism-related genes in this pathogen. Further transcriptomic analyses of pear trees indicated that strain Nl4 inoculation was associated with changes in the expression of genes associated with secondary metabolite biosynthesis, signal transduction, and cutin, suberine, and wax biosynthesis. Together, these data highlighted *P. polymyxa* strain Nl4 as a promising biocontrol agent against pear Valsa canker and investigated the possible mechanisms of strain Nl4 on control of this devastating disease.

KEYWORDS

pear Valsa canker, *Valsa pyri*, *Paenibacillus polymyxa*, biological control, antagonistic mechanism

Introduction

Pear Valsa canker is one of the most damaging diseases affecting pears, resulting in severe yield losses and associated economic harm to growers. This disease, which is caused by the fungus *Valsa pyri*, can cause the bark of pear trees to turn reddish-brown, soft, and rotten following infection (Wang et al., 2014; Yin et al., 2015). While fungicides are the most

commonly used tools to control pear Valsa canker, food safety concerns have increasingly led to the need to limit the application of these pesticides. There is thus a clear need for the development of alternative or complementary approaches to controlling this disease, with endophyte-based biocontrol representing a particularly attractive disease control strategy.

Several different endophyte have been reported to be effective agents in the bicontrol of pear Valsa canker, such as *Bacillus subtilis*, *Bacillus velezensis*, *Bacillus amyloliquefaciens*, *Lysobacter enzymogenes*, and *Penicillium citrinum* (Cheng et al., 2017; Song et al., 2020; Liu R. et al., 2021; Yu et al., 2021; Yuan et al., 2021). *Bacillus velezensis* strains D4 and P2-1, for example, can readily inhibit *V. pyri* growth (Liu R. et al., 2021; Yuan et al., 2022), while *B. subtilis* strain 168-produced dipicolinic acid (DPA) can exert antifungal activity through the suppression of chitin synthesis (Song et al., 2020). Despite these promising results, the availability of biocontrol agents in preventing pear Valsa canker remains limited, hampering the effective control of this disease in agronomic practice.

Paenibacillus polymyxa is a *Bacillus* species that has previously been reported to be an effective biocontrol agent capable of inhibiting several plant diseases (Daud et al., 2019). For example, *P. polymyxa* strain HX-140 was found to readily inhibit the growth of *F. oxysporum* f. sp. *cucumerinum*, which causes cucumber Fusarium wilt (Zhai et al., 2021). Moreover, *P. polymyxa* strain JY1-5 effectively controlled tomato gray mold caused by *Botrytis cinere* (Zhang et al., 2021), while *P. polymyxa* strain APEC128 readily antagonized the development of apple anthracnose caused by *Colletotrichum gloeosporioides* and *Colletotrichum acutatum* (Kim et al., 2016). To date, however, there have not been any studies describing the use of *P. polymyxa* strains for the biocontrol of pear Valsa canker.

Prior studies have demonstrated that the induction of antifungal defense mechanisms is one of the primary mechanisms whereby *P. polymyxa* can exert its antifungal activity. For example, Liu H. et al. (2021) found that the treatment of peppers with *P. polymyxa* strain SC2 resulted in the induction of systemic responses tied to the upregulation of specific transcription factors (Liu H. et al., 2021). In cucumber roots, *P. polymyxa* strain NSY50 can similarly induce the expression of *PR1* and *PR5*, thereby conferring enhanced antifungal resistance (Du et al., 2017), while *P. polymyxa* strain AC-1 can regulate salicylic acid to coordinate the induction of plant resistance mechanisms (Hong et al., 2016). These previous studies thus highlight a range of mechanisms underlying the *P. polymyxa*-mediated biocontrol of plant diseases, providing a foundation for the use of these bacteria in agricultural contexts.

In the present study, 120 different bacterial isolates from pear branches were screened for the ability to inhibit *V. pyri* growth. Among these strains, *P. polymyxa* strain Nl4 was found to exhibit robust antifungal activity against *V. pyri* and several other pathogenic fungi. Strain Nl4 had protease, cellulose and β-1, 3-glucanase activity. In addition, *P. polymyxa* strain Nl4 was able to drive enhanced plant growth probably through phosphorus solubilization. Further analyses of the ability of this endophytic bacterial strain to colonize pear twigs were additionally conducted, while transcriptomic analyses were used to explore the potential mechanisms underlying the strain NI4-mediated biocontrol of pear Valsa canker caused *V. pyri*.

Materials and methods

Pathogenic fungal isolates

The *V. pyri*, *Valsa mali*, *C. gloeosporioides* and *Botryosphaeria dothidea* strains used for the present study (Yuan et al., 2022) were cultured in potato dextrose agar (PDA; potato extracts 200 g L^{-1}, glucose 20 g L^{-1}, and agar 15 g L^{-1}) and grow at 25°C.

Isolation and screening of potentially antagonistic bacteria

Healthy one-year-old branches were harvested in June 2021 from an "Enli" pear tree in Zhengzhou (Henan province, China) to isolate endophytic bacteria with the procedure as the same as reported previously (Yuan et al., 2022). The ability of all isolated endophytes to inhibit the growth of *V. pyri* was assessed using a dual culture screening approach as detailed previously by Yuan et al. (2022). Briefly, after overnight culture in LB broth (peptone 10 g L^{-1}, yeast extract 5 g L^{-1}, and sodium chloride 10 g L^{-1}), 3 μl of bacteria were inoculated on PDA medium on each side of a Petri dish (2 cm from the center), with a mycelial plug (diameter: 5 mm) being placed in the center of this plate. Plates to which no bacteria were added served as controls. Plates were incubated at 25°C, and pathogen colony diameter was measured at 6 days post-inoculation (dpi). This screening assay was repeated in triplicate, with three replicates per assay. Following preliminary screening, the antifungal activity of identified antagonistic strains against other fungal pathogens (*V. mali*, *C. gloeosporioides*, and *B. dothidea*) was additionally assessed.

Hyphal morphological characterization was performed with an ultra-depth three-dimensional microscope (KEYENCE, Japan) after dual culture for 2 days. This assay was repeated three times, with at least 10 hyphae being analyzed for each replicate assay.

Identification of antagonistic strain

Morphological and molecular approaches were employed to identify selected antagonistic endophytic bacterial strains. Morphological identification was performed as reported previously (Holt et al., 1994), while molecular identification was performed *via* the 16S rDNA sequencing of this strain using appropriate primers (Fan et al., 2016; Supplementary Table 1).

After amplification, PCR products were sequenced by Bgi Genomics Co., Ltd., Beijing, China, with a BLAST comparison being used to compare these sequences in the NCBI nucleotide collection database. Similar sequences from other isolates were used to conduct multiple sequence alignment using MEGA 7.0 software, after which a phylogenetic tree was constructed with the neighbor-joining approach with 1,000 bootstrap replicates.

Antifungal activity of culture filtrate of antagonistic strain against *Valsa pyri* mycelial growth

Culture filtrate was harvested from antagonistic bacteria following culture for 2 days at 28°C, 200 rpm. Filtrate was sterilized by passing them through a 0.22 μm filter and was combined with PDA medium at final culture filtrate concentrations of 2%, 4%, 8%, or 16%. The diameters of *V. pyri* colonies grown on PDA medium supplemented with these various culture filtrate concentrations were assessed at 6 dpi, with filtrate-free PDA serving as a control. This analysis was repeated in triplicate, with three replicates per assay.

Secreted enzyme activity analyses

The secreted protease, cellulase, and β-1, 3-glucanase activity of strain Nl4 was, respectively, assessed using skim milk medium, CMC medium, and aniline blue medium after incubating these plates for 3 days at 28°C (Zhai et al., 2021). This analysis was repeated in triplicate with two replicates per analysis.

Antifungal activity of *Paenibacillus polymyxa* strain Nl4 against *Valsa pyri in vivo*

The ability of *P. polymyxa* strain NI4 to control *V. pyri* infection of pear twigs (Zhongli no. 1) was assessed as reported previously with some modification (Yuan et al., 2021). Briefly, 1-year-old pear twigs were collected, rinsed with sterilized water, disinfected using 75% ethanol, and cut into 10 cm lengths. A sterile borer was used to generate a punch (diameter: 5 mm) in the center of each of these twigs, after which each twig was sprayed evenly with 1 ml of a strain Nl4 cell suspension (1×10^8 CFU ml^{-1}). After dry, twigs were then inoculated with *V. pyri* mycelial plugs (diameter: 5 mm). Sterile water and carbendazim (CBZ, 0.8 g L^{-1}; Tianjin Hanbang Plant Protective Agent Co., Ltd., Tianjing, China) treatments, respectively, served as negative and positive controls. Following inoculation, twigs were incubated at 25°C. At 7 dpi, vernier calipers were used to measure lesion length. This analysis was repeated in triplicate, with 10 inoculation sites per replicate experiment.

Paenibacillus polymyxa strain Nl4 colonization of pear twig wounds

A sterile borer was used to punch pear twigs as above, with 20 μl of strain NI4 suspension (1×10^8 CFU ml^{-1}) being applied to each wound. These twigs were then incubated at 25°C, with ~0.05 g of wounded tissue being harvested and ground to isolate bacterial colonies at 0 (3 h post-inoculation),1, 2, 3, 4, 5, 6, 7, 8, 9, and 10 dpi. For each sample, 0.1 ml of each prepared dilution was applied to NA medium (peptone 10 g L^{-1}, beef extract 3 g L^{-1}, sodium chloride 5 g L^{-1}, and agar 15 g L^{-1}) plates, with bacterial colonies being counted at 2 dpi following culture at 28°C. This analysis was repeated two times, with three replicates per assay.

Effect of *Paenibacillus polymyxa* strain Nl4 on plant growth

Germinated tomato seedlings were sown in seedling pots in a growth chamber at 25°C under 60% ± 5% relative humidity with a 16 h light/8 h dark photoperiod. On day 10 after transplantation, these seedlings were irrigated with a 5 ml suspension of strain NI4 (1×10^8 CFU ml^{-1}) at a range of concentrations (1×, 10×, 50×). An equivalent volume of LB broth medium served as a negative control. Tomato plant growth was assessed at 10 dpi based on plant height, fresh weight, and dry weight. This analysis was repeated in triplicate, with six plants per replicate.

Potential plant growth promoting traits of *Paenibacillus polymyxa* strain Nl4

Indole acetic acid (IAA) production was detected using Salkowski colorimetric method (Glickmann and Dessaux, 1995). Strain Nl4 was inoculated in 20 ml LB broth supplemented with 0.5 mg ml^{-1} l-Tryptophane at 28°C, 200 rpm. The supernatant of strain Nl4 was mixed with Salkowski reagent in a ratio of 1:2 for IAA assay. Phosphate solubilization assay was performed by placing stain Nl4 on Bacterial Organo-phosphorus Medium and Norganic Phosphorus Medium purchased from Hope Bio-Tcehnology Co., Ltd. (Qingdao, China) for growth 3 days.

Transcriptome analysis

To examine changes in global *V. pyri* gene expression in response to antagonistic bacteria, wild-type *V. pyri* strain lfl-XJ was harvested from PDA medium to extract RNA following dual culture for 2 days with strain NI4, as above. *V. pyri* grown on PDA medium in the absence of strain NI4 served as a control for these analyses. To assess strain NI4 treatment-associated changes in global gene expression in pear twigs, healthy twigs were sprayed with a suspension of strain NI4 (1×10^8 CFU ml^{-1}), and bark samples were collected from these twigs on day two

post-spraying. LB-treated pear twigs served as a control for these analyses. Trizol was used to extract total RNA from these samples based on provided directions (TransGen Biotech, Beijing, China), after which transcriptomic sequencing and downstream analyses were performed by Nanjing Personalbia Gene Technology Co., Ltd. (Nanjing, Jiangsu, China). A NEB Next Ultra Directional RNA Library Prep Kit for Illumina (NEB, CA, United States) was used to prepare sequencing libraries, while an Illumina Novaseq 6000 instrument was used for sequencing. Differentially expressed genes (DEGs) were those exhibiting a fold change $|\log_2 (\text{fold change})| > 1$ and an adjusted $p < 0.05$. Gene ontology (GO) annotations were assessed with the topGO software (Alexa and Rahnenfuhrer, 2010), while KEGG pathway enrichment analyses were conducted with the clusterProfiler package (Yu et al., 2012).

Quantitative real-time PCR assay

A quantitative real-time PCR (qRT-PCR) approach was used to validate RNA-seq results by analyzing the expression of several randomly selected genes. Samples were collected as the same as above, after which first-strand cDNA was prepared with the MonScript™ RTIII All-in-One Mix with dsDNase Kit (Monad, Suzhou, China). All qPCR analyses were performed with the Light CyclerR 96 PCR Detection System and a ChemoHS qPCR Kit (Monad, Suzhou, China) based on provided directions using the primers listed in Supplementary Table 1. The *Ppactin* and *Vpactin* genes served as normalization controls for analyses of pear and *V. pyri* gene expression, respectively, with the $2^{-\Delta\Delta Ct}$ method (Livak and Schmittgen, 2001) being used to quantify relative gene expression. Analyses were repeated two times with three replicates per analysis.

Results

Antagonistic strain screening and isolation

In total, 120 bacteria were isolated from pear branches. The majority of these bacterial strains did not exhibit clear inhibition zones in dual culture tests with *V. pyri* (Supplementary Figure 1), with just five strains exhibiting significant antagonistic activity. Of these strains, stain NI4 exhibited the most robust antagonist activity, inhibiting ~75.9% of *V. pyri* mycelial growth (Figure 1A), with a 7.8 mm inhibition zone. Further analyses of the impact of strain NI4 on *V. pyri* hyphae revealed that these hyphae were abnormally stretched and deformed with a black shadow-like appearance in the context of strain NI4-mediated inhibition (Figure 1B). Statistical analyses suggested that the average *V. pyri* hyphal diameter that grown in the presence of strain NI4 was just 4.1 μm, which was significantly reduced relative to that observed for control *V. pyri* (Figure 1C).

The ability of strain NI4 to inhibit the growth of three other major fruit pathogens was also measured, revealing that this bacterium were able to significantly inhibit *V. mali*, *B. dothidea*, and *C. gloeosporioides* growth by 74.6%, 74.9%, and 69.8%, respectively. Together, these data thus suggested that strain NI4 exhibited broad-spectrum antifungal activity *in vitro*.

Strain NI4 culture filtrate suppressed *Valsa pyri* growth

To establish whether culture filtrate prepared from strain NI4 would similarly possess antagonistic activity against *V. pyri*, culture filtrate of strain NI4 were added to PDA medium at final concentrations of 2%, 4%, 8%, or 16%. Subsequent results demonstrated that these strain NI4 filtrate significantly inhibited

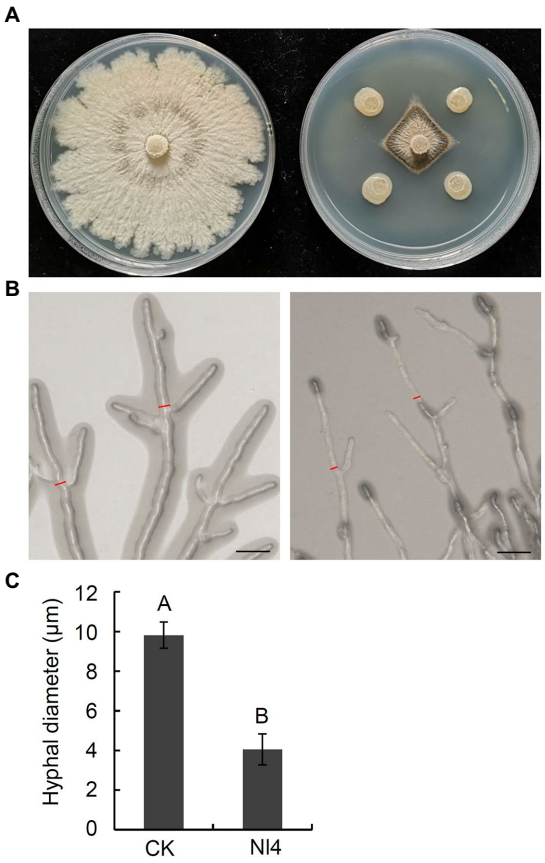

FIGURE 1
Antifungal activity of strain NI4 against *Valsa pyri*. **(A)** Effect of strain NI4 on mycelial growth of *V. pyri*. The picture was taken at 6dpi. Left, *V. pyri* CK; Right, *V. pyri* antagonized with strain NI4. **(B)** Effect of strain NI4 on hyphal morphology of *V. pyri*. Hyphal morphology of *V. pyri* was observed at 2days after antagonism with strain NI4. Bar=20mm. **(C)** Hyhal diameter of *V. pyri*. Values are means ± SD from three replicates. The measure position of hyphae diameter was indicated in **(B)** with red line. Different uppercase letters indicate significant differences between CK and treatment according to Student's *t*-test ($p<0.01$).

V. pyri mycelial growth in a dose-dependent fashion (Figures 2A,B). Specifically, the inhibition of *V. pyri* mediated by 2%, 4%, 8%, and 16% culture filtrate preparations were 39.5%, 49.7%, 55.7%, and 60.1%, respectively (Figure 2C). As such, culture filtrate prepared from strain NI4 exhibited robust antifungal activity against *V. pyri*.

Analysis of the secreted enzyme activity of strain Nl4

Next, secreted enzyme activity analyses were conducted for strain NI4, revealing that it was capable of forming a clear transparent circle on skim milk medium, CMC medium, and aniline blue medium (Figure 3). These results thus indicated that enzymes or metabolites produced by strain NI4 exhibited protease, cellulase, and β-1, 3-glucanase activity, potentially accounting for the ability of strain Nl4 to degrade *V. pyri* hyphae.

Identification of strain Nl4

Biochemical and physiological analyses of strain NI4 were next performed (Supplementary Table 2). This bacterium was identified as a gram-positive strain that yielded positive Voges-Proskauer (VP), nitrate reductase, starch hydrolysis, and gelatin liquefaction test results and a negative citrate test (Supplementary Table 2). Strain Nl4 was capable of growing on media containing sucrose, xylose, or mannitol as a carbon source, but could not grow on medium containing more than 5% sodium chloride.

A phylogenetic tree constructed based on the partial 16S rDNA sequence of strain NI4 (accession number: ON763838), together with closely related sequences, suggested this strain to be most closely related to *P. polymyxa* (Figure 4). As such, strain Nl4 was identified as *P. polymyxa*.

Colonization of *Paenibacillus polymyxa* strain Nl4 in pear twigs wounds

At 0 dpi, 6.47×10^5 CFU/wound strain NI4 colonies were observed in wound sites on pear twigs, rapidly expanding over 10-fold to 6.63×10^6 CFU at 1 dpi (Figure 5). The peak number of NI4 colonies was observed in pear branches at 5 dpi (4.28×10^7 CFU; 66.19-fold higher than 0 dpi), after which the number of colonies remained largely consistent with slight fluctuations (Figure 5). At 10 dpi, a high number of strain Nl4 colonies was still present in pear twig wound sites (Figure 5). These results thus demonstrated the ability of strain NI4 to readily colonize wounded pear twigs.

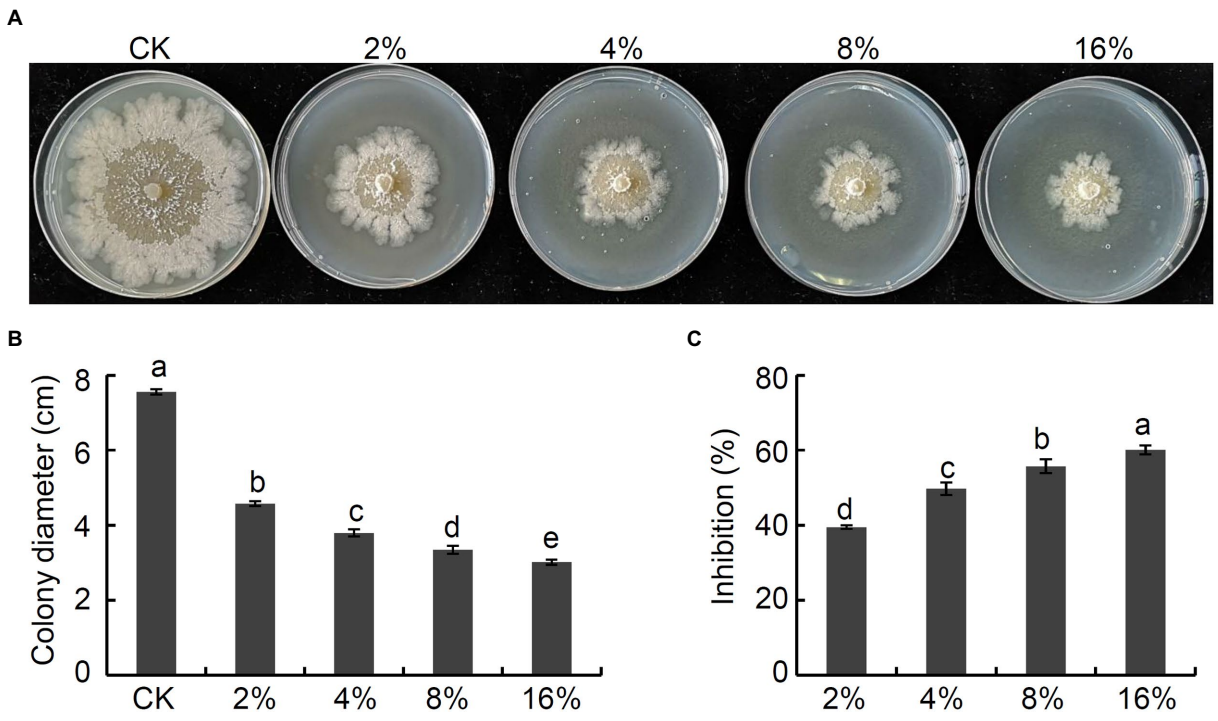

FIGURE 2
Antifungal activity of culture filtrate of strain Nl4 against *V. pyri*. **(A)** Effect of culture filtrate of strain Nl4 on mycelial growth of *V. pyri*. The picture was taken at 6dpi. **(B)** Statistical analysis of colony diameter. **(C)** Inhibition of strain Nl4 culture filtrate on mycelial growth of *V. pyri*. Each data represents the mean±SD of three replicates. Letters above the bars indicate statistical significance and different lowercase letters indicate significant different means ($p<0.05$) based on Student's t-test.

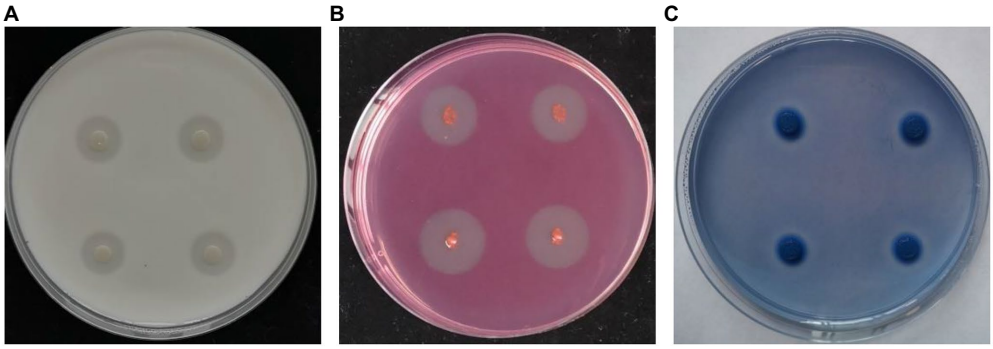

FIGURE 3
Secreted enzyme activity of strain Nl4. Protease **(A)**, cellulose **(B)**, and β-1, 3-glucanase **(C)** activities of strain Nl4 were analyzed on skim milk medium, CMC medium, and aniline blue medium, respectively. The pictures were taken at 3dpi at 28°C.

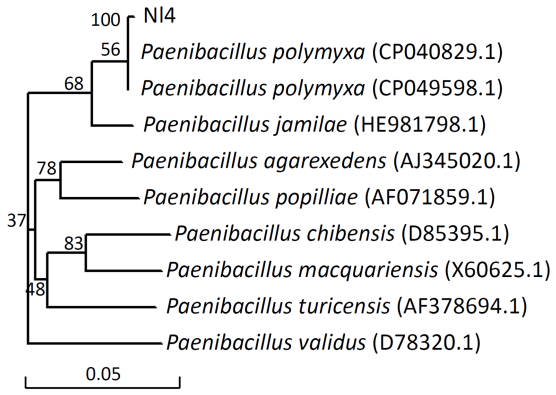

FIGURE 4
Phylogenetic analysis of strain Nl4 and its relatives based on 16S rDNA.

Antifungal activity of *Paenibacillus polymyxa* strain Nl4 against *Valsa pyri in vivo*

To assess the ability of *P. polymyxa* strain NI4 to inhibit the development of pear Valsa canker caused by *V. pyri*, a suspension of NI4 was applied to pear twigs that were then inoculated with *V. pyri*. On day 7 following *V. pyri* inoculation, control pear twigs exhibited brown lesions at the inoculated site, while twigs that had been treated with a suspension of strain NI4 cells exhibited less symptoms of disease (Figure 6A). Overall, strain NI4 treatment was associated with a reduction in disease incidence to just 6.7% as compared to the ~96.7% disease incidence observed in control twigs (Figure 6B). Pear twigs treated with CBZ as a positive control remained free of disease (Figures 6A,B). Average lesion size values were also significantly reduced in treated pear twigs relative to those observed on control twigs (Figure 6C). These data thus supported the ability of *P. polymyxa* strain Nl4 to suppress the development and severity of pear Valsa canker caused by *V. pyri*.

PGP traits of *Paenibacillus polymyxa* strain Nl4

To explore the plant growth promoting (PGP) characteristics of *P. polymyxa* strain NI4, different proportions of strain NI4 cell suspensions were applied to tomato seedling roots. As shown in Table 1, strain NI4 treatment was associated with significant increases in plant height, with plants treated with 1x, 10x, and 50x strain NI4 cell suspensions exhibiting respective heights of 10.18, 10.94, and 10.48 cm, respectively, as compared to a control plant height of just 7.54 cm (Table 1). An increase in total plant biomass was similarly observed following strain NI4 treatment (Table 1). Further results showed that strain Nl4 could not produce IAA but had the ability to dissolve organo-phosphorus (Supplementary Figure 2).

Transcriptome analysis of *Valsa pyri* treated with *Paenibacillus polymyxa* strain Nl4

Next, transcriptome analyses of *V. pyri* that were or were not exposed to *P. polymyxa* strain NI4 were conducted, with an R^2 of 0.816–1.000 among treatments (Supplementary Figure 3), reaffirming the reproducibility of the data derived from this analysis. In total, comparisons of control and *P. polymyxa* strain NI4-treated *V. pyri* revealed 2,585 DEGs of which 1,610 and 975 were, respectively, upregulated and downregulated (Figure 7A; Supplementary Figure 4). GO analyses indicated that these DEGs were primarily associated with molecular functions including oxidoreductase activity and catalytic activity, biological processes including oxidation–reduction and carbohydrate metabolic processes, and cellular component terms including intrinsic component of membrane, integral component of membrane and membrane among cellular component (Figure 7B). Subsequent analysis indicated that 1,002 of these DEGs were associated with the catalytic activity annotation while 1,778 were associated with

the membrane component annotation. KEGG analyses further revealed these DEGs to be enriched for the biosynthesis and metabolism of multiple carbohydrates, amino acids, and lipids (Figure 7C).

Further analysis indicated that the fatty acid metabolism, biosynthesis of unsaturated fatty acids, glycerophospholipid metabolism, glycosphingolipid biosynthesis and steroid biosynthesis, which associated with cell membrane, were enriched in *V. pyri* at the stress of strain Nl4. Among them, eight genes (*VP1G_09796*, *VP1G_00957*, *VP1G_08690*, *VP1G_05245*, *VP1G_07256*, *VP1G_08986*, *VP1G_04775* and *VP1G_11014*) involved in fatty acid metabolism, three genes (*VP1G_00733*, *VP1G_03079* and *VP1G_08598*) involved in unsaturated fatty acids biosynthesis, three genes (*VP1G_06941*, *VP1G_04418* and *VP1G_09142*) involved in glycerophospholipid metabolism, one gene (*VP1G_07179*) involved in glycosphingolipid biosynthesis and two genes (*VP1G_04184* and *VP1G_04418*) involved in steroid biosynthesis were downregulated. In order to alleviate oxidative damages of strain Nl4 on the cell membrance, plenty of genes involved in antioxidant response were significantly activated in *V. pyri*. For example, the genes *VP1G_01209* encoding catalase-related peroxidase and *VP1G_08485* encoding L-ascorbate peroxidase were greatly upregulated. In addition, homolog genes of glutathione S-transferase (GST, *VP1G_08389*, *VP1G_09397*, *VP1G_05587* and *VP1G_04014*) and ABC transporter proteins (*VP1G_01031* and *VP1G_05741*) were also significantly upregulated, to eliminate ROS stress.

These data suggested that *P. polymyxa* strain Nl4 was able to suppress *V. pyri* growth primarily *via* impacting the membrane and energy metabolism activity of this pathogen.

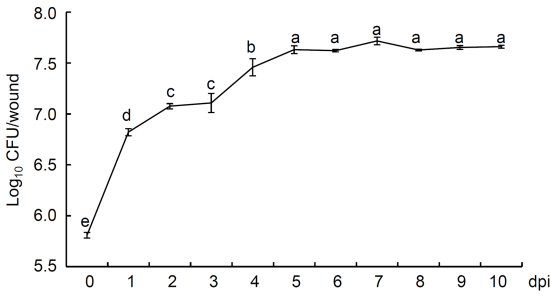

FIGURE 5
Population dynamics of *Paenibacillus polymyxa* strain Nl4 in wounds of pear twig. Population densities were expressed as Log_{10} CFU/wound. Each data represents the mean±SD of three biological replicates. Different lowercase letters indicate significant differences according to Student's *t*-test ($p<0.05$).

Transcriptome analysis of pear tree treated with *Paenibacillus polymyxa* strain Nl4

A transcriptomic analysis of pear trees treated with *P. polymyxa* strain Nl4 was additionally conducted, revealing 396 and 466 DEGs that were, respectively, upregulated and downregulated following such treatment relative to control tree samples (Figure 8A; Supplementary Figure 5). GO analyses revealed these DEGs to

TABLE 1 Effect of *P. polymyxa* strain Nl4 on tomato growth promotion.

Treatment	Plant height (cm)	Fresh weight (g)	Dry weight (g)
CK	7.54 ± 0.63b	0.54 ± 0.21b	0.038 ± 0.016b
1 × Nl4	10.18 ± 0.77a	0.87 ± 0.15a	0.056 ± 0.004a
10 × Nl4	10.94 ± 0.36a	0.96 ± 0.13a	0.0619 ± 0.010a
50 × Nl4	10.48 ± 0.80a	0.94 ± 0.20a	0.0562 ± 0.008a

Data represents the mean ± SD of six biological replicates. Different lowercase letters indicate significant differences according to Student's *t*-test ($p < 0.05$).

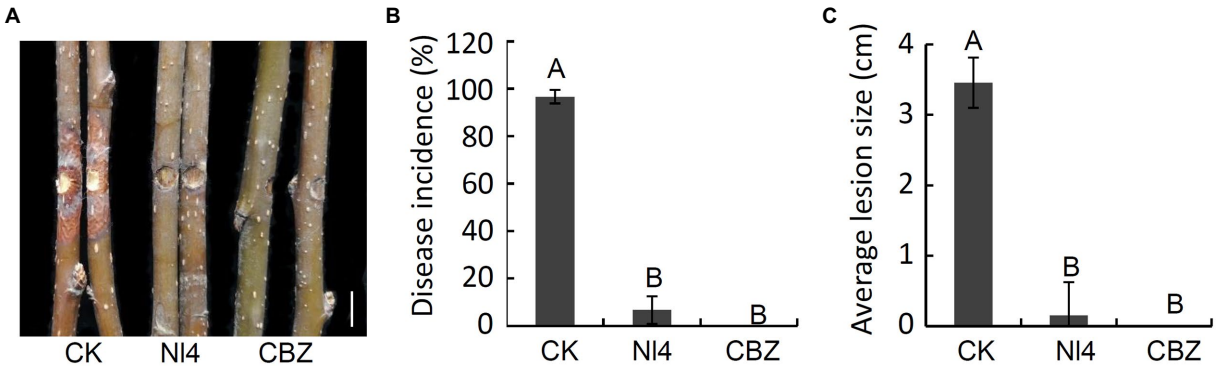

FIGURE 6
Biocontrol activity of *P. polymyxa* strain Nl4 in controlling pear Valsa canker caused by *V. pyri*. **(A)** Suppression of strain Nl4 cell suspension on pear Valsa canker. Sterile distilled water or carbendazim (CBZ) treatment was used as the negative and positive control, respectively. Bar=1cm. **(B)** Statistical analysis of the disease incidence. **(C)** Statistical analysis of disease lesion size. Each data represents the mean±SD of three replicates. Disease lesion size and disease incidence were measured at 7dpi. Letters above the bars indicate statistical significance and different uppercase letters indicate significant different means ($p<0.01$) based on Student's t-test.

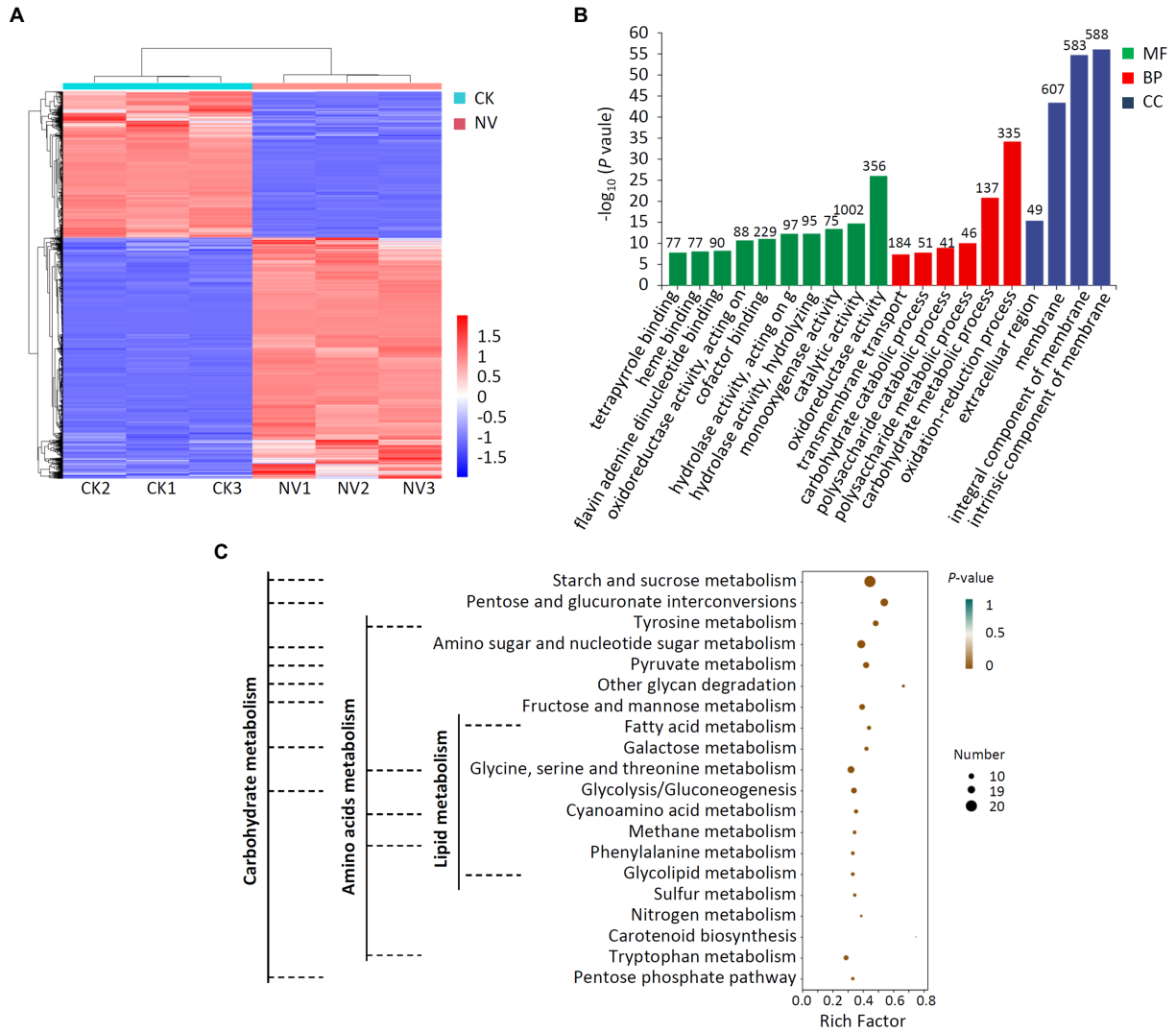

FIGURE 7
Transcriptome analysis of DEGs in *V. pyri* treated with *P. polymyxa* strain Nl4. **(A)** Heat map analysis. CK, untreated *V. pyri*; NV, strain Nl4 treated *V. pyri*. Red indicates highly expressed genes, and blue indicates low expressed genes. **(B)** GO annotation analyses of DEGs. The number above the column represents the number of DEGs. **(C)** KEGG pathway enrichment analyses of the DEGs. Rich factor=DEGs number/total gene number identified from transcriptome of a certain process.

be mainly associated with 20 different annotated subcategories, with many of these genes being enriched for GO terms pertaining to hydrolase activity, acting on glycosyl bonds, hydrolyzing O-glycosyl compounds, regulating cell wall organization or biogenesis, and impacting the extracellular region (Figure 8B). KEGG enrichment analyses further revealed these DEGs to be enriched for secondary metabolite biosynthesis pathways including phenylpropanoid biosynthesis, sesquiterpenoid and triterpenoid biosynthesis, isoquinoline alkaloid biosynthesis, glucosinolate biosynthesis, carotenoid biosynthesis, steroid biosynthesis, tropane, piperidine and pyridine alkaloid biosynthesis, and flavonoid biosynthesis (Figure 8C). Moreover, these DEGs were also enriched for cutin, suberine, and wax biosynthesis, plant hormone signal transduction, and MAPK signaling pathway activity.

After *P. polymyxa* strain Nl4 treatment, 33 genes in pear related to secondary metabolism were upregulated by 1.02–4.65 times by comparing with the control (Table 2). Some potential defense-related genes were also upregulated in pear after Nl4 treatment (Table 3). In addition, the expression of several transcription factors involved in plant disease resistance were increased, such as homologs of *WRKY 75* (*Ppy14g1309.1* and *Ppy06g1207.1*), *WRKY 40* (*Ppy09g1858.1* and *Ppy08g0450.1*). Furthermore, some genes involved in plant hormone signal transduction were upregulated. For example, gibberellin receptor *GID1C* (*Ppy12g1496.1*) was upregulated with a 1.58-fold time. ACO homolog gene in pear (*Ppy10g0793.1*) involved in the biosynthesis of ethylene was upregulated with a 1.67-fold time.

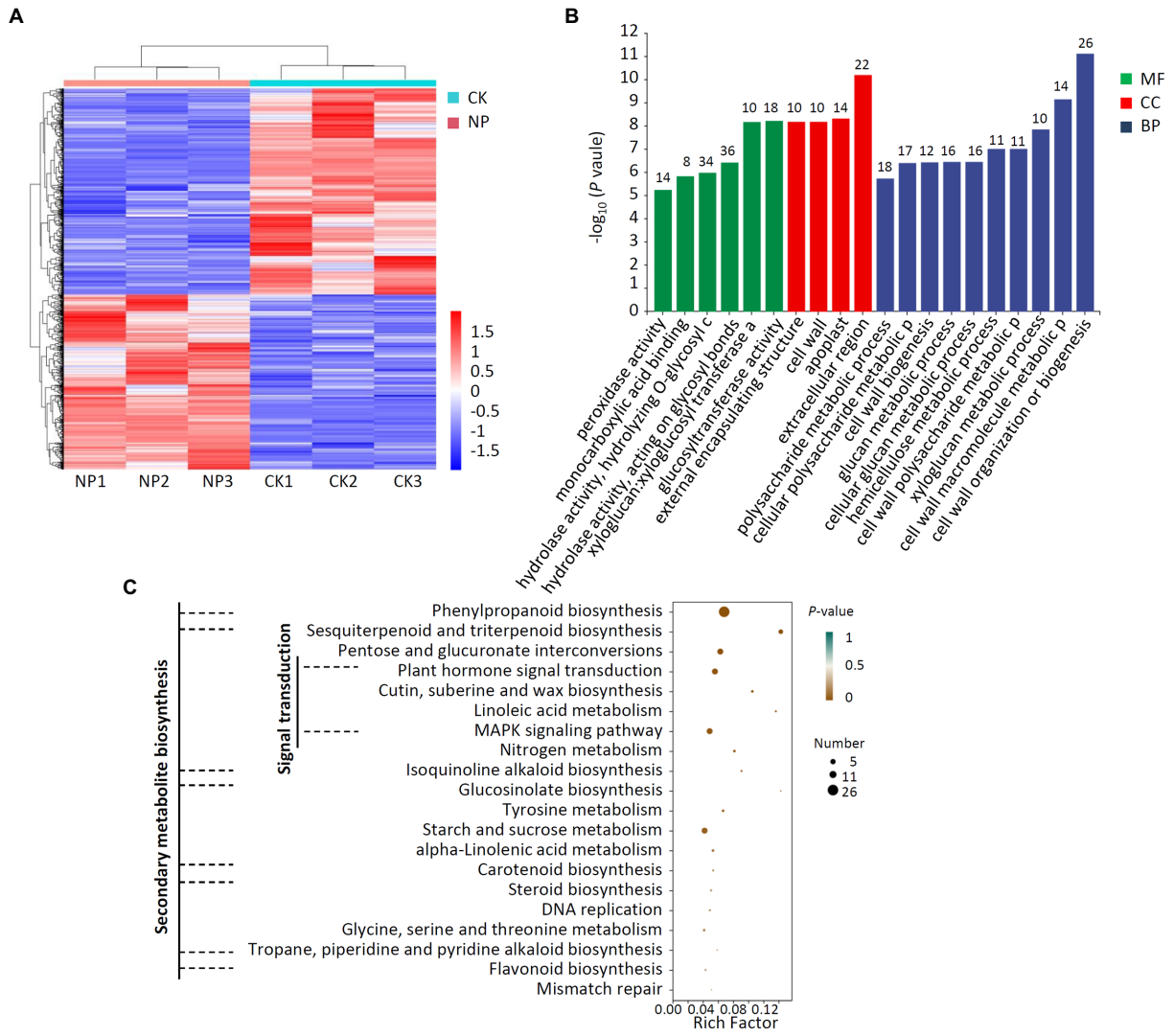

FIGURE 8
Transcriptome analysis of DEGs in pear twigs treated with *P. polymyxa* strain Nl4. **(A)** Heat map analysis. CK, untreated pear twigs; NP, strain Nl4 treated pear twigs. Red indicates highly expressed genes, and blue indicates low expressed genes. **(B)** GO annotation analyses of DEGs. The number above the column represents the number of DEGs. **(C)** KEGG pathway enrichment analyses of the DEGs. Rich factor=DEGs number/total gene number identified from transcriptome of a certain process.

Together, these results suggest that *P. polymyxa* strain Nl4 can regulate pear resistance by mainly altering the expression of resistance-related genes associated with secondary metabolite biosynthesis, signal transduction, and cutin, suberine, and wax biosynthesis.

Validation the results of RNA-sequencing by qRT-PCR analysis

The result of qRT-PCR analysis showed that the expression of 10 randomly selected genes exhibited a similar expression pattern with RNA-sequencing (Figure 9), which suggested the transcriptome data in this study were reliable.

Discussion

Pear Valsa canker is a devastating disease caused by *V. pyri* that can adversely impact pear tree yields. Endophyte-based biocontrol strategies of this disease represent an attractive alternative to chemical fungicide application, and prior studies have demonstrated the promise of such approaches (Song et al., 2020; Yuan et al., 2021). However, relatively few biocontrol strains with antagonistic activity against pear Valsa canker have been described to date. As such, in the present study, 120 bacteria were isolated from pear branches and screened for the ability to inhibit *V. pyri* growth in a dual culture test. Of the isolated strains, *P. polymyxa* strain Nl4 was most readily able to inhibit this fungal pathogen, suppressing *V. pyri* mycelial growth and inducing hyphal

10.3389/fmicb.2022.950742

TABLE 2 List of upregulated gene related to secondary metabolism in pear twigs at the present of *Paenibacillus polymyxa* strain Nl4.

Gene	log_2 (fold change)	Description
Ppy14g0888.1	1.06	4-Coumarate-CoA ligase-like
Ppy07g2039.1	1.07	Caffeoyl shikimate esterase
Ppy07g1936.1	1.39	Caffeoyl shikimate esterase
Ppy02g1609.1	1.26	Peroxidase 73-like
Ppy01g1477.1	1.96	Peroxidase P7-like
Ppy14g0094.1	1.49	Peroxidase 57-like
Ppy15g0912.1	1.50	Peroxidase 16-like
Ppy15g2378.1	1.42	Peroxidase 10-like
Ppy05g2964.1	1.74	Polyphenol oxidase
Ppy09g1129.1	1.14	Polyphenol oxidase IV
Ppy05g2960.1	2.16	Polyphenol oxidase IV
Ppy10g1746.1	2.28	polyphenol oxidase
Ppy16g0851.1	2.17	Flavanone 3-hydroxylase-like
Ppy11g1345.1	3.12	Secoisolariciresinol dehydrogenase-like
Ppy10g1848.1	2.72	Nerolidol synthase 1-like
Ppy10g1852.1	3.15	(3S,6E)-Nerolidol synthase 1-like
Ppy10g0228.1	1.02	Beta-amyrin synthase-like
Ppy03g1922.1	4.65	(−)-Germacrene D synthase-like
Ppy07g0648.1	3.05	Squalene monooxygenase-like
Ppy07g0087.1	2.36	Squalene monooxygenase-like
Ppy13g2150.1	1.51	3-Isopropylmalate dehydratase large subunit
Ppy06g1930.1	2.74	Eucoanthocyanidin reductase-like
Ppy17g0031.1	1.23	Aspartokinase 2
Ppy01g0522.1	2.13	(−)-Isopiperitenone reductase-like
Ppy13g0036.1	1.67	Serine carboxypeptidase-like
Ppy03g0799.1	2.87	Probable inactive 2-oxoglutarate-dependent dioxygenase
Ppy10g0822.1	1.35	Cytochrome P450 94A1-like
Ppy11g1877.1	1.43	Cytochrome P450 CYP736A12-like
Ppy09g1129.1	1.14	UDP-Glycosyltransferase
Ppy11g0487.1	1.84	UDP-Glycosyltransferase superfamily protein
Ppy02g0042.1	2.85	UDP-Glycosyltransferase
Ppy08g1972.1	2.61	7-Deoxyloganetin glucosyltransferase-like
Ppy12g0470.1	1.41	Probable glycosyltransferase At5g03795

TABLE 3 List of upregulated gene related to defense-related in *Paenibacillus polymyxa* strain Nl4 treated pear twigs.

Gene	log_2 (fold change)	Description
Ppy05g0926.1	2.92	Pathogenesis-related protein 1-like
Ppy05g0923.1	1.46	Basic form of pathogenesis-related protein 1-like
Ppy04g0597.1	1.34	Pathogenesis-related protein 5-like
Ppy06g0674.1	1.88	Pathogenesis-related protein 5-like
Ppy13g1587.1	1.74	Pathogenesis-related protein 10
Ppy13g1585.1	1.37	Pathogenesis-related protein 10b
Ppy08g1541.1	1.36	Pathogenesis-related protein 10b
Ppy06g1893.1	1.14	Protein SGT1-like
Ppy14g1921.1	1.26	Protein SGT1-like
Ppy07g0357.1	1.02	TMV resistance protein N-like
Ppy10g1810.1	1.67	Disease resistance RPP13-like protein 4
Ppy00g1277.1	1.34	Salicylic acid methyltransferase
Ppy00g0673.1	2.00	Salicylic acid methyltransferase
Ppy11g1304.1	1.53	Ankyrin repeat-containing protein NPR4-like
Ppy11g1309.1	1.99	Ankyrin repeat-containing protein NPR4-like

malformations. Notably, *P. polymyxa* strain Nl4 also exhibited broad-spectrum antifungal activity, inhibiting the growth of a range of plant pathogens in line with prior studies (Zhang et al., 2018; Slama et al., 2019). This endophytic bacterial strain was able to significantly reduce pear Valsa canker disease incidence and lesion size, exhibiting efficacy similar to that for positive control CBZ treatment. Together, these findings suggested that *P. polymyxa* strain Nl4 represents a promising biocontrol resource with the potential to combat *V. pyri*-induced pear Valsa canker.

The ability of biocontrol strains to colonize and survive in host plant tissues is critical to their agronomic utility. *P. polymyxa* strain Nl4 was initially isolated from pear branches, and it was also successfully re-isolated after being used to inoculate pear twigs. Moreover, strain NI4 rapidly proliferated after application to pear twigs, reaching peak density at 5 dpi with bacterial counts were 66.19-fold higher than at 0 dpi, after which this population remained stable throughout the remainder of the study period. These data thus indicate that *P. polymyxa* strain NI4 can readily colonize and survive on pear twigs, emphasizing the need for further studies exploring the impact of different environmental variables on this activity.

P. polymyxa is capable of promoting plant growth, primarily *via* nitrogen fixation (Puri et al., 2016), phosphate solubilization (Mohd Din et al., 2020), IAA (Mei et al., 2014), iron acquisition (Zhou et al., 2016), or improvements in chlorophyll content (Liu

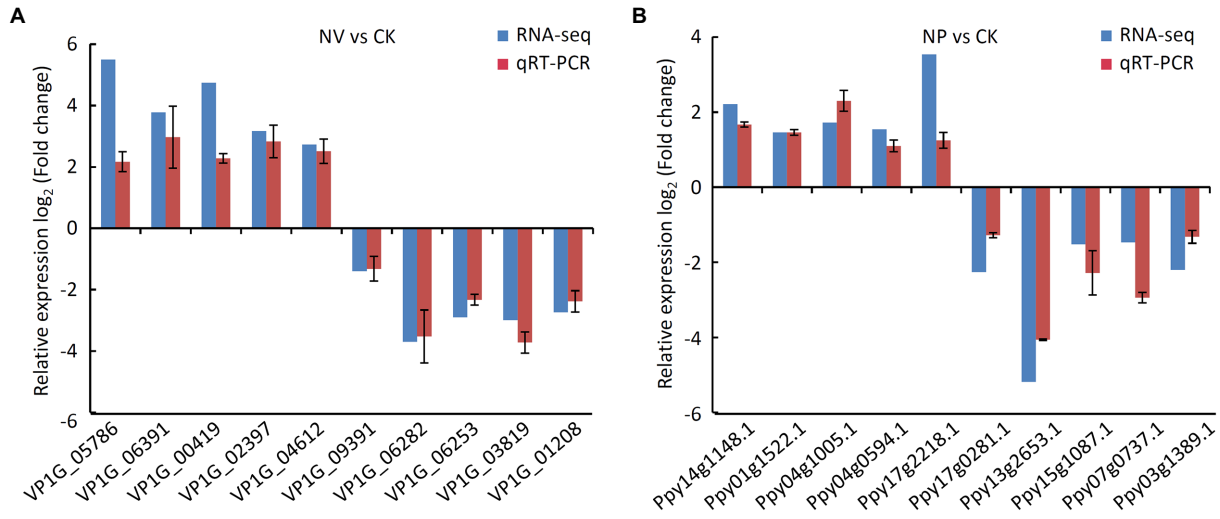

FIGURE 9
Validation the results of RNA-seq by qRT-PCR assay. **(A)** qRT-PCR assay in *V. pyri*. CK, untreated *V. pyri*; NV, strain Nl4-treated *V. pyri*. **(B)** qRT-PCR assay in pear twigs. CK, LB-treated pear twigs; NP, strain Nl4-treated pear twigs.

H. et al., 2021). PGP train analyses in the present study suggested that *P. polymyxa* strain Nl4 was able to solubilize phosphorus, suggesting that this may be the mechanism underlying the ability of this biocontrol agent to accelerate plant growth.

Cell wall disruption can adversely impact fungal cell growth and morphological characteristics, potentially promoting cell death (Bowman and Free, 2006). Given their importance, cell walls commonly serve as targets for antifungal treatment. Here, strain NI4 culture filtrate was found to mediate antifungal activity against *V. pyri*, suggesting that the culture filtrate contained antimicrobial compounds. Secretions produced by strain NI4 also exhibited robust protease, cellulase, and β-1, 3-glucanase activity, with all three of these enzymes being capable of breaking down fungal cell walls (Park et al., 2012; Zhai et al., 2021). Cell membranes are important for the cell to cope with different environment stress, such as chemical substances. Previous study had proven that components of fungal cell membrane, such as ergosterol was one of the main targets of antifungal agent (Jordá and Puig, 2020). In this study, transcriptomic analyses revealed that 1,778 total DEGs that were expressed in *V. pyri* in response to strain NI4 exposure were annotated as being associated with the cell membrane, suggesting that the *V. pyri* membrane may be a primary target of *P. polymyxa* strain Nl4. Strain Nl4-induced damage also caused 1,385 DEGs exhibiting oxidoreductase activity and catalytic activity in *V. pyri*. Together, these data thus suggest that the antifungal activity of *P. polymyxa* strain Nl4 against *V. pyri* may be related to its ability to inhibit cell wall and membrane synthesis, in line with similar antagonistic mechanisms that have previously been reported for other strains exhibiting antifungal activity (Yang et al., 2020; Liu R. et al., 2021).

A number of plant secondary metabolites have been shown to contribute to plant resistance (Bennett and Wallsgrove, 1994; Piasecka et al., 2015). In transcriptomic analyses of pear trees treated with *P. polymyxa* strain NI4, many of the identified DEGs were enriched in secondary metabolite biosynthesis pathways including the phenylpropanoid biosynthesis, sesquiterpenoid and triterpenoid biosynthesis, and isoquinoline alkaloid biosynthesis pathways. Phenylpropanoids are synthesized from phenylalanine, and can enable plants to resist a range of abiotic and biotic stressors (Geng et al., 2020; Yadav et al., 2020). Chen et al. (2021) found that *Pichia galeiformis* was capable of enhancing postharvest citrus resistance to the pathogen *P. digitatum via* the activation of the phenylpropanoid biosynthesis pathway. Here, 16 DEGs in pear trees were identified to associate with phenylpropanoid biosynthesis pathway following strain Nl4 treatment. Among them, 4-coumarate-CoA ligase (4CL, *Ppy14g0888.1*) is a rate-limiting enzyme involved in the phenylpropanoid metabolism to produce flavonoids, cinnamate and lignin (Hu et al., 2010). The flavonoid biosynthesis pathway is a branch of the phenylpropanoid biosynthesis pathway, with flavonoids serving as inducible phytoalexins that confer resistance to pathogens (Samanta et al., 2011; Nemesio-Gorriz et al., 2016; Ullah et al., 2017). In the present study, flavonoid biosynthesis was similarly enriched in pear twigs following strain NI4 treatment, with a 2.74-fold and 2.17-fold increase in leucoanthocyanidin reductase (LAR, *Ppy06g1930.1*) and flavanone 3-hydroxylase-like (F3H, *Ppy16g0851.1*) gene expression, respectively.

Lignin and lignan as a class of secondary metabolites belong to phenylpropane derivatives. Many studies have confirmed that lignin is an inducible physical barrier against pathogen infection by reinforcing plant cell wall (Shadle et al., 2003). Peroxidase (POD) is a key enzyme involved in lignin formation (Ali et al., 2006). In this study, we found that the expression of five PODs genes (*Ppy02g1609.1*, *Ppy01g1477.1*,

Ppy14g0094.1, *Ppy15g0912.1* and *Ppy15g0912.1*) was significantly increased in *P. polymyxa* strain Nl4 treated pear when compared with control. Other study also found a similar result in citrus treated with antagonistic strain (Chen et al., 2021). Gene encoding caffeoyl shikimate esterase-like (CSE, *Ppy07g2039.1* and *Ppy07g1936.1*), as an enzyme function in the lignin biosynthetic pathway through hydrolyzing caffeoyl shikimate into caffeate (Vanholme et al., 2013), were also upregulated. In addition, Gene encoding secoisolariciresinol dehydrogenase-like (SDH, *Ppy11g1345.1*) involved in the biosynthesis of lignan showed higher upregulation by increasing to 3.12-fold.

CYP450s and glycosyltransferase (UGTs) are considered to be involved in the biosynthesis of triterpene saponins that participate in plant defense (Rahimi et al., 2019). CYP450s can catalyze the carboxylation, hydroxylation, dehydrodehydration, alkylation and kekylation of triterpene backbones to form the intermediate of triterpene saponins (Thimmappa et al., 2014). UGTs function at the last step in triterpene saponin biosynthesis by glycosylation (Augustin et al., 2012). In this study, two CYP450s genes (*Ppy10g0822.1* and *Ppy11g1877.1*) and five UGTs genes (*Ppy09g1129.1*, *Ppy11g0487.1*, *Ppy02g0042.1*, *Ppy08g1972.1* and *Ppy12g0470.1*) were upregulated in pear. Other plant secondary metabolites regulated by strain NI4 including sesquiterpenoids and isoquinoline alkaloids can also confer pathogen resistance (Bennett and Wallsgrove, 1994; Morrissey, 2009). Together, these data suggest that *P. polymyxa* strain Nl4 can induce pear antifungal defenses primarily through the regulation of secondary metabolite biosynthesis pathways.

Conclusion

In conclusion, *P. polymyxa* Nl4 was herein identified as a promising biocontrol agent capable of preventing pear Valsa canker caused by *V. pyri*. Preliminary transcriptomic analyses were conducted to explore the mechanisms whereby *P. polymyxa* strain NI4 can suppress *V. pyri* growth and induce plant defense responses, providing a robust foundation for future efforts to apply this bacterium as a good biocontrol agent.

Data availability statement

The data presented in the study are deposited in NCBI, accession number PRJNA851571 (https://www.ncbi.nlm.nih.gov/sra/PRJNA851571) and PRJNA851531 (https://www.ncbi.nlm.nih.gov/sra/PRJNA851531).

Author contributions

HY and HT designed the research. HY, MY, BS, and ZW performed the experiments with help from TH, GQ, HH, and LW. HY analyzed the data and wrote the manuscript. HT provided the funding. All authors contributed to the article and approved the submitted version.

Funding

This work obtained the financial support of the National Key R&D Program of China (no. 2017YFE0135600), the Agricultural Science and Technology Innovation Program (CAAS-ASTIP-2016-RIP), and the Central Public-Interest Scientific Institution Basal Research Fund (no. ZGS202110).

Conflict of interest

The authors declare that the research was conducted in the absence of any commercial or financial relationships that could be construed as a potential conflict of interest.

Publisher's note

All claims expressed in this article are solely those of the authors and do not necessarily represent those of their affiliated organizations, or those of the publisher, the editors and the reviewers. Any product that may be evaluated in this article, or claim that may be made by its manufacturer, is not guaranteed or endorsed by the publisher.

Supplementary materials

The Supplementary materials for this article can be found online at: https://www.frontiersin.org/articles/10.3389/fmicb.2022.950742/full#supplementary-material

SUPPLEMENTARY FIGURE 1
The endophyte strain Nl7 did not show antagonistic activity against *V. pyri*.

SUPPLEMENTARY FIGURE 2
PGP traits of strain Nl4. **(A)** IAA assay. Landy medium was used as negative control and IAA (10 mg L^{-1}) was used as positive control. **(B)** Phosphate solubilization assay. Left, inorganic phosphorus; Right, organo-phosphorus.

SUPPLEMENTARY FIGURE 3
Correlation heatmap between *V. pyri* CK and *V. pyri* treated with *P. polymyxa* strain Nl4 in transcriptome analysis. CK, untreated *V. pyri*; NV, strain Nl4 treated *V. pyri*.

SUPPLEMENTARY FIGURE 4
Transcriptome pattern in *V. pyri* at the present of *P. polymyxa* strain Nl4. Downregulated DEGs are shown with blue dots, while the upregulated DEGs are shown in red. Those that are not significantly altered are shown in grey in the center.

SUPPLEMENTARY FIGURE 5
Transcriptome pattern in pear twigs at the present of *P. polymyxa* strain Nl4. Downregulated DEGs are shown with blue dots, while the upregulated DEGs are shown in red. Those that are not significantly altered are shown in grey in the center.

References

Alexa, A., and Rahnenfuhrer, J. (2010). TopGO: enrichment analysis for gene ontology. R package, version 2.22.0.

Ali, M. B., Khatun, S., Hahn, E. J., and Paek, K. Y. (2006). Enhancement of phenylpropanoid enzymes and lignin in *Phalaenopsis orchid* and their influence on plant acclimatisation at different levels of photosynthetic photon flux. *Plant Growth Regul.* 49, 137–146. doi: 10.1007/s10725-006-9003-z

Augustin, J. M., Drok, S., Shinoda, T., Sanmiya, K., Nielsen, J. K., Khakimov, B., et al. (2012). UDP glycosyltransferases from the UGT73C subfamily in *Barbarea vulgaris* catalyze sapogenin 3-O-glucosylation in saponin-mediated insect resistance. *Plant Physiol.* 160, 1881–1895. doi: 10.1104/pp.112.202747

Bennett, R. N., and Wallsgrove, R. M. (1994). Secondary metabolites in plant defence mechanisms. *New Phytol.* 127, 617–633. doi: 10.1111/j.1469-8137.1994.tb02968.x

Bowman, S. M., and Free, S. J. (2006). The structure and synthesis of the fungal cell wall. *Bioessays* 28, 799–808. doi: 10.1002/bies.20441

Chen, O., Deng, L., Ruan, C., Yi, L., and Zeng, K. (2021). *Pichia galeiformis* induces resistance in postharvest citrus by activating the phenylpropanoid biosynthesis pathway. *J. Agric. Food Chem.* 69, 2619–2631. doi: 10.1021/acs.jafc.0c06283

Cheng, C., Zhao, Y., Li, H., He, F., Cao, S., Yang, X., et al. (2017). Control effect of HSAF from *Lysobacter enzymogenes* OH11 on pear valsa canker. *Chinese J. Biol. Control* 33, 114–120. doi: 10.16409/j.cnki.2095-039x.2017.01.016

Daud, N. S., Rosli, M. A., Azam, Z. M., Othman, N. Z., and Sarmidi, M. R. (2019). *Paenibacillus polymyxa* bioactive compounds for agricultural and biotechnological applications. *Biocatal. Agric. Biotechnol.* 18:101092. doi: 10.1016/j.bcab.2019.101092

Du, N., Shi, L., Yuan, Y., Sun, J., Shu, S., and Guo, S. (2017). Isolation of a potential biocontrol agent *Paenibacillus polymyxa* NSY50 from vinegar waste compost and its induction of host defense responses against *Fusarium* wilt of cucumber. *Microbiol. Res.* 202, 1–10. doi: 10.1016/j.micres.2017.04.013

Fan, H., Zeng, L., Yang, P., Guo, Z., and Bai, T. (2016). First report of banana soft rot caused by *Klebsiella variicola* in China. *Plant Dis.* 100:517. doi: 10.1094/PDIS-05-15-0586-PDN

Geng, D., Shen, X., Xie, Y., Yang, Y., Bian, R., Gao, Y., et al. (2020). Regulation of phenylpropanoid biosynthesis by MdMYB88 and MdMYB124 contributes to pathogen and drought resistance in apple. *Hortic. Res.* 7:102. doi: 10.1038/s41438-020-0324-2

Glickmann, E., and Dessaux, Y. (1995). A critical examination of the specificity of the Salkowski reagent for indolic compounds produced by phytopathogenic bacteria. *Appl. Environ. Microbiol.* 61, 793–796. doi: 10.1128/aem.61.2.793-796.1995

Holt, J. G., Krieg, N. R., Sneath, P. H., Staley, J. T., and Williams, S. T. (1994). *Bergey's manual of determinative bacteriology. 9th Edn.* Baltimor: William & Wilkins.

Hong, C. E., Kwon, S. Y., and Park, J. M. (2016). Biocontrol activity of *Paenibacillus polymyxa* AC-1 against *pseudomonas syringae* and its interaction with *Arabidopsis thaliana*. *Microbiol. Res.* 185, 13–21. doi: 10.1016/j.micres.2016.01.004

Hu, Y., Gai, Y., Yin, L., Wang, X., Feng, C., Feng, L., et al. (2010). Crystal structures of a *Populus tomentosa* 4-coumarate: CoA ligase shed light on its enzymatic mechanisms. *Plant Cell* 22, 3093–3104. doi: 10.1105/tpc.109.072652

Jordá, T., and Puig, S. (2020). Regulation of ergosterol biosynthesis in *Saccharomyces cerevisiae*. *Genes* 11:795. doi: 10.3390/genes11070795

Kim, Y. S., Balaraju, K., and Jeon, Y. (2016). Biological control of apple anthracnose by *Paenibacillus polymyxa* APEC128, an antagonistic rhizobacterium. *Plant Pathology J.* 32, 251–259. doi: 10.5423/PPJ.OA.01.2016.0015

Liu, H., Li, Y., Ge, K., Du, B., Liu, K., Wang, C., et al. (2021). Interactional mechanisms of *Paenibacillus polymyxa* SC2 and pepper (*Capsicum annuum* L.) suggested by transcriptomics. *BMC Microbiol.* 21, 70–16. doi: 10.1186/s12866-021-02132-2

Liu, R., Li, J., Zhang, F., Zheng, D., Chang, Y., Xu, L., et al. (2021). Biocontrol activity of *Bacillus velezensis* D4 against apple Valsa canker. *Biol. Control* 163:104760. doi: 10.1016/j.biocontrol.2021.104760

Livak, K., and Schmittgen, T. (2001). Analysis of relative gene expression data using real-time quantitative PCR and the $2^{-\Delta\Delta CT}$ method. *Methods* 25, 402–408. doi: 10.1006/meth.2001.1262

Mei, L., Liang, Y., Zhang, L., Wang, Y., and Guo, Y. (2014). Induced systemic resistance and growth promotion in tomato by an indole-3-acetic acid-producing strain of *Paenibacillus polymyxa*. *Ann. Appl. Biol.* 165, 270–279. doi: 10.1111/aab.12135

Mohd Din, A. R. J., Rosli, M. A., Mohamad Azam, Z., Othman, N. Z., and Sarmidi, M. R. (2020). *Paenibacillus polymyxa* role involved in phosphate solubilization and growth promotion of *Zea mays* under abiotic stress condition. *Proc. Natl. Acad. Sci., India, Sect. B Biol. Sci.* 90, 63–71. doi: 10.1007/s40011-019-01081-1

Morrissey, J. P. (2009). *Biological activity of defence-related plant secondary metabolites. Plant-derived natural products*. New York: Springer, 283–299.

Nemesio-Gorriz, M., Hammerbacher, A., Ihrmark, K., Källman, T., Olson, Å., Lascoux, M., et al. (2016). Different alleles of a gene encoding leucoanthocyanidin reductase (*PaLAR3*) influence resistance against the fungus *Heterobasidion parviporum* in *Picea abies*. *Plant Physiol.* 171, 2671–2681. doi: 10.1104/pp.16.00685

Park, J. K., Kim, J. D., Park, Y. I., and Kim, S. K. (2012). Purification and characterization of a 1, 3-β-D-glucanase from *Streptomyces torulosus* PCPOK-0324. *Carbohydr. Polym.* 87, 1641–1648. doi: 10.1016/j.carbpol.2011.09.058

Piasecka, A., Jedrzejczak-Rey, N., and Bednarek, P. (2015). Secondary metabolites in plant innate immunity: conserved function of divergent chemicals. *New Phytol.* 206, 948–964. doi: 10.1111/nph.13325

Puri, A., Padda, K. P., and Chanway, C. P. (2016). Evidence of nitrogen fixation and growth promotion in canola (*Brassica napus* L.) by an endophytic diazotroph *Paenibacillus polymyxa* P2b-2R. *Biol. Fertil. Soils* 52, 119–125. doi: 10.1007/s00374-015-1051-y

Rahimi, S., Kim, J., Mijakovic, I., Jung, K. H., Choi, G., Kim, S. C., et al. (2019). Triterpenoid-biosynthetic UDP-glycosyltransferases from plants. *Biotechnol. Adv.* 37:107394. doi: 10.1016/j.biotechadv.2019.04.016

Samanta, A., Das, G., and Das, S. K. (2011). Roles of flavonoids in plants. *Carbon* 100, 12–35.

Shadle, G. L., Wesley, S. V., Korth, K. L., Chen, F., Lamb, C., and Dixon, R. A. (2003). Phenylpropanoid compounds and disease resistance in transgenic tobacco with altered expression of l-phenylalanine ammonia-lyase. *Phytochemistry* 64, 153–161. doi: 10.1016/S0031-9422(03)00151-1

Slama, H. B., Cherif-Silini, H., Chenari Bouket, A., Qader, M., Silini, A., Yahiaoui, B., et al. (2019). Screening for *Fusarium* antagonistic bacteria from contrasting niches designated the endophyte *Bacillus halotolerans* as plant warden against *Fusarium*. *Front. Microbiol.* 9:3236. doi: 10.3389/fmicb.2018.03236

Song, X., Han, M., He, F., Wang, S., Li, C., Wu, G., et al. (2020). Antifungal mechanism of dipicolinic acid and its efficacy for the biocontrol of pear Valsa canker. *Front. Microbiol.* 11:958. doi: 10.3389/fmicb.2020.00958

Thimmappa, R., Geisler, K., Louveau, T., O'Maille, P., and Osbourn, A. (2014). Triterpene biosynthesis in plants. *Annu. Rev. Plant Biol.* 65, 225–257. doi: 10.1146/annurev-arplant-050312-120229

Ullah, C., Unsicker, S. B., Fellenberg, C., Constabel, C. P., Schmidt, A., Gershenzon, J., et al. (2017). Flavan-3-ols are an effective chemical defense against rust infection. *Plant Physiol.* 175, 1560–1578. doi: 10.1104/pp.17.00842

Vanholme, R., Cesarino, I., Rataj, K., Xiao, Y., Sundin, L., Goeminne, G., et al. (2013). Caffeoyl shikimate esterase (CSE) is an enzyme in the lignin biosynthetic pathway in *Arabidopsis*. *Science* 341, 1103–1106. doi: 10.1126/science.1241602

Wang, X., Zang, R., Yin, Z., Kang, Z., and Huang, L. (2014). Delimiting cryptic pathogen species causing apple Valsa canker with multilocus data. *Ecol. Evol.* 4, 1369–1380. doi: 10.1002/ece3.1030

Yadav, V., Wang, Z., Wei, C., Amo, A., Ahmed, B., Yang, X., et al. (2020). Phenylpropanoid pathway engineering: an emerging approach towards plant defense. *Pathogens* 9:312. doi: 10.3390/pathogens9040312

Yang, X., Zhang, L., Xiang, Y., Du, L., Huang, X., and Liu, Y. (2020). Comparative transcriptome analysis of *Sclerotinia sclerotiorum* revealed its response mechanisms to the biological control agent, *Bacillus amyloliquefaciens*. *Sci. Rep.* 10, 12576–12512. doi: 10.1038/s41598-020-69434-9

Yin, Z., Liu, H., Li, Z., Ke, X., Dou, D., Gao, X., et al. (2015). Genome sequence of Valsa canker pathogens uncovers a potential adaptation of colonization of woody bark. *New Phytol.* 208, 1202–1216. doi: 10.1111/nph.13544

Yu, F., Feng, Y., Han, J., Sheng, Q., Sun, L., and Luo, M. (2021). Screening of antagonistic bacteria against *Valsa pyri* from agricultural plant Jiaosu and their control effects on pear canker. *J. Agric. Sci. Technol.* 23, 125–135. doi: 10.13304/j.nykjdb.2021.0226

Yu, G., Wang, L., Han, Y., and He, Q. (2012). ClusterProfiler: an R package for comparing biological themes among gene clusters. *OMICS* 16, 284–287. doi: 10.1089/omi.2011.0118

Yuan, H., Shi, B., Huang, T., Zhou, Z., Wang, L., Hou, H., et al. (2021). Biological control of pear Valsa canker caused by *Valsa pyri* using *Penicillium citrinum*. *Horticulturae* 7:198. doi: 10.3390/horticulturae7070198

Yuan, H., Shi, B., Wang, L., Huang, T., Zhou, Z., Hou, H., et al. (2022). Isolation and characterization of *Bacillus velezensis* strain P2-1 for biocontrol of apple postharvest decay caused by *Botryosphaeria dothidea*. *Front. Microbiol.* 12:808938. doi: 10.3389/fmicb.2021.808938

Zhai, Y., Zhu, J., Tan, T., Xu, J., Shen, A., Yang, X., et al. (2021). Isolation and characterization of antagonistic *Paenibacillus polymyxa* HX-140 and its biocontrol potential against *Fusarium* wilt of cucumber seedlings. *BMC Microbiol.* 21, 75–12. doi: 10.1186/s12866-021-02131-3

Zhang, F., Li, X., Zhu, S., Ojaghian, M. R., and Zhang, J. (2018). Biocontrol potential of *Paenibacillus polymyxa* against *Verticillium dahliae* infecting cotton plants. *Biol. Control* 127, 70–77. doi: 10.1016/j.biocontrol.2018.08.021

Zhang, Q., Xing, C., Li, S., He, L., Qu, T., and Chen, X. (2021). In vitro antagonism and biocontrol effects of *Paenibacillus polymyxa* JY1-5 against *Botrytis cinerea* in tomato. *Biol. Control* 160:104689. doi: 10.1016/j.biocontrol.2021.104689

Zhou, C., Guo, J., Zhu, L., Xiao, X., Xie, Y., Zhu, J., et al. (2016). *Paenibacillus polymyxa* BFKC01 enhances plant iron absorption via improved root systems and activated iron acquisition mechanisms. *Plant Physiol. Biochem.* 105, 162–173. doi: 10.1016/j.plaphy.2016.04.025

frontiers | Frontiers in Microbiology

ORIGINAL RESEARCH
published: 22 July 2022
doi: 10.3389/fmicb.2022.912632

Lactic Acid Bacteria as Potential Biocontrol Agents for Fusarium Head Blight Disease of Spring Barley

*Micheal B. Byrne[1], Ganesh Thapa[2], Flona M. Doohan[2] and James I. Burke[1]**

[1] School of Agriculture and Food Science, University College Dublin, Dublin, Ireland, [2] School of Biology and Environmental Science, University College Dublin, Dublin, Ireland

Fusarium head blight (FHB) is a devastating disease encountered by spring-grown barley. Traditionally, synthetic chemicals have been used to control this disease on small grain cereals. A move toward biological control agents as part of sustainable agriculture is pertinent due to the evolutionary mechanisms employed by fungal diseases to circumvent current protection strategies. This study evaluated the effect of six lactic acid bacteria isolates on the development of FHB under *in vitro* and glasshouse conditions. The relative expression of *Fusarium* marker genes and transcription factors under *Fusarium* infection was examined. Dual-culture assays observed inhibition zones of up to 10 and 17% of total plate area for *L. amylovorus* FST 2.11 and *L. brevis* R2Δ, respectively. Detached leaf assays validated the antifungal activity and showed the potential of all test isolates to significantly inhibit sporulation of *Fusarium culmorum* and *Fusarium graminearum* strains. Spray inoculation of lactic acid bacteria to barley spikelets prior to *Fusarium* spore application significantly reduced disease severity for five candidates ($P < 0.05$) under glasshouse conditions. Mycotoxin analysis revealed the ability of *L. amylovorus* DSM20552 to significantly reduce deoxynivalenol content in spikelets ($P < 0.05$). A preliminary gene expression study showed the positive influence of lactic acid bacteria on the expression of important defense-related marker genes and transcription factors upon FHB. These results indicate the potential of lactic acid bacteria to be included as part of an integrated pest management strategy for the management of FHB disease. This strategy will reduce FHB severity and deoxynivalenol (DON) contamination of spring barley, leading to high acceptance in the grain market.

Keywords: biological control, *Fusarium* head blight, lactic acid bacteria, barley (*Hordeum vulgare* L.), *pathogenesis-related* (PR) genes

OPEN ACCESS

Edited by:
Xiaodan Wang,
China Agricultural University, China

Reviewed by:
Fuguo Xing,
Institute of Food Science and Technology (CAAS), China
M. Y. Sreenivasa,
University of Mysore, India

***Correspondence:**
James I. Burke
jimmy.burke@ucd.ie

Specialty section:
This article was submitted to Microbe and Virus Interactions with Plants, a section of the journal Frontiers in Microbiology

Received: *04 April 2022*
Accepted: *07 June 2022*
Published: *22 July 2022*

Citation:
Byrne MB, Thapa G, Doohan FM and Burke JI (2022) Lactic Acid Bacteria as Potential Biocontrol Agents for Fusarium Head Blight Disease of Spring Barley. Front. Microbiol. 13:912632. doi: 10.3389/fmicb.2022.912632

INTRODUCTION

Barley (*Hordeum vulgare* L.) is among the world's first domesticated land plants that has underpinned the development of present-day civilizations. It is one of the most important food staples considered to be the premium grain used by malting and brewing industries (Ullrich, 2010; CGIAR, 2012; Murphy, 2016). The Irish brewing and distilling sector has shown a growth rate of 4% between 2014 and 2019 with a 22% increase in the number of micro-breweries. The number of distilleries has increased to 38 in 2020 with global sales at 20 million nine-liter cases

(Umego and Barry-Ryan, 2022). Therefore, it is imperative that we provide an active concern for world barley production and the threats associated with the escalation of crop losses as we enter an era of uncertainty surrounding food security. FHB is a serious spoilage disease encountered by barley, wheat (*Triticum aestivum*), and other small grain cereals worldwide (McMullen et al., 1997; Wegulo et al., 2015; Gunupuru et al., 2018). Primary agents of the disease vary across geographical regions with *Fusarium graminearum*, *Fusarium culmorum*, *Fusarium poae,* and *Fusarium avenaceum* encountered by European cereal growers (Bottalico and Perrone, 2002; Wegulo et al., 2015; Beccari et al., 2017). *Fusarium* species are also the causal organism of *Fusarium* foot rot and *Fusarium* seedling blight of small grain cereals resulting in reduced germination and poor plant establishment leading to intensified yield and quality losses (Brennan et al., 2003; Goswami and Kistler, 2004; Khan et al., 2006; Scherm et al., 2013). Accordingly, barley's worth as a seed source for malt production for brewing and other food industries declines (Parry et al., 1995; Scherm et al., 2013; Hückelhoven et al., 2018). In barley, Fusaria of the FHB complex secure our attention as they produce a wide range of mycotoxins including: DON, HT-2 toxin, T-2 toxin, aflatoxin, and ochratoxin, known instigators of chronic and acute mycotoxicosis in humans and animals (Placinta et al., 1999; Haidukowski et al., 2005; Nielsen et al., 2014; Bolechová et al., 2015). The consequence of extreme disease outbreaks resulting in an FHB epidemic has been seen with extensive economic and sociological impacts (Jones, 2000; McMullen et al., 2012).

To circumvent additional costs associated with reduced yield, poorer quality, and extra costs of cleaning grain, synthetic fungicides have traditionally been applied to prevent FHB disease outbreaks (Smiley et al., 2005; Blandino et al., 2012; Matny, 2015). However, the efficacy of available fungicides is uncertain due to the evolving nature of *Fusarium*, changing weather patterns, and the inherent variability of cultivar resistance (Simpson et al., 2001; Magan et al., 2002; Blandino et al., 2012; Talas and McDonald, 2015). Even with the introduction of disease predictive models allowing for optimal timing of fungicide applications, their employment only remains practical for a one-off application at mid-anthesis, with further treatment costs failing to be justified by yield and quality improvements (McMullen et al., 1997; D'Angelo et al., 2014). Extensive field studies on azole-based fungicides to manage FHB and mycotoxin accumulation presented reductions between 40 and 70%, respectively (Paul et al., 2008, 2018; Willyerd et al., 2012; D'Angelo et al., 2014). However, with increscent fungicide applications, over time, gradual resistance among the target organisms is a real possibility (Ferrigo et al., 2016). Notably, the application of the fungicide azoxystrobin 2 days post-artificial inoculation of wheat spikelets with *Fusarium* spp. resulted in enhanced DON production per unit of pathogen (Simpson et al., 2001). Another study quantified that sub-lethal levels of prothioconazole increased DON production in wheat (Audenaert et al., 2010). Consequently, there has been a renewed focus on the implementation of integrated pest management (IPM) systems as both an economically and ecologically justified means to reduce the risks to human health and the environment (Union, 2009; Pretty and Bharucha, 2015; Cowger et al., 2016).

To date, research has focused on the development of proficient biological control agents (BCAs), with the aim of contriving new commercially applicable FHB antagonists (Wachowska and Głowacka, 2014; Xue et al., 2014; Wang et al., 2015). A potential group of 22 endophytes to control *F. graminearum* (30–51% inhibition) and *F. culmorum* (15–53% inhibition) *in vitro*, including the discovery of three novel endophytic species, i.e., *Aureobasidium proteae, Phoma glomeramycota* and *Sarocladium kiliense*, have been reported (Comby et al., 2017). Recently, the mode of action of the known antifungal species *Bacillus amyloliquefaciens* Y1 has been identified as the antifungal compound cyclo(D-PRO-L-VAL), which was characterized using H1 and C13 nuclear magnetic resonance techniques (Jamal et al., 2017). Furthermore, it has been shown that detoxification of mycotoxin-infused produce, including grain, is possible through the addition of biological agents prior to and during the processing of foodstuffs (Petchkongkaew et al., 2008; Tian et al., 2016). Field trials gave comparable results for reductions in DON accumulation and FHB severity following applications of *Bacillus* subtilis strain RC218 (Palazzini et al., 2016; Cantoro et al., 2021). Several strains of lactic acid bacteria (LAB) have similarly shown promise through their enhancement of organoleptic properties and ability to mitigate fungal contamination of foodstuffs, most notably their incorporation into starter cultures during malting and the formulation of probiotics (Schnürer and Magnusson, 2005; Kedia et al., 2007; Franco et al., 2011; Rathore et al., 2012; Nakkarach and Withayagiat, 2018). The versatile use potential was further confirmed to reduce mycotoxin accumulation and gushing when applied to barley *in situ* (Lowe and Arendt, 2004; Peyer et al., 2016). It is considered that their role in fungal inhibition is through the production of organic acids, proteinaceous compounds, and other low molecular weight compounds (Lynch et al., 2016; Siedler et al., 2019). Despite making major progress, the role of many BCAs in the regulation of plant defense responses, mechanistic of LAB-mediated resilience to biotic stresses, viz., FHB disease of barley, remains limited (Miedaner et al., 2018; Gómez-Lama Cabanás et al., 2021).

As a pathogen-associated molecular pattern (PAMP) is conserved molecules among pathogens and PAMP-triggered immunity (PTI) contributes to basal and non-host resistance, the transfer of pattern recognition receptors (PRRs) might confer resistance to current pathogens in crops by recognition of undetected epitopes (Schoonbeek et al., 2015). Hence, expression analysis of selected PRRs, transcription factors, kinase, and R genes was performed on FHB infection in barley to ascertain its role in resistance. Interestingly, silencing of the chitin elicitor-binding protein (CEBiP) orthologous gene in barley increases susceptibility to the fungus *Magnaporthe oryzae* (Tanaka et al., 2010), suggesting that CEBiP may be involved in chitin perception. *TaMPK3*, which encodes a MAP kinase, involved in resistance to *Mycosphaerella graminicola* (Rudd et al., 2008). A wheat pore-forming toxin-like (PFT) homolog of *HvPFT* gene was highly expressed and regulatory FHB-resistant gene in Sumai 3 (He et al., 2018). The transcription factor *HvWRKY23*

regulates flavonoid glycoside and hydroxycinnamic acid amide biosynthetic genes in barley to combat FHB (Karre et al., 2019), whereas *TaWRKY70* in wheat *QTL-2DL* regulates downstream metabolite biosynthetic genes to resist *Fusarium graminearum* infection spread within spike (Kage et al., 2017). Expression of salicylate-responsive *pathogenesis-related 1* (*HvPR1*) was strongly induced by *Fusarium graminearum* strain Fg-IFA65GFP in barley leaves (Koch et al., 2016). The homolog ubiquitin ligase gene *PUB23*-like was highly induced in response to *Fusarium* PAMP treatment in *Arabidopsis* (Trujillo et al., 2008). The wheat homologs of *HvLOX2, HvCOI1, HvICS1, HvPAL1, HvNPR1,* and *HvNPR3* were reported to have a regulatory role in FHB resistance (Thapa et al., 2018). The wheat homolog of *HvCamBP* is a particularly good marker due to robust upregulation upon PAMP treatment (Schoonbeek et al., 2015), whereas the CRISPR/Cas9 editing of susceptibility *SWEET1* gene provides the potential for the development of FHB-resistant barley (Ahmad et al., 2020). As most of the genes get upregulated upon FHB infection, their selection in gene for expression analysis may reveal a resistance mechanism and can be used as PTI marker genes in barley.

The research evaluated the ability of six LAB isolates to inhibit *Fusarium* spp. and the *Fusarium* infection of spring barley through *in vitro* and glasshouse experiments. *In vitro* dual-culture assays were followed by detached leaf assays. FHB trials were established under glasshouse conditions, and a gene expression study examined the potential priming capabilities of starter cultures of LAB on the regulation of spring barley defense gene expression.

MATERIALS AND METHODS

Plant Material

The Spring barley cv. "Sanette" used for *in vitro* and glasshouse studies was kindly provided by Gold Crop Ltd. (Cluide, Dunleer, Co., Louth, Ireland).

Lactic Acid Bacteria, *Fusarium,* and Their Culture

LAB isolates (**Table 1**) were chosen based on their ability to inhibit the growth of *F. culmorum* strain TMW4.2043 *in vitro* (Axel et al., 2016), which reported that *F. culmorum* strain 126 TMW4.2043 growth was inhibited by these selected LABs depending upon the synthesis of antifungal-active acids such as 3-phenyllactic acid, 4-hydroxyphenyllactic acid and 2-hydroxyisocaproic acid in quantities between 0.1 and 360 mg/kg. *L. reuteri* M13, lacking antifungal activity, was selected as a negative control (Lynch et al., 2016; Peyer et al., 2016). LAB were re-cultured regularly on de Man, Rogosa, and Sharpe (MRS) agar-filled Petri plates (M.R.S AGAR, Oxoid Ltd., Hampshire, United Kingdom) as per Meroth et al. (2003). Cultures were incubated at 30°C (*L. amylovorus* and *L. brevis* strains) and 37°C (*L. reuteri* strains) for 48 h under static conditions, and they were stored short term at 4°C. Single colonies were sub-cultured and used to inoculate 10 ml of de man, Rogosa, and Sharpe broth (MRS broth, Oxoid Ltd., Hampshire, United Kingdom). After a 24-h period, bacteria were sub-cultured at 1% into MRS broth at the respective temperatures for a further 48 h. Growth was observed through the assessment of the optical density of MRS broth at 620 nm (OD620) (Kedia et al., 2007). *Fusarium graminearum* strain GZ3639 and *Fusarium culmorum* strain FCF 200 were obtained from the UCD School of Biology and Environmental Science fungal collection (the former kindly provided by Robert Proctor, USDA). Fresh asexual macroconidia of both *Fusarium* spp. were cultured, and conidia were prepared as per the method outlined by Brennan et al. (2003). Following incubation, cultures were washed, and spores were counted using a haemocytometer (Hycor Biomedical) and adjusted to the 2×10^5 spores/ml using 0.2% Tween 20 (VWR Chemicals, Pennsylvania, United States).

Fungicide Preparation

The fungicide Fandango® (Bayer CropScience Ltd., Dublin, Ireland) was used as a comparative treatment based on its commercial use against foliar, spikelet, and stem base diseases of small grain cereals. It was prepared as per manufacturers' recommendations at the rate of 1.25 L/ha (Bayer CropScience Ltd., Dublin, Ireland).

Dual-Culture Assay

Antifungal activity of the selected LAB against *F. graminearum* strain GZ3639 was observed using a modified version of the dual-culture assay (Khan et al., 2006). Potato dextrose agar (PDA; Oxoid Ltd., United Kingdom) plates were inoculated with mycelial plugs (10 mm diameter) from 7-day-old *Fusarium* cultures placed at the center of each plate. Three sterile 1.0-cm Whatman filter paper disks (Whatman plc, Buckinghamshire, United Kingdom) were equidistantly placed at the perimeter of each plate 26 mm from mycelial plugs. Ten microliter aliquots of LAB (log CFU/ml = 9) were pipetted onto each disk (MRS broth was used as a negative control). Plates were incubated at 21°C ± 1°C in darkness. The antifungal activity was evaluated by measuring the area of the inhibition surrounding individual filter paper disks 168 h post-incubation, using ImageJ software (NIH, United States). A total of three trials were completed. Each trial consisted of three biological replications for each treatment and control.

Detached Leaf Assay

This experiment was a modification of the detached leaf assay (Chen et al., 2006). Four seeds were sown in 4-cm pots containing John Innes Number 2 compost (John Innes

TABLE 1 | Lactic acid bacteria.

Species	Isolate code	References
Lactobacillus amylovorus	FST 2.11	UCC, Cork, Ireland
Lactobacillus amylovorus	DSM 20552 (–)	UCC, Cork, Ireland
Lactobacillus reuteri	R29 (+)	Axel et al., 2016
Lactobacillus reuteri	*M13 (–)*	Lynch et al., 2016
Lactobacillus amylovorus	*DSM20053 (–)*	UCC, Cork Ireland
Lactobacillus brevis	*R2*Δ (+)	Axel et al., 2016

Manufacturer Association, Berkshire, United Kingdom) and grown at 20°C ± 4°C under artificial light conditions of 16-h light/8-h dark cycle at 150 μmol m-2 s-1. The relative humidity was maintained at 50% ± 5%. Seedlings were thinned to two per pot 7 days after germination. After 21–25 days, second true leaves, growth stage 12 (Zadoks et al., 1974), were detached. Leaf sections (6 cm) were placed adaxial side up in square Petri dishes on 10% plant nutrient agar (Duchefa, Netherlands), pH 5.7, comprising 0.67 μM benzimidazole (Oxoid Ltd., Hampshire, United Kingdom). Treatments were positioned centrally along the midrib of each leaf section. They consisted of 10 μl containing 1×10^6 *F. graminearum* strain GZ3639 conidia ml^{-1} 0.02% Tween 20 and 20 μl aliquot of the chosen LAB. The negative control treatment combination was 10 μl of 0.02% (v/v) Tween 20 and 20 μl of MRS broth. The positive fungal control treatment combination was 10 μl of 1×10^6 *F. graminearum* strain GZ3639 conidia ml^{-1} 0.02% Tween 20 and 20 μl of MRS broth. The fungicide Fandango® was incorporated as a comparative treatment. The same inoculation method and pattern were followed for *F. culmorum* experiment wherein *F. culmorum* spores were used. The treated leaves in plates were incubated under the conditions. The number of conidia per leaf section was determined at 5 dpi as per Chen et al. (2006). Starting at 48 hpi, mycelial spread was measured using ImageJ computer software (NIH, United States). Disease severity was assessed per the relative lesion area (RLA) at 48, 72, 96, and 120 h post-inoculation. RLA was calculated using the formula %RLA = 100 × (total area of lesions)/(total leaf area). A total of three replicate trials were completed. Each replicate trial consisted of 12 biological replicates for each treatment and control.

FHB Severity and Mycotoxin Analysis

An adult plant experiment was conducted to establish the effects of LAB on FHB development and mycotoxin accumulation. Four pre-germinated seedlings were transferred at 10-cm spacings into 3-L containers of John Innes Number 3 compost (John Innes Manufacturer Association, Berkshire, United Kingdom). Plants were placed in an unlit, ventilated greenhouse. Natural light levels were maintained under shading engaged at 60,000 lux m−1 and retracted at 50,000 lux m-1. Seedlings were culled to two per container after 20 days. Plants were irrigated three times weekly along with an added liquid feed of 18–18–18 at a dilution of 1:1,000 weekly with a granular feed of 22-5-6 + 2 Mg + TE (4–5 months, Osmocote® Topdress FT, Everris International BV, Netherlands, containing 22% nitrogen, 2.2% phosphorous, 5% potassium, 1.2% magnesium and trace elements) applied 14 days after transplanting and ca.1 week prior to applications of biocontrol agents.

Spray inoculations (4 ml) of LAB isolates at a concentration of log CFU/ml = 9 (onto secondary tillers) were made ca. 24 h prior to mid-anthesis. Control heads were treated with MRS broth. At mid-anthesis [growth stage 65 (Zadoks et al., 1974)], heads were treated with 4 ml of 0.02% (v/v) Tween 20 (control) or 4 ml of 0.02% (v/v) Tween 20 (mock) supplemented with 2×10^5 conidia ml^{-1} of *F. graminearum* strain GZ3639. Directly after inoculations, all treated heads were enclosed in resealable bags for 3 days. A total of three trials were completed. Each trial consisted of eight biological replicates for each treatment/control arranged in a randomized block design. Disease severity was estimated by counting the number of infected spikelets per ear and expressing this as a percentage of total spikelet infections at 5, 10, and 14 dpi. *Fusarium* infection was identified as brown discolored lesions with premature blanching of individual spikelets (McCallum and Tekauz, 2002; McMullen et al., 2012). The treated spikelets were harvested at plant senescence (growth stage 99 (Zadoks et al., 1974). A total of three biological replicates were completed. Each biological replicate consisted of 32 trials for each treatment and control. Spikelets were dried in a desiccator with silica gel beads for 14 days. Spikelets were triturated using a Glen Creston Hammer Mill and sieved through a 1.0-mm mesh sieve. Sieved samples were bulked according to the treatment per replicate. Mycotoxin testing was carried out for DON, aflatoxin, ZEA T-2 toxin, and ochratoxin by© Sciantec Analytical Laboratories using specific R-Biopharm RIDASCREEN® enzyme-linked immunosorbent assay (ELISA) tests. The absorbance value measured at 450 nm with the RIDA®SOFT Win (Art. No. Z9999) software package (R-Biopharm, Darmstadt, Germany) was used to deduce the toxin content of each sample.

Analysis of Defense Gene Expression in Adult Barley Plants

A separate experiment used quantitative reverse transcriptase-polymerase chain reaction (qRT-PCR) analysis to elucidate the effect of LAB isolates on the regulation of important defense genes and transcription factors in flowering barley heads (**Table 2**). Spikelets were treated with the same LAB, *Fusarium,* and control treatments detailed above. The treated spikelets were harvested at 12-, 24-, 48-, 72- and 120-h time points post-fungal inoculation. RNA was extracted using Trizol™ reagent according to the manufacturers' specifications (Thermo Fischer Scientific, Massachusetts, United States) (Chomczynski, 1993). Reverse transcription of total RNA was performed as previously described (Meroth et al., 2003; Walter et al., 2008). Accumulated threshold cycle (Ct) values were obtained by qPCR, and the barley genes *HvActin* and *HvU-61* were used as housekeeping genes to calculate the relative expression of the selected defense genes. The formula described previously (Livak and Schmittgen, 2001) was used to calculate relative gene expression: $2\text{-}\Delta$ (Ct target gene—Ct housekeeping gene). This gene expression study was based on an FHB experiment comprised of three biological replicates with 32 trials for each treatment in each biological replicate. Each treatment time point consisted of 3–4 pooled spikelets from two separate plants per replicate. All real-time RT-PCR analyses were performed two times (two cDNAs generated from independent reverse transcriptions from each individual sample of RNA) for all the treatments.

Statistical Analysis

All data from *in vitro* and glasshouse experiments were analyzed in R v4.0.2 (R Core Team). Normality was tested using the Shapiro–Wilk test. Non-normal data were analyzed by a pairwise

TABLE 2 | List of genes and primers used for real-time expression studies.

Genes/Annotation	Forward primer (5′-3′)	Reverse primer (5′-3′)	References
Hvtub/tubulinα-2 chain	GTCCACCCACTCCCTCCTTG	CGGCGGCAGATGTCATAGATG	Ali et al., 2014
HvActin/actin	CCACGAGACGACCTACAAC	CACTGAGCACGATGTTTCC	Ferdous et al., 2015
HvGADPH/glycolytic glyceraldehye-3-phosphate dehydrogenase	GCCAAGACCCAGTAGAGC	CACATTTATTCCCATAGACAAAGG	
HvPR1/pathogenesis-related protein	ACTACTACCTTTCACCCCACAAC	GATCCTCTGGTTGGCGTA	
HvPFT3B/pore-forming protein-like	CACGTTCGACACCATCCTG	GATGAACACCGAGTAGCTCC	
FgActin/Fusarium graminearumγ-actin	ATGGTGTCACTCACGTTGTCC	CAGTGGTGGAGAAGGTGTAACC	Brown et al., 2011
HcWRKY70/transcription factor	GACAATCCCTCCACACCAAG	TCACTCCTGCTCCACCTAG	
HvCAMBP1/calmodulin-binding protein	CGCGTTCGAGGAGAAACAAG	CGTACCTTGACCAGCCTTGT	
HvWRKY23/WRKY transcription factor	GAGCGTAGACGTCAGCACCA	CACGGATGCTAATGGCCACC	
HvPUB23/ubiquitin ligase protein	CGTTCATCAGAATGCTCAGCTG	TTCTCTTTTGTAGGCACGAACCA	
HvLOX2/lipoxygenase for jasmonic acid synthesis	GCACCGCCTGCTGCACCCGC	CGGCTGACGAGGTCCTCCGGCG	
HvCOI1/coronatine-insensitive protein 1	CATTGTGCGAGTGAACTGTGACA	CGCGGAAACCAGACAAGCT	
HvICS1/isochorismate synthase 1	CGGACGGCCCCGCCGAGGAC	CGCGGCGGTCGACGCGGCGGGA	
HvPAL1/phenylalanine ammonia lyase 1	CGACGAGGTCAAGCGCATGGT	CGGCTGCTCTCCTTGACGCGG	Dempsey et al., 2011
HvNPR1/regulatory receptor protein 1	CGCGGACGTGGAGGCGCTCCGC	CCGGTTGCCCTCGGCGCCGCCG	
HvNPR3/regulatory receptor protein3	ATGGAGCCGTCGTCGTCCATCA	TCCGCCACGTCGACGTCGGCGT	Zhang et al., 2006
HvMPK3/MAP kinase 3	ACCCTTACCTAGAGCGGC TTC	ACTCCAGGGCTTCGTTGAATA	

Kruskal–Wallis test. Correlations of data were tested using Spearman's rank correlation coefficient analysis. Data from gene expression studies were analyzed using GraphPad Prism6® (GraphPad Software, San Diego, California, United States).

RESULTS

Assessment of the Inhibitory Effect of Lactic Acid Bacteria Against *Fusarium graminearum* in Dual Cultures

Dual-culture assays assessed the capacity of six *Lactobacillus* strains to inhibit the spread of mycelium from *Fusarium graminearum* GZ3639. The maximum inhibition was provided by *L. brevis* R2Δ with an average reduction of 17% in mycelial growth ($p < 0.05$) (**Table 3**). Both *L. amylovorus* FST 2.11 and *L. amylovorus* DSM 20053 significantly reduced mycelial spread compared with the control ($P < 0.05$). The three remaining *Lactobacillus* isolates, namely, *L. amylovorus DSM 20552, L. reuteri M13* and *L. reuteri* R29, failed to significantly inhibit mycelial spread compared with the control ($p > 0.05$). No clear zone of inhibition was observed at the point of contact between the control (MRS broth) and the fungus. In addition to mycelial impedance, it was observed that *L. amylovorus* FST 2.11 altered hyphal color from cream/light pink to a bright pink/red hue (**Figure 1**).

Assessment of the Ability of Lactic Acid Bacteria to Inhibit *Fusarium* Infection, as Determined Using a Detached Leaf Assay

Based on the mycelial growth inhibition *in vitro* assay, the selected LAB was assessed *in plant* for the fungal spread and sporulation suppression of *F. graminearum* and *F. culmorum* using a modified leaf detachment assay (Chen et al., 2006). No *Fusarium*-like lesions appeared on control treatments (MRS broth and Tween 20). On all other treatments, at 120 hours post-inoculation (hpi), all leaves displayed brown necrotic lesions typical of *Fusarium* infection (Koch et al., 2013). Lesion area on leaves treated with the positive control of both test fungi was significantly larger than that of the negative control at 120 hpi, although these differences were only significant from 72 hpi onward ($p < 0.001$). The positive control across both *Fusarium* spp. resulted in the highest average relative lesion area, as compared to all other treatments (**Figure 2A**). Lesion size was expressed as a percentage of infection to control treatment 10 μl of 0.02% (v/v) Tween 20 and 20 μl of MRS broth. For the leaves treated with LAB in combination with *F. culmorum*, the most effective isolates minimizing lesion size

TABLE 3 | Percentage of growth inhibition of *F. graminearum* by six *Lactobacillus species* under *in vitro* dual-culture conditions.

Bacterial *spp.*	Isolate	Average area of fungal inhibition (mm^2)	% Inhibition of fungal mycelium (after 7 days)
L. brevis	R2Δ	485.2425	17.16 *
L. amylovorus	DSM 20053	255.42	9.03 *
L. amylovorus	FST 2.11/ DSM19280	296.6725	10.49 *
L. amylovorus	DSM 20552	101.5875	3.59
L. reuteri	R29	58.46	2.06
L. reuteri	M13	142.7625	5.04
MRS broth		4.7525	0.16

**Indicates a significant difference in the% inhibition of fungal mycelium compared with the control treatment (P < 0.05).*

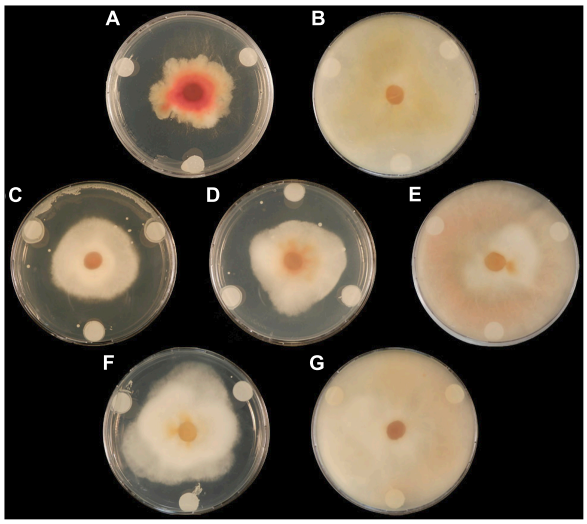

FIGURE 1 | The effect of lactic acid bacteria on radial growth of *F. graminearum* GZ3639 on potato dextrose agar plates at 7 days. Treatments **(A)** (*L. amylovorus* FST 2.11), **(C)** (*L. brevis* R2Δ), and **(D)** (*L. amylovorus* DSM 20053) displayed clear zones of fungal inhibition compared with the control ($P < 0.05$), whereas treatments **(B)** (*L. reuteri* M13), **(E)** (*L. reuteri* R29), and **(F)** (*L. amylovorus* DSM 20552) displayed lowered antifungal activity ($P > 0.05$). Control treatment **(G)** (MRS broth) displayed no inhibition.

were *L. amylovorus* DSM 20053 (24%), *L. amylovorus* FST 2.11 (26%) and *L. brevis* R2Δ (32%).

The fungicide Fandango® provided significantly higher levels of disease suppression compared with all LAB isolates ($P < 0.001$) except *L. amylovorus* DSM 20552. Against *F. graminearum*, all LAB isolates significantly reduced diseased lesion area compared with the positive control (MRS + *F. graminearum*) ($P < 0.05$). The effect of LAB on sporulation of both *Fusarium* species was examined. Leaves treated with the positive control resulted in significantly greater spore quantities than those of the negative control ($P < 0.001$). All LAB isolates displayed an ability to reduce sporulation of *F. graminearum* compared with the positive control ($P < 0.001$) (**Figure 2D**). Leaves treated with Fandango® + *Fusarium graminearum* resulted in a larger lesioned area than that of the negative control of MRS + Tween 20 ($p > 0.05$). Leaves inoculated with the test fungus *F. graminearum* and MRS broth brought about the largest relative lesion area (68%), while *L. brevis* R2Δ and *L. amylovorus* DSM 20552 were the LAB that caused the greatest lesion inhibition at 24 and 23%, respectively (**Figure 2C**). Compared with the positive control, sporulation of *F. graminearum* saw the biggest reduction by *L. amylovorus* FST 2.11 with an average spore count of 2.3 per detached leaf ($p < 0.001$). Subsequent bacteria which significantly reduced sporulation of *F. graminearum* included *L. reuteri* R29 and *L. amylovorus* DSM 20053 with average spore counts of 2.61 and 3.00 per detached leaf, respectively ($p < 0.001$).

Comparable results were observed for detached leaves co-inoculated with *F. culmorum and* LAB (**Figures 2B,D**). The positive treatment resulted in the highest levels of spore production which were significantly higher (504.22) than most LAB treatments ($P < 0.001$). The exception was *L. amylovorus* DSM 20552 which did not have a significantly reduced spore count ($p > 0.05$). LAB isolates with the greatest inhibition of spore count included *L. amylovorus* FST 2.11 and *L. amylovorus* DSM 20053 which did not differ significantly when compared with the negative control ($p > 0.05$). No correlations between treatments were found for LAB co-inoculations against both test fungi.

Evaluation of the Effect of Lactic Acid Bacteria Treatments on FHB Development and Mycotoxin Accumulation Under Greenhouse Conditions

An FHB experiment assessed the impact of *L. amylovorus* FST 2.11, *L. amylovorus* DSM 20552, *L. amylovorus* DSM 20053, *L. reuteri* M13, *L. brevis* R2Δ, and *L. reuteri* R29 (**Table 1**) on disease development and mycotoxin accumulation in grain. Disease severity scoring was assessed at 5, 10, and 14 dai and used to calculate the area under disease pressure curve (AUDPC) (Jeger and Viljanen-Rollinson, 2001; Legzdina and Buerstmayr, 2004; Legzdina et al., 2013). Disease symptoms were minimal but not completely absent on spikelets treated with Tween 20 (mock). This is likely due to the heightened levels of background infection after unnatural levels of inoculum were applied to the neighboring plants. The majority of LAB treatments significantly reduced FHB severity compared with the positive control of MRS + *F. graminearum* (**Figure 3**). The exception was heads treated with *L. reuteri* R29, which showed no significant reduction compared with the positive control ($\boldsymbol{P} > 0.05$). A noteworthy observation was the deleterious effect that early inoculations of MRS broth, and MRS broth containing bacterial cultures, had on spike maturation. In some cases, heads treated more than 24 h before mid-anthesis commenced premature cessation.

Spikelets were analyzed for the mycotoxins DON, aflatoxin, ochratoxin A, T-2 toxin, and zearalenone (**Figure 4**). Correlation of mycotoxin accumulation was moderate to strong between the three trials ($r > 0.55$) across all treatments. DON was the highest recorded mycotoxin at 204.4 μg/kg. Ochratoxin A levels were undetectable using ELISA. Mycotoxin accumulation of DON, T-2 toxin, ZEA, and aflatoxin was not significantly different across treatments from three replications ($p > 0.05$). Although mycotoxin accumulation was generally higher in the samples treated with MRS broth and *Fusarium* than in samples treated with LAB and *Fusarium*, no significant differences were found in mycotoxin accumulation between LAB treatments, once *P*-values were adjusted for multiple comparison testing.

The Effect of Lactic Acid Bacteria on Defense Gene Expression in Spikelet Tissue

Quantitative real-time PCR (qRT-PCR) was used to quantitatively determine the effect of LAB isolates on the

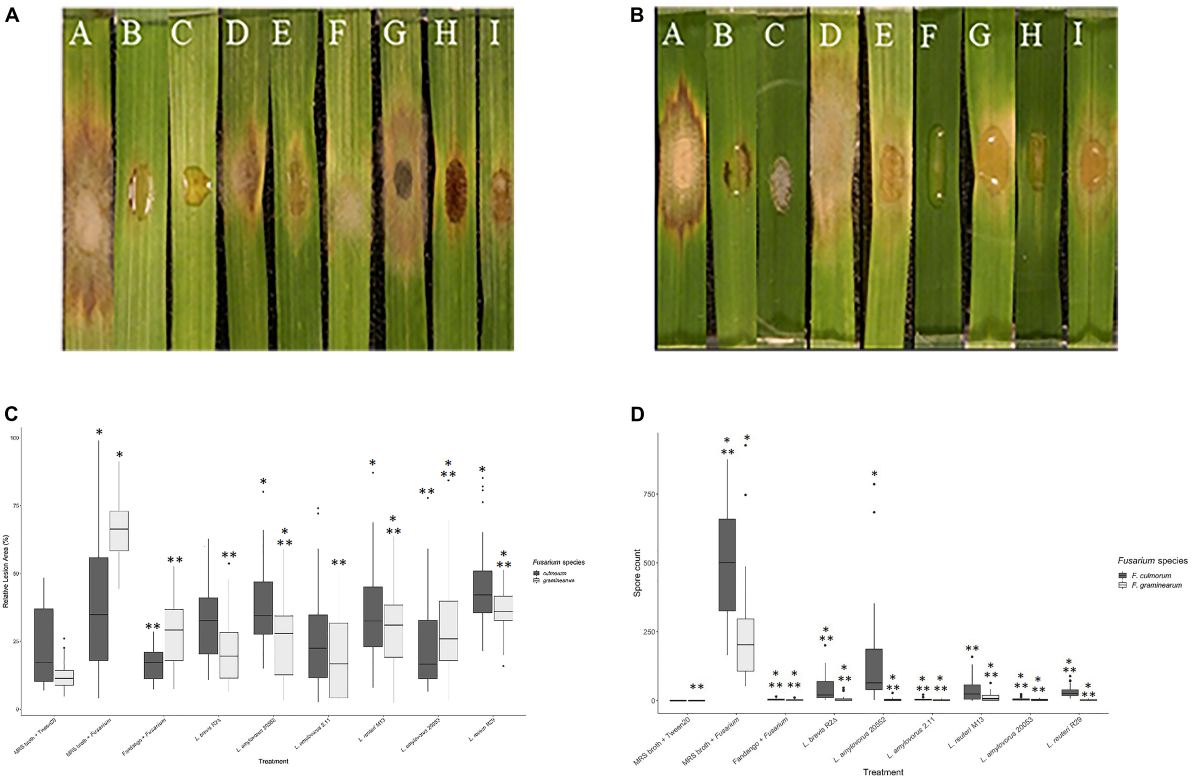

FIGURE 2 | Effect of lactic acid bacteria on the mycelial growth of *Fusarium spp.* using detached leaf assay. **(A)** Treatments were applied simultaneously. Disease estimation was calculated by measuring the relative lesion area at 120 h post-inoculation. * Indicates treatments significantly different than the control MRS broth + Tween 20 (*F. graminearum*). ** Indicates treatments significantly different than the control MRS broth + *F. graminearum*. **(B)** Symptomatic diseased lesions on barley leaves. The barley leaves were treated with *F. graminearum* and controls [(A) MRS broth + *F. graminearum*, (B) Fandango® + *F. graminearum* (C) MRS broth + Tween 20]. MRS broth and lactic acid bacteria [(D) *L. reuteri* R29, (E) *L. brevis* R2Δ, (F) *L. amylovorus* FST2.11, (G) *L. reuteri* M13, (H) *L. amylovorus* DSM 20053, and (I) *L. amylovorus* DSM 20552]. The effects of the treatments above were observed 120 h post-inoculation. **(C)** Symptomatic diseased lesions on barley leaves treated with *F. culmorum* and controls [(A) MRS broth + *F. culmorum*, (B) Fandango® + *F. culmorum* (C) MRS broth + Tween 20]. MRS broth and lactic acid bacteria [(D) *L. reuteri* R29, (E) *L. brevis* 2Δ, (F) *L. amylovorus* FST 2.11, (G) *L. reuteri* M13, (H) *L. amylovorus* DSM 20053, and (I) *L. amylovorus* DSM 20552]. The effects of treatments above observed 120 h post-inoculation. **(D)** An assessment of LAB treatments on sporulation of *Fusarium spp.* by detached leaf assay. Conidia production was determined 5 days post-inoculation. *** Indicates treatments significantly different than the control MRS broth + Tween 20 (*F. culmorum*). **** Indicates treatments significantly different than the control MRS broth + *F. culmorum*. * Indicates treatments significantly different than the control MRS broth + Tween 20 (*F. graminearum*). ** Indicates treatments significantly different than the control MRS broth + *F. graminearum*.

expression of 11 important defense-related genes (**Table 2**). All genes were expressed in barley spikelets treated with 0.2% Tween 20 and MRS broth (mock). The target gene expression was quantified relative to that of the barley housekeeping genes *HvActin* and *HvU-61*. Responsiveness of defense-related genes following LAB and *Fusarium* applications showed that different treatments triggered variable expression levels across the time points. One notable trend was the increased quantity of *HvPUB23, HvICS1, HvWRKY23, HvActin, HvCAMBP1,* and *HvCOI1* transcripts from 72 to 120 hpi. Spray inoculations of spikelets with LAB and *F. graminearum* resulted in no significant changes in the expression of *HvSWEET1, HvNPR3, HvPR1, HvLOX2,* and *HvMPK3* compared with those treated with the positive or negative controls (**Figure 5**). Levels of mRNA accumulation of *HvICS1* were found to progressively increase from 12 hpi to 120 hpi (**Figure 6A**). Significant differences in *HvICS1* expression levels were not noted until 120 hpi where *L. amylovorus* FST 2.11-treated spikelets had significantly more transcripts as compared to all other LAB treatments and controls ($p < 0.05$). Significant changes triggered by LAB treatments on the expression of *HvCOI1* were noted from 12 hpi ($p < 0.05$) (**Figure 6B**). At 120 hpi, all LAB treatments brought about significant changes in levels of *HvCOI1* expression compared with the positive control of MRS broth + *F. graminearum*. Of the six LAB isolates, only *L. amylovorus* FST 2.11 expressed higher levels of *HvCOI1* expression ($P < 0.05$), the remainder expressing lower levels compared with the positive control at 120 hpi ($p < 0.05$). Three treatments of *L. amylovorus* FST 2.11, *L. amylovorus* DSM 20053, and *L. brevis* R2Δ did induce *HvCOI1* expression compared with the negative control of MRS broth + Tween 20 ($p < 0.05$), but only *L. amylovorus* FST 2.11 expressed higher levels of *HvCOI1* compared with the positive control treatment ($p < 0.05$). The remaining LAB treatments all provided lower levels of *HvCOI1* expression compared with the negative control, with *L. reuteri* M13 significantly lower ($p \leq 0.006$).

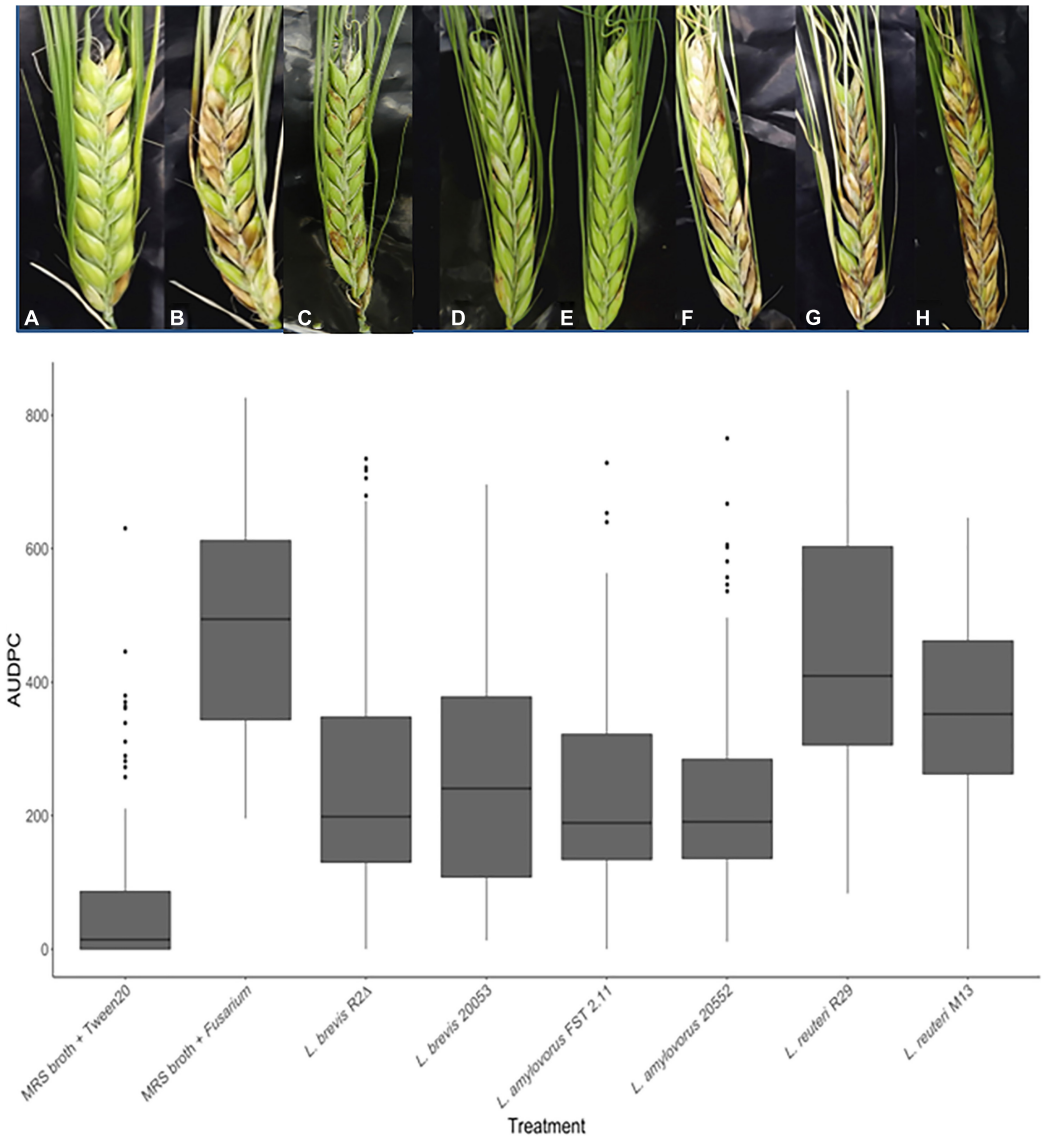

FIGURE 3 | FHB symptoms of spring barley cultivar "Sanette" assessed following LAB and control treatments at 14 days post-inoculation. Chosen spikelets received LAB [(C) (*L. amylovorus* DSM 20552)], [(D) (*L. amylovorus* DSM 20053)], [(E) (*L. brevis* R2Δ)], [(F) (*L. amylovorus* FST 2.11)], [(G) (*L. reuteri* M13)], [(H) (*L. reuteri* R29)] or MRS broth (A,B). Conidia of *F. graminearum* (B) or Tween 20 (mock) (A) were spray applied at mid-anthesis. Disease severity means were analyzed using the Kruskal–Wallis H test. * Indicates treatments significantly different from the control MRS broth + Tween 20. ** Indicates treatments significantly different than the control MRS broth + *F. graminearum/F. culmorum.*

The expression of transcription factor *HvWRKY23* from 12 to 120 hpi was inconsistent with induction and downregulation (**Figure 6C**). From 12 to 72 hpi, no significant effect of treatments was observed. At 120 hpi, a significant reduction in expression levels was noted when the control treatment MRS + *F. graminearum* was compared with LAB treatments of *L. brevis* R2Δ, *L. amylovorus* DSM20053 and *L. amylovorus* DSM20552 ($P < 0.05$). At the same time point, expression levels of *HvWRKY23* were also significantly greater for spikelets treated with MRS broth + *F. graminearum* compared with the mock treatment of MRS broth + Tween 20 ($P \leq 0.01$). The expression levels of *HvPUB23* were examined with significant differences only observed at 120 hpi. Accumulation of mRNA was significantly greater in *L. reuteri* R29 when compared with *L. reuteri* M13 ($P \leq 0.014$), *L. amylovorus* DSM 20053 ($P \leq 0.022$), *L. amylovorus* DSM 2055 ($P \leq 0.013$), MRS broth + *F. graminearum* ($P \leq 0.046$) and MRS broth + Tween 20 ($P \leq 0.017$). Differences in expression levels of *L. reuteri* R29, *L. brevis R2*Δ, and *L. amylovorus* FST 2.11 were not significant ($P > 0.05$). The relative gene expression of *FgActin*, monitored as an indicator of fungal activity, revealed a general incline from 12 to 120 hpi (**Figure 6D**). LAB treatments of *L. reuteri* M13 and *L. reuteri* R29 provided the highest levels of *FgActin* although these differences were not significant ($p > 0.05$). Two treatments,

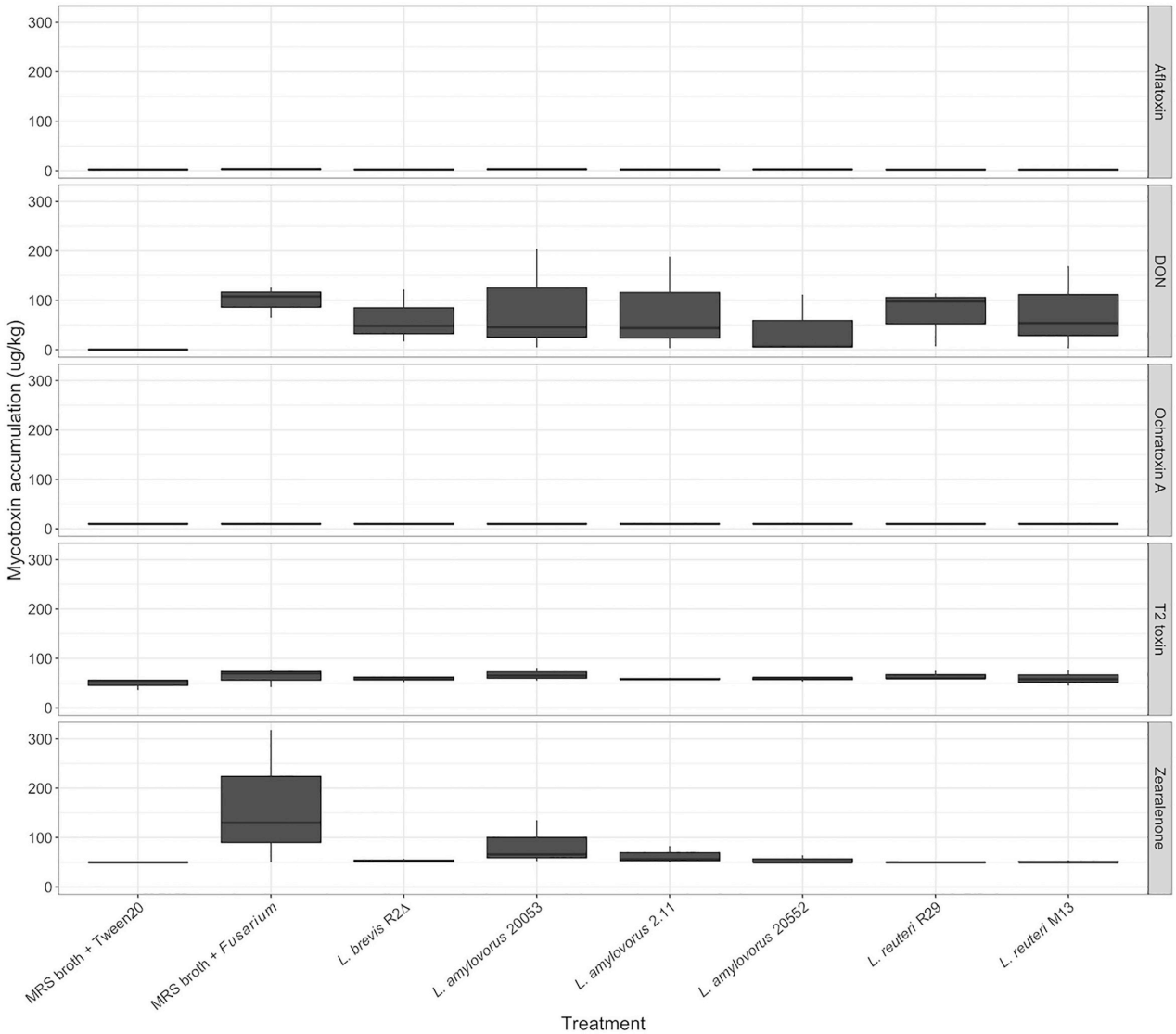

FIGURE 4 | Mycotoxin accumulation in pooled FHB grain samples. Mycotoxin means were separated using the Kruskal–Wallis H test.

namely, *L. amylovorus* DSM 20552 and the mock, were shown to significantly reduce levels of *FgActin* mRNA accumulation compared with that of MRS broth + *F. graminearum*-treated heads ($p < 0.05$).

DISCUSSION

Management of fungal diseases caused by several *Fusarium* spp. including *F. graminearum* has remained a ceaseless challenge since the realization of their impact on yield and quality of grain. Indeed, the incessant threat of cool damp weather, particularly at flowering, and increased concern regarding fungicide use to combat the pathogens that cause head blight, foot rot, and seedling blight mean we must reconsider our options (Arendrup et al., 2013; Shi et al., 2020). In addition to yield losses, it is the propensity of many *Fusarium* spp. to contaminate grain with mycotoxins that impacts the health of humans and animals who consume the affected grain which causes much consternation (Koch et al., 2013; Gallo et al., 2015; Tibola et al., 2016). Reforming our approach to these challenges by providing both economically and environmentally driven alternatives to existing fungicide solutions will allow for sustainably driven tillage systems. Hence, the use of LAB as BCAs to protect crops becomes imminent, as BCAs are cheaper, are environment friendly, leave no toxic residue, and are easy to handle, apply, manufacture and multiply in the soil (Sharma et al., 2013; Mittholiya et al., 2020). There has been a report of *in vivo* efficacy of LAB as BCAs against *Fusarium oxysporum* protection in tomato when used as seed treatment (Hamed et al., 2011). *Lactobacillus coryniformis* subsp. *coryniformis* strain Si3 was also reported to produce PLA, cyclo(Phe-Pro), cyclo(Phe-4-OH-Pro)

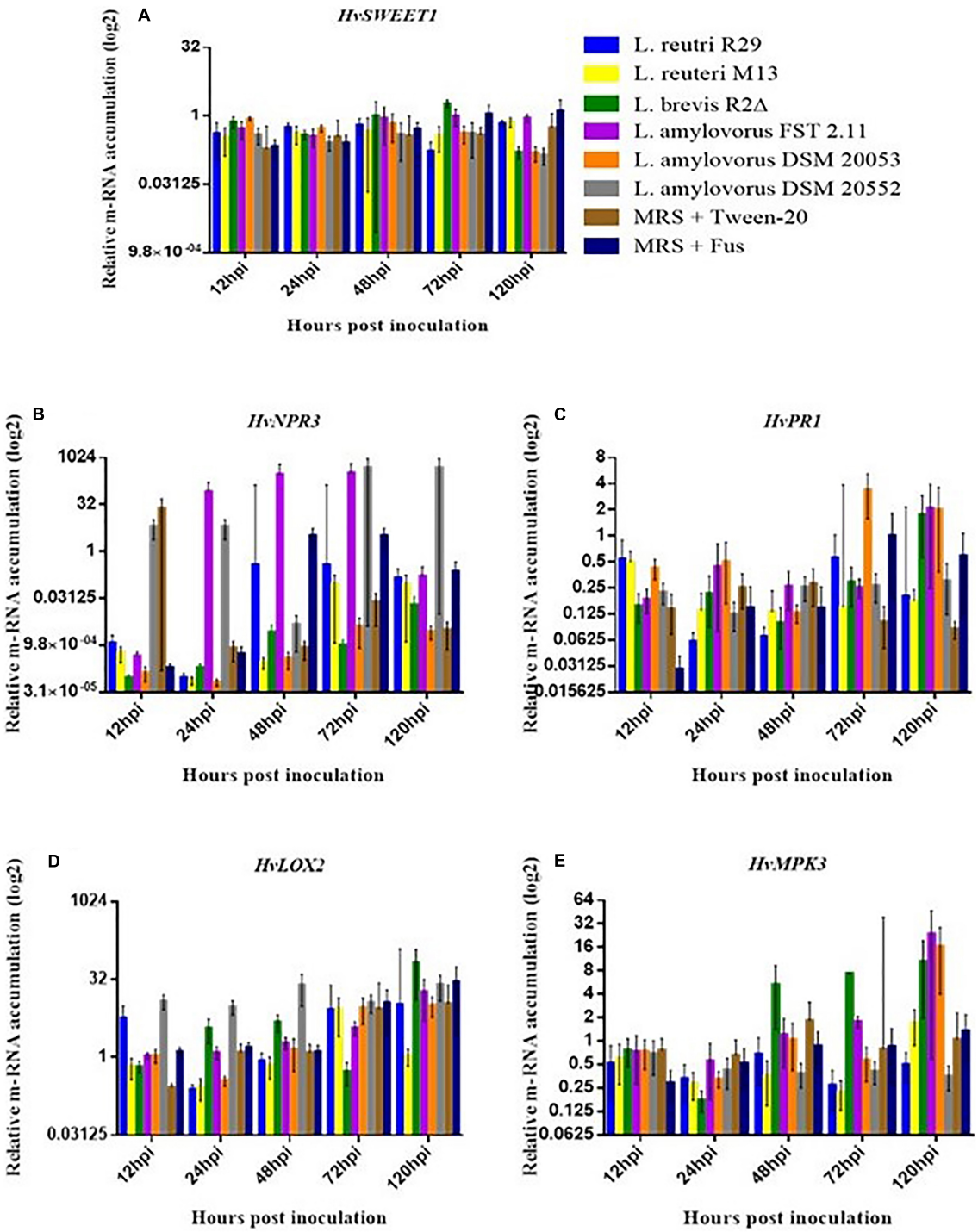

FIGURE 5 | Relative gene expression level in barley head tissue harvested at 12, 24, 48, 72, and 120 hpi of fungal inoculation. **(A)** *HvSEEWT1,* **(B)** *HvNPR3,* **(C)** *HvPR1,* **(D)** *HvLOX2* and **(E)** *HvMPK3*. Error bars indicate ± SEM (n = 8). Asterisks show significant differences between expression levels (*P, 0.05).

in vitro inhibiting *Fusarium graminearum, Fusarium culmorum, Fusarium sporotrichioides* and *Rhodotorula mucilaginosa* (Magnusson and Schnürer, 2001). Furthermore, the LAB were found to live in positive dynamic and assembly as epiphyte and endophyte with *Origanum vulgare* L (Pontonio et al., 2018), which open a door for natural BCAs. Hence, herein the research project to investigate the potential of LAB to be used as BCAs to control FHB in barley was taken up.

Dual-culture assays revealed that three of the tested LABs, namely, *L. amylovorus* FST 2.11, *L. amylovorus* DSM 20053,

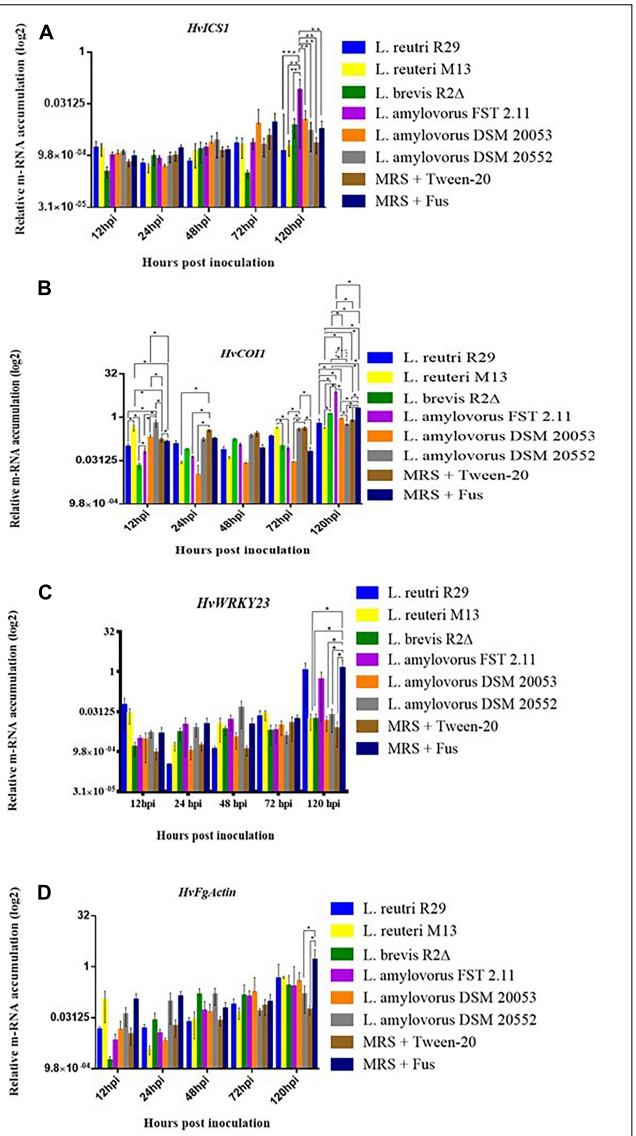

FIGURE 6 | Relative gene expression level in barley head tissue harvested at 12, 24, 48, 72, and 120 hpi of fungal inoculation. **(A)** *HvICS1,* **(B)** *HvCOI1,* **(C)** *HvWRKY23* and **(D)** *FgActin*. Error bars indicate ± SEM (n = 8). Asterisks show significant differences between expression levels (*P, 0.05).

and *L. brevis* R2Δ, can reduce the mycelial growth of the test fungus. For the majority, these results agree with the antifungal potential of the selected isolates as shown in previous studies (Lynch et al., 2016; Peyer et al., 2016) with the exception of *L. reuteri* R29 with a diminished antifungal activity. This may be explained by the specificity of *L. reuteri* R29 to *F. culmorum* strain TMW4.2043 (Axel et al., 2016); therefore, the antifungal activity of this LAB isolate could be fungi-specific. In addition, it is acknowledged that growth media and their components used in dual-culture assays may alter the antifungal activity of the test organism (Fiddaman and Rossall, 1994; Wang and Liu, 2008). The result of this assay carried out on a PDA medium can be further validated by carrying out the same assay on nutrient-limited media. These Petri dish assays did not examine the specific manner of antifungal activity, although previous work has noted the production of carboxylic acids by *L. brevis* R2Δ as the basis for the observed antifungal activity (Axel et al., 2016). These experiments agree with the study where *L. reuteri* M13 provided low to absent levels of fungal inhibition (Lynch et al., 2016). A possible reason for mycelium inhibition by the LAB examined could include the production of secondary metabolites which may directly inhibit mycelium spread as seen in other fungal pathogens (Allioui et al., 2016). Other explanations for mycelium inhibition could be the alteration of the growth media such as a change in pH and thus reducing its affinity to support mycelial growth. Alternatively, the LAB could potentially play a hyperparasitic role in the presence of *Fusarium*. Direct competition for space may also have led to a reduction in Fusarium growth needed to acquire nutrients from the media.

A modified detached leaf assay was used as an auxiliary study to quantify the antifungal potential of the selected agents while eliminating the effect of the growth media used in the dual-culture assay. The three aforesaid LAB which provided the most effective control of mycelial spread on dual culture presented similarly in the detached leaf assay. The reduction in differences in the antifungal activity between the best (*L. brevis* R2Δ) and worst (*L. reuteri* R29) performing isolate could be due to the removal of an artificial growth medium. The difference in the induction of host differences in leaves not seen in dual-culture assay may be due to the variation in the inherent potential of LABs to produce antifungal substances, such as cyclic dipeptides, proteinaceous compounds, organic acids, fatty acids, and reuterin (Crowley et al., 2013; Gajbhiye and Kapadnis, 2016). The biocontrol mechanisms of LAB can vary with strains *in vitro* but may have different performance in leaf surfaces. This means that all strains of LABs do not have the same potential to circumvent fungal spoilage owing to different capabilities to produce antifungal metabolites (Lačanin et al., 2017; Russo et al., 2017; Sadiq et al., 2019). The biocontrol mechanism of LAB strains is not limited to the antifungal activity, and it can extend up to interaction with fungal mycotoxins, resulting in inactivation or removal through cell wall binding (Blagojev et al., 2012; Ahlberg et al., 2015; Juodeikiene et al., 2018). The *in vitro* inhibitory mechanism of LAB strains PM411 and TC92 against *Pseudomonas syringae* pv. actinidiae in kiwifruit, *Xanthomonas arboricola* pv. pruni in Prunus and *Xanthomonas fragariae* in strawberry was reported to be pH-lowering effect and the production of lactic acid rather than the production of antifungal activity. However, both strains showed similar survival rates on leaf surfaces (Daranas Boadella et al., 2019). There are reports of LAB having antifungal activity but with variation. Recently, 10 different genotypes of *Lactobacillus plantarum* confirmed having antifungal activity, but all of them were genetically heterogeneous (Dong et al., 2017). In addition, the presence of naturally occurring saprophytes on detached leaves could have a synergistic effect when co-inoculated with the chosen LAB. Although these experiments did not examine the exact mode of inhibition, as a proxy to further trials they give ample evidence to show potential for *in planta* investigations. To allow for a clearer understanding of biocontrol agents, test fungus and plant, biofilm investigations

along with whole leaf clearing and live–dead staining techniques could be explored (Bruzzese and Hasan, 1983; Bais et al., 2004).

Though there are more *in vitro* studies examining the potential of biocontrol agents *in vivo*, there is a need to find biocontrol agents that provide control at levels similar to or exceeding that of commercially available fungicides, and glasshouse studies were established (Palazzini et al., 2007; Matarese et al., 2012). To date, few studies have examined the relationship between LAB-mediated protection against FHB and mycotoxin accumulation (Oliveira et al., 2014; Baffoni et al., 2015; Zhao et al., 2017, 2019). In this study, LAB isolates of *L. amylovorus* DSM 20552, *L. amylovorus* DSM 20053, and *L. brevis* R2Δ provided evidence to be most suited as spray inoculations for the control of FHB *in planta* and reduction in the levels of mycotoxins on an individual basis. The main reason for these LAB isolates providing FHB resistance is the reduction in DON accumulation, the main virulence factor for *Fusarium*, inhibiting disease spread within barley heads (Sella et al., 2014; Gunupuru et al., 2017). Synergy studies have shown that when combined, LAB compounds have a higher relative antifungal activity (Niku-Paavola et al., 1999; Ndagano et al., 2011). Future glasshouse studies applying combinations of these isolates would offer more insight as to the potentially deleterious or beneficial effects co-inoculations might have on FHB control and mycotoxin moderation.

Previous studies have clearly shown that biocontrol agents alter plant defense systems upon host–agent contact (Khan et al., 2006; Palazzini et al., 2018; Köhl et al., 2019). The rough exploration of the changes in defense pathways was taken up in this study, as it may prove to be beneficial for rapid *in vitro* selection of future biocontrol agents (Conn et al., 2008). The gene expression of *FgActin* showed the increase in mRNA level of *Fusarium* indicating FHB development with time. But interestingly, *L. amylovorus* DSM 20552 and the mock were shown to significantly reduce levels of *FgActin* mRNA accumulation compared with that of MRS broth + *F. graminearum*-treated heads, suggesting the inhibition of FHB development. The *HvICS1* transcript level increment was found progressively from 12 hpi to 120 hpi. This can be related to FHB development with time, and the increase in *HvICS1* seems logical as *HvICS1* is the important gene for SA (salicylic acid) synthesis and SA signaling has been proven to confer FHB resistance (Makandar et al., 2012; Hao et al., 2018; Thapa et al., 2018). This may suggest that *HvICS1* plays a role in SA accumulation upon FHB infection in barley, which, in turn, confers a basal resistance to *F. graminearum* by modulating the accumulation of H_2O_2, O^{-2} and reactive oxygen-associated enzymatic activities (Antalová et al., 2020). The significant changes triggered by LAB treatments on the expression of *HvCOI1* at 12 hpi ($p < 0.05$) do suggest toward the role of LAB in priming barley heads against FHB with time. This is because coronatine-insensitive protein 1(COI1) is a reported receptor of jasmonic acid (JA) signaling and has been known to play a crucial role in FHB resistance in plants (Makandar et al., 2010; Kazan and Gardiner, 2018; Srivastava et al., 2018).

To conclude, this study has explored the effectiveness of *Lactobacillus* isolates as biocontrol agents *in vitro* and under glasshouse conditions. Several isolates provide promising evidence with *L. brevis* R2Δ, *L. amylovorus* DSM 20552, and *L. amylovorus* FST 2.11 showing the most promise regarding mycelial spread *in vitro*, disease severity, and mycotoxin accumulation. Gene expression results add to the burgeoning library recording the underlying interactions between LAB biocontrol agents and their host, resulting in FHB resistance. This work provides a step forward in developing new biological approaches to combat important fungal pathogens during a time when available chemical controls are declining. These results show that LAB control of fungal pathogens is species-specific and caution must be noted with regard to variance in biocontrol properties if the pathogen changes. These LAB can be exploited for their antifungal activity and can be considered useful to control the pathogens and crop improvement. In summary, the results illustrate the potential for a multi-pronged approach to control FHB through direct fungal inhibition, toxin reduction, and host defense pathway induction. This provides an alternative stronghold leading to sustainable agriculture, green control of pathogens, food security, environment friendly, and circular bioeconomy.

DATA AVAILABILITY STATEMENT

The original contributions presented in this study are included in the article/**Supplementary Material**, further inquiries can be directed to the corresponding author.

AUTHOR CONTRIBUTIONS

JB obtained funding for the project. MB, GT, and JB designed all the experiments. JB and GT provided guidance during the experiment implementation. MB and GT carried out all the experiments. FD and JB reviewed the final manuscript. All authors contributed to the article and approved the submitted version.

FUNDING

We thank the Irish Department of Agriculture, Food, and Marine for funding provided under the Research Stimulus Fund (RSF) (Grant No. 11SF 317).

ACKNOWLEDGMENTS

We would like to thank the assistance of Elke Arendt and Claudia Axel, University College Cork, for the provision of the culture strains for laboratory, glasshouse, and field trials.

SUPPLEMENTARY MATERIAL

The Supplementary Material for this article can be found online at: https://www.frontiersin.org/articles/10.3389/fmicb.2022.912632/full#supplementary-material

REFERENCES

Ahlberg, S. H., Joutsjoki, V., and Korhonen, H. J. (2015). Potential of lactic acid bacteria in aflatoxin risk mitigation. *Int. J. Food Microbiol.* 207, 87–102.doi: 10.1016/j.ijfoodmicro.2015.04.042

Ahmad, S., Wei, X., Sheng, Z., Hu, P., and Tang, S. (2020). CRISPR/Cas9 for development of disease resistance in plants: recent progress, limitations and future prospects. *Brief. Funct. Genomics* 19, 26–39. doi: 10.1093/bfgp/elz041

Ali, S. S., Gunupuru, L. R., Kumar, G., Khan, M., Scofield, S., Nicholson, P., et al. (2014). Plant disease resistance is augmented in uzu barley lines modified in the brassinosteroid receptor BRI1. *BMC Plant Biol.* 14:227. doi: 10.1186/s12870-014-0227-1

Allioui, N., Siah, A., Brinis, L., Reignault, P., and Halama, P. (2016). Identification of Qol fungicide-resistant genotypes of the wheat pathogen *Zymoseptoria tritici* in Algeria. *Phytopathol. Mediterr.* 55, 89–97.

Antalová, Z., Bleša, D., Martinek, P., and Matušinsky, P. (2020). Transcriptional analysis of wheat seedlings inoculated with *Fusarium culmorum* under continual exposure to disease defence inductors. *PLoS One* 15:e0224413. doi: 10.1371/journal.pone.0224413

Arendrup, M., Dzajic, E., Jensen, R., Johansen, H., Kjaldgaard, P., Knudsen, J., et al. (2013). Epidemiological changes with potential implication for antifungal prescription recommendations for fungaemia: data from a nationwide fungaemia surveillance programme. *Clin. Microbiol. Infect.* 19, e343–e353. doi: 10.1111/1469-0691.12212

Audenaert, K., Callewaert, E., Höfte, M., De Saeger, S., and Haesaert, G. (2010). Hydrogen peroxide induced by the fungicide prothioconazole triggers deoxynivalenol (DON) production by *Fusarium graminearum*. *BMC Microbiol.* 10:112. doi: 10.1186/1471-2180-10-112

Axel, C., Brosnan, B., Zannini, E., Peyer, L. C., Furey, A., Coffey, A., et al. (2016). Antifungal activities of three different Lactobacillus species and their production of antifungal carboxylic acids in wheat sourdough. *Appl. Microbiol. Biotechnol.* 100, 1701–1711. doi: 10.1007/s00253-015-7051-x

Baffoni, L., Gaggia, F., Dalanaj, N., Prodi, A., Nipoti, P., Pisi, A., et al. (2015). Microbial inoculants for the biocontrol of *Fusarium* spp. in durum wheat. *BMC Microbiol.* 15:242. doi: 10.1186/s12866-015-0573-7

Bais, H. P., Fall, R., and Vivanco, J. M. (2004). Biocontrol of *Bacillus subtilis* against infection of Arabidopsis roots by *Pseudomonas syringae* is facilitated by biofilm formation and surfactin production. *Plant Physiol.* 134, 307–319. doi: 10.1104/pp.103.028712

Beccari, G., Prodi, A., Tini, F., Bonciarelli, U., Onofri, A., Oueslati, S., et al. (2017). Changes in the Fusarium head blight complex of malting barley in a three-year field experiment in Italy. *Toxins* 9:120. doi: 10.3390/toxins9040120

Blagojev, N., Škrinjar, M., Vesković-Moraèanin, S., and Šošo, V. (2012). Control of mould growth and mycotoxin production by lactic acid bacteria metabolites. *Rom. Biotechnol. Lett.* 17, 7219–7226.

Blandino, M., Haidukowski, M., Pascale, M., Plizzari, L., Scudellari, D., and Reyneri, A. (2012). Integrated strategies for the control of Fusarium head blight and deoxynivalenol contamination in winter wheat. *Field Crops Res.* 133, 139–149. doi: 10.1016/j.fcr.2012.04.004

Bolechová, M., Benešová, K., Běláková, S., Čáslavský, J., Pospíchalová, M., and Mikulíková, R. (2015). Determination of seventeen mycotoxins in barley and malt in the Czech Republic. *Food Control* 47, 108–113. doi: 10.1016/j.foodcont.2014.06.045

Bottalico, A., and Perrone, G. (2002). Toxigenic *Fusarium* species and mycotoxins associated with head blight in small-grain cereals in Europe. *Eur. J. Plant Pathol.* 108, 611–624.doi: 10.1023/A:1020635214971

Brennan, J., Fagan, B., Van Maanen, A., Cooke, B., and Doohan, F. (2003). Studies on *in vitro* growth and pathogenicity of European *Fusarium* fungi. *Eur. J. Plant Pathol.* 109, 577–587. doi: 10.1023/A:1024712415326

Brown, N. A., Bass, C., Baldwin, T. K., Chen, H., Massot, F., Carion, P. W., et al. (2011). Characterisation of the *Fusarium graminearum*-wheat floral interaction. *J. Pathog.* 2011:626345. doi: 10.4061/2011/626345

Bruzzese, E., and Hasan, S. (1983). A whole leaf clearing and staining technique for host specificity studies of rust fungi. *Plant Pathol.* 32, 335–338. doi: 10.1111/j.1365-3059.1983.tb02841.x

Cantoro, R., Palazzini, J. M., Yerkovich, N., Miralles, D. J., and Chulze, S. N. (2021). *Bacillus velezensis* RC 218 as a biocontrol agent against *Fusarium graminearum*: effect on penetration, growth and TRI5 expression in wheat spikes. *BioControl* 66, 259–270. doi: 10.1007/s10526-020-10062-7

CGIAR (2012). *Consultative Group on International Agricultural Research*. Montpellier: CGIAR.

Chen, X., Steed, A., Harden, C., and Nicholson, P. (2006). Characterization of *Arabidopsis thaliana–Fusarium graminearum* interactions and identification of variation in resistance among ecotypes. *Mol. Plant Pathol.* 7, 391–403. doi: 10.1111/j.1364-3703.2006.00349.x

Chomczynski, P. (1993). A reagent for the single-step simultaneous isolation of RNA, DNA and proteins from cell and tissue samples. *Biotechniques* 15, 532–534, 536–537.

Comby, M., Gacoin, M., Robineau, M., Rabenoelina, F., Ptas, S., Dupont, J., et al. (2017). Screening of wheat endophytes as biological control agents against *Fusarium* head blight using two different *in vitro* tests. *Microbiol. Res.* 202, 11–20. doi: 10.1016/j.micres.2017.04.014

Conn, V., Walker, A., and Franco, C. (2008). Endophytic actinobacteria induce defense pathways in *Arabidopsis thaliana*. *Mol. Plant Microbe Interact.* 21, 208–218. doi: 10.1094/MPMI-21-2-0208

Cowger, C., Weisz, R., Arellano, C., and Murphy, P. (2016). Profitability of integrated management of Fusarium head blight in North Carolina winter wheat. *Phytopathology* 106, 814–823. doi: 10.1094/PHYTO-10-15-0263-R

Crowley, S., Mahony, J., and Van Sinderen, D. (2013). Current perspectives on antifungal lactic acid bacteria as natural bio-preservatives. *Trends Food Sci. Technol.* 33, 93–109. doi: 10.1016/j.tifs.2013.07.004

D'Angelo, D., Bradley, C., Ames, K., Willyerd, K., Madden, L., and Paul, P. (2014). Efficacy of fungicide applications during and after anthesis against Fusarium head blight and deoxynivalenol in soft red winter wheat. *Plant Dis.* 98, 1387–1397. doi: 10.1094/PDIS-01-14-0091-RE

Daranas Boadella, N., Roselló Prados, G., Cabrefiga Olamendi, J., Donati, I., Francés Ortega, J., Badosa Romañó, E., et al. (2019). Biological control of bacterial plant diseases with *Lactobacillus plantarum* strains selected for their broad-spectrum activity. *Ann. Appl. Biol.* 174, 92–105. doi: 10.1111/aab.12476

Dempsey, D. M. A., Vlot, A. C., Wildermuth, M. C., and Klessig, D. F. (2011). Salicylic acid biosynthesis and metabolism. *Arabidopsis Book* 9:e0156. doi: 10.1199/tab.0156

Dong, A.-R., Lo, R., Bansal, N., and Turner, M. S. (2017). A genetic diversity study of antifungal *Lactobacillus plantarum* isolates. *Food Control* 72, 83–89. doi: 10.1016/j.foodcont.2016.07.026

Ferdous, J., Li, Y., Reid, N., Langridge, P., Shi, B.-J., and Tricker, P. J. (2015). Identification of reference genes for quantitative expression analysis of microRNAs and mRNAs in barley under various stress conditions. *PLoS One* 10:e0118503. doi: 10.1371/journal.pone.0118503

Ferrigo, D., Raiola, A., and Causin, R. (2016). *Fusarium* toxins in cereals: occurrence, legislation, factors promoting the appearance and their management. *Molecules* 21:627. doi: 10.3390/molecules21050627

Fiddaman, P., and Rossall, S. (1994). Effect of substrate on the production of antifungal volatiles from *Bacillus subtilis*. *J. Appl. Bacteriol.* 76, 395–405. doi: 10.1111/j.1365-2672.1994.tb01646.x

Franco, T., Garcia, S., Hirooka, E., Ono, Y., and Dos Santos, J. (2011). Lactic acid bacteria in the inhibition of *Fusarium graminearum* and deoxynivalenol detoxification. *J. Appl. Microbiol.* 111, 739–748. doi: 10.1111/j.1365-2672.2011.05074.x

Gajbhiye, M. H., and Kapadnis, B. P. (2016). Antifungal-activity-producing lactic acid bacteria as biocontrol agents in plants. *Biocontrol Sci. Technol.* 26, 1451–1470. doi: 10.1080/09583157.2016.1213793

Gallo, A., Giuberti, G., Frisvad, J. C., Bertuzzi, T., and Nielsen, K. F. (2015). Review on mycotoxin issues in ruminants: occurrence in forages, effects of mycotoxin ingestion on health status and animal performance and practical strategies to counteract their negative effects. *Toxins* 7, 3057–3111. doi: 10.3390/toxins7083057

Gómez-Lama Cabanás, C., Fernández-González, A. J., Cardoni, M., Valverde-Corredor, A., López-Cepero, J., Fernández-López, M., et al. (2021). The banana root endophytome: differences between mother plants and suckers and evaluation of selected bacteria to control *Fusarium oxysporum* f.sp. *cubense*. *J. Fungi* 7:194. doi: 10.3390/jof7030194

Goswami, R. S., and Kistler, H. C. (2004). Heading for disaster: *Fusarium graminearum* on cereal crops. *Mol. Plant Pathol.* 5, 515–525. doi: 10.1111/j.1364-3703.2004.00252.x

Gunupuru, L., Perochon, A., and Doohan, F. (2017). Deoxynivalenol resistance as a component of FHB resistance. *Trop. Plant Pathol.* 42, 175–183. doi: /10.1007/s40858-017-0147-3

Gunupuru, L. R., Arunachalam, C., Malla, K. B., Kahla, A., Perochon, A., Jia, J., et al. (2018). A wheat cytochrome P450 enhances both resistance to deoxynivalenol and grain yield. *PLoS One* 13:e0204992. doi: 10.1371/journal.pone.0204992

Haidukowski, M., Pascale, M., Perrone, G., Pancaldi, D., Campagna, C., and Visconti, A. (2005). Effect of fungicides on the development of *Fusarium* head blight, yield and deoxynivalenol accumulation in wheat inoculated under field conditions with *Fusarium graminearum* and *Fusarium culmorum*. *J. Sci. Food Agric.* 85, 191–198. doi: 10.1002/jsfa.1965

Hamed, H. A., Moustafa, Y. A., and Abdel-Aziz, S. M. (2011). In vivo efficacy of lactic acid bacteria in biological control against *Fusarium oxysporum* for protection of tomato plant. *Life Sci. J.* 8, 462–468.

Hao, Q., Wang, W., Han, X., Wu, J., Lyu, B., Chen, F., et al. (2018). Isochorismate-based salicylic acid biosynthesis confers basal resistance to *Fusarium graminearum* in barley. *Mol. Plant Pathol.* 19, 1995–2010. doi: 10.1111/mpp.12675

He, Y., Zhang, X., Zhang, Y., Ahmad, D., Wu, L., Jiang, P., et al. (2018). Molecular characterization and expression of PFT, an FHB resistance gene at the Fhb1 QTL in wheat. *Phytopathology* 108, 730–736. doi: 10.1094/PHYTO-11-17-0383-R

Hückelhoven, R., Hofer, K., Coleman, A., and Heß, M. (2018). Fusarium infection of malting barley has to be managed over the entire value chain. *J. Plant Dis. Protect.* 125, 1–4. doi: 10.1007/s41348-017-0101-0

Jamal, Q., Cho, J.-Y., Moon, J.-H., and Kim, K. Y. (2017). Purification and antifungal characterization of cyclo (D-Pro-L-Val) from *Bacillus amyloliquefaciens* Y1 against *Fusarium graminearum* to control head blight in wheat. *Biocatal. Agric. Biotechnol.* 10, 141–147. doi: 10.1016/j.bcab.2017.01.003

Jeger, M., and Viljanen-Rollinson, S. (2001). The use of the area under the disease-progress curve (AUDPC) to assess quantitative disease resistance in crop cultivars. *Theor. Appl. Genet.* 102, 32–40. doi: 10.1007/s001220051615

Jones, R. (2000). Assessments of Fusarium head blight of wheat and barley in response to fungicide treatment. *Plant Dis.* 84, 1021–1030. doi: 10.1094/PDIS.2000.84.9.1021

Juodeikiene, G., Bartkiene, E., Cernauskas, D., Cizeikiene, D., Zadeike, D., Lele, V., et al. (2018). Antifungal activity of lactic acid bacteria and their application for *Fusarium* mycotoxin reduction in malting wheat grains. *Lwt* 89, 307–314. doi: 10.1016/j.lwt.2017.10.061

Kage, U., Yogendra, K. N., and Kushalappa, A. C. (2017). TaWRKY70 transcription factor in wheat QTL-2DL regulates downstream metabolite biosynthetic genes to resist *Fusarium graminearum* infection spread within spike. *Sci. Rep.* 7:42596. doi: 10.1038/srep42596

Karre, S., Kumar, A., Yogendra, K., Kage, U., Kushalappa, A., and Charron, J.-B. (2019). *HvWRKY23* regulates flavonoid glycoside and hydroxycinnamic acid amide biosynthetic genes in barley to combat Fusarium head blight. *Plant Mol. Biol.* 100, 591–605. doi: 10.1007/s11103-019-00882-2

Kazan, K., and Gardiner, D. M. (2018). Transcriptomics of cereal–*Fusarium graminearum* interactions: what we have learned so far. *Mol. Plant Pathol.* 19, 764–778. doi: 10.1111/mpp.12561

Kedia, G., Wang, R., Patel, H., and Pandiella, S. S. (2007). Use of mixed cultures for the fermentation of cereal-based substrates with potential probiotic properties. *Process Biochem.* 42, 65–70.

Khan, M. R., Fischer, S., Egan, D., and Doohan, F. M. (2006). Biological control of Fusarium seedling blight disease of wheat and barley. *Phytopathology* 96, 386–394. doi: 10.1094/PHYTO-96-0386

Koch, A., Biedenkopf, D., Furch, A., Weber, L., Rossbach, O., Abdellatef, E., et al. (2016). An RNAi-based control of *Fusarium graminearum* infections through spraying of long dsRNAs involves a plant passage and is controlled by the fungal silencing machinery. *PLoS Pathog.* 12:e1005901. doi: 10.1371/journal.ppat.1005901

Koch, A., Kumar, N., Weber, L., Keller, H., Imani, J., and Kogel, K.-H. (2013). Host-induced gene silencing of cytochrome P450 lanosterol C14α-demethylase–encoding genes confers strong resistance to *Fusarium* species. *Proc. Natl. Acad. Sci. U.S.A.* 110, 19324–19329. doi: 10.1073/pnas.1306373110

Köhl, J., Kolnaar, R., and Ravensberg, W. J. (2019). Mode of action of microbial biological control agents against plant diseases: relevance beyond efficacy. *Front. Plant Sci.* 10:845. doi: 10.3389/fpls.2019.00845

Lačanin, I., Mounier, J., Pawtowski, A., Dušková, M., Kameník, J., and Karpíšková, R. (2017). Assessment of the antifungal activity of *Lactobacillus* and *Pediococcus* spp. for use as bioprotective cultures in dairy products. *World J. Microbiol. Biotechnol.* 33:188. doi: 10.1007/s11274-017-2354-y

Legzdina, L., Bleidere, M., Usele, G., Vilcane, D., Beinarovica, I., Mezaka, I., et al. (2013). "Phenotypic evaluation of spring barley RIL mapping populations for pre-harvest sprouting, Fusarium head blight and β-glucans," in *Advance in Barley Sciences*, eds G. Zhang, C. Li, and X. Liu (Dordrecht: Springer), 441–452.

Legzdina, L., and Buerstmayr, H. (2004). Comparison of infection with Fusarium head blight and accumulation of mycotoxins in grain of hulless and covered barley. *J. Cereal Sci.* 40, 61–67.

Livak, K. J. and Schmittgen, T. D. (2001). Analysis of relative gene expression data using real-time quantitative PCR and the $2^{-\Delta\Delta CT}$ method. *Methods* 25, 402–408. doi: 10.1006/meth.2001.1262

Lowe, D. P., and Arendt, E. K. (2004). The use and effects of lactic acid bacteria in malting and brewing with their relationships to antifungal activity, mycotoxins and gushing: a review. *J. Inst. Brew.* 110, 163–180. doi: 10.1002/j.2050-0416.2004.tb00199.x

Lynch, K., Zannini, E., Guo, J., Axel, C., Arendt, E., Kildea, S., et al. (2016). Control of *Zymoseptoria tritici* cause of septoria tritici blotch of wheat using antifungal *Lactobacillus* strains. *J. Appl. Microbiol.* 121, 485–494. doi: 10.1111/jam.13171

Magan, N., Hope, R., Colleate, A., and Baxter, E. (2002). Relationship between growth and mycotoxin production by *Fusarium* species, biocides and environment. *Eur. J. Plant Pathol.* 108, 685–690. doi: 10.1023/A:1020618728175

Magnusson, J., and Schnürer, J. (2001). *Lactobacillus coryniformis* subsp. *coryniformis* strain Si3 produces a broad-spectrum proteinaceous antifungal compound. *Appl. Environ. Microbiol.* 67, 1–5. doi: 10.1128/AEM.67.1.1-5.2001

Makandar, R., Nalam, V., Chaturvedi, R., Jeannotte, R., Sparks, A. A., and Shah, J. (2010). Involvement of salicylate and jasmonate signaling pathways in Arabidopsis interaction with *Fusarium graminearum*. *Mol. Plant Microbe Interact.* 23, 861–870. doi: 10.1094/MPMI-23-7-0861

Makandar, R., Nalam, V. J., Lee, H., Trick, H. N., Dong, Y., and Shah, J. (2012). Salicylic acid regulates basal resistance to Fusarium head blight in wheat. *Mol. Plant Microbe Interact.* 25, 431–439. doi: 10.1094/MPMI-09-11-0232

Matarese, F., Sarrocco, S., Gruber, S., Seidl-Seiboth, V., and Vannacci, G. (2012). Biocontrol of *Fusarium* head blight: interactions between *Trichoderma* and mycotoxigenic *Fusarium*. *Microbiology* 158, 98–106. doi: 10.1099/mic.0.052639-0

Matny, O. (2015). Fusarium head blight and crown rot on wheat & barley: losses and health risks. *Adv. Plants Agric. Res.* 2:00039. doi: 10.15406/apar.2015.02.00039

McCallum, B., and Tekauz, A. (2002). Influence of inoculation method and growth stage on fusarium head blight in barley. *Can. J. Plant Pathol.* 24, 77–80. doi: 10.1080/07060660109506976

McMullen, M., Bergstrom, G., De Wolf, E., Dill-Macky, R., Hershman, D., Shaner, G., et al. (2012). A unified effort to fight an enemy of wheat and barley: Fusarium head blight. *Plant Dis.* 96, 1712–1728. doi: 10.1094/PDIS-03-12-0291-FE

McMullen, M., Jones, R., and Gallenberg, D. (1997). Scab of wheat and barley: a re-emerging disease of devastating impact. *Plant Dis.* 81, 1340–1348. doi: 10.1094/PDIS.1997.81.12.1340

Meroth, C. B., Walter, J., Hertel, C., Brandt, M. J., and Hammes, W. P. (2003). Monitoring the bacterial population dynamics in sourdough fermentation processes by using PCR-denaturing gradient gel electrophoresis. *Appl. Environ. Microbiol.* 69, 475–482. doi: 10.1128/AEM.69.1.475-482.2003

Miedaner, T., Schmid, J. E., Flath, K., Koch, S., Jacobi, A., Ebmeyer, E., et al. (2018). A multiple disease test for field-based phenotyping of resistances to Fusarium head blight, yellow rust and stem rust in wheat. *Eur. J. Plant Pathol.* 151, 451–461. doi: 10.1007/s10658-017-1386-3

Mittholiya, S., Chittora, D., and Sharma, K. (2020). "Role of lactic acid bacteria as biological control agent," in *Innovative Research on Science, Humanities, Engineering & Management*, eds R. Shyam and R. K. Kaswan (Paris: RFI), 21.

Murphy, B. R. (2016). *Unlocking the Potential of Endophytes in Cereal Crops*. Doctoral thesis. Dublin: Trinity College of Dublin.

Nakkarach, A., and Withayagiat, U. (2018). Comparison of synbiotic beverages produced from riceberry malt extract using selected free and encapsulated probiotic lactic acid bacteria. *Agric. Nat. Resour.* 52, 467–476. doi: 10.1016/j.anres.2018.11.013

Ndagano, D., Lamoureux, T., Dortu, C., Vandermoten, S., and Thonart, P. (2011). Antifungal activity of 2 lactic acid bacteria of the *Weissella* genus isolated from food. *J. Food Sci.* 76, M305–M311. doi: 10.1111/j.1750-3841.2011.02257.x

Nielsen, L., Cook, D., Edwards, S., and Ray, R. (2014). The prevalence and impact of Fusarium head blight pathogens and mycotoxins on malting barley quality in UK. *Int. J. Food Microbiol.* 179, 38–49. doi: 10.1016/j.ijfoodmicro.2014.03.023

Niku-Paavola, M. L., Laitila, A., Mattila-Sandholm, T., and Haikara, A. (1999). New types of antimicrobial compounds produced by *Lactobacillus plantarum*. *J. Appl. Microbiol.* 86, 29–35. doi: 10.1046/j.1365-2672.1999.00632.x

Oliveira, P. M., Zannini, E., and Arendt, E. K. (2014). Cereal fungal infection, mycotoxins, and lactic acid bacteria mediated bioprotection: from crop farming to cereal products. *Food Microbiol.* 37, 78–95. doi: 10.1016/j.fm.2013.06.003

Palazzini, J., Roncallo, P., Cantoro, R., Chiotta, M., Yerkovich, N., Palacios, S., et al. (2018). Biocontrol of *Fusarium graminearum* sensu stricto, reduction of deoxynivalenol accumulation and phytohormone induction by two selected antagonists. *Toxins* 10:88. doi: 10.3390/toxins10020088

Palazzini, J. M., Dunlap, C. A., Bowman, M. J., and Chulze, S. N. (2016). *Bacillus velezensis* RC 218 as a biocontrol agent to reduce *Fusarium* head blight and deoxynivalenol accumulation: genome sequencing and secondary metabolite cluster profiles. *Microbiol. Res.* 192, 30–36. doi: 10.1016/j.micres.2016.06.002

Palazzini, J. M., Ramirez, M. L., Torres, A. M., and Chulze, S. N. (2007). Potential biocontrol agents for Fusarium head blight and deoxynivalenol production in wheat. *Crop Prot.* 26, 1702–1710. doi: 10.1016/j.cropro.2007.03.004

Parry, D., Jenkinson, P., and Mcleod, L. (1995). Fusarium ear blight (scab) in small grain cereals—a review. *Plant Pathol.* 44, 207–238. doi: 10.1111/j.1365-3059.1995.tb02773.x

Paul, P., Lipps, P., Hershman, D., Mcmullen, M., Draper, M., and Madden, L. (2008). Efficacy of triazole-based fungicides for Fusarium head blight and deoxynivalenol control in wheat: a multivariate meta-analysis. *Phytopathology* 98, 999–1011. doi: 10.1094/PHYTO-98-9-0999

Paul, P. A., Bradley, C. A., Madden, L. V., Dalla Lana, F., Bergstrom, G. C., Dill-Macky, R., et al. (2018). Effects of pre-and postanthesis applications of demethylation inhibitor fungicides on Fusarium head blight and deoxynivalenol in spring and winter wheat. *Plant Dis.* 102, 2500–2510. doi: 10.1094/PDIS-03-18-0466-RE

Petchkongkaew, A., Taillandier, P., Gasaluck, P., and Lebrihi, A. (2008). Isolation of *Bacillus* spp. from Thai fermented soybean (Thua-nao): screening for aflatoxin B1 and ochratoxin A detoxification. *J. Appl. Microbiol.* 104, 1495–1502. doi: 10.1111/j.1365-2672.2007.03700.x

Peyer, L. C., Axel, C., Lynch, K. M., Zannini, E., Jacob, F., and Arendt, E. K. (2016). Inhibition of *Fusarium culmorum* by carboxylic acids released from lactic acid bacteria in a barley malt substrate. *Food Control* 69, 227–236. doi: 10.1016/j.foodcont.2016.05.010

Placinta, C., D'mello, J. F., and Macdonald, A. (1999). A review of worldwide contamination of cereal grains and animal feed with *Fusarium* mycotoxins. *Anim. Feed Sci. Technol.* 78, 21–37. doi: 10.1016/S0377-8401(98)00278-8

Pontonio, E., Di Cagno, R., Tarraf, W., Filannino, P., De Mastro, G., and Gobbetti, M. (2018). Dynamic and assembly of epiphyte and endophyte lactic acid bacteria during the life cycle of *Origanum vulgare* L. *Front. Microbiol.* 9:1372. doi: 10.3389/fmicb.2018.01372

Pretty, J., and Bharucha, Z. P. (2015). Integrated pest management for sustainable intensification of agriculture in Asia and Africa. *Insects* 6, 152–182. doi: 10.3390/insects6010152

Rathore, S., Salmerón, I., and Pandiella, S. S. (2012). Production of potentially probiotic beverages using single and mixed cereal substrates fermented with lactic acid bacteria cultures. *Food Microbiol.* 30, 239–244. doi: 10.1016/j.fm.2011.09.001

Rudd, J. J., Keon, J., and Hammond-Kosack, K. E. (2008). The wheat mitogen-activated protein kinases TaMPK3 and TaMPK6 are differentially regulated at multiple levels during compatible disease interactions with *Mycosphaerella graminicola*. *Plant Physiol.* 147, 802–815. doi: 10.1104/pp.108.119511

Russo, P., Arena, M. P., Fiocco, D., Capozzi, V., Drider, D., and Spano, G. (2017). *Lactobacillus plantarum* with broad antifungal activity: a promising approach to increase safety and shelf-life of cereal-based products. *Int. J. Food Microbiol.* 247, 48–54. doi: 10.1016/j.ijfoodmicro.2016.04.027

Sadiq, F. A., Yan, B., Tian, F., Zhao, J., Zhang, H., and Chen, W. (2019). Lactic acid bacteria as antifungal and anti-mycotoxigenic agents: a comprehensive review. *Compr. Rev. Food Sci. Food Saf.* 18, 1403–1436. doi: 10.1111/1541-4337.12481

Scherm, B., Balmas, V., Spanu, F., Pani, G., Delogu, G., Pasquali, M., et al. (2013). *Fusarium culmorum*: causal agent of foot and root rot and head blight on wheat. *Mol. Plant Pathol.* 14, 323–341. doi: 10.1111/mpp.12011

Schnürer, J., and Magnusson, J. (2005). Antifungal lactic acid bacteria as biopreservatives. *Trends Food Sci. Technol.* 16, 70–78.

Schoonbeek, H. J., Wang, H. H., Stefanato, F. L., Craze, M., Bowden, S., Wallington, E., et al. (2015). Arabidopsis EF-Tu receptor enhances bacterial disease resistance in transgenic wheat. *New Phytol.* 206, 606–613. doi: 10.1111/nph.13356

Sella, L., Gazzetti, K., Castiglioni, C., Schäfer, W., and Favaron, F. (2014). *Fusarium graminearum* possesses virulence factors common to Fusarium head blight of wheat and seedling rot of soybean but differing in their impact on disease severity. *Phytopathology* 104, 1201–1207. doi: 10.1094/PHYTO-12-13-0355-R

Sharma, A., Diwevidi, V., Singh, S., Pawar, K. K., Jerman, M., Singh, L., et al. (2013). Biological control and its important in agriculture. *Int. J. Biotechnol. Bioeng. Res.* 4, 175–180.

Shi, S., Zhao, J., Pu, L., Sun, D., Han, D., Li, C., et al. (2020). Identification of new sources of resistance to crown rot and Fusarium head blight in Wheat. *Plant Dis.* 104, 1979–1985. doi: 10.1094/PDIS-10-19-2254-RE

Siedler, S., Balti, R., and Neves, A. R. (2019). Bioprotective mechanisms of lactic acid bacteria against fungal spoilage of food. *Curr. Opin. Biotechnol.* 56, 138–146.

Simpson, D. R., Weston, G. E., Turner, J. A., Jennings, P., and Nicholson, P. (2001). Differential control of head blight pathogens of wheat by fungicides and consequences for mycotoxin contamination of grain. *Eur. J. Plant Pathol.* 107, 421–431.

Smiley, R. W., Gourlie, J. A., Easley, S. A., and Patterson, L.-M. (2005). Pathogenicity of fungi associated with the wheat crown rot complex in Oregon and Washington. *Plant Dis.* 89, 949–957. doi: 10.1094/PD-89-0949

Srivastava, A. K., Orosa, B., Singh, P., Cummins, I., Walsh, C., Zhang, C., et al. (2018). SUMO suppresses the activity of the jasmonic acid receptor CORONATINE INSENSITIVE1. *Plant Cell* 30, 2099–2115. doi: 10.1105/tpc.18.00036

Talas, F., and McDonald, B. A. (2015). Genome-wide analysis of *Fusarium graminearum* field populations reveals hotspots of recombination. *BMC Genomics* 16:996. doi: 10.1186/s12864-015-2166-0

Tanaka, S., Ichikawa, A., Yamada, K., Tsuji, G., Nishiuchi, T., Mori, M., et al. (2010). *HvCEBiP*, a gene homologous to rice chitin receptor *CEBiP*, contributes to basal resistance of barley to *Magnaporthe oryzae*. *BMC Plant Biol.* 10:288. doi: 10.1186/1471-2229-10-288

Thapa, G., Gunupuru, L. R., Hehir, J. G., Kahla, A., Mullins, E., and Doohan, F. M. (2018). A pathogen-responsive leucine rich receptor like kinase contributes to *Fusarium* resistance in cereals. *Front. Plant Sci.* 9:867. doi: 10.3389/fpls.2018.00867

Tian, Y., Tan, Y., Liu, N., Liao, Y., Sun, C., Wang, S., et al. (2016). Functional agents to biologically control deoxynivalenol contamination in cereal grains. *Front. Microbiol.* 7:395. doi: 10.3389/fmicb.2016.00395

Tibola, C. S., Fernandes, J. M. C., and Guarienti, E. M. (2016). Effect of cleaning, sorting and milling processes in wheat mycotoxin content. *Food Control* 60, 174–179. doi: 10.4315/0362-028X-47.6.489

Trujillo, M., Ichimura, K., Casais, C., and Shirasu, K. (2008). Negative regulation of PAMP-triggered immunity by an E3 ubiquitin ligase triplet in *Arabidopsis*. *Curr. Biol.* 18, 1396–1401. doi: 10.1016/j.cub.2008.07.085

Ullrich, S. E. (2010). *Barley: Production, Improvement, and Uses*. Hoboken, NJ: John Wiley & Sons.

Umego, E. C., and Barry-Ryan, C. (2022). Overview of the Irish brewing and distilling sector: processing inputs supply and quality requirements. *BrewingScience* 75, 9–16.

Union, E. (2009). Regulation (EC) No 1107/2009 of the European parliament and of the council of 21 October 2009 concerning the placing of plant protection products on the market and repealing council directives 79/117/EEC and 91/414/EEC. *Off. J. Eur. Union* 52, 1–50.

Wachowska, U., and Głowacka, K. (2014). Antagonistic interactions between *Aureobasidium pullulans* and *Fusarium culmorum*, a fungal pathogen of winter wheat. *BioControl* 59, 635–645.

Walter, S., Brennan, J. M., Arunachalam, C., Ansari, K. I., Hu, X., Khan, M. R., et al. (2008). Components of the gene network associated with genotype-dependent response of wheat to the *Fusarium mycotoxin* deoxynivalenol. *Funct. Integr. Genomics* 8, 421–427. doi: 10.1007/s10142-008-0089-4

Wang, L.-Y., Xie, Y.-S., Cui, Y.-Y., Xu, J., He, W., Chen, H.-G., et al. (2015). Conjunctively screening of biocontrol agents (BCAs) against fusarium root rot and fusarium head blight caused by *Fusarium graminearum*. *Microbiol. Res.* 177, 34–42. doi: 10.1016/j.micres.2015.05.005

Wang, Z.-W., and Liu, X.-L. (2008). Medium optimization for antifungal active substances production from a newly isolated *Paenibacillus* sp. using response surface methodology. *Bioresour. Technol.* 99, 8245–8251. doi: 10.1016/j.biortech.2008.03.039

Wegulo, S. N., Baenziger, P. S., Nopsa, J. H., Bockus, W. W., and Hallen-Adams, H. (2015). Management of Fusarium head blight of wheat and barley. *Crop Prot.* 73, 100–107.

Willyerd, K., Li, C., Madden, L., Bradley, C., Bergstrom, G., Sweets, L., et al. (2012). Efficacy and stability of integrating fungicide and cultivar resistance to manage Fusarium head blight and deoxynivalenol in wheat. *Plant Dis.* 96, 957–967.

Xue, A. G., Chen, Y., Voldeng, H. D., Fedak, G., Savard, M. E., Längle, T., et al. (2014). Concentration and cultivar effects on efficacy of CLO-1 biofungicide in controlling Fusarium head blight of wheat. *Biol. Control* 73, 2–7.

Zadoks, J. C., Chang, T. T., and Konzak, C. F. (1974). A decimal code for the growth stages of cereals. *Weed Res.* 14, 415–421.

Zhang, Y., Cheng, Y. T., Qu, N., Zhao, Q., Bi, D., and Li, X. (2006). Negative regulation of defense responses in Arabidopsis by two *NPR1* paralogs. *Plant J.* 48, 647–656. doi: 10.1111/j.1365-313X.2006.02903.x

Zhao, H., Vegi, A., and Wolf-Hall, C. (2017). Screening of lactic acid bacteria for anti-*Fusarium* activity and optimization of incubation conditions. *J. Food Prot.* 80, 1648–1656. doi: 10.4315/0362-028X.JFP-17-100

Zhao, Y., Cheng, C., Jiang, T., Xu, H., Chen, Y., Ma, Z., et al. (2019). Control of wheat fusarium head blight by heat-stable antifungal factor (HSAF) from *Lysobacter enzymogenes*. *Plant Dis.* 103, 1286–1292. doi: 10.1094/PDIS-09-18-1517-RE

Conflict of Interest: The authors declare that the research was conducted in the absence of any commercial or financial relationships that could be construed as a potential conflict of interest.

Publisher's Note: All claims expressed in this article are solely those of the authors and do not necessarily represent those of their affiliated organizations, or those of the publisher, the editors and the reviewers. Any product that may be evaluated in this article, or claim that may be made by its manufacturer, is not guaranteed or endorsed by the publisher.

frontiers | Frontiers in Microbiology

TYPE Original Research
PUBLISHED 04 August 2022
DOI 10.3389/fmicb.2022.906784

OPEN ACCESS

EDITED BY
Qunqing Wang,
Shandong Agricultural University,
China

REVIEWED BY
Cong Jiang,
Northwest A&F University, China
Xiao-Lin Chen,
Huazhong Agricultural University, China
Haifeng Zhang,
Nanjing Agricultural University,
China
Yuemin Pan,
Anhui Agricultural University,
China

*CORRESPONDENCE
Wei Tang
tangw@fafu.edu.cn
Zonghua Wang
wangzh@fafu.edu.cn

†These authors have contributed equally to this work

SPECIALTY SECTION
This article was submitted to Microbe and Virus Interactions with Plants, a section of the journal Frontiers in Microbiology

RECEIVED 29 March 2022
ACCEPTED 11 July 2022
PUBLISHED 04 August 2022

CITATION
Zhang J, Chen X, Yang Z, Xu H, Weng S, Wang Z and Tang W (2022) Endoplasmic reticulum membrane protein MoScs2 is important for asexual development and pathogenesis of *Magnaporthe oryzae*. *Front. Microbiol.* 13:906784. doi: 10.3389/fmicb.2022.906784

Endoplasmic reticulum membrane protein MoScs2 is important for asexual development and pathogenesis of *Magnaporthe oryzae*

Jun Zhang[1†], Xuehang Chen[1†], Zifeng Yang[1], Huxiao Xu[1], Shuning Weng[1], Zonghua Wang[1,2*] and Wei Tang[1,2,3*]

[1]State Key Laboratory of Ecological Pest Control for Fujian and Taiwan Crops, Ministerial and Provincial Joint Innovation Centre for Safety Production of Cross-Strait Crops, College of Plant Protection, Fujian Agriculture and Forestry University, Fuzhou, China, [2]Institute of Oceanography, Minjiang University, Fuzhou, China, [3]Fujian Key Laboratory for Monitoring and Integrated Management of Crop Pests, Fuzhou, China

Most secretory proteins are folded and modified in the endoplasmic reticulum (ER). In *Saccharomyces cerevisiae*, the absence of Scs2 protein will lead to the separation of the endoplasmic reticulum and plasma membrane, resulting in endoplasmic reticulum dysfunction, but its function is not clear in rice blast fungus or even filamentous fungus. In this study, we report the identification and characterization of *MoSCS2* in the pathogenesis of the rice blast fungus *Magnaporthe oryzae*. Protein subcellular localization showed that MoSCS2 is mainly localized in the endoplasmic reticulum. Compared to the wild-type strain Guy11, the deletion mutant Δ*Moscs2* showed a significant reduction in growth and conidiation. *MoSCS2* deficiency also resulted in abnormal conidial morphology and septum formation. The Δ*Moscs2* mutant shows delayed appressorium formation, and the appressorium of Δ*Moscs2* mutant could not form huge turgor pressure to penetrate the host epidermal cell wall. Pathogenicity and plant leave infection assays showed that knockout of *MoSCS2* significantly inhibited the expansion of the invasive hyphae in host cells, ultimately leading to the decline of pathogenicity. Moreover, *MoSCS2* gene is also involved in the regulation of cell wall and endoplasmic reticulum stress response. In conclusion, *MoSCS2* plays an important role in the growth, asexual production, conidia morphogenesis, infection-related morphogenesis and pathogenicity of *M. oryzae*.

KEYWORDS

***Magnaporthe oryzae*, ER-PM, tail-anchored protein, pathogenesis, asexual development**

Introduction

Magnaporthe oryzae, an intriguing ascomycete fungal pathogen causes the most devastating rice blast disease (Talbot, 2003). It spreads rapidly between hosts by wind and rain and impacts rice production worldwide, especially in the changing climate (Pringle and Taylor, 2002). It has become a model organism for studying the interaction between

pathogens on plants and the plants they infect (Ebbole, 2007; Dean et al., 2012). The fungus produces pyriform conidia, which is important for fungal pathogenesis, partially because conidia are the primary inoculums and facilitate disease dissemination in the host (Howard et al., 1991). Conidia are produced by the apex of the conidiophores where two round mitotic divisions and the formation of two septa. Finally, the conidia form a three-celled structure by nuclear migration and positioning. During the appropriate environment condition, germination and differentiation of the conidium result in a specialized infection structure on the hydrophobic surface, appressorium (Dean, 1997). Interestingly, the appressorium can generate an enormous turgor pressure to mechanically penetrate plant tissues (Oses-Ruiz et al., 2017). Subsequently, invasive hyphae (IH) are produced by the penetration peg that can rapidly penetrate the cuticle and underlying plant cells (Yi and Valent, 2013). After colonization for 1 week, a large number of infection diseases appear on the leaf surface, where conidia are produced and enter new invasive breeding (Howard and Valent, 1996). To promote infection, *M. oryzae* secretes a large number of effector proteins during rice–pathogen interaction to inhibit plant defense response (Fernandez and Orth, 2018). There are two different secretory pathways of effector proteins during infection. Secretion of apoplastic effectors takes place within the traditional ER-Golgi secretory pathway, in contrast, the exocyst complex is responsible for delivering cytoplasmic effectors (Giraldo et al., 2013). In eukaryotic cells, proteins secreted by ribosomes are processed and modified within the ER (Liu et al., 2014). Upon reaching the Golgi apparatus, mature proteins are packed into secretory vesicles, then they can release their contents into the extracellular space by fusion with the cytoplasmic membrane (Cui et al., 2015). As is known to us the ER contacts numerous organelles. There is a special connection between the ER and the plasma membrane (PM), which is called ER-PM (Stefan et al., 2013). The ER-PM junction plays an important role in many physiological processes, such as lipid metabolism and control of calcium (Ca^{2+}) dynamics (Spang, 2018). In yeast cells, the cortical ER (cER) is extensively associated with PM, and this association requires several tethering proteins that staple them together (West et al., 2011).

There are at least six proteins that act as tethers contribute to ER–PM contact sites: two VAMP-associated proteins (Ssc2/22), three extended synaptotagmins (*Tcb1/2/3*), and the putative ion channel (*Ist2*; Loewen and Levine, 2005; Stefan et al., 2011; Manford et al., 2012). Ist2 is related to the TMEM16-anoctamin family of ion channels and phospholipid scramblases, the deletion of *Ist2* results in a significantly lower proportion of cER structures, while the overexpression of *Ist2* results in the increase of ER-PM contact sites (Kunzelmann et al., 2016). Scs2 and Scs22 are homologs of the yeast vesicle-associated membrane protein (VAMP)-associated protein (VAP; Kato et al., 2017). They were anchored in the ER through the C-terminal (transmembrane domain) and contained the MSP (Major SPERM Protein) domain at the N-terminal (Quon et al., 2018). The MSP domain of Scs2/22 can bind to plasma membrane proteins containing FFAT (two phenylalanines in an acidic tract) or FFAT-like motifs (Loewen and Levine, 2005; Manford et al., 2012), In yeast cells, Scs2/22 are associated with cER inheritance, deletion of Scs2/22 will cause a loss of cER associated with the PM (Loewen et al., 2007). Scs2/22 also has a PH domain that interacts with phosphoinositides at the PM (Kaiser et al., 2005). At the ER-PM contact sites, Scs2 interacts with the oxysterol-binding homology protein Osh3 to activate Sac1 which is located in ER. The interaction between Scs2 and Septin Shs1 can form an ER diffusion barrier to prevent intact ER proteins from diffusing between the ERs of the mother and the daughter cells (Luedeke et al., 2005; Chao et al., 2014). Tcb1/2/3 bind to the PM by means of lipid-binding C2 domains, while TCB1/2/3 also has an SMP domain, which participates in the exchange of phospholipids and diglycerol esters between the PM and ER (Giordano et al., 2013). Tcb1/2/3 was homologous to the extended synaptotagmin-like proteins E-syt1/2/3 (Min et al., 2007). The absence of all six proteins results in a massive reduction in ER-PM contacts and morphological changes in ER (Manford et al., 2012). Meanwhile, misregulation of phosphoinositol signaling at PM occurs in cells lacking the ER-PM adaptor protein (Zhang et al., 2012), and the activation of unfolded protein response is constitutive in the ER (Luedeke et al., 2005). In conclusion, ER-PM contact sites play an important role in cell signal transduction organelle morphology and endoplasmic reticulum function.

Previous studies have demonstrated that MCS (Membrane Contact Sites) between ER and PM play an important role in eukaryotic cells, and this connection is critical for the transport of substances such as protein lipids and ions between ER and PM (Mentlak et al., 2012), it can provide a platform for material exchange and signal transduction between organelles (Stefan et al., 2013). The cER and PM make extensive contacts, and the ER-localized PI phosphatase Sac1 reversely regulated the level of phosphatidylinositol-4-phosphate (PI4P; Stefan et al., 2011). It is observed in yeast cells that Scs2/ Scs22 contribute to the ER-PM junction and Sac1-mediated PI4P turnover (Loewen et al., 2007; Stefan et al., 2011).

In this study, we identified Scs2 orthologous protein in *M. oryzae*. To investigate the importance of Scs2 in *M. oryzae*, we analyzed the functions of Scs2 in the different developmental stages. Based on our studies, we demonstrate that Scs2 is located in the ER and plays a crucial role in vegetative growth, asexual reproduction infection-related morphogenesis and pathogenicity of *M. oryzae*.

Materials and methods

Strains and culture conditions

The *M. oryzae* strain Guy11 was used as WT for transformation in this study. All strains were cultured on CM agar plates (CM: 10 g D-glucose, 2 g peptone, 1 g yeast extract, 1 g casamino acids, 50 ml

20 × nitrate salts, 1 ml trace elements, 1 ml vitamin solution, 15 g agar, add distilled water to 1 l) at 28°C (Talbot et al., 1993). Liquid CM medium was used to harvest the mycelia for protoplast preparation, genomic DNA, RNA and protein extraction.

The protoplast-mediated transformation of *M. oryzae* was performed for gene deletion and complementation assays by using hygromycin B and bleomycin as a selective marker as described (Sweigard et al., 1992). Hygromycin B (250 mg/ml, Calbiochem, La Jolla, CA) or bleomycin (200 mg/ml, Invitrogen, Carlsbad, CA) was used for transformant selection on TB3 medium (3 g of yeast extract, 3 g of casamino acids, 200 g of sucrose, 7.5 g of agar in 1 l of distilled water).

Targeted gene deletion and complementation

The gene-deletion mutants were generated using the standard one-step gene replacement strategy as described (Tang et al., 2015; Pan et al., 2019). Two 1.0 kb of sequences flanking the targeted gene was PCR amplified from *M. oryzae* genomic DNA using the primer pairs (Supplementary Table S1) respectively; the hygromycin phosphotransferase (*hph*) cassette were PCR amplified from pCX62 using the primer pair HYG F(F)/HYG R(R; Supplementary Table S1). The double-joint PCR approach was used to generate the gene replacement construct for the *MoSCS2* gene which contained the flanking sequences and *hph* cassette for each gene were transformed into protoplasts of the WT Guy11 (Yu et al., 2004). Putative mutants were firstly screened by PCR and further confirmed by Southern blotting analysis (Supplementary Figure S1; Supplementary Table S1). One mutant strain for either gene disruption (Δ*Moscs2#3*) was randomly selected for further analysis (Supplementary Figures S1C,D). The complement fragments, which contain the entire *MoSCS2* gene and the native promoter regions, were amplified by PCR with primers (Supplementary Table S1) and inserted into pYF11 (Bleomycin resistance) to generate *MoSCS2-GFP* or *MoSCS2*$^{\Delta TMD}$-*GFP* fusion constructs which were used to complement the respective mutant strains. Transformants expressing the constructs were identified by PCR and confirmed by fluorescent microscopy.

Assays for vegetative growth, conidiation, and appressorium formation

Small agar blocks were cut from the edge of 4-day-old cultures and placed onto fresh media (CM and SDC) for culturing in the dark at 28°C for 7 days, and colony diameter was measured by ruler before photographing. To assay for defects in ER stress responses, the growth rate was measured with cultures grown on CM with 2 mM DTT or 0.2 μg/ml TM. For conidiation, strain blocks were maintained on straw decoction and corn (SDC: 100 g of straw, 40 g of corn powder, 15 g of agar in 1 l of distilled water) agar media at 28°C for 7 days in the dark followed by 3 days continuous illumination under fluorescent light. Calcofluor White (CFW) staining was performed by using fluorescent brightener 28 (10 μg/ml, Sigma-Aldrich) for the microscopy of conidia and viewed under the fluorescence microscope. Appressorium formation on artificial hydrophobic surface and infection on barley epidermal cells were measured as described previously (Tang et al., 2019). For appressorium induction on rice leaves, conidial suspension (5×10^4 spores per milliliter) was dropped on rice leaves and directly observed under microscopy.

Pathogenicity and plant leave infection assays

Plant infection and injection assays were performed as described (Zhang and Xu, 2014). Conidia were resuspended to a concentration of 5×10^4 spores per milliliter in 5 ml of 0.2% (w/v) gelatine solution. For detached barley leaves inoculation, 5-day-old barley (*Hordeum vulgare* cv. Golden Promise) leaves were cut and laid into 15 cm dishes under humid conditions, and 20 μl of the conidial suspension was placed onto each inoculation site of barley leaves followed by incubation at 28°C for 5 days and photographed. For spray inoculation on rice, a conidial suspension was sprayed onto 2-week-old seedlings of rice (*O. sativa* cv. CO39). For injected inoculation, conidial suspension was injected into the rice sheath by using 1 ml syringe. Inoculated plants were kept in a growth chamber at 25°C with 90% humidity and in the dark for the first 24 h, followed by a 12-h/12-h light/dark cycle for 7 days to examine the lesion formation. Host-derived ROS was detected by staining with DAB (3,3-diaminobenzidine, D-8001, Sigma-Aldrich, United States) as described (Wang et al., 2019). For microscopic observation of hyphal expansion in plant cells, the same concentration of conidial suspension was injected into the detached rice sheaths followed by incubation at 28°C for 36 h, and rice sheaths were observed and photographed under a light microscope (Tang et al., 2019).

Protein subcellular localization

A Nikon A1 plus confocal microscope (Nikon, Tokyo, Japan) was used to observe fluorescent light of transformants expressing MoScs2-GFP or MoScs2$^{\Delta TMD}$-GFP. The emission wavelength and excitation wavelength is 525.0 nm and 488.0 nm for GFP fluorescence.

Stress response

Mycelia plugs were placed onto CM agar plates with 2 mM DTT, 0.2 μg/ml TM, 400 μg/ml CFW, 400 μg/ml CR, 0.005% SDS and cultured in the dark at 28°C for 7 days to determine their effects on fungal growth. The inhibition rate was determined by

the percent decrease in the colony diameter. The experiment was repeated three times with three replicates each time.

Results

Identification and characterization of MoSCS2 in *Magnaporthe oryzae*

Scs2 orthologs are well conserved in fungi. We performed a BLASTP search of the *M. oryzae* genome[1] using the sequence of Scs2/Scs22 from *Saccharomyces cerevisiae* as a query and named *MoSCS2* (MGG_06183). *MoSCS2* is predicted to encode a 285-amino-acid (aa) protein, respectively. Domain prediction reveals that MoSCS2 possesses a motile sperm domain (108 aa) at the N-terminus and a transmembrane domain (TMD; 20 aa) at the C-terminus (Supplementary Figure S1A).

Targeted gene deletion and complementation of MoSCS2

To test the function of *MoSCS2*, we generated a construct for gene replacement and transformed into the wild-type (WT) Guy11. At least five independent *MoSCS2* deletion mutants with identical phenotypes were verified by PCR and confirmed by Southern blot analysis using gene-specific primers and probes (Supplementary Figure S1; Supplementary Table S1). Therefore, one mutant strain (Δ*Moscs2#3*) was randomly selected for further analysis (Supplementary Figures S1C,D). To ascertain that the observed phenotypes of the gene disruption mutants were due to the deletion of the *MoSCS2* gene, the complementation of transformants was generated by transforming the native promoter-driven MoScs2-GFP fusion constructs into the corresponding mutant. The complemented strains with GFP signals were achieved and recovered all the phenotypic defects. One of which was randomly selected for further study.

MoScs2 is an ER-localized protein in *Magnaporthe oryzae*

To further clarify the localization characteristics of *MoSCS2* in different growth and development stages of *M. oryzae*, we constructed the GFP fusion protein expression vector of *MoSCS2* (pYF11::*MoSCS2*). We then co-expressed the ER-targeted MoLhs1-RFP in the fluorescent strain expressing MoScs2-GFP strain. Co-localization between MoScs2-GFP and MoLhs1-RFP supported our assumption that *MoSCS2* can be expressed in vegetative mycelia, conidia, appressorium, and infection mycelia (Figures 1A,B). These results suggested that MoScs2 was localized in the ER during each growth and development stage of *M. oryzae*.

1 http://fungidb.org/fungidb/

MoSCS2 is important for hyphae growth, conidiation and conidia morphology

To investigate the role of MoScs2 in vegetative growth, analyses were carried out in *M. oryzae* to determine the effects of disrupting *MoSCS2* on growth and morphology, and the growth phenotype was compared with WT and its corresponding complemented strains. After incubation at 28°C for 7 days, a recognizable change in colony morphology was observed in Δ*Moscs2* mutant colonies. As compared to the WT, the Δ*Moscs2* developed significantly slower, and a reduced number of aerial hyphae was evident (Figure 2). These results indicated that *MoSCS2* has an important role in vegetative hyphal growth.

To investigate the role of *MoSCS2* in asexual development, quantifying conidium production of the corresponding strains on SDC media was carried out as well. Compared with the WT and Δ*Moscs2/MoSCS2*, the Δ*Moscs2#3* produced considerably fewer conidia and reduced approximately 60% in conidiation (Figures 3A,B).

In addition, part of the conidia produced by the Δ*Moscs2* mutant showed aberrant morphology (Figure 3C). The conidial length of the Δ*Moscs2* mutant was significantly shorter (Figure 3D), further examination by CFW staining showed that over 90% of conidia of the Δ*Moscs2* mutant showed abnormal morphology which had only one or no septum, while the conidia of the WT were pyriform and 85% possessed two septa (Figures 3C,D). These results indicated that the loss of *MoSCS2* affects conidiogenesis and conidial morphology.

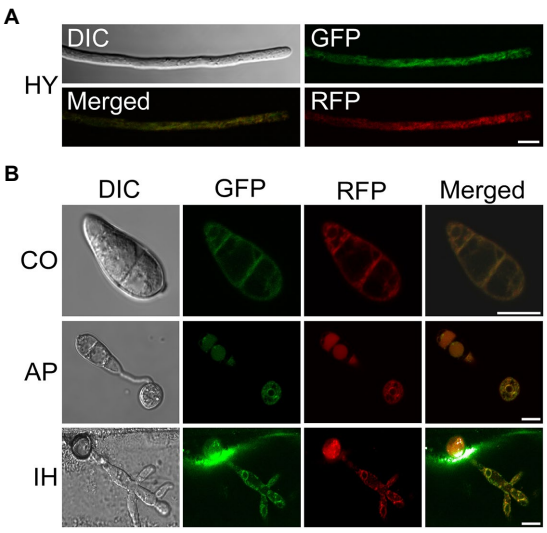

FIGURE 1
Subcellular localization of MoScs2 at different developmental stages of *M. oryzae*. **(A)** Hyphae (HY) co-localization of MoScs2-GFP together with the MoLhs1-RFP endoplasmic reticulum marker. **(B)** Conidia (CO), appressorium (AP) and invasive hyphae (IH) co-localization of MoScs2-GFP together with the MoLhs1-RFP endoplasmic reticulum marker. Localization of MoScs2-GFP were examined by Nikon laser confocal. Scale bar=10 μm. DIC, Differential interference contrast.

10.3389/fmicb.2022.906784

Deletion of *MoSCS2* impaired the pathogenicity of *Magnaporthe oryzae*

To further test the role of *MoSCS2* in pathogenesis, conidial suspensions (5×10^4 spores/ml) from the wild-type strain Guy11, the Δ*Moscs2* mutant and complemented strain were sprayed onto susceptible rice seedlings of CO-39. It was found that the Δ*Moscs2* mutant produced significantly fewer lesions than wild-type strains after 7 days of inoculation. Additionally, the lesions produced by Δ*Moscs2* mutant were also smaller and less expansive, in contrast to the fully expanded necrotic lesions produced by wild-type strain Guy11 and the complemented strain (Figure 4A). We obtained similar results from infection assays with seedlings of barley or by using the injection inoculation on rice (Figures 4B,C). The results demonstrate that *MoSCS2* plays a vital role in pathogenicity.

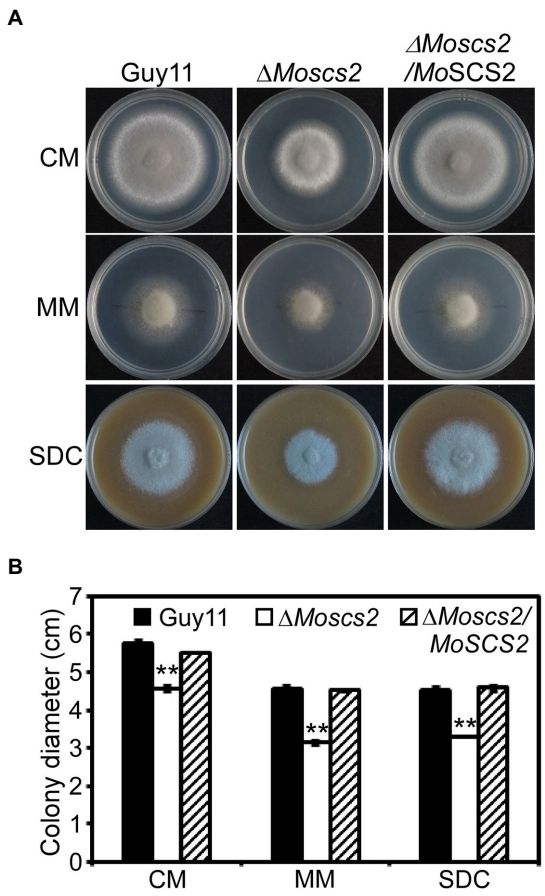

FIGURE 2
Effects of MoScs2 on hyphal growth. **(A)** Colony morphology and diameter of WT, Δ*Moscs2*, and the complemented strain cultured on CM, SDC, and MM. Photographs were taken after 7days of incubation. **(B)** Statistical representation of average growth characteristics of the Δ*Moscs2* mutant compared to Guy11 and the complemented strain. Data used for statistical computation were obtained from three independent biological experiments with each time four replicates each time. Experiments were repeated with similar results. Asterisks represent a significant difference between Guy11 and the Δ*Moscs2* strain (Duncan's new multiple range test, $p<0.01$).

A reduction in pathogenicity in Δ*Moscs2* mutant was attributed to defects in penetration and invasive hyphae growth

We inoculated rice leaf sheath and barley epidermal cells with the conidial suspensions. Following 36 h of incubation with rice leaf sheaths containing spore suspensions, invasive hyphae formed freely and expanded into neighboring cells in the wild type and the complementation strains. By contrast, the Δ*Moscs2* mutant showed restricted invasive hyphal growth, which was confined to the first plant cells (Figure 4D).

Furthermore, a similar result was observed when inoculations were done on barley epidermal cells. After incubation with spore suspensions for 36 h, compared with the WT and complemented strains, fewer invasive hyphae were observed in the Δ*Moscs2* mutant, and the branches are significantly reduced. We classify the invasive hyphae into 4 types (type 1, no penetration; type 2, with penetration peg; type 3, with a single invasive hypha; type 4, with extensive hyphal growth). In WT and the complemented strains, approximately 80% of cells displayed type 4, 15% showed type 3 and 5% showed type 2. Nonetheless, less than 20% of cells showed type 4 and type 3, and 80% showed type 1 and type 2 in the Δ*Moscs2* mutant (Figure 4E). Taken together, these results suggest that *MoSCS2* is required for appressorial penetration and invasive hyphal growth. Moreso, these data suggest that the limited invasive hyphal extension of the mutant may be the cause of a significant reduction in pathogenicity.

MoSCS2 is involved in the regulation of appressorium development, turgor pressure and host-produced reactive oxygen species (ROS) accumulation

To further investigate whether the compromised pathogenicity of the Δ*Moscs2* mutant was related to the defects in appressorium development, spores of WT, the Δ*Moscs2* mutant and the complemented strains were inoculated onto artificial hydrophobic surfaces. After inoculation for 8 h, compared with the WT and complemented strains, the majority of the Δ*Moscs2* mutant produced unmelanized appressoria. The appressorium formation of the Δ*Moscs2* mutant appeared to be delayed, and the conidia germination rate was lower than that of the WT. However, the appressorium formation and maturation were similar in all the strains by 24 h (Figure 5A). These results indicated that deletion of *MoSCS2* gene delayed appressorium development, but did not affect the appressorium formation.

The huge appressorium turgor pressure is essential for *M. oryzae* to penetrate the plant epidermal cell and causes disease. To further clarify whether the deletion of *MoSCS2* gene affects the turgor pressure in appressorium and leads to attenuation of pathogenicity, we tested the appressorium turgor pressure by cytolysis assays. We treated appressoria with 1 M, 2 M, 3 M, and 4 M glycerol, respectively. Our results

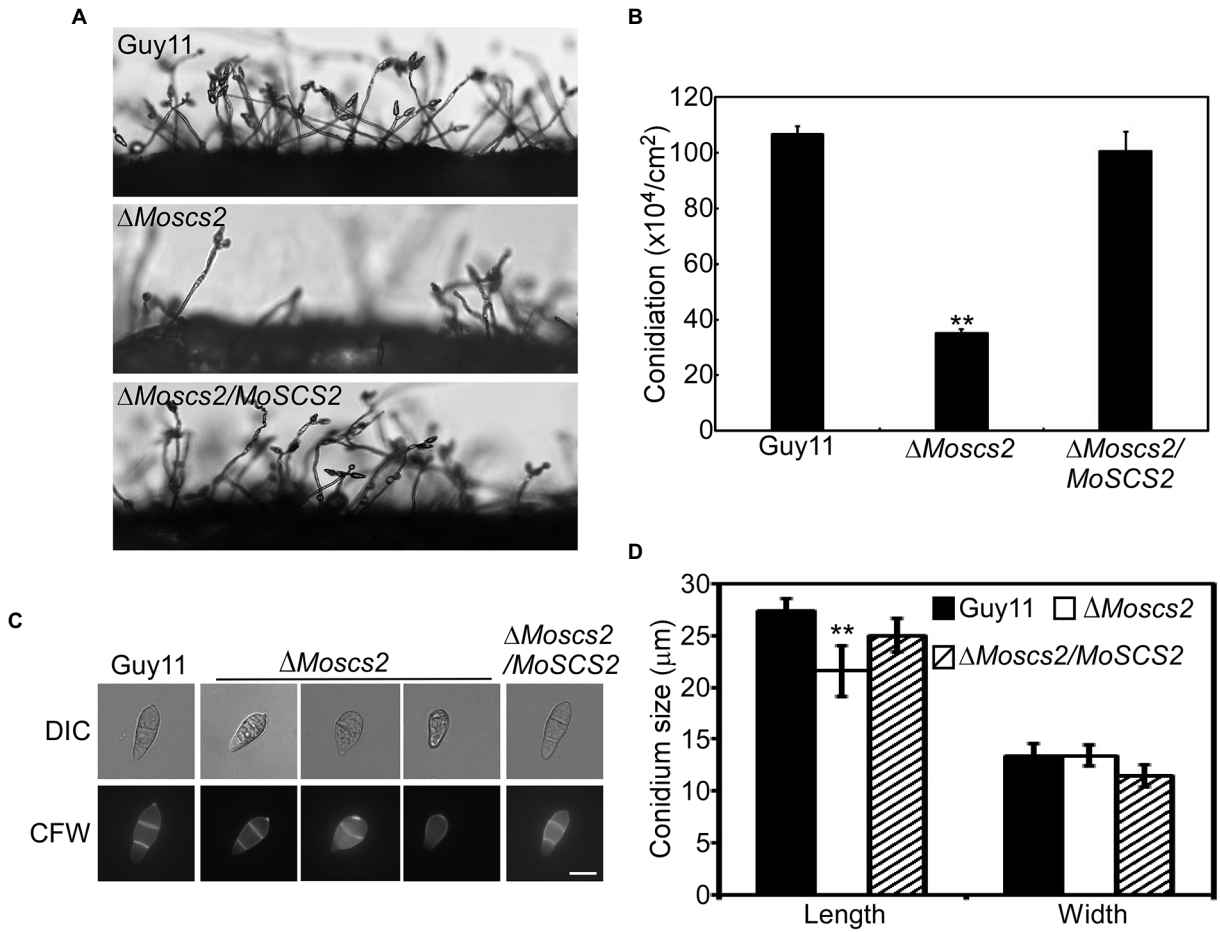

FIGURE 3
MoScs2 is important for asexual development. **(A)** Conidia formation was observed under a light microscope after 24h incubation at room temperature after induction of conidiation on coverslips. **(B)** Statistical representation of the conidiation characteristics of the Δ*Moscs2* mutant, the WT and the complemented strain. **(C)** Conidium shape comparison. The conidia of the indicated strains were stained with Calcofluor white (CFW) and photographed. **(D)** Statistical analysis of the conidium size of the indicated strains. Error bars represent SD of three replicates and asterisks represent a significant difference between Guy11 and the Δ*Moscs2* strain (Duncan's new multiple range test, $p<0.01$). Scale bar=10 μm.

showed that the Δ*Moscs2* mutant displayed a higher collapsed rate than the WT and complemented strains. Moreover, the collapse rate of appressorium in the Δ*Moscs2* mutant was twice that of the others at 1 M and 2 M glycerol (Figure 5B), indicating MoScs2 is important for normal turgor of appressorium. Moreover, 3,3′-diaminobenzidine (DAB) staining assays of the penetrated plant cells showed the accumulation of ROS at the infection site of the Δ*Moscs2* mutant, but not the wild type and complemented strains (Figure 5C). These results indicated that deletion of *MoSCS2* affects appressorium development, turgor pressure and host-produced ROS accumulation.

MoScs2 contribute to ER morphology

We further determined whether the deletion of *MoSCS2* contributes to ER morphology by using Lhs1-RFP transgenic strains. Lhs1 is an endoplasmic reticulum protein, a RFP-labeled LHS1 was expressed in both WT and the Δ*Moscs2* mutant to monitor ER morphology. Compared with the WT, the ER morphology of about 56 ± 3.9% vegetative mycelium and 63 ± 3.6% conidia of the Δ*Moscs2* mutant was abnormal (Figures 6A,B), with a majority of the ER appearing to be invaginated or diffuse. This result indicated that the deletion of *MoSCS2* gene would affect the ER morphology.

MoScs2 is involved in the regulation of ER stress response

Dithiothreitol (DTT) and tunicamycin (TM) are typical inducers that disturb ER homeostasis and induce ER stress. To investigate whether MoScs2 is important for the ER stress response, we test the sensitivity of the Δ*Moscs2* mutant strains towards DTT and TM. When exposed to 2.0 mM DTT, the

10.3389/fmicb.2022.906784

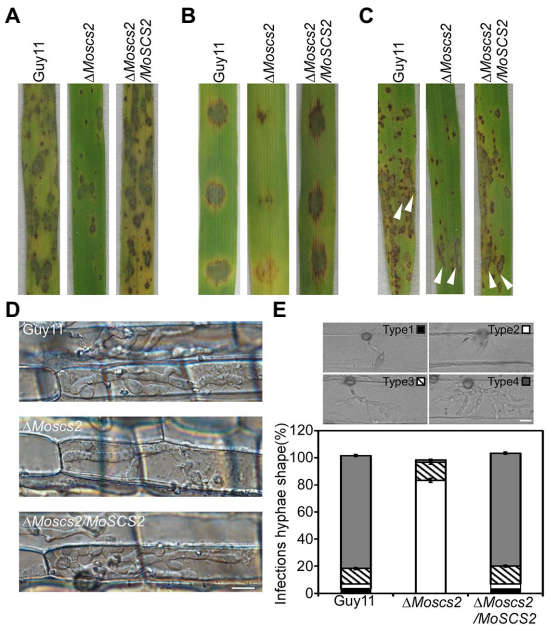

FIGURE 4
MoScs2 is crucial for the pathogenicity of *M. oryzae*. **(A)** Rice seedlings were sprayed with conidial suspension from the indicated strains and examined at 7 dpi. **(B)** Detached barley leaves were drop-inoculated with conidial suspensions and examined at 5 dpi. **(C)** Pathogenicity was tested by injection with conidia of the indicated strains. **(D)** Excised rice sheath from 4-week-old rice seedlings was inoculated with conidial suspensions. Infectious growth was observed at 1.5 dpi. **(E)** Statistical analysis for each type (type 1, no penetration; type 2, with penetration peg; type 3, with a single invasive hypha; type 4, with extensive hyphal growth) of infectious hyphal shape, for each tested strain; more than 30 infected sites were counted per replicate. Experiments were repeated with similar results. Scale bar=10 μm.

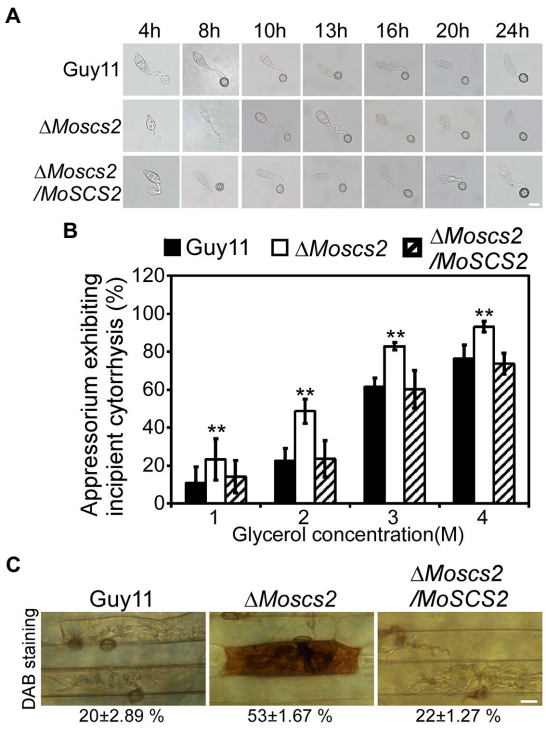

FIGURE 5
Effects of MoScs2 on appressorium development and turgor pressure of *M. oryzae*. **(A)** Appressorium formation were tested on artificial hydrophobic surface of the indicated strains at different time-points. **(B)** Collapsed appressoria were observed in mutant strain. For each glycerol concentration, at least 60 appressoria were observed and the numbers of collapsed appressoria were counted. Error bars represent SD of three replicates and asterisks represent a significant difference between Guy11 and the Δ*Moscs2* strain (Duncan's new multiple range test, $p<0.01$). **(C)** DAB-staining of the indicated strains-infected barley epidermis cells. Percentage of DAB-stained barley epidermis cells infected by the strains were shown at the bottom of the micrograph. Scale bar=10 μm.

Δ*Moscs2* mutant exhibited remarkably heightened sensitivity to DTT (Figure 7A). The deletion of both *MoSCS2* caused severe inhibitory hyphal growth (42% inhibition rate). Similarly, when exposed to 0.2 μg/ml TM, the Δ*Moscs2* mutant heightened significantly sensitivity compared with the WT and the complemented strain with a 50% inhibition rate (Figure 7B). These data suggest that *MoSCS2* is involved in the regulation of ER stress response.

MoScs2 is involved in the regulation of cell wall stress responses

To investigate the contribution of *MoSCS2* genes in cell wall stress responses, the vegetative growth of all strains was monitored and measured on CM medium with the addition of cell wall stressors Calcofluor white (CFW), Sodium Dodecyl Sulfate (SDS), and Congo Red (CR). Following 7 days post-inoculation, our results indicated that the inhibition rate of the three cell wall stressors against the Δ*Moscs2* mutant was lower than that of the

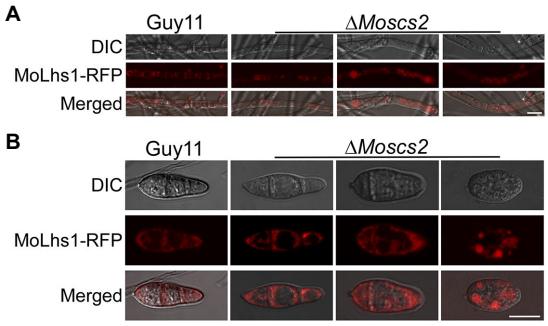

FIGURE 6
MoScs2 is involved in the regulation of ER morphology. ER marker protein MoLhs1-RFP was introduced into the indicated strain and hyphae **(A)** and conidia **(B)** of the resulting transformants were observed under an epifluorescence microscope. Scale bar=10 μm.

WT and the complemented strain (Figures 8A,B). The above results indicated that MoScs2 is involved in the regulation of cell wall stress responses of *M. oryzae*.

Functional characterization of MoScs2 transmembrane domain

To clarify the function of a transmembrane domain (TMD) of *MoSCS2* during vegetative growth, domain deletion constructs were fused with GFP to generate the MoScs2$^{\Delta TMD}$-GFP (loss of the transmembrane domain) which were transformed into the Δ*Moscs2* mutant. The resulting transformants (Δ*Moscs2*/*MoSCS2*$^{\Delta TMD}$) were evaluated for GFP signals and analyzed. The wild-type (Guy11), Δ*Moscs2* mutant, and Δ*Moscs2*/*MoSCS2*$^{\Delta TMD}$ strains were inoculated on CM, MM, and SDC media. After 7 days, compared with the wild-type strain, the Δ*Moscs2*/*MoSCS2*$^{\Delta TMD}$ showed a reduced hyphal growth rate similar to that of the Δ*Moscs2* mutant (Figures 9A,B). We also observed the localization of the transmembrane domain deletion transformant. Compared with the MoScs2-GFP strain, the GFP signal of the Δ*Moscs2*/*MoSCS2*$^{\Delta TMD}$ mutant was diffused in the conidia. We further test the pathogenicity of these mutants on rice and found that the Δ*Moscs2*/*MoSCS2*$^{\Delta TMD}$ mutants displayed pathogenic defects similar to that of the Δ*Moscs2* mutant (Figure 9D). The above results indicate that the TMD of *MoSCS2* is pivotal for the growth, pathogenicity and subcellular localization in *M. oryzae* (Figure 9C).

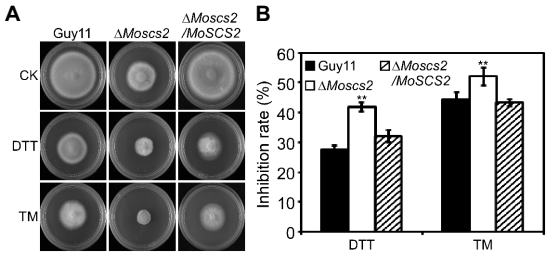

FIGURE 7
The Δ*Moscs2* mutant heightened sensitivity to ER stress. **(A)** Growth of Guy11, the Δ*Moscs2* mutant and complemented strains in CM media supplemented with TM or DTT. **(B)** Colony diameters were determined in each independent biological experiment after 7days. Measurements of growth inhibition rate are relative to the growth rate of each untreated control. Error bars represent SD of three replicates and asterisks represent a significant difference between Guy11 and the Δ*Moscs2* strain (Duncan's new multiple range test, $p<0.01$).

Discussion

In *S. cerevisiae*, the absence of Scs2 protein will lead to the separation of ER and plasma membrane, resulting in the ER dysfunction, but its function remains unkonwn in rice blast fungus or even filamentous fungus. In this study, we focused on the characteristics of *MoSCS2* in *M. oryzae* and its effect on the vegetative growth, asexual reproduction, and pathogenicity of *M. oryzae*. To elucidate the function of *MoSCS2* in *M. oryzae*, *MoSCS2* gene was deleted by homologous recombination, and the morphological characterization and pathogenicity of wild-type strain Guy11, *MoSCS2* deletion mutant and its complementary transformant were analyzed.

In yeast cells, Scs2/Scs22 localizes to both the nuclear and cytoplasmic ER structures in addition to the cER (Loewen et al., 2007). After the deletion of Scs2/Scs22, the cER was significantly reduced and PI4P accumulation level was higher (Manford et al., 2012). What we found in *M. oryzae* is that MoScs2 was localized in the ER. And compared to wild-type strain Guy11, the growth rate of Δ*Moscs2* mutant is significantly slower, and the asexual

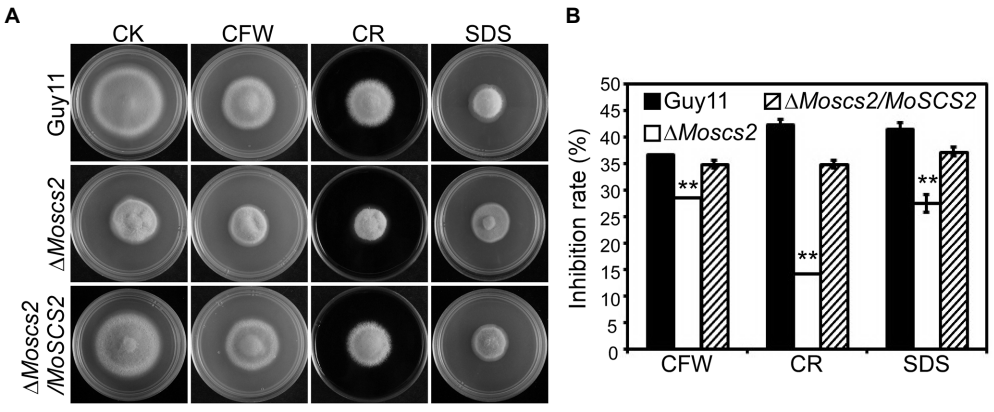

FIGURE 8
(A) Effects of MoScs2 on cell wall integrity of *M. oryzae*. Growth of Guy11, the Δ*Moscs2* mutant and complemented strains in CM media supplemented with CFW, CR or SDS. **(B)** Colony diameters were determined in each independent biological experiment after 7days. Measurements of growth inhibition rate are relative to the growth rate of each untreated control. Error bars represent SD of three replicates and asterisks represent a significant difference between Guy11 and the Δ*Moscs2* strain (Duncan's new multiple range test, $p<0.01$).

10.3389/fmicb.2022.906784

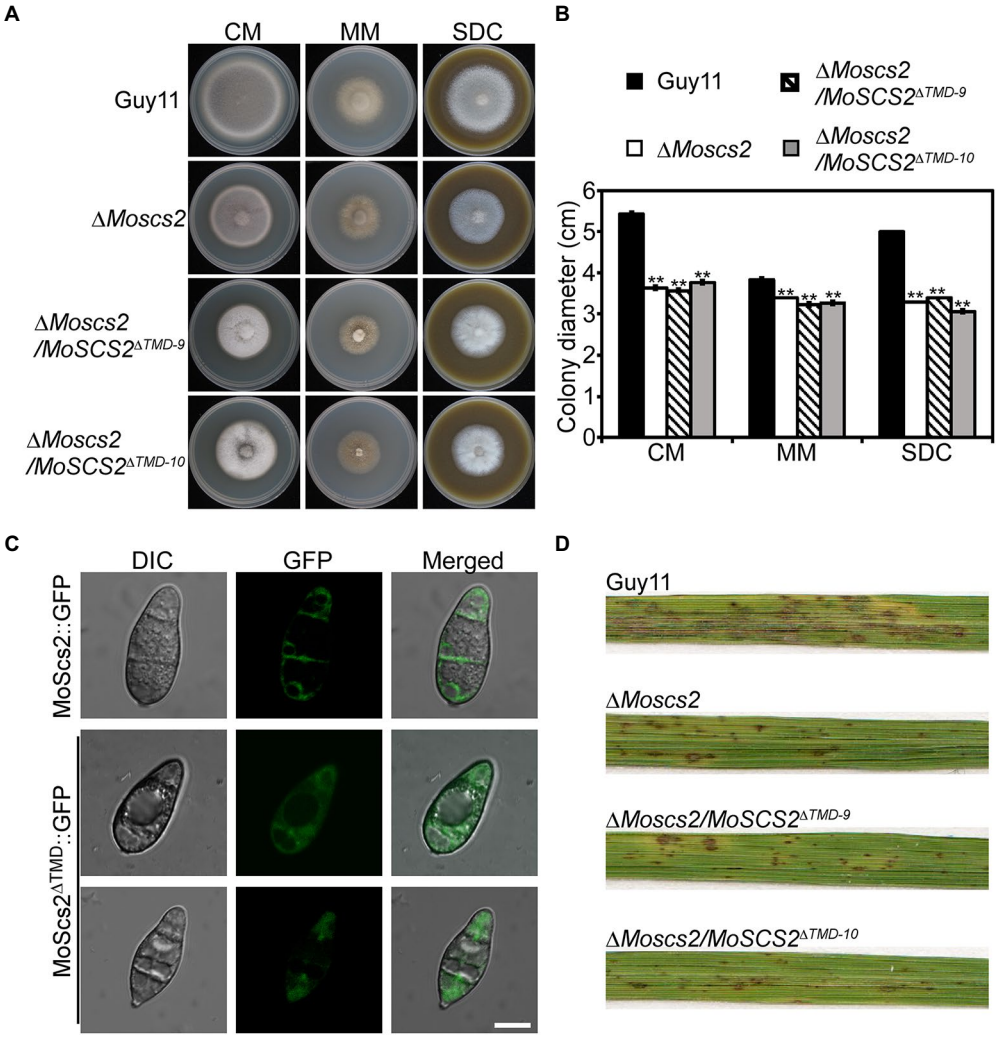

FIGURE 9
Functions of TMD domain of MoScs2 in *M. oryzae*. **(A)** The wild-type (Guy11), Δ*Moscs2* mutant, and Δ*Moscs2/MoSCS2*$^{\Delta TMD}$ strains were inoculated on CM, MM, and SDC media and cultured at 28°C in the dark for 7days and then photographed. **(B)** Statistical analyses of the colony diameter of Guy11, the Δ*Moscs2* mutant, Δ*Moscs2/MoSCS2*$^{\Delta TMD}$ strains on different media. Error bars represent the standard deviations; asterisks denote statistical significances ($p<0.01$). **(C)** Subcellular localization of the MoScs2$^{\Delta TMD}$-GFP fusion proteins. Conidia of the transformant expressing MoScs2-GFP or MoScs2$^{\Delta TMD}$-GFP were examined by differential interference contrast (DIC) and epifluorescence microscopy. Scale bar=10 μm. **(D)** Two-week-old rice seedlings were sprayed with conidial suspensions of the wild-type (Guy11), Δ*Moscs2* mutant, and Δ*Moscs2/MoSCS2*$^{\Delta TMD}$ strains. Diseased leaves were photographed 7days after inoculation.

reproduction ability of the mutant is significantly reduced. Further experiments showed that the deletion of *MoSCS2* also affected the septum formation of the conidia, and delayed the appressorium development. Plant leaves infection assays showed that knockout of *MoSCS2* significantly inhibited the expansion of the invasive hyphae in cells. This result may reflect the important role of MoScs2 during invasive growth. Moreover, the appressorium of Δ*Moscs2* mutant could not form huge turgor pressure to penetrate the host epidermal cell wall, and invasive hyphal growth was limited in host cells, probably ultimately leading to the pathogenic defects.

ER is known to be the main intracellular organelle responsible for protein synthesis and secretion. Based on the phenotype of Δ*Moscs2* mutant, we speculated that the impaired ER morphology of the mutant may lead to ER dysfunction. To test this hypothesis, we treated Δ*Moscs2* mutant with DTT and TM which could disturb ER homeostasis and induce ER stress, respectively. Then we found that the mutant was more sensitive to the ER pressure inducers. The above results all confirmed that the ER homeostasis was compromised in the Δ*Moscs2* mutant. In addition, there is evidence that ROS are critical components during the host-pathogen interaction, and play key roles in rice against *M. oryzae* (Kou et al., 2019). According to our research, DAB staining assays of the penetrated plant cells showed the accumulation of ROS at the infection site of the Δ*Moscs2* mutant. This result suggests that *MOSCS2* is involved in regulating host-driven ROS scavenging

during infection. The rice blast fungus secretes a large number of effectors into rice cells to suppress plant immunity. We speculate that the ER dysfunction in the Δ*Moscs2* mutant may lead to a defective secretory efficiency and then disturb the effector secretion to suppress immunity. It would be interesting to determine the secretion of known effector proteins in the Δ*Moscs2* mutant in future research.

Scs2 contains a single transmembrane domain (TMD) and a cytoplasmic MSP domain (Manford et al., 2012). Moreover, the mutant Scs2 protein lacking its TMD localized in the nucleus rather than the ER (Manford et al., 2012). According to our results, the pathogenicity of the Δ*Moscs2* mutant reduced after the function of the ER was impaired. To clarify the cause, we knock out the TMD of *MoSCS2* in *M. oryzae*. Based on the phenotype analysis we found that the Δ*Moscs2*/*MoSCS2*$^{\Delta TM^D}$ mutant was unable to restore the defective phenotype and the protein localization. These results suggest that the TMD domain plays an important role in the function of *MoSCS2*.

In conclusion, our study illustrates that MoScs2 plays an important role in the growth, asexual development, conidia morphogenesis, appressorium formation and pathogenicity of *M. oryzae*, but its specific pathogenic mechanism needs further study.

Data availability statement

The original contributions presented in the study are included in the article/Supplementary material; further inquiries can be directed to the corresponding authors.

Author contributions

ZW and WT designed this study. JZ, XC, ZY, HX, and SW performed experiments and analyzed all data. JZ, WT, and ZW wrote the initial manuscript. All authors contributed to the article and approved the submitted version.

Funding

This research was funded by the National Natural Science Foundation of China (No. U1805232), the Special Fund Project for Science and Technology Innovation of Fujian Agriculture and Forestry University (No. CXZX2020014A), and the Program of Fujian Key Laboratory for Monitoring and Integrated Management of Crop Pests, Fuzhou 350013, China (No. MIMCP-202101).

Conflict of interest

The authors declare that the research was conducted in the absence of any commercial or financial relationships that could be construed as a potential conflict of interest.

Publisher's note

All claims expressed in this article are solely those of the authors and do not necessarily represent those of their affiliated organizations, or those of the publisher, the editors and the reviewers. Any product that may be evaluated in this article, or claim that may be made by its manufacturer, is not guaranteed or endorsed by the publisher.

Supplementary material

The Supplementary material for this article can be found online at: https://www.frontiersin.org/articles/10.3389/fmicb.2022.906784/full#supplementary-material

References

Chao, J. T., Wong, A. K., Tavassoli, S., Young, B. P., Chruscicki, A., Fang, N. N., et al. (2014). Polarization of the endoplasmic reticulum by ER-septin tethering. *Cell* 158, 620–632. doi: 10.1016/j.cell.2014.06.033

Cui, H. T., Tsuda, K., and Parker, J. E. (2015). Effector-triggered immunity: From pathogen perception to robust defense. *Annu. Rev. Plant Biol.* 66, 487–511. doi: 10.1146/annurev-arplant-050213-040012

Dean, R. A. (1997). Signal pathways and appressorium morphogenesis. *Annu. Rev. Phytopathol.* 35, 211–234. doi: 10.1146/annurev.phyto.35.1.211

Dean, R., Van Kan, J. A. L., Pretorius, Z. A., Hammond-Kosack, K. E., Di Pietro, A., Spanu, P. D., et al. (2012). The top 10 fungal pathogens in molecular plant pathology. *Mol. Plant Pathol.* 13:804. doi: 10.1111/j.1364-3703.2012.00822.x

Ebbole, D. J. (2007). *Magnaporthe* as a model for understanding host-pathogen interactions. *Annu. Rev. Phytopathol.* 45, 437–456. doi: 10.1146/annurev.phyto.45.062806.094346

Fernandez, J., and Orth, K. (2018). Rise of a cereal killer: The biology of *Magnaporthe oryzae* biotrophic growth. *Trends Microbiol.* 26, 582–597. doi: 10.1016/j.tim.2017.12.007

Giordano, F., Saheki, Y., Idevall-Hagren, O., Colombo, S. F., Pirruccello, M., Milosevic, I., et al. (2013). PI(4,5)P(2)-dependent and Ca(2+)-regulated ER-PM interactions mediated by the extended synaptotagmins. *Cell* 153, 1494–1509. doi: 10.1016/j.cell.2013.05.026

Giraldo, M. C., Dagdas, Y. F., Gupta, Y. K., Mentlak, T. A., Yi, M., Martinez-Rocha, A. L., et al. (2013). Two distinct secretion systems facilitate tissue invasion by the rice blast fungus *Magnaporthe oryzae*. *Nat. Commun.* 4:1996. doi: 10.1038/ncomms2996

Howard, R. J., Ferrari, M. A., Roach, D. H., and Money, N. P. (1991). Penetration of hard substrates by a fungus employing enormous turgor pressures. *Proc. Natl. Acad. Sci. U. S. A.* 88, 11281–11284. doi: 10.1073/pnas.88.24.11281

Howard, R. J., and Valent, B. (1996). Breaking and entering: host penetration by the fungal rice blast pathogen *Magnaporthe grisea*. *Annu. Rev. Microbiol.* 50, 491–512. doi: 10.1146/annurev.micro.50.1.491

Kaiser, S. E., Brickner, J. H., Reilein, A. R., Fenn, T. D., Walter, P., and Brunger, A. T. (2005). Structural basis of FFAT motif-mediated ER targeting. *Structure* 13, 1035–1045. doi: 10.1016/j.str.2005.04.010

Kato, T., Kubo, A., Nagayama, T., Kume, S., Tanaka, C., Nakayama, Y., et al. (2017). Genetic analysis of the regulation of the voltage-gated calcium channel homolog Cch1 by the gamma subunit homolog Ecm7 and cortical ER protein Scs2 in yeast. *PLoS One* 12:e0181436. doi: 10.1371/journal.pone.0181436

Kou, Y., Qiu, J., and Tao, Z. (2019). Every coin has two sides: reactive oxygen species during Rice(−) *Magnaporthe oryzae* interaction. *Int. J. Mol. Sci.* 20:1191. doi: 10.3390/ijms20051191

Kunzelmann, K., Cabrita, I., Wanitchakool, P., Ousingsawat, J., Sirianant, L., Benedetto, R., et al. (2016). Modulating Ca(2)(+) signals: a common theme for TMEM16, Ist2, and TMC. *Pflugers Arch.* 468, 475–490. doi: 10.1007/s00424-015-1767-4

Liu, Y., Soetandyo, N., Lee, J. G., Liu, L., Xu, Y., Clemons, W. M. Jr., et al. (2014). USP13 antagonizes gp78 to maintain functionality of a chaperone in ER-associated degradation. *elife* 3:e01369. doi: 10.7554/eLife.01369

Loewen, C. J. R., and Levine, T. P. (2005). A highly conserved binding site in vesicle-associated membrane protein-associated protein (VAP) for the FFAT motif of lipid-binding proteins. *J. Biol. Chem.* 280, 14097–14104. doi: 10.1074/jbc.M500147200

Loewen, C. J. R., Young, B. P., Tavassoli, S., and Levine, T. P. (2007). Inheritance of cortical ER in yeast is required for normal septin organization. *J. Cell Biol.* 179, 467–483. doi: 10.1083/jcb.200708205

Luedeke, C., Frei, S. B., Sbalzarini, I., Schwarz, H., Spang, A., and Barral, Y. (2005). Septin-dependent compartmentalization of the endoplasmic reticulum during yeast polarized growth. *J. Cell Biol.* 169, 897–908. doi: 10.1083/jcb.200412143

Manford, A. G., Stefan, C. J., Yuan, H. L., Macgurn, J. A., and Emr, S. D. (2012). ER-to-plasma membrane tethering proteins regulate cell signaling and ER morphology. *Dev. Cell* 23, 1129–1140. doi: 10.1016/j.devcel.2012.11.004

Mentlak, T. A., Kombrink, A., Shinya, T., Ryder, L. S., Otomo, I., Saitoh, H., et al. (2012). Effector-mediated suppression of chitin-triggered immunity by *magnaporthe oryzae* is necessary for rice blast disease. *Plant Cell* 24, 322–335. doi: 10.1105/tpc.111.092957

Min, S. W., Chang, W. P., and Sudhof, T. C. (2007). E-Syts, a family of membranous Ca2+−sensor proteins with multiple C2 domains. *Proc. Natl. Acad. Sci. U. S. A.* 104, 3823–3828. doi: 10.1073/pnas.0611725104

Oses-Ruiz, M., Sakulkoo, W., Littlejohn, G. R., Martin-Urdiroz, M., and Talbot, N. J. (2017). Two independent S-phase checkpoints regulate appressorium-mediated plant infection by the rice blast fungus *Magnaporthe oryzae*. *Proceed. National Acad. Sci. 114.2* 114, E237–e244. doi: 10.1073/pnas.1611307114

Pan, Y., Pan, R., Tan, L., Zhang, Z., and Guo, M. (2019). Pleiotropic roles of O-mannosyltransferase MoPmt4 in development and pathogenicity of *Magnaporthe oryzae*. *Curr. Genet.* 65, 223–239. doi: 10.1007/s00294-018-0864-2

Pringle, A., and Taylor, J. (2002). The fitness of filamentous fungi. *Trends Microbiol.* 10, 474–481. doi: 10.1016/S0966-842X(02)02447-2

Quon, E., Sere, Y. Y., Chauhan, N., Johansen, J., Sullivan, D. P., Dittman, J. S., et al. (2018). Endoplasmic reticulum-plasma membrane contact sites integrate sterol and phospholipid regulation. *PLoS Biol.* 16:e2003864. doi: 10.1371/journal.pbio.2003864

Spang, A. (2018). The endoplasmic reticulum-the caring mother of the cell. *Curr. Opin. Cell Biol.* 53, 92–96. doi: 10.1016/j.ceb.2018.06.004

Stefan, C. J., Manford, A. G., Baird, D., Yamada-Hanff, J., Mao, Y. X., and Emr, S. D. (2011). Osh proteins regulate Phosphoinositide metabolism at ER-plasma membrane contact sites. *Cell* 144, 389–401. doi: 10.1016/j.cell.2010.12.034

Stefan, C. J., Manford, A. G., and Emr, S. D. (2013). ER-PM connections: sites of information transfer and inter-organelle communication. *Curr. Opin. Cell Biol.* 25, 434–442. doi: 10.1016/j.ceb.2013.02.020

Sweigard, J. A., Chumley, F. G., and Valent, B. (1992). Disruption of a *Magnaporthe grisea* cutinase gene. *Mol. Gen. Genet.* 232, 183–190. doi: 10.1007/BF00279995

Talbot, N. J. (2003). On the trail of a cereal killer: exploring the biology of *Magnaporthe grisea*. *Annu. Rev. Microbiol.* 57, 177–202. doi: 10.1146/annurev.micro.57.030502.090957

Talbot, N. J., Ebbole, D. J., and Hamer, J. E. (1993). Identification and characterization of MPG1, a gene involved in pathogenicity from the rice blast fungus *Magnaporthe grisea*. *Plant Cell* 5, 1575–1590.

Tang, W., Jiang, H., Zheng, Q., Chen, X., Wang, R., Yang, S., et al. (2019). Isopropylmalate isomerase MoLeu1 orchestrates leucine biosynthesis, fungal development, and pathogenicity in *Magnaporthe oryzae*. *Appl. Microbiol. Biotechnol.* 103, 327–337. doi: 10.1007/s00253-018-9456-9

Tang, W., Ru, Y., Hong, L., Zhu, Q., Zuo, R., Guo, X., et al. (2015). System-wide characterization of bZIP transcription factor proteins involved in infection-related morphogenesis of *Magnaporthe oryzae*. *Environ. Microbiol.* 17, 1377–1396. doi: 10.1111/1462-2920.12618

Wang, L., Cai, X., Xing, J., Liu, C., Hendy, A., and Chen, X. L. (2019). URM1-mediated ubiquitin-Like modification is required for oxidative stress adaptation During infection of the Rice blast fungus. *Front. Microbiol.* 10:2039. doi: 10.3389/fmicb.2019.02039

West, M., Zurek, N., Hoenger, A., and Voeltz, G. K. (2011). A 3D analysis of yeast ER structure reveals how ER domains are organized by membrane curvature. *J. Cell Biol.* 193, 333–346. doi: 10.1083/jcb.201011039

Yi, M., and Valent, B. (2013). Communication between filamentous pathogens and plants at the biotrophic interface. *Annu. Rev. Phytopathol.* 51, 587–611. doi: 10.1146/annurev-phyto-081211-172916

Yu, J. H., Hamari, Z., Han, K. H., Seo, J. A., Reyes-Dominguez, Y., and Scazzocchio, C. (2004). Double-joint PCR: a PCR-based molecular tool for gene manipulations in filamentous fungi. *Fungal Genet. Biol.* 41, 973–981. doi: 10.1016/j.fgb.2004.08.001

Zhang, D., Vjestica, A., and Oliferenko, S. (2012). Plasma membrane tethering of the cortical ER necessitates its finely reticulated architecture. *Curr. Biol.* 22, 2048–2052. doi: 10.1016/j.cub.2012.08.047

Zhang, S., and Xu, J. R. (2014). Effectors and effector delivery in *Magnaporthe oryzae*. *PLoS Pathog.* 10:e1003826. doi: 10.1371/journal.ppat.1003826

frontiers | Frontiers in Microbiology

TYPE Original Research
PUBLISHED 10 August 2022
DOI 10.3389/fmicb.2022.978920

OPEN ACCESS

EDITED BY
Qunqing Wang,
Shandong Agricultural University, China

REVIEWED BY
Qiya Yang,
Jiangsu University, China
Elsherbiny A. Elsherbiny,
Mansoura University, Egypt

*CORRESPONDENCE
Guangyuan Wang
gywang@qau.edu.cn

SPECIALTY SECTION
This article was submitted to Microbe and Virus Interactions with Plants, a section of the journal Frontiers in Microbiology

RECEIVED 27 June 2022
ACCEPTED 21 July 2022
PUBLISHED 10 August 2022

CITATION
Liu Z, Tian J, Yan H, Li D, Wang X, Liang W and Wang G (2022) Ethyl acetate produced by *Hanseniaspora uvarum* is a potential biocontrol agent against tomato fruit rot caused by *Phytophthora nicotianae*. *Front. Microbiol.* 13:978920. doi: 10.3389/fmicb.2022.978920

Ethyl acetate produced by *Hanseniaspora uvarum* is a potential biocontrol agent against tomato fruit rot caused by *Phytophthora nicotianae*

Ziyu Liu[1], Junjie Tian[1], Hao Yan[2], Delong Li[2], Xue Wang[3], Wenxing Liang[2] and Guangyuan Wang[1]*

[1]Shandong Province Key Laboratory of Applied Mycology, College of Life Sciences, Qingdao Agricultural University, Qingdao, China, [2]The Key Laboratory of Integrated Crop Pest Management of Shandong Province, College of Plant Health and Medicine, Qingdao Agricultural University, Qingdao, China, [3]Yantai Agricultural Technology Extension Center, Yantai, China

In this study, an oomycete strain FQ01 of *Phytophthora nicotianae*, which could cause destructive postharvest disease, was isolated. At present, chemical fungicides are the main reagents used for controlling *Phytophthora* diseases. It is necessary to find new control techniques that are environmentally friendly. The biocontrol activity of *Hanseniaspora uvarum* MP1861 against *P. nicotianae* FQ01 was therefore investigated. Our results revealed that the volatile organic compounds (VOCs) released by the yeast strain MP1861 could inhibit the development of *P. nicotianae* FQ01. The major component of the VOCs produced by the yeast strain MP1861 was identified to be ethyl acetate (70.8%). Biocontrol experiments showed that *Phytophthora* disease in tomato fruit could be reduced by 95.8% after the yeast VOCs treatment. Furthermore, ethyl acetate inhibited the mycelial growth of the oomycete strain FQ01, and damaged the pathogen cell membrane. This paper describes the pioneering utilization of the yeast strain MP1861 for biocontrol of postharvest fruit rot in tomato caused by *P. nicotianae*.

KEYWORDS

postharvest fruit rot, ethyl acetate, VOCs, *Hanseniaspora uvarum*, *Phytophthora nicotianae*

Introduction

Phytophthora is a genus of oomycete plant pathogens that are notorious for their devastating effects on crops, vegetables, pasture plants and trees. The *Phytophthora* complex has been found to include ~120 species (Panabieres et al., 2016). *Phytophthora nicotianae*, first isolated from tobacco, is an important pathogen because it causes severe damage to a particularly large number of host plants (Panabieres et al., 2016). More than 255 plant species can be infected by *P. nicotianae*, including tomato, tobacco, potato, citrus, and eggplant (Chowdappa et al., 2016; Panabieres et al., 2016). At present, the application of fungicides, such as formanyl, hymexazol, and dimethomorph, is the main

method to prevent the occurrence of plant diseases caused by *P. nicotianae* (Han et al., 2019). However, systematic use of chemicals can lead to pathogen resistance to fungicides and pesticide residues, which in turn pollute environmental ecosystems and endanger human health and livestock. Therefore, to effectively prevent agricultural losses caused by *P. nicotianae*, it is necessary to find new ways to reduce the use of and replace fungicides.

In recent years, microbes acting as agents for the biological control of plant diseases have been recognized as among the most promising alternatives to fungicides because of their effectiveness and environmental friendliness. To date, many antagonistic bacteria and fungi, such as *Bacillus atrophaeus* (Rajaofera et al., 2018), *Pseudomonas fluorescens* (Sukhada et al., 2011), *Trichoderma* spp. (Bae et al., 2016), and *Glomus mosseae* (Sukhada et al., 2011), have been reported as biocontrol agents against *P. nicotianae*. However, the utilization of antagonistic yeasts to manage plant diseases caused by *P. nicotianae* has rarely been reported.

Antagonistic yeasts have many advantages, such as high safety, wide antimicrobial spectrum, strong stress resistance, genetic stability, cultivability, and low nutrient requirements (Cai et al., 2015). Many plant diseases have been found to be controlled by antagonistic yeasts. For example, *Sporidiobolus pararoseus* could protect table grape from decay caused by *Aspergillus niger* (Li et al., 2017); *Metschnikowia fructicola* antagonized the pathogen *Botrytis* causing rot in stored grapes (Kurtzman and Droby, 2001); *Aureobasidium pullulans* provided improved biocontrol against the pathogen *Geotrichum citri-aurantii* causing sour rot in citrus (Klein and Kupper, 2018); *Candida oleophila* reduced papaya anthracnose caused by *Colletotrichum gloeosporioides* (Gamagae et al., 2003). These examples clearly indicate the potential applicability of antagonistic yeasts in biological control and also highlight the limited knowledge of the control of *P. nicotianae* with such organisms. Therefore, it is of great significance to screen new antagonistic yeasts for protecting plants from *Phytophthora* infection.

Hanseniaspora uvarum, a kind of apiculate yeast with a lemon-shaped cell morphology, is widely distributed on the surface of mature fruit, plant leaves, fermented beverages, soils and many other environments (Guaragnella et al., 2019). Previous studies demonstrated that *H. uvarum* had potential for controlling postharvest decay of strawberry (Cai et al., 2015). The volatile organic compounds (VOCs) from *H. uvarum* had been shown to inhibit the growth of the pathogenic fungus *B. cinerea* (Wang L. Y. et al., 2019). Further study revealed that *H. uvarum* could reduce the natural decay of grape berries without impairing quality parameters (Liu et al., 2010). These findings clearly showed that *H. uvarum* has promising potential in the biological control of plant diseases.

In this study, the yeast strain MP1861 of *H. uvarum* was identified as a potential biocontrol strain against *P. nicotianae*. Evaluating the antifungal efficacy of the VOCs from the yeast strain MP1861 and analysis of the active components in the VOCs were further conducted. Ours findings promoted the application of antagonistic yeast in the control of *Phytophthora* diseases. To our knowledge, the present work represents the first report of utilization of antagonistic yeast to manage postharvest fruit disease caused by *P. nicotianae*.

Materials and methods

Yeast and oomycete strains

H. uvarum MP1861 isolated from the leaves of *Kalopanax septemlobus* and *P. nicotianae* FQ01 isolated from rotten tomato fruit were maintained on YPD (1% yeast extract, 2% peptone, 2% dextrose and 2% agar) and PDA (20% potato extract, 2% dextrose, and 2% agar) slants at 4°C, respectively.

Assay of the pathogenicity of *P. nicotianae* FQ01

After growth on PDA plate at 26°C for 3 days, five mm diameter mycelial agar plugs of the pathogen FQ01 were transferred to tobacco leaves, tomato fruit, potato tuber, cucumber, and eggplant, respectively, followed by incubation at 26°C for 4 days. Finally, the lesions caused by the pathogen FQ01 were investigated.

Isolating and screening the yeast strains with biocontrol activities

Plant samples, including roots, stems, leaves, fruit, and flowers, were collected from Laoshan National Forest Park in Qingdao, China. Yeast strains were isolated using the procedures as previously described (Wang et al., 2018). Briefly, five grams of plant sample was suspended in 50 ml YPD medium supplemented with 0.01% chloramphenicol and then incubated at 28°C, 180 rpm, for 2 days. The culture was diluted to 10^{-6} using sterilized water. Then, 200 μl of the diluted cell culture was evenly plated on an YPD plate and grown at 28°C for 2 d. The obtained yeast colonies were maintained at 4°C.

Antifungal activities of the obtained yeast strains were performed using the dual culture method (Rajaofera et al., 2018). In brief, the pathogen FQ01 was inoculated in the center of PDA plate, and the isolated yeasts were inoculated around the pathogen. After inoculation at 26°C for 4 d, the growth

inhibitions of the pathogen FQ01 on PDA plate by different yeast strains were observed.

Morphological characterization

After growth on YPD plates at 26°C for 48 h, the morphological characterization of the yeast strain MP1861 was performed. The oomycete strain FQ01 was first grown on PDA plates at 26°C for 4 d. Then, ∼10 mycelial plugs (0.5 cm diameter) of the oomycete strain FQ01 were transferred into clarified V8 juice followed by incubation at 26°C for 48 h. After 3–4 washes using ultrapure water, the actively growing mycelia were covered by ultrapure water and incubated at room temperature for 3–7 d. Finally, the sporangia and chlamydospores produced by the oomycete strain FQ01 were recorded.

Phylogenetic analysis of different microorganisms

DNA extraction from the oomycete strain FQ01 and the antagonistic yeast MP1861 were carried out with Fungi Genomic DNA Purification Kit (Sangon Biotech, China) according to the manufacturer's instructions, respectively. ITS region of the oomycete strain FQ01 was amplified using PCR with the universal fungal primers ITS1 and ITS4 (Garcia-Estrada et al., 2020). D1/D2 26S rDNA region of the antagonistic yeast MP1861 was amplified using PCR with the primers NL1 and NL4 (Wang et al., 2018). The generated fragments were sequenced. The obtained sequences were blasted using BLASTN. Phylogenetic tree based on a neighbor-joining analysis was constructed using MEGA 4.0 (Tamura et al., 2007).

Pathogen inhibition by the VOCs emitted from the antagonistic yeast

The mycelial inhibition by the VOCs emitted from the yeast strain MP1861 was performed in closed Petri dishes according to previously methods (Huang et al., 2011) with appropriate modifications. In brief, the pathogen FQ01 was incubated on PDA plate at 26°C for 3 days. Then, a mycelial agar plug (0.5 cm diameter) from the colony margin of *P. nicotianae* FQ01 was transferred onto one PDA plate (6.0 cm diameter). Meanwhile, the other PDA plate was inoculated with 100 μl yeast cells (3.0×10^4 cells/mL). The two plates were then sealed with parafilm. Subsequently, the sealed plates were placed at 26°C for 4 d. The colony diameter of *P. nicotianae* FQ01 in each plate was measured. The inhibition of mycelial growth by the VOCs produced by the yeast strain MP1861 was calculated according to the formula $[(D_{ck} - D_{VOCs}) / D_{ck}] \times 100$ %, where D_{ck} and D_{VOCs} indicate the average diameter of *P. nicotianae* colonies grown on PDA without or with the VOCs treatment, respectively.

GC/MS analysis

VOCs were first adsorbed by solid-phase microextraction (SPME) (Supelco, 57329-U). The VOCs adsorbed above were then analyzed by a TSQ8000 mass spectrometer (Thermo Fisher). Briefly, a fused-silica fiber coated with divinylbenzene (DVB), carboxen (CAR), and polydimethylsiloxane (PDMS) was traversed into the sampling headspace bottle *via* a silicone septum. After adsorption at 40°C for 60 min, the fiber was inserted into a GC injector to desorb the volatile compounds at 250°C for 5 min. The released components were then separated by a TG-5SILMS GC column (Thermo Fisher, 30 m × 0.25 mm × 0.25 μm). The carrier gas of the GC was helium, and the gas flow rate was 1.3 mL per min. The temperature program in the GC oven consisted of 40°C for 2.0 min, raising to 100°C at 3°C per min and then to 240°C at 20°C per min, 240°C for 5.0 min. The electron ionization (EI) applied was fixed at 70 eV, and the ion source temperature used in the MS was set at 230°C. The m/z scan range was 40–400 amu. The results obtained above were searched against the database of the National Institute of Standards and Technology (NIST).

Fluorescence microscopy to evaluate the toxicity of ethyl acetate to the oomycete strain FQ01

To investigate the damage caused by ethyl acetate to *P. nicotianae* FQ01, we performed a propidium iodide (PI) fluorescence assay. In brief, the hyphal cells of *P. nicotianae* FQ01 were treated with different concentrations of ethyl acetate (Sangon Biotech) from 0 to 7.18 g/L at 26°C for 24 h, respectively. Then, the treated mycelia were stained with PI fluorescent probe (1 mg/L, Solarbio) 30 min at room temperature in the dark (Jing et al., 2017; Han et al., 2019). Finally, the treated mycelia were photographed using an EVOS M5000 fluorescence imaging system (Thermo Fisher).

Control of *Phytophthora* disease on tomato fruit by the VOCs from the yeast strain MP1861

The inhibitory assay of *Phytophthora* disease on tomato fruit by the volatiles of *H. uvarum* MP1861 was performed in double closed Petri plates. First, the surface of sixteen healthy tomato fruit (3.0–3.5 cm length and 2.0–3.0 cm diameter)

were disinfected using 70% ethanol. After rinsing in sterile distilled water, the fruit was dried at room temperature on an ultra-clean workbench. Each fruit was poked once with a toothpick, followed by inoculation with one mycelial plug (0.5 cm diameter) of the oomycete strain FQ01. The treated fruit were arranged on a glass Petri plate (3.0 cm height and 15.0 cm diameter). Meanwhile, the other Petri plate containing PDA medium was inoculated with 200 μl yeast cell suspension (1.0×10^9 cells/mL) on the medium surface (Qin et al., 2017). An equal amount of sterile distilled water was used as the control. The two glass Petri dishes were then sealed with parafilm. The closed Petri plates were incubated at 26°C for 3 d. Finally, the lesions on tomato fruit and the ethyl acetate production in the closed Petri plates were investigated. There were three replicate trials in each test. The inhibition rate of the VOCs on tomato fruit disease was calculated by equation $[(L_{ck} - L_{VOCs}) / L_{ck}] \times 100\%$. L_{ck} and L_{VOCs} indicate the average area of lesions infected by *P. nicotianae* FQ01 on tomato fruit without or with the VOCs treatment, respectively.

Statistical analysis

Data represent the mean values ± standard deviation (SD). The obtained data were calculated by the one-way ANOVA for statistical tests. A value of $p < 0.05$ was considered to be statistically significant.

Results

Identification and pathogenicity investigation of the pathogen FQ01

The pathogen FQ01 was isolated from rotten tomato, which could cause postharvest loss of tomato fruit. The sporangia produced by the pathogen FQ01 were ovoid and obturbinate with a prominent papilla (Figures 1A,B). The pathogen FQ01 could also produce abundant spherical chlamydospores (Figure 1C). The ITS region of the pathogen FQ01 was sequenced. The obtained sequence has been stored in GenBank (accession No. OL824731). A phylogenetic tree according to the ITS region of the pathogen FQ01 was further constructed. The results revealed that the pathogen FQ01 was clustered in one branch with *P. nicotianae* (Figure 1D). These observations clearly showed that the pathogen FQ01 was *P. nicotianae*.

We further investigated the host range of the pathogen FQ01. The results showed that the pathogen FQ01 could infect tobacco leaves, tomato fruit, cucumber, eggplant fruit and potato tuber (Figure 1E), indicating that a variety of plants could be infected by the pathogen FQ01, especially postharvest fruit.

Screening the antagonistic yeast strains for biocontrol of *P. nicotianae* FQ01

We first isolated and purified more than 50 yeast strains from different plant samples. After testing the inhibitory activities of the isolated yeast strains against *P. nicotianae* FQ01, one candidate, labeled MP1861, exhibited the best biocontrol ability against the pathogen FQ01. As shown in Figure 2A, the growth of *P. nicotianae* FQ01 was strongly inhibited by the yeast strain MP1861.

To identify the yeast strain MP1861, the colony and cell morphological characteristics were investigated. As shown in Figure 2B, the colonies of the yeast strain MP1861 were white, round, smooth, and sticky. The cells of the yeast strain MP1861 exhibited a typical lemon shape (Figure 2C). A dendrogram based on the D1/D2 26S rDNA region of the yeast strain MP1861 (GenBank accession No. OL906093) was further constructed. According to the results of the phylogenetic analysis, the yeast strain MP1861 was identified as *H. uvarum* (Figure 2D).

Inhibition of *P. nicotianae* FQ01 growth by the VOCs from *H. uvarum* MP1861

A schematic representation for testing the inhibition of *P. nicotianae* FQ01 growth by the VOCs from *H. uvarum* MP1861 was shown in Figure 3A. The VOCs emitted by *H. uvarum* MP1861 could effectively inhibit the mycelial growth of *P. nicotianae* FQ01 (Figure 3B). The average colony diameter of the pathogen FQ01 reached 5.35 mm in the negative control treatment group and 1.10 mm in the antagonistic yeast treatment group (Figure 3C). The VOCs from *H. uvarum* MP1861 showed a growth inhibition rate of 79.4 % against *P. nicotianae* FQ01 (Figure 3C).

Identification of the VOCs emitted by *H. uvarum* MP1861

Results of GC/MS analysis showed that seven major components were identified in the VOCs released from *H. uvarum* MP1861, and their retention times were 2.20, 7.18, 17.45, 23.33, 24.28, 26.13, and 27.31 min (Figure 4A). However, only three components matched with more than 80% probability against the mass spectrometry database: ethyl acetate (2.20 min, probability 93.53%), 1-butanol, 3-methyl-, acetate (7.18 min, probability 83.47%) and phenylethyl alcohol (17.45 min, probability 86.31%) (Figure 4A). The MS spectra of these peaks (retention time: 2.20, 7.18, and 17.45 min) have been supplied in Supplementary Figure S1. It is worth noting that ethyl acetate was the most abundant component among the volatile gases detected above, accounting for 70.8% (Figure 4A).

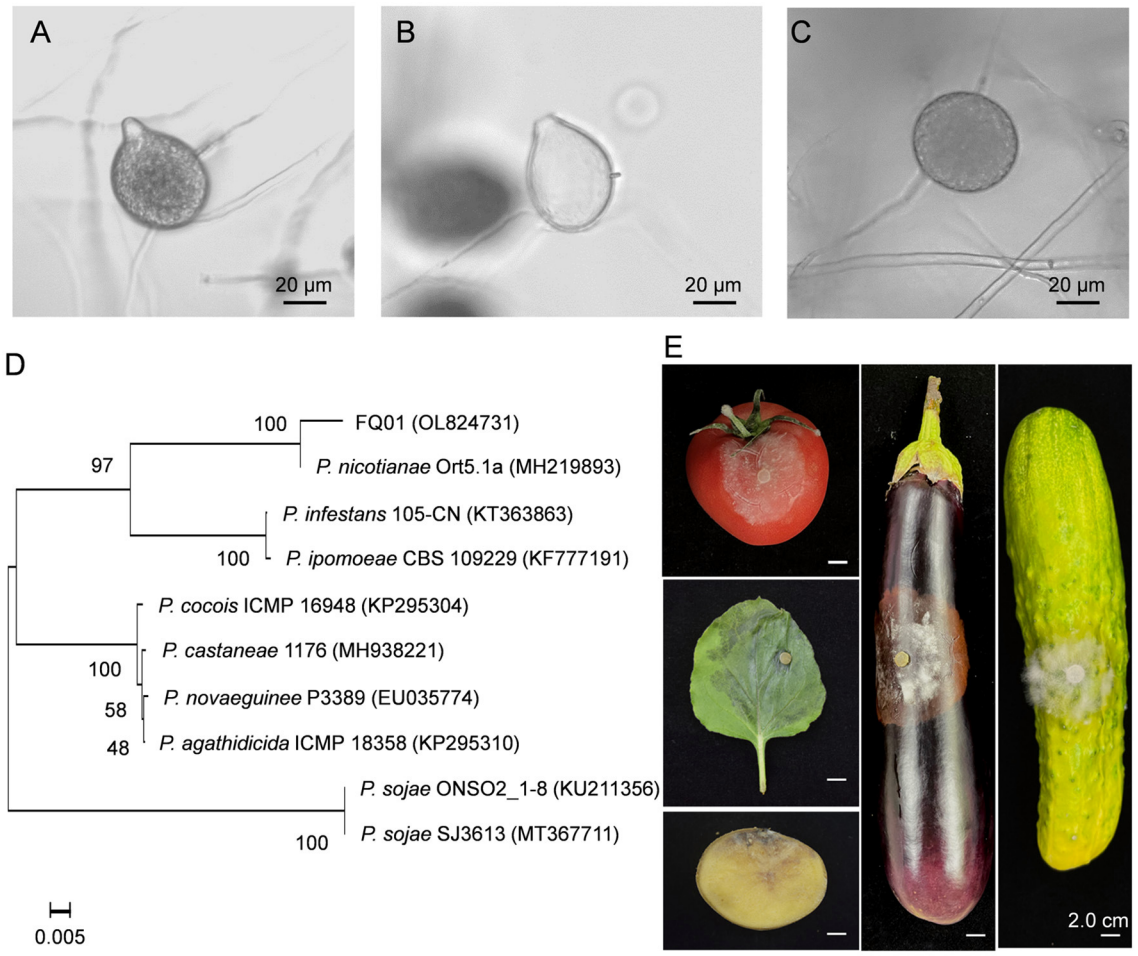

FIGURE 1
Identification of the pathogen FQ01. **(A)** Sporangial morphology before the release of zoospores. **(B)** Sporangial shell after the release of zoospores. **(C)** Chlamydospore morphology. **(D)** Phylogenetic tree of the pathogen FQ01 and other *Phytophthora* strains based on a neighbor-joining analysis of ITS sequence. **(E)** Symptoms of plant diseases caused by *P. nicotianae* FQ01 infection.

When the yeast strain MP1861 and the oomycete strain FQ01 were coincubated for 2 days, the main component among the VOCs was still ethyl acetate (Figure 4C). However, ethyl acetate was not detected in the VOCs produced by *P. nicotianae* FQ01 (Figure 4B).

Confirmation of the growth inhibition of *P. nicotianae* FQ01 by ethyl acetate

Since ethyl acetate was the main component of the VOCs produced by the yeast strain MP1861 (Figure 4A), the impact of ethyl acetate on the growth of *P. nicotianae* FQ01 was further investigated. The procedure used in this study is shown in Figure 5A. The results revealed that with the increase in ethyl acetate content in the Petri dish airspace, the mycelial growth of the oomycete strain FQ01 was gradually inhibited. When the ethyl acetate content in the Petri dish airspace reached 184 mg/L, the mycelial growth of the oomycete strain FQ01 was completely inhibited (Figures 5B,C). However, the ethyl acetate concentrations tested in this study did not show inhibitory effect on the growth of the yeast strain MP1861 (Figures 5B,C). The ethyl acetate concentration in the VOCs released by the yeast strain MP1861 reached 344 mg/L (Figure 5D), which exceeded the tolerance of the oomycete strain FQ01 to ethyl acetate (Figures 5B,C).

Plasma membrane damage of *P. nicotianae* by ethyl acetate

The toxicity of ethyl acetate to *P. nicotianae* FQ01 was investigated and the results showed that the mycelia

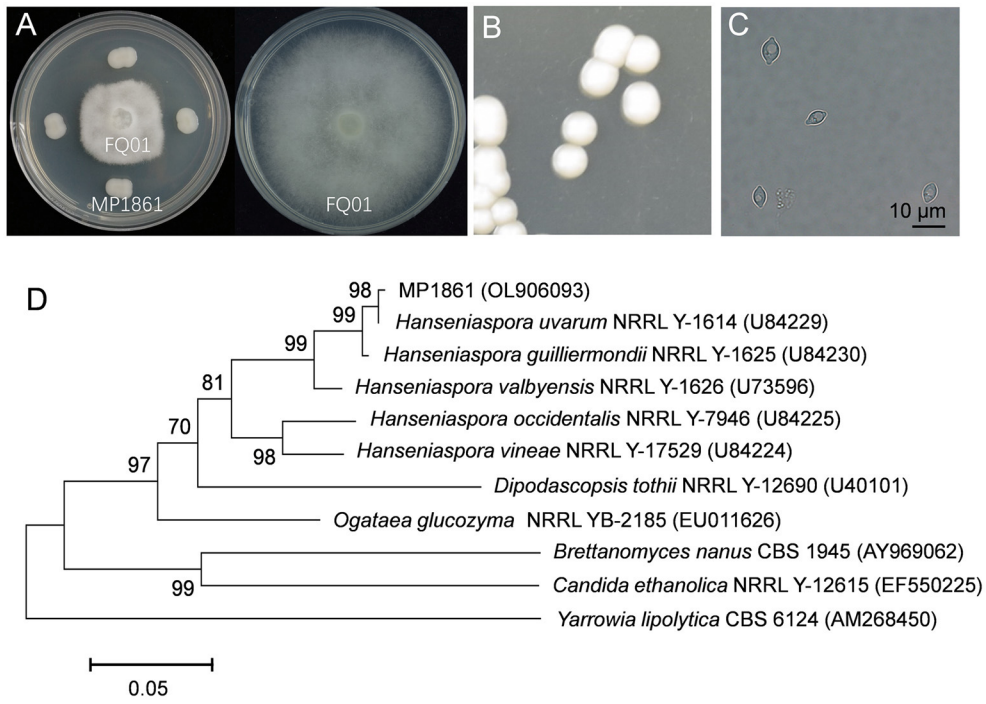

FIGURE 2
Identification of the antagonistic yeast strain MP1861. **(A)** Inhibition of *Phytophthora* growth by the yeast strain MP1861. **(B)** Colonies of the yeast strain MP1861 after growth on YPD plates at 26°C for 2 d. **(C)** Cell morphological characteristics of the yeast strain MP1861. **(D)** Phylogenetic relationship of the yeast strain MP1861 and other yeasts according to a neighbor-joining analysis of D1/D2 26S rDNA region.

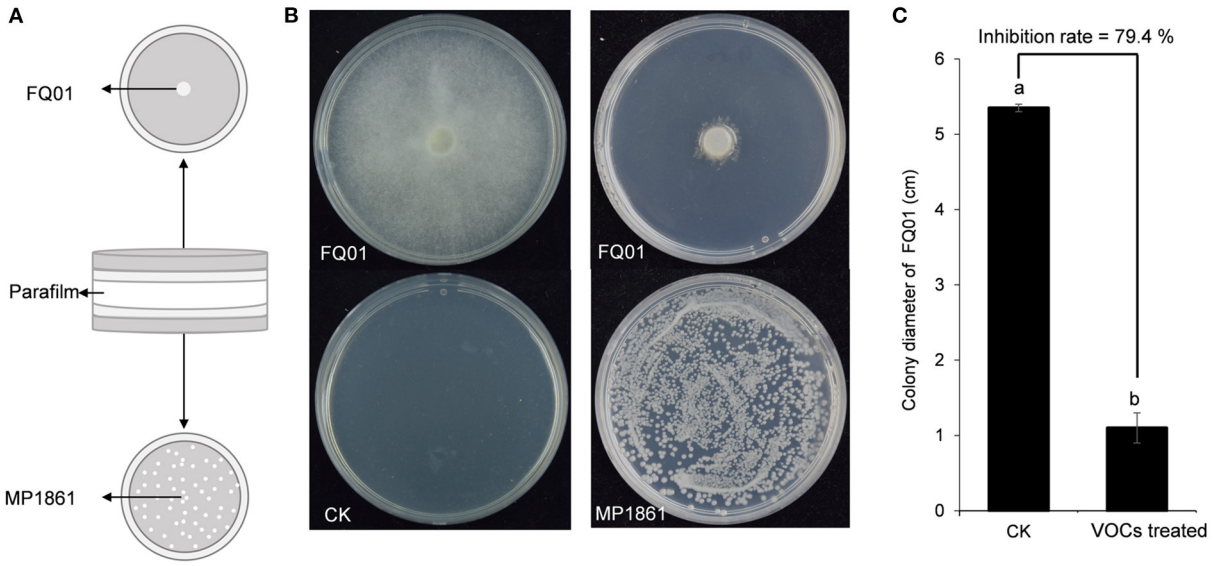

FIGURE 3
Graphical representation of VOCs released by the yeast strain MP1861 against the oomycete strain FQ01. **(A)** Schematic depiction of the method used in this study. **(B)** Mycelial growth of the pathogen FQ01 grown on PDA plates for 4 d. For the VOCs treated group, each plate was inoculated with 100 μl of yeast seed (3.0×10^4 cells/mL). **(C)** Colony diameter of the pathogen FQ01. Data are calculated as the mean values ± SD, $n = 3$. The different letters a and b on the chart indicate significant difference at the 0.05 level.

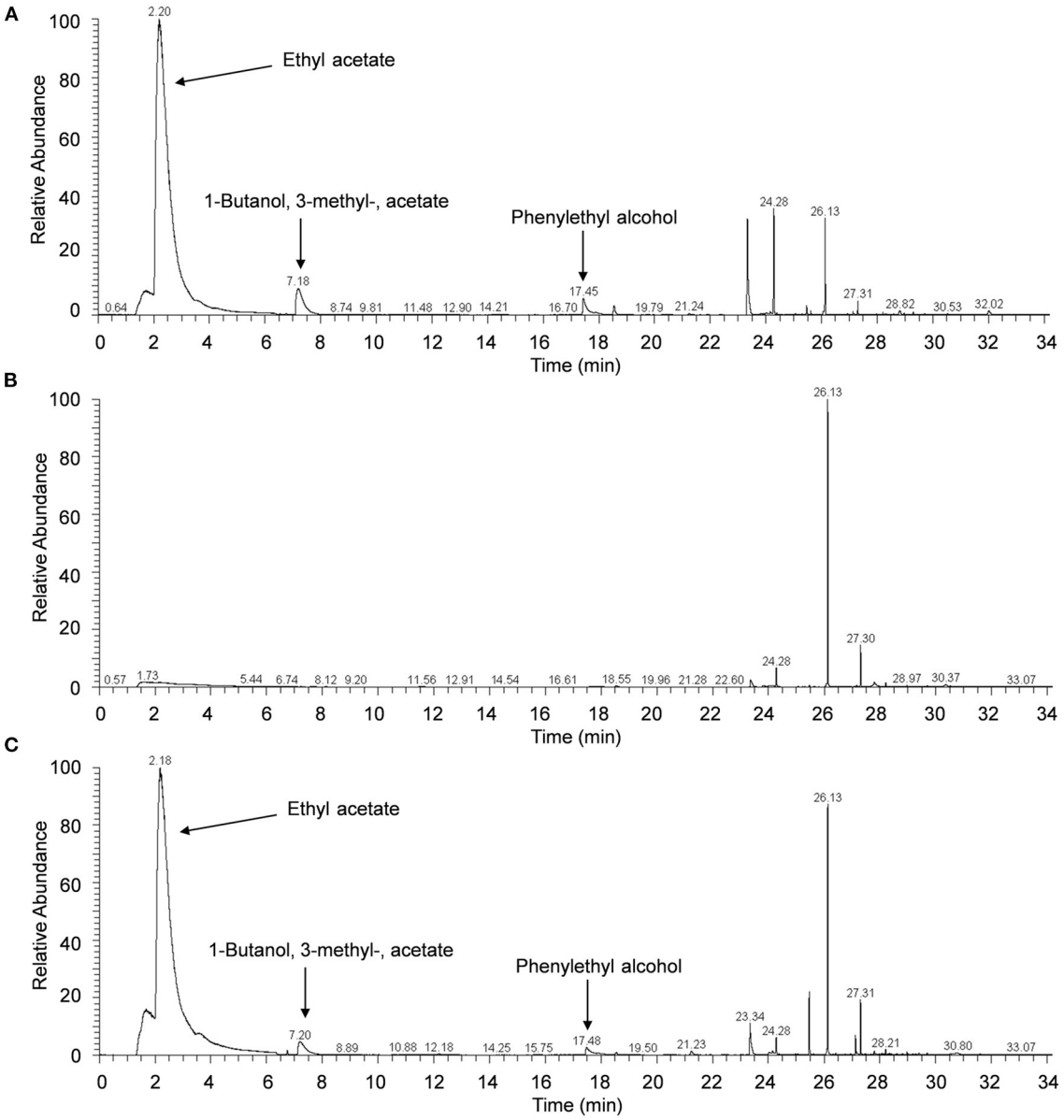

FIGURE 4
Chromatograms of VOCs. **(A)** The VOCs released from *H. uvarum* MP1861. **(B)** The VOCs produced by *P. nicotianae* FQ01. **(C)** The VOCs produced by coculture of the yeast and oomycete.

of the pathogen FQ01 could not be stained by PI after being treated with low dose (<3.59 g/L) of ethyl acetate (Figure 6A), indicating that low dose of ethyl acetate showed weak toxicity to *P. nicotianae* FQ01. However, a strong red color was observed in the mycelia treated with 5.38 g/L ethyl acetate (Figure 6B), indicating that the plasma membrane integrity of the oomycete strain FQ01 was damaged by ethyl acetate.

Effects of *H. uvarum* MP1861 VOCs on control of tomato fruit rot caused by *P. nicotianae* FQ01

The ability of the VOCs from *H. uvarum* MP1861 to suppress the pathogen FQ01-mediated disease development on tomato fruit was investigated. As shown in Figure 7A, all the tomato fruit inoculated with the oomycete strain FQ01 in the

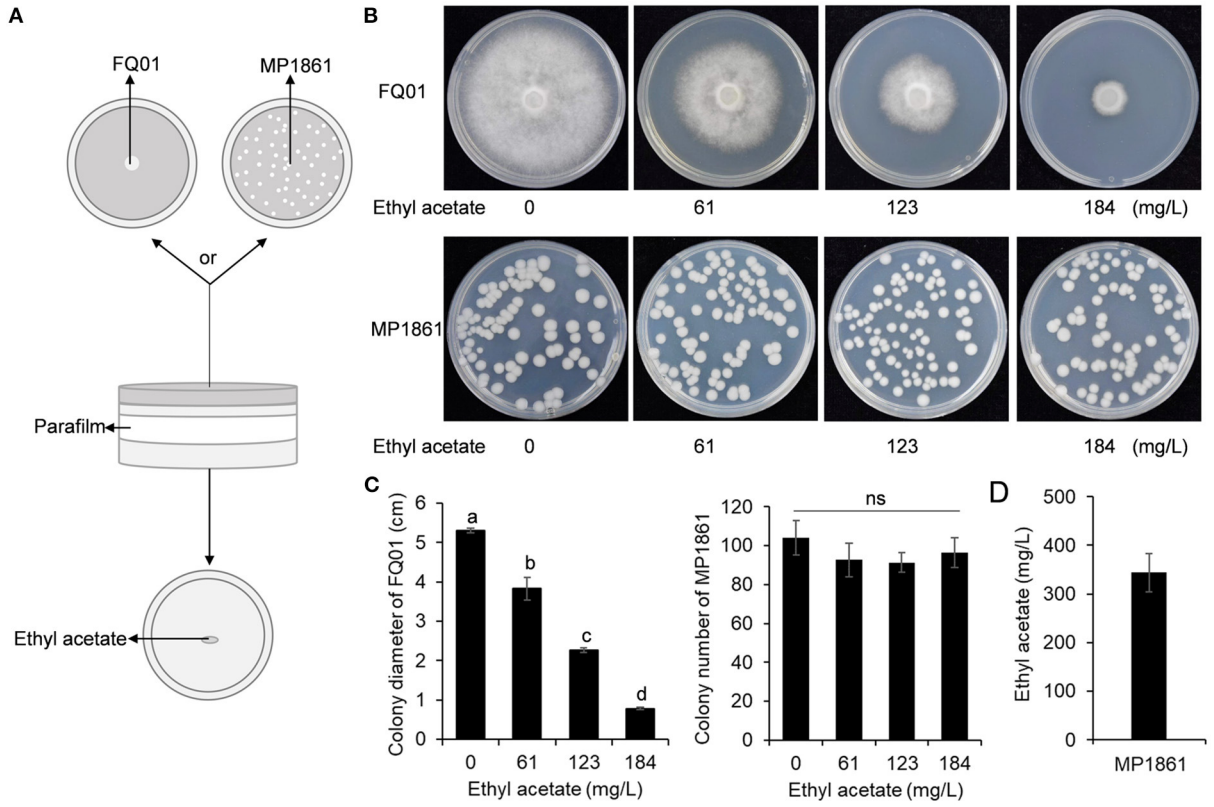

FIGURE 5
Antifungal activity of ethyl acetate in the airspace against *P. nicotianae* FQ01. **(A)** Procedure used in this study. **(B)** Colonies of the oomycete strain FQ01 and the yeast strain MP1861 grown on PDA plates for 4 d. **(C)** Colony diameter of the pathogen FQ01 and colony number of the yeast strain MP1861. Three experiments were carried out. Different letters (a, b, c, and d) labeled on the columns are significant difference at $p < 0.05$. Probability values of more than 0.05 were marked as ns (no significance). **(D)** Ethyl acetate production in the VOCs of the yeast strain MP1861.

Petri plate showed severe symptoms of *Phytophthora* disease in the blank control group. Compared with those in the CK group, the lesions in the tomato fruit after biofumigation with the VOCs of *H. uvarum* MP1861 were basically confined to the inoculation area (Figure 7B). The inhibition rate of the VOCs on tomato fruit disease were 95.8% (Figure 7C). The concentration of ethyl acetate in the Petri plates containing *H. uvarum* MP1861 reached 430 mg/L (Figure 7D), indicating that the VOCs produced by the yeast strain MP1861 could protect tomato from *Phytophthora* pathogen infection.

Discussion

Species of the genus *Phytophthora* are considered plant destroyers that can cause widespread damage in many agricultural species and even in native ecosystems worldwide. The established methods for effective control of the plant diseases caused by *Phytophthora* rely mainly on extensive use of fungicides (Panabieres et al., 2016). However, in terms of food safety and environmental friendliness, these methods are no longer suitable given the current situation. In recent years, the demand for safe agricultural products has increased. Therefore, the utilization of biological control agents as replacements for chemical pesticides has attracted great interest. Numerous previous researches have indicated that selected strains of many antagonistic bacteria and filamentous fungi, including *B. atrophaeus* (Rajaofera et al., 2018), *P. fluorescens* (Sukhada et al., 2011), *G. mosseae* (Sukhada et al., 2011) and *Trichoderma* spp. (Bae et al., 2016), were effective agents for biocontrol of plant diseases caused by *P. nicotianae*. Our study revealed that antagonistic yeast was also an important source for screening biocontrol agent against *P. nicotianae* similar to antagonistic bacteria and filamentous fungi.

A large number of studies have shown that the biological control mechanisms of antagonistic yeasts against plant pathogens include competition for nutrients and space (Zhao et al., 2008; Zhang et al., 2011; Cheng et al., 2019), secretion of extracellular cell wall-degrading enzymes (Chanchaichaovivat

et al., 2008; Zhang et al., 2011), restriction of spore germination and germ tube growth of pathogens (Droby et al., 2002), induction of disease resistance in host plants (Droby et al., 2002; Zhao et al., 2008; Apaliya et al., 2017), etc. In this study, it was found that the VOCs produced by *H. uvarum* MP1861 could effectively suppress the mycelial growth of *P. nicotianae* FQ01. Consistent with our observations, production of VOCs with antifungal activities have been reported in various yeasts e.g., *Candida intermedia* (Huang et al., 2011), *Hanseniaspora osmophila* (Delgado et al., 2021), *Starmerella bacillaris* (Lemos Junior et al., 2020), *Wickerhamomyces anomalus*, *Metschnikowia pulcherrima* and *Saccharomyces cerevisiae* (Oro et al., 2018). In another report, the VOCs produced by *H. uvarum* reduced *B. cinerea* infection of strawberry (Qin et al., 2017). These findings suggest that biosynthesis of antifungal VOCs by antagonistic yeasts is one of the important mechanisms for controlling plant pathogens.

VOCs are substances with a low molecular weight (<300 Da), high vapor pressure (≥0.01 kPa at 20°C), and low water solubility (Pagans et al., 2006; Delgado et al., 2021). The VOCs synthesized by microbes contains a variety of compounds such as esters, alcohols and aromatic compounds (de Boer et al., 2019). The present study revealed that the volatiles produced by *H. uvarum* MP1861 contained ethyl acetate, isopentyl alcohol (1-butanol, 3-methyl-, acetate), and phenylethyl alcohol. Similarly, these volatiles were also detected in *C. intermedia* C410 (Huang et al., 2011) and *H. osmophila* 337 (Delgado et al., 2021). According to previous researches (Huang et al., 2011; Qin et al., 2017), these volatiles have been demonstrated antifungal activities. Compared with the yeast strains reported above, the yeast strain MP1861 had the highest content (70.8

A

Strain	Ethyl acetate (g/L)						
	0	0.35	0.90	1.78	3.59	5.38	7.18
FQ01	–	–	–	–	w	+	+

B

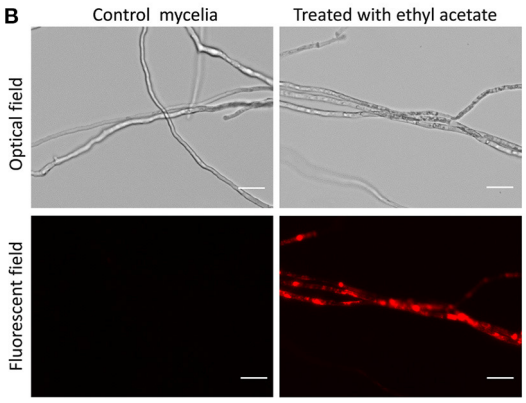

FIGURE 6
PI staining of the pathogen FQ01. **(A)** Effect of different ethyl acetate concentration on PI staining. –, negative; w, weak; +, positive. **(B)** Images of the pathogen FQ01 after PI staining. Mycelia treated with 5.38 g/L ethyl acetate. Bars represent 20 μm.

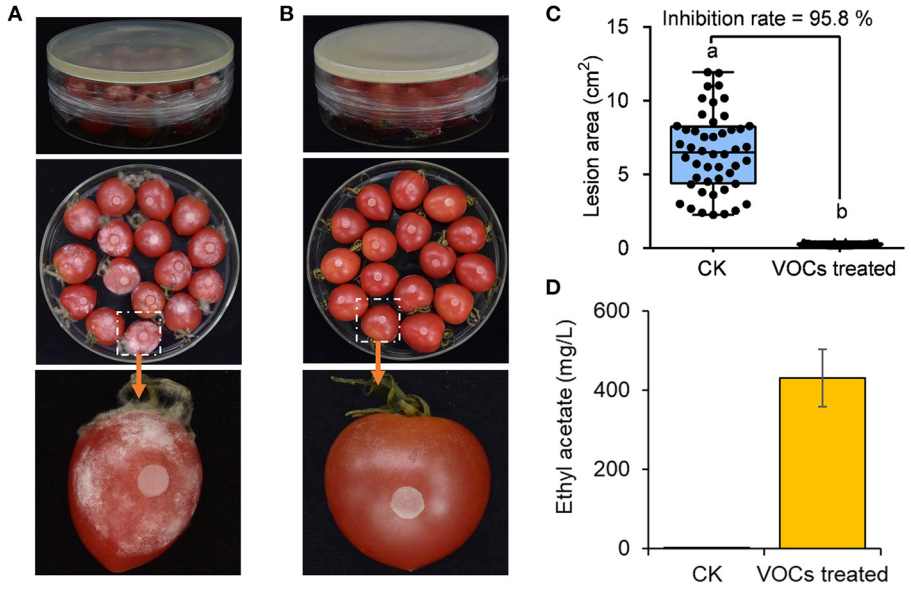

FIGURE 7
Evaluation of the efficacy of the VOCs from the yeast strain MP1861 on *Phytophthora* disease development. **(A)** Blank control group. **(B)** Group treated with *H. uvarum* MP1861 VOCs. **(C)** Statistics of the areas of 48 lesions on tomato fruit. Different letters, a and b, means a significant difference at the level of $p < 0.05$. **(D)** Ethyl acetate contents in the closed Petri dishes. Data are given as the mean values ± SD, $n = 3$.

%) of ethyl acetate in the VOCs. Our study revealed that ethyl acetate was the main antifungal component in the VOCs of *H. uvarum* MP1861.

P. nicotianae was found to be sensitive to both esters and oils. It was found that garlic essential oil could strongly inhibit the growth of *P. nicotianae,* and one of the major components in garlic essential oil is diallyl disulfide, which could destroy the cell membrane of *Phytophthora* and cause cell death (Wang Y. C. et al., 2019). The cell membrane integrity of *P. nicotianae* could also be destroyed by essential oil from *Chrysanthemum indicum* L., in which the major components are monoterpenes and sesquiterpenes (Han et al., 2019). In another study, eugenol, a major component in *Syringa oblata* essential oil, inhibited the mycelial growth of *Phytophthora* by impairing its cell membrane (Jing et al., 2017). We found that ethyl acetate also destroyed the cell membrane of *P. nicotianae*, leading to cell death. These observations confirmed the inhibitory effects of oils and esters on *P. nicotianae*.

Ethyl acetate has been widely used in food, beverage, solvent and other fields (Zhang et al., 2020). However, ethyl acetate isn't 100% safe. It can cause heat/sparks/open flames/hot surfaces. Exposure to ethyl acetate even at low concentration causes dizziness, irritation and even cancer (Zhu et al., 2017). In addition, this component can be toxic if ingested or inhaled and can cause severe internal organ damage with long-term or repeated exposure. Control of plant diseases using the antagonistic yeast strain MP1861 can avoid the potential harm caused by direct application of ethyl acetate in the environment. Biological control of plant disease using antagonistic yeast involves a tritrophic interaction between host, pathogen and yeast, all of which are influenced by environmental factors such as temperature, pH, ultraviolet light, nutrition, and osmotic and oxidative stress (Sui et al., 2015). The influence of environmental factors on the production of ethyl acetate by *H. uvarum* MP1861 will be further investigated.

Conclusion

The current work demonstrated that the VOCs released by *H. uvarum* MP1861 exhibited bioactivity against *P. nicotianae* FQ01. Ethyl acetate was identified to be the most abundant component in the VOCs produced by the yeast strain MP1861, which exhibited strong anti-oomycete activity against *P. nicotianae* FQ01 by breaking the *Phytophthora* cell membrane integrity. The yeast strain MP1861 significantly decreased the incidence of decay on tomato fruit caused by *P. nicotianae*. This study provided a novel antagonistic yeast strain MP1861 of *H. uvarum* and a useful information about the antagonistic properties of *H. uvarum* MP1861. Further studies are warranted to focus on the application of *H. uvarum* MP1861 in the control of *Phytophthora* diseases in agricultural production.

Data availability statement

The original contributions presented in the study are included in the article/Supplementary material, further inquiries can be directed to the corresponding author/s.

Author contributions

ZL and GW designed the experiments and wrote the first draft of the manuscript. ZL and JT performed the experiments. ZL, JT, HY, and XW organized the database and performed the statistical analysis. DL, GW, and WL reviewed and edited the manuscripts. All authors provided comments on the manuscript and approved the submitted version.

Funding

This work was financially supported by the Shandong Provincial Natural Science Foundation (ZR2019MC052, ZR2020KC003), the National Natural Science Foundation of China (31972213), the Key Research and Development Program of Shandong Province (2019YQ017), Shandong Province Double-Hundred Talent Plan (WST2018008), and Taishan Scholar Construction Foundation of Shandong Province (tshw20130963).

Conflict of interest

The authors declare that the research was conducted in the absence of any commercial or financial relationships that could be construed as a potential conflict of interest.

Publisher's note

Supplementary material

The Supplementary Material for this article can be found online at: https://www.frontiersin.org/articles/10.3389/fmicb.2022.978920/full#supplementary-material

SUPPLEMENTARY FIGURE S1
MS spectra of three peaks. **(A)** Ethyl acetate peak at 2.20 min. **(B)** 1-butanol, 3-methyl-, acetate peak at 7.18 min. **(C)** Phenylethyl alcohol peak at 17.45 min.

References

Apaliya, M. T., Zhang, H., Yang, Q., Zheng, X., Zhao, L., Kwaw, E., et al. (2017). *Hanseniaspora uvarum* enhanced with trehalose induced defense-related enzyme activities and relative genes expression levels against *Aspergillus tubingensis* in table grapes. *Postharvest Biol. Technol.* 132, 162–170. doi: 10.1016/j.postharvbio.2017.06.008

Bae, S.-J., Mohanta, T. K., Chung, J. Y., Ryu, M., Park, G., Shim, S., et al. (2016). *Trichoderma* metabolites as biological control agents against *Phytophthora* pathogens. *Biol. Control* 92, 128–138. doi: 10.1016/j.biocontrol.2015.10.005

Cai, Z. K., Yang, R., Xiao, H. M., Qin, X. J., and Si, L. Y. (2015). Effect of preharvest application of *Hanseniaspora uvarum* on postharvest diseases in strawberries. *Postharvest Biol. Technol.* 100, 52–58. doi: 10.1016/j.postharvbio.2014.09.004

Chanchaichaovivat, A., Panijpan, B., and Ruenwongsa, P. (2008). Putative modes of action of *Pichia guilliermondii* strain R13 in controlling chilli anthracnose after harvest. *Biol. Control* 47, 207–215. doi: 10.1016/j.biocontrol.2008.07.018

Cheng, L. L., Nie, X. B., Jiang, C. X., and Li, S. L. (2019). The combined use of the antagonistic yeast *Hanseniaspora uvarum* with beta-aminobutyric acid for the management of postharvest diseases of kiwifruit. *Biol. Control* 137, 104019. doi: 10.1016/j.biocontrol.2019.104019

Chowdappa, P., Kumar, B. J. N., Kumar, S. P. M., Madhura, S., Bhargavi, B. R., and Lakshmi, M. J. (2016). Population structure of *Phytophthora nicotianae* reveals host-specific lineages on brinjal, ridge gourd, and tomato in south India. *Phytopathology* 106, 1553–1562. doi: 10.1094/PHYTO-04-14-0099-R

de Boer, W., Li, X., Meisner, A., and Garbeva, P. (2019). Pathogen suppression by microbial volatile organic compounds in soils. *FEMS Microbiol. Ecol.* 95, fiz105. doi: 10.1093/femsec/fiz105

Delgado, N., Olivera, M., Cádiz, F., Bravo, G., Montenegro, I., Madrid, A., et al. (2021). Volatile organic compounds (VOCs) produced by *Gluconobacter cerinus* and *Hanseniaspora osmophila* displaying control effect against table grape-rot pathogens. *Antibiotics* 10, 663. doi: 10.3390/antibiotics10060663

Droby, S., Vinokur, V., Weiss, B., Cohen, L., Daus, A., Goldschmidt, E. E., et al. (2002). Induction of resistance to *Penicillium digitatum* in grapefruit by the yeast biocontrol agent *Candida oleophila*. *Phytopathology* 92, 393–399. doi: 10.1094/PHYTO.2002.92.4.393

Gamagae, S. U., Sivakumar, D., Wijeratnam, R. S. W., and Wijesundera, R. L. C. (2003). Use of sodium bicarbonate and *Candida oleophila* to control anthracnose in papaya during storage. *Crop Prot.* 22, 775–779. doi: 10.1016/S0261-2194(03)00046-2

Garcia-Estrada, R. S., Cruz-Lachica, I., Osuna-Garcia, L. A., and Marquez, I. (2020). First report of eggplant fruit rot caused by *Phytophthora nicotianae* Breda de Haan in Mexico. *Plant Dis.* 105, 513. doi: 10.1094/PDIS-07-20-1574-PDN

Guaragnella, N., Chiara, M., Capece, A., Romano, P., Pietrafesa, R., Siesto, G., et al. (2019). Genome sequencing and comparative analysis of three *Hanseniaspora uvarum* indigenous wine strains reveal remarkable biotechnological potential. *Front. Microbiol.* 10, 3133. doi: 10.3389/fmicb.2019.03133

Han, X. B., Zhao, J., Cao, J. M., and Zhang, C. S. (2019). Essential oil of *Chrysanthemum indicum* L.: potential biocontrol agent against plant pathogen *Phytophthora nicotianae*. *Environ. Sci. Pollut. Res. Int.* 26, 7013–7023. doi: 10.1007/s11356-019-04152-y

Huang, R., Li, G. Q., Zhang, J., Yang, L., Che, H. J., Jiang, D. H., et al. (2011). Control of postharvest *Botrytis fruit* rot of strawberry by volatile organic compounds of *Candida intermedia*. *Phytopathology* 101, 859–869. doi: 10.1094/PHYTO-09-10-0255

Jing, C., Gou, J. L., Han, X. B., Wu, Q., and Zhang, C. S. (2017). *In vitro* and *in vivo* activities of eugenol against tobacco black shank caused by *Phytophthora nicotianae*. *Pesticide Biochem. Phys.* 142, 148–154. doi: 10.1016/j.pestbp.2017.07.001

Klein, M. N., and Kupper, K. C. (2018). Biofilm production by *Aureobasidium pullulans* improves biocontrol against sour rot in citrus. *Food Microbiol.* 69, 1–10. doi: 10.1016/j.fm.2017.07.008

Kurtzman, C. P., and Droby, S. (2001). *Metschnikowia fructicola*, a new ascosporic yeast with potential for biocontrol of postharvest fruit rots. *Syst. Appl. Microbiol.* 24, 395–399. doi: 10.1078/0723-2020-00045

Lemos Junior, W. J. F., Binati, R. L., Felis, G. E., Slaghenaufi, D., Ugliano, M., and Torriani, S. (2020). Volatile organic compounds from *Starmerella bacillaris* to control gray mold on apples and modulate cider aroma profile. *Food Microbiol.* 89, 103446. doi: 10.1016/j.fm.2020.103446

Li, Q. F., Li, C. L., Li, P. X., Zhang, H. Y., Zhang, X. Y., Zheng, X. F., et al. (2017). The biocontrol effect of *Sporidiobolus pararoseus* Y16 against postharvest diseases in table grapes caused by *Aspergillus niger* and the possible mechanisms involved. *Biol. Control* 113, 18–25. doi: 10.1016/j.biocontrol.2017.06.009

Liu, H. M., Guo, J. H., Cheng, Y. J., Liu, P., Long, C. A., and Deng, B. X. (2010). Inhibitory activity of tea polyphenol and *Hanseniaspora uvarum* against *Botrytis cinerea* infections. *Lett. Appl. Microbiol.* 51, 258–263. doi: 10.1111/j.1472-765X.2010.02888.x

Oro, L., Feliziani, E., Ciani, M., Romanazzi, G., and Comitini, F. (2018). Volatile organic compounds from *Wickerhamomyces anomalus*, *Metschnikowia pulcherrima* and *Saccharomyces cerevisiae* inhibit growth of decay causing fungi and control postharvest diseases of strawberries. *Int. J. Food Microbiol.* 265, 18–22. doi: 10.1016/j.ijfoodmicro.2017.10.027

Pagans, E., Font, X., and Sanchez, A. (2006). Emission of volatile organic compounds from composting of different solid wastes: abatement by biofiltration. *J. Hazard. Mater.* 131, 179–186. doi: 10.1016/j.jhazmat.2005.09.017

Panabieres, F., Ali, G. S., Alagui, M. B., Dalio, R. J. D., Gudmestad, N. C., Kuhn, M. L., et al. (2016). *Phytophthora nicotianae* diseases worldwide: new knowledge of a long-recognised pathogen. *Phytopathol. Mediterr.* 55, 20–40. doi: 10.14601/Phytopathol_Mediterr-16423

Qin, X., Xiao, H., Cheng, X., Zhou, H., and Si, L. (2017). *Hanseniaspora uvarum* prolongs shelf life of strawberry via volatile production. *Food Microbiol.* 63, 205–212. doi: 10.1016/j.fm.2016.11.005

Rajaofera, M. J. N., Jin, P. F., Fan, Y. M., Sun, Q. Q., Huang, W. K., Wang, W. B., et al. (2018). Antifungal activity of the bioactive substance from *Bacillus atrophaeus* strain HAB-5 and its toxicity assessment on *Danio rerio*. *Pesticide Biochem. Phys.* 147, 153–161. doi: 10.1016/j.pestbp.2017.06.006

Sui, Y., Wisniewski, M., Droby, S., and Liu, J. (2015). Responses of yeast biocontrol agents to environmental stress. *Appl. Environ. Microbiol.* 81, 2968–2975. doi: 10.1128/AEM.04203-14

Sukhada, M., Manjula, R., and Rawal, R. D. (2011). Evaluation of arbuscular mycorrhiza and other biocontrol agents against *Phytophthora parasitica* var. nicotianae infecting papaya (*Carica papaya* cv. Surya) and enumeration of pathogen population using immunotechniques. *Biol. Control* 58, 22–29. doi: 10.1016/j.biocontrol.2011.03.013

Tamura, K., Dudley, J., Nei, M., and Kumar, S. (2007). MEGA4: molecular evolutionary genetics analysis (MEGA) software version 4.0. *Mol. Biol. Evol.* 24, 1596–1599. doi: 10.1093/molbev/msm092

Wang, G. Y., Bai, T. T., Miao, Z. G., Ning, W. G., and Liang, W. X. (2018). Simultaneous production of single cell oil and fumaric acid by a newly isolated yeast *Aureobasidium pullulans* var. *aubasidani* DH177. *Bioprocess Biosyst. Eng.* 41, 1707–1716. doi: 10.1007/s00449-018-1994-0

Wang, L. Y., Dou, G. X., Guo, H. N., Zhang, Q. Q., Qin, X. J., Yu, W., et al. (2019). Volatile organic compounds of *Hanseniaspora uvarum* increase strawberry fruit flavor and defense during cold storage. *Food Sci. Nutr.* 7, 2625–2635. doi: 10.1002/fsn3.1116

Wang, Y. C., Wei, K. K., Han, X. B., Zhao, D. L., Zheng, Y. F., Chao, J. M., et al. (2019). The antifungal effect of garlic essential oil on *Phytophthora nicotianae* and the inhibitory component involved. *Biomolecules* 9, 632. doi: 10.3390/biom9100632

Zhang, D., Spadaro, D., Valente, S., Garibaldi, A., and Gullino, M. L. (2011). Cloning, characterization and expression of an exo-1,3-β-glucanase gene from the antagonistic yeast, *Pichia guilliermondii* strain M8 against grey mold on apples. *Biol. Control* 59, 284–293. doi: 10.1016/j.biocontrol.2011.06.018

Zhang, S., Guo, F., Yan, W., Dong, W., Zhou, J., Zhang, W., et al. (2020). Perspectives for the microbial production of ethyl acetate. *Appl. Microbiol. Biotechnol.* 104, 7239–7245. doi: 10.1007/s00253-020-10756-z

Zhao, Y., Tu, K., Shao, X., Jing, W., and Su, Z. (2008). Effects of the yeast *Pichia guilliermondii* against *Rhizopus nigricans* on tomato fruit. *Postharvest Biol. Technol.* 49, 113–120. doi: 10.1016/j.postharvbio.2008.01.001

Zhu, X., Zhang, S., Yang, Y., Zheng, C., Zhou, J., Gao, X., et al. (2017). Enhanced performance for plasma-catalytic oxidation of ethyl acetate over $La_{1-x}Ce_xCoO_{3+\delta}$ catalysts. *Appl. Catal. B Environ.* 213, 97–105. doi: 10.1016/j.apcatb.2017.04.066

frontiers | Frontiers in Microbiology

TYPE Original Research
PUBLISHED 02 September 2022
DOI 10.3389/fmicb.2022.994716

OPEN ACCESS

EDITED BY
Maofeng Jing,
Nanjing Agricultural University,
China

REVIEWED BY
Huijun Wu,
Nanjing Agricultural University,
China
Jie Wang,
Tobacco Research Institute (CAAS), China

*CORRESPONDENCE
Hongyan Wang
sdauwhy@163.com

SPECIALTY SECTION
This article was submitted to Microbe and Virus Interactions With Plants, a section of the journal Frontiers in Microbiology

RECEIVED 15 July 2022
ACCEPTED 08 August 2022
PUBLISHED 02 September 2022

CITATION
Chen Q, Qiu Y, Yuan Y, Wang K and Wang H (2022) Biocontrol activity and action mechanism of *Bacillus velezensis* strain SDTB038 against Fusarium crown and root rot of tomato.
Front. Microbiol. 13:994716.
doi: 10.3389/fmicb.2022.994716

Biocontrol activity and action mechanism of *Bacillus velezensis* strain SDTB038 against Fusarium crown and root rot of tomato

Qiqi Chen, Yue Qiu, Yazhen Yuan, Kaiyun Wang and Hongyan Wang*

Department of Plant Protection, Shandong Agricultural University, Tai'an, Shandong, China

Fusarium crown and root rot of tomato is a soilborne diseases that has brought serious harm and economic losses to tomato production in facilities in recent years. The disease has been reported in more than 30 countries worldwide, but there are few reports on its biological control. A *Bacillus velezensis* strain SDTB038 with biocontrol effects was isolated and identified in a previous study and is considered one of the most important PGPRs. Seven secondary metabolite biosynthesis gene clusters were found in strain SDTB038 by whole genome sequencing, explaining its biocontrol effects. Results indicated that different concentrations of SDTB038 fermentation broth inhibited the mycelial growth of Fusarium crown and root rot of tomato. Strain SDTB038 could generate indole acetic acid and promote healthy growth of tomatoes, while the effect of 10^8 CFU/ml SDTB038 concentration on promoting tomato growth was the most obvious. *B. velezensis* SDTB038 significantly reduced the accumulation of ROS in tomato plants, induced the up-regulation of antifreeze genes, and promoted the rapid recovery of tomato plants at low temperatures in a pot experiment. At the same time, SDTB038 had good control effect on Fusarium crown and root rot of tomato, and 10^8 CFU/ml SDTB038 fermentation broth had the best control effect, which was 42.98%. In summary, the strain *B. velezensis* SDTB038 may be a promising bacterial agent for biological control of Fusarium crown and root rot of tomato, and an important source of potential antimicrobial compounds.

KEYWORDS

***Bacillus velezensis*, Fusarium crown and root rot, tomato, control mechanism, genome analysis**

Introduction

Tomato (*Solanum lycopersicum*) is a common gardening crop. In recent years, the tomato planting area has increased, along with yields (Cheng et al., 2021). However, the frequent occurrence of tomato diseases affects yield and quality, and soilborne diseases are particularly difficult to control because they are persistent and widespread (Borisade et al.,

2017). Fusarium crown and root rot of tomato caused by *Fusarium oxysporum* f. sp. *radicis-lycopersici* is a severe soilborne disease (Mousa et al., 2021). *F. oxysporum* is the pathogen causing this disease and tomato Fusarium wilt, but the pathogens show different specializations. Tomato Fusarium wilt is caused by *F. oxysporum* f. sp. *lycopersici*. Although both of these pathogens can cause plant wilting, there are great differences in the associated symptoms, infection period, conditions and host infection (Bharti et al., 2017). Fusarium crown and root rot of tomato easily occurs under low temperature and high humidity, and the pathogen is mainly transmitted through soil, diseased plants, diseased seeds or compost (Rekah et al., 2000). The disease has seriously restricted the development of facility production of tomato (Deng et al., 2022). Although it is a very damaging pathogen to tomatoes, the management strategies for controlling the pathogen are limited (Cao et al., 2018), and there is an urgent need for a better way to control this disease to ensure production safety, reduce losses and increase outputs (Chu et al., 2021).

Fusarium crown and root rot of tomato are mainly controlled by biological control, which had proven the best method and received increasing attention from the agricultural industry in recent years. Plant growth-promoting rhizobacteria (PGPR) are bacteria that are good for crops and can stabilize the soil, promote plant growth and inhibit or reduce plant damage caused by disease (Joly et al., 2021). PGPR are considered promising biocontrol agents and utilize the plant rhizosphere and other areas as attachment points; these organisms have a control effect on pathogens, which could reduce the incidence of diseases (Riaz et al., 2021). The main biological control mechanisms include competition and plant growth promotion (Zhang et al., 2021). *Bacillus* had become one of the most studied PGPRs in recent years due to its wide variety of sources, high natural survival rate, inhibition of a variety of plant pathogens and environmental friendliness (Aly et al., 2022). Moreover, because it could produce secondary metabolites with antimicrobial activity, it promoted plant growth as a biological agent to control diseases over large areas (Ma et al., 2022).

Bacillus velezensis is an important PGPR that can effectively control soilborne diseases and ensure the normal growth of plants. Dhouib et al. (2019) showed that *B. velezensis* is a good biocontrol strain and could effectively control tomato verticillium wilt. Vignesh et al. (2022) showed that *B. velezensis* NKMV-3 isolated from the rhizosphere had a good biocontrol effect against *Alternaria solani*. Through genome-wide prediction, we found that the strain had seven gene clusters for secondary metabolite biosynthesis. Secondary metabolites are closely related to antimicrobial activity. *B. velezensis* had antimicrobial activity and could produce indoleacetic acid, which has good biocontrol potential (Yan Y. et al., 2021). Therefore, *B. velezensis* has good biocontrol potential against many tomato diseases, but there are few reports of its effects on Fusarium crown and root rot of tomato.

Low temperature is one of the most common abiotic stresses in plants around the world. Inhibition of plant growth and weakening of plant light cooperation have become one of the main factors restricting agricultural production (Wang et al., 2020). Under low temperature conditions, plants respond to external conditions through a series of biochemical reactions, such as leaf wilting, weakened photosynthesis, large accumulation of reactive oxygen species (ROS) in plant cells and reduced enzyme activity (Han et al., 2020). However, in order to reduce the oxidative damage caused by ROS accumulation in plant cells [mainly superoxide anion (O^{2-}) and hydrogen peroxide (H_2O_2)], biological or non-biological factors could be used to regulate the content of related enzymes in plants or induced the expression of antifreeze genes (Liu et al., 2016). Improving the freezing resistance of crops, eliminating the accumulation of ROS in them and protecting the healthy growth of crops are a key goal of agricultural production.

In view of the above facts, this study aimed to determine the inhibitory activity of SDTB038 fermentation broth with different concentrations against *F. oxysporum* f. sp. *radicis-lycopersici*, the promoting effect of SDTB038 on tomato seed germination and plant growth, the colonization dynamics of SDTB038 in soil and plants, and the field control effect of SDTB038 fermentation broth on Fusarium crown and root rot of tomato. The SDTB038 strain reduced the accumulation of low-temperature-induced ROS in tomato leaves, promoted the rapid recovery of plants at low temperature, and increased the expression of stress resistance genes. The whole genome of SDTB038 was sequenced, and its biosynthetic gene clusters were predicted. The reasons for the biocontrol potential of *B. velezensis* SDTB038 were explained at the genomic level, and the biocontrol mechanisms were preliminarily explored, providing a theoretical reference for future studies and further applications.

Materials and methods

Whole-genome sequencing analysis of SDTB038

DNA extraction and quality detection of *B. velezensis* SDTB038. A strain of *B. velezensis* SDTB038 with biocontrol potential was isolated in our laboratory and preserved in the China General Microbiological Culture Collection Center (CGMCC) under CGMCC no. 19215 (Yan H. et al., 2021). *B. velezensis* SDTB038 was cultured to logarithmic phase. Genomic DNA was extracted using a bacterial DNA kit (Tiangen). The concentration of genomic DNA extracted from SDTB038 was determined by an Epoch2 enzyme-labeled instrument (BioTek, United States). The qualified samples are transferred to Beijing concentration were sent to Novogene Co., Ltd. for detection.

Gene prediction and annotation. GeneMarkS software (verison4.17)[1] was used for coding genes expection, statistical genes expection results. The predicted genes were compared with GO, KEGG, COG and other functional databases by BLAST. The

1 http://topaz.gatech.edu/

annotations of identity and coverage ≥40%, e-value ≤$1e^{-5}$ in the sequence BLAST results were selected, and the detailed information obtained by merging all gene annotations was sorted out.

Isolation and identification of pathogens

Using the conventional tissue separation method (Mousa et al., 2021), the isolated tissue was cultured at 25°C for 2–3 days, and the marginal mycelia were selected and transferred to a new PDA plate for preliminary purification. A single spore was selected for purification and cultivation, and the colony and spore morphology were observed (Khaskheli et al., 2020). The isolated and purified strains were cultured on PDA plates and exhibited round colonies, white, villous mycelium, and the colony color changed to light pink later. Under the microscope, the two heads of macroconidia were pointed, slightly curved, sickle-shaped, with septa; microconidia were elliptical, septate. A spore suspension was prepared according to Nekoval et al. (2022). After root injury, each tomato seedling was irrigated with 10 ml spore suspension, and the symptoms were observed after the disease.

According to the Phanta Max Super-Fidelity DNA Polymerase (Vazyme Biotech Co., Ltd., Nanjing, China) kit requirements, *ITS* gene sequences were amplified and sequenced by Sangon Biotech (Shanghai) Co., Ltd. The sequencing results were analyzed by the Blast program in the NCBI database, and the strains were preliminarily classified and identified (Obunukwu et al., 2018). MEGA 7.0 software was used to construct a phylogenetic tree, and the *Sprl* gene fragments of the tomato Fusarium wilt pathogen and other isolates were amplified with Sprlf and Sprlr primers for verification (Table 1). *Sprl* gene fragments of the tomato wilt pathogen (FOL) and isolated strain (FO-1) were amplified by PCR and detected by 2% agarose gel electrophoresis.

Antimicrobial effects of SDTB038

A single colony of SDTB038 was cultured in sterilized LB. The seed solution was prepared at 25 ± 1°C at 180 r/min for 12 h (Cejas et al., 2012). The seed solution was transferred to a new sterilized conical flask with a 1% inoculation amount and cultured at constant temperature for 14 h. The fermentation broth was adjusted to 10^{10} CFU/ml with sterilized liquid LB and then diluted to 10^9, 10^8, 10^7, 10^6, 10^5 and 10^4 CFU/ml. A sterile punch (d = 5 mm) was used to remove a plug from the edge of the pathogen colony and transfer it to the center of a PDA plate. One microliter of fermentation broth was extracted with a pipette and placed on both sides of the mycelial plug (Villarino et al., 2021). With LB as the control, the mycelia grew to 3/4 of the plate at 25°C, and the test effects were observed.

TABLE 1 Primers and sequences used for PCR.

Primer name	Sequences (5′-3′)
Sprlf	GATGGTGGAACGGTATGACC
Sprlr	CCATCACACAAGAACACAGGA

Determination of the growth temperature of SDTB038

The preparation of the biocontrol bacterium SDTB038 seed liquid was as described above. A 10 ml sterile centrifuge tube was added to 3.92 ml sterile liquid LB and 80 μl seed liquid in each tube, and the same amount of liquid LB was added as a control. After sealing the membrane, the tube was placed in a constant temperature oscillator at different temperatures (5, 10, 15, 20, 25, 30, 35, 40, 45, 50°C) and 180 rpm. After 12, 24 and 48 h of culture, the OD value at 600 nm wavelength was measured by microplate reader and the ΔOD600 was calculated.

Determination of the production capacity of growth-promoting substances of SDTB038

Detection of IAA secretion activity: SDTB038 was cultured in 20 ml liquid LB containing 1% L-tryptophan (Buy from Beijing Solarbio Science & Technology Co., Ltd.) for 2 days (180 rpm/min, 25°C) without biocontrol bacteria as a control. Two milliliters of supernatant, was added to 4 ml of Salkowski reagent and two drops of phosphoric acid. The mixture became red, proving that SDTB038 could secrete IAA (Jangir et al., 2018).

Phosphate dissolution activity test: sterile filter paper (5 mm) was placed in the center of NBRIP plate, and 2 μl bacterial solution was added dropwise on the filter paper. Cultured at 25°C for 7 days, if transparent halos appear around colonies, SDTB038 can dissolve phosphate.

Water culture experiment with tomato seedlings

Tomato seeds were germinated in a seedling tray containing sterile matrix soil, cultured in a light incubator at 25°C ± 1°C, and managed with normal watering and fertilization. When the seedlings had formed two leaves and one center, cultivated seedlings were transplanted into the greenhouse of Shandong Agricultural University for hydroponics cultures (Gao et al., 2018). A white plastic square box was used in the hydroponic container, and the container was filled with sterilized Hoagland nutrient solution. The tomato seedlings were fixed with a foam floating plate, and three seedlings were transplanted into each box (the substrate attached to the rhizosphere was carefully removed when the seedlings were transplanted into sterile water). The following seven treatments were set up (30 ml per

box per treatment): A: CK (water control) B: 0.01 mg/l S-inducible hormone treatment (spray); C: LB treatment; D: 10^7 CFU/ml SDTB038; E: 10^8 CFU/ml SDTB038; F: 10^9 CFU/ml SDTB038; G: 10^{10} CFU/ml SDTB038. After transplanting, the seedlings were treated once every 7 days for the first time continuously treated 3 times, and the nutrient solution was replaced once every 7 days. Three repetitions were performed per treatment (Souri and Tohidloo, 2019). The height, stem thickness, root length and effective leaf number of tomato seedlings were measured and recorded at 7, 14, 21 and 40 d after the first test group, and the fresh weight and dry weight of plants and roots were weighed at 40 d. After 30 min of treatment at 105°C in an oven to devitalize the green tissues, samples were dried to constant weight at 80°C to determine the dry weight (Singh et al., 2016).

Real-time PCR detection and histochemical detection of H_2O_2 and O^{2-}

Two treatments were established in the experiment: 1: LB control, 15 ml liquid LB medium was applied to each plant; 2: Application of SDTB038 fermentation broth, 15 ml 10^8 CFU/ml SDTB038 fermentation broth was applied to each plant. Colonization at room temperature for 48 h, was allowed under a 4°C low temperature treatment. There were three replicates per treatment, and three plants per replicate. After treatment, the leaves of the control and treatment groups were taken at 0, 3, 6, 9, 12 h, 1 h rewarming and 3 h rewarming and stored at −80°C for total RNA extraction. An RNA extraction kit and reverse transcriptase kit were used for total RNA extraction from tomato leaves and reverse transcription. The qRT-PCR used SYBR Green Mix reagent kits according to the manufacturer's instructions (The kits are purchased from Vazyme Biotech Co., Ltd., Nanjing, China). QRT-PCR primers were designed by Shanghai Sangon Biological Technology and Services Co., Ltd. (Shanghai, China; Table 2).

The *in situ* formation of H_2O_2 and O^{2-} in the leaf was detected according to the method of Zhang et al. (2019). Diaminobenzidine (DAB) and nitroblue tetrazolium (NBT) were purchased from Beijing Solebo Technology Co., Ltd. After staining, the cells were allowed to stand for 12 h to decolorize. Each treatment was repeated three times (Han et al., 2020). At the same time, a hydrogen peroxide kit and superoxide ion kit were used to measure the H_2O_2 and O^{2-} contents. Kits were purchased from Suzhou Geruisi Biotechnology Co., Ltd.

Determination of the H_2O_2 content:approximately 0.1 g tomato leaves were weighed, 1 ml acetone was added, the mixture was homogenized in an ice bath, transferred to an EP tube, brought to constant volume of 1 ml with acetone, and centrifuged at 12000 rpm and 4°C for 10 min; the supernatant was retained and placed on ice for subsequent measurement.

Determination of the O^{2-} content:approximately 0.1 g tomato leaves were weighed, 1 ml of extract was added, the mixture was homogenized in an ice bath, and then centrifuged at 12000 rpm and 4°C for 10 min; the supernatant was retained as crude body fluid and placed on ice for subsequent measurement.

SDTB038 colonization test

Determination of natural resistance of the biocontrol strain SDTB038. Preparation of drug-containing plates containing kanamycin, rifampicin and ampicillin at final concentrations (All purchased from Beijing Solarbio Science & Technology Co., Ltd.) of 20, 50 and 100 mg/l, and the plates without drug additions were used as the control. The SDTB038 fermentation broth was diluted in 100 µl, absorbed by a pipette and evenly coated on the plate. SDTB038 was cultured at 25°C for 12 h to examine the growth of SDTB038.

Determination of rifampicin resistance of soil microbial populations. Tow grams of soil was dissolved in water and diluted 100 times. Then, 100 µl of the soil suspension before and after dilution was evenly coated on the LB plate containing 100 mg/l rifampicin, and the LB plate without rifampicin was used as the control. The growth of the soil microbial population on LB plates containing rifampicin was observed at 25°C for 10–12 h (Schreiter et al., 2018).

Induction of rifampicin-resistant strains. The concentrations of the rifampicin resistance induction series were set as follows: 0.1, 0.5, 1.0, 2.0, 4.0, 8.0, 16.0, 25.0, 50.0, 100.0 and 200.0 mg/l. Single colonies were picked and cultured in liquid LB containing 0.1 mg/l rifampicin for 12 h, streaked

TABLE 2 Primers used for qRT-PCR.

Gene name	Forward primers (5′-3′)	Reverse primers (5′-3′)
SIMPK3	GCAACTCCCACAACATCC	TCTGCTCTTCTCCTATCCCT
SIHSP17.7	CACCGAAGGAGGAAGGAAAGTGG	TTTGCGTTCTCTGGAAGTC
SLMYB7	CAGATGCCCAAATTCGCAGG	CTGCTGCAGGGTGAACAAAC
SICPK8	CTCTAGAATGAGTAGCTCAACGTCAACGC	GGGTACCTTAAGACCCTTTTTCTTCAGAG
SIHY5	GGCTCTAGAATGCAAGAGCAAGCGACG	CCATGGGCTTCCTCCCTTCCTGTGCACC
SOD	GGCACCATCCTCTTCACTC	GCACCATGCTCCTTACCAG
CAT	GATGAGCACACTTTGGAGCA	TGCCCTTCTATTGTGGTTCC

on LB plates containing the same concentration of rifampicin and cultured at 25°C. Single colonies with the same shape as the original colonies were selected and transferred to liquid LB plates containing lower concentrations of rifampicin to continue shaking culture until the induced strains could grow normally on LB plates containing 200 mg/l rifampicin (Stoll et al., 2021; Huang et al., 2022).

Determination of the genetic stability of rifampicin resistance of the SDTB038 strain. After rifampin resistance induction, the resistant marker strain was transferred to an ordinary LB plate for 3 generations by the streaking method, and then transferred to the LB plate containing 200 mg/l rifampin to detect its genetic stability (Rathore et al., 2016).

Morphological observation, physiological and biochemical characterization and molecular biological identification of the rifampicin-labeled strain. Morphological characteristics: Rifampicin-resistant labeled strains and wild-type strains were lined up on LB plates at the same time, and single colonies were cultured on LB plates for later observation and recording (Wang et al., 2022).

Molecular biological identification: Total DNA of labeled and wild-type strains was extracted by a bacterial DNA kit (Vazyme Biotech Co., Ltd., Nanjing, China). The primers were sequenced by Sangon Biotechnology (Shanghai) Co., Ltd. The 16S rRNA gene and *gyrB* gene were amplified by using universal primer sets (27F and 1492R; UP1f and UP2r; Table 3), and DNMAN was used to compare the gene sequences of the two strains to determine the relationship between rifampicin-resistant marker strains and wild strains (Soergel et al., 2012).

SDTB038 colonization and SEM observation. Thirty ml of rifampin-resistant marker strain fermentation broth was inoculated in each pot by the root irrigation method. With the plants watered with 30 ml sterile liquid LB as the control, the rhizosphere soil, root tissue, stem base and leaves of tomato plants were taken 1, 2, 3, 4, 5, 6, 7, 14, 21, 28 and 60 d after root irrigation. The labeled strains were recovered from a plate containing 100 mg/l rifampicin, and the colonization of the labeled strains at different times and in different plant parts was analyzed (Chu et al., 2021). Scanning electron microscopy was performed according to a previous method (Guo et al., 2017). The colonization of strain SDTB038 in roots and stems of tomato seedlings at 7 d and 60 d was observed by scanning electron microscopy.

Field test

The field experiment site was located in Fangcun Beibudong Village, Daiyue District, Taian City, Shandong Province, China. Tomato is the main greenhouse vegetable in Fangcun Village, and it is planted in both spring and autumn. The greenhouse selected in this experiment had been in tomato cultivation for more than 20 years. The test site had good soil and fertility conditions, tillage measures in place, and easy-access to irrigation. The tomato seedlings were planted on August 31, 2020. The plant spacing in the shed was approximately 55 cm, and the row spacing was approximately 1.1 m. Two thousand tomato seedlings were planted per mu.

The experiment used a randomized block distribution, with a total of 20 plots. The plot area was 21 m^2, and each treatment set had 5 replicates, with the treatment interval of a plot for the isolation zone. The following four treatments were set: 1: blank control, no application of biocontrol bacteria and pesticides; 2: LB control, 10 ml liquid LB medium was applied to each strain; 3: Microbial fertilizer treatment (content of *Bacillus subtilis* in microbial fertilizer ≥20 billion CFU/g, 0.5 g per plant); 4: Chemical treatment, 75 g/ha 10% difenoconazole water dispersible granules (Buy from Shandong Biao Biotechnology Co., Ltd.); 5: Application of SDTB038 fermentation broth, each strain was treated with 10 ml 10^8 CFU/ml SDTB038 fermentation broth. The base of the stem was sprayed with a 3 WBD-20 electric sprayer in the difenoconazole treatment, and 450 l/ha water was used for each treatment. The fermentation broth of biocontrol bacteria was used to irrigate the roots (Luo et al., 2019). A total of 3 applications of biocontrol bacteria were made, at transplanting (August 31); before cooling (November 21); and 7 days after the second treatment. After the obvious onset of disease in the control treatment, the disease incidence under each treatment was checked and recorded, and the disease index (DI) and disease control effect (DCE) were calculated.

Disease classification standards are as follows: level 0: plant health, no disease; level 1: roots brown, not soft rot, not constricted, leaves healthy, root no obvious lesion; level 2: the root became brown with obvious constriction, the tip or leaf became yellow, and the root became brown; level 3: the roots became brown and rotten, the leaves became yellow, and the roots became brown or even black; level 4: root and root rot, whole seedling necrosis (Ma and Wehner, 2015).

TABLE 3 Primers and sequences used for PCR.

Primer name	Sequences (5′-3′)
27F	AGAGTTTGATCMTGGCTCAG
1492R	TACGGYTACCTTGTTACGACTT
UP1f	GAAGTCATCATGACCGTTCTGCAYGCNGGNGGNAARTTYGA
UP2r	AGCAGGGTACGGATGTGCGAGCCRTCNACRTCNGCRTCNGTCAT

Disease index (%) = (∑ number of plants of all grades × representative value of disease classification)/highest disease level × all number of observed plants × 100.

Control effect (%) = ∑ (blank group disease index−treatment group disease index)/blank group disease index × 100.

Data analysis

The data obtained in the antibacterial effect test of lipopeptide crude extract were used to calculate the median lethal concentration (EC_{50}) by ANOVA in Excel and SPSS 18.0 software. Indoor germination, greenhouse growth and field test data were statistically analyzed by Duncan New Complex Range (DMRT), and expressed as mean ± standard deviation (SD).

Results

Genome-wide sequencing analysis of strain SDTB038

Genome-wide data for *B. velezensis* SDTB038. To understand the strain SDTB038 more thoroughly and comprehensively, we further analyzed its complete genome (Figure 1A) and submitted it. The total number of base pairs contained in the complete genome of SDTB038 was 3,929,791, and the GC content was 47.26%. The whole gene sequences of strain SDTB038 were submitted to the National Center for Biotechnology Information (NCBI) database with the accession numbers SUB6310808. The number of genes annotated by specific genes in each database was as follows NR (3944), GO (2707), COG (2900), KEGG (3833), Swiss-Prot (3314), pfam (2707), TCDB (450), and CAZy (159).

Gene functional annotation results from the main databases. Gene Ontology (GO) is a widely used and important tool in the field of bioinformatics. It is an international standardized classification system for gene function descriptions. It describes our understanding of the biological field from three aspects (Figure 1B). The biological process (BP) genes are further subdivided into 24 subfunctions, with genes involving metabolic and cellular processes numbering at 1602 and 1,559, respectively. Genes in cell components (CCs) were subdivided into 10 subfunctions, with the largest number of genes in cells and cell parts, both with 1,036; the genes in molecular functions (MFs) were also subdivided in 10 subfunctions, and the number of genes involved in catalytic activity reached 1,550. Based on GO annotation, the most abundant genes of strain SDTB038 in BP, CC and MF were metabolism, catalysis and cell function.

Kyoto Encyclopedia of Genes and Genomes (KEGG) is a database for genome deciphering with which the possible metabolic processes or functions of SDTB038 were obtained by comparative analysis. ABC transporters (127), two-component systems (114) and other pathways had a high correlation with the genome of strain SDTB038. In addition, by comparison with known functional sequences, these pathways were divided into six categories, as shown in Figure 1C. SDTB038 had the highest abundance of genes involved in metabolism.

Cluster of Orthologous Groups of proteins (COG) is constructed according to the phylogenetic relationships of coding proteins in the complete genome. The biological function of SDTB038 was also revealed by COG annotation. A total of 3,337 genes were annotated to 25 COG families (Figure 1D), which were related to metabolism, cell process and signaling, genetic information storage and processing. The analysis showed that SDTB038 had a strong metabolic function, and the annotated genes related to metabolic function accounted for 42.97%. The large proportion of genes involved in cell processes and signaling was mainly related to cell membrane, wall, and capsule biosynthesis and signal transduction mechanisms, accounting for more than 5.5%. The number of genes related to genetic information storage and processing was second only to those in metabolic function, accounting for 22.95% of the total annotated genes, of which transcription-related genes accounted for 8.6%. In addition, the conventional function accounted for 9.14%, and the unknown function accounted for 6.23%, indicating that the potential abilities of the biocontrol bacterium SDTB038 remains to be further developed.

Gene clusters for secondary metabolite synthesis. Gene clusters associated with secondary metabolite synthesis were annotated using the antiSMASH6.0.1 database. The results showed that SDTB038 contained biosynthesis gene clusters including those for macrolactin H, bacillaene, fengycin, difficidin, *bacillus* bactin, bacilysin and surfactin. Although that surfactin showed 86% similarity to the reported secondary metabolite synthesis gene cluster, the similarity of other gene clusters was 100% (Table 4). The results showed that the SDTB038 genome has genes that can be used for the biosynthesis, regulation and transport of antimicrobial substances, and there were many genes beneficial to plant growth, that were related to antimicrobial and growth-promoting potential.

Isolation and identification of pathogens

The results showed that FOL failed to amplify the target band, and the isolated strain (FO-1) amplified the target band at the position of nearly 1,000 bp, which was consistent with the results of Hirano and Arie. After Blast comparison, the *ITS* gene of the isolated strain was 100% similar to that of *F. oxysporum* AM4. In the *ITS* gene system tree (Supplementary Figure S1), the isolates (FO-1) and *F. oxysporum* AM4 were clustered in the same branch.

After root inoculation, the stem base exhibited light brown stripe rot and brown depressions, and the plants showed lodging.

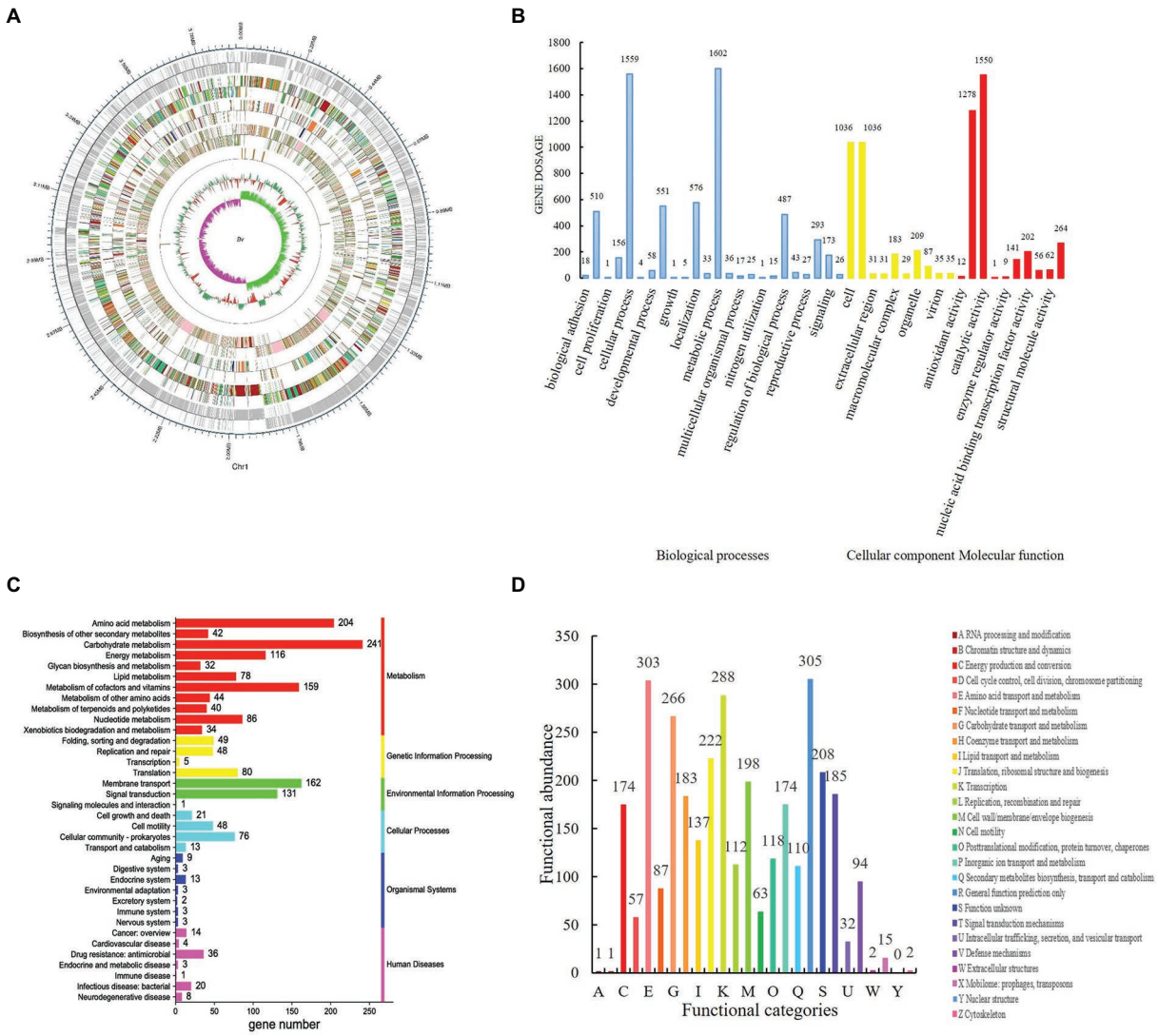

FIGURE 1
Genome-wide analysis of *Bacillus velezensis* SDTB038. **(A)** genome circular map of SDTB038 strain; **(B)** Gene Ontology (GO) sub-classification of SDTB038. Blue: biological process; Yellow: cellular components; Red: molecular functions; **(C)** Statistical chart of KEGG secondary function classification. Red: metabolism; Yellow: genetic information processing; Green: environmental information processing; Light blue: cellular process; Dark blue: organismal system; Light red: human disease. **(D)** Functional classification map of strain SDTB038 in COG.

TABLE 4 Biosynthetic gene clusters of secondary metabolite in strain of SDTB038 genome.

Gene cluster type	Metabolite	Gene cluster ID similarity (%)	Gene location Start – end	Size(bp)
nrps	surfactin	BGC0000433(86%)	323,410–387,387	63,978
transatpks	macrolactin H	BGC0000181(100%)	1,384,086–1,471,921	87,836
transatpks-nrps	bacillaene	BGC0001089(100%)	1,691,450–1,792,015	100,566
transatpks-nrps	fengycin	BGC0001095(100%)	1,865,757–2,000,046	134,290
transatpks	difficidin	BGC0000176(100%)	2,282,382–2,376,174	93,793
bacteriocin-nrps	bacillibactin	BGC0000309(100%)	3,000,878–3,052,669	51,792
other	bacilysin	BGC0001184(100%)	3,588,979–3,630,397	41,419

The pathogenic fungi were isolated from the diseased plants. The isolated and purified strains were similar to the original strain in morphology and biological identification results. According to the growth morphology and molecular biology identification results, the isolated strain was identified as F. *oxysporum* f. sp. *radicis-lycopersici* (FORL).

Antifungal effect of SDTB038

The results showed that the inhibition zone width of SDTB038 fermentation broth with different concentrations was 5.68–7.66 mm, which indicated that SDTB038 had activity against FORL. The statistical analysis of the antifungal band width showed that the effect of SDTB038 at 10^7 and 10^8 CFU/ml concentrations was significantly higher than that of other concentrations (Table 5). The maximum inhibition zone width was 7.66 ± 0.23 mm at 10^8 CFU/ml (Supplementary Figure S2).

SDTB038 at different concentrations had good control effects on Fusarium crown and root rot of tomato pathogens, and SDTB038 at 10^7 and 10^8 CFU/ml had the best control effect.

Determination of the growth temperature of SDTB038

The growth curves of SDTB038 cultured at different temperatures for 12, 24 and 48 h are shown in Figure 2. Under 20°C, the activity of SDTB038 cultured for 12, 24, 48 h was low and the growth rate was slow. Between 20°C and 30°C, the growth rate of SDTB038 cultured in three periods was the fastest, and the growth rate reached the peak around 25°C. When the temperature was higher than 30°C, the growth rate of SDTB038 cultured in three periods decreased significantly. The growth rate is slow to flat after 40°C. The tests indicated that the optimal growth temperature range of SDTB038 was 25–30°C. When the temperature was lower than 20°C or higher than 35°C, the growth rate of SDTB038 decreased significantly. Although the growth slowed down at low temperature, SDTB038 could still grow at 5°C, it indicated that SDTB038 could colonize in tomato roots at low temperature.

Indole acetic acid production capacity of SDTB038

SDTB038 was cultured in 20 ml liquid LB containing 1% L-tryptophan for 2 days. Two milliliters of supernatant were taken, was added to 4 ml Salkowski reagent and two drops of orthophosphoric acid. After bathing in 28°C water bath for 2.5 h, it was found that the mixture showed light pink, while the control group without biocontrol bacteria showed light yellow. Meanwhile, transparent halos were not observed on NBRIP plates. Therefore, the experiment showed that SDTB038 could produce indoleacetic acid, promote seed germination and plant growth, prevent and treat diseases, and have plant health effects. However, SDTB038 had no phosphorus-solubilizing effect.

TABLE 5 Antibacterial activity of SDTB038 gradient fermentation broth.

Fermentation broth concentration (CFU/mL)	Bacteriostatic diameter (mm)
$_{10}10$	5.78 ± 0.21c
10^9	6.72 ± 0. 11b
10^8	7.66 ± 0. 23a
10^7	7.43 ± 0. 09a
10^6	5.68 ± 0.24c
10^5	6.25 ± 0.37bc

Values are means ± SD of 3 experiments. The lowercases represent significant level ($p = 0.05$) according to the Duncan's test.

Hydroponic culture experiment with tomato seedlings

In the greenhouse hydroponic experiment, it can be seen from Figure 3A that 10^7–10^{10} CFU/ml SDTB038 resulted no significant difference in plant height at the statistical level at 7 and 14 days after treatments. Among them, 10^8 CFU/ml had the best effect after processing for approximately 7 days, and the plant height of tomato was 4.05 cm; 10^7 CFU/ml had the best effect after processing for approximately 14 days, and the plant height of tomato was 4.39 cm. At 21 d after treatment, the 10^7 and 10^8 CFU/ml SDTB038 treatments resulted in plant height that were significantly higher than those under the water, LB and S-inducible control treatments, and the plant height of the 10^8 CFU/ml SDTB038 treatment group was 4.87 cm. After 40 days of treatment, the height under the 10^8 CFU/ml SDTB038 treatment was obviously higher than that of the water and LB control treatments, at 6.53 cm. Except for the 10^8 CFU/ml treatment, there was no obvious change among the other treatments.

The effect of each treatment on the stem diameter of tomato seedlings was mainly reflected in the early stage of treatment (7 and 14 d after treatment). After approximately 7 days, the 10^7, 10^8 and 10^{10} CFU/ml SDTB038 treatments resulted in a significantly larger diameter than those under the clean water, LB and S-selectin control treatments; on the 14th day after treatment, the diameter under the 10^8 CFU/ml SDTB038 treatment was obviously different from that under water, LB and the S-induced control. There was no obvious change between treatments at 21 and 40 days after treatment (Figure 3B).

The fermentation broth treatment had little effect on the number of effective leaves. In the statistical analysis results, there was no difference in the effect between the two groups in the first 7 days; After processing for approximately 14 days, the number of effective leaves in the 10^7 CFU/ml SDTB038 experimental group was obviously higher than that in the water, liquid LB and S-inducible control treatments. However, 21 d after treatment, there was no obvious change between the treatment with 10^7–10^9 CFU/ml SDTB038 fermentation broth and the control treatment with clear water, liquid LB and S-selectin. There was no obvious change among treatments 40 days after treatment (Figure 3C).

The effect of each treatment on root length was mainly reflected in the later treatment stage (21 and 40 d). There was no

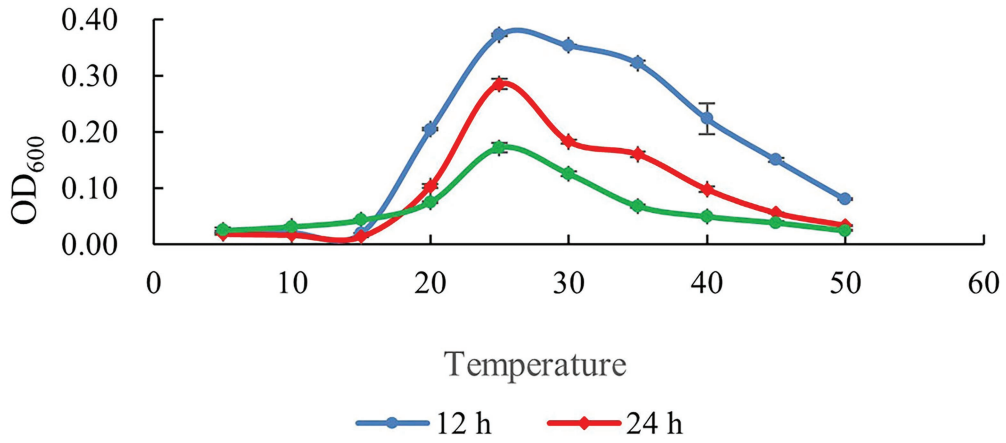

FIGURE 2
Determination of growth temperature of SDTB038. Blue: growth curve of SDTB038 cultured for 12h; Red: growth curve of SDTB038 cultured for 24h; Green: growth curve of SDTB038 cultured for 48h.

obvious change in the statistical level between the seven groups at 7 and 14 d after treatment. Twenty-one days after treatment, the promoting effect of S-selectin treatment on root length was significantly higher than that of the other treatments. After processing for approximately 40 days, water, liquid LB treatment and inducer treatment effects were better. However, when the fresh weight and dry weight of seedling roots were measured, it was found that although the seedling roots in the water treatment, liquid LB treatment and S-selectin treatment were longer than those in the fermentation broth treatment at 40 d after treatment, the weighing measurement results (Table 6) showed that the fresh weight of roots under the 10^8 CFU/ml SDTB038 fermentation broth treatment was 1.13 g, which was 59.15%, 73.85% and 24.18% higher those under the water treatment, liquid LB treatment and S-selectin treatment, which were 0.71 g, 0.65 g and 0.91 g, respectively (Figures 3D,E). Statistical analysis showed that 10^8 CFU/ml SDTB038 fermentation broth had the same effect on roots as the s-selectin treatment, but resulted in significantly higher weight than that under the water and liquid LB treatments. After drying the seedling roots to constant weight, the root dry weight under the 10^8 CFU/ml SDTB038 fermentation broth treatment was 0.065 g, which was 51.16%, 62.50% and 47.73% higher than the 0.043 g, 0.040 g and 0.044 g of the water, liquid LB and S-inducible treatments, respectively. At the statistical level, the 10^8 CFU/ml SDTB038 fermentation broth treatment resulted in significantly higher weight than the water, liquid LB and S-inducible treatments.

SDTB038 can induce cryogenic genes and reduce active reactive oxygen species accumulation in tomato

Through low-temperature stress treatment of tomato, we studied the expression of antifreeze genes in strain SDTB038. The *SIMPK3* gene regulates ROS homeostasis by activating the cell antioxidant system and regulating the transcription of stress-related genes, thus acting as a positive regulator in the low-temperature stress response. The expression of *SIMPK3* in tomato tissues at 0, 3, 6 and 9 h after applying SDTB038 fermentation broth was not different from that in the control group. The expression of *SIMPK3* in tomato tissues was upregulated 12 h after low temperature treatment. After rewarming, *SIMPK3* gene expression gradually decreased (Figure 4A). The *SIHSP17.7* gene and *SLMYB7* gene could improve the regulation of cells under low temperature in tomato and regulate the ROS content in plants. After 12 h of low-temperature treatment, the expression levels of the *SIHSP17.7* gene and *SLMYB7* gene were upregulated in tomato plants treated with SDTB038 fermentation broth. The expression of both genes increased gradually at 1 h after rewarming. After 3 h of rewarming, the expression levels of the *SIHSP17.7* gene and *SLMYB7* gene gradually decreased and returned to normal levels (Figures 4B,C). There was no obvious change in the expression of the *SICPK8* gene and *SIHY5* gene between tomato tissues at different time points (Figures 4D,E).

By measuring the activity of superoxide dismutase (SOD) and catalase (CAT), it was found that both were increased at 0 h, which may have been due to the application of SDTB038 fermentation broth to promote the production of SOD and CAT enzymes. At 3 and 6 h, *SOD* and *CAT* were affected by low-temperature stress, downregulating their expression. At low temperature for 9 and 12 h, both of the expression levels were upregulated, with a significant difference from those under the liquid LB treatment, because the application of SDTB038 fermentation broth promoted the expression of antifreeze genes (Figures 5A,B).

At the same time, we evaluated the accumulation of ROS in leaves at low temperature. The contents of H_2O_2 and O^{2-} were

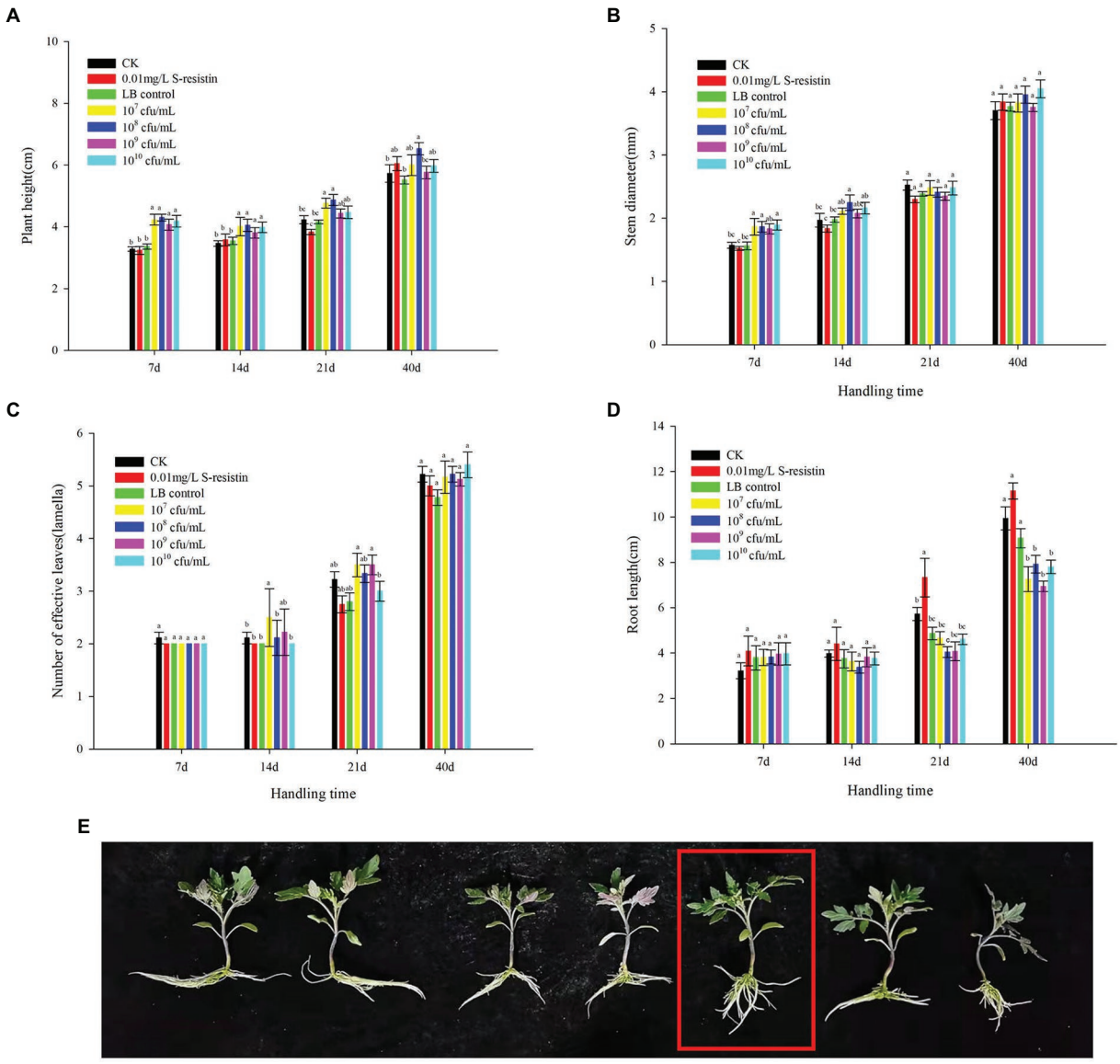

FIGURE 3
Effects of SDTB038 on tomato seedlings. **(A)** Plant height; **(B)** Stem diameter; **(C)** Number of effective leaves; **(D)** Root length; **(E)** Effects of fermentation broth on root length of tomato plants. The different lowercases represent significant level (p=0.05) according to the Duncan's test.

detected by kits. The contents of H_2O_2 and O^{2-} and in tomato plants treated with liquid LB gradually increased and ROS accumulated under low temperature conditions. However, the contents of H_2O_2 and O^{2-} in tomato plants treated with SDTB038 fermentation broth increased first and then decreased, and the contents of H_2O_2 and O^{2-} were the lowest at the low temperature treatment for 12 h (Figures 5C,D). At the same time, H_2O_2 and O^{2-} were detected by staining, and the staining increased first and then decreased, which was consistent with the content determination (Figure 6). It can be concluded that strain SDTB038 could promote the expression of antifreeze genes and reduce the accumulation of ROS under low temperature conditions.

Colonization test of strain SDTB038

Natural resistance of the biocontrol strain SDTB038. In the natural resistance test of biocontrol bacteria, the control plate without antibiotics grew single colonies on the surface of the medium after 12 h of culture, and no single colonies grew on the plate with different concentrations of rifampicin, ampicillin and kanamycin. Therefore, SDTB038 had no natural resistance to antibiotics such as rifampicin.

Rifampicin resistance in soil microbial populations. In the resistance test of the soil microbial population to rifampicin, on the control plate without rifampicin, the soil suspension before and after dilution showed the growth of soil microorganisms. In

TABLE 6 Effects of SDTB038 on fresh and dry weight of tomato seedlings.

Treatment	Fresh weight		Dry weight	
	Root(g)	Aerial parts (g)	Root (g)	Aerial parts (g)
1	0.71 ± 0.06bc	1.38 ± 0.12b	0.043 ± 0.004b	0.12 ± 0.014bc
2	0.91 ± 0.06abc	1.47 ± 0.08ab	0.044 ± 0.003b	0.12 ± 0.006bc
3	0.65 ± 0.04c	1.18 ± 0.09b	0.040 ± 0.002b	0.10 ± 0.009c
4	1.02 ± 0.11ab	1.69 ± 0.11ab	0.058 ± 0.006ab	0.15 ± 0.008ab
5	1.13 ± 0.13a	1.91 ± 0.12a	0.065 ± 0.006a	0.17 ± 0.009a
6	0.86 ± 0.13abc	1.61 ± 0.22ab	0.051 ± 0.007ab	0.15 ± 0.019ab
7	1.05 ± 0.21ab	1.99 ± 0.35a	0.060 ± 0.012ab	0.17 ± 0.028a

1. Water control; 2. 0.1 mg/l S-dactin; 3. LB control; 4. 10^7 CFU/ml fermentation broth; 5. 10^8 CFU/ml fermentation broth; 6. 10^9 CFU/ml fermentation broth; 7. 10^{10} CFU/ml fermentation broth. Values are means ± SD of three experiments. The different lowercases represent significant level ($p = 0.05$) according to the Duncan's test.

terms of surface morphology, mainly bacterial microorganisms were present, while there was no trace of microbial growth on the rifampicin plate with 100 mg/l.

Morphological observation, physiological and biochemical characterization and molecular biological identification of the rifampicin-labeled strain. After the genetic stability test of the resistant strains that could grow normally on 200 mg/l rifampicin plates, the colony morphology was observed by streaking. Under the same culture time and conditions, compared with the wild-type strain, the growth of the rifampicin-labeled strain was slower, but that of the single colony was the same as that of the wild-type strain, which was white on the medium plate, with smooth and neat edges, and wrinkled bulges in the middle.

The physiological and biochemical results showed that the rifampin-labeled strain was gram-positive bacterium that could hydrolyze gelatin and starch, did not produce pyocyanin, hydrogen sulfide or fluorescent pigments, and could not use citric acid or malonic acid. The rifampin-labeled strain was positive in the V-P test, contact enzyme test, nitrate reduction test and anaerobic growth test, and negative in the methyl red test, which was the same as the results of the previous determination of wild strains in the laboratory. DNAMAN software was used to compare the 16S rRNA gene and *gyrB* gene fragments of rifampicin-resistant marker strains and wild strains, and the results showed 100% identity.

Colonization characteristics of SDTB038. The dynamic colonization results of SDTB038 in different parts of tomato rhizosphere soil and tomato plants are shown in Supplementary Figure S3. The bacterial amount decreased with time in the early stage and gradually stabilized in the later stage.

SDTB038 had the highest amount of recovered bacteria in rhizosphere soil on the first day after root irrigation, which was 2.05×10^9 CFU/g. On the 4th day, it decreased to the first low of 3.42×10^7 CFU/g and increased on the 5th day. Subsequently, with increasing culture time, colony colonization decreased gradually. At the later stage of the experiment (28, 40, and 60 d), the colonization rate of biocontrol bacteria in tomato rhizosphere soil tended to be stable at 2.89×10^6 CFU/g and 5.91×10^6 CFU/g. However, the colonization rate of SDTB038 in tomato roots was 2.24×10^8 CFU/g on the first day after root irrigation, and rapidly decreased to the first low value on the third day. The colonization amount was 1.92×10^7 CFU/g, and then slowly increased. The colonization amount increased to 1.23×10^8 CFU/g on the sixth day, but then sharply decreased to a new low value of 2.00×10^7 CFU/g on the seventh day. On the 14th day, the colonization amount of biocontrol bacteria peaked 3.89×10^9 CFU/g and then decreased over time and gradually stabilized on the days 40 and 60.

The colonization of SDTB038 in the stem bases of tomato was detected on the 2nd day after root irrigation, and the amount of bacteria was 5.00×10^6 CFU/g. There was a low value on the 4th day, and the amount of bacteria was 3.67×10^6 CFU/g. The colonization continued to increase over the next 2 days, a new low value appeared on the 7th day, and the amount of bacteria was 1.52×10^6 CFU/g. The colonization of biocontrol bacteria peaked 14th day, and the amount of bacteria was 4.07×10^9 CFU/g. After 21 days, the amount of bacteria decreased sharply, and then the colonization became stable. The colonization of SDTB038 in tomato leaves was divided into two parts, original leaves and new leaves, after 14 days of colonization. It can be seen from the figure that the colonization of biocontrol bacteria in the original true leaves and new leaves was similar to that in roots and stems, and peaked at 14 d after treatment. The colonization amount in the original true leaves was 9.13×10^7 CFU/g, and that in the new leaves was 2.07×10^9 CFU/g. The change trends of the two were consistent. The colonization amount decreased sharply at 21 d after treatment, and then stabilized after 21 d. On the 60th day, the original true leaf colonization rate was 6.56×10^4 CFU/g, and the new leaf colonization rate was 4.51×10^4 CFU/g.

Scanning electron microscopy observations. Supplementary Figure S4 shows our SEM (5,000 × SEM) observations. Supplementary Figures S4A,B shows the electron microscopy images and figures of tomato roots after 7 d of fermentation broth treatment and LB control treatment, respectively. Supplementary Figures S4C,D shows the electron microscopy images and figures of tomato the stem base after 7 d of fermentation broth treatment and LB control treatment, respectively. Supplementary Figures S4E,F shows the electron microscopy images and figures of tomato roots after 60 d of fermentation broth treatment and LB control treatment, respectively. Supplementary Figures S4G,H shows the electron microscopy images and figures of tomato the stem base after 60 d of fermentation broth treatment and LB control treatment, respectively. As shown in Supplementary Figure S4, compared with the control treatment, a large amount of *Bacillus* adhesion was observed in the root and stem base of tomato in the fermentation broth treatment group.

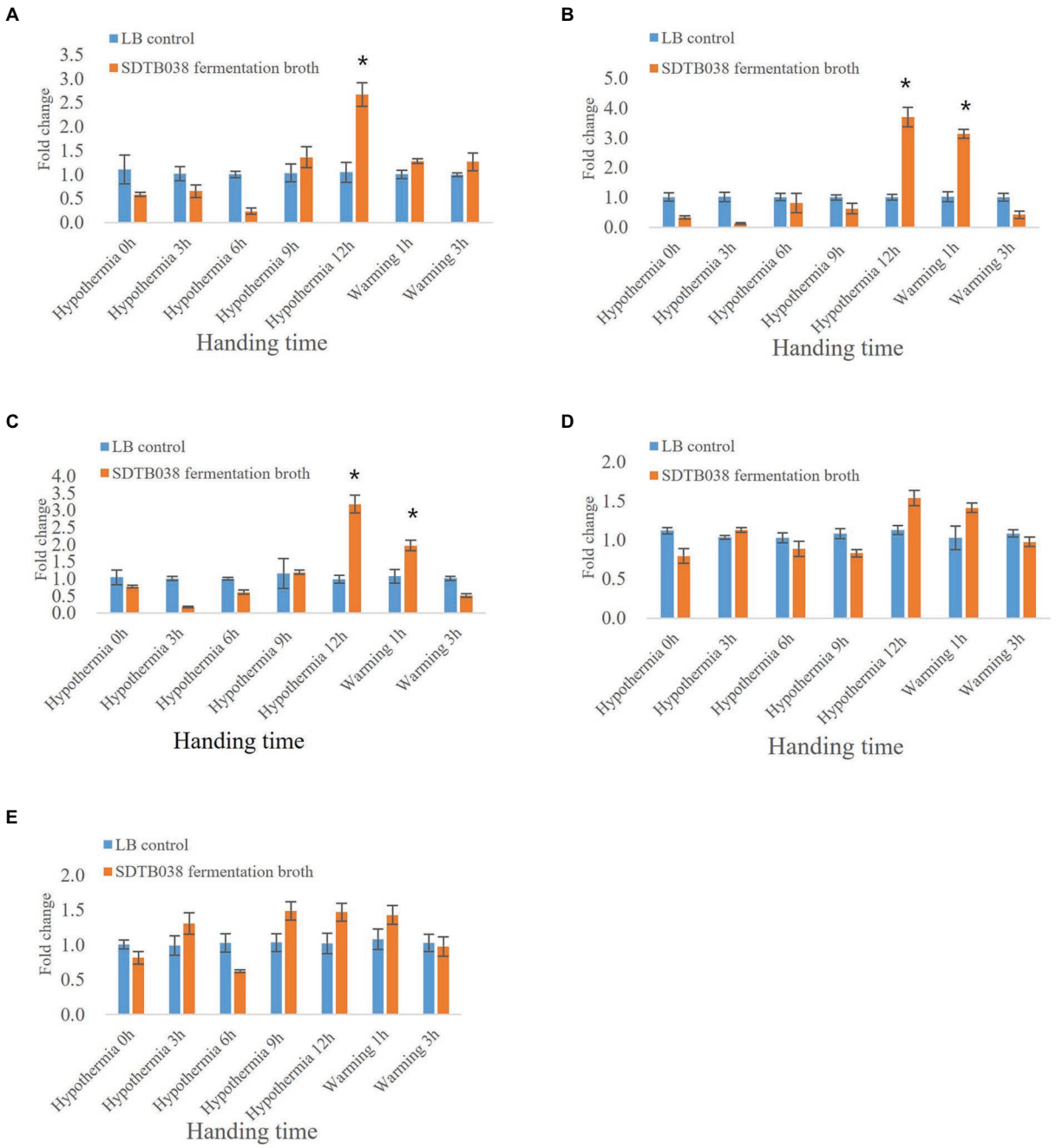

FIGURE 4
Expression of SDTB038 on antifreeze genes at low temperature. **(A)** *SlMPK3* gene expression; **(B)** *SlHSP17.7* gene expression; **(C)** *SLMYB7* gene expression; **(D)** *SlCPK8* gene expression; **(E)** *SlHY5* gene expression. Asterisks indicate significant differences between tomato plants inoculated with SDTB038 broth and those inoculated with liquid LB. The different lowercases represent significant level (p=0.05) according to the Duncan's test.

Field efficacy of SDTB038 against Fusarium crown and root rot of tomato

In the field efficacy tests, the disease indexes of the water treatment, LB treatment and microbial fertilizer treatment were 33.61, 32.78 and 27.37%, respectively. The disease index of the SDTB038 with 10^8 CFU/ml was 19.16%, which was 42.99, 41.55 and 30% lower than that of water treatment, LB control and microbial fertilizer treatment, respectively. The disease index of difenoconazole treatment was 12.22%, which was 63.64, 62.72 and 55.3% lower than that of clean water, LB control and microbial fertilizer treatment, respectively. The control effect of the difenoconazole treatment was 63.63%, significantly higher than 10^8 CFU/ml SDTB038 bacterial liquid and microbial fertilizer

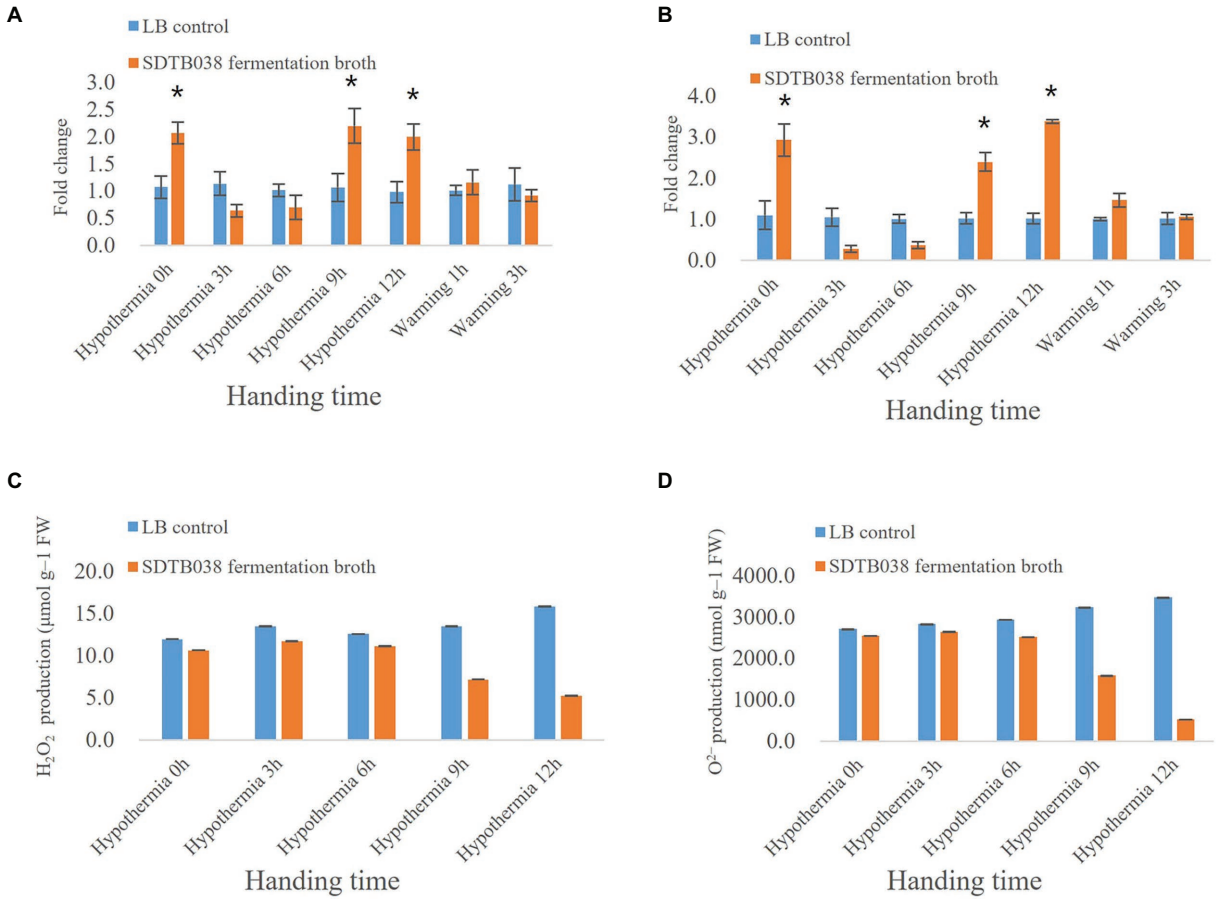

FIGURE 5
Expression of enzyme activity genes and changes of H_2O_2 and O^{2-} Content. **(A)** *CAT* expression; **(B)** *SOD* expression; **(C)** Changes of H_2O_2 Content; **(D)** Changes of O^{2-} Content. Asterisks indicate significant differences between tomato plants inoculated with SDTB038 broth and those inoculated with liquid LB. The different lowercases represent significant level (p=0.05) according to the Duncan's test.

treatment. The control effect of SDTB038 at 10^8 CFU/ml was 42.98%, which was significantly higher than that of microbial fertilizer treatments (control effect was 19.33). The above results showed that SDTB038 could better control Fusarium crown and root rot of tomato compared with microbial fertilizer containing *B. subtilis* (Table 7).

Discussion

Genome-wide sequencing analysis is of great significance to understand the mechanisms of microbial control and disease prevention. This method can locate functional genes and predict the gene clusters for secondary metabolite synthesis, which is conducive to the rapid identification of organisms with biocontrol potential and the development of engineered strains (Chun et al., 2019). These methods help reveal biocontrol mechanisms at the genome level, and lays the foundation for the in-depth study and utilization of biocontrol bacteria (Chen et al., 2007). Wang et al. (2019) proved that WRN014 and other *B. velezensis* strains had potential as growth-promoting bacteria and biopesticides through whole-gene sequencing. A *B. velezensis* YYC strain was isolated from the tomato rhizosphere by Yan Y. et al. (2021), who found that the genome size was 3,973,236 bp and consisted of 4,034 genes in total, with a mean GC content of 46.52%. In this study, the whole genome of SDTB038 was sequenced by combining second-generation and third-generation sequencing technology. The genome size was 3,929,791 bp, and its GC content was 47.26%. In addition, through software prediction, seven biosynthetic gene clusters of secondary metabolites were found, proving that *B. velezensis* can reduce or even eliminate the accumulation of ROS under low temperature stress. The strain could produce indole acetic acid and surfactin, which play a role in the prevention and treatment of diseases (Figure 7).

Fusarium crown and root rot of tomato is a soilborne disease that has spread all over the world and seriously threatens tomato quality and production (Chu et al., 2021). After decades of research abroad, a variety of resources have been identified, including microorganisms such as *B. amyloliquefaciens*, *B. cereus*, and *Rhizobium*. Debbi et al. (2018) verified that

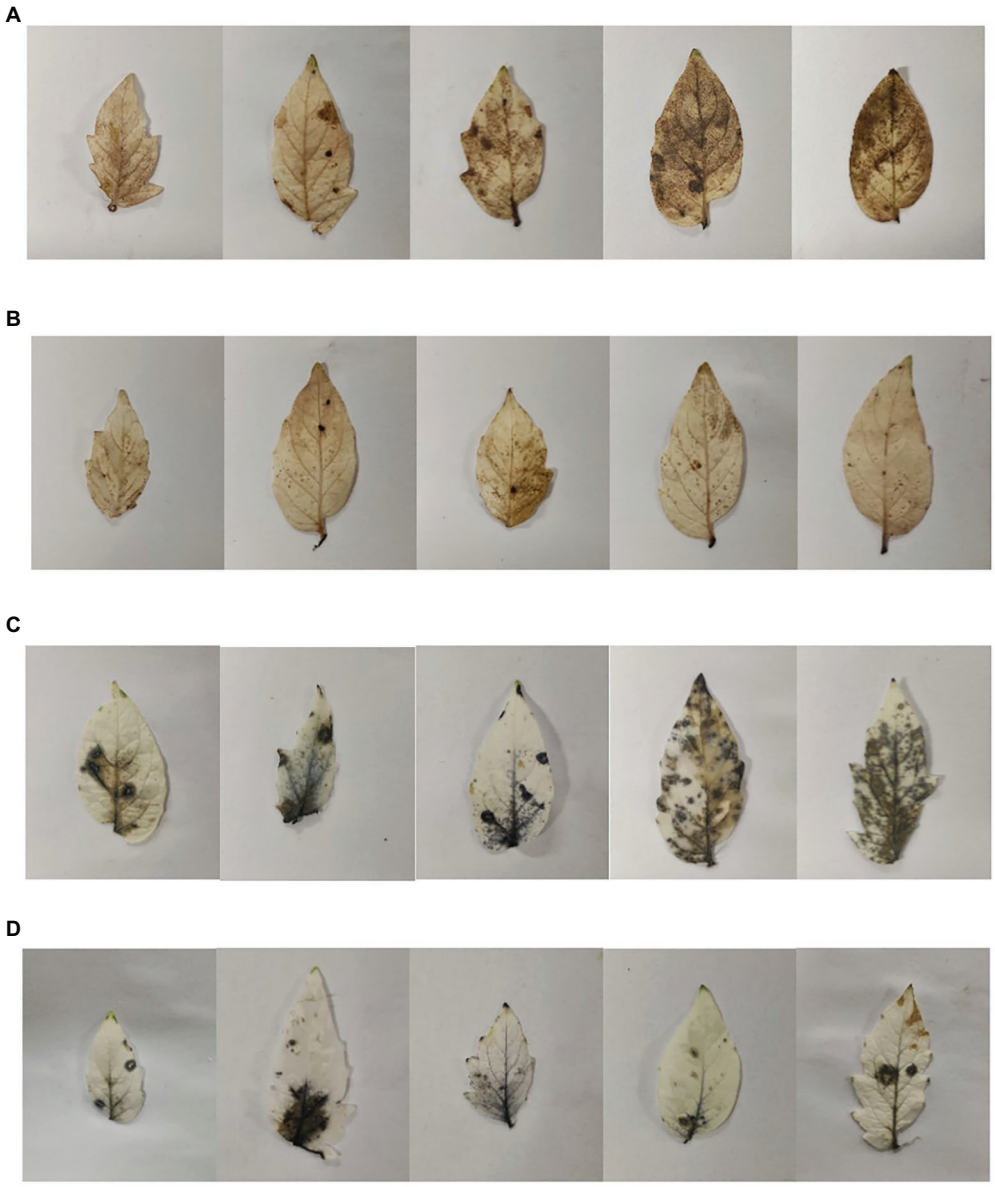

FIGURE 6
Comparison of ROS accumulation in leaves. **(A)** LB control H_2O_2 staining; **(B)** SDTB038 fermentation broth H_2O_2 staining; **(C)** LB control O^{2-} staining; **(D)** SDTB038 fermentation broth O^{2-} staining.

TABLE 7 The disease index and control effect of Fusarium crown and root rot of tomato.

Treatment	Index(%)	Control effect(%)
1	33.61 ± 1. 82	
2	32.78 ± 2.78	
3	27.37 ± 1.32	19.33 ± 4.33a
4	12.22 ± 1.82	63.63 ± 5.42b
5	19.16 ± 2.20	42.98 ± 6.56c

1. Water control; 2. LB control; 3. microbial fertilizer; 4. 75 g ha^{-1} Difenoconazole (10% water dispersible granules); 5. 10^8 CFU/ml fermentation broth. The different lowercases represent significant level ($p = 0.05$) according to the Duncan's test.

Trichoderma harzianum had different degrees of inhibition of FORL, indicating its potential as part of a biocontrol strategy against the disease. Moreover, *B. velezensis* is considered an important PGPR, could product many bioactive primary metabolic products, and inhibiting plant diseases and harmful substances (Rabbee et al., 2019). Rabbee et al. (2019) showed that *B. velezensis* played an important role in inhibiting pathogens and promoting plant growth. Our research was similar to that of Liu et al. (2020), who found that *B. velezensis* produced antimicrobial substance that showed antimicrobial activity against pathogenic fungi and bacteria. Results indicated

that different concentrations of SDTB038 fermentation broth inhibited the mycelial growth of Fusarium crown and root rot of tomato.

PGPR are beneficial bacteria that can colonize and promote plant growth, and inhibit or reduce the threat of plant diseases (Sarwar et al., 2020). Tests have indicated that plant rhizosphere bacteria can promote the dissolution of phosphorus and potassium, inhibit pathogen, improve stress resistance, and produce IAA and other plant hormones, thereby increasing crop yields (Agha et al., 2022). The study of PGPR, mainly including *Mesorhizobium* and *Allorhizobium,* intracellular PGPR, and *Bacillus*, *Pseudomonas* and *Azotobacter* extracellular PGPR (Li et al., 2020), has attracted the attention of scholars at home and abroad. To screen salt-tolerant *Bacillus* strains and growth-promoting microorganisms, Medeiros and Bettiol (2021) evaluated: the production of iron carriers and indoleacetic acid (IAA) and solubilization of phosphate. A study found that SDTB038 could produce indole acetic acid. However, SDTB038 had no phosphorus-solubilizing effect. Through greenhouse hydroponic experiments, the results showed that SDTB038 had plant growth promoting effects, we speculate that indole acetic acid may play a role in regulating plant growth.

Low temperature is one of the adverse factors affecting plant growth, resulting in loss of plant (mainly crop) economy and yield. Overall, the increase and decrease in ROS in plant cells is a dynamic equilibrium process. However, when plants receive low temperature stress, this balance will be broken, resulting in a large accumulation of ROS in plants, thereby causing damage to cells (Zhang et al., 2019). Therefore, it is very important to control the production of ROS in plants and eliminate the accumulation of ROS under low temperature (Wang et al., 2020). Heidari et al. (2021) showed that oxidative stress can be induced under low temperature, and EBR treatment may increase antioxidant enzymes and improve tomato growth by reducing the content of reactive oxygen species. Wang et al. (2020) found that endogenous melatonin could reduce the content of ROS and increase antioxidant enzymes in tomato leaves under low-temperature stress, while exogenous melatonin could not reduce the content of ROS. Han et al. (2020) showed that *SlHY5* improved the tolerance of plants to low temperature and can be used to promote the improvement of cold resistance in tomato. However, in this experiment, the tomato plants treated with SDTB038 fermentation broth failed to induce the up-regulation of *SlHY5* gene, which could not induce low temperature tolerance in these tomatoes. At the same time, our results are similar to those of Wang et al. (2017), who found that the *SIMPK3* gene can increase tomato tolerance to low temperature, and regulate plant hormone concentrations and antioxidant enzyme activity

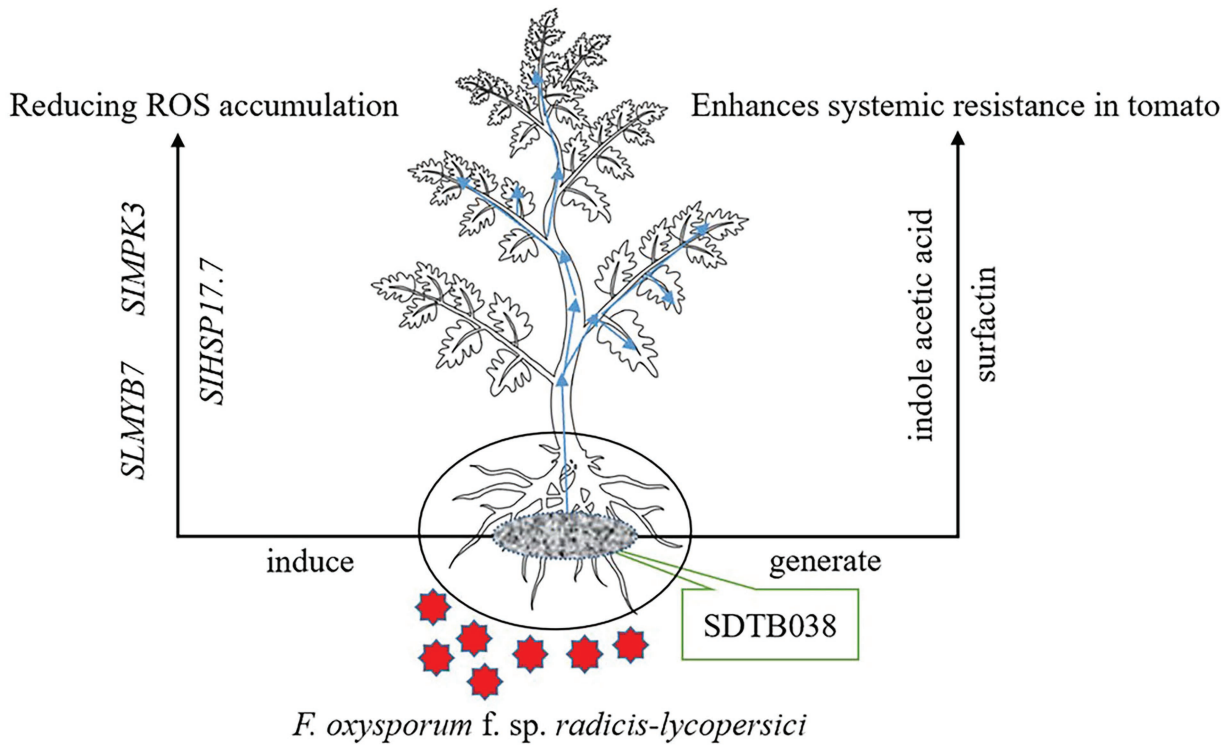

FIGURE 7
SDTB038 action mechanism diagram. Strain SDTB038 colonizes in tomato roots and can be moved to the rhizomes and leaves, which can induce the expression of antifreeze genes, produce indoleacetic acid and surfactin, and prevent and treat diseases.

to enhance the cold tolerance of tomato plants. Experimental studies have shown that SDTB038 can induce the expression of *SIHSP17.7* and *SLMYB7* genes, and regulate ROS contents in plants by regulating nonenzymatic antioxidant systems such as those involving SOD and CAT.

The colonization process of biocontrol bacteria involves biofilm formation, flagella, fimbriae, motility, chemotaxis and so on. It is closely related to light, temperature and soil microorganisms (Abdallah et al., 2020). Huang et al. (2022) systematically explored the potential adhesion substances of PGPR strains, and the adhesion process required for root colonization was clarified. This helps strengthen rhizosphere stability. In this experiment, the colonization dynamics of rifampicin-resistant marker strains in rhizosphere soil and tomato roots, stems and leaves were also studied. The results indicated that SDTB038 could colonize normally in soil and plants and grow steadily. Yan H. et al. (2021) showed that *B. velezensis* had good antibacterial activity, which could effectively control potato late blight in greenhouse and field, and promote the growth of potato plants, the field control effect was 42.43%. Zhou et al. (2021) found that the combination of *Trichoderma virens* (Tvien6) and *B. velezensis* (X5) could control tomato bacterial wilt. *B. velezensis* (X5) could promote tomato plant growth and enhance defense enzyme activity. In this study, it was found through field experiments that SDTB038 had good control effects on Fusarium crown and root rot of tomato. The control effect of 10^8 CFU/ml SDTB038 fermentation broth was the best, which was 42.98%.

Conclusion

In the present study, we investigated the ability of *B. velezensis* SDTB038 to promote tomato plant growth and prevent Fusarium crown and root rot of tomato. *B. velezensis* had antifungal activity against the Fusarium crown and root rot pathogen of tomato according to whole genome prediction. It could produce indole acetic acid, had a stable colonization state, induce the expression of antifreeze genes in tomato plants under low temperature and reduce the accumulation of ROS. Meanwhile, it was found through field experiments that SDTB038 had good control effects on Fusarium crown and root rot of tomato. The control effect of 10^8 CFU/ml SDTB038 fermentation broth was the best, which was 42.98%.

Data availability statement

The data provided in the study are stored in the National Center for Biotechnology Information (NCBI) database, with registration number SUB6310808.

Author contributions

QC and YQ performed the experiments, analyzed the data, and wrote the manuscript. YY collected pathogen isolates. KW revised the manuscript. HW designed the experiments, supervised the project, and wrote the manuscript. All authors contributed to the article and approved the submitted version.

Funding

This research was supported by the National Natural Science Foundation of China (32102259) and the Central Guidance of Local Science and Technology Development Special Foundation of Shan-dong Province (YDZX2021088).

Conflict of interest

The authors declare that the research was conducted in the absence of any commercial or financial relationships that could be construed as a potential conflict of interest.

Publisher's note

Supplementary material

The Supplementary material for this article can be found online at: https://www.frontiersin.org/articles/10.3389/fmicb.2022.994716/full#supplementary-material

References

Abdallah, D. B., Krier, F., Jacques, P., Tounsi, S., and Frikha-Gargouri, O. (2020). Agrobacterium tumefaciens C58 presence affects *bacillus velezensis* 32a ecological fitness in the tomato rhizosphere. *Environ. Sci. Pollut. R.* 27, 28429–28437. doi: 10.1007/s11356-020-09124-1

Agha, S. I., Jahan, N., Azeem, S., Parveen, S., Tabassum, B., Raheem, A., et al. (2022). Characterization of broad-spectrum biocontrol efficacy of *bacillus velezensis* against *Fusarium oxysporum* in *Triticum aestivum* L. *Not. Bot. Horti Agrobo.* 50:12590. doi: 10.15835/nbha50112590

Aly, A. A., El-Mahdy, O. M., Habeb, M. M., Elhakem, A., Asran, A. A., Youssef, M. M., et al. (2022). Pathogenicity of *bacillus* strains to cotton seedlings and their effects on Some biochemical components of the infected seedlings. *Plant Pathol. J* 38, 90–101. doi: 10.5423/PPJ.OA.11.2021.0173

Bharti, P., Jyoti, P., Kapoor, P., Sharma, V., Shanmugam, V., and Yadav, S. K. (2017). Host-induced silencing of pathogenicity genes enhances resistance to *Fusarium oxysporum* wilt in tomato. *Mol. Biotechnol.* 59, 343–352. doi: 10.1007/s12033-017-0022-y

Borisade, O., Uwaidem, Y., and Salami, A. (2017). Preliminary report on *Fusarium oxysporum* f. sp. *lycopersici* (Sensu lato) From Some tomato producing Agroecological areas in southwestern Nigeria and susceptibility of F1-resistant tomato hybrid (F1-Lindo) to infection. *Annual Res. Rev. Biol.* 18, 1–9. doi: 10.9734/arrb/2017/34626

Cao, Y., Pi, H., Chandrangsu, P., Li, Y., Wang, Y., Zhou, H., et al. (2018). Antagonism of two plant-growth promoting *bacillus velezensis* isolates Against *Ralstonia solanacearum* and *Fusarium oxysporum*. *Sci. Rep-UK.* 8:4360. doi: 10.1038/s41598-018-22782-z

Cejas, I., Vives, K., Laudat, T., Gonzalez-Olmedo, J., Engelmann, F., Martinez-Montero, M. E., et al. (2012). Effects of cryopreservation of *Phaseolus vulgaris* L. seeds on early stages of germination. *Plant Cell Rep.* 31, 2065–2073. doi: 10.1007/s00299-012-1317-x

Chen, X. H., Koumoutsi, A., Scholz, R., Eisenreich, A., Schneider, K., Heinemeyer, I., et al. (2007). Comparative analysis of the complete genome sequence of the plant growth-promoting bacterium *bacillus amyloliquefaciens* FZB42. *Nat. Biotechnol.* 25, 1007–1014. doi: 10.1038/nbt1325

Cheng, H., Zhang, D., Ren, L., Song, Z., Li, Q., Wu, J., et al. (2021). Bio-activation of soil with beneficial microbes after soil fumigation reduces soil-borne pathogens and increases tomato yield. *Environ. Pollut.* 283:117160. doi: 10.1016/j.envpol.2021.117160

Chu, D., Ilyas, N., Peng, L., Wang, X., Wang, D., Xu, Z., et al. (2021). Genomic insights on fighting bacterial wilt by a novel *bacillus amyloliquefaciens* strain Cas02. *Microb. Biotechnol.* 15, 1152–1167. doi: 10.1111/1751-7915.13925

Chun, B. H., Kim, K. H., Jeong, S. E., and Jeon, C. O. (2019). Genomic and metabolic features of the *bacillus amyloliquefaciens* group- *B. amyloliquefaciens*, *B. velezensis*, and *B. siamensis*- revealed by pan-genome analysis. *Food Microbiol.* 77, 146–157. doi: 10.1016/j.fm.2018.09.001

Debbi, A., Boureghda, H., Monte, E., and Hermosa, R. (2018). Distribution and genetic variability of *Fusarium oxysporum* associated with tomato diseases in Algeria and a biocontrol strategy with indigenous *Trichoderma* spp. *Front. Microbiol.* 9:282. doi: 10.3389/fmicb.2018.00282

Deng, Y., Liu, R., Zheng, M., Cai, C., Diao, J., and Zhou, Z. (2022). Hexaconazole application saves the loss of Grey Mold disease but hinders tomato fruit ripening in healthy plants. *J. Agric. Food Chem.* 70, 3948–3957. doi: 10.1021/acs.jafc.2c00109

Dhouib, H., Zouari, I., Ben Abdallah, D., Belbahri, L., Taktak, W., Triki, M. A., et al. (2019). Potential of a novel endophytic *bacillus velezensis* in tomato growth promotion and protection against Verticillium wilt disease. *Biol. Control* 139:104092. doi: 10.1016/j.biocontrol.2019.104092

Gao, Y., Liang, J., Xiao, R., Zang, P., Zhao, Y., and Zhang, L. (2018). Effect of four trace elements on *Paenibacillus polymyxa* Pp-7250 proliferation, activity and colonization in *ginseng*. *AMB Express* 8:164. doi: 10.1186/s13568-018-0694-0

Guo, T., Wang, X.-W., Shan, K., Sun, W., and Guo, L.-Y. (2017). The Loricrin-Like protein (LLP) of *Phytophthora infestans* is required for oospore formation and plant infection. *Front. Plant Sci.* 8:142. doi: 10.3389/fpls.2017.00142

Han, N., Fan, S., Zhang, T., Sun, H., Zhu, Y., Gong, H., et al. (2020). *SlHY5* is a necessary regulator of the cold acclimation response in tomato. *Plant Growth Regul.* 91, 1–12. doi: 10.1007/s10725-020-00583-7

Heidari, P., Entazari, M., Ebrahimi, A., Ahmadizadeh, M., Vannozzi, A., Palumbo, F., et al. (2021). Exogenous EBR ameliorates endogenous hormone contents in tomato species under low-temperature stress. *Horticulturae* 7:84. doi: 10.3390/horticulturae7040084

Huang, R., Feng, H., Xu, Z., Zhang, N., Liu, Y., Shao, J., et al. (2022). Identification of Adhesins in plant beneficial Rhizobacteria *bacillus velezensis* SQR9 and their effect on root colonization. *Mol. Plant Microbe* 35, 64–72. doi: 10.1094/MPMI-09-21-0234-R

Jangir, M., Pathak, R., Sharma, S., and Sharma, S. (2018). Biocontrol mechanisms of *bacillus* sp., isolated from tomato rhizosphere, against *Fusarium oxysporum* f. sp. *lycopersici*. *Biol. Control* 123, 60–70. doi: 10.1016/j.biocontrol.2018.04.018

Joly, P., Calteau, A., Wauquier, A., Dumas, R., Beuvin, M., Vallenet, D., et al. (2021). From strain characterization to field authorization: highlights on *bacillus velezensis* strain B25 beneficial properties for plants and its activities on Phytopathogenic fungi. *Microorganisms* 9:1924. doi: 10.3390/microorganisms9091924

Khaskheli, M. A., Wu, L., Chen, G., Chen, L., Hussain, S., Song, D., et al. (2020). Isolation and characterization of root-associated bacterial Endophytes and their biocontrol potential against major fungal Phytopathogens of Rice (*Oryza sativa* L.). *Pathogens* 9:172. doi: 10.3390/pathogens9030172

Li, H., Qiu, Y., Yao, T., Ma, Y., Zhang, H., and Yang, X. (2020). Effects of PGPR microbial inoculants on the growth and soil properties of *Avena sativa*, *Medicago sativa*, and *Cucumis sativus* seedlings. *Soil Tillage Res.* 199:104577. doi: 10.1016/j.still.2020.104577

Liu, S., Li, H., Lv, X., Ahammed, G. J., Xia, X., Zhou, J., et al. (2016). Grafting cucumber onto luffa improves drought tolerance by increasing ABA biosynthesis and sensitivity. *Sci. Rep.* 6:20212. doi: 10.1038/srep20212

Liu, Y., Teng, K., Wang, T., Dong, E., Zhang, M., Tao, Y., et al. (2020). Antimicrobial *bacillus velezensis* HC6: production of three kinds of lipopeptides and biocontrol potential in maize. *J. Appl. Microbiol.* 128, 242–254. doi: 10.1111/jam.14459

Luo, L., Wang, P., Zhai, Z., Su, P., Tan, X., Zhang, D., et al. (2019). The effects of *Rhodopseudomonas palustris* PSB06 and CGA009 with different agricultural applications on rice growth and rhizosphere bacterial communities. *AMB Express* 9, 173. doi: 10.1186/s13568-019-0897-z

Ma, Q., Cong, Y., Feng, L., Liu, C., Yang, W., Xin, Y., et al. (2022). Effects of mixed culture fermentation of *bacillus amyloliquefaciens* and *Trichoderma longibrachiatum* on its constituent strains and the biocontrol of tomato Fusarium wilt. *J. Appl. Microbiol.* 132, 532–546. doi: 10.1111/jam.15208

Ma, S., and Wehner, T. C. (2015). Flowering stage resistance to bacterial fruit blotch in the watermelon Germplasm collection. *Crop Sci.* 55, 727–736. doi: 10.2135/cropsci2014.01.0071

Medeiros, C. A. A., and Bettiol, W. (2021). Multifaceted intervention of *bacillus* spp. against salinity stress and Fusarium wilt in tomato. *J. Appl. Microbiol.* 131, 2387–2401. doi: 10.1111/jam.15095

Mousa, M. A. A., Abo-Elyousr, K. A. M., Abdel Alal, A. M. K., and Alshareef, N. O. (2021). Management Fusarium wilt disease in tomato by combinations of *bacillus amyloliquefaciens* and peppermint oil. *Agronomy* 11:2536. doi: 10.3390/agronomy11122536

Nekoval, S., Zakharchenko, A., Sadovaya, A., Churikova, A., and Fedoryanskaya, I. (2022). Assessment of mutant tomato lines as a starting material for breeding varieties resistant to *Alternaria alternata*. *Saudi J. Biol. Sci.* 29, 1061–1072. doi: 10.1016/j.sjbs.2021.09.066

Obunukwu, G. M., Dike, K. S., and Nwakwasi, G. E. (2018). Isolation and identification of microbial Deteriogens of fresh tomatoes stored at ambient temperature. *Microbio. Res. J. Intern.* 26, 1–8. doi: 10.9734/mrji/2018/45193

Rabbee, M. F., Ali, M. S., Choi, J., Hwang, B. S., Jeong, S. C., and Baek, K. H. (2019). *Bacillus velezensis*: A valuable member of bioactive molecules within plant microbiomes. *Molecules* 24:46. doi: 10.3390/molecules24061046

Rathore, M. S., Mastan, S. G., Yadav, P., Bhatt, V. D., Shekhawat, N. S., and Chikara, J. (2016). Shoot regeneration from leaf explants of *Withania coagulans* (stocks) Dunal and genetic stability evaluation of regenerates with RAPD and ISSR markers. *S. Afr. J. Bot.* 102, 12–17. doi: 10.1016/j.sajb.2015.08.003

Rekah, Y., Shtienberg, D., and Katan, J. (2000). Disease development following infection of tomato and basil foliage by airborne conidia of the soilborne pathogens *Fusarium oxysporum* f. sp. *radicis-lycopersici* and *F. oxysporum* f. sp. *basilici*. *Phytopathology* 90, 1322–1329. doi: 10.1094/phyto.2000.90.12.1322

Riaz, R., Khan, A., Khan, W. J., Jabeen, Z., Yasmin, H., Naz, R., et al. (2021). Vegetable associated *bacillus* spp. suppress the pea (Pisum sativum L.) root rot caused by Fusarium solani. *Biol. Control* 158:104610. doi: 10.1016/j.biocontrol.2021.104610

Sarwar, S., Khaliq, A., Yousra, M., Sultan, T., Ahmad, N., Khan, M. Z., et al. (2020). Screening of siderophore-producing PGPRs isolated from groundnut (arachis hypogaea L.) rhizosphere and their influence on iron release in soil. *Commun. Soil Sci. Plan.* 51, 1680–1692. doi: 10.1080/00103624.2020.1791159

Schreiter, S., Babin, D., Smalla, K., and Grosch, R. (2018). Rhizosphere competence and biocontrol effect of *pseudomonas* sp. RU47 independent from plant species and soil type at the field scale. *Front. Microbiol.* 9:97. doi: 10.3389/fmicb.2018.00097

Singh, V. K., Khan, A. W., Jaganathan, D., Thudi, M., Roorkiwal, M., Takagi, H., et al. (2016). QTL-seq for rapid identification of candidate genes for 100-seed weight and root/total plant dry weight ratio under rainfed conditions in chickpea. *Plant Biotechnol. J.* 14, 2110–2119. doi: 10.1111/pbi.12567

Soergel, D. A., Dey, N., Knight, R., and Brenner, S. E. (2012). Selection of primers for optimal taxonomic classification of environmental 16S rRNA gene sequences. *ISME J.* 6, 1440–1444. doi: 10.1038/ismej.2011.208

Souri, M. K., and Tohidloo, G. (2019). Effectiveness of different methods of salicylic acid application on growth characteristics of tomato seedlings under salinity. *Chem. Biol. Technol. Ag.* 6:26. doi: 10.1186/s40538-019-0169-9

Stoll, A., Salvatierra-Martinez, R., Gonzalez, M., and Araya, M. (2021). The role of Surfactin production by *bacillus velezensis* on colonization, biofilm formation on tomato root and leaf surfaces and subsequent protection (ISR) against *Botrytis cinerea*. *Microorganisms* 9:2251. doi: 10.3390/microorganisms9112251

Vignesh, M., Shankar, S. R. M., Mubarak Ali, D., and Hari, B. N. V. (2022). A novel Rhizospheric bacterium: *bacillus velezensis* NKMV-3 as a biocontrol agent Against *Alternaria* leaf blight in tomato. *Appl. Biochem. Biotechnol.* 194, 1–17. doi: 10.1007/s12010-021-03684-9

Villarino, M., De Cal, A., Melgarejo, P., and Larena, I. (2021). Development of a multiplex PCR for the identification of *Fusarium solani* and *F. oxysporum* in a single step. *J. Plant Dis. Protect.* 128, 1275–1290. doi: 10.1007/s41348-021-00475-6

Wang, B., Gao, Z., Shi, Q., and Gong, B. (2022). *SAMS1* stimulates tomato root growth and P availability via activating polyamines and ethylene synergetic signaling

under low-P condition. *Environ. Exp. Bot.* 197:104844. doi: 10.1016/j.envexpbot.2022.104844

Wang, J., Xing, J., Lu, J., Sun, Y., Zhao, J., Miao, S., et al. (2019). Complete genome sequencing of *bacillus velezensis* WRN014, and comparison with genome sequences of other *bacillus velezensis* strains. *J. Microbiol. Biotechnol.* 29, 794–808. doi: 10.4014/jmb.1901.01040

Wang, M., Zhang, S., and Ding, F. (2020). Melatonin mitigates chilling-induced oxidative stress and photosynthesis inhibition in tomato plants. *Antioxidants-Basel* 9:218. doi: 10.3390/antiox9030218

Wang, L., Zhao, R., Zheng, Y., Chen, L., Li, R., Ma, J., et al. (2017). *SlMAPK1/2/3* and antioxidant enzymes are associated with H_2O_2-induced chilling tolerance in tomato plants. *J. Agric. Food Chem.* 65, 6812–6820. doi: 10.1021/acs.jafc.7b01685

Yan, H., Qiu, Y., Yang, S., Wang, Y., Wang, K., Jiang, L., et al. (2021). Antagonistic activity of *bacillus velezensis* SDTB038 against *Phytophthora infestans* in potato. *Plant Dis.* 105, 1738–1747. doi: 10.1094/PDIS-08-20-1666-RE

Yan, Y., Xu, W., Chen, W., Hu, Y., and Wang, Z. (2021). Complete genome sequence of *bacillus velezensis* YYC, a bacterium isolated from the tomato rhizosphere. *Arch. Microbiol.* 204:44. doi: 10.1007/s00203-021-02709-5

Zhang, Z., Cao, B., Gao, S., and Xu, K. (2019). Grafting improves tomato drought tolerance through enhancing photosynthetic capacity and reducing ROS accumulation. *Protoplasma* 256, 1013–1024. doi: 10.1007/s00709-019-01357-3

Zhang, J., Chen, J., Hu, L., Jia, R., Ma, Q., Tang, J., et al. (2021). Antagonistic action of Streptomyces pratensis S10 on *Fusarium graminearum* and its complete genome sequence. *Environ. Microbiol.* 23, 1925–1940. doi: 10.1111/1462-2920.15282

Zhou, Y., Yang, L., Wang, J., Guo, L., and Huang, J. (2021). Synergistic effect between Trichoderma virens and *bacillus velezensis* on the control of tomato bacterial wilt disease. *Horticulturae* 7:439. doi: 10.3390/horticulturae7110439

frontiers | Frontiers in Microbiology

TYPE Original Research
PUBLISHED 08 September 2022
DOI 10.3389/fmicb.2022.972928

OPEN ACCESS

EDITED BY
Qunqing Wang,
Shandong Agricultural University,
China

REVIEWED BY
Ramesh Raju Vetukuri,
Swedish University of Agricultural Sciences,
Sweden
Weilin Cao,
Shandong Agricultural University,
China
Junliang Yin,
Yangtze University,
China

*CORRESPONDENCE
Li-Na Yang
yikeshu1114@126.com
Jiasui Zhan
Jiasui.zhan@slu.se

SPECIALTY SECTION
This article was submitted to Microbe and Virus Interactions With Plants, a section of the journal Frontiers in Microbiology

RECEIVED 19 June 2022
ACCEPTED 10 August 2022
PUBLISHED 08 September 2022

CITATION
Yang L-N, Ouyang H, Nkurikiyimfura O, Fang H, Waheed A, Li W, Wang Y-P and Zhan J (2022) Genetic variation along an altitudinal gradient in the *Phytophthora infestans* effector gene *Pi02860*. *Front. Microbiol.* 13:972928. doi: 10.3389/fmicb.2022.972928

Genetic variation along an altitudinal gradient in the *Phytophthora infestans* effector gene *Pi02860*

Li-Na Yang[1]*, Haibing Ouyang[2], Oswald Nkurikiyimfura[3], Hanmei Fang[3], Abdul Waheed[3], Wenyang Li[3], Yan-Ping Wang[4] and Jiasui Zhan[5]*

[1]Fujian Key Laboratory on Conservation and Sustainable Utilization of Marine Biodiversity, Fuzhou Institute of Oceanography, Minjiang University, Fuzhou, China, [2]Department of Plant Pathology, Nanjing Agricultural University, Nanjing, China, [3]Institute of Plant Pathology, Fujian Agriculture and Forestry University, Fuzhou, China, [4]College of Chemistry and Life Sciences, Sichuan Provincial Key Laboratory for Development and Utilization of Characteristic Horticultural Biological Resources, Chengdu Normal University, Chengdu, China, [5]Department of Forest Mycology and Plant Pathology, Swedish University of Agricultural Sciences, Uppsala, Sweden

Effector genes, together with climatic and other environmental factors, play multifaceted roles in the development of plant diseases. Understanding the role of environmental factors, particularly climate conditions affecting the evolution of effector genes, is important for predicting the long-term value of the genes in controlling agricultural diseases. Here, we collected *Phytophthora infestans* populations from five locations along a mountainous hill in China and sequenced the effector gene *Pi02860* from >300 isolates. To minimize the influence of other ecological factors, isolates were sampled from the same potato cultivar on the same day. We also expressed the gene to visualise its cellular location, assayed its pathogenicity and evaluated its response to experimental temperatures. We found that *Pi02860* exhibited moderate genetic variation at the nucleotide level which was mainly generated by point mutation. The mutations did not change the cellular location of the effector gene but significantly modified the fitness of *P. infestans*. Genetic variation and pathogenicity of the effector gene were positively associated with the altitude of sample sites, possibly due to increased mutation rate induced by the vertical distribution of environmental factors such as UV radiation and temperature. We further found that *Pi02860* expression was regulated by experimental temperature with reduced expression as experimental temperature increased. Together, these results indicate that UV radiation and temperature are important environmental factors regulating the evolution of effector genes and provide us with considerable insight as to their future sustainable action under climate and other environmental change.

KEYWORDS

adaptation, agriculture, population genetics, plant pathogen, virulence factor, climate change, natural selection, molecular evolution

Introduction

Plant diseases have deleterious effects on ecological integrity and agricultural productivity, greatly threatening natural sustainability and global food security. For example, damage caused by plant diseases such as chestnut blight and Dutch elm disease to primary and secondary forests not only reduces species richness and the associated ecological services (Martín et al., 2013) but has also restructured ecological landscapes in North America and Europe (Raum, 2020). From a social-economic perspective, 13–20% of global agricultural harvest (Burdon et al., 2020) corresponding to ~US$220 billion is lost due to plant disease epidemics annually. Moreover, it is of great concern that the ecological and societal impact of plant diseases may be further aggravated by global climate change (Cavicchioli et al., 2019).

Effector proteins, either directly secreted into the apoplast or translocated into host cells, play critical roles in the antagonistic interaction between hosts and pathogens (Lo Presti et al., 2015; Wang et al., 2017). They are mainly involved in the regulation of the host's immunity system but also take part in nutrient uptake of pathogens from hosts (Uhse and Djamei, 2018). To broaden their host range and increase their successful colonization and reproduction, both expression level and profile of pathogen effector genes are strictly regulated during antagonistic interactions, and show waves of concerted expression at diverse stages of infection and reproduction according to the surrounding environment and genetic background of hosts (Wang et al., 2011; Soyer et al., 2014; Ren et al., 2020). For example, some effector genes are upregulated to promote host susceptibility (Boevink et al., 2016) and subdue the host immune system (Turnbull et al., 2017), while others are down regulated to avoid host recognition (Lo Presti et al., 2015).

It has been found that plant pathogens encode a large number of effectors in order to ensure successful colonization and reproduction by suppressing host defence immunity (Franceschetti et al., 2017). The specialized location of many effector genes in the gene-sparse, repeat-rich regions of the genome provide them with unique niches for quick evolution (Haas et al., 2009; Raffaele and Kamoun, 2012; Dong et al., 2015) and hence the ability to defeat host defence immunity involved in gene-for-gene interactions (Fry, 2008; Vleeshouwers et al., 2011). The arm race between host resistance genes and pathogen effector genes is particularly intense in agricultural ecosystems due to the strong directional selection generated by farming practices associated with crop intensification and genetic homogenization (Zhan et al., 2014, 2015). It is widely documented that pathogens in agricultural ecosystems are equipped with an array of mutation mechanisms to drive their escape from host immunity. For example, *Phytophthora infestans Avr1* and *Avr4* were removed from the effector repertoire by pseudogenization to escape the corresponding R1 and R4 detection in host (van Poppel et al., 2008; Shen et al., 2021; Waheed et al., 2021). *Phytophthora infestans Avr2* escapes host immunity by protein disordering through which shifts the effector from an avirulent type to virulent type (Yang et al., 2020). On the other hand, *P. infestans Avr3a* overcomes R3a recognition by potato crop through point mutations in two residues ($K^{80}I^{103}$ to $E^{80}M^{103}$) where protein (effector)-protein (receptor) interactions take place (Boutemy et al., 2011; Yaeno et al., 2011).

As an important part of the disease triangle, climatic conditions can regulate the growth and development of pathogens and hosts as well as their interactions (Juroszek et al., 2020). In addition to host resistance and the biology of pathogens, recent studies have shown that the evolution and performance of effector genes are also affected by climate conditions. For example, the effector function of *P. syringae AvrRpt2* to *Arabidopsis RPS2* resistance disappeared when plants were grown for 3 weeks under 28°C (Wang et al., 2009). The strong association of annual mean temperature in the collection sites with nucleotide diversity and/or population differentiation of *Avr1* (Shen et al., 2021), *Avr2* (Yang et al., 2020), *Avr3a* (Yang et al., 2018) and *Avr4* (Waheed et al., 2021) in *P. infestans* further supports that local air temperature could influence the evolution of effector genes.

Our knowledge about the evolution of effector genes is fragmented. Most research on this part of genome has focused on molecular characterization and functional analysis. Population genetic analysis of the spatial distribution of effector genes to understand their evolutionary history, mechanisms and future trajectory is limited. Climate changes in the planet have accelerated in the past decades due to the human activities including agricultural production. It is predicted that average air temperature would increase ~5°C by the end of the century (Tollefson, 2020). UV radiation, another important determinant of disease epidemics and pathogen evolution, is also expected to increase associated with the current wave of climate change due to the thinning ozone layer associated with emission of some industrial gases (Bais et al., 2015). Knowledge of how and to what extent these climate and climate related factors may impact the evolution and performance of effector genes is important to understand future ecological and agricultural sustainability under changing climates.

In this manuscript, we used a population genetic approach to study the evolution of *Pi02860*, one of confirmed effector gene in the interaction of *P. infestans* with potato host (Yang et al., 2016b) and how ecological factors may influence its evolution. *P. infestans* is one of the most widespread oomycete plant pathogens causing late blight disease of potato and tomato. Genome analysis revealed that *P. infestans* codes many effectors that are delivered into plant cells during infection where they interfere with host immunity (Haas et al., 2009). *Pi02860* is one of the effectors that are specifically upregulated at ~2 days after infecting potato plants (Yang et al., 2016b). It is found that this effector significantly suppressed the cell death triggered by pathogen-associated molecular pattern INF1 and strongly enhanced the colonization ability of *P. infestans* (Yang et al., 2016b). It interacted with the host susceptibility protein NRL1 and enhanced the assembly of NRL1 with SWAP70, a positive

regulator of immunity, to promote proteasome-mediated degradation of the latter and, thus, suppress immunity (Yang et al., 2016b; He et al., 2018).

The specific objectives of the study were to answer four questions: (i) what is the genetic variation of *Pi02860*? (ii) How is the genetic diversity generated? (iii) What are the pathogenicity and cellular consequences of the observed mutations? and (iv) how may climatic or climate-related factors such as UV radiation and air temperature affect the performance and spatial distribution of genetic variation in the effector gene? Altitude change provides a strong reflection of climatic gradients across short spatial distances, offering a great opportunity to study the influence of climate conditions particularly UV light and temperature on the biology and ecology of species (Körner, 2007). For example, UV intensity increases 10–20% and temperature decreases ~6.5°C for every 1,000 m elevation. To achieve our objectives, we sampled >300 isolates from five altitudinal sites along a mountainous hill and sequenced the effector gene *Pi02860*. Genetic variation, mechanisms responsible for the generation of this variation, cellular localization, altitudinal distribution and expression of the effector gene under different experimental temperatures were analysed. A total of 21 nucleotide haplotypes mainly generated by point mutations were found in the collections. The spatial distribution of the effector gene was associated with the altitude of collection sites and the expression of the effector was strongly regulated by experimental temperatures.

Materials and methods

Phytophthora infestans collections

Phytophthora infestans isolates were collected in a single day during the 2016 late blight epidemic season from a single potato cultivar (Hui-2) grown in five fields along along a mountainous hill located at Huize, Yunnan. The altitudes of the five fields ranged from 1,976 to 2,677 m and were designated as A–E from lower to higher altitude, respectively (Table 1). One hundred *P. infestans* infected plants each at least 1-m apart were selected from each field and one infected leaf was sampled from the upper canopy of each plant. The sampled leaves were transferred to the laboratory within 24 h for *P. infestans* isolation. A single isolate was secured from each sample, resulting in a collection of a total of 354 isolates with 59–87 isolates originating from each of the five fields. The isolates were purified three times by sequential transfers of a single sporangium to a fresh rye B plate supplemented with ampicillin (100 μg/ml) and rifampicin (50 μg/ml). Detailed information on the sample collection and *P. infestans* isolation can be found in our previous publications (Zhu et al., 2015; Yang et al., 2016a).

TABLE 1 Sample size, and genetic variation of *Phytophthora infestans Pi02860* sequences collected from five altitudinal locations.

Population	Size	Altitude (m)	S	H	PH	HD	Π
A	65	1,976	3	5	1	0.5817	0.00165
B	86	2,124	4	5	1	0.5499	0.00165
C	59	2,471	7	6	3	0.6791	0.00232
D	77	2,591	23	10	6	0.6702	0.00228
E	67	2,677	8	10	6	0.6739	0.00274
Total	354		35	21	17	0.6240	0.00231

S, number of segregating sites; H, number of haplotypes; PH, number of private haplotypes, i.e., which only present in one population; HD, haplotype diversity; π, nucleotide diversity.

Pi02860 sequencing

Phytophthora infestans isolates were cultured on rye B agar at 18°C in the dark. Mycelia (~100 mg) were harvested after 15 days cultivation, transferred into sterile, 2 ml centrifuge tubes and lyophilized with a vacuum freeze dryer (Alpha1-2, Christ, Germany). The lyophilized mycelia were ground to powder with a mixer mill (MM400, Retsch, Germany). Total DNA was extracted using a Plant gDNA Miniprep Kit (GD 2611, Biomiga, China) according to the manufacturer's instructions. The genomic DNA was suspended in 50 μl of ultrapure water and stored at −20°C until use.

A pair of *Pi02860* specific primers (For: 5′-ACTCACCGT CACCCTCATTC-3′ and Rev: 5′-AACTTTGACTCCGACCG TTG-3′) were designed according to the conserved upstream and downstream of the reference sequence (PITG_02860) downloaded from NCBI and used to amplify the *Pi02860* effector gene. PCR reactions were carried out in a 25 μl reaction volume using a thermal cycler (Applied Biosystems 2720). The reaction cocktail contained 1 × PCR buffer, 0.2 mM dNTPs, 1 unit of TransStart KD Plus DNA Polymerase, 0.2 μM of primers and 20 ng of template DNA. PCR amplification was started with an initial denaturation step of 94°C for 2 min, followed by 30 cycles of amplification at 95°C for 30 s, annealing at 55°C for 30 s, extension at 72°C for 50 s, and ended with a further extension cycle at 72°C for 10 min. The PCR products were separated by 1% agarose gel electrophoresis and sent to Sangon Biotech company for sequencing using an ABI3730 automated DNA sequencer (Applied Bio-Systems, United States).

Plant preparation

Nicotiana benthamiana and a universal susceptible potato variety Desiree were grown in a greenhouse at 20°C in 60% humidity. The greenhouse was supplemented with 16 h-light at the intensity of 120–150 μmol m^{-2} s^{-1}, nutrient and water were supplied at necessary. *Nicotiana benthamiana* plants were used for agroinfiltration at 4–5 weeks old and potato leaves at 5–6 weeks old were used for *P. infestans* infection analysis.

Vector construction

After removing those with mutations in the start codon or translating to the same isoforms, 16 *Pi02860* haplotypes without a signal peptide were amplified from genomic DNAs of corresponding *P. infestans* isolates. PCR products were ligated into pEarlyGate 104 (N-terminal GFP tag) using a Vazyme ClonExpressII One Step Cloning Kit, and then transformed into *Agrobacterium tumefaciens* strain AGL1. The Avr3a and INF1 constructs with N-terminal GFP tag were kindly provided by Dr. Qin He from Huazhong Agricultural University, Wuhan, China.

Agroinfiltration, infection assays, HR suppression and cellular localization

Agrobacterium tumefaciens strain AGL1 transformed with the vector constructed above was grown overnight in LB medium containing selective antibiotics at 28°C, pelleted, resuspended in infiltration buffer (10 mM MES, 10 mM $MgCl_2$), and adjusted to the required optical density measured at 600 nm (OD_{600}) before being infiltrated into *N. benthamiana* leaves (generally 0.005–0.01 for cellular localization purposes, 0.25 for infection assays, and 0.5 for hypersensitive reaction assays). For co-expression, agrobacterial cultures carrying the appropriate vector constructs were mixed prior to infiltration.

Phytophthora infestans strain 88,069 (Yang et al., 2021) was used for plant infection. It was cultured on rye agar at 18°C for 2 weeks before sporangia collection. The inoculum concentration was adjusted to 40,000 sporangia per ml, and 10 µl droplets were inoculated onto the abaxial side of leaves of intact *N. benthamiana* plants which were transiently expressed with *Pi02860* haplotypes in sealed boxes. The average lesion diameter was pictured at 6–8 days after inoculation (DAIs).

Cellular localization of *Pi02860* effectors was investigated on *N. benthamiana* plants by confocal imaging. In this analysis, *N. benthamiana* cells were imaged at 2 DAIs using a Nikon Ti-E inverted microscope with Plan Apo 40X/0.95 dry objective. GFP was excited by 488-nm light shed from an argon laser, and 500–530 nm emissions were captured. To minimize potential artifacts of ectopic protein expression, only single optical images from leaf cells expressing low levels of the protein fusions were collected and analysed.

Analyses of thermal-mediated *Pi02860* expression

Fifteen *P. infestans* isolates with different *Pi02860* haplotypes were inoculated onto the detached leaves of the universal susceptible potato cultivar at low (10°C), near optimum (18°C) (near optimum) and high (25°C) temperature of the pathogen infection (Yang et al., 2016a). Three 6-mm leaf disks were excised from the inoculation sites 2 DAIs. RNA was extracted from the leaf disks using the *EasyPure* plant RNA Kits (TransGen Biotech) according to the manufacturer's instructions. RNA was quantified using a Nanodrop 1000 (Thermo Scientific) and cDNA was synthesized using TransScript One-Step gDNA Removal and cDNA Synthesis SuperMix (TransGen Biotech) according to the manufacturer's instructions. QRT-PCR was performed using TransStart Top Green qPCR SuperMix (TransGen Biotech) and run on a QuantStudio 5 Real-Time PCR Instrument (Applied Biosystems) using QuantStudio Design & Analysis software v1.4.2 with specific primers (For: GTGTCGCCTGGTCTAATCC, Rev: TTCTCTCTTCATTGGCTTCG). The expression of the effector gene was analyzed using the ΔΔCt method (McLellan et al., 2013) normalized with the housekeeping gene ActinA.

Data analyses

Before analysis, all *Pi02860* nucleotide sequences were visually assessed to remove potential artifacts (Yang et al., 2013). *Pi02860* isoforms were deduced from nucleotide sequences and multiple sequence alignments were performed by the ClustalW implemented in MEGA 7.0.21 (Kumar et al., 2016). Nucleotide haplotypes were reconstructed with the PHASRE algorithm implemented in DnaSP 5.10 (Librado and Rozas, 2009). The DnaSP 5.10 program was also used to estimate haplotype diversity, nucleotide diversity, the rates of non-synonymous substitutions and synonymous substitutions. Haplotype and nucleotide diversities were estimated for each of the five populations (elevations) as well as the combined population by pooling the sequences for individual populations. A median joining (MJ) network illustrating genealogical relationships among haplotypes was generated using PopART 1.7 (Leigh and Bryant, 2015). The population scaled recombination rates were assessed by INTERVAL program implemented in LDHAT package at the interface of RDP4 (McVean et al., 2002, 2004). The mean lesion size (INF1 cell death suppression) in each population was calculated with the formula as follows:

$$Y = \sum(w_i p_i)$$

where w_i and p_i represent the frequency and the observed lesion size (INF1 cell death suppression) of haplotype *i* and Y is the mean lesion size (INF1 cell death suppression) in the population. Associations of sequence diversity with biological characteristics of the effector gene and altitude were evaluated by Pearson's correlation (Lawrence and Lin, 1989). Duncan's multiple range and LSD tests (Ott and Longnecker, 2015) were applied to determine the differences in lesion size, INF1 induced cell death and gene expression using the SAS software. A Chi-square test for haplotype homogeneity among different altitudes was conducted by SPSS 19.0.

10.3389/fmicb.2022.972928

Results

Sequence variation in *Pi02860* effector gene

A total of 35 variable sites were detected in the 354 full nucleotide sequences, representing 3–23 sites from each of the five populations (Table 1). These variable sites formed 21 nucleotide haplotypes. Nearly all sequence variations were generated by point mutations (Supplementary Table 1). Besides that, an early termination stop codon was generated by point mutation at the 107th nucleotide in Hap_8, causing truncation within the RXLR motif (Figure 1; Supplementary Table 1). Pseudo genes generated by deletions in the start codon were found in two isolates (Supplementary Table 1).

Altitudinal distribution of *Pi02860* gene

Among the 21 nucleotide haplotypes, Hap_1 to Hap_4 were major haplotypes with a frequency ranging from 0.00 to 62.79% in individual populations (Supplementary Table 2) and ranging from 2.26 to 54.24% in the combined population. Hap_1, Hap_2, and Hap_3 were observed in all five populations while Hap_4, was observed in four of the five populations (Figure 2). Other haplotypes were detected only once and were private to each population (Table 1; Figure 2). The pathogen populations from different altitudes varied significantly in the frequency of both nucleotide haplotypes (Supplementary Table 2) and isoforms (Supplementary Table 3) by the homogeneity test, with a value of p of 0.009 and 0.044, respectively. The haplotype diversity of nucleotide sequences in the five populations ranged from 0.5499 to 0.6791 with a mean of 0.6240 when sequences from the five sites were combined. Nucleotide diversity in the populations ranged from 0.00165 to 0.00274 with a grand mean of 0.00231 (Table 1). Populations collected from the lowest altitudes (A and B) had the least number of haplotypes and lowest haplotype nucleotide diversity while population E from the highest altitude displayed the greatest number of haplotypes and highest nucleotide diversity (Table 1).

Haplotype network

Hap_4 was identical to T30-4, the reference sequence. Hap_1, Hap_2 and Hap_3 had one SNP in 30^{T-C} or 143^{G-A} compared to the

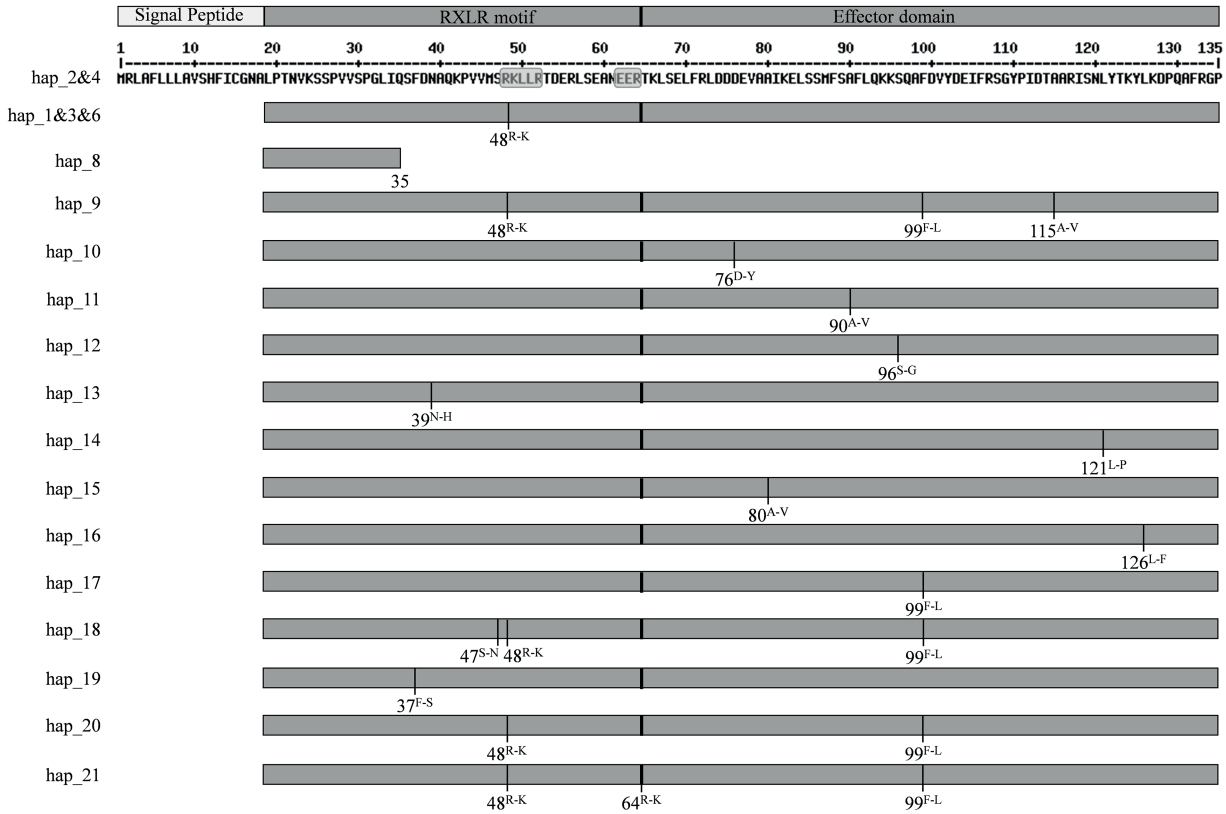

FIGURE 1
Sketch showing the *Pi02860* structural domain and the mutation position in each of nucleotide haplotypes. Hap_5 and Hap_7 were removed due to a mutation in start codon.

10.3389/fmicb.2022.972928

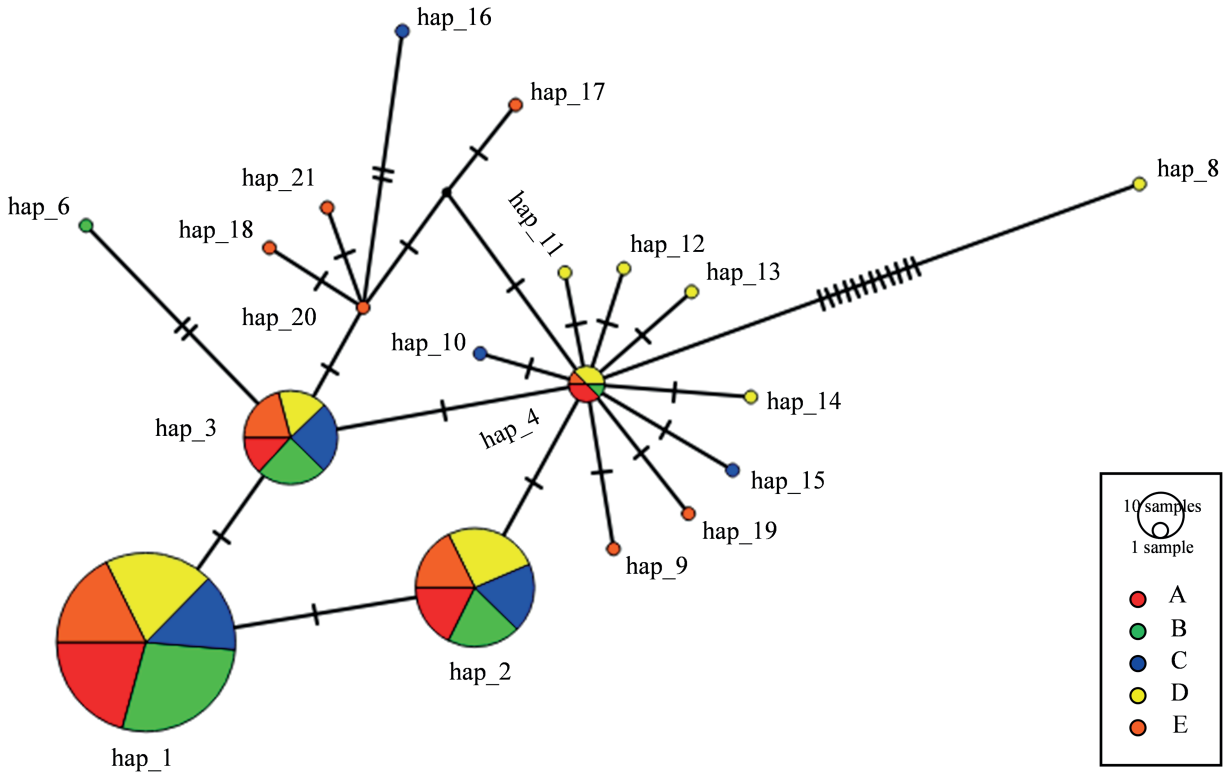

FIGURE 2
Haplotype network of *Pi02860* gene. Nucleotide haplotypes are named with Hap followed by a number. Size of the circles indicates haplotype frequencies in the population. Colors correspond to the respective populations. Each tick mark represents a step of nucleotide substitution. Hap_5 and Hap_7 have a mutation in start codon and were removed from haplotype network construction.

reference sequence (Supplementary Table 1). Due to some synonymous mutations, Hap_1 and Hap_3 were translated to the same amino acid isoform, accounting for 68.93% of the combined population while Hap_2 and Hap_4 were translated to another isoform, accounting for 26.27% of the combined population (Supplementary Table 3). All dominant haplotypes were one or two steps away from each other except Hap_8 which has an early termination at the 36th amino acid position and some rare haplotypes (Figure 2).

Association between sequence variation and altitude

Haplotype richness of *Pi02860* was positively associated with altitude ($p = 0.049$, Figure 3A). The haplotype diversity and nucleotide diversity of the effector gene were also positively correlated with altitude, with a value of p of 0.037 and 0.013, respectively (Figures 3B,C). Both synonymous mutation (dS) and non-synonymous mutation (dN) rates were positively correlated with altitude, but only the correlation with synonymous mutation was significant (Figures 3D,E). Population recombination rate was negatively correlated with altitude but was not significant (Figure 3F).

The subcellular localization of *Pi02860* haplotypes

Sixteen vectors were constructed to transiently express *Pi02860* haplotypes without a signal peptide in *N. benthamiana* for subcellular localization analysis. Two of the 21 haplotypes which are considered as pseudogenes due to a point mutation in the start codon were removed from the cellular localization analysis. Three haplotypes (Hap_1, Hap_3, and Hap_6) translate into one identical isoform and two haplotypes (Hap_2 and Hap_4) translate into another identical isoform (Figure 1). Only one vector was constructed for each of these two isoforms. Confocal images showed that non-synonymous mutation at these nucleotide sites (37th, 39th, 47th, 48th, 64th, 76th, 80th, 90th, 96th, 99th, 115th, 121st and 126th) did not change the subcellular localization of the *Pi02860* effector. All GFP-tagged *Pi02860* haplotypes were found to localize in the cytoplasm and nucleus (Figure 4).

Virulence analysis of *Pi02860* haplotypes

GFP-tagged expression revealed all *Pi02860* haplotypes including the truncated haplotype promoted the lesion size of co-expressed host *N. benthamiana* and there was also a significant

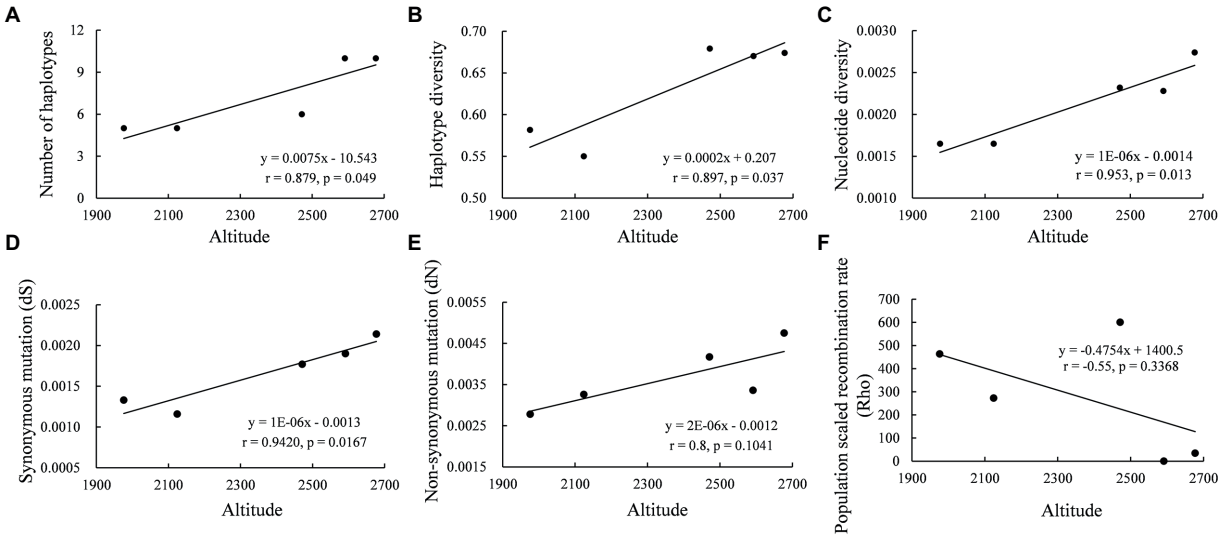

FIGURE 3
Correlations between the altitude of the collection sites of the pathogen and the genetic variation of *Pi02860* gene: **(A)** the number of haplotypes; **(B)** haplotype diversity; **(C)** nucleotide diversity; **(D)** synonymous mutation; **(E)** nonsynonymous mutation; **(F)** population scaled recombination rate of *Pi02860* and altitude.

difference in pathogenicity among the effector haplotypes (Figure 5). Hap_2 and Hap_4, which translate into isoform identical to the wild type *Pi02860* effector (T30-4), produced lesions larger than Hap_8, *Avr3a* and the negative control (EV). Hap_1, Hap_3 and Hap_6 which have one SNP in $48^{K\text{-}R}$ compared to the wild type *Pi02860* effector, as well as other haplotypes except Hap_8, produced larger lesions than Hap_2 and Hap _4 did. Hap_8, which has a terminal truncation starting at the 36^{th} amino acid position, produced significantly smaller lesions than other haplotypes including *Avr3a* (Figure 5). The altitude of collection site was negatively associated with the lesion size of the pathogen but was not significant (Figure 6A).

Pi02860 haplotypes varied significantly in suppressing INF1 cell death (Figure 7). Although there was no significantly correlation, the suppression of INF1 cell death caused by effector haplotypes largely mirrored the lesion sizes they produced on *N. benthamiana* (Figures 5, 7). In this expression analysis, Hap_2 and Hap _4 had the strongest suppression on cell death elicited by INF1, followed by Hap_1 Hap _3 and Hap _6, the most dominant *Pi02860* effector haplotypes. Hap_8 had nearly no effect on INF1 cell death suppression. The average of INF1 cell death suppression in the *P. infestans* populations was positively and significantly correlated with altitude (Figure 6B).

Thermal-mediated expression polymorphisms in *Pi02860* effector gene

QRT-PCR analysis of *Pi02860* expression at 2DAIs on susceptible potato plants showed that the transcription accumulation varied substantially among isolates with different effector haplotypes and among experimental temperatures (Figure 8). In all but isolate DQS9-14 of Hap_2, AH8-7 of Hap_3, DQS9-1 of Hap_12 and BKY-2 of Hap_6, *Pi02860* effector was expressed mostly at 10°C, followed by at 18°C. The effector was least expressed at 25°C. At 18°C, the nearly optimum infection temperature of the pathogen, the expression of *Pi02860* gene in seven isolates was upregulated >3 times with the highest upregulation of ~20 times in isolate BHYW-9 of Hap_1 whereas the expression in other isolates was <2 times (Figure 8). At 10°C, seven isolates were upregulated for ~20 times with the most upregulation of >300 times in isolate CHZ-62 of Hap_11. At 25°C, only three isolates were upregulated >2 times.

Discussion

Due to their critical roles in host-pathogen interactions, pathogen effectors are important proteins regulating disease initiation and epidemics in natural and agricultural ecosystems (Uhse and Djamei, 2018). Population genetic analysis of effector genes would provide useful insights on how these important proteins evolve and what ecological functions they play. In addition to their roles in regulating host pathogen interaction, it has been documented that effector genes also have other ecological functions such as antimicrobial activities (Snelders et al., 2020). To maintain these multifaceted functions, effector genes are expected to have a higher evolvability equipped by high genetic variation for quick adaptation to constantly changing biotic and abiotic environments. Indeed, previous studies have reported that the genetic variation in effector genes is higher than many other functional genes in *P. infestans* and other pathogen species,

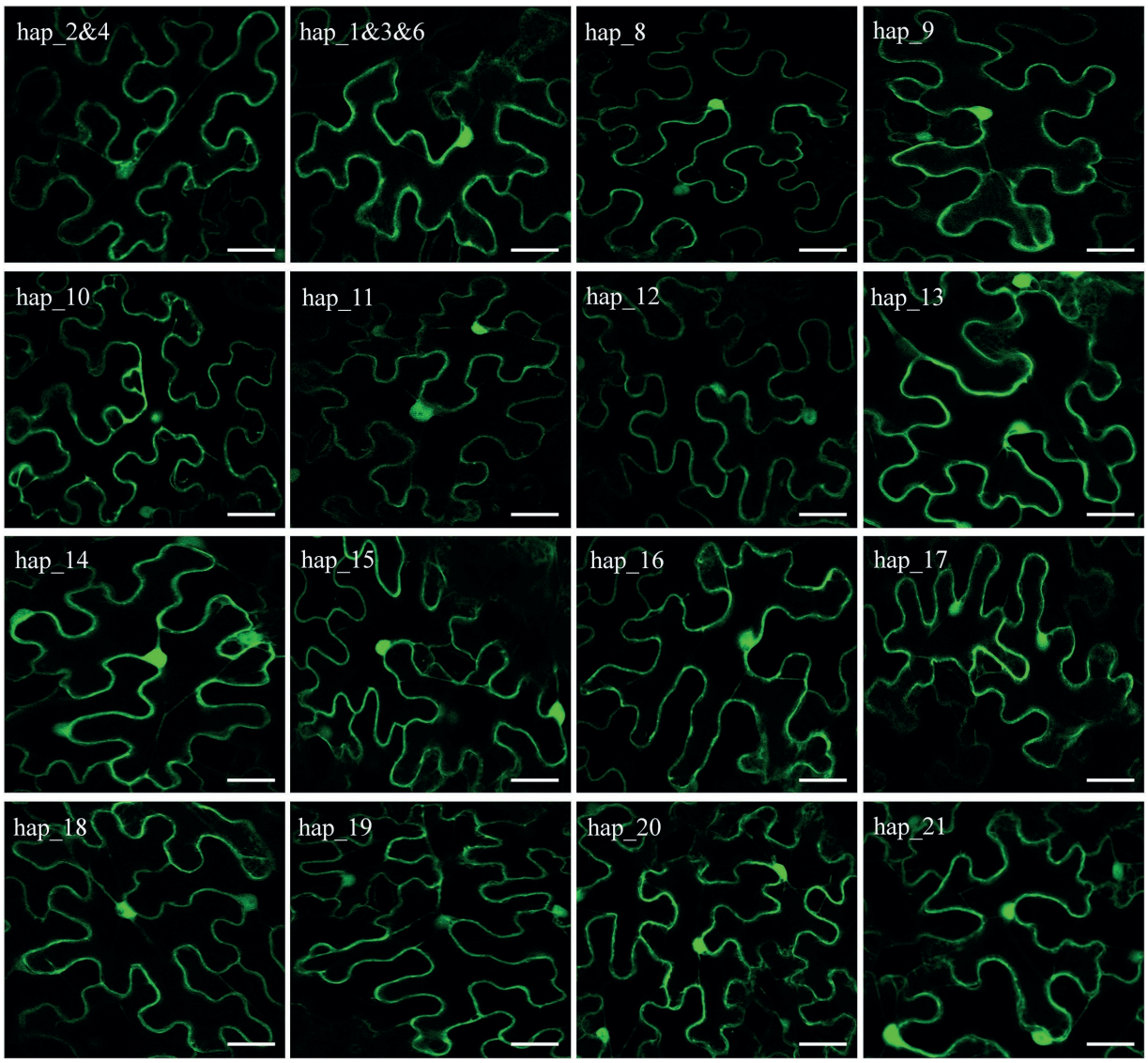

FIGURE 4
Confocal images showing that GFP-*Pi02860* effectors are localized in the cytoplasm and nucleus. Scale bars are 20μm.

possibly due to a synergic effect of recombination (Yang et al., 2018; Dale et al., 2019), plasticity (Timilsina et al., 2020) and multiple mutation mechanisms including pseudogenization, point mutation, deletion, insertion and truncation (Shen et al., 2021; Waheed et al., 2021). The physical locations of many effector genes in the sparse regions of genomes enriching with transposable elements provide unique opportunity for mutations to occur with a minimum fitness penalty to pathogen species (Haas et al., 2009; Dong et al., 2015). In this study, we found >20 nucleotide haplotypes in ~350 *Pi02860* sequences analysed. This is much higher than the genetic variation of other functional genes in this species. For example, we only identified < 10 nucleotide haplotypes in the 165 eEF1a sequences (Wang et al., 2021b) and two nucleotide haplotypes in the 140 ATP6 sequences (Zhang et al., 2017). However, the genetic variation found in *Pi02860* is much lower than other effector genes of the pathogen such as *Avr1, Avr2*, *Avr3a* and *Avr4* (Yang et al., 2018, 2020; Shen et al., 2021; Waheed et al., 2021). In addition, only point mutation and deletion were found in the current study. On the other hand, many variation mechanisms including pseudogenization, point mutation, deletion, insertion and truncation were found in *Avr1*, *Avr2*, *Avr3a* and *Avr4* of *P. infestans*.

These differences in genetic variation and mutation mechanisms between the *Pi02860* and other effector genes of *P. infestans* may reflect differences in interactions with host resistance genes. The corresponding resistance genes of effectors *Avr1*, *Avr2*, *Avr3a* and *Avr4* in our previous publications have been used commercially over a wide spatial scale in the past decades. Due to the constant interaction with host immunity systems, it is expected that this group of effector genes have become equipped

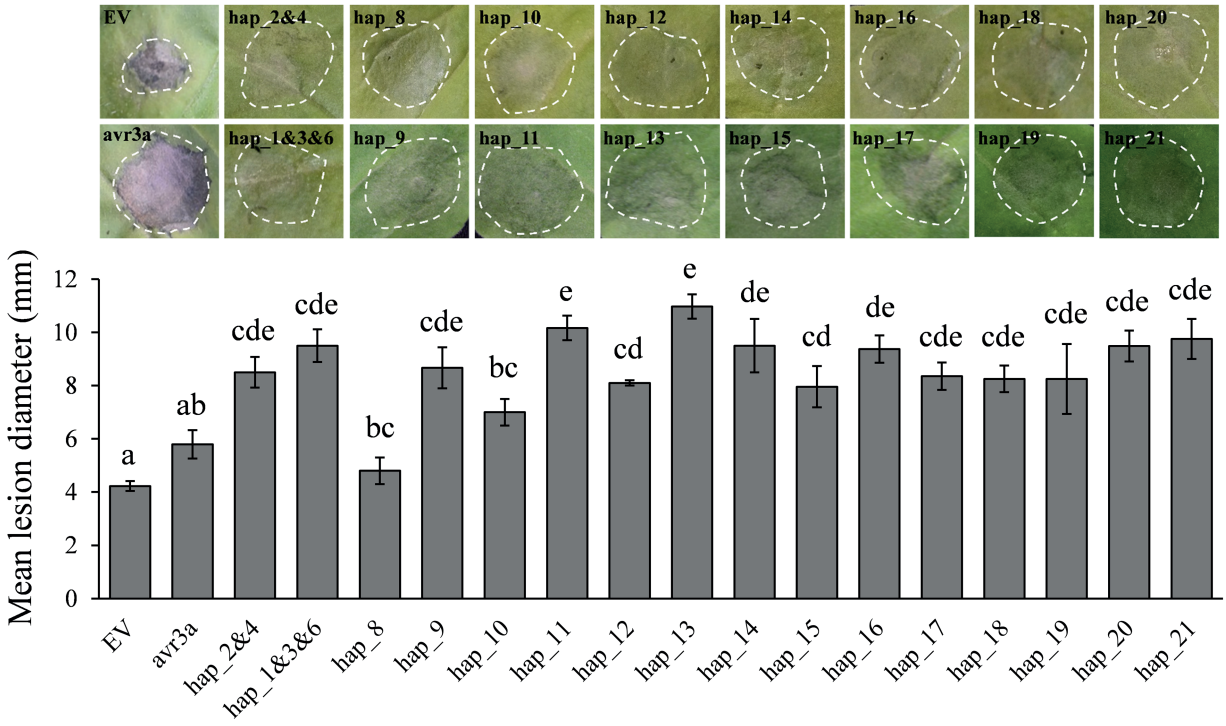

FIGURE 5
Transient overexpression of *Pi02860* haplotypes in *N. benthamiana* increases *P. infestans* lesion diameter to various degrees compared with free GFP. Bottom: statistical test; Top: representative images of pathogen expression. EV and avr3a are negative and positive controls, respectively. Hap_1 to Hap_21 are the codes of 21 haplotypes detected. Hap_2 and 4 are deduced into the same isoform and Hap_1, 3 and 6 are deduced into another the same isoform, thus only one vector was constructed for each of the two haplotype groups. Results shown are derived from the mean of at least three independent biological replicates.

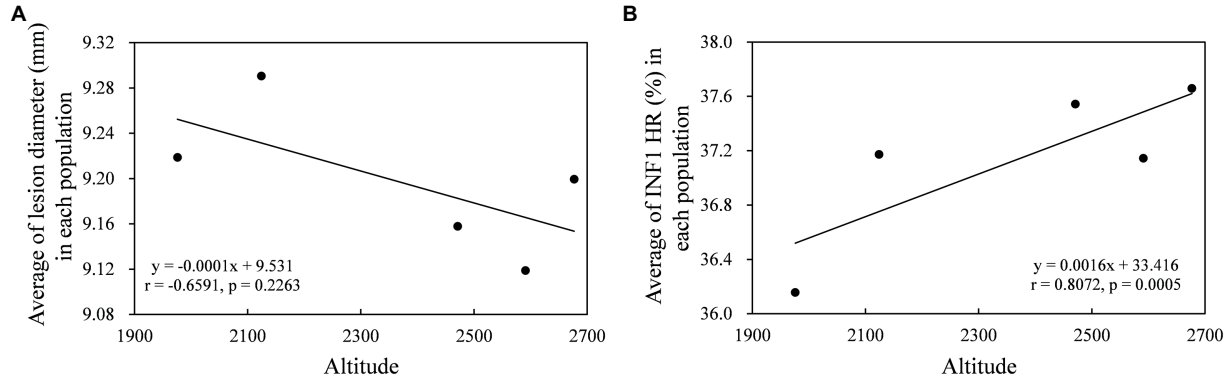

FIGURE 6
Correlation between the altitude of the collection sites and lesion size **(A)** and INF1 suppression **(B)** of pathogen population.

with higher genetic variation to maintain the pathogen's co-evolutionary pace with the host. On the other hand, *Pi02860* is only a candidate effector gene with some documented functions (Yang et al., 2016b; He et al., 2018) of regulating host immunity responses. No corresponding resistance gene has been identified in the potato host or has been used commercially. In this case, standing genetic variation in the effector gene is not essential for reproduction and transmission of the pathogen and therefore would be gradually purged out either due to random genetic drift (Lynch et al., 2016) or genetic load (Kirkpatrick and Jarne, 2000) incurred to the pathogen in its presence. It is documented that plant pathogens have optimized their effector reservoirs over their co-evolution journey with their hosts. Some effectors play a more important and common role in pathogen virulence than others.

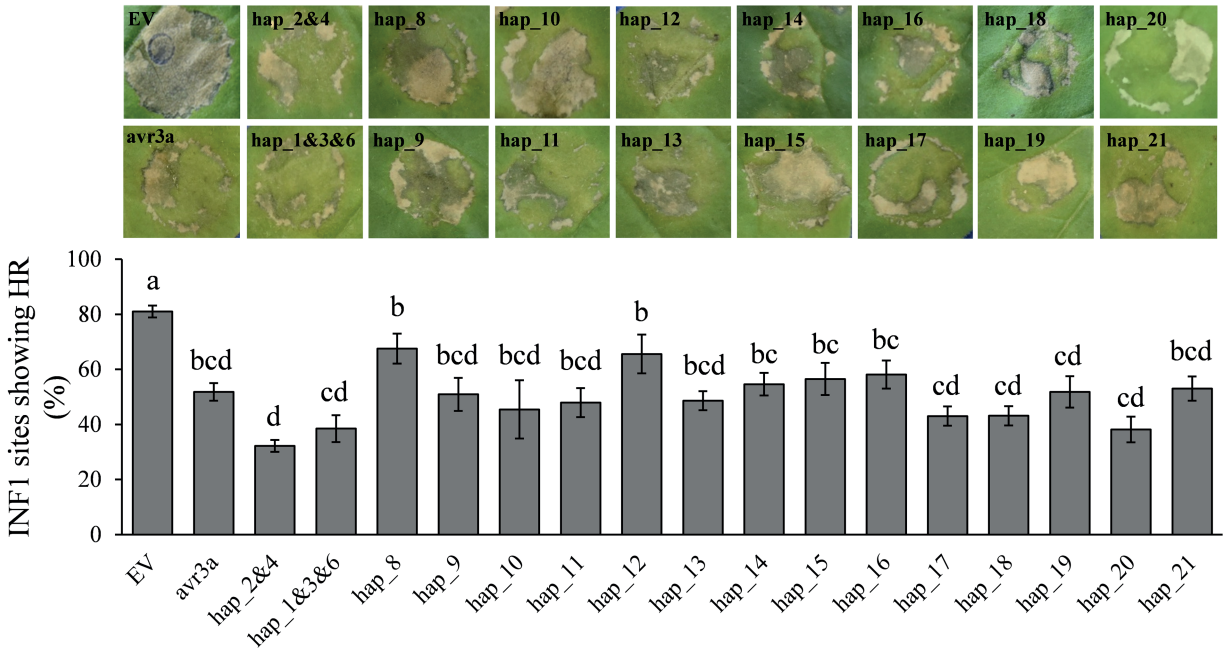

FIGURE 7
Transient overexpression of GFP-*Pi02860* haplotypes in *N. benthamiana* suppresses the HR (hypersensitive response) triggered by the elicitin INF1. Top: images of pathogen expression: Bottom: statistical test. EV and avr3a are negative and positive controls, respectively. Hap_1 to Hap_21 are the codes of 21 haplotypes detected. Hap_2 and 4 are deduced into the same isoform and Hap_1, 3 and 6 are deduced into another the same isoform, thus only one vector was constructed for each of the two haplotype groups. Results shown are derived from the mean of at least three independent biological replicates.

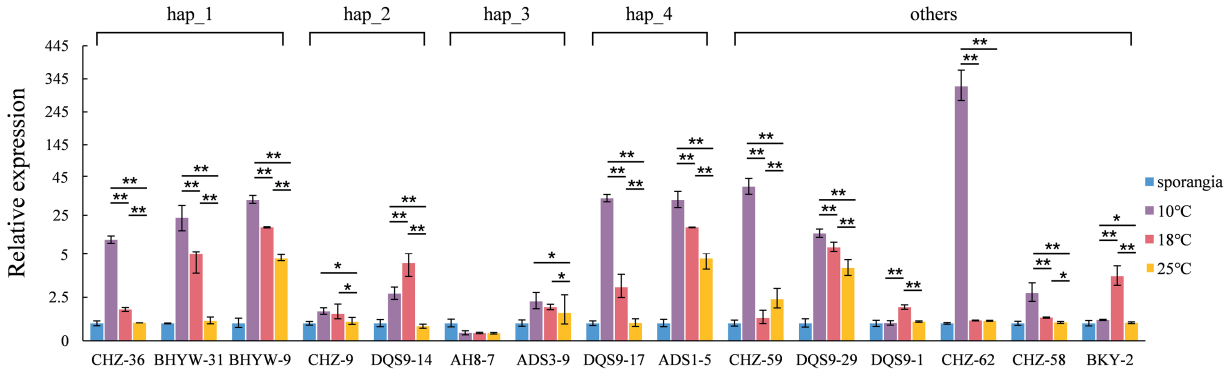

FIGURE 8
The expression of *Pi02860* haplotypes under 10, 18 and 25°C.

This group of effectors are more conserved in sequence structure and are regard as core effectors (Chepsergon et al., 2021). It is possible that *Pi02860* is also one of such core effectors.

We found mutations in the effector domain of *Pi02860* did not change its subcellular localization. The effectors were only found in the nucleus and cytoplasm, confirming that *Pi02860* is a cytoplasmic effector (Yang et al., 2016b). However, mutations in this region dramatically affect the fitness of the pathogen as indicated by the statistical difference among the nucleotide haplotypes in their ability to suppress the host's immunity response and the amount of disease they produced (Figures 5, 7). Overall, these mutations reduce the ability of the pathogen to inhibit host immunity responses, leading to less disease even though the positive correlation between the two parameters is not significant (Figure 6). This reduction in immunity suppression is more obvious for the haplotype with the C-terminal truncation (Hap_8), further suggesting that *Pi02860* may be a core effector which is crucial for *P. infestans* pathogenicity and its loss from the genome may lead to a severe fitness penalty to the pathogen.

In addition to host resistance, other ecological factors may also contribute to the evolution of effector genes. Previously, it was reported that microbial community structure in the plant root rhizosphere can affect the evolutionary outcome of effector genes in a plant pathogen (Bever et al., 2012). Here, we found that abiotic factors may also contribute to the evolution of the effector gene in *P. infestans*. Genetic variation of *Pi02860* in terms of haplotype richnesss, haplotype diversity and nucleotide diversity increased as the altitude of the sample collection sites increased (Figures 2B,C, 3A). This spatial pattern of genetic variation is also linked to the fitness of the pathogen (Figure 6). Mutation rate, particularly the synonymous mutation rate, also increased as the altitude of the collection site increased (Figures 3D–F). Because no resistance gene corresponding to *Pi02860* was used in the fields and the isolates included in the study were sampled from the same potato variety on the same day at the same region, the observed difference in the genetic variation among altitudinal *Pi02860* effector is unlikely to have been caused by natural selection for host adaptation. Rather, it more likely reflects an elevated mutation rate caused by the vertical distribution of climatic conditions such as UV radiation and temperature. UV radiation is a major mutagenic agent which promotes the generation of genetic variation in species by inducing structural change of genetic material in the genome. For example, the mutation rate in bacteria increased hundreds of times after exposed to UV radiation (Shibai et al., 2017). In clear skies, UV radiation increases by 10–20% in response to a 1,000 m increase in altitude (Blumthaler et al., 1992; Schmucki and Philipona, 2002; Narayanan et al., 2010).

Temperature is an important environmental factor with crucial impacts on nearly all biological and evolutionary processes of species (Townsley and Yildiz, 2015; Huot et al., 2017; Garbelotto et al., 2021). Recently, it was reported that temperature can regulate the population genetic structure and evolution of effector genes (Velásquez et al., 2018; Waheed et al., 2021). In the current study, we found the expression of *Pi02860* was regulated by experimental temperatures. The effector gene demonstrated a higher expression level at a lower temperature (10°C) compared to the near optimum infection temperature of the pathogen (~19°C), and the expression level was further reduced as the experimental temperature increased to 25°C (Figure 8). Air temperature at the earth surface is negatively correlated with altitude (Legates and Willmott, 1990) and it is possible that changes in temperature may also contribute to the observed association of genetic variation in *Pi02860* with altitude. Recombination increases genetic variation of species by reshuffling genetic material among genomes and reducing the purging effect of natural selection (Gossmann et al., 2014). Both UV radiation and temperature can affect the recombination rate of species (Boyko et al., 2005; Shibai et al., 2017). Recombination events regulated by vertical distributions of temperature may also contribute to the observed association of genetic variation with altitude, but this hypothesis is rejected by the association analysis between recombination rate and the altitudes of collection sites. We found neither putative recombination events by the seven algorithms (RDP, GENECONV, Bootscan, MaxChi, Chimaera, SiScan and 3Seq) embedded in the RDP4 suite (Martin et al., 2015) nor association between recombination rate and altitude. However, intragenic recombination has been documented in several other effector genes of the pathogen sampled from the region (Yang et al., 2020; Shen et al., 2021; Waheed et al., 2021).

Many genetic and ecological factors influence the generation and maintenance of genetic variation. To minimize this effect, we sampled from the same potato variety along a hill on the same day. Our results indicate that in additional to host, climatic conditions associated with altitudinal distribution also contribute to the evolution of effector gene *Pi02860*. It has to point out that only one effector was reported in the current manuscript, further studies involving more effector genes and pathogen species are needed to confirm the altitudinal pattern. However, our results are complementary to other evolutionary phenomena that also show altitudinal effect on pathogen evolution at both the genic and organismic level (Santini and Ghelardini, 2015; Wang et al., 2021a). Further studies involving more effector genes are needed and may therefore, have many important implications for future agricultural and ecological sustainability caused by ongoing climate changes.

Data availability statement

The *Pi02860* haplotype sequence data presented in the study has been deposited in NCBI. The GenBank accession numbers of hap_1, 2, 3, 4, 6, 9, 10, 11, 12, 13, 14, 15, 16, 17, 18, 19, 20, 21 are OP222576, OP222577, OP222578, OP222579, OP222580, OP222581, OP222582, OP222583, OP222584, OP222585, OP222586, OP222587, OP222588, OP222589, OP222590, OP222591, OP222592, and OP222593. The GenBank accession numbers of hap_5, 7, 8 are OP222594, OP222595, and OP222596.

Author contributions

L-NY and HO performed the experiments, analysed data and wrote the manuscript. ON, AW, and Y-PW collected pathogen isolates. HF and WL genotyped pathogen isolates. JZ conceived, designed and supervised the experiments, analysed the data and wrote the manuscript. All authors contributed the article and approved the submitted version.

Funding

This work was supported by the National Natural Science Foundation of China (grant no. 31901861).

Acknowledgments

We thank Jeremy Burdon for comments and language proofreading.

Conflict of interest

The authors declare that the research was conducted in the absence of any commercial or financial relationships that could be construed as a potential conflict of interest.

The reviewer RV declared a shared affiliation with one of the authors JZ to the handling editor at the time of review.

Publisher's note

Supplementary material

The Supplementary material for this article can be found online at: https://www.frontiersin.org/articles/10.3389/fmicb.2022.972928/full#supplementary-material

References

Bais, A. F., McKenzie, R. L., Bernhard, G., Aucamp, P. J., Ilyas, M., Madronich, S., et al. (2015). Ozone depletion and climate change: impacts on UV radiation. *Photochem. Photobiol. Sci.* 14, 19–52. doi: 10.1039/C4PP90032D

Bever, J. D., Platt, T. G., and Morton, E. R. (2012). Microbial population and community dynamics on plant roots and their feedbacks on plant communities. *Annu. Rev. Microbiol.* 66, 265–283. doi: 10.1146/annurev-micro-092611-150107

Blumthaler, M., Ambach, W., and Rehwald, W. (1992). Solar UV-A and UV-B radiation fluxes at two alpine stations at different altitudes. *Theor. Appl. Climatol.* 46, 39–44. doi: 10.1007/BF00866446

Boevink, P. C., McLellan, H., Gilroy, E. M., Naqvi, S., He, Q., Yang, L., et al. (2016). Oomycetes seek help from the plant: *Phytophthora infestans* effectors target host susceptibility factors. *Mol. Plant* 9, 636–638. doi: 10.1016/j.molp.2016.04.005

Boutemy, L. S., King, S. R., Win, J., Hughes, R. K., Clarke, T. A., Blumenschein, T. M., et al. (2011). Structures of phytophthora RXLR effector proteins a conserved but adaptable fold underpins functional diversity. *J. Biol. Chem.* 286, 35834–35842. doi: 10.1074/jbc.M111.262303

Boyko, A., Filkowski, J., and Kovalchuk, I. (2005). Homologous recombination in plants is temperature and day-length dependent. *Mutat. Res. Fundam. Mol. Mech. Mutagen.* 572, 73–83. doi: 10.1016/j.mrfmmm.2004.12.011

Burdon, J. J., Barrett, L., Yang, L. N., He, D. C., and Zhan, J. (2020). Maximizing world food production through disease control. *Bioscience* 70, 126–128. doi: 10.1093/biosci/biz149

Cavicchioli, R., Ripple, W. J., Timmis, K. N., Azam, F., Bakken, L. R., Baylis, M., et al. (2019). Scientists' warning to humanity: microorganisms and climate change. *Nat. Rev. Microbiol.* 17, 569–586. doi: 10.1038/s41579-019-0222-5

Chepsergon, J., Motaung, T. E., and Moleleki, L. N. (2021). "Core" RxLR effectors in phytopathogenic oomycetes: a promising way to breeding for durable resistance in plants? *Virulence* 12, 1921–1935. doi: 10.1080/21505594.2021.1948277

Dale, A. L., Feau, N., Everhart, S. E., Dhillon, B., Wong, B., Sheppard, J., et al. (2019). Mitotic recombination and rapid genome evolution in the invasive forest pathogen *Phytophthora ramorum*. *mBio* 10, e02452-18. doi: 10.1128/mBio.02452-18

Dong, S., Raffaele, S., and Kamoun, S. (2015). The two-speed genomes of filamentous pathogens: waltz with plants. *Curr. Opin. Genet. Dev.* 35, 57–65. doi: 10.1016/j.gde.2015.09.001

Franceschetti, M., Maqbool, A., Jiménez-Dalmaroni, M. J., Pennington, H. G., Kamoun, S., and Banfield, M. J. (2017). Effectors of filamentous plant pathogens: commonalities amid diversity. *Microbiol. Mol. Biol. Rev.* 81, e00066-16. doi: 10.1128/MMBR.00066-16

Fry, W. (2008). *Phytophthora infestans*: the plant (and R gene) destroyer. *Mol. Plant Pathol.* 9, 385–402. doi: 10.1111/j.1364-3703.2007.00465.x

Garbelotto, M., Schmidt, D., and Popenuck, T. (2021). Pathogenicity and infectivity of *Phytophthora ramorum* vary depending on host species, infected plant part, inoculum potential, pathogen genotype, and temperature. *Plant Pathol.* 70, 287–304. doi: 10.1111/ppa.13297

Gossmann, T. I., Santure, A. W., Sheldon, B. C., Slate, J., and Zeng, K. (2014). Highly variable recombinational landscape modulates efficacy of natural selection in birds. *Genome Biol. Evol.* 6, 2061–2075. doi: 10.1093/gbe/evu157

Haas, B. J., Kamoun, S., Zody, M. C., Jiang, R. H., Handsaker, R. E., Cano, L. M., et al. (2009). Genome sequence and analysis of the Irish potato famine pathogen *Phytophthora infestans*. *Nature* 461, 393–398. doi: 10.1038/nature08358

He, Q., Naqvi, S., McLellan, H., Boevink, P. C., Champouret, N., Hein, I., et al. (2018). Plant pathogen effector utilizes host susceptibility factor NRL1 to degrade the immune regulator SWAP70. *Proce. Natl. Acad. Sci.* 115, E7834–E7843. doi: 10.1073/pnas.1808585115

Huot, B., Castroverde, C. D. M., Velásquez, A. C., Hubbard, E., Pulman, J. A., Yao, J., et al. (2017). Dual impact of elevated temperature on plant defence and bacterial virulence in *Arabidopsis*. *Nat. Commun.* 8, 1808–1812. doi: 10.1038/s41467-017-01674-2

Juroszek, P., Racca, P., Link, S., Farhumand, J., and Kleinhenz, B. (2020). Overview on the review articles published during the past 30 years relating to the potential climate change effects on plant pathogens and crop disease risks. *Plant Pathol.* 69, 179–193. doi: 10.1111/ppa.13119

Kirkpatrick, M., and Jarne, P. (2000). The effects of a bottleneck on inbreeding depression and the genetic load. *Am. Nat.* 155, 154–167. doi: 10.1086/303312

Körner, C. (2007). The use of 'altitude' in ecological research. *Trends Ecol. Evol.* 22, 569–574. doi: 10.1016/j.tree.2007.09.006

Kumar, S., Stecher, G., and Tamura, K. (2016). MEGA7: molecular evolutionary genetics analysis version 7.0 for bigger datasets. *Mol. Biol. Evol.* 33, 1870–1874. doi: 10.1093/molbev/msw054

Lawrence, I., and Lin, K. (1989). A concordance correlation coefficient to evaluate reproducibility. *Biometrics* 45, 255–268. doi: 10.2307/2532051

Legates, D. R., and Willmott, C. J. (1990). Mean seasonal and spatial variability in global surface air temperature. *Theor. Appl. Climatol.* 41, 11–21. doi: 10.1007/BF00866198

Leigh, J. W., and Bryant, D. (2015). Popart: full-feature software for haplotype network construction. *Methods Ecol. Evol.* 6, 1110–1116. doi: 10.1111/2041-210X.12410

Librado, P., and Rozas, J. (2009). DnaSP v5: a software for comprehensive analysis of DNA polymorphism data. *Bioinformatics* 25, 1451–1452. doi: 10.1093/bioinformatics/btp187

Lo Presti, L., Lanver, D., Schweizer, G., Tanaka, S., Liang, L., Tollot, M., et al. (2015). Fungal effectors and plant susceptibility. *Annu. Rev. Plant Biol.* 66, 513–545. doi: 10.1146/annurev-arplant-043014-114623

Lynch, M., Ackerman, M. S., Gout, J. F., Long, H., Sung, W., Thomas, W. K., et al. (2016). Genetic drift, selection and the evolution of the mutation rate. *Nat. Rev. Genet.* 17, 704–714. doi: 10.1038/nrg.2016.104

Martin, D. P., Murrell, B., Golden, M., Khoosal, A., and Muhire, B. (2015). RDP4: detection and analysis of recombination patterns in virus genomes. *Virus Evol.* 1:vev003. doi: 10.1093/ve/vev003

Martín, J. A., Witzell, J., Blumenstein, K., Rozpedowska, E., Helander, M., Sieber, T. N., et al. (2013). Resistance to Dutch elm disease reduces presence of xylem endophytic fungi in elms (*Ulmus* spp.). *PLoS One* 8:e56987. doi: 10.1371/journal.pone.0056987

McLellan, H., Boevink, P. C., Armstrong, M. R., Pritchard, L., Gomez, S., Morales, J., et al. (2013). An RxLR effector from *Phytophthora infestans* prevents

re-localisation of two plant NAC transcription factors from the endoplasmic reticulum to the nucleus. *PLoS Pathog.* 9:e1003670. doi: 10.1371/journal.ppat.1003670

McVean, G, Awadalla, P., and Fearnhead, P. (2002). A coalescent-based method for detecting and estimating recombination from gene sequences. *Genetics* 160, 1231–1241. doi: 10.1093/genetics/160.3.1231

McVean, G. A., Myers, S. R., Hunt, S., Deloukas, P., Bentley, D. R., and Donnelly, P. (2004). The fine-scale structure of recombination rate variation in the human genome. *Science* 304, 581–584. doi: 10.1126/science.1092500

Narayanan, D. L., Saladi, R. N., and Fox, J. L. (2010). Ultraviolet radiation and skin cancer. *Int. J. Dermatol.* 49, 978–986. doi: 10.1111/j.1365-4632.2010.04474.x

Ott, R. L., and Longnecker, M. T. (2015). *An introduction to statistical methods and data analysis* Cengage Learning. Boston: Duxbury Press.

Raffaele, S., and Kamoun, S. (2012). Genome evolution in filamentous plant pathogens: why bigger can be better. *Nat. Rev. Microbiol.* 10, 417–430. doi: 10.1038/nrmicro2790

Raum, S. (2020). Land-use legacies of twentieth-century forestry in the UK: a perspective. *Landsc. Ecol.* 35, 2713–2722. doi: 10.1007/s10980-020-01126-1

Ren, F., Yan, D. H., Wu, G., Sun, X., Song, X., and Li, R. (2020). Distinctive gene expression profiles and effectors consistent with host specificity in two formae speciales of *Marssonina brunnea*. *Front. Microbiol.* 11:276. doi: 10.3389/fmicb.2020.00276

Santini, A., and Ghelardini, L. (2015). Plant pathogen evolution and climate change. *CABI Rev.* 2015, 1–8. doi: 10.1079/PAVSNNR201510035

Schmucki, D. A., and Philipona, R. (2002). Ultraviolet radiation in the Alps: the altitude effect. *Opt. Eng.* 41, 3090–3095. doi: 10.1117/1.1516820

Shen, L. L., Wheed, A., Wang, Y. P., Nkurikiyimfura, O., Wang, Z. H., Yang, L. N., et al. (2021). Multiple mechanisms drive the evolutionary adaptation of *Phytophthora infestans* effector Avr1 to host resistance. *J. Fungi* 7, 789. doi: 10.3390/jof7100789

Shibai, A., Takahashi, Y., Ishizawa, Y., Motooka, D., Nakamura, S., Ying, B. W., et al. (2017). Mutation accumulation under UV radiation in *Escherichia coli*. *Sci. Rep.* 7, 14531–14512. doi: 10.1038/s41598-017-15008-1

Snelders, N. C., Rovenich, H., Petti, G. C., Rocafort, M., van den Berg, G. C., Vorholt, J. A., et al. (2020). Microbiome manipulation by a soil-borne fungal plant pathogen using effector proteins. *Nat. Plants* 6, 1365–1374. doi: 10.1038/s41477-020-00799-5

Soyer, J. L., El Ghalid, M., Glaser, N., Ollivier, B., Linglin, J., Grandaubert, J., et al. (2014). Epigenetic control of effector gene expression in the plant pathogenic fungus *Leptosphaeria maculans*. *PLoS Genet*. 10:e1004227. doi: 10.1371/journal.pgen.1004227

Timilsina, S., Potnis, N., Newberry, E. A., Liyanapathiranage, P., Iruegas-Bocardo, F., White, F. F., et al. (2020). Xanthomonas diversity, virulence and plant–pathogen interactions. *Nat. Rev. Microbiol.* 18, 415–427. doi: 10.1038/s41579-020-0361-8

Tollefson, J. (2020). How hot will earth get by 2100? *Nature* 580, 443–445. doi: 10.1038/d41586-020-01125-x

Townsley, L., and Yildiz, F. H. (2015). Temperature affects c-di-GMP signalling and biofilm formation in Vibrio cholerae. *Environ. Microbiol.* 17, 4290–4305. doi: 10.1111/1462-2920.12799

Turnbull, D., Yang, L., Naqvi, S., Breen, S., Welsh, L., Stephens, J., et al. (2017). RXLR effector AVR2 up-regulates a brassinosteroid-responsive bHLH transcription factor to suppress immunity. *Plant Physiol.* 174, 356–369. doi: 10.1104/pp.16.01804

Uhse, S., and Djamei, A. (2018). Effectors of plant-colonizing fungi and beyond. *PLoS Pathog.* 14:e1006992. doi: 10.1371/journal.ppat.1006992

van Poppel, P. M., Guo, J., van de Vondervoort, P. J., Jung, M. W., Birch, P. R., Whisson, S. C., et al. (2008). The *Phytophthora infestans* avirulence gene Avr4 encodes an RXLR-dEER effector. *Mol. Plant-Microbe Interact.* 21, 1460–1470. doi: 10.1094/MPMI-21-11-1460

Velásquez, A. C., Castroverde, C. D. M., and He, S. Y. (2018). Plant–pathogen warfare under changing climate conditions. *Curr. Biol.* 28, R619–R634. doi: 10.1016/j.cub.2018.03.054

Vleeshouwers, V. G., Raffaele, S., Vossen, J. H., Champouret, N., Oliva, R., Segretin, M. E., et al. (2011). Understanding and exploiting late blight resistance in the age of effectors. *Annu. Rev. Phytopathol.* 49, 507–531. doi: 10.1146/annurev-phyto-072910-095326

Waheed, A., Wang, Y. P., Nkurikiyimfura, O., Li, W. Y., Liu, S. T., Lurwanu, Y., et al. (2021). Effector Avr4 in *Phytophthora infestans* escapes host immunity mainly through early termination. *Front. Microbiol.* 12:646062. doi: 10.3389/fmicb.2021.646062

Wang, Y., Bao, Z., Zhu, Y., and Hua, J. (2009). Analysis of temperature modulation of plant defense against biotrophic microbes. *Mol. Plant Microbe Interact.* 22, 498–506. doi: 10.1094/MPMI-22-5-0498

Wang, S., Boevink, P. C., Welsh, L., Zhang, R., Whisson, S. C., and Birch, P. R. (2017). Delivery of cytoplasmic and apoplastic effectors from *Phytophthora infestans* haustoria by distinct secretion pathways. *New Phytol.* 216, 205–215. doi: 10.1111/nph.14696

Wang, Q., Han, C., Ferreira, A. O., Yu, X., Ye, W., Tripathy, S., et al. (2011). Transcriptional programming and functional interactions within the *Phytophthora sojae* RXLR effector repertoire. *Plant Cell* 23, 2064–2086. doi: 10.1105/tpc.111.086082

Wang, Y. P., Waheed, A., Liu, S. T., Li, W. Y., Nkurikiyimfura, O., Lurwanu, Y., et al. (2021a). Altitudinal heterogeneity of UV adaptation in *Phytophthorainfestans* is associated with the spatial distribution of a DNA repair gene. *J. Fungi* 7, 245. doi: 10.3390/jof7040245

Wang, Y. P., Wu, E. J., Lurwanu, Y., Ding, J. P., He, D. C., Waheed, A., et al. (2021b). Evidence for a synergistic effect of post-translational modifications and genomic composition of eEF-1α on the adaptation of *Phytophthora infestans*. *Ecol. Evol.* 11, 5484–5496. doi: 10.1002/ece3.7442

Yaeno, T., Li, H., Chaparro-Garcia, A., Schornack, S., Koshiba, S., Watanabe, S., et al. (2011). Phosphatidylinositol monophosphate-binding interface in the oomycete RXLR effector AVR3a is required for its stability in host cells to modulate plant immunity. *Proc. Natl. Acad. Sci.* 108, 14682–14687. doi: 10.1073/pnas.1106002108

Yang, X., Chockalingam, S. P., and Aluru, S. (2013). A survey of error-correction methods for next-generation sequencing. *Brief. Bioinform.* 14, 56–66. doi: 10.1093/bib/bbs015

Yang, L. N., Liu, H., Duan, G. H., Huang, Y. M., Liu, S., Fang, Z. G., et al. (2020). The *Phytophthora infestans* AVR2 effector escapes R2 recognition through effector disordering. *Mol. Plant Microbe Interact.* 33, 921–931. doi: 10.1094/MPMI-07-19-0179-R

Yang, L. N., Liu, H., Wang, Y. P., Seematti, J., Grenville-Briggs, B. J., Wang, Z., et al. (2021). Pathogen-mediated stomatal opening: A previously overlooked pathogenicity strategy in the oomycete pathogen *Phytophthora infestans*. *Front. Plant Sci.* 12:668797. doi: 10.3389/fpls.2021.668797

Yang, L., McLellan, H., Naqvi, S., He, Q., Boevink, P. C., Armstrong, M., et al. (2016b). Potato NPH3/RPT2-like protein StNRL1, targeted by a *Phytophthora infestans* RXLR effector, is a susceptibility factor. *Plant Physiol.* 171, 645–657. doi: 10.1104/pp.16.00178

Yang, L., Ouyang, H. B., Fang, Z. G., Zhu, W., Wu, E. J., Luo, G. H., et al. (2018). Evidence for intragenic recombination and selective sweep in an effector gene of *Phytophthora infestans*. *Evol. Appl.* 11, 1342–1353. doi: 10.1111/eva.12629

Yang, L. N., Zhu, W., Wu, E. J., Yang, C., Thrall, P. H., Burdon, J. J., et al. (2016a). Trade-offs and evolution of thermal adaptation in the Irish potato famine pathogen *Phytophthora infestans*. *Mol. Ecol.* 25, 4047–4058. doi: 10.1111/mec.13727

Zhan, J., Thrall, P. H., and Burdon, J. J. (2014). Achieving sustainable plant disease management through evolutionary principles. *Trends Plant Sci.* 19, 570–575. doi: 10.1016/j.tplants.2014.04.010

Zhan, J., Thrall, P. H., Papaïx, J., Xie, L., and Burdon, J. J. (2015). Playing on a pathogen's weakness: using evolution to guide sustainable plant disease control strategies. *Annu. Rev. Phytopathol.* 53, 19–43. doi: 10.1146/annurev-phyto-080614-120040

Zhang, J. F., Wu, E. J., Luo, H. H., Zhu, W., and Zhan, J. (2017). Correlation analyses between *ATP6* sequences of *Phytophthora infestans* and geographical factors. *Jiangsu J. Agric. Sci.* 45, 75–78. doi: 10.15889/j.issn.1002-1302.2017.08.021

Zhu, W., Yang, L. N., Wu, E. J., Qin, C. F., Shang, L. P., Wang, Z. H., et al. (2015). Limited sexual reproduction and quick turnover in the population genetic structure of *Phytophthora infestans* in Fujian, China. *Sci. Rep.* 5, 1–11. doi: 10.1038/srep10094

frontiers | Frontiers in Microbiology

TYPE Original Research
PUBLISHED 15 September 2022
DOI 10.3389/fmicb.2022.994941

OPEN ACCESS

EDITED BY
Ryan Kessens,
Corteva Agriscience™, United States

REVIEWED BY
Hari S. Gaur,
Sharda University,
India
Maria Lurdes Inacio,
Instituto Nacional Investigaciao Agraria e Veterinaria (INIAV), Portugal

*CORRESPONDENCE
Xiaowei Huang
xwhuang@ynu.edu.cn

†These authors have contributed equally to this work

SPECIALTY SECTION
This article was submitted to Microbe and Virus Interactions With Plants, a section of the journal Frontiers in Microbiology

RECEIVED 15 July 2022
ACCEPTED 22 August 2022
PUBLISHED 15 September 2022

CITATION
Zhao Y, Zhou Q, Zou C, Zhang K and Huang X (2022) Repulsive response of *Meloidogyne incognita* induced by biocontrol bacteria and its effect on interspecific interactions. *Front. Microbiol.* 13:994941. doi: 10.3389/fmicb.2022.994941

Repulsive response of *Meloidogyne incognita* induced by biocontrol bacteria and its effect on interspecific interactions

Yanli Zhao[1,2†], Qinying Zhou[1†], Chenggang Zou[1], Keqin Zhang[1] and Xiaowei Huang[1,3*]

[1]State Key Laboratory for Conservation and Utilization of Bio-Resources, and College of Life Science, Yunnan University, Kunming, China, [2]Institute of Medicinal Plants, Yunnan Academy of Agricultural Sciences, Kunming, China, [3]School of Medicine, Yunnan University, Kunming, China

The aversive behavior of *Caenorhabditis elegans* is an important strategy that increases their survival under pathogen infection, and the molecular mechanisms underlying this behavior have been described. However, whether this defensive response occurs in plant-parasitic nematodes (PPNs), which have quite different life cycles and genomic sequences from the model nematode, against biocontrol microbes and affects interspecific interactions in ecological environments remains unclear. Here, we showed that *Meloidogyne incognita*, one of the most common PPNs, engaged in lawn-leaving behavior in response to biocontrol bacteria such as *Bacillus nematocida* B16 and *B. thuringiensis* Bt79. Genomic analysis revealed that the key genes responsible for the aversive behavior of *C. elegans*, such as serotonin-and TGF-β-related genes in canonical signaling pathways, were homologous to those of *M. incognita*, and the similarity between these sequences ranged from 30% to 67%. Knockdown of the homologous genes impaired avoidance of *M. incognita* to varying degrees. Calcium ion imaging showed that the repulsive response requires the involvement of the multiple amphid neurons of *M. incognita*. *In situ* hybridization specifically localized *Mi-tph-1* of the serotonin pathway to ADF/NSM neurons and *Mi-dbl-1* of the TGF-β pathway to AVA neurons. Our data suggested that the repulsive response induced by different biocontrol bacteria strongly suppresses the invasion of tomato host plants by *M. incognita*. Overall, our study is the first to clarify the pathogen-induced repulsive response of *M. incognita* and elucidate its underlying molecular mechanisms. Our findings provide new insights into interspecific interactions among biocontrol bacteria, PPNs, and host plants.

KEYWORDS

plant parasitic nematodes, *Meloidogyne incognita*, biocontrol bacteria, repulsive response, host plant, interspecific interactions

Introduction

Plant parasitic nematodes (PPNs) are some of the most devastating agricultural pests. Root-knot nematodes (*Meloidogyne* spp.) are the most omnivorous PPNs, and they can parasitize more than 5,500 host plants and cause over $100 billion agriculture losses worldwide annually (Wang et al., 2021b). *Meloidogyne* preferentially invades plant roots and forms root galls, which impede the normal uptake of water and nutrients, and further facilitates the infection of some other soil-borne phytopathogens (Makhubu et al., 2021).

PPNs accomplish their life cycles through a robust chemosensory system, which allows them to sense a variety of chemical signals from soil and plants, and their responses to these signals are mediated *via* the synergistic functions of chemoreceptors, neuropeptides, and molecular signaling pathways. For example, root exudates secreted by plants strongly attract the second-stage juveniles (J2s) of *Meloidogyne*, which play an indispensable role when nematodes migrate in soil and search for suitable feeding sites on plants (Oota et al., 2020). During this process, chemical gradients of volatile chemicals such as pinene, limonene, and tridecane, and organic acids, such as malic acid, oxalic acid, and lactic acid have been reported to be tracked by *Meloidogyne* (Wang et al., 2021a). *Meloidogyne* also shows a chemotactic response toward fats and their derivatives, including low concentrations of lauric acid from crown daisy (Dong et al., 2014). A few phytohormones, such as zeatin, ethylene, jasmonic acid, salicylic acid, and abscisic acid, contribute to the development of feeding cells and alter the attractiveness of plant roots (Wubben et al., 2004; Swiecicka et al., 2009; Fudali et al., 2013; Cabrera et al., 2014; Kirwa et al., 2018). However, repellents, such as dibutyl phthalate, palmitic acid and linoleic acid derived from plant roots, induce repulsive response in *M. incognita* J2 and thus provide protection against parasitism by PPNs (Yang et al., 2016; Dong et al., 2018).

In *C. elegans*, pathogen-induced aversive behavior is an important defense strategy that confers resistance to virulent bacteria, in addition to innate immunity. Pathogen-induced aversive behavior also keeps the nematodes away from predators or tainted food. Several canonical molecular signaling pathways, such as the serotonin or TGF-β pathways, are responsible for the pathogen-induced aversive behavior of *C. elegans* (Shivers et al., 2009; Melo and Ruvkun, 2012; Zhang and Zhang, 2012). However, whether PPNs use their chemosensory system to induce the similar repulsive response in the presence of biocontrol bacteria, or whether this response affects their ability to infect host plants and subsequently alter the efficiency of biocontrol agents remains unclear (Zhou et al., 2019).

In 2008, the draft genomes of *M. incognita* and *M. hapla* were published, and bioinformatic analyses have suggested that the size of the genomes of these two root-knot nematodes is significantly reduced compared with the genome of *C. elegans*; this reduction is especially pronounced for families of genes involved in stress responses and innate immunity, such as glutathione transferase, cytochrome P450, immune effector elements, G protein-coupled receptors, and chitin-degrading enzymes, which might be attributed to the parasitic lifestyle of *Meloidogyne* within host plants (Abad et al., 2008; Opperman et al., 2008). The significant differences in the genome sequences of *Meloidogyne* and *C. elegans* suggest that the repulsive response of *M. incognita* might differ from that of *C. elegans*, or even be stronger than that of *C. elegans* to compensate for the loss of genes involved in stress resistance and innate immunity. Previous studies had shown that *Bacillus* and *Pseudomonas* spp. were the most common populations that colonized the rhizosphere and could effectively antagonize root-knot nematodes for their nematocidal activity (Zhu et al., 2021; Antil et al., 2022; Gowda et al., 2022). Here, the repulsive response of *M. incognita* against two species of biocontrol bacteria, including *B. nematocida* B16 and *B. thuringiensis* Bt79, was investigated and the signal pathways underlying this behavior were elucidated. Our findings provide new insights into interspecific interactions among biocontrol bacteria, PPNs, and host plants and have implications for the development of new biocontrol strategies.

Materials and methods

Preparation of *Meloidogyne incognita*

A pure isolate of *M. incognita* was maintained on tomatoes (*Solanum lycopersicum* cv. Jingfen Champion) in the greenhouse at Yunnan University, Kunming, China. Egg masses were collected from infected plants and hatched in distilled water. The freshly hatched *M. incognita* J2s were used in subsequent experiments.

Repulsive response assay

Chemotactic assays were used to test the repulsive response of *M. incognita* on pluronic gel medium of PF-127 (Sigma-Aldrich, St. Louis, United States; Figure 1A). In the avoidance assay, 4 ml of 23% (w/v) PF-127 (liquid at 4°C) was added to a 6 cm diameter Petri dish at room temperature for the gel to solidify. Five μl of bacterial culture and LB fluid medium without bacteria, which were used as the sample and control groups, respectively, were added to opposite sides at a distance of 2 cm from the center of the plate. Approximately 100 *M. incognita* J2s were added to the center of the plate, and the lid was closed. After 6, 12, and 24 h, the numbers on both sides were counted under stereomicroscope (Nikon Co, Tokyo, Japan). The avoidance index (AI) was calculated using the following formula: (number of nematodes on the control side – number of nematodes on the sample side) /total number of nematodes; the index ranged from −1.0 to 1.0 (Shivakumara et al., 2018; Kuang et al., 2020). Locomotion, including the crawling pattern and movement tracks, was also assessed on PF-127 medium under the stereomicroscope.

10.3389/fmicb.2022.994941

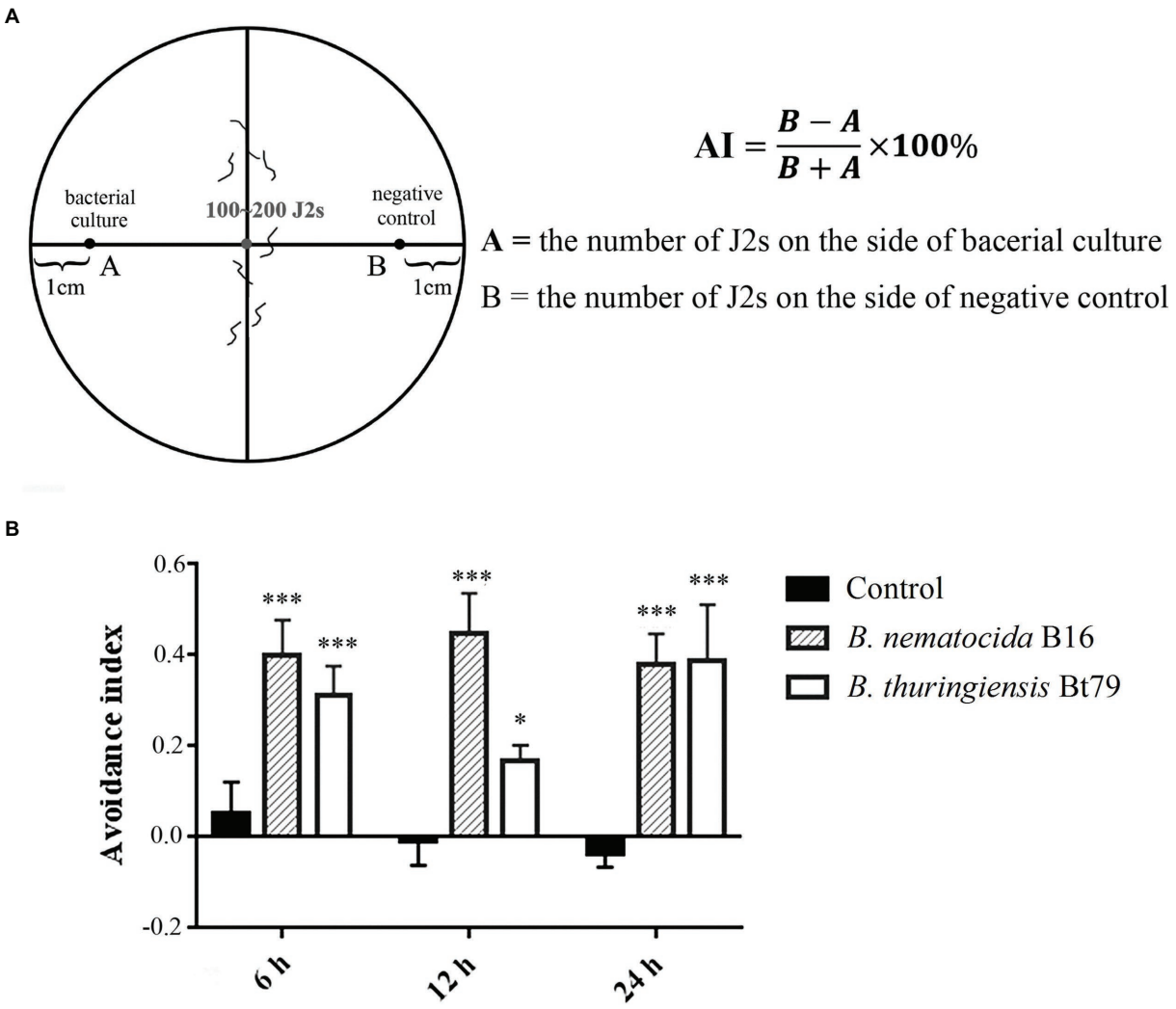

FIGURE 1
Repulsive response of *Meloidogyne incognita* second-stage juveniles (J2s) induced by different biocontrol bacteria. **(A)** Schematic diagram of the chemotaxis assay of *M. incognita* J2s on PF-127 medium. **(B)** Avoidance index of *M. incognita* J2s against different biocontrol bacteria. *p<0.05 and ***p<0.001.

Calcium imaging

Fura-2-AM (Beyotime, Shanghai, China), a fluorescent indicator with high affinity for Ca^{2+}, was used to detect the intracellular Ca^{2+} concentration (Shuang et al., 2010). Approximately 300 freshly hatched J2s were soaked in 500 μl of M9 buffer containing 2 μl of 20 mM Fura-2-AM and 10 μl of 0.5% resorcinol, and they were incubated in the dark at room temperature on a rotary mixer for 6 h and then washed several times with sterile M9 buffer. A fluorescent microscope of Nikon E800 (Nikon Co, Tokyo, Japan) was used to record the fluorescence intensity in the head neurons under 330–350 nm excitation wavelengths before and after the bacterial culture of *B. nematocida* B16 and *B. thuringiensis* Bt79 was added near J2. The software ImageJ was used to quantify the mean fluorescence intensity.

cDNA cloning of target genes from *Meloidogyne incognita*

Total RNA was extracted from 10,000 J2s by Trizol reagent (Tiangen Co., Tianjin, China). Synthesis of cDNA was performed using random primers with the Prime Script RT Reagent Kit (Takara, Dalian, China). The target cDNA of *Mi-tph-1*, *Mi-mod-1*, *Mi-dbl-1*, and *Mi-sma-6* was amplified using EX Taq DNA polymerase (Takara, Dalian, China). The components of the PCR reaction were 0.5 μl of each primer, 0.5 μl of cDNA, 2.5 μl of 10 × Ex Taq buffer, 2 μl of dNTP mix, 0.2 μl of Ex Taq DNA Polymerase, and 18.8 μl of double distilled water. The primers are shown in Table 1. The amplified fragment was then cloned into pGEM-T Easy Vector (Promega, Madison, United States), and the inserted fragment was confirmed by sequencing.

In vitro silencing of target genes

Purified PCR products were used as the template to synthesize the dsRNA of each target gene using the MEGAscript™ SP6 Transcription Kit following the method described by Shivakumara et al. (2018) (Thermo Fisher, Waltham, MA, United States). RNA interference (RNAi) treatment of nematodes was performed following a previously described method (Bakhetia et al., 2005) with minor modifications. Briefly, the freshly hatched J2s were immersed in soaking buffer with 1 mg/ml dsRNA supplemented with 0.1 mg/ml FITC, 0.1% resorcinol, 20 mM octopamine, 30 mM spermidine, and 1% gelatin on a rotary mixer in the dark at room temperature for 24 h. Fluorescein isothiocyanate (Beyotime, Shanghai, China) was used as a tracer to assess the uptake efficiency of dsRNA by observing the fluorescence intensity. *Meloidogyne incognita* J2s incubated in the soaking buffer without dsRNA probes were used as the negative control. After that, the soaked nematodes were recovered in the nuclease-free water for another 12 h. Real-time qPCR was used to evaluate the efficiency of the transcriptional knockdown of target genes.

In situ hybridization

Probe preparation and hybridization were performed using the DIG-High Prime DNA Labeling and Detection Starter Kit I (Roche, Basel, Switzerland). The probes of *Mi-tph-1* and *Mi-dbl-1* were generated by PCR using previously designed primers (see Table 1) to amplify a 200–250 base pair region from cDNA cloned in pGEM-TEasy. PCR products were then visualized on a 1.2% (w/v) agarose gel, and sequences were verified as described above. One microgram of purified PCR product was added to an RNAase-free PCR tube and mixed with ddH_2O to a volume of 16 µl. dsDNA was denatured in a boiling water bath for 10 min. The PCR tube was then quickly inserted into an ice-water mixture for 5 min to prevent the renaturation of DNA. Next, 4 µl of DIG-High Prime was added to the above PCR tube. The probe was then labeled with DIG-11-dUTP after incubation at 37°C for 20 h and at 65°C for 10 min to end the reaction. The labeled probe could be immediately used or stored at −20°C for standby application.

TABLE 1 The primers used to amplify cDNA of the target genes or the dsDNA probes for ISH.

Gene	Primer sequence 5′–3′
Mi-tph-1	GCAGAACTGTTGCTCCTCAT
Mi-tph-1 R	AGCTACTGGACGTACACGAA
Mi-mod-1	GCAAGACATGGGCTCGTTAA
Mi-mod-1 R	GGGACATAAGCCTGTAGAAT
Mi-dbl-1	ATGGGTATGCTAAACTTGTG
Mi-dbl-1 R	CGATGCGTCTTCTTCCTCTT
Mi-sma-6	CGTGTAATGCTTGGCGTTTT
Mi-sma-6 R	ATTTCCCCATATCTTCCTTT
IS-Mi-tph-1	AGCTACTGGACGTACACGAA
IS-Mi-tph-1 R	TGCATGCCAAGAATTTTTAG
IS-Mi-dbl-1	TGGCAGGATTGGATTGTTGC
IS-Mi-dbl-1 R	GGCTTTAACAACGAGCGCAT
IS-Ce-tph-1	CCGAACGGAAAACTTGGGGA
IS-Ce-tph-1 R	CCTGCCAAGAAATCACGAGC
IS-Ce-dbl-1	AACAATGATCGATTTCAAATCGAATC
IS-Ce-dbl-1 R	GGTTCGGACAGGTCACTGAA

Fixation, permeabilization, probe hybridization, and detection were conducted following the procedures of Kimber et al. (2002) with slight modifications. In short, freshly hatched *M. incognita* J2s were thoroughly washed in sterile water and fixed in 4% paraformaldehyde overnight at 4°C. After fixation, the nematodes were washed twice in M9 buffer and permeabilized using 5 mg/ml proteinase K for 25 min on a rotator at room temperature, followed by incubation in an ice bath for 20 min, incubation in methanol for 1 min (−20°C), and incubation in acetone for 1 min (−20°C).

The permeabilized nematodes were thoroughly washed with M9 buffer and resuspended in 1,000 µl of hybridization buffer for prehybridization at 42°C for 2 h. Five µl of digoxigenin-labeled dsDNA probe was diluted with 50 µl of double distilled water and heat-denatured at 95°C for 10 min, followed by an ice bath for 2 min to maintain the melted state of the probe. The denatured probe was then added to the prehybridization system for hybridization at 42°C overnight, and DIC-labeled DNA was added to the control group. The nematodes were washed two times with 2× saline sodium citrate (SSC) with 0.1% SDS at room temperature and then twice with 0.2 × SSC/0.1% SDS at 42°C, followed by one wash with maleic acid buffer for 3 min at room temperature. Hybridization was conducted for 30 min at room temperature in 1 × blocking solution diluted by maleic acid buffer. The antibody of alkaline phosphatase-conjugated anti-digoxigenin was diluted 1:5,000 by 1 × blocking solution and incubated at room temperature for 2 h, followed by washing with maleic acid buffer for 2 min and 2–5 min by detection buffer. After overnight incubation in a color substrate solution of nitroblue tetrazolium salt and 5-bromo-4-chloro-3-indolyl phosphate (NBT/BCIP) diluted 1:50 by detection buffer, the nematodes were washed twice with 0.1 × M9 buffer for 1 min each wash. The nematode specimens were then mounted on a glass slide covered with a cover slip and observed under a microscope.

Infection assay of tomato root tips

The infection assay was performed on PF-127 medium to evaluate the effect of the repulsive response induced by different biocontrol bacteria on infection of the plant roots (Dash et al., 2017). Using a pipette, ~300 J2s were added to 1.5 cm posterior to the root tips of tomato seedlings on 23% PF-127 medium in a Petri

dish with a diameter of 3 cm. Approximately 5 μl bacterial culture was added near the root tips. Roots were stained by acid fuchsin at 48 h after inoculation, and the number of *M. incognita* J2s that invaded the host plant roots was counted.

Statistical analysis

At least three technical and biological replicates were performed for all assays. All data were expressed as mean ± standard deviation. Statistical analyses were performed using one-or two-way ANOVA and *t*-tests.

Results

Repulsive response of *Meloidogyne incognita* induced by biocontrol bacteria

To determine whether the repulsive response of PPNs could be induced by biocontrol bacteria, a PF-127 chemotactic assay was conducted, and the AI was calculated for *M. incognita* J2s after sensing the volatile molecules secreted by the bacterial strains (Figure 1A). Compared with the negative control (blank media), the lawn-leaving behavior of *M. incognita* was observed after 6 h of exposure to the two biocontrol bacteria, and the AI was 0.40 ± 0.08 against *B. nematocida* B16 and 0.3 ± 0.06 against *B. thuringiensis* Bt79. As the time course was extended, the AI was increased to 0.45 ± 0.09 at 12 h and slightly decreased to 0.38 ± 0.09 at 24 h against *B. nematocida* B16. To *B. thuringiensis* Bt79, the AI was firstly decreased to 0.17 ± 0.03 at 12 h and increased to 0.39 ± 0.12 again at 24 h (Figure 1B). Thus, the PF-127 chemotactic assay demonstrated that *M. incognita* J2s can escape efficiently from the different biocontrol bacteria, which is similar with the defensive response of *C. elegans* against its bacterial pathogens (Zhang et al., 2005).

Identification of the candidate genes responsible for repulsive response of *Meloidogyne incognita*

The repulsive response of *M. incognita* J2 was observed after 6 h of exposure to biocontol bacteria, suggesting that it might involve learning-associated avoidance. We analyzed the homology of key genes of *C. elegans* in canonical signaling pathways, such as *tph-1* encoding serotonin synthase, *mod-1* encoding the GPCR receptor in the serotonin pathway, and *dbl-1* and *sma-6* encoding the ligand and receptor of the TGF-β pathway, respectively, to the genomic sequence of *M. incognita*. Alignment to these four genes revealed low similarities (30%–67%) in amino acid sequences between *M. incognita* and *C. elegans* (Table 2), which urged us to further validate their roles in repulsive response of *M. incognita*.

Involvement of candidate genes in the repulsive response of *Meloidogyne incognita*

To validate whether the homologous genes of *M. incognita* play the similar roles in repulsive response against biocontol bacteria, RNAi targeting of *Mi-tph-1* and *Mi-mod-1* in the serotonin pathway, as well as *Mi-dbl-1* and *Mi-sma-6* in the TGF-β pathway, was conducted by soaking *M. incognita* J2s in buffer containing dsRNA probes and FITC. In this reaction system, the green fluorescence of FITC was detected in esophagus and intestinal tract of *M. incognita* J2, suggesting that dsRNA of the target gene was successfully absorbed by *M. incognita* (Figure 2A). To determine the efficiency of gene knockdown, we used qRT-PCR to analyze transcription levels and found that the expression of each gene, including *Mi-tph-1*, *Mi-mod-1, Mi-dbl-1*, and *Mi-sma-6*, was significantly down-regulated as expected ($p < 0.001$; Figure 2B).

Next, the PF-127 chemotactic assay was performed again for the roles of the candidate genes in repulsive response. Knockdown of genes in either the serotonin or TGF-β pathway weakened the lawn-leaving behavior of *M. incognita* to varying degrees: the AIs of *Mi-tph-1* RNAi decreased from 0.59 ± 0.16 to-0.01 ± 0.15 and from 0.40 ± 0.18 to 0.12 ± 0.24 when *M. incognita* J2s was exposed to *B. nematocida* B16 and *B. thuringiensis* Bt79, respectively (Figure 3A); knockdown of the receptor gene *Mi-mod-1* also attenuated aversive response, and the AIs decreased to-0.03 ± 0.12 and 0.08 ± 0.03 against *B. nematocida* B16 and *B. thuringiensis* Bt79, respectively (Figure 3B). Similarly, RNAi of the other two genes in the TGF-β signaling pathway, *Mi-dbl-1* and *Mi-sma-6*, caused deficiencies in the lawn-leaving behavior against *B. nematocida* and *B. thuringiensis* (Figures 3C,D). Overall, our data indicate that both the serotonin and TGF-β pathways of *M. incognita* play the same roles in the repulsive response to biocontrol bacteria as in *C. elegans* despite their relatively low homology of gene sequences.

RNAi of *Mi-tph-1* and *Mi-mod-1* also altered the movements of *M. incognita*, and no similar effect has been described for alterations to the serotonin pathway of *C. elegans*. To confirm the potentially new function of the serotonin pathway in *M. incognita*, we tracked the movements of nematodes with *Mi-tph-1* and

TABLE 2 Homology of key genes in canonical pathways related to learning-associated avoidance between *Meloidogyne incognita* and *Caenorhabditis elegans*.

Pathway	Gene name	Homology to *C. elegans*	Gene number in *M. incognita*
Serotonin	*tph-1*	67%	Minc3s00501g13379
	mod-1	51%	Minc3s00015g00995
TGF-β	*dbl-1*	30%	Minc3s00127g05444
	sma-6	42%	Minc3s01231g21921

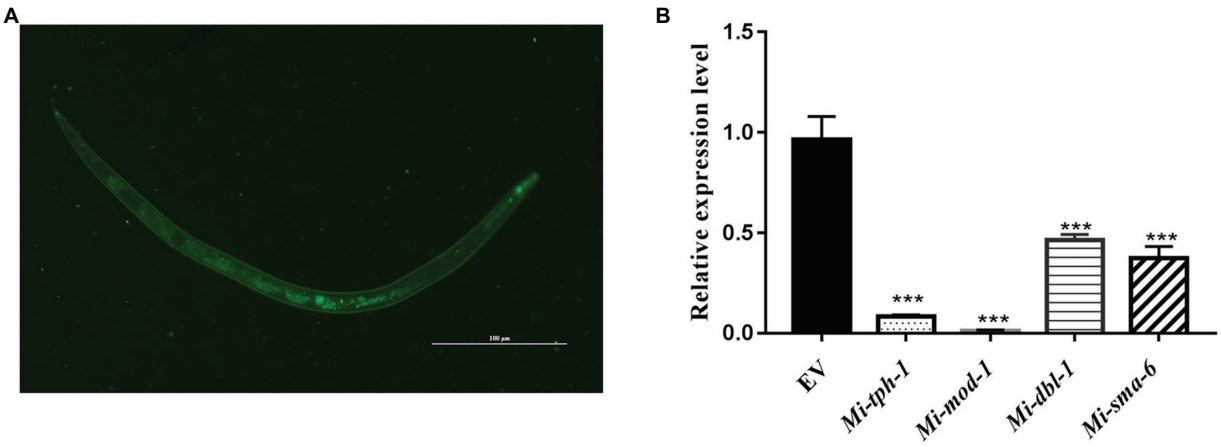

FIGURE 2
Expression levels of target genes in the RNAi treatment of *Meloidogyne incognita* second-stage juveniles (J2s). **(A)** dsRNA uptake of *M. incognita* J2s determined by the green fluorescence of FITC in the stylet, esophageal gland, and intestine. **(B)** Relative expressional levels of target genes, including *Mi-tph-1*, *Mi-mod-1*, *Mi-dbl-1* and *Mi-sma-6*, quantified by qRT-PCR. EV refers to the control group with empty vector. ***$p<0.001$.

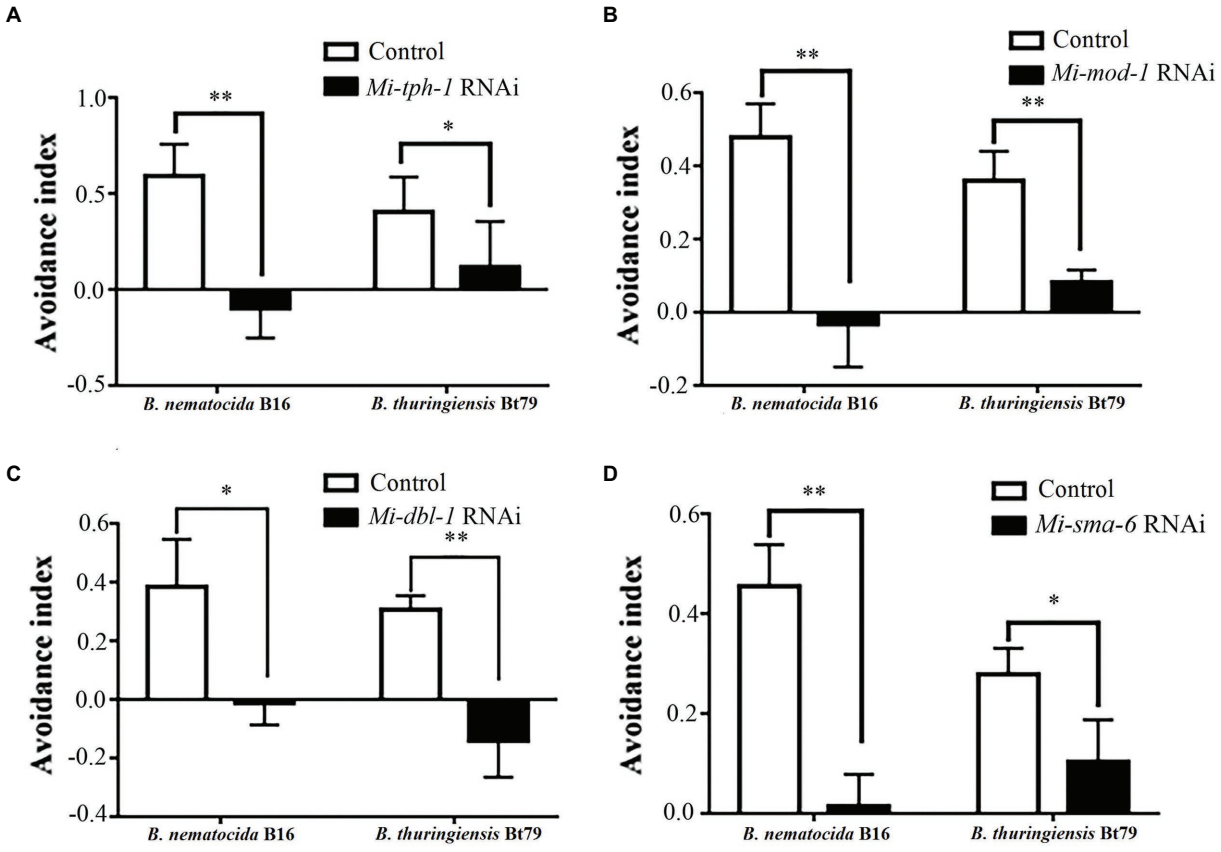

FIGURE 3
Avoidance index of *Meloidogyne incognita* against different biocontrol bacteria after RNAi treatment of target genes. RNAi of *Mi-tph-1* **(A)**, *Mi-mod-1* **(B)**, *Mi-dbl-1* **(C)**, and *Mi-sma-6* **(D)**. *$p<0.05$ and **$p<0.01$.

Mi-mod-1 knocked down by RNAi. Compared with the control group of *M. incognita* with only empty vector, which displayed crooked movement trajectories on PF-127 medium, the movement patterns of *M. incognita* with either *Mi-tph-1* or *Mi-mod-1* knocked down were altered; specifically, the swing amplitude of the body was reduced, and the traces of the nematodes were more flattened (Figure 4A). No differences in body rigidity and movement patterns were observed in N2, *tph-1(mg280)*, and *mod-1(ok103)* of *C. elegans* (Figure 4B).

Neuronal localization of the serotonin and TGF-β pathways in *Meloidogyne incognita*

To identify the neuron(s) involved in the repulsive response of *M. incognita* against biocontrol bacteria, we measured intracellular changes in Ca^{2+} using Fura-2-AM imaging. Once the bacterial culture of either *B. nematocidal* B16 or *B. thuringiensis* Bt79 was sensed by *M. incognita* J2 and the repulsive response was stimulated, the fluorescence enhancement of Ca^{2+} was detected in multiple amphid neurons of *M. incognita* J2 (Figure 5A), which was further supported by a statistical significance of the average fluorescence intensities within the amphid neurons at 0 min and 5 min (Figure 5B).

As previous studies have reported that the aversive behavior of *C. elegans* depends on the functioning of *tph-1* in ADF neurons and *dbl-1* in AVA neurons (Zhang et al., 2005; Zhang and Zhang, 2012), we characterized their neuronal localization in *M. incognita*. ISH revealed that these two genes exhibited similar expressional patterns in the amphid neurons, with *Mi-tph-1* mainly localized in ADF/NSM neurons (Figures 6A,B) and *Mi-dbl-1* in AVA neurons (Figures 6C,D).

Repulsive response of *Meloidogyne incognita* suppresses their invasion into host plants

Infection experiments was designed to investigate whether the repulsive response affects the colonization of PPNs within host plants or alters the efficiency of biocontrol bacteria (Figure 7A). Treatment of either *B. nematocida* B16 or *B. thuringiensis* Bt79 significantly decreased the number of nematodes inside tomato roots 48 h (Figure 7B). Statistical analysis to 10 samples in each treatment suggested that the average numbers of nematodes in the root tips were 1.30 ± 1.34 and 2.07 ± 1.62 in the groups treated with *B. nematocida* B16 and *B. thuringiensis* Bt79, which were 4.42 and 2.78 times lower than that of the control (5.75 ± 2.44), respectively (Figure 7C).

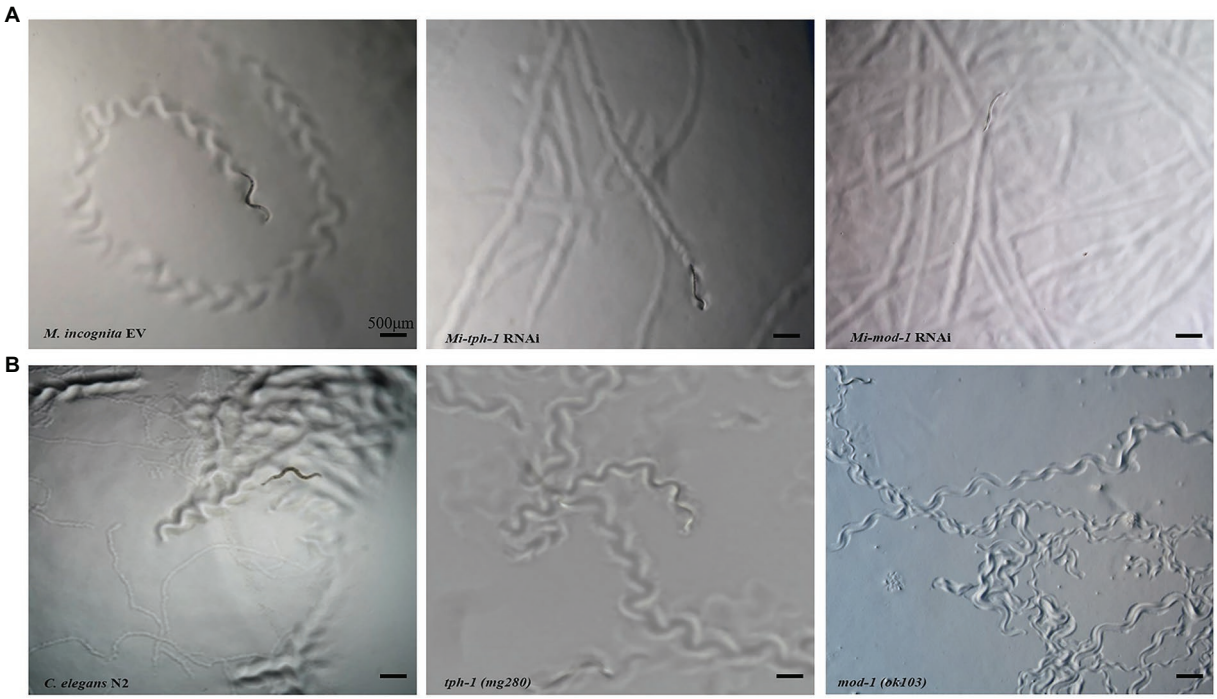

FIGURE 4
Effects of inactivating the serotonin signaling pathway on the movement trajectory of *Meloidogyne incognita*. **(A)** Movement traces of the control with empty vector, *Mi-tph-1* RNAi, and *Mi-mod-1* RNAi of *M. incognita*. **(B)** Movement traces of the wild type nematodes (N2), *tph-1(mg280)*, and *mod-1(ok103)* of *Caenorhabditis elegans*.

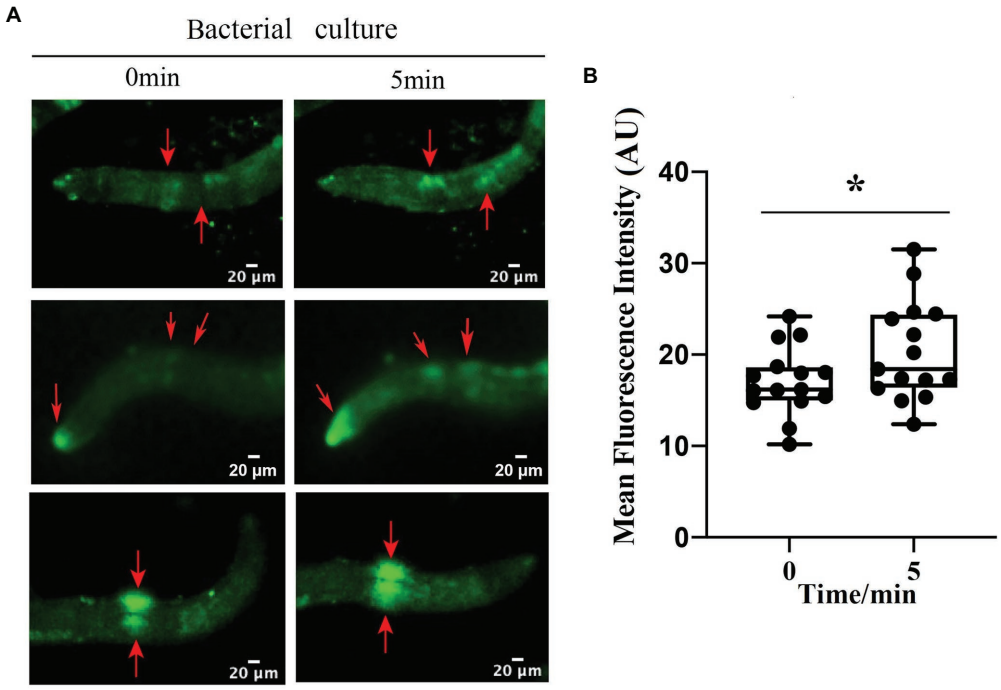

FIGURE 5
Involvement of multiple amphid neurons in the repulsive response of *Meloidogyne incognita*. **(A)** Images of intracellular Ca^{2+} measurements on the amphid neurons using Fura-2-AM. **(B)** Quantitative analysis to the mean fluorescence intensity in the amphid neurons before and after adding the bacterial culture (n=15). *p<0.05.

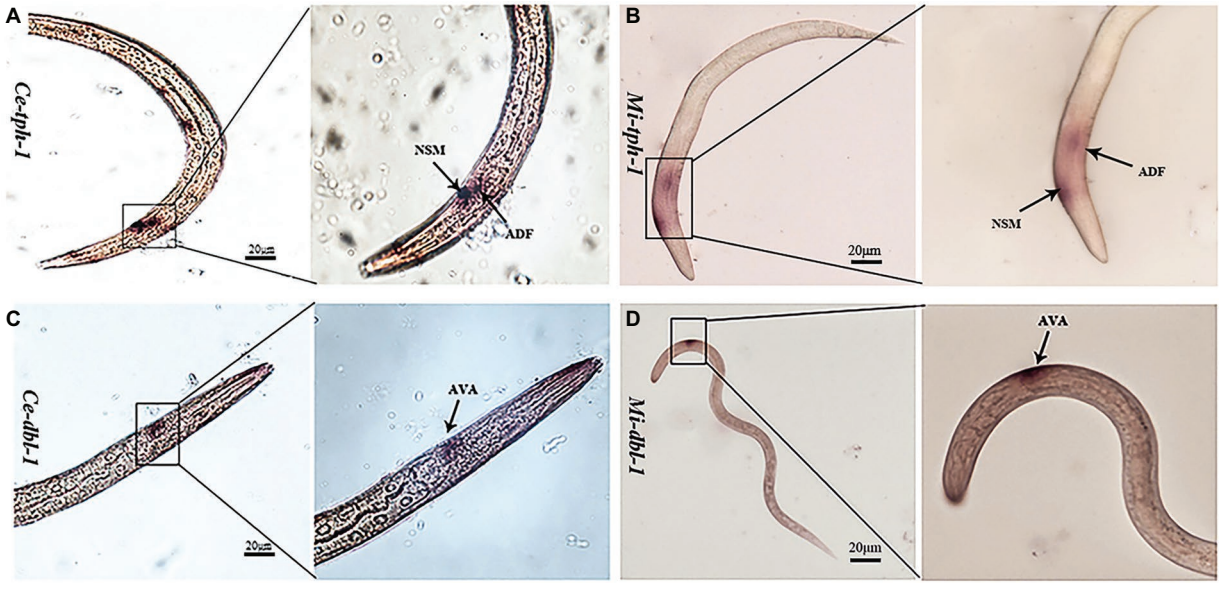

FIGURE 6
Comparisons of the neuronal localization. *In situ* hybridization with the DIG-labeled probes of *Ce-tph-1 in Caenorhabditis elegans* **(A)** and *Mi-tph-1* in *Meloidogyne incognita* **(B)** on NSM and ADF neurons, *Ce-dbl-1 in C. elegans* **(C)** and *Mi-dbl-1* in *M. incognita* **(D)** on AVA neurons.

Discussion

In natural ecosystems, rhizosphere microbiota participates in interactions between nematodes and plants. The symbiotic bacteria of plants, such as *Bacterillus* and *Pseudomonas*, synthesize hundreds of compounds to either stimulate plant growth or enhance the resistance to nematodes (Santoyo, 2021). Additionally, a few non-virulence bacteria, acting as the food of

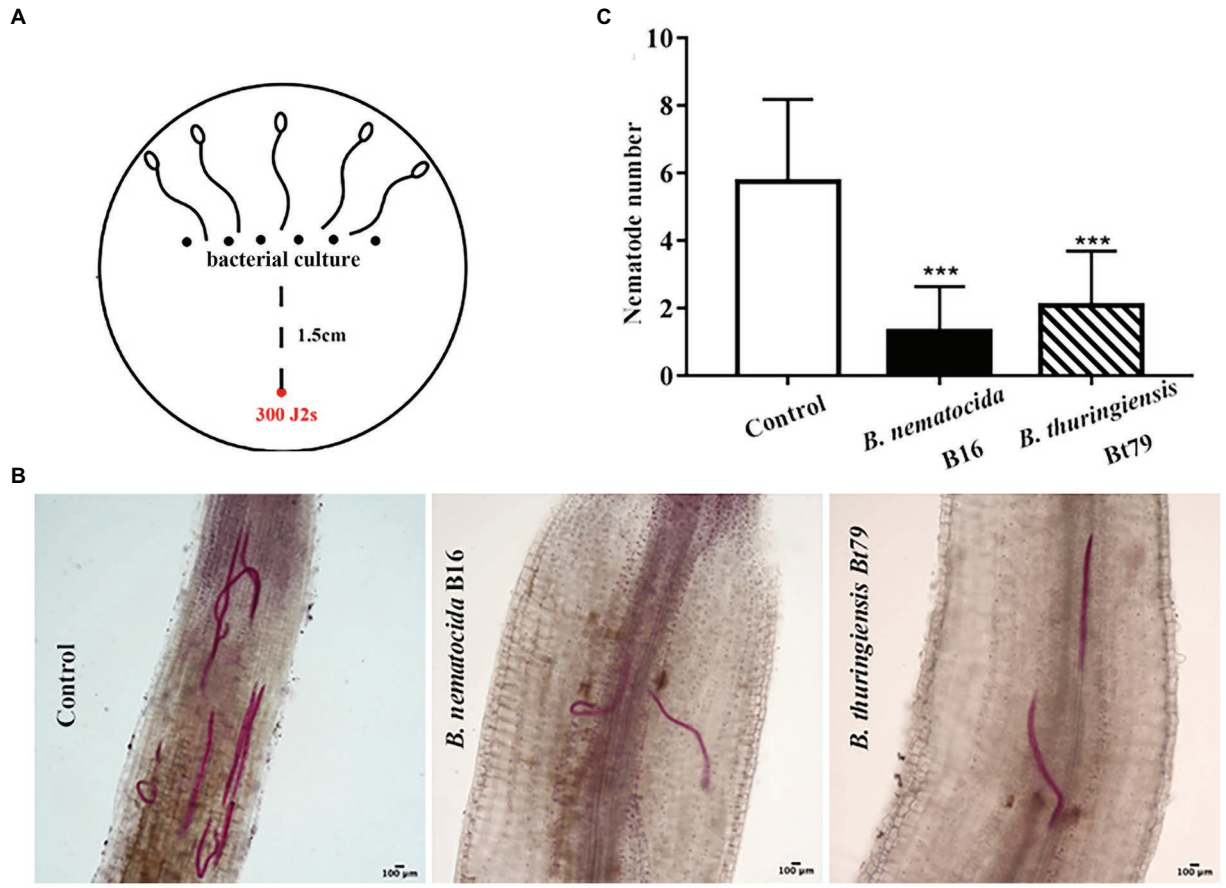

FIGURE 7
Induction of the repulsive response of *Meloidogyne incognita* by biocontrol bacteria suppresses the invasion of *M. incognita* into host plants. **(A)** Schematic diagram of the assay for evaluating the effects of repulsive response on the invasion of *M. incognita* second-stage juveniles (J2s) into tomato roots. **(B)** Stained nematodes that have invaded tomato roots after 48h. **(C)** The numbers of nematodes inside tomato roots (n =10). ***p<0.001.

bacterivorous nematodes, have developed a strategy to mobilize their ally of nematode-trapping fungi to help them kill nematodes (Wang et al., 2014).

The biocontrol bacteria, *B. nematocidal* and *B. thuringiensis*, can induce the repulsive response of *M. incognita* J2s after 6h of exposure to inhibit their invasion of host plants. But what's interesting is that the AI index for *B. thuringiensis* Bt79 was once decreased at 12h, and then continued to increase at 24h. This change trend seems different from that of *B. nematocidal* B16, which retains a constant increase at all time points. It may be due to the differential volatile compounds between *B. nematocidal* and *B. thuringiensis*.

The pathogenic bacterium *P. aeruginosa* PA14 can stimulate learning-associated avoidance in *C. elegans* after 4h of exposure, and this might increase their survival rate during infection (Zhang et al., 2005). A few molecular mechanisms have been suggested to underlie these behaviors. First, serotonin from ADF chemosensory neurons is increased by transcriptional and post-transcriptional mechanisms. After binding to its receptor MOD-1, a serotonin-gated chloride channel localized to the sensory interneurons AIY and AIZ, serotonin promotes the aversive learning of *C. elegans* against *P. aeruginosa* PA14 (Zhang et al., 2005; Melo and Ruvkun, 2012). The module DBL-1/SMA-6 in the TGF-β signaling pathway is also thought to be required for the lawn-escaping behavior of *C. elegans*. After aversive training with *P. aeruginosa* PA14, the repressed activity of AVA interneurons triggers an increase in the expression of the ligand DBL-1, which binds to the type I TGF-β receptor SMA-6 on ASI neurons, promotes olfactory plasticity, and induces a strong aversive response (Zhang and Zhang, 2012). In light of differences in the genomic sequences between *M. incognita* and *C. elegans* and limitations in current research techniques, the genes, molecular pathways, and neural circuits involved in the repulsive response of *M. incognita* require further study.

Sequence alignment of the genes involved in the above two classical pathways between *C. elegans* and *M. incognita* revealed a similarity >50% for genes in the serotonin pathway

and 30%–42% for genes in the TGF-β signaling pathway. Silencing of the key genes in both pathways decreased the AIs of *M. incognita* J2 against biocontrol bacteria, which confirmed that they played similar roles in the repulsive response of *M. incognita*. Ca^{2+} imaging with Fura-2-AM and ISH showed that both sets of genes functioned in the same neural circuits in *M. incognita* as in *C. elegans*. However, the contributions of these signaling pathways vary to the repulsive response induced by the different biocontrol bacteria. Additionally, a novel role of serotonin pathway has also been suggested to modulate the muscle tone of *M. incognita*, as decreased body swing amplitude and more flattened traces were observed following RNAi of *Mi-tph-1* and *Mi-mod-1*, and such changes are absent in *C. elegans*. We speculate that this might be explained by the fact that the reduced genome of *M. incognita* possesses genes that are responsible for more biological activities.

The repulsive response of *M. incognita* induced by biocontrol bacteria likely affects interspecific interactions among bacteria, PPNs, and host plants. In agriculture, the control of PPNs is fairly difficult because the nematodes generally inhabit soil and attack the underground parts of plants. Chemical nematicides have long been thought to be the most effective approach for controlling PPNs. Due to their high toxicity, as well as the ease with which they form residues and can be abused, the use of chemical nematicides can have deleterious effects on the environment and cause the serious pollution for agricultural products. Therefore, biological control, which is a more environmentally friendly alternative that exploits the interactions between nematode-antagonistic microorganisms and their hosts, provides a more robust complementary approach. Nematode-antagonistic microorganisms employ different strategies to alleviate PPN infections in plants. Theoretical studies of their interactions are of great value to improve the efficacy of biocontrol by enhancing the virulence factors of biocontrol microorganisms and weakening the defensive response of PPNs.

Since semiochemicals have been successfully used to control pests (Park et al., 2003; Lee et al., 2004), and the infection efficiencies of *M. incognita* can be greatly reduced *via* induction of the repulsive response by biocontrol bacteria, we believe the results of our study provide new insights into the biocontrol control of PPNs.

Data availability statement

The original contributions presented in the study are included in the article/supplementary material, further inquiries can be directed to the corresponding author.

Author contributions

XH conceived and designed the study. YZ and QZ conducted experiments, searched the literature and wrote the manuscript. XH, CZ, and KZ revised the manuscript. XH and CZ supplied funding. All authors contributed to the article and approved the submitted version.

Funding

This work was supported by the National Natural Science Foundation of China (grant number 32170184, 32060632, and U1802233) and the Department of Science and Technology of Yunnan Province (grant number 2019FA046).

Acknowledgments

We would like to acknowledge the State Key Lab for Conservation and Utilization of Bio-Resources for supplying the experimental platform.

Conflict of interest

The authors declare that the research was conducted in the absence of any commercial or financial relationships that could be construed as a potential conflict of interest.

Publisher's note

All claims expressed in this article are solely those of the authors and do not necessarily represent those of their affiliated organizations, or those of the publisher, the editors and the reviewers. Any product that may be evaluated in this article, or claim that may be made by its manufacturer, is not guaranteed or endorsed by the publisher.

References

Abad, P., Gouzy, J., Aury, J. M., Castagnone-Sereno, P., Danchin, E. G. J., Deleury, E., et al. (2008). Genome sequence of the metazoan plant-parasitic nematode *Meloidogyne incognita*. *Nat. Biotechnol.* 26, 909–915. doi: 10.1038/nbt.1482

Antil, S., Kumar, R., Pathak, D. V., Kumar, A., Panwar, A., and Kumari, A. (2022). Plant growth-promoting rhizobacteria – *Bacillus cereus* KMT-5 and *B. megaterium* KMT-8 effectively suppressed *Meloidogyne javanica* infection. *Appl. Soil Ecol.* 174:104419. doi: 10.1016/j.apsoil.2022.104419

Bakhetia, M., Charlton, W., Atkinson, H. J., and Mc Pherson, M. J. (2005). RNA interference of dual oxidase in the plant nematode Meloidogyne incognita. *Mol. Plant Microbe.* 18, 1099–1106. doi: 10.1094/MPMI-18-1099

Cabrera, J., Barcala, M., Fenoll, C., and Escobar, C. (2014). Transcriptomic signatures of transfer cells in early developing nematode feeding cells of *Arabidopsis* focused on auxin and ethylene signaling. *Front. Plant Sci.* 5:107. doi: 10.3389/fpls.2014.00107

Dash, M., Dutta, T. K., Phani, V., Papolu, P. K., Shivakumara, T. N., and Rao, U. (2017). RNAi-mediated disruption of neuropeptide genes, *nlp-3* and *nlp-12*, cause multiple behavioral defects in *Meloidogyne incognita*. *Biochem. Biophys. Res. Commun.* 490, 933–940. doi: 10.1016/j.bbrc.2017.06.143

Dong, L. L., Li, X. L., Huang, L., Gao, Y., Zhong, L. N., Zheng, Y. Y., et al. (2014). Lauric acid in crown daisy root exudate potently regulates root-knot nematode chemotaxis and disrupts mi-flp-18 expression to block infection. *J. Exp. Bot.* 65, 131–141. doi: 10.1093/jxb/ert356

Dong, L., Li, X., Huang, C., Lu, Q., Li, B., Yao, Y., et al. (2018). Reduced *Meloidogyne incognita* infection of tomato in the presence of castor and the involvement of fatty acids. *Sci. Hortic.* 237, 169–175. doi: 10.1016/j.scienta.2018.03.066

Fudali, S. L., Wang, C. L., and Williamson, V. M. (2013). Ethylene signaling pathway modulates attractiveness of host roots to the root-knot nematode *Meloidogyne hapla*. *Mol. Plant Microbe In.* 26, 75–86. doi: 10.1094/mpmi-05-12-0107-r

Gowda, M. T., Meena, B. R., Krishnan, N., Manjunath, M., Sellaperumal, C., Rai, A. B., et al. (2022). Antimicrobial peptides producing native *bacillus* spp. for the management of root-knot nematode *Meloidogyne incognita* infecting okra (*Abelmoschus esculentus* L. Moench). *Biol. Control* 171:104951. doi: 10.1016/j.biocontrol.2022.104951

Kimber, M. J., Fleming, C. C., Prior, A., Jones, J. T., Halton, D. W., and Maule, A. G. (2002). Localisation of *Globodera pallid* FMRFamide-related peptide encoding genes using in situ hybridisation. *Int. J. Parasitol.* 32, 1095–1105. doi: 10.1016/s0020-7519(02)00084-x

Kirwa, H. K., Murungi, L. K., Beck, J. J., and Torto, B. (2018). Elicitation of differential responses in the root-knot nematode *Meloidogyne incognita* to tomato root exudate cytokinin, flavonoids, and alkaloids. *J. Agric. Food Chem.* 66, 11291–11300. doi: 10.1021/acs.jafc.8b05101

Kuang, M. S., Liu, T. T., Wu, H. B., Lan, H. P., Wen, Y. X., Wu, H. B., et al. (2020). Constituents leached by tomato seeds regulate the behavior of root-knot nematodes and their antifungal effects against seed-borne fungi. *J. Agric. Food Chem.* 68, 9061–9069. doi: 10.1021/acs.jafc.0c01797

Lee, B. H., Annis, P. C., Tumaalii, F., and Choi, W. S. (2004). Fumigant toxicity of essential oils from the Myrtaceae family and 1, 8-cineole against 3 major stored-grain insects. *J. Sto. Pro. Res.* 40, 553–564. doi: 10.1016/j.jspr.2003.09.001

Makhubu, F. N., Khosa, M. C., and McGaw, L. J. (2021). South African plants with nematicidal activity against root-knot nematodes: a review. *S. Afr. J. Bot.* 139, 183–191. doi: 10.1016/j.sajb.2021.02.010

Melo, J., and Ruvkun, G. (2012). Inactivation of conserved *C. elegans* genes engages pathogen-and xenobiotic-associated defenses. *Cell* 149, 452–466. doi: 10.1016/j.cell.2012.02.050

Oota, M., Tsai, A. Y., Aoki, D., Matsushita, Y., Toyoda, S., Fukushima, K., et al. (2020). Identification of naturally occurring polyamines as root-knot nematode attractants. *Mol. Plant* 13, 658–665. doi: 10.1016/j.molp.2019.12.010

Opperman, C. H., Bird, D. M., Williamson, V. M., Rokhsar, D. S., Burke, M., Cohn, J., et al. (2008). Sequence and genetic map of *Meloidogyne hapla*: A compact nematode genome for plant parasitism. *Proc. Natl. Acad. Sci. U. S. A.* 105, 14802–14807. doi: 10.1073/pnas.0805946105

Park, I. K., Lee, S. G., Choi, D. H., Park, J. D., and Ahn, Y. J. (2003). Insecticidal activities of constituents identified in the from leaves of *Chamaecyparis obtusa* against *Callosobruchus chinensis* (L.) and *Sitophilus oryzae* (L.). *J. Sto. Pro. Res.* 39, 375–384. doi: 10.1016/S0022-474X(02)00030-9

Santoyo, G. (2021). How plants recruit their microbiome? New insights into beneficial interactions. *J. Adv. Res.* doi: 10.1016/j.jare.2021.11.020 (in press).

Shivakumara, T. N., Dutta, T. K., and Rao, U. (2018). A novel in vitro chemotaxis bioassay to assess the response of *Meloidogyne incognita* towards various test compounds. *J. Nematol.* 50, 487–494. doi: 10.21307/jofnem-2018-047

Shivers, R. P., Kooistra, T., Chu, S. W., Pagano, D. J., and Kim, D. H. (2009). Tissue-specific activities of an immune signaling module regulate physical response to pathogenic and nutritional bacteria in *C. elegans*. *Cell Host Microbe* 6, 321–330. doi: 10.1016/j.chom.2009.09.001

Shuang, S. M., Qiao, X. N., Wang, D. D., Fan, L., Lu, D. T., Mu, L. X., et al. (2010). Analytical behavior of Fura-2 and its determination of $[Ca^{2+}]_i$ in lymphocytes treated with cefotaxime. *J. Meas. Sci. Instru.* 1, 395–400. doi: 10.3969/j.issn.1674-8042.2010.04.21

Swiecicka, M., Filipecki, M., Lont, D., Vliet, J. V., Qin, L., Goverse, A., et al. (2009). Dynamics in the tomato root transcriptome on infection with the potato cyst nematode *Globodera rostochiensis*. *Mol. Plant Pathol.* 10, 487–500. doi: 10.1111/j.1364-3703.2009.00550.x

Wang, J. X., Ding, Z. J., Bian, J., Bo, T. T., and Liu, Y. J. (2021a). Chemotaxis response of *Meloidogyne incognita* to volatiles and organic acids from root exudates. *Rhizosphere* 17:100320. doi: 10.1016/j.rhisph.2021.100320

Wang, S., Fan, H. Y., Zhao, D., Zhu, X. F., Wang, Y. Y., Liu, X. Y., et al. (2021b). Multifunctional efficacy of the nodule endophyte *Pseudomonas fragi* in stimulating tomato immune response against *Meloidogyne incognita*. *Biol. Control* 164:104773. doi: 10.1016/j.biocontrol.2021.104773

Wang, X., Li, G. H., Zou, C. G., Ji, X. L., Liu, T., Zhao, P. J., et al. (2014). Bacteria can mobilize nematode-trapping fungi to kill nematodes. *Nat. Commun.* 5:5776. doi: 10.1038/ncomms6776

Wubben, M. J. E., Rodermel, S. R., and Baum, T. J. (2004). Mutation of a UDP-glucose-4-epimerase alters nematode susceptibility and ethylene responses in *Arabidopsis* roots. *Plant J.* 40, 712–724. doi: 10.1111/j.1365-313x.2004.02257.x

Yang, G. D., Zhou, B. L., Zhang, X. Y., Zhang, Z. J., Wu, Y. Y., Zhang, Y. M., et al. (2016). Effects of tomato root exudates on *Meloidogyne incognita*. *PLoS One* 11:e0154675. doi: 10.1371/journal.pone.0154675

Zhang, Y., Hang, L., and Bargmann, C. I. (2005). Pathogenic bacteria induce aversive olfactory learning in *Caenorhabditis elegans*. *Nature* 438, 179–184. doi: 10.1038/nature04216

Zhang, X., and Zhang, Y. (2012). DBL-1, a TGF-β, is essential for *Caenorhabditis elegans* aversive olfactory learning. *Proc. Natl. Acad. Sci. U. S. A.* 109, 17081–17086. doi: 10.1073/pnas.1205982109

Zhou, Q. Y., Zhu, M., Huang, H., and Huang, X. W. (2019). Chemosensory system of plant parasitic nematodes. *Sci. Sin. Vitae* 49, 828–838. doi: 10.1360/SSV-2019-0092

Zhu, M., Chen, Y., Zhao, N. H., Bai, H., Zhang, K. Q., and Huang, X. W. (2021). Multiple olfactory pathways contribute to the lure process of *Caenorhabditis elegans* by pathogenic bacteria. *Sci. China Life Sci.* 64, 1346–1354. doi: 10.1007/s11427-020-1842-7

frontiers | Frontiers in Microbiology

TYPE Review
PUBLISHED 28 September 2022
DOI 10.3389/fmicb.2022.1018504

OPEN ACCESS

EDITED BY
Maofeng Jing,
Nanjing Agricultural University, China

REVIEWED BY
Jia Li,
Nanjing Agricultural University, China
Shitou Xia,
Hunan Agricultural University, China
Guan-Feng Wang,
Shandong University, China

*CORRESPONDENCE
Wenya Yuan
wyyuan@hubu.edu.cn
Haitao Zhang
zht@hubu.edu.cn

†These authors have contributed equally to this work and share first authorship

SPECIALTY SECTION
This article was submitted to Microbe and Virus Interactions with Plants,
a section of the journal Frontiers in Microbiology

RECEIVED 13 August 2022
ACCEPTED 09 September 2022
PUBLISHED 28 September 2022

CITATION
Zhang B, Liu M, Wang Y, Yuan W and Zhang H (2022) Plant NLRs: Evolving with pathogen effectors and engineerable to improve resistance. *Front. Microbiol.* 13:1018504. doi: 10.3389/fmicb.2022.1018504

Plant NLRs: Evolving with pathogen effectors and engineerable to improve resistance

Biaoming Zhang†, Mengting Liu†, Yanchao Wang†, Wenya Yuan* and Haitao Zhang*

State Key Laboratory of Biocatalysis and Enzyme Engineering, School of Life Sciences, Hubei University, Wuhan, China

Pathogens are important threats to many plants throughout their lifetimes. Plants have developed different strategies to overcome them. In the plant immunity system, nucleotide-binding domain and leucine-rich repeat-containing proteins (NLRs) are the most common components. And recent studies have greatly expanded our understanding of how NLRs function in plants. In this review, we summarize the studies on the mechanism of NLRs in the processes of effector recognition, resistosome formation, and defense activation. Typical NLRs are divided into three groups according to the different domains at their N termini and function in interrelated ways in immunity. Atypical NLRs contain additional integrated domains (IDs), some of which directly interact with pathogen effectors. Plant NLRs evolve with pathogen effectors and exhibit specific recognition. Meanwhile, some NLRs have been successfully engineered to confer resistance to new pathogens based on accumulated studies. In summary, some pioneering processes have been obtained in NLR researches, though more questions arise as a result of the huge number of NLRs. However, with a broadened understanding of the mechanism, NLRs will be important components for engineering in plant resistance improvement.

KEYWORDS

plant immunity, NLR, pathogen effector, resistosome, engineering, interaction

Introduction

A large number of microbes are pathogens for plants, which cause different kinds of diseases. However, plants have developed many strategies to acquire resistance to most of the pathogens after a long time of evolution. It is well known that there are two layers of innate immunity in plants. The first layer is composed of membrane-anchored receptors that can interact with small conserved molecules called pathogen-associated molecular patterns (PAMPs) or microbe-associated molecular patterns (MAMPs). Therefore, these receptors are named as pattern recognition receptors (PRRs) and initiate PAMP-triggered immunity (PTI) (Jones and Dangl, 2006). The level of PTI is usually weak and non-specific, which can easily be overcome by pathogen effectors

(Jones and Dangl, 2006; Zhang and Wang, 2013). Comparatively, the second layer of plant immunity is controlled by special intracellular receptors that can recognize the effectors and trigger severe resistance, which is known as effector-triggered immunity (ETI) (Jones and Dangl, 2006; van Wersch et al., 2019).

Based on the phenotype after pathogen invasion, plant disease resistance can be classified as qualitative resistance and quantitative resistance. Genetically speaking, qualitative resistance is conferred by a single *resistance* (*R*) gene or a pair of related *R* genes, in a few cases, in plants. The *R* genes can confer resistance to pathogens that carry *avirulence* (*avr*) genes in the way known as the "gene for gene" hypothesis. Meanwhile, quantitative resistance is controlled by multiple different genes or loci in the genome. Usually, qualitative resistance is pathogen race-specific and can be even complete resistance, while quantitative resistance is pathogen race-nonspecific and partial resistance. Qualitative resistance is also simple and easy to manipulate. As a result, it is widely used in mechanism studies and crop improvement. To date, the number of cloned plant *R* genes is more than 300 (Kourelis and van der Hoorn, 2018). Although these *R* genes encode many different kinds of proteins, a large portion of the proteins belongs to nucleotide binding, leucine-rich repeat proteins (NLRs), which are also the most common intracellular receptors in ETI (Kourelis and van der Hoorn, 2018).

Plant NLRs harbor similar structural similarities that they all have an NB-ARC (nucleotide-binding adaptor, APAF-1, R proteins, and CED-4) domain and a leucine-rich repeat (LRR) domain. The N-termini of the typical NLRs are different, but only a few domains or motifs exist in this region, such as the Toll/interleukin receptor (TIR) domain, coiled-coil (CC) motif, or resistance to powdery mildew 8 (RPW8) domain. Based on these domains, the typical NLRs can be grouped into three groups, TIR-NLRs (TNLs), CC-NLRs (CNLs), and RPW8-NLRs (RNLs) (Maruta et al., 2022). Many TNLs and CNLs can interact with effectors directly or indirectly and are called "sensor" NLRs (sNLRs); by contrast, many RNLs function redundantly at downstream of TNLs and CNLs and are called "helper" NLRs (hNLRs) instead (Jubic et al., 2019). Intriguingly, not all hNLRs are RNLs. A special family of CNLs named as NRC (NB-LRR protein required for HR-associated cell death) family also belongs to hNLRs (Jubic et al., 2019).

However, there are still some atypical NLRs, which include additional integrated domains (IDs), such as WRKY, kinase, heavy metal-associated (HMA), and zinc-finger BED (zf-BED) domains (Brueggeman et al., 2008; Le Roux et al., 2015; Maqbool et al., 2015; Sarris et al., 2015; Marchal et al., 2018; Ji et al., 2020; Zhang et al., 2020). Some IDs interact with corresponding pathogen effectors, and thereby they are recognized as "integrated decoys" (Jones et al., 2016; Kroj et al., 2016). Such atypical NLRs are also named as NLRs with integrated domains (NLR-IDs), and many of them function together with other NLRs as NLR pairs (also called paired NLRs) (Jones et al., 2016). In this review, we summarize the research on the mechanism of NLRs in accordance with their classification. We then discuss about the recent attempts at NLR engineering, which brings us into a new research field.

Most CNLs interact indirectly with effectors to confer resistance

The significant feature of CNLs is that most of them recognize the cognate effectors in an indirect manner. There are two models for describing this kind of recognition. The first is the "guard" model, in which the pathogen effectors interact with and modify their target proteins in plant cells, while the NLRs can monitor the integrity and modification of these target proteins. As a result, the NLRs are called "guarders" and the target proteins are "guardees". Once the guardees changed their status, the NLRs trigger resistance in plants. The most well-known guardees are Arabidopsis RPM1-interacting protein 4 (RIN4) and PBS1, which are involved in the resistance mediated by many NLRs (Duxbury et al., 2021). The effectors AvrB and AvrRpm1 can target RIN4 and induce its phosphorylation to increase the activity of plasma membrane (PM) H^+-ATPases and regulate the stomata re-opening (Liu et al., 2009). Then phosphorylated RIN4 activates the CNL RPM1 to confer resistance in Arabidopsis (Chung et al., 2011; Liu et al., 2011). The effector AvrRpt2 also targets and cleaves RIN4 into fragments to suppress PTI (Afzal et al., 2011). Whereas the Arabidopsis CNL RPS2 can interact with intact RIN4 and become active to trigger plant defense response after RIN4 is cleaved (Axtell and Staskawicz, 2003). Similarly, another CNL RPS5 interacts with and guards PBS1 in Arabidopsis. The effector AvrPphB can cleave PBS1, leading to the activation of RPS5 (Shao et al., 2003; Ade et al., 2007).

The second is the "decoy" model, which is a derivative and modification of the "guard" model. Compared with "guardees", which usually are functional proteins and involved in defense response, many "decoys" barely have any significant function besides interacting with pathogen effectors (Jones et al., 2016; van Wersch et al., 2019). When the decoys are targeted and modified by the effectors, the NLRs recognize and interact with decoys to trigger defense reactions (Duxbury et al., 2021). One example is the Arabidopsis CNL ZAR1, which recognizes multiple decoys to confer resistance to diverse pathogens. The effector AvrAC of *Xanthomonas campestris* pathovar *campestris* uridylylates many proteins in Arabidopsis, such as BIK1 and RIPK, to attenuate their function in immunity (Feng et al., 2012). Whereas, PBL2, a homolog of BIK1, acts as a decoy and can be uridylylated by AvrAC, though it is not required for AvrAC virulence. And the uridylylated PBL2, $PBL2^{UMP}$, can be recruited to the preformed complex of ZAR1 and RKS1 to trigger immunity (Wang et al., 2015). Nevertheless, it is

difficult to make a distinction between "guardee" and "decoy" for certain proteins. Taking PBS1 as an example, although its homologs participate in PTI and also can be cleaved by the effector AvrPphB, PBS1 has the weakest function in PTI. As a result, PBS1 is also regarded as a "decoy" for AvrPphB (Zhang et al., 2010).

The sophisticated indirect interaction between CNLs and effectors is well-proved by the structure information of ZAR1. Before $PBL2^{UMP}$ is recognized by the pre-active complex of ZAR1-RKS1, ZAR1 binds ADP through its NB domain and remains inactive. After the interaction between $PBL2^{UMP}$ and RKS1, ADP is released and the conformation of the ZAR1 NB domain is changed (Wang et al., 2019b). With the exchange of ADP by dATP or ATP, the activated ZAR1-RKS1-$PBL2^{UMP}$ complexes further oligomerize as a pentameric resistosome to confer resistance (Wang et al., 2019a). In contrast, the corresponding effector AvrAC is not a component in the ZAR1 resistosome.

Meanwhile, a few CNLs have been found to interact directly with pathogen effectors or PAMPs. In tomatoes, a Solanaceae domain (SD) exists at the terminus of the CNL Sw-5. The Sw-5 SD physically interacts with a conserved region in the viral movement protein NSm from tospoviruses and activates Sw-5 to initiate a defense response (Li et al., 2019). In barley, proteins encoded by several alleles of the *Mla* gene can interact with many natural AVR_A effectors of barley powdery mildew pathogen in tobacco (Saur et al., 2019).

The precise function of CNLs has been studied in plants. However, the results are different and some kind of controversial from each other. In barley, the CC domain alone is sufficient to induce cell death for MAL10 (Maekawa et al., 2011; Bai et al., 2012). And self-association of the CC domain is found to be essential for MAL10-triggered immunity (Maekawa et al., 2011). In potatoes, the Rx protein triggers a hypersensitive response (HR) through its NB domain instead of the CC domain (Rairdan et al., 2008). Whereas in Arabidopsis, both the CC and NB-ARC domains are required for HR-inducing of RPS5 (Qi et al., 2012). After the discovery of the ZAR1 resistosome, the CC domain is recognized as the key element for the CNL resistosome. The CC domains formed a helical barrel in the ZAR1 resistosome, and the biochemical function of the whole resistosome has been clarified as a cation-selective channel permeable to calcium ion (Ca^{2+}) last year (Wang et al., 2019a; Bi et al., 2021). When ZAR1 resistosome is activated, it can be localized into the PM and cause Ca^{2+} influx, which results in perturbation of organelles structures, induction of reactive oxygen species (ROS), and cell death in plants (Figure 1A; Bi et al., 2021). Likewise, the Ca^{2+} influx is also increased in RPM1-mediated resistance and leads to hydrogen peroxide (H_2O_2) accumulation and HR in Arabidopsis (Grant et al., 2000). However, whether other CNLs, such as Rx, function in the same way still remains unclear now.

Many TNLs directly recognize effectors to confer resistance

The TIR domain is a well-known structure that can be found not only in plants but also in animals and bacteria. Moreover, TIR domains are critical components of innate immune proteins in both plants and animals (Ve et al., 2015). Unlike that TIR domains occur in many structurally different proteins in animals, they mainly exist in TNLs, TIR-NB (TN) proteins, which lack LRRs, and TIR-only (or named as TX) proteins in plants (Nandety et al., 2013; Ve et al., 2015). The TIR domains are involved in protein–protein interactions, including self-association. In plants, overexpression of TIR regions of several TNLs can trigger HR in an effector-independent manner. Mutations disrupting the TIR self-association affect its auto-activation and the HR reaction (Bernoux et al., 2011). Moreover, chimeric NLRs that are constructed from TIR domains of plant TNLs and other domains of mammalian NLRC4 can trigger HR in plants when co-expressed with other inflammasome components (Duxbury et al., 2020). As a result, the induced proximity of TIR domains is crucial for plant defense (Duxbury et al., 2021).

However, the function of TIR is influenced by other domains in TNLs. It has been reported that the TIR-triggered HR can be inhibited by NB-ARC domains (Bernoux et al., 2011; Schreiber et al., 2016). Cryo-electron microscopy (cryo-EM) structure information has revealed that TNLs, like tobacco ROQ1, bind ADP to keep NB-ARC domains in a closed state and inhibit self-association (Martin et al., 2020; Maruta et al., 2022). An exception is Arabidopsis RPP1, which binds ATP instead of ADP and maintains inactive by NB-ARC associated with LRR (Ma et al., 2020). Nevertheless, after the cognate effectors are recognized through the C-JIDs (C-terminal jelly roll/Ig-like domains) and LRR domains, conformations of NB-ARC domains are changed and TNLs assemble as polymers, which leads to the proximity of TIRs to trigger immunity (Ma et al., 2020; Martin et al., 2020).

Though the LRR domains participate in effector recognition, C-JIDs are the key determinants. Many studies have also revealed that truncation, deletion, or mutation in the C-JIDs impairs TNL-mediated immunity (Dodds et al., 2001; Saucet et al., 2021). Some TNLs even contain more than one C-JIDs. The *Ma* gene in Myrobalan plum encodes a TNL with five C-JIDs located at the C-terminus and confers complete-spectrum and high-level resistance to root-knot nematode (RKN) (Claverie et al., 2011; Maruta et al., 2022). While Arabidopsis RPS4, which forms an NLR pair with RPP1, is an exception (Birker et al., 2009; Narusaka et al., 2009). The C-JID of RPS4 is involved in the maintenance of its inactive state and cannot interact with the corresponding effectors (Saucet et al., 2021). In addition, the TNL N protein recognizes the 50 kDa helicase (p50) effector of the *Tobacco mosaic virus* (TMV)

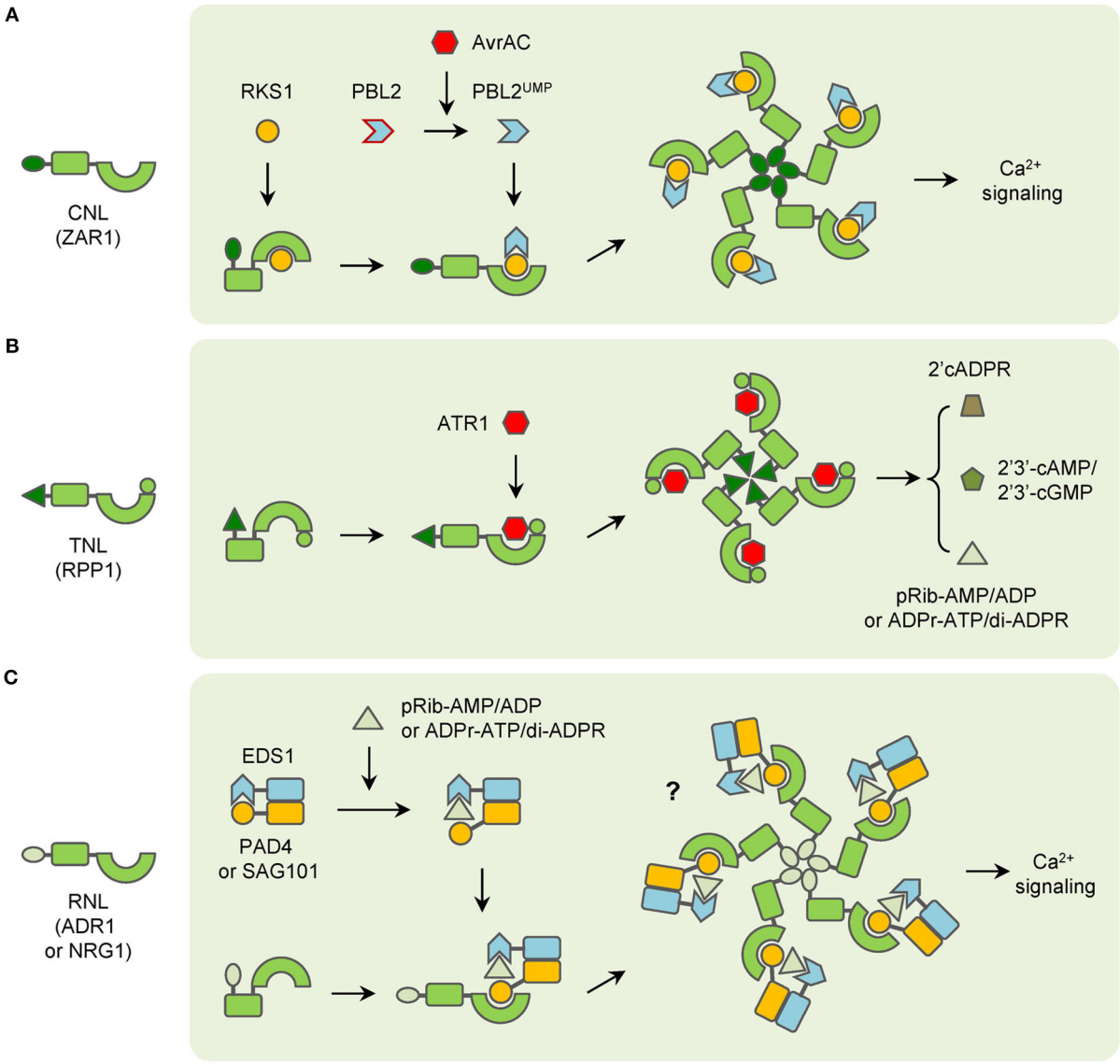

FIGURE 1
Functioning models of three groups of typical NLRs. **(A)** CNLs (ZAR1 as an example) recognize pathogen effectors indirectly and form resistosomes with associated proteins to trigger immunity. **(B)** TNLs (RPP1 as an example) directly interact with pathogen effectors and then form resistosomes in plants immunity. **(C)** RNLs (ADR1 and NRG1 as examples) function with EDS1 complexes, which are activated by TNLs-generated small molecules to trigger immunity.

through its TIR domain in an indirect manner. The N receptor-interacting protein 1 (NRIP1) interacts with both N and p50 and forms a complex in plant defense response (Caplan et al., 2008).

The biochemical function of TIR domains was unknown for a long time until it was first characterized in human protein SARM1 (sterile alpha and TIR motif containing 1), which belonged to Toll-like receptor (TLR) proteins. The SARM1-TIR domain has intrinsic NADase (nicotinamide adenine dinucleotide nucleosidase) activity and contains an essential glutamic acid residue (Essuman et al., 2017). Recently, TIR domains of many plant TNLs have been found to possess NAD^+ cleavage activity and produce cyclic adenosine diphosphate ribose (cADPR), cyclization variant of cADPR (v-cADPR), and nicotinamide (NAM) (Wan et al., 2019). Notably, the NADase activity is dependent on the self-association of TIR domains in both animals and plants (Horsefield et al., 2019; Wan et al., 2019). The self-association has also been confirmed by the cryo-EM structures of RPP1 and ROQ1. After

interacting with corresponding effectors, both TNLs assemble as tetrameric resistosomes. In each resistosome, two asymmetric TIR homodimers form a holoenzyme with two active sites at the groove in the homodimer (Ma et al., 2020; Martin et al., 2020). However, the characterization of chimeric NLRC4 that fused with plant and animal TIR domains has shown that the NADase activity is essential but not sufficient for plant defense reaction (Duxbury et al., 2020). And recently, it has been found that the plant TIR domains are bifunctional enzymes, which also synthesize 2',3'-cAMP/cGMP with DNA or RNA and lead to cell death (Yu et al., 2022).

In brief, for many TNLs, the NB-ARC and LRR domains stay in a closed state and inhibit the self-association of TIR domains to keep TNLs inactive without the presence of cognate effectors. When the effectors appear, they can interact with the C-JIDs and LRR domains of TNLs. After recognition, the conformation of NB-ARC domains is changed and they participate in self-association and lead to the oligomerization of TNLs. Then the assembly of activated TNLs induces the proximity of TIR domains to make up the holoenzymes and generate certain molecules. The molecules of the resistosomes then transduce the signaling to other downstream components in plant immunity (Figure 1B).

Most RNLs are crucial downstream components of NLR signaling

There are two families of RNLs, the ADR1 (ACTIVATED DISEASE RESISTANCE 1) family and the NRG1 (N REQUIREMENT GENE 1) family (Duxbury et al., 2021). Neither of the two families is involved in the recognition of pathogen effectors. Instead, they function at the downstream of CNLs and TNLs (Jubic et al., 2019). Some TNLs prefer the ADR1 family to transduce signaling in immunity. For example, a triple mutant of the *ADR1* gene family fully suppresses the gain-of-function mutant *snc1*-mediated auto-immunity in Arabidopsis, which indicates that ADR1 family proteins function redundantly downstream of the TNL SNC1 (Dong et al., 2016). Similar results have been found for RPP2 and RRS1 (Saile et al., 2020). While most of the TNLs prefer the NRG1 family in signaling transduction. Mutants of the *NRG1* family lead to impaired HR in tobacco and Arabidopsis which express different TNLs (Castel et al., 2019). Interestingly, the resistance mediated by the TNL WRR4A is attenuated when both *ADR1* and *NRG1* gene families are mutated in Arabidopsis, which suggests that ADR1 and NRG1 family proteins are fully redundant in WRR4A-conferred resistance (Saile et al., 2020). Similarly, the requirement of ADR1 family proteins has also been found in some CNLs-mediated immunity (Bonardi et al., 2011).

Another important constituent of NLR signaling is the EDS1 (enhanced disease susceptibility 1) family, which contains EDS1, PAD4 (phytoalexin deficient 4), and SAG101 (senescence-associated gene 101) (Duxbury et al., 2021; Maruta et al., 2022). Though these proteins contain N-terminal lipase-like domains, they do not possess catalytic activity. In fact, EDS1 can form heterodimers with either PAD4 or SAG101 (Wagner et al., 2013). The EDS1-PAD4 and EDS1-SAG101 dimers are involved in both PTI and ETI, especially in TNL signaling (Dongus and Parker, 2021).

Recent studies have found that RNLs and EDS1 family proteins constitute complexes to regulate TNL signaling. In Arabidopsis, EDS1 and SAG101 interact with NRG1, not ADR1 after the effector XopQ activate ROQ1-triggered immunity (Lapin et al., 2019; Sun et al., 2021). A member of the ADR1 family, ADR1-L1, interacts with EDS1-PAD4 heterodimer in TX protein RBA1-triggered immunity, and the interaction is reduced if the NADase activity is mutated in RBA1 (Wu et al., 2021). As a result, the molecules produced by TIR domains are expected to transduce the signals from activated TNLs to downstream EDS1-PAD4 and EDS1-SAG101 complexes, like second messengers. However, it remains unsure what the product is until two groups of compounds are reported very recently. The 2′-(5″-phosphoribosyl)- 5′-adenosine mono-/di-phosphate (pRib-AMP/ADP) are produced after RBA1 is activated. They bind to the EDS1-PAD4 complex and lead to conformational changes, which promote the interaction with ADR1 in immunity (Huang et al., 2022). Similarly, ADP-ribosylated ATP (ADPr-ATP) and ADPr-ADPR (di-ADPR) are generated by TIR domains of RPP1 and RPS4. They can bind to the EDS1-SAG101 complex and induce the interaction with NRG1A (also named as NRG1.1), a member of the NRG1 family (Jia et al., 2022).

Notably, the RPW8 domains at the N-terminus of RNLs belong to an ancient class of CC domains that are also called the CC-R domain. The CC-R domains are homologous to the 4HB domain in animal MLKL (mixed lineage kinase domain like), which causes a rapid influx of Ca^{2+} and necroptotic cell death after being activated (Gong et al., 2017; Jubic et al., 2019). After the structure of the NRG1.1 CC-R domain was discovered, it has been found that the CC-R domain resembles the four-helical bundle of the ZAR1 CC domain. And both NRG1.1 and ADR1 have been found to form Ca^{2+}-permeable channels in plants (Jacob et al., 2021). In addition, ADR1 and NRG1 family members trigger auto-immunity if the MHD motifs are modified (Roberts et al., 2013; Wu et al., 2019). Nonetheless, whether EDS1-PAD4-ADR1 or EDS1-SAG101-NRG1 complex would form a resistosome similar to ZAR1 in plant immunity is still not confirmed. In summary, many RNLs possess the same biochemical function as CNLs, but the function is regulated by the interaction with EDS1-PAD4 or EDS1-SAG101 heterodimers after the second messengers are derived by pathogen effector-activated TNLs (Figure 1C). However, a report has shown that overexpression of NRG1 alone can trigger resistance to HopQ1-carrying *Pseudomonas syringae*

pv. *tomato* (*Pto*) DC3000 in Arabidopsis. Given that the TNL-encoding gene *Roq1* does not exist in the Arabidopsis genome, NRG1 is considered to recognize the effector HopQ1 directly (Brendolise et al., 2018). This report has indicated that RNLs may have additional functions in plant immunity. Meanwhile, the mechanism of RNLs function in CNL-mediated immunity is still largely unknown.

Atypical NLRs confer resistance in diverse manners

Compared with classical NLRs, many atypical NLRs have extra domains or motifs, which also play important roles in plant immunity. A large portion of atypical NLRs are members in NLR pairs. In Arabidopsis, RPS4 and RRS1 function as an NLR pair to confer resistance to PopP2 from *Ralstonia solanacearum* and AvrRps4 from *Pseudomonas syringae* pv. *pisi* (Narusaka et al., 2009). Structurally, RPS4 is a common TNL while RRS1 contains an additional WRKY domain at the C-terminus. TIR domains of RPS4 can form homodimers and induce HR. However, the HR can be abolished by the RRS1 TIR domain because the TIR domains of RRS1 and RPS4 form a more stable heterodimeric complex (Williams et al., 2014). Though overexpression of *RPS4* induces weak HR, *RPS4* autoactive alleles, which contain mutations in the NB-ARC domain cause increased HR in the presence of RRS1-R1. These results strongly suggest that RRS1 plays a sophisticated role in regulating RPS4-mediated immunity (Guo et al., 2021). The effector PopP2 possesses acetyltransferase activities and acetylates many WRKY transcription factors (TFs), which leads to a reduction of WRKY-DNA interaction and suppression of PTI in Arabidopsis. Meanwhile, RRS1-R1 uses the WRKY domain as an 'integrated decoy' to detect the appearance of PopP2, and its acetylation further activates the RRS1-R/RPS4 complex (Le Roux et al., 2015; Sarris et al., 2015). The effector AvrRps4 is hydrolyzed into two fragments after entering the plant cell and the C-terminal fragment ($AvrRps4^{C}$) can interact with the WRKY domain of RRS1-R1 (Sohn et al., 2009, 2012; Mukhi et al., 2021). Without AvrRps4, the WRKY domain of RRS1 interacts with the domain 4 (DOM4) and results in the inactive (pre-activation) state of the RRS1/RPS4 complex (Ma et al., 2018; Guo et al., 2020). After recognition of AvrRps4 by RRS1 WRKY domain, the interaction between RRS1 TIR and its C-terminus is enhanced, which releases the RPS4 TIR from the heterodimer with RRS1 TIR (Sarris et al., 2015; Guo et al., 2020). In summary, RRS1 is a 'sensor NLR' that detects effectors *via* its WRKY domain, the RPS4 is an 'executor NLR' that triggers plant immunity after being activated. In the pre-activation state, RRS1 and RPS4 form the heterodimer, and RRS1 TIR inhibits the activity of RPS4 TIR. The effectors can interact with or modify the RRS1 WRKY domain to enhance the proximity of RRS1 TIR to its C terminus. As a result, the RPS4 TIR is released and initiates plant immunity (Figure 2A).

Meanwhile, in rice, many NLRs use heavy metal associated (HMA) domains as integrated decoys. *Pia*-mediated resistance to rice blast is conferred by the CNL pair RGA4/RGA5 (Okuyama et al., 2011). RGA5 contains an HMA domain at the C-terminus, which interacts with the effectors AVR1-CO39 and AVR-Pia of the fungus *Magnaporthe oryzae* (Cesari et al., 2013). RGA4 acts as an executor NLR, which can induce strong HR in tobacco leaves. RGA5 interacts with RGA4 and represses the HR when co-expressed in the absence of cognate effectors. And if AVR-Pia is co-expressed additionally, the HR can be resumed because of the recognition by the RGA5 HMA domain (Figure 2B; Cesari et al., 2014). The HMA domains also exist in NLR pairs encoded by *Pik* and its alleles, such as *Pikm* and *Pikp* (Ashikawa et al., 2008; Yuan et al., 2011). The HMA domains exist between the CC and NB-ARC domains in Pikp-1 and Pikm-1 and interact with AVR-Pik variants (Maqbool et al., 2015; De la Concepcion et al., 2018). Unlike RGA4, Pikp-1 or Pikp-2 alone cannot induce HR in tobacco. However, co-expression of Pikp-1, Pikp-2, and their corresponding effector AVR-PikD induces significant HR in tobacco (Figure 2C; Maqbool et al., 2015). Pikm-1 has variations in the HMA domain and binds more effectors than Pikp-1 (De la Concepcion et al., 2018). AVR-Pia, AVR1-CO39, and AVR-PikD are different in sequence but similar in structure and all belong to the MAX (*Magnaporthe* Avrs and ToxB like) effector family (de Guillen et al., 2015). The structural similarity among the MAX effectors also leads to the discovery that *Pikp* confers partial resistance to *M. oryzae* expressing AVR-Pia, which is caused by the "mis-matched" interaction between AVR-Pia and Pikp-1 HMA domain (Varden et al., 2019). Intriguingly, although AVR-Pia (or AVR1-CO39) and AVR-PikD are recognized by the HMA domains, the interactions occur at opposite surfaces of HMA domains, which is possibly the result of convergent evolution for rice to cope with varied pathogen effectors (Guo et al., 2018; Varden et al., 2019).

In a few pieces of literature, the "executor NLR" is also called "helper NLR" (Adachi et al., 2019; De la Concepcion et al., 2019). However, this might lead to confusion with RNLs and NRCs in some cases. In most NLR pairs, the two NLRs often interact with each other in the recognition of pathogen effectors. And NLRs such as RPS4 and RGA4 are capable to induce HR alone, instead of functioning at the downstream of the sensor NLRs. Based on these features, we prefer to group them into "executor NLRs" here. To further distinguish helper NLR and executor NLR in NLR pairs, we refer readers to recent reviews (van Wersch et al., 2019; Sun et al., 2020).

Besides participating in NLR pairs, a few atypical NLRs function as "singletons" without partner NLRs. Due to the lack of knowledge, the function of their IDs is unknown yet. The zf-BED is commonly found in chromatin-associated proteins and transposases (Aravind, 2000). Nevertheless,

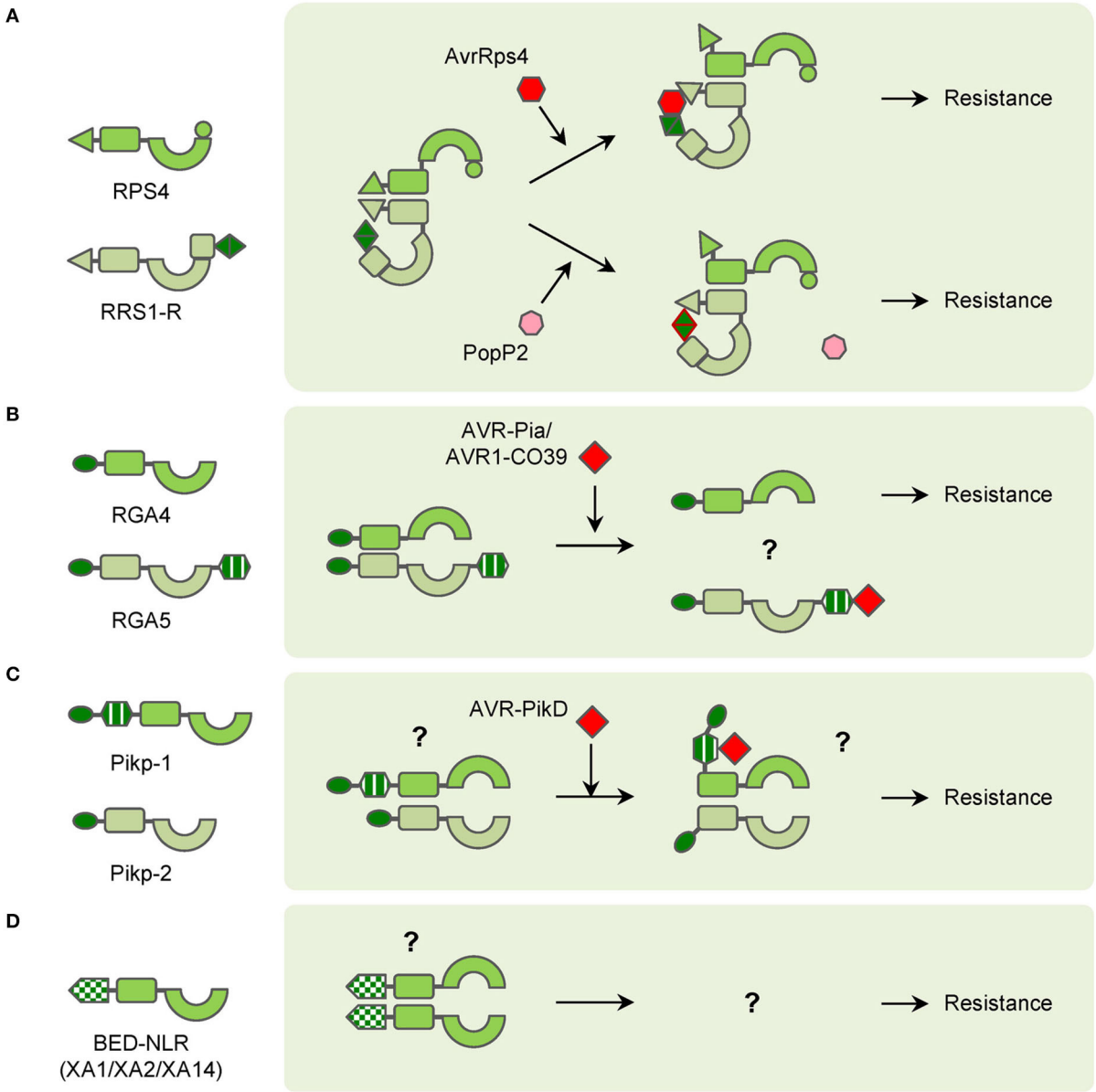

FIGURE 2
Diagrams of interactions between pathogen effectors and atypical NLRs in NLR pairs or singletons. **(A)** RPS4/PPS1-R NLR pair functions in different ways with pathogen effectors AvrRps4 and PopP2 to confer resistance. **(B)** RGA4/RGA5 NLR pair recognizes pathogen effectors AVR-Pia and AVR1-CO39 through the RGA5 HMA domain to confer resistance. **(C)** Pikp-1/Pipk-2 NLR pair interacts with pathogen effector AVR-PikD through Pikp-1 HMA domain to confer resistance. **(D)** BED-NLRs (XA1/XA2/XA14 as examples) probably form polymers to confer resistance.

several NLRs in rice and wheat contain zf-BED domains for resistance to different pathogens. In wheat, *Yr5*, *Yr7*, and *YrSP* are three allelic yellow stripe rust *R* genes. The zf-BED domains are located at the N-terminus of the Yr5, Yr7, and YrSP proteins. Mutation in the zf-BED domain of Yr7 attenuates its resistance, though the mechanism is unclear (Marchal et al., 2018). In rice, *Xa1*, *Xa2*, *Xa14*, and *Xo1* are all allelic *R* genes for resistance to *Xanthomonas oryzae* pv. *oryzae* (*Xoo*) and *Xanthomonas oryzae* pv. *oryzicola* (*Xoc*) (Yoshimura et al., 1998; Ji et al., 2020, Read et al., 2020; Zhang et al., 2020). The proteins encoded by these genes are homologous to Yr5 and Yr7, and they also harbor zf-BED domains at N-terminus (Ji et al., 2020; Zhang et al., 2020). The zf-BED domains of XA1, XA2, and XA14 interact with themselves and also one another, which indicates homodimers and heterodimers may be formed in the resistance process (Figure 2D; Zhang et al., 2020). It has been reported that many transcription activator-like effectors (TALEs) are

crucial for *Xa1*-mediated resistance, but the physical interaction between them is still uncovered yet (Zhao et al., 2016; Zhang et al., 2022).

NLRs can be engineered for improved resistance

After a long time of evolution, plants have evolved many strategies to cope with various pathogens. For NLRs that recognize effectors indirectly, the guardees or decoys are the determinants of their resistance. RIN4 is targeted by lots of bacterial effectors to disturb plant PTI, and many NLRs guard RIN4 for triggering ETI for resistance (Ray et al., 2019). Besides RKS1, ZAR1 can interact with many other different ZAR1-ASSOCIATED KINASEs (ZRKs), which probably function as sensors for diverse effectors (Liang and Zhou, 2018). As a result, modification of the guardees or decoys can lead to changes in pathogen recognition in theory. In the past few years, this has been proved by the engineering of PBS1. When the AvrPphB cleavage site is replaced by sites for other pathogen protease, PBS1 confers resistance to new pathogens (Kim et al., 2016). Such a strategy is also applicable to crops. Modification of the PBS1 ortholog in soybean can lead to significant resistance to soybean mosaic virus (SMV) (Figure 3A; Pottinger et al., 2020).

In contrast, for NLRs that directly interact with pathogen effectors, duplication and recombination of their encoding genes for generating orthologs and paralogs are easily found in most plant genomes. Thus, many NLR-encoding genes are allelic and mediate resistance with specific spectrums. It is easy to understand that the variations in the domains which are involved in pathogen effector recognition are key for the resistance specificity. It has also been found for a long time that mutation or changes in this region can lead to the changement in resistance (Ellis et al., 1999; Dodds et al., 2001). And domain-swapping has been used in many studies for generating new NLRs for a long time. Taking the flax *L* locus as an example, it contains several allelic genes that confer resistance to different strains of flax rust fungus *Melampsora lini*, which carry different effectors (Ellis et al., 1999). A recombinant chimeric protein based on L5 and L6 has exhibited a novel and expanded spectrum in tobacco (Figure 3B; Ravensdale et al., 2012). Random mutagenesis is another strategy to select synthetic NLRs with expanded spectrums (Harris et al., 2013; Segretin et al., 2014). In potatoes, the CNL R3a confers resistance to the late blight pathogen *Phytophthora infestans* (*P. infestans*). R3a recognizes the effector AVR3a of *P. infestans* but responds weakly to its allele AVR3a^{EM}. A random mutant library has been generated and many clones with expanded responses to AVR3a^{EM} have been obtained (Figure 3B; Segretin et al., 2014). However, there are still disadvantages to domain-swapping and random mutagenesis. The efficiency and effectiveness are unpredictable until the chimeras or mutants are tested. Usually, plenty of recombinants should be employed to fully cover the whole variations, and only a small number of them could meet the objectives. And due to the limitation of template sequences, new spectrums are commonly limited within the species which the templet NLRs confer resistance to.

Recently, with the application of structural biology technology, detailed interactions between certain NLRs and pathogen effectors have been uncovered. These results have greatly facilitated the attempts of NLR engineering. The most well-known examples are the modification of NLRs for rice blast resistance. The structure of the AVR-PikD bound Pikp-1 HMA domain has been used in screening mutations of Pikp-1 for expanded effector recognition, and one mutation has displayed increased affinity to many AVR-Pik variants in tobacco (De la Concepcion et al., 2019). Because of the conservation of HMA domains, RGA5 has been engineered to recognize AVR-PikD based on structural information of the Pikp-1_HMA/AVR-PikD complex without affecting AVR-Pia recognition. The engineered RGA5 indeed interacts with both AVR-Pia and AVR-PikD in tobacco, while it only confers resistance to *M. oryzae* isolates carrying AVR-Pia in rice (Cesari et al., 2022). Furthermore, the HMA domain of RGA5 has been modified for interacting with the noncorresponding effectors. Though the *M. oryzae* effector AvrPib initiates *Pib*- not *Pia*-mediated resistance, it belongs to the MAX family and folds into a structure similar to AVR1-CO39. As a result, structure-guided engineering of the RGA5 HMA domain is carried out and a designed RGA5-HMA2 domain that interacts with AvrPib instead of AVR1-CO39 is found. Remarkably, the designed NLR RGA5^{HMA2}, which carries the RGA5-HMA2 domain, confers significant resistance to *M. oryzae* isolates carrying AVR-Pib in the presence of RGA4 in rice (Figure 3C; Liu et al., 2021). All these attempts have shed light on the future that NLRs can be designed as predicted for improved plant immunity.

Future perspectives and challenges

The researches on NLRs have obtained great progress in recent years, especially in the discoveries and functional characterizations of NLR resistosomes, as well as the interactions between different IDs and their cognate effectors. However, the number of NLRs in plants is plentiful and most of them are still unclear or uncovered yet. Even for the well-characterized ZAR1, whether it forms the same resistosome in resistance to pathogens carrying other effectors, such as HopZ1a, HopF2, HopBA1, HopO1, and HopX1, is still unknown (Martel et al., 2020). Lately, the CNL PigmR has been reported to guard the deubiquitinase PICI1 (PigmR-interacting and chitin-induced protein 1) from being degraded by *M. oryzae* effector Avr-Pi9 to initiate immunity in rice (Zhai et al., 2022). The interaction occurs between the CC domain of PigmR and PICI1, and this raises the question of detailed complex

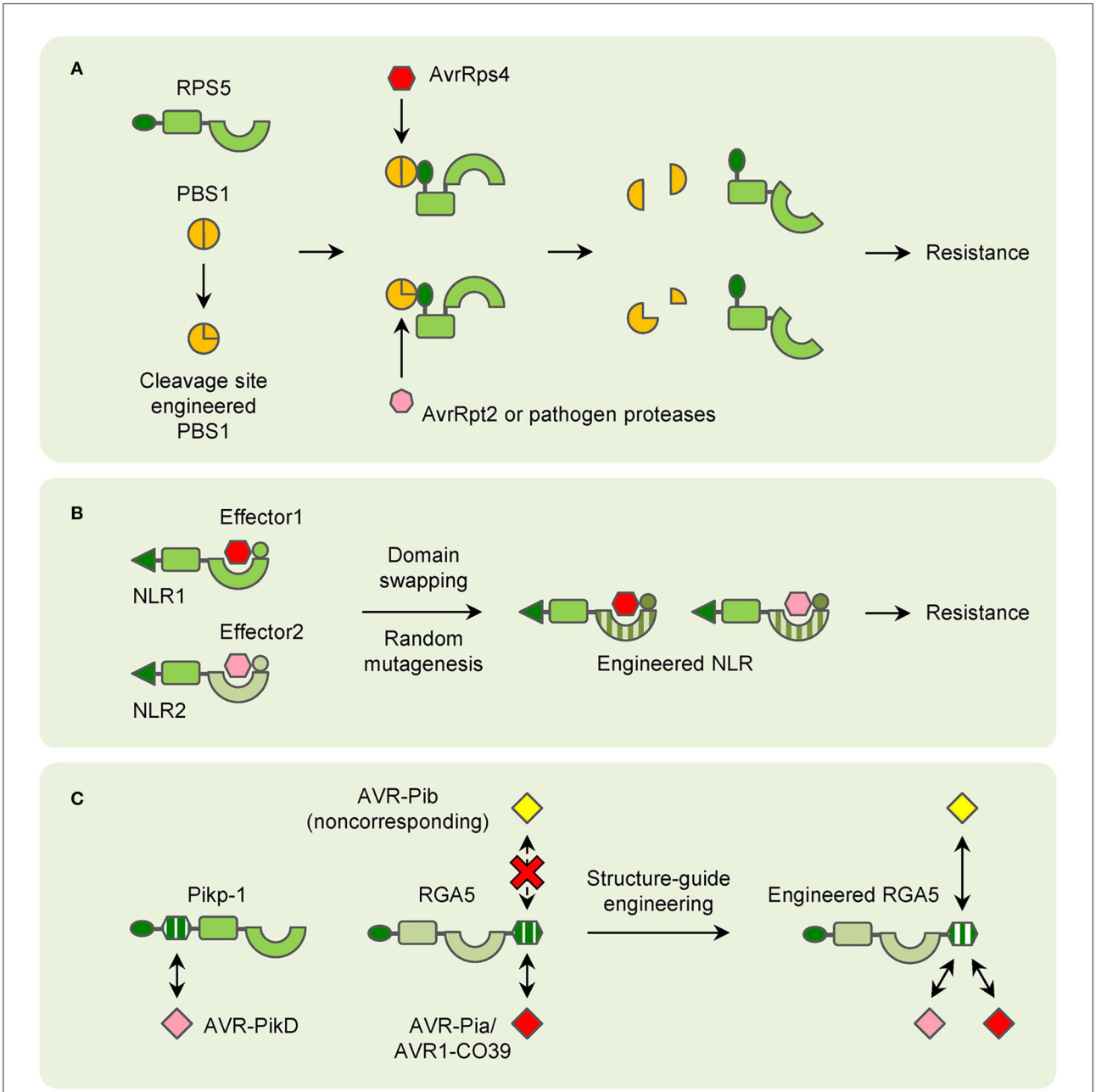

FIGURE 3
Models of NLR engineering in plants. **(A)** Modification of decoy proteins (PBS1 as an example) to confer resistance to new pathogen effectors. **(B)** Domain-swapping and random mutagenesis of NLRs to enlarge the resistance spectrums. **(C)** Structure-guide engineering of NLRs to confer resistance to noncorresponding effectors.

composition in the possible resistosome. RNLs function at the downstream of both PTI and ETI, and more studies may be carried out according to the existing results for each RNL. Current researches have shown that the relationship between PTI and ETI is more complicated than expected. Some NLR-mediated ETI responses have been reported to enhance ROS production and key components of PTI signaling in Arabidopsis (Ngou et al., 2021). Meanwhile, PRRs mutants have been found to be impaired in ETI response mediated by certain NLRs (Ngou et al., 2021, (Yuan et al., 2021)). These data raise the possibility that the PTI and ETI pathways mutually potentiate plant immunity. However, whether similar results could be found for all the NLRs are unsure. Furthermore, the whole structures of atypical NLRs are also important questions and should be different from each other. In addition, whether the IDs in some atypical NLRs, such as BED-NLRs, function as decoys is still uncertain, which should be illustrated first.

Recently, AvrPiz-t, another MAX effector from rice blast fungus, has been found to suppress rice immunity by exploiting ROD1 (RESISTANCE OF RICE TO DISEASES1) (Gao et al., 2021). AvrPiz-t also has the conserved structure of MAX effectors, and whether an engineered RGA5 or Pikp-1, which recognizes AvrPiz-t, could be designed is an intriguing question. Though still there are many questions to be fixed, the attempts at NLR engineering have already pointed out the direction in the future. The difficulties in studying an NLR structure are its high molecular weight and polymerization, and they could be solved with the help of developed cryo-EM technology. In general, with the accumulation of researches on the characterization and engineering of NLRs, designed plant immunity will be possible and benefit crop production in the future.

Author contributions

HZ conceived the manuscript. BZ, ML, and YW prepared the original draft and figures. HZ and WY reviewed and edited the manuscript. All authors have read and approved the final manuscript.

Funding

This work was supported by grants from the National Natural Science Foundation of China (32101747 and 31872811).

Conflict of interest

The authors declare that the research was conducted in the absence of any commercial or financial relationships that could be construed as a potential conflict of interest.

Publisher's note

All claims expressed in this article are solely those of the authors and do not necessarily represent those of their affiliated organizations, or those of the publisher, the editors and the reviewers. Any product that may be evaluated in this article, or claim that may be made by its manufacturer, is not guaranteed or endorsed by the publisher.

References

Adachi, H., Derevnina, L., and Kamoun, S. (2019). NLR singletons, pairs, and networks: evolution, assembly, and regulation of the intracellular immunoreceptor circuitry of plants. *Curr. Opin. Plant Biol.* 50, 121–131. doi: 10.1016/j.pbi.2019.04.007

Ade, J., DeYoung, B. J., Golstein, C., and Innes, R. W. (2007). Indirect activation of a plant nucleotide binding site-leucine-rich repeat protein by a bacterial protease. *Proc. Natl. Acad. Sci. U.S.A.* 104, 2531–2536. doi: 10.1073/pnas.0608779104

Afzal, A. J., da Cunha, L., and Mackey, D. (2011). Separable fragments and membrane tethering of *Arabidopsis* RIN4 regulate its suppression of PAMP-triggered immunity. *Plant Cell.* 23, 3798–3811. doi: 10.1105/tpc.111.088708

Aravind, L. (2000). The BED finger, a novel DNA-binding domain in chromatin-boundary-element-binding proteins and transposases. *Trends Biochem. Sci.* 25, 421–423. doi: 10.1016/s0968-0004(00)01620-0

Ashikawa, I., Hayashi, N., Yamane, H., Kanamori, H., Wu, J., Matsumoto, T., et al. (2008). Two adjacent nucleotide-binding site-leucine-rich repeat class genes are required to confer *Pikm*-specific rice blast resistance. *Genetics.* 180, 2267–2276. doi: 10.1534/genetics.108.095034

Axtell, M. J., and Staskawicz, B. J. (2003). Initiation of *RPS2*-specified disease resistance in *Arabidopsis* is coupled to the AvrRpt2-directed elimination of RIN4. *Cell.* 112, 369–377. doi: 10.1016/s0092-8674(03)00036-9

Bai, S., Liu, J., Chang, C., Zhang, L., Maekawa, T., Wang, Q., et al. (2012). Structure-function analysis of barley NLR immune receptor MLA10 reveals its cell compartment specific activity in cell death and disease resistance. *PLoS Pathog.* 8, e1002752. doi: 10.1371/journal.ppat.1002752

Bernoux, M., Ve, T., Williams, S., Warren, C., Hatters, D., Valkov, E., et al. (2011). Structural and functional analysis of a plant resistance protein TIR domain reveals interfaces for self-association, signaling, and autoregulation. *Cell Host Microbe.* 9, 200–211. doi: 10.1016/j.chom.2011.02.009

Bi, G., Su, M., Li, N., Liang, Y., Dang, S., Xu, J., et al. (2021). The ZAR1 resistosome is a calcium-permeable channel triggering plant immune signaling. *Cell.* 184, 3528–3541. doi: 10.1016/j.cell.2021.05.003

Birker, D., Heidrich, K., Takahara, H., Narusaka, M., Deslandes, L., Narusaka, Y., et al. (2009). A locus conferring resistance to *Colletotrichum higginsianum* is shared by four geographically distinct Arabidopsis accessions. *Plant J.* 60, 602–613. doi: 10.1111/j.1365-313X.2009.03984.x

Bonardi, V., Tang, S., Stallmann, A., Roberts, M., Cherkis, K., and Dangl, J. L. (2011). Expanded functions for a family of plant intracellular immune receptors beyond specific recognition of pathogen effectors. *Proc. Natl. Acad. Sci. U.S.A.* 108, 16463–16468. doi: 10.1073/pnas.1113726108

Brendolise, C., Martinez-Sanchez, M., Morel, A., Chen, R., Dinis, R., Deroles, S., et al. (2018). NRG1-mediated recognition of HopQ1 reveals a link between PAMP- and Effector-triggered Immunity. *bioRxiv.* 293050. doi: 10.1101/293050

Brueggeman, R., Druka, A., Nirmala, J., Cavileer, T., Drader, T., Rostoks, N., et al. (2008). The stem rust resistance gene *Rpg5* encodes a protein with nucleotide-binding-site, leucine-rich, and protein kinase domains. *Proc. Natl. Acad. Sci. U.S.A.* 105, 14970–14975. doi: 10.1073/pnas.0807270105

Caplan, J. L., Mamillapalli, P., Burch-Smith, T. M., Czymmek, K., and Dinesh-Kumar, S. P. (2008). Chloroplastic protein NRIP1 mediates innate immune receptor recognition of a viral effector. *Cell.* 132, 449–462. doi: 10.1016/j.cell.2007.12.031

Castel, B., Ngou, P. M., Cevik, V., Redkar, A., Kim, D. S., Yang, Y., et al. (2019). Diverse NLR immune receptors activate defence via the RPW8-NLR NRG1. *New Phytol.* 222, 966–980. doi: 10.1111/nph.15659

Cesari, S., Kanzaki, H., Fujiwara, T., Bernoux, M., Chalvon, V., Kawano, Y., et al. (2014). The NB-LRR proteins RGA4 and RGA5 interact functionally and physically to confer disease resistance. *EMBO J.* 33, 1941–1959. doi: 10.15252/embj.201487923

Cesari, S., Thilliez, G., Ribot, C., Chalvon, V., Michel, C., Jauneau, A., et al. (2013). The rice resistance protein pair RGA4/RGA5 recognizes the *Magnaporthe oryzae* effectors AVR-Pia and AVR1-CO39 by direct binding. *Plant Cell.* 25, 1463–1481. doi: 10.1105/tpc.112.107201

Cesari, S., Xi, Y., Declerck, N., Chalvon, V., Mammri, L., Pugniere, M., et al. (2022). New recognition specificity in a plant immune receptor by molecular engineering of its integrated domain. *Nat. Commun.* 13, 1524. doi: 10.1038/s41467-022-29196-6

Chung, E. H., da Cunha, L., Wu, A. J., Gao, Z., Cherkis, K., Afzal, A. J., et al. (2011). Specific threonine phosphorylation of a host target by two unrelated type III effectors activates a host innate immune receptor in plants. *Cell Host Microbe.* 9, 125–136. doi: 10.1016/j.chom.2011.01.009

Claverie, M., Dirlewanger, E., Bosselut, N., Van Ghelder, C., Voisin, R., Kleinhentz, M., et al. (2011). The *Ma* gene for complete-spectrum resistance to

Meloidogyne species in *Prunus* is a TNL with a huge repeated C-terminal post-LRR region. *Plant Physiol.* 156, 779–792. doi: 10.1104/pp.111.176230

de Guillen, K., Ortiz-Vallejo, D., Gracy, J., Fournier, E., Kroj, T., and Padilla, A. (2015). Structure analysis uncovers a highly diverse but structurally conserved effector family in phytopathogenic fungi. *PLoS Pathog.* 11, e1005228. doi: 10.1371/journal.ppat.1005228

De la Concepcion, J. C., Franceschetti, M., MacLean, D., Terauchi, R., Kamoun, S., and Banfield, M. J. (2019). Protein engineering expands the effector recognition profile of a rice NLR immune receptor. *Elife.* 8, e47713. doi: 10.7554/eLife.47713

De la Concepcion, J. C., Franceschetti, M., Maqbool, A., Saitoh, H., Terauchi, R., Kamoun, S., et al. (2018). Polymorphic residues in rice NLRs expand binding and response to effectors of the blast pathogen. *Nat. Plants* 4, 576–585. doi: 10.1038/s41477-018-0194-x

Dodds, P. N., Lawrence, G. J., and Ellis, J. G. (2001). Six amino acid changes confined to the leucine-rich repeat beta-strand/beta-turn motif determine the difference between the *P* and *P2* rust resistance specificities in flax. *Plant Cell.* 13, 163–178. doi: 10.1105/tpc.13.1.163

Dong, O. X., Tong, M., Bonardi, V., El Kasmi, F., Woloshen, V., Wunsch, L. K., et al. (2016). TNL-mediated immunity in *Arabidopsis* requires complex regulation of the redundant *ADR1* gene family. *New Phytol.* 210, 960–973. doi: 10.1111/nph.13821

Dongus, J. A., and Parker, J. E. (2021). EDS1 signalling: At the nexus of intracellular and surface receptor immunity. *Curr. Opin. Plant Biol.* 62, 102039. doi: 10.1016/j.pbi.2021.102039

Duxbury, Z., Wang, S., MacKenzie, C. I., Tenthorey, J. L., Zhang, X., Huh, S. U., et al. (2020). Induced proximity of a TIR signaling domain on a plant-mammalian NLR chimera activates defense in plants. *Proc. Natl. Acad. Sci. U.S.A.* 117, 18832–18839. doi: 10.1073/pnas.2001185117

Duxbury, Z., Wu, C. H., and Ding, P. (2021). A comparative overview of the intracellular guardians of plants and animals: NLRs in innate immunity and beyond. *Annu. Rev. Plant Biol.* 72, 155–184. doi: 10.1146/annurev-arplant-080620-104948

Ellis, J. G., Lawrence, G. J., Luck, J. E., and Dodds, P. N. (1999). Identification of regions in alleles of the flax rust resistance gene *L* that determine differences in gene-for-gene specificity. *Plant Cell* 11, 495–506. doi: 10.1105/tpc.11.3.495

Essuman, K., Summers, D. W., Sasaki, Y., Mao, X., DiAntonio, A., and Milbrandt, J. (2017). The SARM1 Toll/interleukin-1 receptor domain possesses intrinsic NAD(+) cleavage activity that promotes pathological axonal degeneration. *Neuron.* 93, 1334–1343. doi: 10.1016/j.neuron.2017.02.022

Feng, F., Yang, F., Rong, W., Wu, X., Zhang, J., Chen, S., et al. (2012). A *Xanthomonas* uridine 5'-monophosphate transferase inhibits plant immune kinases. *Nature.* 485, 114–118. doi: 10.1038/nature10962

Gao, M., He, Y., Yin, X., Zhong, X., Yan, B., Wu, Y., et al. (2021). Ca(2+) sensor-mediated ROS scavenging suppresses rice immunity and is exploited by a fungal effector. *Cell.* 184, 5391–5404. doi: 10.1016/j.cell.2021.09.009

Gong, Y. N., Guy, C., Olauson, H., Becker, J. U., Yang, M., Fitzgerald, P., et al. (2017). ESCRT-III acts downstream of MLKL to regulate necroptotic cell death and its consequences. *Cell.* 169, 286–300. doi: 10.1016/j.cell.2017.03.020

Grant, M., Brown, I., Adams, S., Knight, M., Ainslie, A., and Mansfield, J. (2000). The *RPM1* plant disease resistance gene facilitates a rapid and sustained increase in cytosolic calcium that is necessary for the oxidative burst and hypersensitive cell death. *Plant J.* 23, 441–450. doi: 10.1046/j.1365-313x.2000.00804.x

Guo, H., Ahn, H. K., Sklenar, J., Huang, J., Ma, Y., Ding, P., et al. (2020). Phosphorylation-regulated activation of the *Arabidopsis* RRS1-R/RPS4 immune receptor complex reveals two distinct effector recognition mechanisms. *Cell Host Microbe* 27, 769–781. doi: 10.1016/j.chom.2020.03.008

Guo, H., Wang, S., and Jones, J. D. G. (2021). Autoactive Arabidopsis RPS4 alleles require partner protein RRS1-R. *Plant Physiol.* 185, 761–764. doi: 10.1093/plphys/kiaa076

Guo, L., Cesari, S., de Guillen, K., Chalvon, V., Mammri, L., Ma, M., et al. (2018). Specific recognition of two MAX effectors by integrated HMA domains in plant immune receptors involves distinct binding surfaces. *Proc. Natl. Acad. Sci. U.S.A.* 115, 11637–11642. doi: 10.1073/pnas.1810705115

Harris, C. J., Slootweg, E. J., Goverse, A., and Baulcombe, D. C. (2013). Stepwise artificial evolution of a plant disease resistance gene. *Proc. Natl. Acad. Sci. U.S.A.* 110, 21189–21194. doi: 10.1073/pnas.1311134110

Horsefield, S., Burdett, H., Zhang, X., Manik, M. K., Shi, Y., Chen, J., et al. (2019). NAD(+) cleavage activity by animal and plant TIR domains in cell death pathways. *Science* 365, 793–799. doi: 10.1126/science.aax1911

Huang, S., Jia, A., Song, W., Hessler, G., Meng, Y., Sun, Y., et al. (2022). Identification and receptor mechanism of TIR-catalyzed small molecules in plant immunity. *Science.* 377, eabq3297. doi: 10.1126/science.abq3297

Jacob, P., Kim, N. H., Wu, F., El-Kasmi, F., Chi, Y., Walton, W. G., et al. (2021). Plant "helper" immune receptors are Ca(2+)-permeable nonselective cation channels. *Science.* 373, 420–425. doi: 10.1126/science.abg7917

Ji, C., Ji, Z., Liu, B., Cheng, H., Liu, H., Liu, S., et al. (2020). *Xa1* allelic *R* genes activate rice blight resistance suppressed by interfering TAL effectors. *Plant Commun.* 1, 100087. doi: 10.1016/j.xplc.2020.100087

Jia, A., Huang, S., Song, W., Wang, J., Meng, Y., Sun, Y., et al. (2022). TIR-catalyzed ADP-ribosylation reactions produce signaling molecules for plant immunity. *Science.* 377, eabq8180. doi: 10.1126/science.abq8180

Jones, J. D., and Dangl, J. L. (2006). The plant immune system. *Nature.* 444, 323–329. doi: 10.1038/nature05286

Jones, J. D., Vance, R. E., and Dangl, J. L. (2016). Intracellular innate immune surveillance devices in plants and animals. *Science.* 354, aaf6395. doi: 10.1126/science.aaf6395

Jubic, L. M., Saile, S., Furzer, O. J., El Kasmi, F., and Dangl, J. L. (2019). Help wanted: helper NLRs and plant immune responses. *Curr. Opin. Plant Biol.* 50, 82–94. doi: 10.1016/j.pbi.2019.03.013

Kim, S. H., Qi, D., Ashfield, T., Helm, M., and Innes, R. W. (2016). Using decoys to expand the recognition specificity of a plant disease resistance protein. *Science.* 351, 684–687. doi: 10.1126/science.aad3436

Kourelis, J., and van der Hoorn, R. A. L. (2018). Defended to the nines: 25 years of resistance gene cloning identifies nine mechanisms for R protein function. *Plant Cell.* 30, 285–299. doi: 10.1105/tpc.17.00579

Kroj, T., Chanclud, E., Michel-Romiti, C., Grand, X., and Morel, J. B. (2016). Integration of decoy domains derived from protein targets of pathogen effectors into plant immune receptors is widespread. *New Phytol.* 210, 618–626. doi: 10.1111/nph.13869

Lapin, D., Kovacova, V., Sun, X., Dongus, J. A., Bhandari, D., von Born, P., et al. (2019). A coevolved EDS1-SAG101-NRG1 module mediates cell death signaling by TIR-domain immune receptors. *Plant Cell* 31, 2430–2455. doi: 10.1105/tpc.19.00118

Le Roux, C., Huet, G., Jauneau, A., Camborde, L., Tremousaygue, D., Kraut, A., et al. (2015). A receptor pair with an integrated decoy converts pathogen disabling of transcription factors to immunity. *Cell.* 161, 1074–1088. doi: 10.1016/j.cell.2015.04.025

Li, J., Huang, H., Zhu, M., Huang, S., Zhang, W., Dinesh-Kumar, S. P., et al. (2019). A plant immune receptor adopts a two-step recognition mechanism to enhance viral effector perception. *Mol. Plant.* 12, 248–262. doi: 10.1016/j.molp.2019.01.005

Liang, X., and Zhou, J. M. (2018). Receptor-like cytoplasmic kinases: central players in plant receptor kinase-mediated signaling. *Annu. Rev. Plant Biol.* 69, 267–299. doi: 10.1146/annurev-arplant-042817-040540

Liu, J., Elmore, J. M., Fuglsang, A. T., Palmgren, M. G., Staskawicz, B. J., and Coaker, G. (2009). RIN4 functions with plasma membrane H+-ATPases to regulate stomatal apertures during pathogen attack. *PLoS Biol.* 7, e1000139. doi: 10.1371/journal.pbio.1000139

Liu, J., Elmore, J. M., Lin, Z. J., and Coaker, G. (2011). A receptor-like cytoplasmic kinase phosphorylates the host target RIN4, leading to the activation of a plant innate immune receptor. *Cell Host Microbe.* 9, 137–146. doi: 10.1016/j.chom.2011.01.010

Liu, Y., Zhang, X., Yuan, G., Wang, D., Zheng, Y., Ma, M., et al. (2021). A designer rice NLR immune receptor confers resistance to the rice blast fungus carrying noncorresponding avirulence effectors. *Proc. Natl. Acad. Sci. U.S.A.* 118, e2110751118. doi: 10.1073/pnas.2110751118

Ma, S., Lapin, D., Liu, L., Sun, Y., Song, W., Zhang, X., et al. (2020). Direct pathogen-induced assembly of an NLR immune receptor complex to form a holoenzyme. *Science.* 370, eabe3069. doi: 10.1126/science.abe3069

Ma, Y., Guo, H., Hu, L., Martinez, P. P., Moschou, P. N., Cevik, V., et al. (2018). Distinct modes of derepression of an *Arabidopsis* immune receptor complex by two different bacterial effectors. *Proc. Natl. Acad. Sci. U.S.A.* 115, 10218–10227. doi: 10.1073/pnas.1811858115

Maekawa, T., Cheng, W., Spiridon, L. N., Toller, A., Lukasik, E., Saijo, Y., et al. (2011). Coiled-coil domain-dependent homodimerization of intracellular barley immune receptors defines a minimal functional module for triggering cell death. *Cell Host Microbe.* 9, 187–199. doi: 10.1016/j.chom.2011.02.008

Maqbool, A., Saitoh, H., Franceschetti, M., Stevenson, C. E., Uemura, A., Kanzaki, H., et al. (2015). Structural basis of pathogen recognition by an integrated HMA domain in a plant NLR immune receptor. *Elife.* 4, e08709. doi: 10.7554/eLife.08709

Marchal, C., Zhang, J., Zhang, P., Fenwick, P., Steuernagel, B., Adamski, N. M., et al. (2018). BED-domain-containing immune receptors confer diverse resistance spectra to yellow rust. *Nat. Plants.* 4, 662–668. doi: 10.1038/s41477-018-0236-4

Martel, A., Laflamme, B., Seto, D., Bastedo, D. P., Dillon, M. M., Almeida, R. N. D., et al. (2020). Immunodiversity of the *Arabidopsis* ZAR1 NLR is conveyed by receptor-like cytoplasmic kinase sensors. *Front. Plant Sci.* 11, 1290. doi: 10.3389/fpls.2020.01290

Martin, R., Qi, T., Zhang, H., Liu, F., King, M., Toth, C., et al. (2020). Structure of the activated ROQ1 resistosome directly recognizing the pathogen effector XopQ. *Science.* 370, eabd9993. doi: 10.1126/science.abd9993

Maruta, N., Burdett, H., Lim, B. Y. J., Hu, X., Desa, S., Manik, M. K., et al. (2022). Structural basis of NLR activation and innate immune signalling in plants. *Immunogenetics.* 74, 5–26. doi: 10.1007/s00251-021-01242-5

Mukhi, N., Brown, H., Gorenkin, D., Ding, P., Bentham, A. R., Stevenson, C. E. M., et al. (2021). Perception of structurally distinct effectors by the integrated WRKY domain of a plant immune receptor. *Proc. Natl. Acad. Sci. U.S.A.* 118, e2113996118. doi: 10.1073/pnas.2113996118

Nandety, R. S., Caplan, J. L., Cavanaugh, K., Perroud, B., Wroblewski, T., Michelmore, R. W., et al. (2013). The role of TIR-NBS and TIR-X proteins in plant basal defense responses. *Plant Physiol.* 162, 1459–1472. doi: 10.1104/pp.113.219162

Narusaka, M., Shirasu, K., Noutoshi, Y., Kubo, Y., Shiraishi, T., Iwabuchi, M., et al. (2009). *RRS1* and *RPS4* provide a dual *Resistance*-gene system against fungal and bacterial pathogens. *Plant J.* 60, 218–226. doi: 10.1111/j.1365-313X.2009.03949.x

Ngou, B. P. M., Ahn, H. K., Ding, P., and Jones, J. D. G. (2021). Mutual potentiation of plant immunity by cell-surface and intracellular receptors. *Nature.* 592, 110–115. doi: 10.1038/s41586-021-03315-7

Okuyama, Y., Kanzaki, H., Abe, A., Yoshida, K., Tamiru, M., Saitoh, H., et al. (2011). A multifaceted genomics approach allows the isolation of the rice *Pia*-blast resistance gene consisting of two adjacent NBS-LRR protein genes. *Plant J.* 66, 467–479. doi: 10.1111/j.1365-313X.2011.04502.x

Pottinger, S. E., Bak, A., Margets, A., Helm, M., Tang, L., Casteel, C., et al. (2020). Optimizing the PBS1 decoy system to confer resistance to potyvirus infection in *Arabidopsis* and soybean. *Mol. Plant Microbe Interact.* 33, 932–944. doi: 10.1094/MPMI-07-19-0190-R

Qi, D., DeYoung, B. J., and Innes, R. W. (2012). Structure-function analysis of the coiled-coil and leucine-rich repeat domains of the RPS5 disease resistance protein. *Plant Physiol.* 158, 1819–1832. doi: 10.1104/pp.112.194035

Rairdan, G. J., Collier, S. M., Sacco, M. A., Baldwin, T. T., Boettrich, T., and Moffett, P. (2008). The coiled-coil and nucleotide binding domains of the Potato Rx disease resistance protein function in pathogen recognition and signaling. *Plant Cell.* 20, 739–751. doi: 10.1105/tpc.107.056036

Ravensdale, M., Bernoux, M., Ve, T., Kobe, B., Thrall, P. H., Ellis, J. G., et al. (2012). Intramolecular interaction influences binding of the Flax L5 and L6 resistance proteins to their AvrL567 ligands. *PLoS Pathog.* 8, e1003004. doi: 10.1371/journal.ppat.1003004

Ray, S. K., Macoy, D. M., Kim, W. Y., Lee, S. Y., and Kim, M. G. (2019). Role of RIN4 in regulating PAMP-triggered immunity and effector-triggered immunity: current status and future perspectives. *Mol. Cells.* 42, 503–511. doi: 10.14348/molcells.2019.2433

Read, A. C., Hutin, M., Moscou, M. J., Rinaldi, F. C., and Bogdanove, A. J. (2020). Cloning of the rice *Xo1* resistance gene and interaction of the Xo1 protein with the defense-suppressing *Xanthomonas* effector Tal2h. *Mol. Plant Microbe Interact.* 33, 1189–1195. doi: 10.1094/MPMI-05-20-0131-SC

Roberts, M., Tang, S., Stallmann, A., Dangl, J. L., and Bonardi, V. (2013). Genetic requirements for signaling from an autoactive plant NB-LRR intracellular innate immune receptor. *PLoS Genet.* 9, e1003465. doi: 10.1371/journal.pgen.1003465

Saile, S. C., Jacob, P., Castel, B., Jubic, L. M., Salas-Gonzales, I., Backer, M., et al. (2020). Two unequally redundant "helper" immune receptor families mediate *Arabidopsis thaliana* intracellular "sensor" immune receptor functions. *PLoS Biol.* 18, e3000783. doi: 10.1371/journal.pbio.3000783

Sarris, P. F., Duxbury, Z., Huh, S. U., Ma, Y., Segonzac, C., Sklenar, J., et al. (2015). A plant immune receptor detects pathogen effectors that target WRKY transcription factors. *Cell.* 161, 1089–1100. doi: 10.1016/j.cell.2015.04.024

Saucet, S. B., Esmenjaud, D., and Van Ghelder, C. (2021). Integrity of the post-LRR domain is required for TIR-NB-LRR function. *Mol. Plant Microbe Interact.* 34, 286–296. doi: 10.1094/MPMI-06-20-0156-R

Saur, I. M., Bauer, S., Kracher, B., Lu, X., Franzeskakis, L., Muller, M. C., et al. (2019). Multiple pairs of allelic MLA immune receptor-powdery mildew AVR_A effectors argue for a direct recognition mechanism. *Elife.* 8, e44471. doi: 10.7554/eLife.44471

Schreiber, K. J., Bentham, A., Williams, S. J., Kobe, B., and Staskawicz, B. J. (2016). Multiple domain associations within the Arabidopsis immune receptor RPP1 regulate the activation of programmed cell death. *PLoS Pathog.* 12, e1005769. doi: 10.1371/journal.ppat.1005769

Segretin, M. E., Pais, M., Franceschetti, M., Chaparro-Garcia, A., Bos, J. I., Banfield, M. J., et al. (2014). Single amino acid mutations in the potato immune receptor R3a expand response to Phytophthora effectors. *Mol. Plant Microbe Interact.* 27, 624–637. doi: 10.1094/MPMI-02-14-0040-R

Shao, F., Golstein, C., Ade, J., Stoutemyer, M., Dixon, J. E., and Innes, R. W. (2003). Cleavage of *Arabidopsis* PBS1 by a bacterial type III effector. *Science.* 301, 1230–1233. doi: 10.1126/science.1085671

Sohn, K. H., Hughes, R. K., Piquerez, S. J., Jones, J. D., and Banfield, M. J. (2012). Distinct regions of the *Pseudomonas syringae* coiled-coil effector AvrRps4 are required for activation of immunity. *Proc. Natl. Acad. Sci. U.S.A.* 109, 16371–16376. doi: 10.1073/pnas.1212332109

Sohn, K. H., Zhang, Y., and Jones, J. D. (2009). The *Pseudomonas syringae* effector protein, AvrRPS4, requires *in planta* processing and the KRVY domain to function. *Plant J.* 57, 1079–1091. doi: 10.1111/j.1365-313X.2008.03751.x

Sun, X., Lapin, D., Feehan, J. M., Stolze, S. C., Kramer, K., Dongus, J. A., et al. (2021). Pathogen effector recognition-dependent association of NRG1 with EDS1 and SAG101 in TNL receptor immunity. *Nat. Commun.* 12, 3335. doi: 10.1038/s41467-021-23614-x

Sun, Y., Zhu, Y. X., Balint-Kurti, P. J., and Wang, G. F. (2020). Fine-tuning immunity: players and regulators for plant NLRs. *Trends Plant Sci.* 25, 695–713. doi: 10.1016/j.tplants.2020.02.008

van Wersch, S., Tian, L., Hoy, R., and Li, X. (2019). Plant NLRs: the whistleblowers of plant immunity. *Plant Commun.* 1, 100016. doi: 10.1016/j.xplc.2019.100016

Varden, F. A., Saitoh, H., Yoshino, K., Franceschetti, M., Kamoun, S., Terauchi, R., et al. (2019). Cross-reactivity of a rice NLR immune receptor to distinct effectors from the rice blast pathogen *Magnaporthe oryzae* provides partial disease resistance. *J. Biol. Chem.* 294, 13006–13016. doi: 10.1074/jbc.RA119.007730

Ve, T., Williams, S. J., and Kobe, B. (2015). Structure and function of Toll/interleukin-1 receptor/resistance protein (TIR) domains. *Apoptosis.* 20, 250–261. doi: 10.1007/s10495-014-1064-2

Wagner, S., Stuttmann, J., Rietz, S., Guerois, R., Brunstein, E., Bautor, J., et al. (2013). Structural basis for signaling by exclusive EDS1 heteromeric complexes with SAG101 or PAD4 in plant innate immunity. *Cell Host Microbe.* 14, 619–630. doi: 10.1016/j.chom.2013.11.006

Wan, L., Essuman, K., Anderson, R. G., Sasaki, Y., Monteiro, F., Chung, E. H., et al. (2019). TIR domains of plant immune receptors are NAD(+)-cleaving enzymes that promote cell death. *Science* 365, 799–803. doi: 10.1126/science.aax1771

Wang, G., Roux, B., Feng, F., Guy, E., Li, L., Li, N., et al. (2015). The decoy substrate of a pathogen effector and a pseudokinase specify pathogen-induced modified-self recognition and immunity in plants. *Cell Host Microbe.* 18, 285–295. doi: 10.1016/j.chom.2015.08.004

Wang, J., Hu, M., Qi, J., Han, Z., Wang, G., Qi, Y., et al. (2019a). Reconstitution and structure of a plant NLR resistosome conferring immunity. *Science.* 364, eaav5870. doi: 10.1126/science.aav5870

Wang, J., Hu, M., Wu, S., Qi, J., Wang, G., Han, Z., et al. (2019b). Ligand-triggered allosteric ADP release primes a plant NLR complex. *Science.* 364, eaav5868. doi: 10.1126/science.aav5868

Williams, S. J., Sohn, K. H., Wan, L., Bernoux, M., Sarris, P. F., Segonzac, C., et al. (2014). Structural basis for assembly and function of a heterodimeric plant immune receptor. *Science.* 344, 299–303. doi: 10.1126/science.1247357

Wu, Z., Li, M., Dong, O. X., Xia, S., Liang, W., Bao, Y., et al. (2019). Differential regulation of TNL-mediated immune signaling by redundant helper CNLs. *New Phytol.* 222, 938–953. doi: 10.1111/nph.15665

Wu, Z., Tian, L., Liu, X., Zhang, Y., and Li, X. (2021). TIR signal promotes interactions between lipase-like proteins and ADR1-L1 receptor and ADR1-L1 oligomerization. *Plant Physiol.* 187, 681–686. doi: 10.1093/plphys/kiab305

Yoshimura, S., Yamanouchi, U., Katayose, Y., Toki, S., Wang, Z. X., Kono, I., et al. (1998). Expression of *Xa1*, a bacterial blight-resistance gene in rice, is induced by bacterial inoculation. *Proc. Natl. Acad. Sci. U.S.A.* 95, 1663–1668. doi: 10.1073/pnas.95.4.1663

Yu, D., Song, W., Tan, E. Y. J., Liu, L., Cao, Y., Jirschitzka, J., et al. (2022). TIR domains of plant immune receptors are 2',3'-cAMP/cGMP synthetases mediating cell death. *Cell.* 185, 2370–2386. doi: 10.1016/j.cell.2022.04.032

Yuan, B., Zhai, C., Wang, W., Zeng, X., Xu, X., Hu, H., et al. (2011). The *Pik-p* resistance to *Magnaporthe oryzae* in rice is mediated by a pair of closely linked CC-NBS-LRR genes. *Theor. Appl. Genet.* 122, 1017–1028. doi: 10.1007/s00122-010-1506-3

Yuan, M., Jiang, Z., Bi, G., Nomura, K., Liu, M., Wang, Y., et al. (2021). Pattern-recognition receptors are required for NLR-mediated plant immunity. *Nature.* 592, 105–109. doi: 10.1038/s41586-021-03316-6

Zhai, K., Liang, D., Li, H., Jiao, F., Yan, B., Liu, J., et al. (2022). NLRs guard metabolism to coordinate pattern- and effector-triggered immunity. *Nature.* 601, 245–251. doi: 10.1038/s41586-021-04219-2

Zhang, B., Han, X., Yuan, W., and Zhang, H. (2022). TALEs as double-edged swords in plant-pathogen interactions: progress, challenges, and perspectives. *Plant Commun.* 3, 100318. doi: 10.1016/j.xplc.2022.100318

Zhang, B., Zhang, H., Li, F., Ouyang, Y., Yuan, M., Li, X., et al. (2020). Multiple alleles encoding atypical NLRs with unique central tandem repeats in rice confer resistance to *Xanthomonas oryzae* pv. *oryzae. Plant Commun.* 1, 100088. doi: 10.1016/j.xplc.2020.100088

Zhang, H., and Wang, S. (2013). Rice versus *Xanthomonas oryzae* pv. *oryzae: a unique pathosystem. Curr. Opin. Plant Biol.* 16, 188–195. doi: 10.1016/j.pbi.2013.02.008

Zhang, J., Li, W., Xiang, T., Liu, Z., Laluk, K., Ding, X., et al. (2010). Receptor-like cytoplasmic kinases integrate signaling from multiple plant immune receptors and are targeted by a Pseudomonas syringae effector. *Cell Host Microbe.* 7, 290–301. doi: 10.1016/j.chom.2010.03.007

Zhao, Y., Huang, J., Wang, Z., Jing, S., Wang, Y., Ouyang, Y., et al. (2016). Allelic diversity in an NLR gene *BPH9* enables rice to combat planthopper variation. *Proc. Natl. Acad. Sci. U.S.A.* 113, 12850–12855. doi: 10.1073/pnas.1614862113

frontiers | Frontiers in Microbiology

TYPE Original Research
PUBLISHED 17 November 2022
DOI 10.3389/fmicb.2022.1068158

OPEN ACCESS

EDITED BY
Maofeng Jing,
Nanjing Agricultural University,
China

REVIEWED BY
Zhuo Zhang,
Hunan Academy of Agricultural Sciences,
China
Zhao-Qing Zeng,
Institute of Microbiology (CAS), China

*CORRESPONDENCE
Han-Cheng Wang
xiaobaiyang126@hotmail.com

SPECIALTY SECTION
This article was submitted to
Microbe and Virus Interactions with Plants,
a section of the journal
Frontiers in Microbiology

RECEIVED 12 October 2022
ACCEPTED 31 October 2022
PUBLISHED 17 November 2022

CITATION
Xiang L-G, Wang H-C, Cai L-T, Guo T, Luo F, Hsiang T and Yu Z-H (2022) Variations in leaf phyllosphere microbial communities and development of tobacco brown spot before and after fungicide application. *Front. Microbiol.* 13:1068158. doi: 10.3389/fmicb.2022.1068158

Variations in leaf phyllosphere microbial communities and development of tobacco brown spot before and after fungicide application

Li-Gang Xiang[1,2], Han-Cheng Wang[2]*, Liu-Ti Cai[2], Tao Guo[3], Fei Luo[3], Tom Hsiang[4] and Zhi-He Yu[3]

[1]College of Agriculture, Yangtze University, Jingzhou, Hubei, China, [2]Guizhou Provincial Academician Workstation of Microbiology and Health, Guizhou Academy of Tobacco Science, Guiyang, Guizhou, China, [3]College of Life Sciences, Yangtze University, Jingzhou, Hubei, China, [4]School of Environmental Sciences, University of Guelph, Guelph, ON, Canada

In recent years, STROBY (50% Kresoxim-methyl) has been widely used to control tobacco brown spot in Guizhou Province, China. As a broad-spectrum fungicide, STROBY targets not only phytopathogens, but also affects many other microorganisms including those pathogenic, beneficial, or neutral to the plant hosts. To understand the effects of STROBY on the phyllosphere microbial communities of tobacco leaves during the development of tobacco brown spot, the fungal and bacterial communities of symptomatic and asymptomatic leaves at four time points, before spraying (August 29) and after spraying (September 3, 8, and 13), were investigated using the Illumina high-throughput sequencing. The results showed that STROBY had significant effects on the phyllosphere microbial communities of tobacco leaves. Microbial communities in asymptomatic leaves were more greatly affected than their counterparts in symptomatic leaves, and fungal communities were more sensitive than bacterial communities. Throughout the experiment, the most common genera in symptomatic leaves were *Alternaria*, *Pseudomonas*, *Pantoea*, and *Sphingomonas*, and in asymptomatic leaves, these were *Golubevia* and *Pantoea*. After spraying, the alpha diversity of fungal communities increased in symptomatic leaves and decreased in asymptomatic leaves, while the alpha diversity of bacteria increased in both types of leaves. Beta diversity showed that in asymptomatic leaves, the fungal communities in the first stage was significantly different from the remaining three stages. In contrast, the fungal communities in symptomatic leaves and the bacterial communities in all leaves did not fluctuate significantly during the four stages. Before spraying (August 29), the dominant functions of the fungal community were animal pathogen, endophyte, plant pathogen, and wood saprotroph. Whereas after spraying (September 3, 8, and 13), the proportion of the above fungal functions decreased and the unassigned functions increased, especially in asymptomatic leaves. This study describes the effects of STROBY application and tobacco brown spot presence in shaping the leaf phyllosphere microbial communities, and provides insights into the microbial community effects on tobacco leaves of a strobilurin fungicide.

KEYWORDS

microbial community, STROBY, tobacco brown spot, leaf phyllosphere, high-throughput sequencing

Introduction

Tobacco brown spot caused by *Alternaria alternata* (Fr.) Keissl, has been confirmed as one of the most harmful fungal diseases that significantly affects the quantity and quality of tobacco (Wang et al., 2015). In China, approximately 100,000 ha of tobacco fields are affected by tobacco brown spot each year, resulting in an economic loss of 1 billion RMB (Liu et al., 2009). Symptoms of tobacco brown spots on leaves include small, round, and yellowish-brown spots in the initial stage, which then gradually develop into large areas (Jing et al., 2018). The most effective and economical method of controlling this disease in the field is the application of fungicides. Fungicides that have been used for the control of tobacco brown spot in China are boscalid (Lei et al., 2021), azoxystrobin, and difenoconazole (Wang et al., 2016). In recent years, a broad-spectrum fungicide, STROBY (50% kresoxim-methyl), has been widely used in Guizhou Province for tobacco spot disease control, especially for tobacco brown spot. STROBY is a Quinone outside Inhibitor (QoI) fungicide (Kolosova et al., 2017; Ge et al., 2021), also commonly called strobilurins. Strobilurins bind to the Qo site of cytochrome b, blocking electron transfer between cytochrome b and cytochrome c1 and inhibiting mitochondrial respiration (Balba, 2007; Mercader et al., 2008). Strobilurins are known to affect Ascomycota, Basidiomycota, and even Oomycota (Grossmann and Retzlaff, 1997), but there are few reports on whether it has an effect on bacteria. In previous studies, STROBY was used to control Botrytis blight of gladiolus (Singh et al., 2011), and powdery mildew of mango, cucumber, and grape (Yu et al., 2008; Reuveni et al., 2018). In addition to its use as a fungicide, STROBY can also be used as a growth-promoting compound to regulate leaf growth in *Arabidopsis* (Van Dingenen et al., 2017) and to promote wound healing in potato tubers (Ge et al., 2021).

The phyllosphere is the aerial or above-ground part of plant, such as stems, leaves, flowers, and fruits (Knief et al., 2010). From a microbial point of view, the environmental conditions of the leaf phyllosphere may be harsh, with limitations on free water, nutrients, favorable temperatures, and relative humidity, as well as fluctuations in UV radiation (Bashir et al., 2022). Anthropogenic factors such as climate warming, chemical and air pollution, and application of fertilizers and pesticides have wide impacts on leaf phyllosphere microorganisms (Xu et al., 2022). Because of the quickly changing environmental conditions of the phyllosphere, the microbial communities are also in flux. Within these communities, some members may be beneficial to the host plant, and improve plant productivity, or defend against phytopathogen invasion, or increase plant stress resistance, while others are plant pathogens that can cause disease once conditions are suitable, but most microorganisms are likely neutral and have no effects on the host (Stone et al., 2018; Thapa and Prasanna, 2018; Liu et al., 2020).

As a broad-spectrum fungicide, STROBY affects not only plant pathogens but also microorganisms that are beneficial or neutral to hosts. Therefore, the objectives of this study were as follows: (i) assess field efficacy of STROBY against tobacco brown spot; (ii) investigate composition and diversity of microbial communities in the leaf phyllosphere before and after STROBY application; and (iii) compare differences in microbial community composition and diversity and response to STROBY pressure between symptomatic and asymptomatic leaves.

Materials and methods

Experimental design

The experiment was conducted in August and September 2020 in a mature tobacco field, Bijie city (26.74 N, 104.02E), Guizhou Province, China. Prior to the experiment, tobacco brown spot had sporadically appeared on the tobacco plants (cultivar Yunyan 105) in the field. On 29 August 2020, nine symptomatic and nine asymptomatic tobacco plants at least 3 m apart from each other were randomly selected for first sampling, and one tobacco leaf was collected from each plant. After the first sampling, the entire tobacco field (50 m × 20 m) was sprayed with a 3,000-fold dilution (300 g/ha) of STROBY® (50% Kresoxim-methyl, BASF), and the tobacco leaves were sprayed on both sides until runoff. The second, third, and fourth samplings were done on September 3, 8, and 13, respectively. The 18 tobacco plants used for sampling were the same ones at all four sampling time points. The letters CBB were used to denote symptomatic leaves and CBJ to denote asymptomatic leaves, followed by the number 0 for the first sampling, 1 for the second sampling, 2 for the third sampling, and 3 for the fourth sampling, and finally followed by 1–3 for biological repetition.

During the entire experiment, environmental conditions were measured with an automatic weather station (Beijing Xinhong Tec. IT, Co., Ltd., Beijing, China) and soil moisture sensor (RainPoint, Walnut, CA, United States). Temperature, relative humidity, rainfall, soil temperature, soil relative humidity, and disease index were the average of the 4 days before sampling and the day of sampling. The calculation method of disease index followed Wu et al. (2015), and the classification of tobacco brown spot followed the Chinese National Standard (GB/T 23222-2008) from the Standardization Administration of China.

Leaf phyllosphere microorganisms were collected as described by Luo et al. (2019), with slight modifications. Three leaves of the same type and time point were mixed for processing giving three samples of symptomatic leaves and three samples of asymptomatic leaves. Each leaf was cut into 5 mm by 5 mm pieces. Five grams of leaf pieces per sample were placed in a 500 ml sterile conical flask with 300 ml phosphate buffer saline (PBS) containing 0.01% Tween-80. Then the flask was shaken at 28°C for 30 min at 180 rpm/min. The PBS buffer was then filtered through a 0.45 μm filter microfiltration membrane, and the membrane was stored at-80°C for further DNA extraction.

DNA extraction, PCR amplification, and high-throughput sequencing

Total genomic DNA from each of the 24 samples was extracted using a FastDNA® Spin Kit (MP Biomedicals, Santa Ana, CA, United States) based on the manufacturer's instruction. The purity and concentration of genomic DNA were assessed using agarose gel electrophoresis and the NanoDrop-2000 (Thermo Fisher Scientific, Waltham, MA, United States). The DNA concentration was diluted to 30 ng/μl for each sample. For PCR amplification, the bacterial hypervariable V4 region of the 16S rRNA gene was amplified using primers 515F/806R (Moreau and Rubin, 2017), and the fungal ITS1 region was amplified using primers ITS1/ITS2 (Zhang et al., 2010). The PCR reaction solutions and thermocycling steps for V4 and ITS1 regions followed Wei et al. (2018). The PCR products were visualized on 2% agarose gel electrophoresis, quantified by NanoDrop-2000, and purified with the Qiagen Gel Extraction Kit (Qiagen, Dusseldorf, Germany). Libraries were generated for each sample as described in Xiang et al. (2022). Finally, the libraries were sequenced on an Illumina NovaSeq PE250 platform at Novogene Bioinformatics Technology Co., Tianjin, China, generating 250 bp paired-end reads.

Bioinformatics analysis

Paired-end raw reads were assigned to samples based on their unique 12-bp barcodes and truncated by cutting off the barcode and primer sequence. Paired-end reads with at least 10 bp overlap and up to 0.25 mismatch rate were merged using FLASH V1.2.7 (http://ccb.jhu.edu/software/FLASH/; Magoč and Salzberg, 2011). QIIME V1.9.1[1] was used to filter raw reads under specific criteria (reads with ambiguous bases or quality scores <20 or the length < 200 bp) to obtain clean reads (Bokulich et al., 2013). Clean reads were compared to the UNITE (V12.01.2017) and Silva (V132) databases using the UCHIME algorithm[2] to detect chimeric sequences for removal (Haas et al., 2011). After a series of operations, the sequences were considered "effective" reads. Sequences with at least 97% similarity were assigned to the same operational taxonomic unit (OTU) using Uparse software V7.0.1001 (Edgar, 2013). Based on the Mothur algorithm, the taxonomic information of each representative sequence of each OTU was annotated using the UNITE and Silva database. To analyze the alpha and beta diversity of the microbial communities for each sample, the OTU abundance was normalized to the sample with the fewest sequences. All alpha indices of microbial communities in the samples were calculated with QIIME V1.7.0, and displayed with R software V2.15.3. The beta diversity of both weighted and unweighted UniFrac distance was calculated with QIIME V1.9.1. The Wilcoxon signed rank test was used to compare the alpha diversity index of symptomatic and asymptomatic leaf microbial communities. Principal co-ordinate analysis (PCoA) with unweighted UniFrac distance was performed based on the Bray–Curtis dissimilarity matrix, and the results were displayed using the WGCNA package, stat packages, and ggplot2 package in R software following Zhou et al. (2018). Linear discriminant analysis effect size (LEfSe) analysis with a threshold of 4.0 in the logarithmic LDA score was used to reveal the significant ranking of biomarkers between samples. Effective reads were compared with the Greengene database using PICRUSt[3] to predict bacterial functionality (Langille et al., 2013), and with FUNGuild database[4] to obtain the fungal trophic mode and guild (Nguyen et al., 2016). The co-occurrence networks of leaf phyllosphere microbial genera and the relationships between environmental factors and microbial genera richness were demonstrated using Spearman's rank analysis based on significant ($p < 0.05$) and strong positive correlations ($r > 0.6$) or strong negative correlations ($r < -0.6$; Li and Wu, 2018).

Results

Environmental conditions and tobacco disease index

During the 5-day period of each sampling interval (August 25–29, August 30 to September 3, September 4–8, and September 9–13), there were no significant differences in average daily temperatures, rainfall, and soil temperature between the four stages; the average daily relative humidity in the first stage was significantly lower than that in the fourth stage; and the average daily soil relative humidity and disease index in the first and second stages were significantly lower than that in the third and fourth stages (Table 1). As asymptomatic plants did not develop disease throughout the experiment, only the disease index of symptomatic plants was counted.

1 http://qiime.org/scripts/split_libraries_fastq.html
2 http://www.drive5.com/usearch/manual/uchime_algo.html
3 http://picrust.github.com/
4 https://github.com/UMNFuN/FUNGuild

10.3389/fmicb.2022.1068158

TABLE 1 Environmental factors and symptomatic tobacco plant disease indices in tobacco fields.

Sampling date	Temperature (°C)	Relative humidity (%)	Rainfall (mm/m²)	Soil temperature (°C)	Soil relative humidity (%)	Disease index
Aug 25	19.0	62.2	0.0	21.7	27.3	17.9
Aug 26	17.6	65.5	0.0	21.1	24.9	18.0
Aug 27	22.2	62.7	0.0	21.7	22.6	18.0
Aug 28	19.2	82.4	1.4	21.6	21.5	18.2
Aug 29	18.3	82.5	13.6	21.1	23.5	18.3
Average	19.3 ± 1.8a	71.1 ± 10.5b	3.0 ± 6.0a	21.4 ± 0.3a	24.0 ± 2.2b	18.1 ± 0.2c
Aug 30	19.1	80.4	0.6	21.2	25.2	20.0
Aug 31	19.8	77.8	3.0	21.3	24.8	20.0
Sep 1	19.6	73.4	0.0	21.5	23.7	20.6
Sep 2	19.9	77.3	0.0	21.5	22.3	20.6
Sep 3	19.0	83.8	19.0	21.2	27.7	20.8
Average	19.5 ± 0.4a	78.5 ± 3.9ab	4.5 ± 8.2a	21.3 ± 0.2a	24.7 ± 2.0b	20.4 ± 0.4c
Sep 4	19.8	81.2	1.2	21.5	30.2	21.6
Sep 5	20.2	81.9	2.2	21.8	28.6	23.2
Sep 6	16.1	89.5	53.6	20.1	33.2	25.7
Sep 7	17.5	74.8	0.0	21.0	32.1	27.4
Sep 8	17.5	79.0	0.0	21.4	31.1	28.3
Average	18.2 ± 1.7a	81.3 ± 5.4ab	11.4 ± 23.6a	21.2 ± 0.7a	31.0 ± 1.8a	25.2 ± 2.8b
Sep 9	18.9	79.1	0.0	21.9	30.6	28.5
Sep 10	17.4	89.8	11.8	20.8	32.5	29.0
Sep 11	16.1	86.5	0.0	20.2	32.5	30.0
Sep 12	16.8	90.8	13.0	20.2	32.9	31.6
Sep 13	16.5	91.0	25.4	19.9	34.4	32.2
Average	17.1 ± 1.1a	87.4 ± 5.0a	10.0 ± 10.6a	20.6 ± 0.8a	32.6 ± 1.4a	30.3 ± 1.6a

Different letters in the same column indicate significant difference at $p < 0.05$ among stage.

Sequence information

After sequence and data processing, a total of 794,733 and 790,491 effective fungal reads were obtained from the symptomatic and asymptomatic leaves, respectively, averaged across three samples each (Supplementary Table S1). The average number of reads in symptomatic and asymptomatic leaves at four sampling time points was 64,000–68,000. For bacterial communities, 833,289 effective reads were obtained from symptomatic leaves, and the average number at four sampling time points ranged from 62,000 to 85,000. The asymptomatic leaves gave 835,795 effective bacterial reads with averages ranging from 66,000 to 78,000 among the four sampling time points. The fungal and bacterial raw sequences of each sample have been deposited in the SRA database under project number PRJNA806570.

Microbial community composition

At the phylum level, the fungal divisions Ascomycota and Basidiomycota were the most abundant in symptomatic and asymptomatic leaves, except for the "Others" group (Figure 1A). The "Others" group in Figures 1, 2 represent all microorganisms that were unidentified or whose relative abundance was less than 0.1%. In symptomatic leaves, the relative abundance of Ascomycota remained at about 94% for 10 days after spraying, while it decreased significantly to 62% on the 15th day after spraying. In asymptomatic leaves, Ascomycota was the dominant fungal division (57%) followed by Basidiomycota (10%) before spraying. On the fifth day after spraying, the relative abundance of Ascomycota decreased significantly to 7%, while the relative abundance of Basidiomycota increased significantly to 36% and became the most dominant phylum. The relative abundance of Proteobacteria gradually increased after spraying, with 38/7, 57/24, 79/15, and 91/32% for symptomatic/asymptomatic leaves at the four sampling time points, respectively (Figure 1B).

At the genus level, *Alternaria* was the dominant genus in symptomatic leaves at the four sampling time points, with the relative abundances between 56 and 92% (Figure 2A). Before spraying, the dominant genus in asymptomatic leaves was *Alternaria* (33%), followed by *Cladosporium* (13%), *Symmetrospora* (5%), *Boeremia* (5%), and *Golubevia* (4%). *Golubevia* was the dominant genus in asymptomatic leaves on the 5, 10, and 15th days after spraying, with relative abundances of 35–36%. The relative abundance of *Alternaria* in asymptomatic leaves was less than 4% at three sampling time points after spraying. For bacterial communities, the "others" group had a high percentage in most samples. *Pseudomonas*, *Pantoea*, and *Sphingomonas* were the

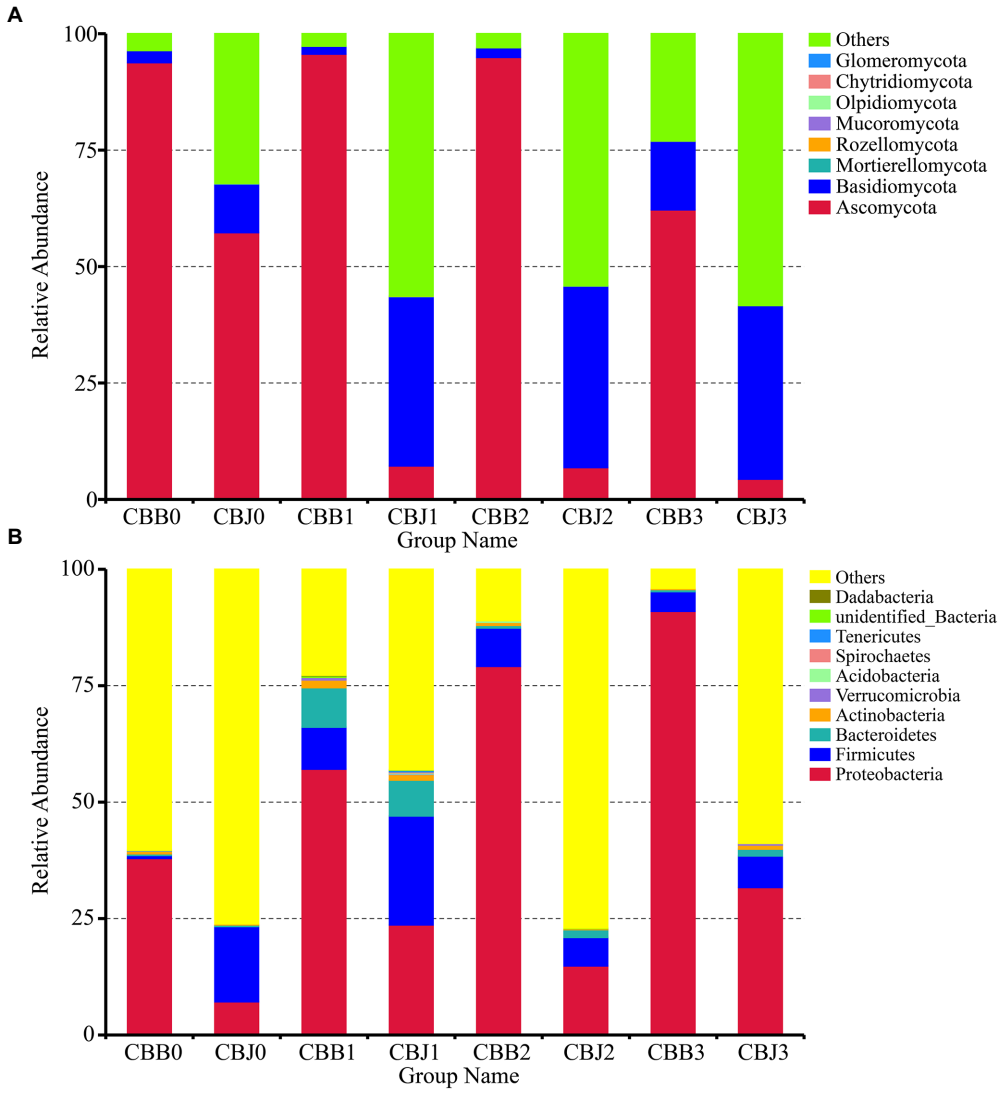

FIGURE 1
Microbial community composition of symptomatic (CBB) and asymptomatic (CBJ) tobacco leaves at four sampling time points (0–3) at the phylum levels (**A** for fungi, **B** for bacteria). The phyla with relative abundance less than 0.01% or without identification were classified as "Others."

common dominant genera in symptomatic leaves at four sampling time points (Figure 2B). In asymptomatic leaves, *Weissella* (15%) and *Pantoea* (6%) were the dominant genera in CBJ0, *Pseudomonas*, *Pantoea*, *Sphingomonas*, *Erwinia*, *Romboutsia*, and unidentified Enterobacteriaceae were the dominant genera in CBJ1, CBJ2, and CBJ3, but their relative abundant was less than 8%.

At the four sampling time points, there were 17, 19, and 11 core fungal OTUs in the symptomatic leaves, asymptomatic leaves, and all leaves, respectively (Figures 3A–C). Among the 11 core fungal OTUs, five OTUs belonged to unidentified fungi, while others belonged to *Alternaria*, *Cladosporium*, *Symmetrosporaceae*, *Stagonosporopsis*, *Golubevia*, and *Didymella*. For bacterial communities, there were 10, four, and four core bacterial OTUs in the symptomatic leaves, asymptomatic leaves, and all leaves at four sampling time points, respectively (Figures 3D–F). Among the four core OTUs in all leaves, three OTUs belonged to unidentified bacteria, and the remaining one belonged to *Pantoea*.

Microbial community diversity

Alpha diversity

Alpha diversity of fungal communities increased in symptomatic leaves and decreased in asymptomatic leaves after STROBY spraying (Figures 4A–F). Before spraying, the Ace index, Chao1 index, Shannon index, Simpson index, and PD_whole_tree index of fungal communities in symptomatic leaves were significantly higher than asymptomatic leaves. At 15 days after spraying, these indices of fungal community in symptomatic

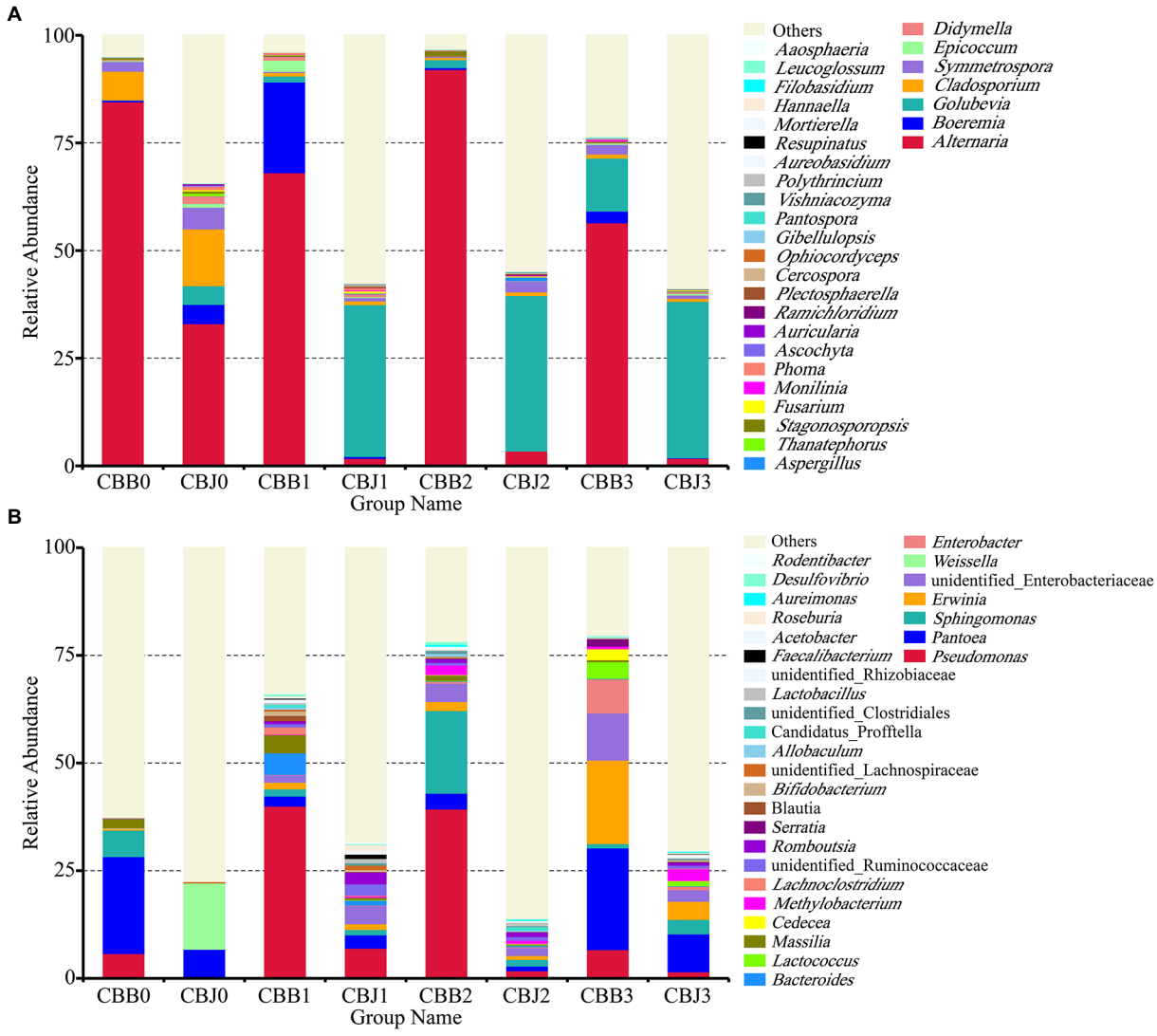

FIGURE 2
Microbial community composition of symptomatic (CBB) and asymptomatic (CBJ) tobacco leaves at four sampling time points (0–3) at the genus leaves (**A** for fungi, **B** for bacteria). The genera with relative abundance less than 0.01% or without identification were classified as "Others".

leaves seemed lower than asymptomatic leaves, but without statistically significant differences between the two types of leaves. Within 5 days after spraying, the Ace index, Chao1 index, Shannon index, and PD_whole_tree index of the bacterial communities increased significantly in symptomatic leaves (Figures 4G–L).

Beta diversity

Weighted and unweighted UniFrac distance metrics were used to estimate microbial beta diversity in the leaf phyllosphere. Dissimilarity coefficients were calculated for all samples and the results confirmed that STROBY could directly affect microbial diversity (Figure 5). Smaller dissimilarity coefficients between samples indicate smaller differences in microbial diversity. Differences between bacterial communities of the different samples were smaller than those of the fungal community. For fungal communities, the CBB0, CBB1, CBB2, and CBB33 differed significantly from CBJ1, CBJ2, and CBJ3. For bacterial communities, only CBJ12 differed from all other samples.

Principal coordinate analysis (PCoA) of Bray-Curtis dissimilarities was performed to explore how microbial community composition varied after spraying. The fungal communities of symptomatic and asymptomatic leaves were clearly clustered separately (Figure 6A). Most symptomatic samples were clustered in first and fourth quadrants (only CBB31 clustered in second quadrant), and most asymptomatic samples were clustered in second and third quadrants (CBJ01 and CBJ03 clustered in first quadrant), indicating significant differences in fungal community composition between symptomatic and asymptomatic leaves. With the exception of CBB02, CBB31, and CBB32, symptomatic leaves were tightly clustered, showing that

10.3389/fmicb.2022.1068158

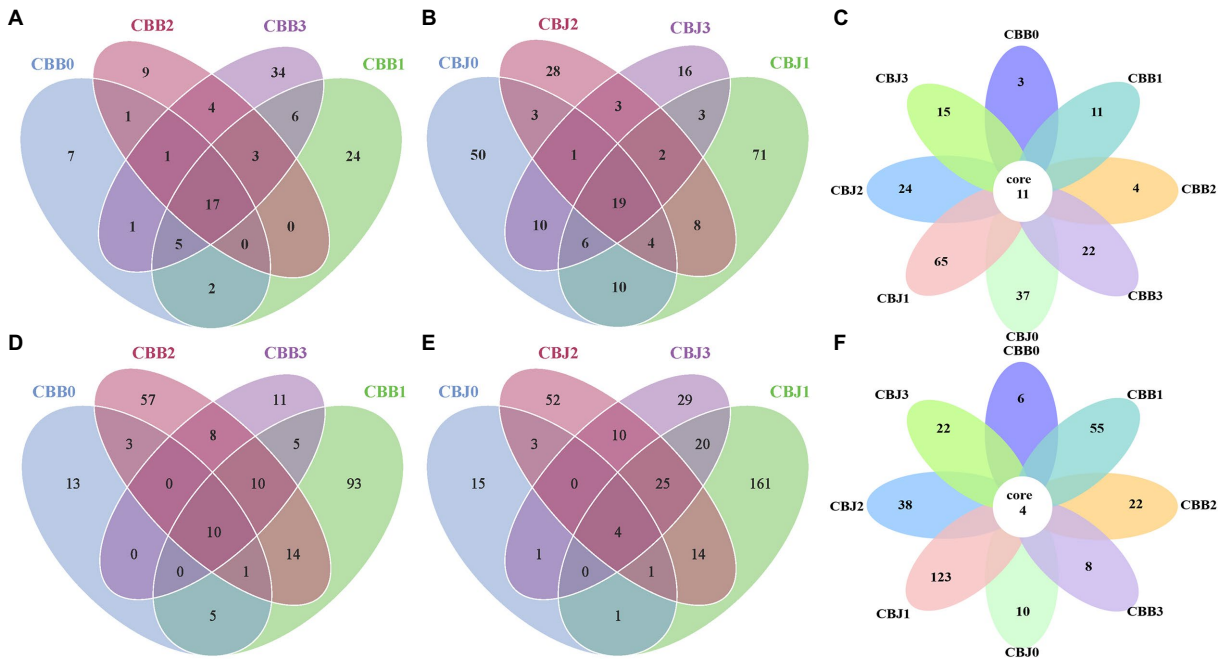

FIGURE 3
Venn diagram showing the number of microbial OTU detached in tobacco leaves (symptomatic leaves CBB; asymptomatic leaves CBJ) at four sampling time points (0–3). **(A–C)** for fungal, **(D–F)** for bacterial. Numbers in the non-overlapping region indicate unique OTUs for the single sample; numbers in the overlapping region indicate shared OTUs for multi-samples; and numbers in the core region indicate shared OTUs for each sample.

no significant changes in the fungal communities of symptomatic leaves until the 15th day after spraying. The group of CBJ0 did not cluster with asymptomatic samples from other sampling time points, indicating that spraying could significantly affect the fungal community composition of asymptomatic leaves. For bacterial communities, most symptomatic samples were clustered in first and fourth quadrants (CBB01 and CBB03 clustered in second quadrant), and most asymptomatic samples were clustered in second and third quadrants (CBJ32 clustered in first quadrant, CBJ12 and CBJ13 clustered in fourth quadrant; Figure 6B). The close sample distance between samples from different sampling time points of the same type of leaves suggested that STROBY application may have little effect on the phyllosphere bacterial communities.

To determine the biomarker in samples, LEfSe was performed to identify taxa that exhibited significant differences among the symptomatic and asymptomatic leaves at different sampling time points (Figure 7). Among the fungal communities, the number of fungal biomarkers was five, one, three, three, and six in CBB1, CBB2, CHJ0, CBJ2, and CBJ3, respectively. In the bacterial communities, a total of 28 bacterial taxa were identified as biomarkers at different sampling points of two types of leaves. The number of bacterial biomarkers in CBB1, CBB2, CBB3, CBJ1, and CBJ3 was four, six, seven, four, and seven, respectively. There were no significantly different fungal biomarkers in CBB0, CBJ1, and CBB3 groups, and no bacterial biomarkers in CBB0, CBJ0, and CBJ2 groups.

Microbial community ecological functions

Fungal ecological functions were predicted using FUNGuild based on community composition (Figure 8A). The dominant fungal functions in symptomatic leaves were animal pathogen, endophyte, plant pathogen, wood saprotroph, and unassigned. For fungal communities in CBJ0 group, the dominant functions were unassigned, followed as animal pathogen, endophyte, plant pathogen, and wood saprotroph. At three sampling time points after spraying, the dominant fungal function in asymptomatic leaves was "unassigned," with relative abundance greater than 95%. Bacterial or archaeal gene families were estimated using PICRUSt (Figure 8B). In this study, metabolism, genetic information processing, and unclassified and environmental information processing were the dominant bacterial community functions common to all samples, only differing in their relative abundance from sample to sample.

Co-occurrence network analysis between microorganisms

Co-occurrence network analysis was used to investigate the interaction of complex microorganisms. A total of 10 strong negative correlations and 154 strong positive correlations were identified from 47 fungal genera (Figure 9A). The co-occurring genera were distributed in Ascomycota (72%), Basidiomycota (26%), and Mortierellomycota (2%). As a genus containing the tobacco brown spot pathogen, *Alternaria* was positively correlated with

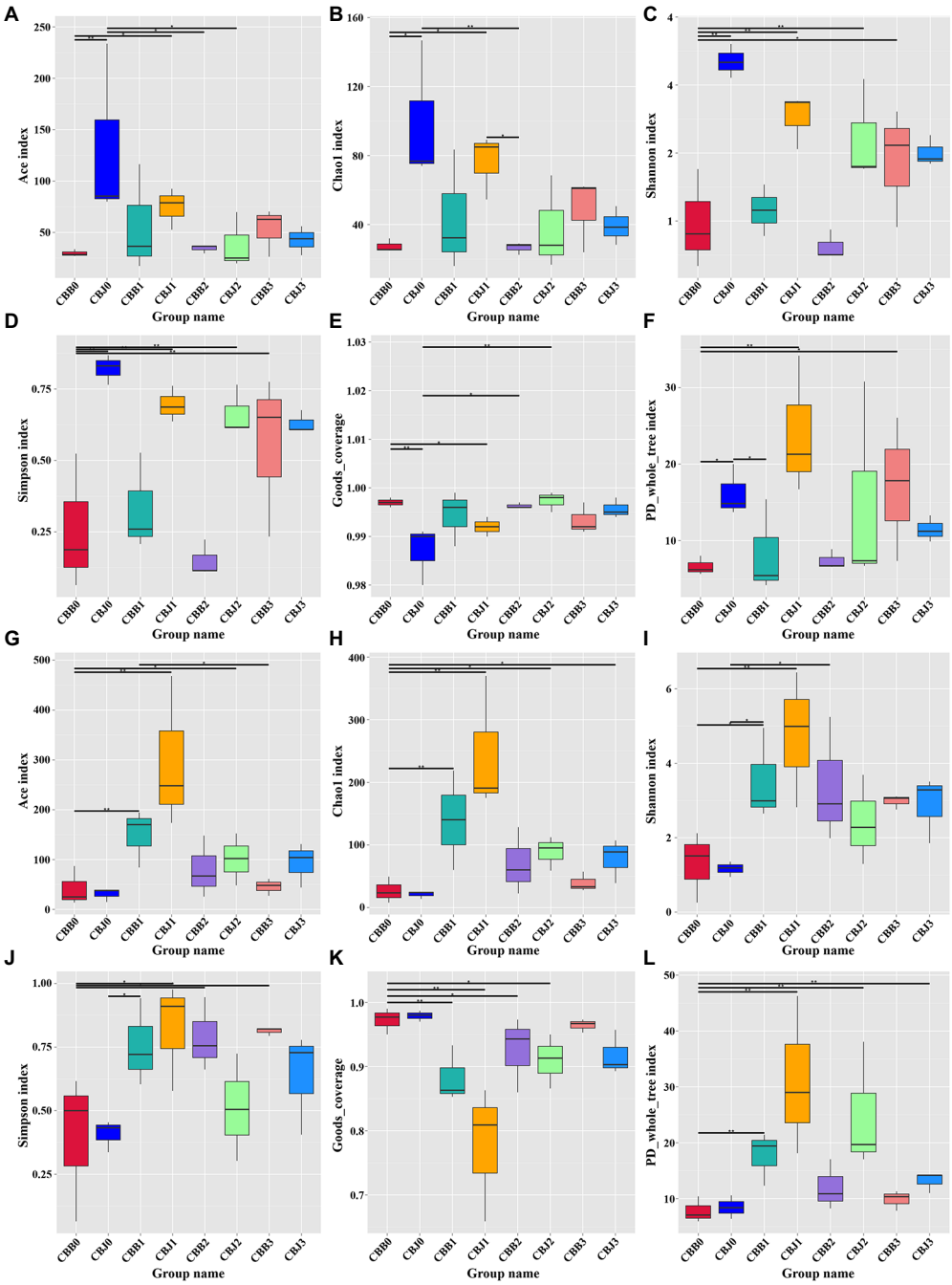

FIGURE 4
Alpha diversity of the microbial (**A–F** for fungal, **G–L** for bacterial) communities in tobacco leaves (symptomatic leaves CBB; asymptomatic leaves CBJ) at four sampling time points (0–3). **(A,G)** Show the Ace index; **(B,H)** show the Chao1 index; **(C,I)** show the Shannon index; **(D,J)** show the Simpson index; **(E,K)** show the Goods_coverage; and **(F,L)** show the PD_whole_tree index. "*" represents a statistical difference between groups (p<0.05), "**" represents a significant statistical difference between groups (p<0.01; Wilcoxon Signed Rank Test).

Stagonosporopsis, and negatively correlated with *Golubevia*, *Aspergillus*, *Plectosphaerella*, and *Fusarium*. The remaining six of the 10 strong negative correlations of fungal communities were *Golubevia-Stagonosporopsis*, *Didymella-Monilinia*, *Aspergillus-Stagonosporopsis*, *Stagonosporopsis-Fusarium*, *Stagonosporopsis-Monilinia*, and *Phoma-Vishniacozyma*. *Ramichloridium*, *Mortierella*, *Plenodomus*, and *Polythrincium* were the top four genera based on the high centrality score. In the bacterial communities, four negative correlations and 212 positive correlations were identified from 48 genera that belong to Proteobacteria (48%), Firmicutes (33%), Bacteroidetes (6%), Actinobacteria (4%), Sporochaetes (2%), Tenericutes (2%), Verrucomicrobia (2%), and unidentified bacteria (2%) (Figure 9B). Four significant negative correlations of bacterial communities occurred in *Erwinia-Weissella*, *Bacteroides-Aureimonas*,

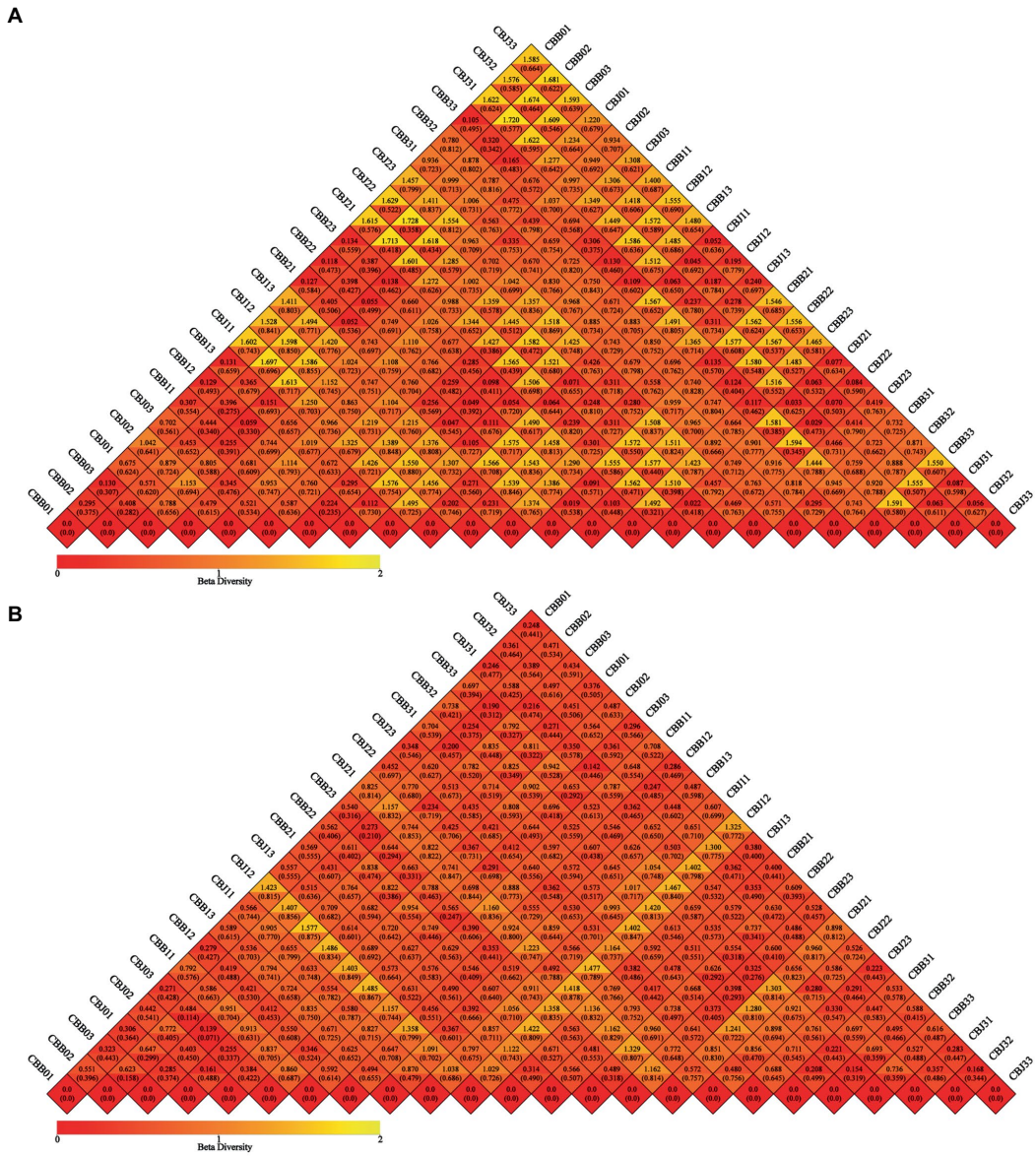

FIGURE 5
Beta diversity heatmap diagram of microbial communities in tobacco leaves (symptomatic leaves CBB; asymptomatic leaves CBJ) at four sampling time points (The first numbers 0–3 in the sample name represent four different sampling time points, respectively. The numbers 1–3 at the end of the sample name represent three biological replicates.). **(A)** For fungal communities, **(B)** for bacterial communities. In the same grid, the upper and lower values represented Weighted Unifrac and Unweighted Unifrac distance value, respectively.

Lactococcus-Massilia, and *Massilia-Aureimonas*. Unidentified Enterobacteriaceae, unidentified Ruminococcaceae, *Paracoccus*, and unidentified Clostridiales were the top four bacterial genera based on the high centrality score.

The relationship between microorganisms and environmental conditions

The relationships between microorganisms and temperature, relative humidity, rainfall, soil temperature, soil relative humidity, and disease index were investigated using Spearman's rank analysis (Figure 10). Temperature was significantly and positively correlated with *Mortierella*, *Verticia*, unidentified Rhizobiaceae, and unidentified Lachnospiraceae, while significantly and negatively correlated with *Vishniacozyma*, *Aureimonas*, *Cedecea*, and *Enterobacter*. Relative humidity and rainfall were significantly and positively correlated with *Roseburia* and *Serratia*. Soil temperature was significantly and positively correlated with *Desulfovibrio* and *Allobaculum*, while significantly and negatively correlated with *Pantoea*. Soil relative humidity was significantly and positively correlated with *Aureimonas*, *Cedecea*, *Methylobacterium*, *Lactococcus*, *Enterobacter*, unidentified

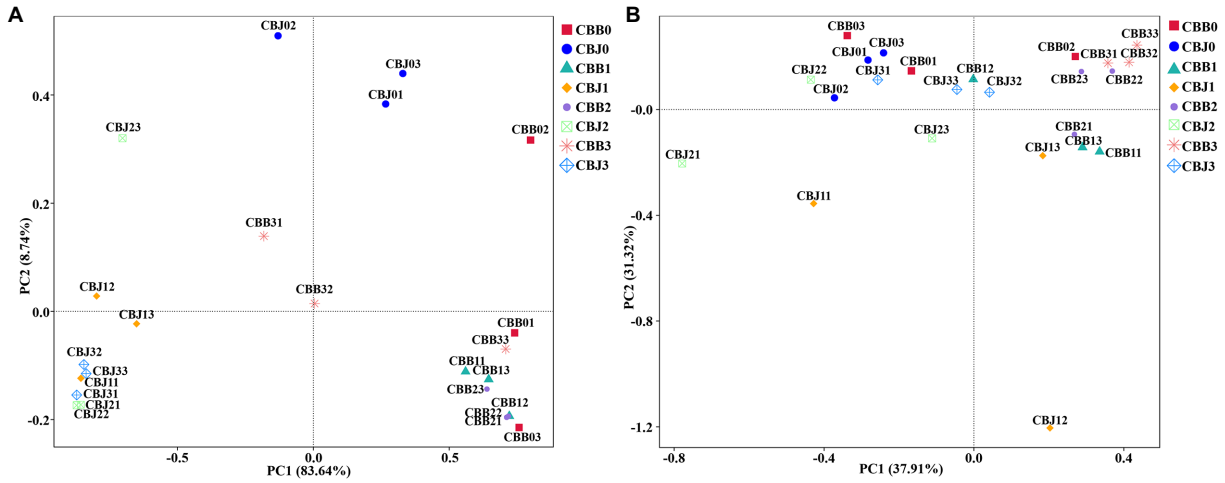

FIGURE 6
Principal coordinate analysis (PCoA) of the microbial communities in tobacco leaves (symptomatic leaves CBB; asymptomatic leaves CBJ) at four sampling time points (The first numbers 0–3 in the sample name represent four different sampling time points, respectively. The numbers 1–3 at the end of the sample name represent three biological replicates.). **(A)** For fungal communities and **(B)** for bacterial communities.

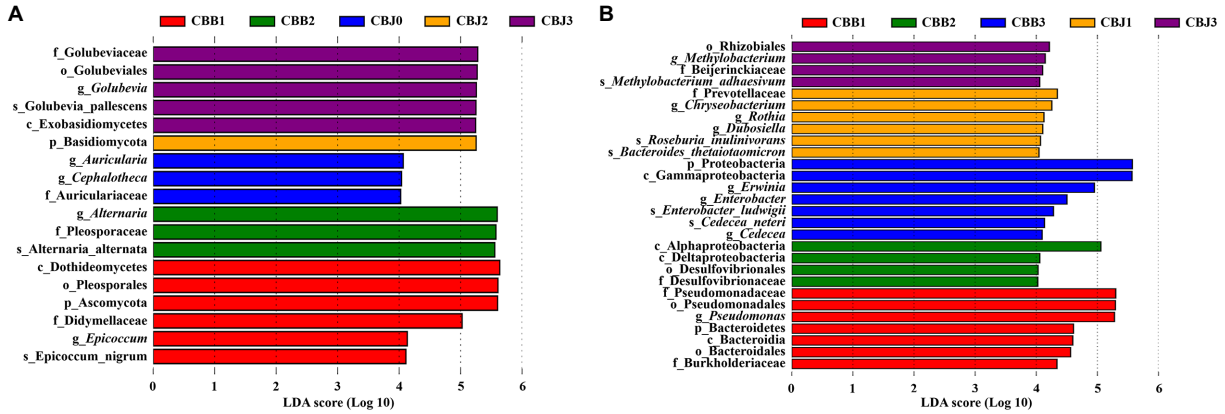

FIGURE 7
LEfSe analysis of microbial communities among tobacco leaves (symptomatic leaves CBB; asymptomatic leaves CBJ) at four sampling time points (0–3). **(A)** For fungal communities and **(B)** for bacterial communities.

Enterobacteriaceae, and *Erwinia*, while significantly and negatively correlated with *Thanatephorus* and *Weissella*. Disease index was significantly and positively correlated with *Plectosphaerella*, *Fusarium*, *Aspergillus*, and *Golubevia*, while significantly and negatively correlated with *Alternaria* and *Massilia*.

Discussion

A single application of STROBY (300 g/ha, 3000x dilution) in mature tobacco fields could prevent the occurrence of tobacco brown spot on asymptomatic plants, but could not prevent the increase of disease index on symptomatic plants (The disease index increased by 12.2 in 15 days). Perhaps if the rate and dose of STROBY are increased within safe limits, its curative effects on tobacco brown spot may be improved.

As expected, the dominant genus in symptomatic leaves was *Alternaria*, because *Alternatia alternata* is the causal agent of tobacco brown spot. However, we also found a high relative abundance of *Alternaria* in asymptomatic leaves. *Alternaria* on asymptomatic leaves may originate from symptomatic leaves and may cause disease on asymptomatic leaves once environmental conditions are suitable. The relative abundance

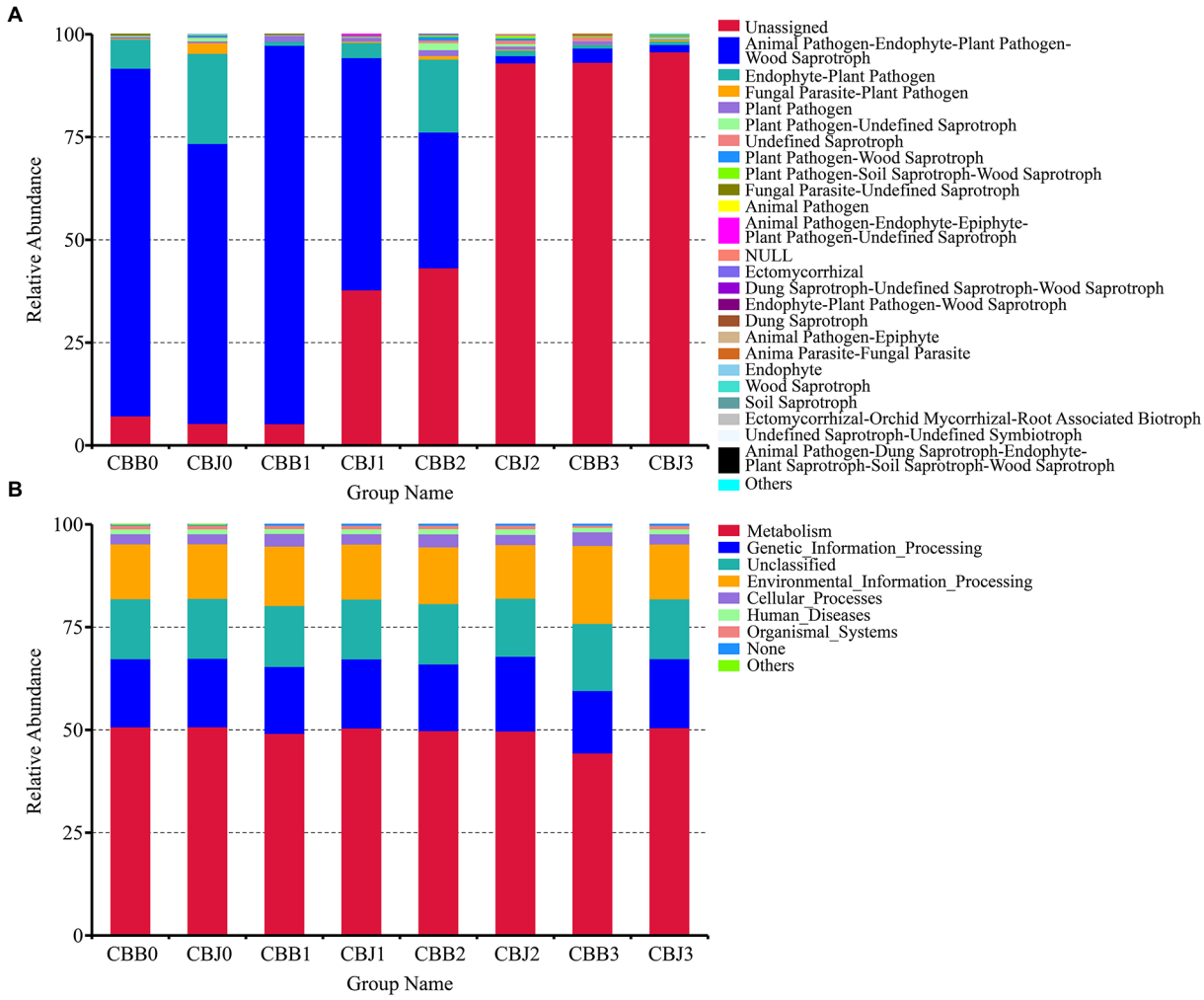

FIGURE 8
Microbial functional categories of tobacco leaves (symptomatic leaves CBB; asymptomatic leaves CBJ) at four sampling time points (0–3). **(A)** For fungal communities and **(B)** for bacterial communities.

of *Alternaria* in asymptomatic leaves was lower than symptomatic leaves before spraying. After spraying, the relative abundance of *Alternaria* showed minor fluctuations among symptomatic leaves, and decreased significantly in asymptomatic leaves. In asymptomatic leaves, spores of *Alternaria* may have landed on the leaf surface, or germinated hyphae may have begun initial invasion, but the STROBY application might have killed them off on asymptomatic leaves or halted further progression. On the contrary, in symptomatic leaves, *Alternaria* may had invaded and grown inside the leaf tissue, so that STROBY was unable to eliminate the established growth. We speculate that our conditions of STROBY application (300 g/ha) was able to preventively affect the occurrence of brown spot but did not have strong curative activity. Similar to *Alternaria*, the relative abundance of *Cladosporium* in asymptomatic leaves decreased significantly after spraying. *Cladosporium* contains a number of potential plant pathogens that can cause diseases in a variety of crops such as cucumber, tomato, and canola (Batta, 2004; Rivas and Thomas, 2005; Idnurm et al., 2021). In contrast to *Alternaria*, *Golubevia* in asymptomatic leaves increased significantly after spraying. The co-occurrence network also demonstrated the same result that *Alternaria* and *Golubevia* had a strong negative correlation. We did not find published reports on the effect of *Golubevia* on plant growth, but it can be detected on many plants (Chen et al., 2020; Qu et al., 2020; Liu et al., 2022). In addition to *Alternaria*, the other common fungal OTUs *Cladosporium*, *Didymella* and *Phoma* have been reported to contain tobacco pathogens (Wang et al., 2014; Yuan et al., 2016; Guo et al., 2020).

The leaf phyllosphere bacterial communities did not have as clear a pattern of variation as the fungal community did. Even among the three replicates of the same group, there were large differences in microorganism composition. Overall, the

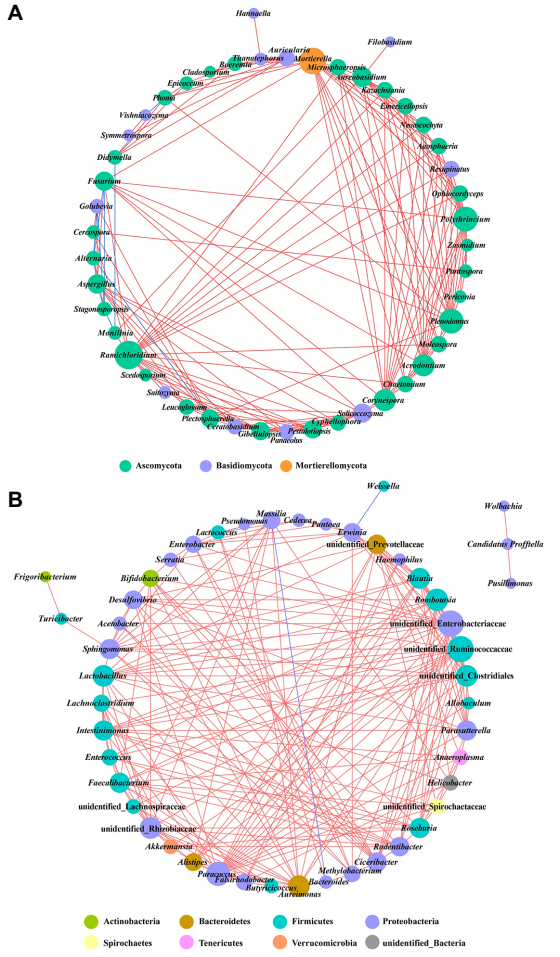

FIGURE 9
Co-occurrence networks of microbial communities at genus level. **(A)** For fungal communities and **(B)** for bacterial communities. Node color represents the phylum of the genus and the size corresponds to the centrality score. Red lines indicate positive relationships, and blue lines indicate negative relationships.

major bacterial genera of the tobacco leaves were *Pseudomonas*, *Pantoea*, *Sphingomonsa*, and *Erwinia*. Within these genera, *Pseudomonas tabaci* (Sinden and Durbin, 1968) and *Pantoea endophytica* (Ilyas et al., 2021) are known as tobacco pathogens.

The alpha diversity results showed that the fungal communities increased in symptomatic leave and decreased in asymptomatic leaves after spraying. We speculated that *Alternaria* as the dominant genus in symptomatic leaves occupied and consumed a large amount of space, nutrients, and free water, resulting in inhibition of the growth of other fungi. When the relative abundance of *Alternaria* decreases, other fungi can grow rapidly, which ultimately lead to an increase in fungal community diversity. Another possible reason was that the fungal community diversity in asymptomatic leaves was significantly higher than symptomatic leaves before spraying. Due to defense mechanisms of plants, many fungi on asymptomatic leaves may not invade the tissues, but only adhered to the leaf surface, so STROBY had a higher effect on them than the fungi in symptomatic leaves. And thereby, the fungal community diversity of asymptomatic leaves decreased after spraying. Additionally, the diversity of bacterial community increased in all leaves after spraying. On the one hand, the STROBY action targets mainly fungal communities such as Ascomycetes, Basidiomycetes, Deuteromycetes, and Oomycetes (Grossmann and Retzlaff, 1997). On the other hand, the resources on tobacco leaves are limited, and once the fungal communities are inhibited, the resources they consume will also be reduced, so more resource will be available for use by bacterial communities.

By using community dissimilarity analysis between consecutive sampling time points, the community change trends were visualized. The change rate of fungal communities was fastest within 5 days after spraying in asymptomatic leaves, and at 10–15 days after spraying in symptomatic leaves. As speculated upon and mentioned above, fungi on symptomatic leaves may invade the inside of leaves through necrotic spot tissue. Since the structural integrity of asymptomatic leaves makes it difficult for fungi to invade the interior, the majority of fungi may only adhere to the leaf surface. Therefore, on asymptomatic leaves, STROBY can directly affect the fungal communities, while on symptomatic leaves, STROBY needs to be absorbed by leaves to affect the fungal communities. These may account for the delayed action of STROBY on fungal communities of symptomatic leaves compared to those of asymptomatic leaves. For the same reasons, the fungal communities of the asymptomatic leaves varied to a greater extent than symptomatic leaves throughout the experiment. This observation is supported by the shift in the function of the phyllosphere microbial community. The relative abundance of plant pathogen, endophyte, and wood saprotroph decreased significantly with 5 days after spraying in asymptomatic leaves and 10–15 days after spraying in symptomatic leaves. Ultimately unassigned fungal communities became dominant and occupied the vast majority of phyllosphere niche. However, the function of phyllosphere bacterial communities did not fluctuate significantly throughout the experiment. This further confirms that STROBY may not have strong direct effects on bacteria.

The co-occurrence network demonstrated the relationship of phyllosphere microbial communities, which may provide crucial details on the interactions (such as parasitism, competition, symbiosis, and mutualism) that exist between different populations (Deng et al., 2012; Vacher et al., 2016). In this study, the node size of the co-occurrence network of the phyllosphere bacterial community was higher than that of the phyllosphere fungal community, indicating that the interactions between phyllosphere bacteria were stronger than between fungi. Among the interactions between microorganisms, the majority was positive interactions,

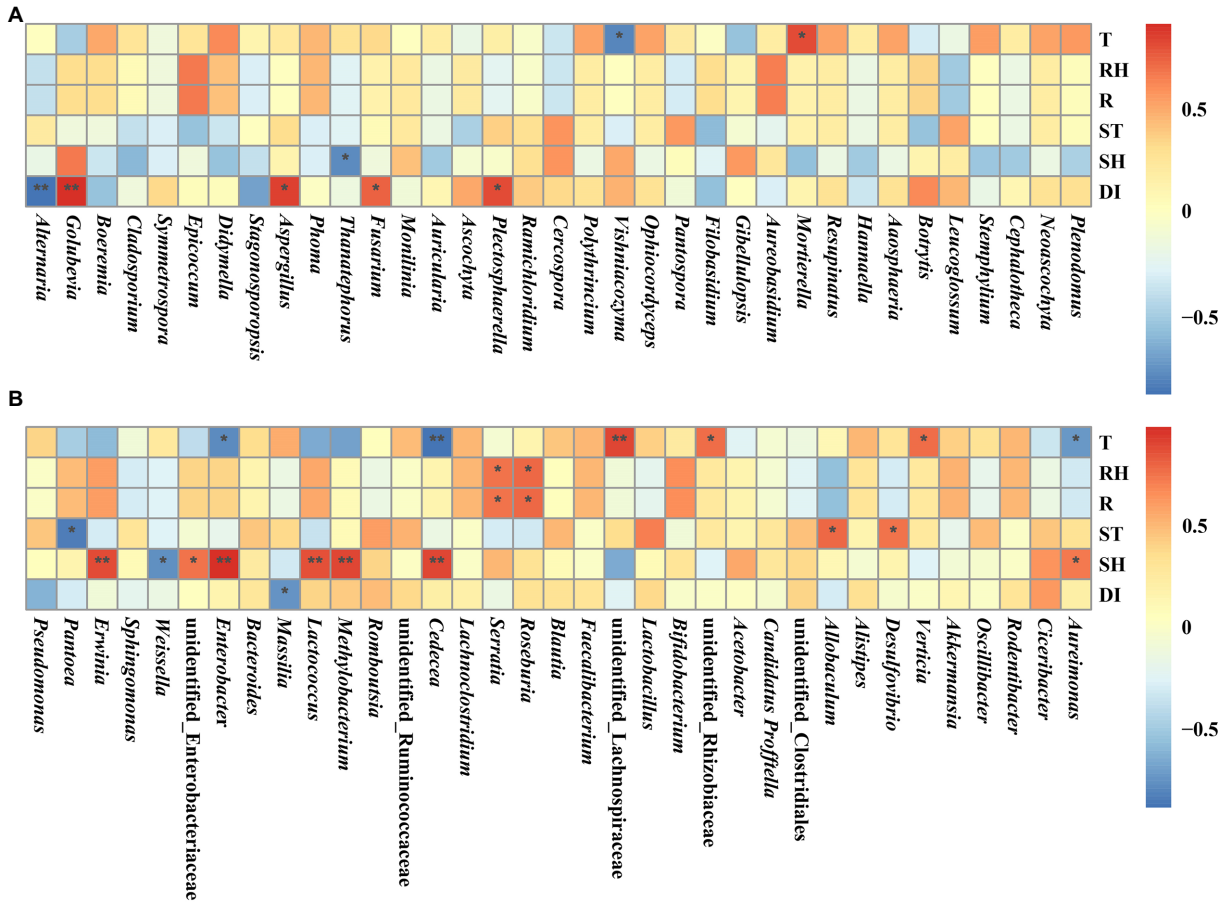

FIGURE 10
Spearman correlation analysis between microbial communities and environmental factors in tobacco leaves at four sampling time points. **(A)** For fungal communities and **(B)** for bacterial communities. Temperature (T), relative humidity (RH), rainfall (R), soil temperature (ST), soil relative humidity (SH), and disease index (DI). "*" represents a statistical difference between groups (p<0.05), "**" represents a significant statistical difference between groups (p<0.01).

showing directly correlated increases or decreases in population, which meant that the most phyllosphere microorganisms were affected the same way by external pressures, and speculatively may be more symbiotic or mutualistic rather than competitive, or did not exert major effects on each other.

Conclusion

This study demonstrated variations in the microbial community of the leaf phyllosphere with and without tobacco brown spot before and after STROBY application. After STROBY application, visible disease did not appear on asymptomatic leaves and the disease index of symptomatic plants disease not increase greatly. *Alternaria* was found to be detectable even on asymptomatic leaves in tobacco fields with greater than 25% incidence of brown spot. In addition to *Alternaria*, fungal genera known to contain plant pathogens such as *Cladosporium*, *Didymella*, *Phoma*, *Pseudomonas*, and *Pantoea* were also found to be present on tobacco leaves. After spraying, the fungal community diversity was significantly reduced in symptomatic leaves. The bacterial community diversity did not change significantly. The effect of STROBY on the structure of leaf phyllosphere fungal communities was significantly higher than bacterial communities, and had the greatest effect on *Alternaria*.

Data availability statement

The datasets presented in this study can be found in online repositories. The names of the repository/repositories and accession number(s) can be found at: https://www.ncbi.nlm.nih.gov/, PRJNA806570.

Author contributions

H-CW and Z-HY contributed to conception. L-GX, L-TC, TG, and FL conducted the study, organized the database,

performed the statistical analysis, and wrote the first draft of the manuscript. H-CW and TH revised the manuscript and wrote some sections. All authors contributed to the article and approved the submitted version.

Funding

This research was financed by China National Tobacco Corporation [110202101048(LS-08) and 110202001035(LS-04)], the "Hundred" Level Innovative Talent Foundation of Guizhou Province (GCC[2022]028-1), National Natural Science Foundation of China (31960550 and 32160522), Guizhou Science Technology Foundation (ZK[2021]Key036), Guizhou Province Technology R&D Program (Grant number: [2019]2398), and Guizhou Tobacco Company (2020XM03 and 2020XM22). The authors declare that this study received funding from Guizhou Tobacco Company. The funder was not involved in the study design, collection, analysis, interpretation of data, the writing of this article or the decision to submit it for publication.

Conflict of interest

The authors declare that the research was conducted in the absence of any commercial or financial relationships that could be construed as a potential conflict of interest.

Publisher's note

Supplementary material

The Supplementary material for this article can be found online at: https://www.frontiersin.org/articles/10.3389/fmicb.2022.1068158/full#supplementary-material

References

Balba, H. (2007). Review of strobilurin fungicide chemicals. *J. Environ. Sci. Health B* 42, 441–451. doi: 10.1080/03601230701316465

Bashir, I., War, A. F., Rafiq, I., Reshi, Z. A., Rashid, I., and Shouche, Y. S. (2022). Phyllosphere microbiome: diversity and functions. *Microbiol. Res.* 254:126888. doi: 10.1016/j.micres.2021.126888

Batta, Y. A. (2004). Cladosporium tenuissimum Cooke (Deuteromycotina: Hyphomycetes) as a causal organism of new disease on cucumber fruits. *Eur. J. Plant Pathol.* 110, 1003–1009. doi: 10.1007/s10658-004-1604-7

Bokulich, N. A., Subramanian, S., Faith, J. J., Gevers, D., Gordon, J. I., Knight, R., et al. (2013). Quality-filtering vastly improves diversity estimates from Illumina amplicon sequencing. *Nat. Methods* 10, 57–59. doi: 10.1038/nmeth.2276

Chen, Q. L., Cai, L., Wang, H. C., Cai, L. T., Goodwin, P., Ma, J., et al. (2020). Fungal composition and diversity of the tobacco leaf phyllosphere during curing of leaves. *Front. Microbiol.* 11:2136. doi: 10.3389/fmicb.2020.554051

Deng, Y., Jiang, Y. H., Yang, Y. F., He, Z. L., Luo, F., and Zhou, J. Z. (2012). Molecular ecological network analyses. *BMC Bioinf.* 13:113. doi: 10.1186/1471-2105-13-113

Edgar, R. C. (2013). UPARSE: highly accurate OTU sequences from microbial amplicon reads. *Nat. Methods* 10, 996–998. doi: 10.1038/nmeth.2604

Ge, X., Zhu, Y., Li, Z., Bi, Y., Yang, J., Zhang, J., et al. (2021). Preharvest multiple fungicide stroby sprays promote wound healing of harvested potato tubers by activating phenylpropanoid metabolism. *Postharvest Biol. Technol.* 171:111328. doi: 10.1016/j.postharvbio.2020.111328

Grossmann, K., and Retzlaff, G. (1997). Bioregulatory effects of the fungicidal strobilurin kresoxim-methyl in wheat (*Triticum aestivum*). *Pestic. Sci.* 50, 11–20. doi: 10.1002/(SICI)1096-9063(199705)50:1<11::AID-PS556>3.0.CO;2-8

Guo, Z., Xie, H., Wang, H., Huang, Y., Chen, Q., Xiang, L., et al. (2020). Leaf spot caused by *Didymella segeticola* on tobacco in China. *Plant Dis.* 104, 1559–1560. doi: 10.1094/PDIS-11-19-2398-PDN

Haas, B. J., Gevers, D., Earl, A. M., Feldgarden, M., Ward, D. V., Giannoukos, G., et al. (2011). Chimeric 16S rRNA sequence formation and detection in sanger and 454-pyrosequenced PCR amplicons. *Genome Res.* 21, 494–504. doi: 10.1101/gr.112730.110

Idnurm, A., Beard, C., Smith, A., Hills, A. L., and Chambers, K. R. (2021). Emergence of *Cladosporium macrocarpum* disease in canola (*Brassica napus*). *Australas. Plant Pathol.* 50, 687–694. doi: 10.1007/s13313-021-00819-8

Ilyas, N., Yang, Y., Liu, W., Li, X., Pu, W., Singh, R. P., et al. (2021). First report of bacterial rot caused by Pantoea endophytica on tobacco in Liuyang, China. *Plant Dis.* 105:4147. doi: 10.1094/PDIS-04-21-0737-PDN

Jing, C., Zhao, J., Han, X., Huang, R., Cai, D., and Zhang, C. (2018). Essential oil of *Syringa oblata* Lindl. As a potential biocontrol agent against tobacco brown spot caused by *Alternaria alternata*. *Crop Prot.* 104, 41–46. doi: 10.1016/j.cropro.2017.10.002

Knief, C., Frances, L., and Vorholt, J. A. (2010). Competitiveness of diverse Methylobacterium strains in the phyllosphere of Arabidopsis thaliana and identification of representative models, including M. Extorquens PA_1. *Microb. Ecol.* 60, 440–452. doi: 10.1007/s00248-010-9725-3

Kolosova, A., Maximova, K., Eremin, S. A., Zherdev, A. V., Mercader, J. V., Abad-Fuentes, A., et al. (2017). Fluorescence polarization immunoassays for strobilurin fungicides kresoxim-methyl, trifloxystrobin and picoxystrobin. *Talanta* 162, 495–504. doi: 10.1016/j.talanta.2016.10.063

Langille, M. G., Zaneveld, J., Caporaso, J. G., McDonald, D., Knights, D., Reyes, J. A., et al. (2013). Predictive functional profiling of microbial communities using 16S rRNA marker gene sequences. *Nat. Biotechnol.* 31, 814–821. doi: 10.1038/nbt.2676

Lei, F. B., Wang, H. C., Dai, Y. F., and Zhang, C. Q. (2021). Sensitivity baseline to boscalid of Alternaria alternata causing tobacco brown spot in Guizhou province. *Chin. J. Pestic. Sci.* 23, 812–816. doi: 10.16801/j.issn.1008-7303.2021.0064

Li, S., and Wu, F. Z. (2018). Diversity and co-occurrence patterns of soil bacterial and fungal communities in seven intercropping systems. *Front. Microbiol.* 9:1521. doi: 10.3389/fmicb.2018.01521

Liu, H., Brettell, L. E., and Singh, B. (2020). Linking the phyllosphere microbiome to plant health. *Trends Plant Sci.* 25, 841–844. doi: 10.1016/j.tplants.2020.06.003

Liu, J., Song, M., Wei, X., Zhang, H., Bai, Z., and Zhuang, X. (2022). Responses of phyllosphere microbiome to ozone stress: abundance, community compositions and functions. *Microorganisms* 10:680. doi: 10.3390/microorganisms10040680

Liu, G. S., Wang, Y. F., and Fu, Y. P., (2009). *Technical Guide for Tobacco Production in China During 2003–2009*. Beijing: China Agriculture Press

Luo, L., Zhang, Z., Wang, P., Han, Y., Jin, D., Su, P., et al. (2019). Variations in phyllosphere microbial community along with the development of angular leaf-spot of cucumber. *AMB Express* 9, 1–13. doi: 10.1186/s13568-019-0800-y

Magoč, T., and Salzberg, S. L. (2011). FLASH: fast length adjustment of short reads to improve genome assemblies. *Bioinformatics* 27, 2957–2963. doi: 10.1093/bioinformatics/btr507

Mercader, J. V., Suárez-Pantaleón, C., Agullo, C., Abad-Somovilla, A., and Abad-Fuentes, A. (2008). Production and characterization of monoclonal antibodies specific to the strobilurin pesticide pyraclostrobin. *J. Agric. Food Chem.* 56, 7682–7690. doi: 10.1021/jf801340u

Moreau, C. S., and Rubin, B. E. R. (2017). Diversity and persistence of the gut microbiome of the giant neotropical bullet ant. *Integr. Comp. Biol.* 57, 682–689. doi: 10.1093/icb/icx037

Nguyen, N. H., Song, Z., Bates, S. T., Branco, S., Tedersoo, L., Menke, J., et al. (2016). FUNGuild: an open annotation tool for parsing fungal community datasets by ecological guild. *Fungal Ecol.* 20, 241–248. doi: 10.1016/j.funeco.2015.06.006

Qu, Z., Zhao, H., Zhang, H., Wang, Q., Yao, Y., Cheng, J., et al. (2020). Bio-priming with a hypovirulent phytopathogenic fungus enhances the connection and strength of microbial interaction network in rapeseed. *NPJ Biofilms Microbiol.* 6, 1–13. doi: 10.1038/s41522-020-00157-5

Reuveni, M., Gur, L., and Farber, A. (2018). Development of improved disease management for powdery mildew on mango trees in Israel. *Crop Prot.* 110, 221–228. doi: 10.1016/j.cropro.2017.07.017

Rivas, S., and Thomas, C. M. (2005). Molecular interactions between tomato and the leaf mold pathogen Cladosporium fulvum. *Annu. Rev. Phytopathol.* 43:395. doi: 10.1146/annurev.phyto.43.040204.140224

Sinden, S. L., and Durbin, R. D. (1968). Glutamine synthetase inhibition: possible mode of action of wildfire toxin from *Pseudomonas tabaci*. *Nature* 219, 379–380. doi: 10.1038/219379a0

Singh, P. J., Sidhu, G. S., Kumar, R., and Thind, T. S. (2011). Superior performance of kresoxim-methyl (Stroby) and trifloxystrobin (Flint) against botrytis blight (*botrytis gladiolorum*) of gladiolus (*gladiolus*× *hortulanus* bailey). *Plant Dis. Res.* 26, 101–105.

Stone, B. W., Weingarten, E. A., and Jackson, C. R. (2018). The role of the phyllosphere microbiome in plant health and function. *Annu. Plant Rev.* 1, 1–24. doi: 10.1002/9781119312994.apr0614

Thapa, S., and Prasanna, R. (2018). Prospecting the characteristics and significance of the phyllosphere microbiome. *Ann. Microbiol.* 68, 229–245. doi: 10.1007/s13213-018-1331-5

Vacher, C., Hampe, A., Porté, A. J., Sauer, U., Compant, S., and Morris, C. E. (2016). The phyllosphere: microbial jungle at the plant-climate interface. *Annu. Rev. Ecol. Syst.* 47, 1–24. doi: 10.1146/annurev-ecolsys-121415-032238

Van Dingenen, J., Antoniou, C., Filippou, P., Pollier, J., Gonzalez, N., Dhondt, S., et al. (2017). Strobilurins as growth-promoting compounds: how Stroby regulates Arabidopsis leaf growth. *Plant Cell Environ.* 40, 1748–1760. doi: 10.1111/pce.12980

Wang, H., Huang, Y., Wang, J., Chen, X., Wei, K., Wang, M., et al. (2016). Activities of azoxystrobin and difenoconazole against *Alternaria alternata* and their control efficacy. *Crop Prot.* 90, 54–58. doi: 10.1016/j.cropro.2016.08.022

Wang, H., Huang, Y., Xia, H., Wang, J., Wang, M., Zhang, C., et al. (2015). Phenotypic analysis of *Alternaria alternata*, the causal agent of tobacco brown spot. *Plant Pathol. J.* 14, 79–85. doi: 10.3923/ppj.2015.79.85

Wang, H. C., Wang, J., Li, W. H., Huang, Y. F., Xia, H. Q., Wang, M. S., et al. (2014). *Cladosporium cladosporioides* identified in China on tobacco seeds. *Plant Dis.* 98:1002. doi: 10.1094/PDIS-12-13-1203-PDN

Wei, Y. J., Wu, Y., Yan, Y. Z., Zou, W., Xue, J., Ma, W. R., et al. (2018). High-throughput sequencing of microbial community diversity in soil, grapes, leaves, grape juice and wine of grapevine from China. *PLoS One* 13:e0193097. doi: 10.1371/journal.pone.0193097

Wu, K., Yuan, S. F., Xun, G. H., Shi, W., Pan, B., Guan, H. L., et al. (2015). Root exudates from two tobacco cultivars affect colonization of *Ralstonia solanacearum* and the disease index. *Eur. J. Plant Pathol.* 141, 667–677. doi: 10.1007/s10658-014-0569-4

Xiang, L. G., Wang, H. C., Wang, F., Cai, L. T., Li, W. H., Hsiang, T., et al. (2022). Analysis of phyllosphere microorganisms and potential pathogens of tobacco leaves. *Front. Microbiol.* 13:843389. doi: 10.3389/fmicb.2022.843389

Xu, N., Zhao, Q., Zhang, Z., Zhang, Q., Wang, Y., Qin, G., et al. (2022). Phyllosphere microorganisms: sources, drivers, and their interactions with plant hosts. *J. Agric. Food Chem.* 70, 4860–4870. doi: 10.1021/acs.jafc.2c01113

Yu, J. H., Choi, G. J., and Kim, H. T. (2008). Effect of foliar uptake of azoxystrobin and kresoxim-methyl on fungicidal activity against cucumber powdery mildew. *Appl. Biol. Chem.* 51, 108–113.

Yuan, G. Q., Liao, T., Tan, H. W., Li, Q. Q., and Lin, W. (2016). First report of leaf spot caused by Phoma sorghina on tobacco in China. *Plant Dis.* 100:1790. doi: 10.1094/PDIS-11-15-1377-PDN

Zhang, Y. J., Zhang, S., Liu, X. Z., Wen, H. A., and Wang, M. (2010). A simple method of genomic DNA extraction suitable for analysis of bulk fungal strains. *Lett. Appl. Microbiol.* 51, 114–118. doi: 10.1111/j.1472-765X.2010.02867.x

Zhou, Y., Ou, Z., Tang, X., Zhou, Y., Xu, H., Wang, X., et al. (2018). Alterations in the gut microbiota of patients with acquired immune deficiency syndrome. *J. Cell. Mol. Med.* 22, 2263–2271. doi: 10.1111/jcmm.13508

frontiers | Frontiers in Microbiology

TYPE Original Research
PUBLISHED 08 December 2022
DOI 10.3389/fmicb.2022.1069517

OPEN ACCESS

EDITED BY
Ryan Kessens,
Corteva Agriscience™, United States

REVIEWED BY
Liming Wu,
Nanjing Agricultural University, China
Eugenio Llorens,
Tel Aviv University, Israel

*CORRESPONDENCE
Yonghong Huang
gstshh@126.com
Yanxin Duan
dyxdyx2007@163.com

SPECIALTY SECTION
This article was submitted to Microbe and Virus Interactions With Plants, a section of the journal Frontiers in Microbiology

RECEIVED 14 October 2022
ACCEPTED 18 November 2022
PUBLISHED 08 December 2022

CITATION
Huang Y, Liu J, Li J, Shan X and Duan Y (2022) Endophytic bacterium *Pseudomonas protegens* suppresses mycelial growth of *Botryosphaeria dothidea* and decreases its pathogenicity to postharvest fruits.
Front. Microbiol. 13:1069517.
doi: 10.3389/fmicb.2022.1069517

Endophytic bacterium *Pseudomonas protegens* suppresses mycelial growth of *Botryosphaeria dothidea* and decreases its pathogenicity to postharvest fruits

Yonghong Huang[1,2,3,4]*, Junping Liu[1,2,3,4], Jinghui Li[1,2,3,4], Xiaoying Shan[1,2,3,4] and Yanxin Duan[1,2,3,4]*

[1]College of Horticulture, Qingdao Agricultural University, Qingdao, China, [2]Laboratory of Quality and Safety Risk Assessment for Fruit, Ministry of Agriculture and Rural Affairs, Qingdao, China, [3]National Technology Centre for Whole Process Quality Control of FSEN Horticultural Products, Qingdao, China, [4]Qingdao Key Laboratory of Modern Agriculture Quality and Safety Engineering, Qingdao, China

Apple (*Malus domestica* Borkh.), one of the most economically important fruits widely consumed worldwide, has been suffering from apple ring rot caused by *Botryosphaeria dothidea*, which dramatically affects its quality and yield. In the present study, we demonstrated that *Pseudomonas protegens*, isolated from Chinese leek (*Allium tuberosum*), significantly suppressed the mycelial growth and propagation of *B. dothidea*, respectively, further displayed a considerably inhibitory effect on the apple ring rot of postharvest fruits. In addition, *P. protegens* significantly improved the total soluble solid/titrable acidity (TSS/TA) ratio and soluble sugar/titrable acidity (SS/TA) ratio and drastically maintained the fruit firmness. Further analysis manifested that *P. protegens* substantially induced the defense-related genes such as MdGLU, MdPAL, MdPOD, MdCAL, and transcription factors related to the resistance to *B. dothidea*, including MdWRKY15, MdPUB29, MdMyb73, and MdERF11 in apple fruits. Meanwhile, *P. protegens* considerably restrained the expressions of the pathogenicity-related genes in *B. dothidea*, including the BdCYP450, BdADH, BdGHY, BdATS, Bdα/β-HY, and BdSTR. By inference, *P. protegens* inhibited the apple ring rot on postharvest fruits by activating the defense system of apple fruit and repressing the pathogenic factor of *B. dothidea*. The study provided a theoretical basis and a potential alternative to manage the apple ring rot on postharvest fruits.

KEYWORDS

biological control, fruit quality, defense-related genes, pathogenicity-related genes, apple ring rot

Introduction

Apple (*Malus domestica* Borkh.) is one of the most widely produced and economically important fruits in temperate regions (Chen et al., 2021). China is the largest producer in the world, with harvested areas of 1.91 million hectares (41.01% of the world total) and 40.50 million tons (46.85% of the world total) in 2020 (FAOSTAT, 2022).[1] In recent years, apple fruit has been among the most widely consumed fruits in the world since they are available the whole year, inexpensive, and convenient to consume. Above all, apple contains a range of nutrients with different biological activities, including polyphenols, vitamins, minerals, lipids, proteins/peptides, and carbohydrates (Koutsos and Lovegrove, 2015; Pollini et al., 2021), which are beneficial for our health, as per the saying, "an apple a day keeps the doctor away" (Davis et al., 2015).

Unfortunately, due to the lack of resistant varieties, continuous cropping, and poor field management, apple orchards in China often suffer from pests and diseases. Apple ring rot, caused by *Botryosphaeria dothidea*, is one of the most destructive apple diseases worldwide, including in China, Japan, South Korea, United States, Australia, and South Africa (Wang et al., 2018). *B. dothidea* infects apple trees, resulting in fruit rot, twig dieback, stem and branch canker, and tree death (Dong and Guo, 2020). Besides, *B. dothidea* often infects the apple fruits during the early growth stages, remains latent, and causes fruit rot during ripening or storage (Yu et al., 2022). The decayed fruit incidence caused by the disease usually ranges between 10 and 20% each year and may reach 70% in seasons with conditions conducive to fungal development (Zhao et al., 2016). According to an investigation, the average occurrence of the disease was as high as 77.6% in 88 apple orchards across seven main apple production areas in China (Guo et al., 2009). Therefore, apple ring rot has seriously impeded the sustainable and healthy development of the apple industry in China.

Currently, chemical fungicides are still the primary strategies for controlling apple ring rot disease (Dai et al., 2017; Song et al., 2018; Fan et al., 2019). However, these fungicides were potentially hazardous to human health, other non-target organisms, and the natural environment. In addition, pathogenic microorganisms may evolve fungicide resistance (Yin and Qiu, 2019). Given the above-described concerns, there is an urgent need to research and develop alternative measures for preventing and controlling the disease.

Biological control is a safe way to control pests and pathogens. Antagonistic microorganisms showed tremendous potential for substituting chemical fungicides to manage plant pathogens (El-Hasan et al., 2017; Fan et al., 2020; Zhao et al., 2021). It is reported that *Pseudomonas* spp. have been widely studied for their biocontrol potential. For example, *P. chlororaphis* significantly reduced the postharvest gray mold on Chinese cherry (Wang C. et al., 2021). *P. fluorescens* drastically suppressed the blue mold disease of postharvest citrus fruits (Wang Z. et al., 2021). *P. segetis* markedly reduced soft rot symptoms in potatoes (Rodriguez et al., 2020). *P. aeruginosa* considerably controlled several pathogens in tomatoes, potatoes, taro, and strawberries (Ghadamgahi et al., 2022). *P. putida* strongly reduced the common bean rust disease severity (Abo-Elyousr et al., 2021). *P. synxantha* significantly reduced brown rot incidence and severity on peaches (Aiello et al., 2019). *P. parafulva* effectively controlled the soybean bacterial pustule (Kakembo and Lee, 2019). In addition, *P. protegens* had intense antifungal activity against various plant pathogens, including *Heterobasidion abietinum*, *Heterobasidion annosum*, *Heterobasidion irregulare*, and *Heterobasidion parviporum* (Pellicciaro et al., 2021), *Calonectria pseudonaviculata* (Yang and Hong, 2018), *Rhizoctonia solani* (Jing et al., 2020), *Fomes fomentarius*, *Ganoderma lucidum*, *Phellinus pini*, *Phellinus tuberculosus*, *Sclerotinia sclerotiorum*, *Alternaria tomatophila* (Prigigallo et al., 2021), *Alternaria alternata*, *Aspergillus niger*, *Penicillium expansum*, *Neofusicoccum parvum* (Andreolli et al., 2019), *Botrytis cinerea*, and *Monilinia fructicola* (Zhang et al., 2020). In our preliminary study, we isolated an endophytic bacterium *P. protegens* from Chinese leek (*Allium tuberosum*). The present study demonstrated the antifungal activity against *B. dothidea* and the inhibitory effect on ring rot on postharvest apple fruits. Further, we primitively uncovered the underlying mechanism from the apple fruit aspect and the pathogen *B. dothidea* aspect to provide a theoretical basis and an alternative for controlling the apple ring rot on postharvest fruits.

Materials and methods

Experiment materials

Apple fruits (*Malus domestica*, cv. Fuji) were purchased from the local market. Fruits in uniform size and color, free of visible disease and mechanical injuries, were selected for the experiments. The endophytic bacterium *P. protegens* isolation NSJ-2101 and the pathogen fungus *B. dothidea* isolate LW-1801 were cultured on the nutrient agar (NA) and potato dextrose agar (PDA) medium, respectively, and kept in our laboratory.

The suppressive effect of the *Pseudomonas protegens* on *Botryosphaeria dothidea* growth

We conducted the experiments using the PDA and potato dextrose broth (PDB) medium.

Potato dextrose agar medium experiment

The PDA medium (20 ml) was poured into a 9-cm-diameter Petri dish. One mycelium disc (0.5 cm in diameter) of the fungus

1 https://www.fao.org/faostat/zh/#data/QCL

B. dothidea was inoculated in the center of the Petri dish. Then one disc of *P. protegens* was inoculated on each side 2 cm from the fungal disc (Pp). Sterilized water (50 μL) was used as the control (CK). All the Petri dishes were inverted and incubated at 28°C in the dark for 3 days. The diameters of the fungal colony were measured daily to evaluate the inhibition of *P. protegens* on the mycelial growth *B. dothidea*. After that, *P. protegens*-treated mycelia and the control mycelia were carefully picked from the Petri dishes and observed under a microscope (EVOS Auto2, Thermo Fisher Scientific, United States) with × 40 magnification. The experiments were repeated three times, and five replicates were included for each sample in each experiment.

Potato dextrose broth medium experiment

Various amount (2.5, 5, and 10 ml) of *P. protegens* culture ($OD_{600} = 0.6$) was added into a 150 ml *Erlenmeyer flask*, respectively. PDB medium was appended until it reached a total volume of 50 ml, making the concentrations of the *P. protegens* 5, 10, and 20%. 50 ml of PDB medium was used as a control. Then, one mycelium disc (0.5-cm-diameter) of *B. dothidea* was put into the *Erlenmeyer flask*. The *Erlenmeyer flask* was incubated at a constant temperature shaking incubator at 28°C, shaking at 200 rpm for 2 days. After centrifugation, the precipitate was collected and weighed to evaluate the suppression of *P. protegens* on the propagation of *B. dothidea*. The experiments were performed in triplicates.

The inhibitory effect of the *Pseudomonas protegens* against the apple ring rot on the postharvest fruit

According to the different ways of inoculating fungus *B. dothidea*, we performed two experiments to test the control effect of *P. protegens* on apple ring rot.

Experiment 1

The apple fruits were surface-sterilized with 1.5% NaOCl for 5 min, washed thrice with distilled water, and air-dried. Then a tiny wound (3 mm width × 5 mm deep) was created at the equator in each apple fruit using a sterile needle. Next, 20 μl of *P. protegens* ($OD_{600} = 0.6$) was added into the small cavity. One hour later, a *B. dothidea* mycelial disc (3 mm in diameter) was inoculated into the wound. Again, 20 μl of the nutrient broth (NB) medium was used as a control. Finally, all the apple fruits were packed into a black plastic box and incubated at 28°C under dark conditions for 3 days. The disease spot diameter was measured to evaluate the inhibitory effect of the *P. protegens* on the apple ring rot incidence on fruits. The experiment was repeated ten times.

Experiment 2

First, the apple fruits were surface-sterilized and air-dried, as in experiment 1. Then the apple fruits were immersed in *P. protegens* culture ($OD_{600} = 0.6$) for 15 min and soaked in *B. dothidea* ($OD_{600} = 0.6$) culture for another 15 min after they were air-dried at room temperature for 1 h (Pp + Bd). In addition, the apple fruits that were soaked in NB medium for 15 min, air-dried at room temperature for 1 h, then dipped in *B. dothidea* culture for 15 min were used as the control (Bd). Next, all the fruits were packed in plastic bags and incubated at 28°C. Finally, the disease symptom, such as mycelial cluster and disease spots, were observed and recorded on 1, 3, 5, 7, and 9 days to evaluate the inhibitory effect of *P. protegens* on apple ring rot. The experiment was performed in triplicate.

The effect of *Pseudomonas protegens* on the apple fruit quality

To fully confirm whether *P. protegens* affected the internal quality of apple fruit, we designed four treatments (CK, Pp, Bd, and Pp + Bd). (1) CK: The apple fruits were soaked in PDB medium for 15 min. (2) Pp: The apple fruits were soaked in *P. protegens* culture ($OD_{600} = 0.6$) for 15 min (Pp). (3) Bd and (4) Pp + Bd were described above. All the fruits were packed in plastic bags and set in an incubator at 28°C. Then, fruits were sampled and peeled 9 days later. Fruit firmness was measured at the fruit's equator with the FHM-5 fruit hardness tester (Takemura Electric Works Ltd., Tokyo, Japan). The pulp at the fruit equator was sampled to determine other internal quality indexes, including total soluble solid (TSS), soluble sugar (SS), titratable acidity (TA), vitamin C (VC), total soluble solid/titrable acidity (TSS/TA) ratio, and soluble sugar/titrable acidity (SS/TA) ratio. TSS content was determined using a PAL-1 type sugar concentration detector (ATAGO, Japan). SS, TA, and VC were determined using the anthrone colorimetric, NaOH titration, and 2, 6-dichloroindophenol colorimetric, respectively (Yang L. et al., 2020). Three replicates were included for each sample at each sampling time point.

The effect of the *Pseudomonas protegens* on the defense-related gene in the apple fruits

To determine whether the reduction of the fruit disease symptom was caused by the *P. protegens* induction of the fruit defense system, we detected the expressions of the defense-related genes and the transcription factors in apple fruits. The defense-related genes contained phenylalanine ammonia-lyase (MdPAL; XM_008368428.3), glucanase (MdGLU; XM_029095631.1), peroxidase (MdPOD; XM_029099288.1), and catalase (MdCAT; XM_008375181.3). The transcription factors included MdWRKY15 (XM_008395555.3), apple U-box E3 ubiquitin ligase 29 (MdPUB29; XM_008350166.3), MdMYB73 (XM_008379837.3), and apple ethylene response factor 11 (MdERF11; NM_001301117.1), which were reported to enhance the resistance of apple fruits to *B. dothidea*.

According to previously described methods, the four treatments (CK, Pp, Bd, and Pp + Bd) were performed on apple fruits. All the fruits were packed in plastic bags and incubated at 28°C. One day later, the fruits were sampled and peeled around the equator with a sterilized paring knife. All the samples were stored at −80°C for later qRT-PCR.

The effect of the *Pseudomonas protegens* on the pathogenic-related gene in the fungus *Botryosphaeria dothidea*

We examined several published pathogenicity-related genes to verify whether the reduced disease symptom in the apple fruits was also associated with the repressed expression of vital gene in *B. dothidea* by *P. protegens*. These genes included cytochrome p450 protein (BdCYP450; BOTSDO04127), alcohol dehydrogenase (BdADH; BOTSDO00477), glycoside hydrolase (BdGHY; BOTSDO02303), aminoacyl-tRNA synthetase (BdATS; BOTSDO01704), alpha/beta hydrolase (Bdα/β-HY; BOTSDO04588) and sugar transporter (BdSTR; BOTSDO09350).

A mycelium disc (0.5 cm in diameter) of *B. dothidea* was inoculated on a layer of sterilized cellophane placed on the newly prepared PDA medium. The Petri dish was incubated at 28°C in an inverted position for 2 days in the dark. Then *P. protegens* (2 ml; OD600 = 0.6) was sprayed on the fungal mycelia (Pp). Sterilized water (2 ml) was used as the control (CK). The Petri dishes continued to be incubated in the same condition. Six hours later, the *P. protegens-treated* and the control mycelia were sampled for qRT-PCR.

qRT-PCR measurement

The abovementioned gene sequences of the apple and the mycelium were retrieved from the apple genome (ASM211411v1) and the *B. dothidea* genome (ASM1150312v2) that were downloaded from the National Center for Biotechnology Information (NCBI) genome website.[2] Then, the special primers were designed using Primer Primer 5 according to the respective gene sequences (Supplementary Table 1) and synthesized in Sangon Biotech (Sangon Biotech, Shanghai, China).

The total RNA of the prepared apple and the mycelia samples were extracted using RNAprep Pure Plant Plus Kit [Tiangen Biotech., Beijing, China]. And the cDNA was synthesized using HiScript RIII RT SuperMix for qPCR (CgDNA wiper; Vazyme Biotech, Nanjing, China). qRT-PCR was performed using ABI7500 Thermal Cycler (Applied Biosystems, Foster City, CA, United States) to detect the relative expressions of the genes mentioned above. The MdActin and the BdTubulin were used as the apple's and mycelia's internal reference genes, respectively. The relative expression was calculated by $2^{-\Delta\Delta CT}$ method (Livak and Schmittgen, 2001). The experiment was performed in three replicates.

Statistical analysis

Analysis of variance (ANOVA) was conducted using SAS 8.0 software (SAS Institute Inc., Cary, NC, United States). A least significance difference test (LSD) was applied to determine the significance between different treatments ($p < 0.05$). Standard errors were calculated for all mean values.

Results

Pseudomonas protegens significantly suppressed the growth of *Botryosphaeria dothidea*

On the PDA medium, the new mycelia grew from all the *B. dothidea* discs on the first day. After that, the control mycelia continued to expand rapidly (Figure 1A), but the growth of the *P. protegens*-treated mycelia gradually slowed down (Figure 1B). As a result, the fungal colony diameter treated with *P. protegens* increased to 1.44, 2.19, and 3.23 cm on day 1, day 2 and day 3, respectively (Figure 1C), reduced by 21.08, 52.90, and 50.34% compared to the control (Figure 1D). Microscopic observation demonstrated that the control mycelia was smooth with distinct borders and intact structure (Figure 1E). In contrast, the *P. protegens*-treated mycelia fragmented with blurred boundaries (Figure 1F), which revealed that *P. protegens* damaged the normal mycelial morphology of *B. dothidea*.

On the PDB medium, the *P. protegens*-treated and the control mycelia showed significantly different growth 2 days later. The mycelia treated with various of concentration *P. protegens* showed almost no increase (Figures 2A–C), but the control mycelia developed quickly (Figure 2D). The increased weight of the mycelia treated with 20, 10, and 5% of *P. protegens* was 0.11, 0.19, and 0.24 g (Figure 2E), respectively, which was reduced by 97.62, 96.14, and 95.06%, compared to the control (Figure 2F). It indicated that *P. protegens* significantly suppressed the mycelia growth of *B. dothidea*.

Pseudomonas protegens significantly inhibited the disease severity of apple ring rot on postharvest fruits

Experiment 1

One day later, the disease symptoms appeared at the inoculation sites on the *P. protegens*-treated and the control fruits. And the disease symptoms developed severity over time. However, the disease spots on the *P. protegens*-treated fruits extended slower

2 https://www.ncbi.nlm.nih.gov/

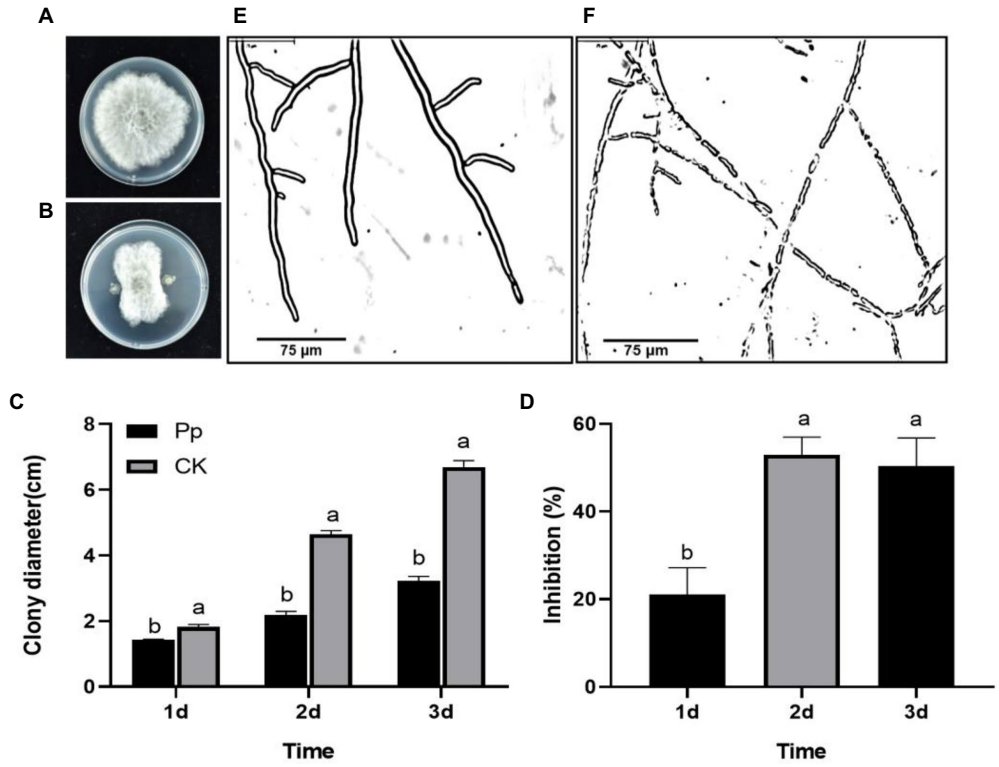

FIGURE 1
The suppression of *Pseudomonas protegens* on the mycelia growth of *Botryosphaeria dothidea* on the PDA medium. The untreated control mycelia **(A)** and the *P. protegens*-treated mycelia **(B)** that were incubated on the PDA medium for 3 days. The comparison of the colony diameter of the different treatments **(C)**. *P. protegens* significantly inhibited the mycelial growth of the fungus *B. dothidea* **(D)**. Compared to the control **(E)**, the *P. protegens* severely damaged the mycelial morphology of *B. dothidea* **(F)**. Lowercase letters indicate a significant difference between treatments ($p<0.05$).

than the control (Figures 3A,B), the disease spot diameter of which expanded to 0.49, 0.77, and 1.76 cm on day 1, day 2, and day 3, respectively (Figure 3C), decreasing by 10.59, 63.66, and 66.05% compared to the control (Figure 3D).

Experiment 2

The greyish-white mycelial cluster grew from the *P. protegens*-treated fruits and the control fruits on the first day. In the subsequent days, the number of the mycelial cluster increased over time. On the fifth day, there were 46.67 mycelial clusters on the control fruits, while only 11.67 on the *P. protegens*-treated fruits, which was decreased by 72.00% compared to the control (Figure 4A). On the seventh day, the disease spot emerged from both the treated and the control fruits, but the size of the disease spots on the *P. protegens*-treated fruits (Figure 4B) was smaller than the control (Figure 4C). The number of disease spots on the control fruits averaged 5.00, whereas 12.33 on the *P. protegens*-treated fruits, 56.46% smaller than the control (Figure 4D). On the ninth day, the disease spots on the control fruits expanded and joined together, forming a large area of rotten tissues. However, there were only 8.70 separated disease spots on the *P. protegens*-treated fruits, denoting that the *P. protegens* substantially inhibited the apple ring disease.

Pseudomonas protegens improved the fruit quality of the postharvest apple fruit to some extent

On the ninth day, we compared the fruit quality indexes, including the TSS, SS, TA, VC, TSS/TA, SS/TA, and the firmness of apple fruits from the four treatments, to evaluate the effect of the *P. protegens* on fruit quality (Figure 5). *P. protegens* significantly improved TSS/TA ratio and SS/TA ratio in the apple fruits without inoculating with *B. dothidea*. Compared to the control (CK), the TSS/TA ratio and SS/TA ratio in the *P. protegens*-treated fruits (Pp) were enhanced by 80.67 and 61.90%, respectively. In addition, the *P. protegens* decreased the TA and VC content by 40.51 and 25.24%, but statistics showed the difference was non-significant. However, *P. protegens* significantly increased the TSS/TA ratio and fruit firmness of the apple fruit inoculated with *B. dothidea*. The TSS/TA ratio and the firmness of the *P. protegens*-treated fruits (Pp + Bd) were 16.11 and 74.03% higher than the control (Bd). Meanwhile, *P. protegens* caused an apparent but non-significant alternation in the SS/TA ratio and TA content, increasing by 21.40% and decreasing by 19.68%, respectively, compared to the control.

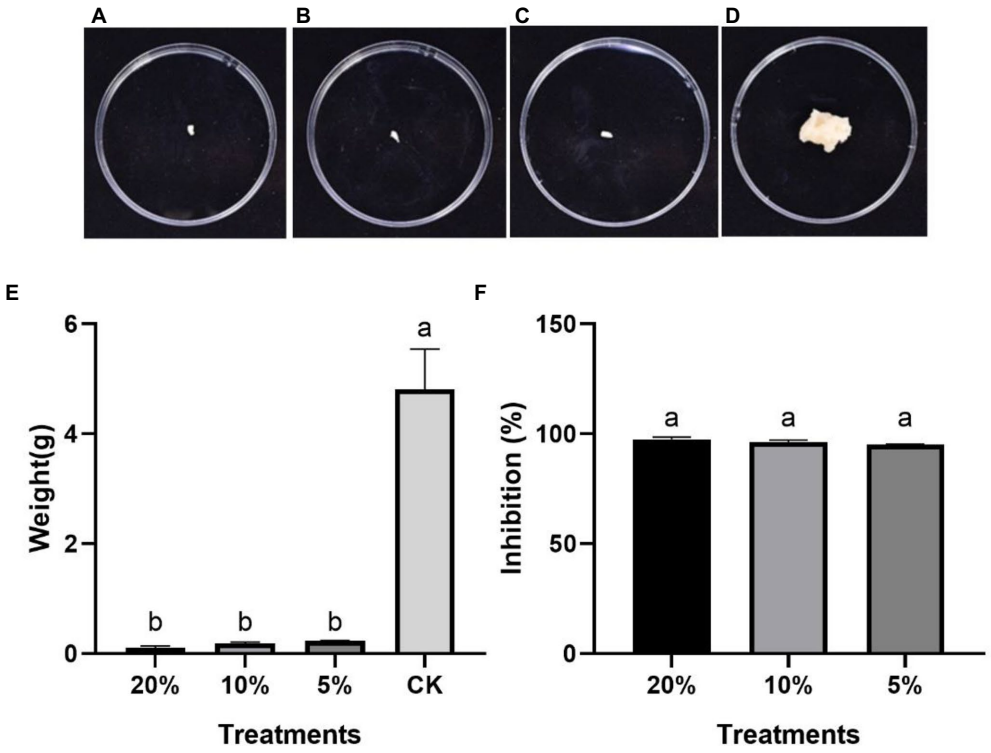

FIGURE 2
The suppression of *P. protegens* on the mycelia growth of *B. dothidea* in the PDB medium. The mycelia incubated with shaking in the PDB medium supplemented with 20% **(A)**, 10% **(B)**, and 5% **(C)** of *P. protegens* and the control mycelia **(D)** for 2 days. **(E)** The weight of mycelia from different treatments **(E)**. The inhibition of various concentrations of *P. protegens* to the fungus *B. dothidea* **(F)**. Lowercase letters indicate a significant difference between treatments ($p<0.05$).

Pseudomonas protegens significantly induced the expressions of defense-related genes in apple fruits

Whether the apple fruits were infected with the pathogen fungus *B. dothidea*, *P. protegens* considerably induced the expressions of defense-related genes such as MdGLU, MdPOD, MdCAT, and MdPAL in apple fruits (Figures 6A–D). In the case of *B. dothidea* infection, the MdGLU, MdPOD, and MdPAL in apple fruits treated with *P. protegens* (Pp + Bd) were 50.00, 357.07, 118.64% higher than the control (Bd). However, in the absence of *B. dothidea*, the MdGLU and MdCAT in *P. protegens*-treated apple fruits (Pp) were increased by 45.44 and 111.53% compared with control (CK).

In addition, *P. protegens* drastically induced the expressions of the transcription factors related to the apple fruit resistance against *B. dothidea*, including the MdPBU29, MdWRKY15, MdERF11, and MdMYB73, regardless of whether the apple fruit was infected with *B. dothidea* or not (Figures 6E–H). Compared to the control (CK), the expressions of these genes in *P. protegens*-treated apple fruits (Pp) were increased by 920.89, 2778.54, 44.81, and 30.14% in the absence of *B. dothidea* infection. While in the presence of *B. dothidea* infection, the expressions of these genes in *P. protegens*-treated apple fruits (Pp + Bd) were 1480.74, 374.78, 45.40, and 249.57% higher than the control (Bd).

Pseudomonas protegens significantly decreased the expressions of pathogenicity-related genes in *Botryosphaeria dothidea*

To determine the inhibitory effect of *P. protegens* on the *B. dothidea*, we tested the expressions of genes related to fungal pathogenicity, including BdCYP450, BdADH, BdGHY, BdATS, Bdα/β-HY, and BdSTR (Figure 7). The analysis revealed that the relative expressions of these genes in *B. dothidea* mycelia treated with the *P. protegens* (Pp) were reduced by 88.47, 70.90, 94.34, 67.38, 46.03, and 64.88% compared to the control (CK) 6 h later, which indicated that the *P. protegens* significantly repressed the pathogenicity-related genes in *B. dothidea*.

Discussion

Our preliminary studies showed that intercropping or rotating with Chinese leek (*Allium tuberosum*) dramatically decreased the incidence and severity of banana *Fusarium* wilt caused by

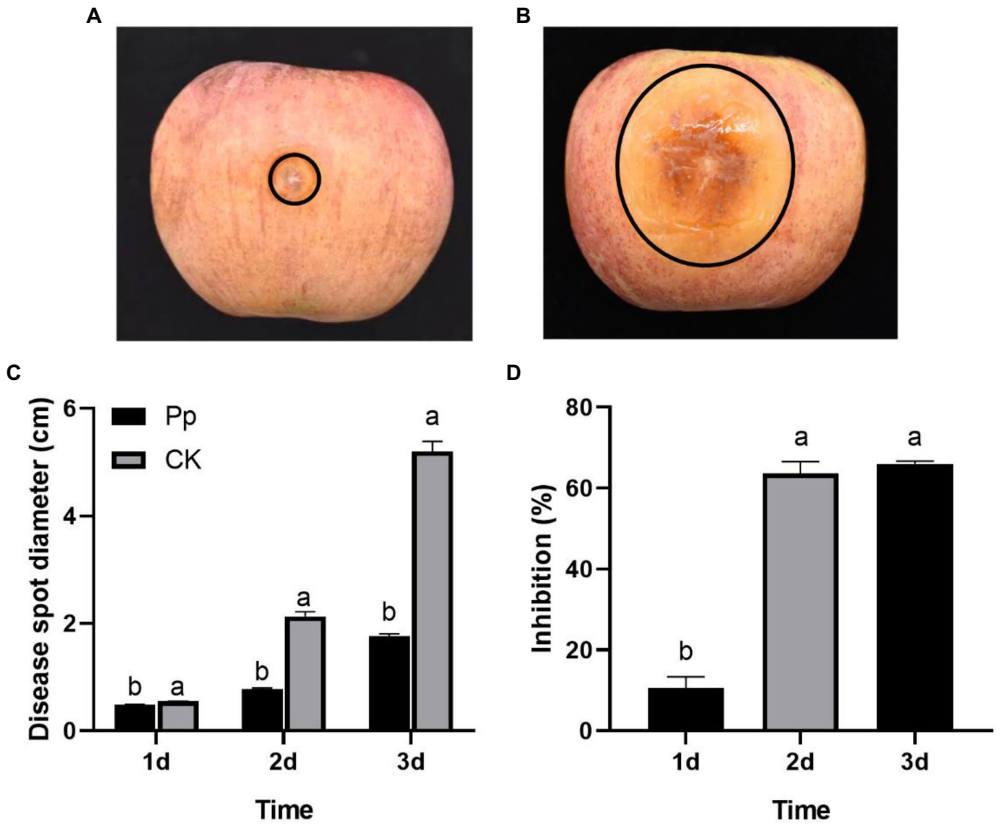

FIGURE 3
The inhibitory effect of *P. protegens* on apple ring rot on postharvest fruits (Experiment 1). The disease symptom on the *P. protegens*-treated fruits **(A)** and the untreated control fruits **(B)** 3 days later. The disease spot diameter of the *P. protegens*-treated fruits was significantly smaller than the untreated control **(C)**, demonstrating that *P. protegens* had potent inhibition on the ring rot disease on postharvest apple fruits **(D)**. Lowercase letters indicate a significant difference between treatments ($p<0.05$).

Fusarium oxysporum f. sp. *cubense* race 4 (Foc4) (Huang et al., 2012). Furthermore, tomato or cucumber intercropped or rotated with Chinese leek significantly reduced root-knot nematode disease (Huang et al., 2016). In addition, we also found that Chinese leek extract (Zhao et al., 2017) and volatiles (Fu et al., 2022) markedly suppressed the apple ring rot on postharvest fruits. Given that fact, we inferred that there were components or endophytic bacterium with antifungal activity in Chinese leek plants. Fortunately, we corroborated that the dimethyl trisulfide, one of the main components of Chinese leek volatiles (Sun et al., 2022a), and the endophytic bacterium *Serratia plymuthica* isolated from Chinese leek (Sun et al., 2022b), showed strong inhibitory effect against *B. dothidea*. In the present study, we validated that another endophytic bacterium *P. protegens*, isolated from Chinese leek, had a significant inhibitory effect on *B. dothidea* and strikingly reduced the apple ring rot on postharvest fruits. These antifungal components and endophytic bacterium were the major factors contributing to the efficient control of Chinese leek on apple ring disease.

Our present study manifested that *P. protegens* was a promising biocontrol agent to inhibit *B. dothidea*, concordant with numerous earlier studies (Jing et al., 2020; Zhang et al., 2020; Pellicciaro et al., 2021; Prigigallo et al., 2021). However, the suppression of *P. protegens* against *B. dothidea* on the PDA medium was substantially lower than that in the PDB medium. The main possible reasons were that there was a distance between *P. protegens* and *B. dothidea* when they were just inoculated on the PDA medium. They contacted and interacted with each other at a later time. At this time, *B. dothidea* had already exhibited vigorous growth, and only the mycelial apex reached the *P. protegens*, limiting the antifungal activity of *P. protegens*. However, *P. protegens* and *B. dothidea* were fully contacted and interacted with each other at the first moment when they were inoculated in the PDB medium. What is more, *B. dothidea* did not thrive at that moment. Consequently, *P. protegens* quickly suppressed the growth of *B. dothidea*. As a result, all these factors brought about the higher repression of *P. protegens* on *B. dothidea* in the PDB medium than in the PDA medium.

Due to the suppression of *P. protegens* on the growth of *B. dothidea*, *P. protegens* showed significant inhibition against apple ring rot on postharvest fruits. We artificially wounded and inoculated the apple fruits with the pathogen fungal disc in the experiment. Generally, in practical production, almost all the

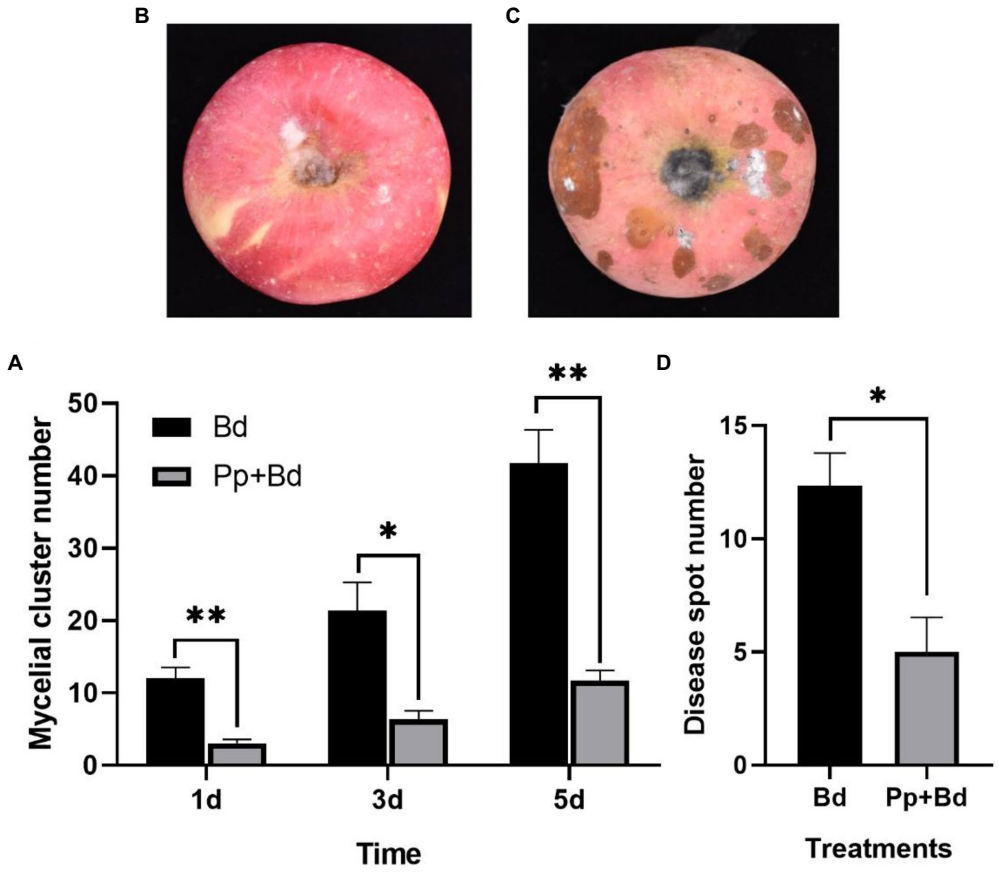

FIGURE 4
The inhibitory effect of *P. protegens* on apple ring on postharvest fruit (Experiment 2). The mycelial cluster number on *P. protegens*-treated fruits was significantly smaller than the control on the first, third, and fifth day **(A)**. In addition, the disease spots on the *P. protegens*-treated fruits **(B)** were smaller than that on the control fruits on the seventh day **(C)**, and the number of the disease spots on the *P. protegens*-treated fruits was also significantly lower than the control **(D)**. $^{*}p < 0.05$, $^{**}p < 0.01$.

apple fruit were intact and not necessarily infected with the fungus. Moreover, the fungal amount contaminating fruits in the field was less than that we inoculated in the laboratory. Accordingly, the *P. protegens* would have a higher inhibitory effect on the disease in actual production. More importantly, *P. protegens* also improved the fruit quality to different extents, killing two birds with one stone.

Our study demonstrated that the *P. protegens* significantly induced the MdGLU, MdPAL, MdPOD, and MdCAT expressions in apple fruit. Previous studies showed that these genes participated in plant resistance to various pathogens. For example, GLU genes in *Panax notoginseng* (Taif et al., 2020) and soybean (Glycine max) (Shi et al., 2020) were vital defense genes against *Fusarium solani* and soybean mosaic virus infection. PAL gene in *Lotus japonicus* (Chen et al., 2017) and soybean (Zhang et al., 2017) affected rhizobial infection progress and resistance to *Phytophthora sojae*. POD gene in potatoes (Yang Y. et al., 2020) and sweet oranges (Li et al., 2020) enhanced the resistance against *Phytophthora infestans*, and *Xanthomonas citri* subsp. *citri* (Li et al., 2020). CAT genes in maize (Jiao et al., 2021) and *Nicotiana tabacum* contributed to resistance against maize chlorotic mottle virus and chili veinal mottle virus infection (Yang T. et al., 2020). In addition, *P. protegens* also significantly induced several transcription factor expressions in apple fruits, including MdERF11, MdMYB73, MdPUB29, and MdWRKY15. Previous studies showed that overexpression of the MdERF11 (Wang et al., 2020), MdMYB73 (Gu et al., 2021), MdPUB29 (Han et al., 2019), and MdWRKY15 (Zhao et al., 2020) in apple fruits significantly increased the fruit resistance to *B. dothidea* infection, whereas silencing these genes in apple fruits resulted in decreased resistance. Therefore, the increased expressions of these genes in apple fruits may be one of the important factors contributing to the disease reduction.

We also found that *P. protegens* significantly repressed the BdCYP450, BdADH, BdGHY, BdATS, Bdα/β-HY, and BdSTR expressions in *B. dothidea*. Previous studies revealed that these genes were involved in fungal development and pathogenicity. For instance, Cytochrome P450s (CYP450) participated in the virulence of *Fusarium graminearum* (Shin et al., 2017) and

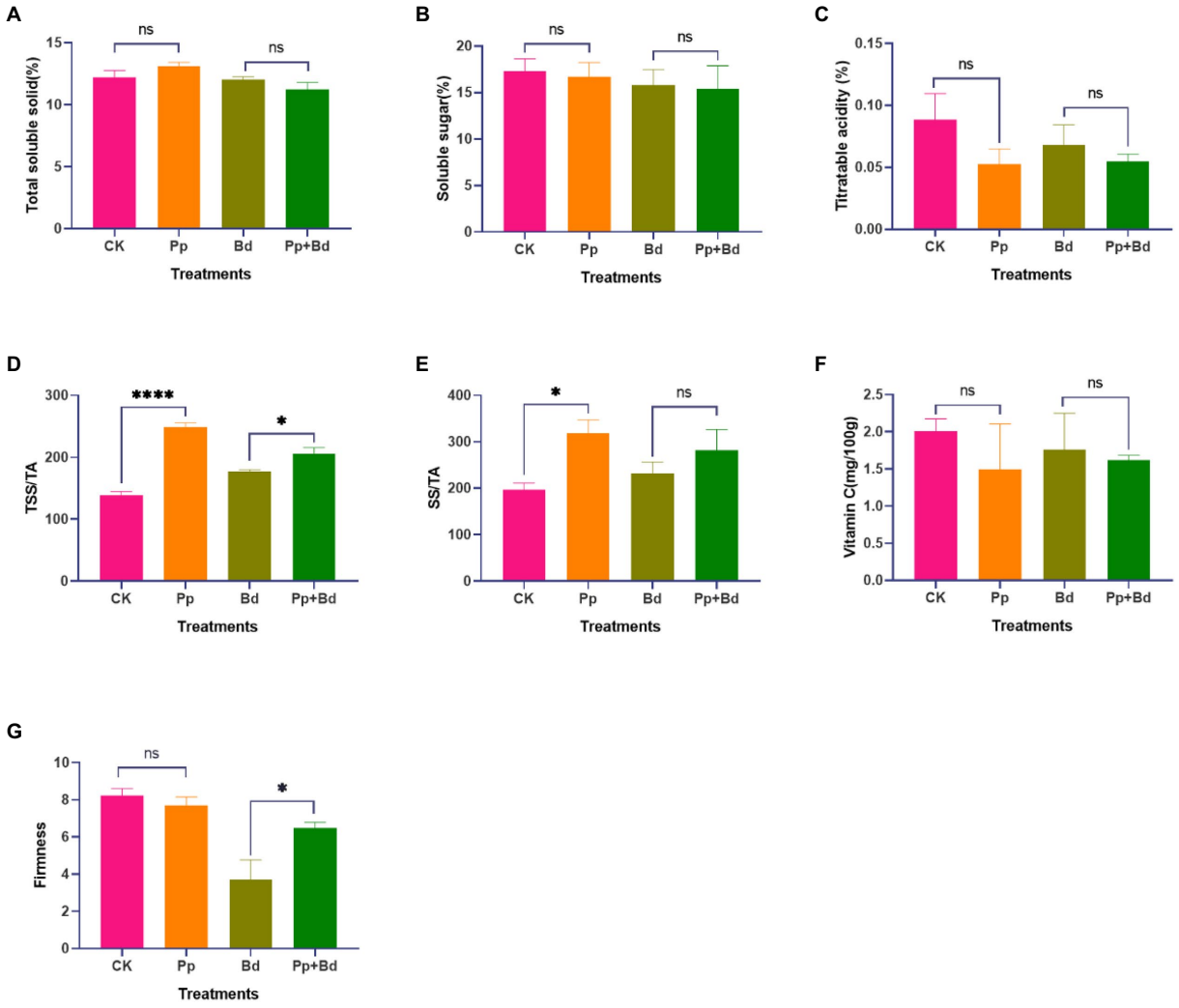

FIGURE 5
The fruit quality indexes of the apple fruits of the four treatments. Nine days later, the fruit quality indexes, including total soluble solid (TSS) **(A)**, titratable acidity (TA) **(B)**, soluble sugar (SS) **(C)**, total soluble solid/titrable acidity (TSS/TA) **(D)**, and soluble sugar/titrable acidity (SS/TA) **(E)**, vitamin C (VC) **(F)**, and firmness **(G)**, were different among the four treatment. $^{*}p<0.05$, $^{****}p<0.0001$, ns $p>0.05$.

Verticillium dahlia (Zhang et al., 2016). Alcohol dehydrogenase (ADH) was required for fungal development, environmental adaptation, and its ability for full pathogenicity in *Botrytis cinerea* (DafaAlla et al., 2021). Glycoside hydrolase (GHY) functioned as an important determinant of virulence in *Coniella vitis* (Qin et al., 2020), *Phytophthora sojae* (Ma et al., 2015), and *Pyricularia oryzae* (Pan et al., 2021). Aminoacyl-tRNA synthetase (ATS) was a vital factor in the cellular viability of *Ustilago maydis* (Ostrowski and Saville, 2017) and germination and blastospore yield in *Beauveria bassiana* (Zhu et al., 2017). Alpha/beta hydrolase (α/β-HY) was involved in the *Fusarium graminearum* pathogenicity (Jiao and Peng, 2018). Sugar Transporter (STR) played an essential role in the germination and mycelial growth of *Metarhizium robertsii* (Dai et al., 2021). From this, the significantly reduced expression of these genes in *B. dothidea* was another important factor contributing to the disease reduction.

Taken together, the molecular mechanism by which *P. protegens* significantly inhibited the apple ring rot on postharvest apple fruit can be explained from two aspects (Figure 8). On the one hand, *P. protegens* induced the defense-related genes, including MdPAL, MdGLU, MdPOD, and MdCAT in apple fruits, and the transcription factors such as MdPUB29, MdWRKY15, MdEFR11, and MdMYB73, which enhanced the apple fruit resistance against pathogen *B. dothidea*. On the other hand, *P. protegens* strongly repressed the pathogenicity-related genes in *B. dothidea*, such as BdCYP450, BdADH, BdGHY, BdATS, Bdα/β-HY, and BdSTR, which reduced the pathogenicity of *B. dothidea* to apple fruits. The two factors, together, contributed to the considerable

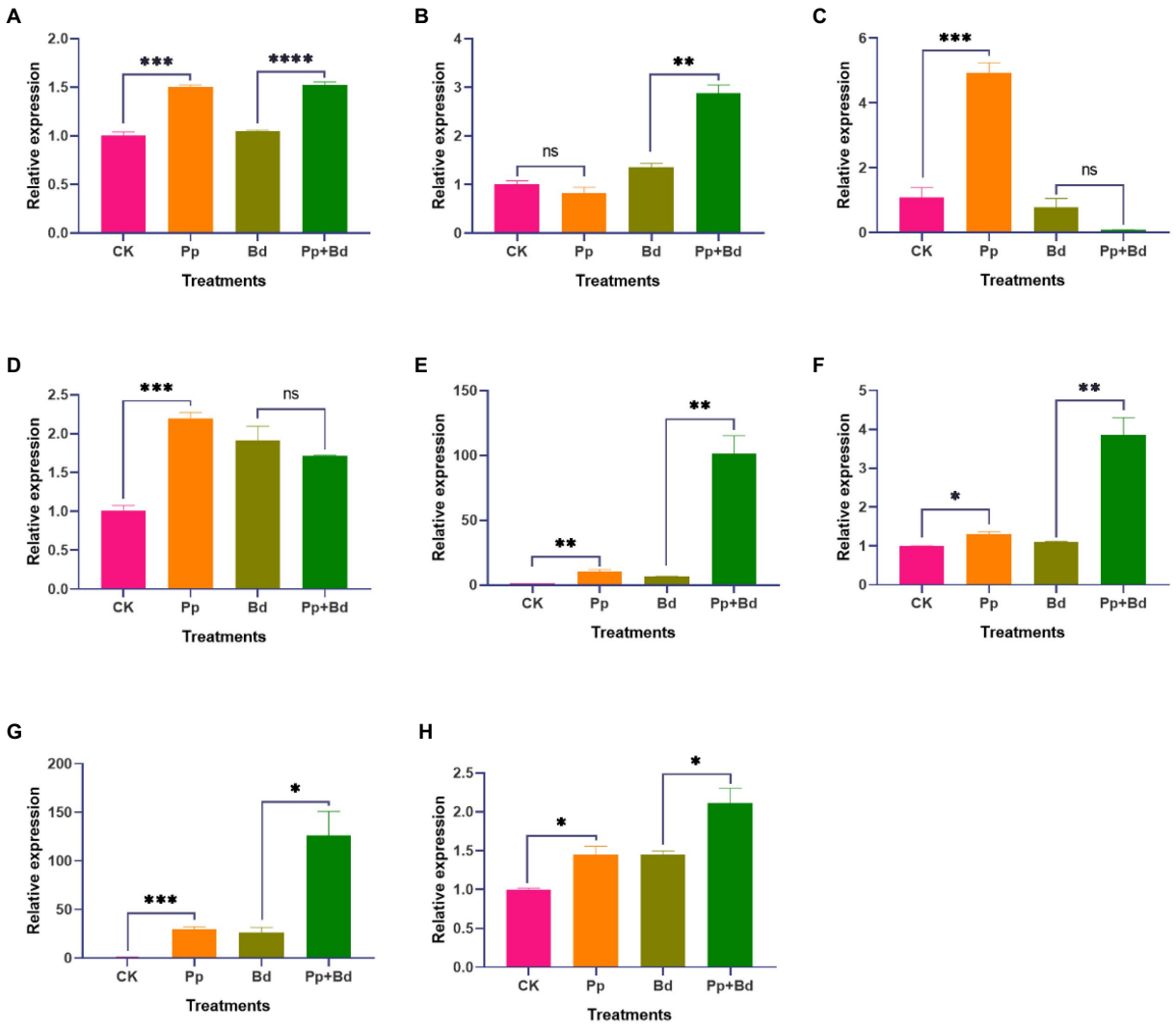

FIGURE 6
The relative expressions of various defense-related genes and the transcription factors, including MdGLU **(A)**, MdCATe **(B)**, MdPOD **(C)**, MdPAL **(D)**, MdPUB29 **(E)**, MdWRKY15 **(F)**, MdERF11 **(G)** and MdMYB73 **(H)** in various treated apple fruits. $^{*}p<0.05$, $^{**}<0.01$, $^{***}p<0.001$, $^{****}p<0.0001$, ns $p>0.05$.

reduction of the ring rot disease on *P. protegens*-treated apple fruits.

Conclusion

P. protegens isolated from Chinese leek strongly suppressed the mycelial growth of the pathogen *B. dothidea*, thus further significantly inhibiting the apple ring rot on postharvest apple fruits. Simultaneously, *P. protegens* also improved the fruit quality to some extent. Furthermore, *P. protegens* significantly induced the defense-related genes in apple fruits and markedly repressed the pathogenicity-related genes in *B. dothidea*. Together, the two-fold factors led to the vast reduction of apple ring rot disease on postharvest apple fruits.

Data availability statement

The original contributions presented in the study are included in the article/Supplementary material, further inquiries can be directed to the corresponding authors.

Author contributions

YH and YD contributed to the conception of the study and wrote and reviewed the manuscript. JpL, JhL, and XS experimented and collected the data. All authors contributed to the article and approved the submitted version.

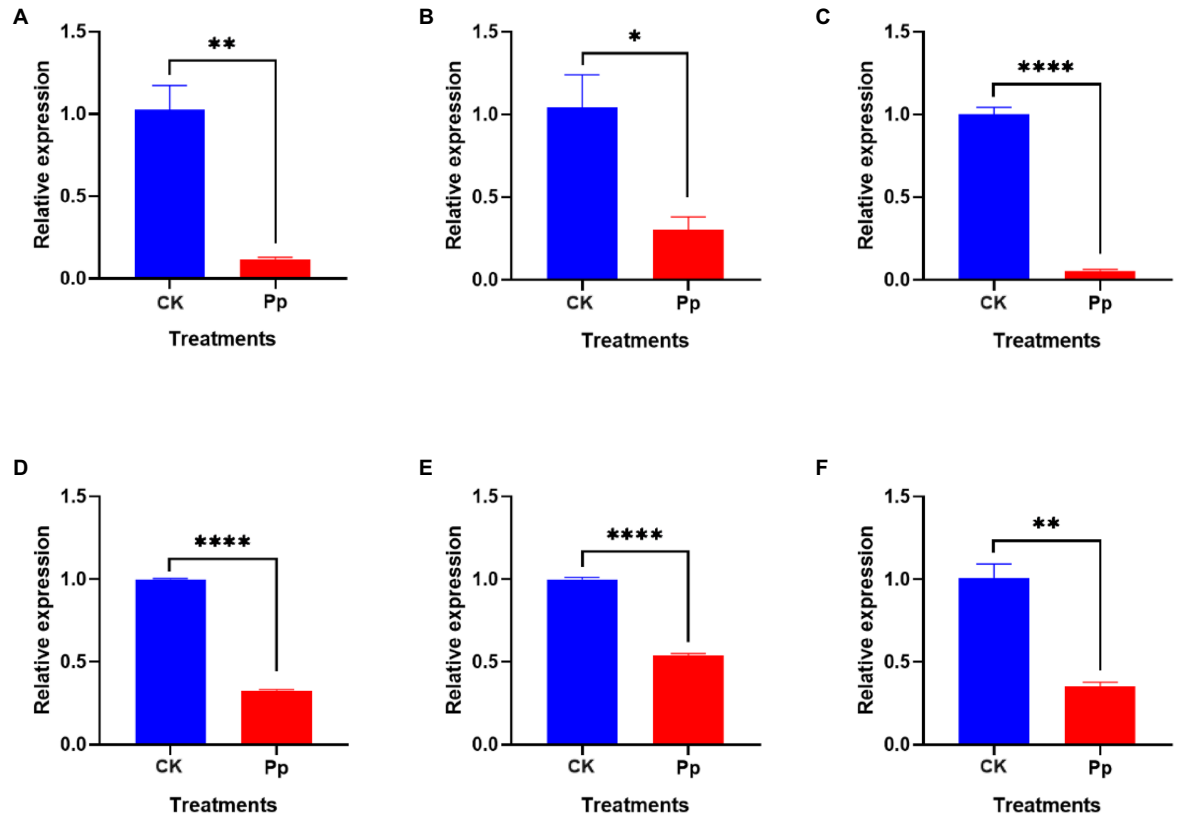

FIGURE 7
The relative expressions of various pathogenicity-related genes, including BdCYP450 **(A)**, BdADH **(B)**, BdGHY **(C)**, BdATS **(D)**, Bdα/β-HY **(E)**, and BdSTR **(F)** in *P. protegens*-treated and the control *B. dothidea*. $^{*}p<0.05$, $^{**}p<0.01$, $^{****}p<0.0001$.

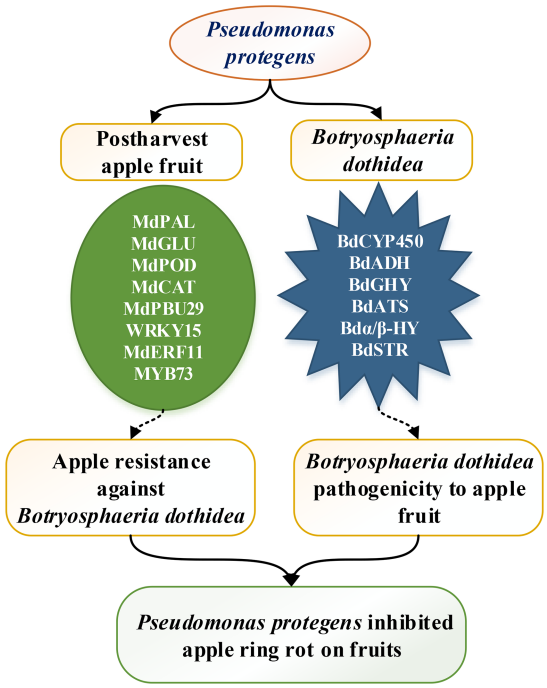

FIGURE 8
The model of *P. protegens* inhibiting the apple ring rot on fruit caused by *B. dothidea*.

Funding

This work was supported by the National Natural Science Foundation of China (31471864), the Natural Science Foundation of Shandong Province (ZR2020MC143 and ZR2020MC136), the Agricultural Variety Improvement Project of Shandong Province 2020LZGC007, and the Qingdao Agricultural University High-level Personnel Startup Fund China (6631115024).

Conflict of interest

The authors declare that the research was conducted in the absence of any commercial or financial relationships that could be construed as a potential conflict of interest.

Publisher's note

Supplementary material

The Supplementary material for this article can be found online at: https://www.frontiersin.org/articles/10.3389/fmicb.2022.1069517/full#supplementary-material

References

Abo-Elyousr, K. A. M., Abdel-Rahim, I. R., Almasoudi, N. M., and Alghamdi, S. A. (2021). Native endophytic pseudomonas putida as a biocontrol agent against common bean rust caused by *Uromyces appendiculatus*. *J. Fungi (Basel)*. 7:745. doi: 10.3390/jof7090745

Aiello, D., Restuccia, C., Stefani, E., Vitale, A., and Cirvilleri, G. (2019). Postharvest biocontrol ability of pseudomonas synxantha against Monilinia fructicola and Monilinia fructigena on stone fruit. *Postharvest Biol. Technol.* 149, 83–89. doi: 10.1016/j.postharvbio.2018.11.020

Andreolli, M., Zapparoli, G., Angelini, E., Lucchetta, G., Lampis, S., and Vallini, G. (2019). Pseudomonas protegens MP12: a plant growth-promoting endophytic bacterium with broad-spectrum antifungal activity against grapevine phytopathogens. *Microbiol. Res.* 219, 123–131. doi: 10.1016/j.micres.2018.11.003

Chen, Y., Li, F., Tian, L., Huang, M., Deng, R., Li, X., et al. (2017). The phenylalanine ammonia Lyase gene LjPAL1 is involved in plant defense responses to pathogens and plays diverse roles in Lotus japonicus-rhizobium symbioses. *Mol. Plant-Microbe Interact.* 30, 739–753. doi: 10.1094/MPMI-04-17-0080-R

Chen, Z., Yu, L., Liu, W., Zhang, J., Wang, N., and Chen, X. (2021). Research progress of fruit color development in apple (Malus domestica Borkh.). *Plant Physiol. Biochem.* 162, 267–279. doi: 10.1016/j.plaphy.2021.02.033

DafaAlla, T., Abdalla, M., El-Arabey, A. A., Eltayb, W. A., and Mohapatra, R. K. (2021). Botrytis cinerea alcohol dehydrogenase mediates fungal development, environmental adaptation and pathogenicity. *J. Biomol. Struct. Dyn*, 1–13. doi: 10.1080/07391102.2021.1971112

Dai, J., Mi, W., Wu, C., Song, H., Bao, Y., Zhang, M., et al. (2021). The sugar transporter MST1 is involved in colonization of rhizosphere and rhizoplane by Metarhizium robertsii. *mSystems* 6, e01277–e01221. doi: 10.1128/mSystems.01277-21

Dai, D. J., Wang, H. D., Wang, Y. P., and Zhang, C. Q. (2017). Management of Chinese hickory (Carya cathayensis) trunk canker through effective fungicide application programs and baseline sensitivity of Botryosphaeria dothidea to trifloxystrobin. *Australas. Plant Pathol.* 46, 75–82. doi: 10.1007/s13313-017-0465-4

Davis, M. A., Bynum, J. P., and Sirovich, B. E. (2015). Association between apple consumption and physician visits: appealing the conventional wisdom that an apple a day keeps the doctor away. *JAMA Intern. Med.* 175, 777–783. doi: 10.1001/jamainternmed.2014.5466

Dong, B. Z., and Guo, L. Y. (2020). An efficient gene disruption method for the woody plant pathogen Botryosphaeria dothidea. *BMC Biotechnol.* 20:14. doi: 10.1186/s12896-020-00608-z

El-Hasan, A., Schöne, J., Höglinger, B., Walker, F., and Voegele, R. T. (2017). Assessment of the antifungal activity of selected biocontrol agents and their secondary metabolites against *Fusarium graminearum*. *Eur. J. Plant Pathol.* 150, 91–103. doi: 10.1007/s10658-017-1255-0

Fan, K., Wang, J., Fu, L., Zhang, G. F., Wu, H. B., Feng, C., et al. (2019). Baseline sensitivity and control efficacy of Pyraclostrobin against Botryosphaeria dothidea isolates in China. *Plant Dis.* 103, 1458–1463. doi: 10.1094/PDIS-07-18-1214-RE

Fan, H., Yao, M., Wang, H., Zhao, D., Zhu, X., Wang, Y., et al. (2020). Isolation and effect of Trichoderma citrinoviride Snef1910 for the biological control of root-knot nematode *Meloidogyne incognita*. *BMC Microbiol.* 20:299. doi: 10.1186/s12866-020-01984-4

FAOSTAT (2022). Food and Agriculture Organization of the United Nations (FAOSTAT). Available online at: https://www.fao.org/faostat/en/#data/QCL (Accessed: February 17, 2022).

Fu, J., Sun, M., Liu, J., Mei, M., and Huang, Y. (2022). Control efficacy of Chinese leek volatiles on postharvest ring rot of apple fruits. *J. Plant Protect.* 49, 975–982. doi: 10.13802/j.cnki.zwbhxb.2022.2020246

Ghadamgahi, F., Tarighi, S., Taheri, P., Saripella, G. V., Anzalone, A., Kalyandurg, P. B., et al. (2022). Plant growth-promoting activity of Pseudomonas aeruginosa FG106 and its ability to act as a biocontrol agent against potato, tomato and Taro pathogens. *Biology.* 11:140. doi: 10.3390/biology11010140

Gu, K. D., Zhang, Q. Y., Yu, J. Q., Wang, J. H., Zhang, F. J., Wang, C. K., et al. (2021). R2R3-MYB transcription factor MdMYB73 confers increased resistance to the fungal pathogen *Botryosphaeria dothidea* in apples via the salicylic acid pathway. *J. Agric. Food Chem.* 69, 447–458. doi: 10.1021/acs.jafc.0c06740

Guo, L. Y., Li, J. Y., Li, B. H., Zhang, X. Z., Zhou, Z. Q., Li, G. X., et al. (2009). Investigations on the occurrence and chemical control of botryosphaeria canker of apple in China (in Chinese). *Plant Prot.* 35, 120–123. doi: 10.3969/j.issn.0529-1542.2009.04.027

Han, P. L., Dong, Y. H., Gu, K. D., Yu, J. Q., Hu, D. G., and Hao, Y. J. (2019). The apple U-box E3 ubiquitin ligase MdPUB29 contributes to activate plant immune response to the fungal pathogen Botryosphaeria dothidea. *Planta* 249, 1177–1188. doi: 10.1007/s00425-018-03069-z

Huang, Y.-H., Mao, Z.-C., and Xie, B.-Y. (2016). Chinese leek (Allium tuberosum Rottler ex Sprengel) reduced disease symptom caused by root-knot nematode. *J. Integr. Agric.* 15, 364–372. doi: 10.1016/s2095-3119(15)61032-2

Huang, Y. H., Wang, R. C., Li, C. H., Zuo, C. W., Wei, Y. R., Zhang, L., et al. (2012). Control of fusarium wilt in banana with Chinese leek. *Eur. J. Plant Pathol.* 134, 87–95. doi: 10.1007/s10658-012-0024-3

Jiao, J., and Peng, D. (2018). Wheat microRNA1023 suppresses invasion of fusarium graminearum via targeting and silencing FGSG_03101. *J. Plant Interact.* 13, 514–521. doi: 10.1080/17429145.2018.1528512

Jiao, Z., Tian, Y., Cao, Y., Wang, J., Zhan, B., Zhao, Z., et al. (2021). A novel pathogenicity determinant hijacks maize catalase 1 to enhance viral multiplication and infection. *New Phytol.* 230, 1126–1141. doi: 10.1111/nph.17206

Jing, X., Cui, Q., Li, X., Yin, J., Ravichandran, V., Pan, D., et al. (2020). Engineering pseudomonas protegens Pf-5 to improve its antifungal activity and nitrogen fixation. *Microb. Biotechnol.* 13, 118–133. doi: 10.1111/1751-7915.13335

Kakembo, D., and Lee, Y. H. (2019). Analysis of traits for biocontrol performance of pseudomonas parafulva JBCS1880 against bacterial pustule in soybean plants. *Biol. Control* 134, 72–81. doi: 10.1016/j.biocontrol.2019.04.006

Koutsos, A., and Lovegrove, J. A. (2015). "An apple a day keeps the doctor away – inter-relationship between apple consumption, the gut microbiota and cardiometabolic disease risk reduction," in *Diet-microbe Interactions in the Gut*. eds. K. Tuohy and D. D. Rio (Amsterdam: Elsevier Inc.), 173–194.

Li, Q., Qin, X., Qi, J., Dou, W., Dunand, C., Chen, S., et al. (2020). CsPrx25, a class III peroxidase in Citrus sinensis, confers resistance to citrus bacterial canker through the maintenance of ROS homeostasis and cell wall lignification. *Hortic. Res.* 7:192. doi: 10.1038/s41438-020-00415-9

Livak, K. J., and Schmittgen, T. D. (2001). Analysis of relative gene expression data using real-time quantitative PCR and the $2^{-\Delta\Delta CT}$ method. *Methods* 25, 402–408. doi: 10.1006/meth.2001.1262

Ma, Z., Song, T., Zhu, L., Ye, W., Wang, Y., Shao, Y., et al. (2015). A *Phytophthora sojae* glycoside hydrolase 12 protein is a major virulence factor during soybean infection and is recognized as a PAMP. *Plant Cell* 27, 2057–2072. doi: 10.1105/tpc.15.00390

Ostrowski, L. A., and Saville, B. J. (2017). Natural antisense transcripts are linked to the modulation of mitochondrial function and teliospore dormancy in Ustilago maydis. *Mol. Microbiol.* 103, 745–763. doi: 10.1111/mmi.13587

Pan, S., Tang, L., Pan, X., Qi, L., and Yang, J. (2021). A member of the glycoside hydrolase family 76 is involved in growth, conidiation, and virulence in rice blast fungus. *Physiol. Mol. Plant Pathol.* 113:101587. doi: 10.1016/j.pmpp.2020.101587

Pellicciaro, M., Lione, G., Giordano, L., and Gonthier, P. (2021). Biocontrol potential of pseudomonas protegens against Heterobasidion species attacking conifers in Europe. *Biol. Control* 157:104583. doi: 10.1016/j.biocontrol.2021.104583

Pollini, L., Cossignani, L., Juan, C., and Manes, J. (2021). Extraction of phenolic compounds from fresh apple pomace by different non-conventional techniques. *Molecules* 26:4272. doi: 10.3390/molecules26144272

Prigigallo, M. I., De Stradis, A., Anand, A., Mannerucci, F., L'Haridon, F., Weisskopf, L., et al. (2021). Basidiomycetes are particularly sensitive to bacterial volatile compounds: mechanistic insight into the case study of *Pseudomonas protegens* volatilome against *Heterobasidion abietinum*. *Front. Microbiol.* 12:684664. doi: 10.3389/fmicb.2021.684664

Qin, J.-X., Li, B.-H., and Zhou, S.-Y. (2020). A novel glycoside hydrolase 74 xyloglucanase CvGH74A is a virulence factor in *Coniella vitis*. *J. Integr. Agric.* 19, 2725–2735. doi: 10.1016/s2095-3119(20)63254-3

Rodriguez, M., Torres, M., Blanco, L., Bejar, V., Sampedro, I., and Llamas, I. (2020). Plant growth-promoting activity and quorum quenching-mediated biocontrol of bacterial phytopathogens by *Pseudomonas segetis* strain P6. *Sci. Rep.* 10:4121. doi: 10.1038/s41598-020-61084-1

Shi, F., Wang, Y., Zhang, F., Yuan, X., Chen, H., Chen, X., et al. (2020). Soybean Endo-1,3-Beta-Glucanase (GmGLU) interaction with soybean mosaic virus-encoded P3 protein may contribute to the Intercelluar movement. *Front. Genet.* 11:536771. doi: 10.3389/fgene.2020.536771

Shin, J. Y., Bui, D. C., Lee, Y., Nam, H., Jung, S., Fang, M., et al. (2017). Functional characterization of cytochrome P450 monooxygenases in the cereal head blight fungus *Fusarium graminearum*. *Environ. Microbiol.* 19, 2053–2067. doi: 10.1111/1462-2920.13730

Song, Y., Li, L., Li, C., Lu, Z., Men, X., and Chen, F. (2018). Evaluating the sensitivity and efficacy of fungicides with different modes of action against *Botryosphaeria dothidea*. *Plant Dis.* 102, 1785–1793. doi: 10.1094/PDIS-01-18-0118-RE

Sun, M., Duan, Y., Liu, J. P., Fu, J., and Huang, Y. (2022a). Efficacy of dimethyl Trisulfide on the suppression of ring rot disease caused by *Botryosphaeria dothidea* and induction of defense-related genes on apple fruits. *Front. Microbiol.* 13:796167. doi: 10.3389/fmicb.2022.796167

Sun, M., Liu, J., Li, J., and Huang, Y. (2022b). Endophytic bacterium *Serratia plymuthica* from Chinese Leek suppressed apple ring rot on postharvest apple fruit. *Front. Microbiol.* 12:802887. doi: 10.3389/fmicb.2021.802887

Taif, S., Zhao, Q., Pu, L., Li, X., Liu, D., and Cui, X. (2020). A β-1,3-glucanase gene from *Panax notoginseng* confers resistance in tobacco to *Fusarium solani*. *Ind. Crop. Prod.* 143:111947. doi: 10.1016/j.indcrop.2019.111947

Wang, J. H., Gu, K. D., Han, P. L., Yu, J. Q., Wang, C. K., Zhang, Q. Y., et al. (2020). Apple ethylene response factor MdERF11 confers resistance to fungal pathogen *Botryosphaeria dothidea*. *Plant Sci.* 291:110351. doi: 10.1016/j.plantsci.2019.110351

Wang, B., Liang, X., Gleason, M. L., Zhang, R., and Sun, G. (2018). Comparative genomics of Botryosphaeria dothidea and B. kuwatsukai, causal agents of apple ring rot, reveals both species expansion of pathogenicity-related genes and variations in virulence gene content during speciation. *IMA Fungus.* 9, 243–257. doi: 10.5598/imafungus.2018.09.02.02

Wang, C., Wang, Y., Wang, L., Fan, W., Zhang, X., Chen, X., et al. (2021). Biocontrol potential of volatile organic compounds from pseudomonas chlororaphis ZL3 against postharvest gray mold caused by *Botrytis cinerea* on Chinese cherry. *Biol. Control* 159:104613. doi: 10.1016/j.biocontrol.2021.104613

Wang, Z., Zhong, T., Chen, K., Du, M., Chen, G., Chen, X., et al. (2021). Antifungal activity of volatile organic compounds produced by *Pseudomonas fluorescens* ZX and potential biocontrol of blue mold decay on postharvest citrus. *Food Control* 120:107499. doi: 10.1016/j.foodcont.2020.107499

Yang, X., and Hong, C. (2018). Biological control of boxwood blight by pseudomonas protegens recovered from recycling irrigation systems. *Biol. Control* 124, 68–73. doi: 10.1016/j.biocontrol.2018.01.014

Yang, Y., Jiang, R., Wang, H., Tian, Z., and Xie, C. (2020). StPOPA, encoding an anionic peroxidase, enhances potato resistance against *Phytophthora infestans*. *Mol. Breed.* 40:16. doi: 10.1007/s11032-019-1093-1

Yang, T., Qiu, L., Huang, W., Xu, Q., Zou, J., Peng, Q., et al. (2020). Chilli veinal mottle virus HCPro interacts with catalase to facilitate virus infection in *Nicotiana tabacum*. *J. Exp. Bot.* 71, 5656–5668. doi: 10.1093/jxb/eraa304

Yang, L., Zhu, Z., Zhang, J., Gao, Y., Wang, X., Liu, G., et al. (2020). Response of kiwifruit yield and fruit quality to chloride-containing fertilizers. *Agron. J.* 112, 1012–1020. doi: 10.1002/agj2.20074

Yin, K., and Qiu, J. L. (2019). Genome editing for plant disease resistance: applications and perspectives. *Philos. Trans. R. Soc. Lond. Ser. B Biol. Sci.* 374:20180322. doi: 10.1098/rstb.2018.0322

Yu, J. Q., Li, X. M., Wang, W. Y., Gu, K. D., Sun, C. H., You, C. X., et al. (2022). Glucose sensor MdHXK1 activates an immune response to the fungal pathogen *Botryosphaeria dothidea* in apple. *Physiol. Plant.* 174:e13596. doi: 10.1111/ppl.13596

Zhang, Q. X., Kong, X. W., Li, S. Y., Chen, X. J., and Chen, X. J. (2020). Antibiotics of *Pseudomonas protegens* FD6 are essential for biocontrol activity. *Australas. Plant Pathol.* 49, 307–317. doi: 10.1007/s13313-020-00696-7

Zhang, D. D., Wang, X. Y., Chen, J. Y., Kong, Z. Q., Gui, Y. J., Li, N. Y., et al. (2016). Identification and characterization of a pathogenicity-related gene VdCYP1 from *Verticillium dahliae*. *Sci. Rep.* 6:27979. doi: 10.1038/srep27979

Zhang, C., Wang, X., Zhang, F., Dong, L., Wu, J., Cheng, Q., et al. (2017). Phenylalanine ammonia-lyase2.1 contributes to the soybean response towards *Phytophthora sojae* infection. *Sci. Rep.* 7:7242. doi: 10.1038/s41598-017-07832-2

Zhao, X. Y., Qi, C. H., Jiang, H., Zhong, M. S., You, C. X., Li, Y. Y., et al. (2020). MdWRKY15 improves resistance of apple to *Botryosphaeria dothidea* via the salicylic acid-mediated pathway by directly binding the MdICS1 promoter. *J. Integr. Plant Biol.* 62, 527–543. doi: 10.1111/jipb.12825

Zhao, J., Wang, S., Zhu, X., Wang, Y., Liu, X., Duan, Y., et al. (2021). Isolation and characterization of nodules endophytic bacteria *Pseudomonas protegens* Sneb1997 and *Serratia plymuthica* Sneb2001 for the biological control of root-knot nematode. *Appl. Soil Ecol.* 164:103924. doi: 10.1016/j.apsoil.2021.103924

Zhao, X., Zhang, G.-l., Li, B.-h., Xu, X.-m., Dong, X.-l., Wang, C.-x., et al. (2016). Seasonal dynamics of Botryosphaeria dothidea infections and symptom development on apple fruits and shoots in China. *Eur. J. Plant Pathol.* 146, 507–518. doi: 10.1007/s10658-016-0935-5

Zhao, G., Zhang, W., Zuo, C., and Huang, Y. (2017). Control effect of chinese leek extract and its main bioactive components on apple ring rot incidence. *Chin. J. Biol. Control.* 33, 273–280. doi: 10.16409/j.cnki.2095-039x.2017.02.019

Zhu, X. G., Chu, Z. J., Ying, S. H., and Feng, M. G. (2017). Lysyl-tRNA synthetase (Krs) acts a virulence factor of *Beauveria bassiana* by its vital role in conidial germination and dimorphic transition. *Fungal Biol.* 121, 956–965. doi: 10.1016/j.funbio.2017.08.003

frontiers | Frontiers in Microbiology

TYPE Original Research
PUBLISHED 04 January 2023
DOI 10.3389/fmicb.2022.1032900

OPEN ACCESS

EDITED BY
Xiuling Yang,
Institute of Plant Protection (CAAS), China

REVIEWED BY
Zhaohui Chu,
Wuhan University, China
Haifeng Zhang,
Nanjing Agricultural University, China

*CORRESPONDENCE
Xiaodan Wang
xdwang@cau.edu.cn

†These authors have contributed equally to this work

SPECIALTY SECTION
This article was submitted to Microbe and Virus Interactions with Plants, a section of the journal Frontiers in Microbiology

RECEIVED 31 August 2022
ACCEPTED 17 November 2022
PUBLISHED 04 January 2023

CITATION
Yang S, Li J, Lu J, Wang L, Min F, Guo M, Wei Q, Wang W, Dong X, Mao Y, Hu L and Wang X (2023) Potato calcineurin B-like protein CBL4, interacting with calcineurin B-like protein-interacting protein kinase CIPK2, positively regulates plant resistance to stem canker caused by *Rhizoctonia solani*.
Front. Microbiol. 13:1032900.
doi: 10.3389/fmicb.2022.1032900

Potato calcineurin B-like protein CBL4, interacting with calcineurin B-like protein-interacting protein kinase CIPK2, positively regulates plant resistance to stem canker caused by *Rhizoctonia solani*

Shuai Yang[1†], Jie Li[2†], Jie Lu[3], Ling Wang[4], Fanxiang Min[1], Mei Guo[1], Qi Wei[1], Wenzhong Wang[1], Xuezhi Dong[1], Yanzhi Mao[1], Linshuang Hu[1] and Xiaodan Wang[2*]

[1]Institute of Industrial Crop, Heilongjiang Academy of Agricultural Sciences, Harbin, China, [2]Department of Plant Pathology, College of Plant Protection, China Agricultural University, Beijing, China, [3]Biotechnology Research Institute, Heilongjiang Academy of Agricultural Sciences, Harbin, China, [4]Institute of Crop Cultivation and Tillage, Heilongjiang Academy of Agricultural Sciences, Harbin, China

Introduction: Calcium sensor calcineurin B-like proteins (CBLs) and their interacting partners, CBL-interacting protein kinases (CIPKs), have emerged as a complex network in response to abiotic and biotic stress perception. However, little is known about how CBL-CIPK complexes function in potatoes.

Methods: In this study, we identified the components of one potato signaling complex, StCBL4–StCIPK2, and characterized its function in defense against *Rhizoctonia solani* causing stem canker in potato.

Results: Expressions of both *StCBL4* and *StCIPK2* from potato were coordinately induced upon *R. solani* infection and following exposure to the defense genes. Furthermore, transient overexpression of *StCBL4* and *StCIPK2* individually and synergistically increased the tolerance of potato plants to *R. solani* in *Nicotiana benthamiana*. Additionally, the transgenic potato has also been shown to enhance resistance significantly. In contrast, susceptibility to *R. solani* was exhibited in *N. benthamiana* following virus-induced gene silencing of *NbCBL* and *NbCIPK2*. Evidence revealed that StCBL4 could interact in yeast and *in planta* with StCIPK2. *StCBL4* and *StCIPK2* transcription was induced upon *R. solani* infection and this expression in response to the pathogen was enhanced in *StCBL4*- and *StCIPK2*-transgenic potato. Moreover, accumulated expression of pathogenesis-related (*PR*) genes and reactive oxygen species (ROS) was significantly upregulated and enhanced in both *StCBL4*- and *StCIPK2*- transgenic potato.

Discussion: Accordingly, *StCBL4* and *StCIPK2* were involved in regulating the immune response to defend the potato plant against *R. solani*. Together, our data demonstrate that *StCBL4* functions in concert with *StCIPK2*, as positive regulators of immunity, contributing to combating stem canker disease in potato.

KEYWORDS

Calcineurin B-like protein, CBL-interacting protein kinases, disease resistance, expression profile, regulation, *Rhizoctonia solani*

Introduction

Plants have evolved tightly regulated signaling pathways that allow them to respond to threats they encounter during exposure to complex and varying environments (Verma et al., 2021). To cope with numerous environmental stimuli, plants rely on a series of complex signal transduction mechanisms to perceive, transduce, and respond to different stresses (Yin et al., 2017). As a secondary messenger in plants, calcium (Ca^{2+}) links various signal pathways together and participates in many biochemical reactions, with altered Ca^{2+} levels observed when plants are exposed to biotic and abiotic stressors (Xu et al., 2022). Importantly, transient changes in intracellular Ca^{2+} concentration are captured by Ca^{2+} sensors that subsequently regulate signaling pathways involved in plant growth and development. Ca^{2+} sensors include two types of Ca^{2+} sensor proteins with distinct structural features and functions: sensor relay proteins and sensor responder proteins. Sensor relay proteins include calmodulin-like proteins (CMLs) and calcineurin B-like proteins (CBLs), while sensor responder proteins include calmodulins (CAMs) and calcium-dependent protein kinases (CDPKs; Tang et al., 2020). Sensor relays (e.g., CMLs and CBLs) lack kinase activity but can specifically target downstream proteins to transmit perceived calcium signals generated in response to various environmental stimuli and developmental processes. In contrast, sensor responder proteins (e.g., CaMs and CDPKs) possess kinase activity and all of the abovementioned sensor relay activities.

As a family of Ca^{2+} sensor proteins, CBLs are generally found in plants, but not in animals or fungi. CBLs contain a crucial structural component consisting of common elongation factor hand domains (EF hands). EF hands function as calcium-binding sites that capture Ca^{2+} while engaging in specific binding interactions with NAF/FISL domains present within C-terminal regions of CBL-interacting protein kinases (CIPKs). CIPKs comprise a group of plant-specific serine/threonine (Ser/Thr) kinases that belong to the SnRK3 protein family. These kinases play crucial roles in signal transduction *via* CBL–CIPK modules (Ma et al., 2020) to thereby control affinities and activities of numerous ion transporters. In contrast, the N-terminal MGCXXS/T motif in some CBL proteins mediates lipid modification *via* myristoylation and palmitoylation that direct CBL-CIPK complex migration to precise cellular membrane target regions where they become anchored to the membrane (Weinl and Kudla, 2009). *Arabidopsis* CBLs include CBL1, 4, 5, and 9, which localize to the plasma membrane (Batistic et al., 2010).

Calcineurin B-like protein–interacting protein kinase complexes of many plant species, including model plants, crop plants, and several horticultural plants, have been extensively studiedconcerning their regulation of diverse responses to abiotic stresses (Dong et al., 2021). One such complex, which was first identified in *Arabidopsis thaliana*, was initially found to participate in the Salt Overly Sensitive (SOS) signaling pathway, whereby CBL4 (SOS3) was shown to interact and form a complex with CIPK24 (SOS2). Once formed, the CBL4-CIPK24 complex was observed to migrate to the plasma membrane, where it activated the Na^+/H^+ antiporter (SOS1) located on the plasma membrane and the vacuolar H^+-ATPase, resulting in enhanced salt tolerance (Ishitani et al., 2000). Subsequently, other complexes were discovered in *Arabidopsis* (CBL1/CBL9-CIPK23) that were observed to localize to the plasma membrane and regulate K^+ in roots and stomatal guard cells by modulating K^+ channel Arabidopsis K^+ Transporter 1 (AKT1) activity (Cheong et al., 2007). Furthermore, overexpression of OsCBL8 and OsCIPK15 in rice was found to enhance salt tolerance (Xiang et al., 2007). Conversely, expression of OsCIPK31 in tobacco plants was found to participate in the generation of diverse signals in response to cold, salt, light, cytokinins, and sugars (Kim et al., 2003). More recently, TaCIPK23 has been shown to participate in wheat abscisic acid (ABA) and drought stress responses by mediating crosstalk between ABA-induced signaling and other pathways associated with adaptation to drought (Cui et al., 2018). In potato, StCIPK10 has been shown to enhance both cellular scavenging of ROS and cellular modulation of corresponding osmoregulatory substances to strengthen plant drought and osmotic stress tolerance (Ma et al., 2021). In addition, differential expression of maize *ZmCBL4*, pea *PsCBL*, Chinese cabbage *BrCBL*, and grapevine *VvCBL* have been reported to occur after exposure of plants to various abiotic stresses (Wang et al., 2007; Jung et al., 2017; Xi et al., 2017).

Compared with studies of abiotic stress responses, studies of biotic stress responses have rarely been reported, although a few studies can be found in the literature. One such study using cultured cells of rice plants demonstrated that an interaction between OsCIPK14/15 and OsCBL4 played a crucial role in the microbe-associated molecular pattern-induced defense signaling pathway (Kurusu et al., 2010). CBL10 and CIPK6 were found to promote ROS generation as part of the tomato immune defense response triggered by an interaction between *Pseudomonas syringae* pv tomato DC3000 and *Nicotiana benthamiana* (De la Torre et al., 2013). OsCIPK30 was shown to play a critical role in enhancing rice tolerance to rice stripe virus (Liu et al., 2017), while the TaCBL4–TaCIPK5 complex was observed to positively modulate wheat resistance to stripe rust fungus through a ROS-dependent mechanism (Liu et al., 2018). Moreover, the

knockdown of CaCIPK1 expression increased the susceptibility of pepper to *Phytophthora capsici*, reduced root activity, and altered the expression of defense-related genes (Ma et al., 2019). Taken together, the abovementioned results obtained from the few research studies reported to date suggest that CBL-CIPK complexes participate in biotic stress responses.

Rhizoctonia solani (teleomorph: *Thanatephorus cucumeris*) is one of the most dominant soil-borne necrotrophic fungal pathogens, due to its broad host range and the lack of crop resistance to this pathogen (Foley et al., 2013). *Rhizoctonia solani* is complex and divided into 14 anastomosis groups (AG1–AG13 and AGBI; Yang et al., 2017). AG3, the most destructive group, causes *Rhizoctonia* disease on potato (*Solanum tuberosum* L.; Woodhall et al., 2013), the fourth most cultivated food crop globally. In recent years, black scurf and stem canker have emerged to become the most severe soil-borne diseases, as evidenced by increasingly reduced crop yields and quality due to these diseases each year. However, efforts to combat these diseases have been hindered by a lack of knowledge about the necrotrophic pathogen infection process and the mechanisms by which plants prevent disease-induced cell death (Yang et al., 2017). In our previous study, transcriptome analysis was performed *via* RNA-Seq to investigate the potato response to *R. solani* infection, leading to the identification of two key genes, which encoded CBL4 and CIPK2 that exhibited up-regulated expression during infection (Yang et al., 2018). In this study, complete DNA sequences of the genes encoding these two proteins were cloned then their expression patterns were characterized in potato. After that, these genes were overexpressed in potato and the heterologous host *N. benthamiana* to determine whether increased expression of these genes could increase plant resistance to *Rhizoctonia* disease. *StCBL4* and *StCIPK2* were involved in regulating the immune response to defend the potato plant against *R. solani*. Therefore, the functional research of *StCBL4* in concert with *StCIPK2*, as both are positive regulators of immunity, will contribute to combating stem canker disease in potato.

Materials and methods

Bacterial strains, plant materials, and growth conditions

The virulent *R. solani* strain (anastomosis group: AG-3PT) used in this study was obtained from Heilongjiang Academy of Agricultural Sciences (HAAS) and cultured in potato dextrose agar (potato 200 g, Dextrose 20 g, agar 17 g, and water 1 L). Cultures were maintained on PDA medium for 1 week at 25°C, and then 5-mm-diameter mycelium plugs were obtained for inoculation of plants. In addition, *Agrobacterium tumefaciens* GV3101 was cultured in LB medium (10 g tryptone, 10 g NaCl, and 5 g yeast extract per liter).

Various potato germplasm resources studied here were grown in a climate-controlled chamber under 16 h light/8 h dark conditions at 23°C. The list of plant varieties is presented in Supplementary Table 1. In addition, *N. benthamiana* plants were grown in a climate-controlled chamber under 14 h light/10 h dark conditions and kept at 25°C and 20°C during light and dark cycles, respectively. All plants were grown on separate trays for subsequent RNA extraction, inoculation, and RT-PCR expression analysis. All experiments involving both control and treated plants were carried out using three independent biological replicate samples.

RNA extraction, gene cloning, and sequence analysis of *StCBL4* and *StCIPK2*

Total RNA was extracted from potato leaves using TRIzol™ Reagent (Invitrogen Co., United Kingdom) according to the manufacturer's instructions. RNA concentrations were measured using a Thermo NanoDrop 1000 spectrophotometer system (Thermo Fisher Scientific Co., United States). cDNA was synthesized using the GoScript™ Reverse Transcription System (Promega Co., United States), and then was used as a template for subsequent PCR amplifications. Based on transcript sequences, cDNA sequences encoding ORFs of *StCBL4* and *StCIPK2* were amplified with primers designed using CE Design V1.04 (Supplementary Table 2) according to amino acid sequence alignments conducted using SMART.[1] Next, multiple sequence alignments were performed using DNAMAN 8.0 software (Lynnon Biosoft Co., United States). Next, a phylogenetic tree was constructed based on alignments of amino acid sequences *via* the neighbor-joining (NJ) method using MEGA 5.0 software. Finally, bootstrap analysis with 1,000 replicates was performed to assess the statistical reliability of each branch of the tree.

Vector construction, subcellular localization, and potato transformation

For transient expression, complete coding sequences (CDSs) of *StCBL4* and *StCIPK2* were cloned into the pCAMBIA1300-35S-HA-RBS vector to generate constructs designated *35S:HA-StCBL4* and *35S:HA-StCIPK2*, respectively. The recombinant constructs were next introduced into *A. tumefaciens* strain GV3101, which was then used to transform *N. benthamiana* plants *via* the *Agrobacterium*-mediated transformation method, with the transformation of empty vector (EV) *35S:HA* serving as a control. To generate constructs for the luciferase complementation assay (LCA), the StCBL4-coding sequence was cloned into the pCAMBIA1300-35S-Cluc-RBS vector, and the StCIPK2-coding sequence was cloned into the pCAMBIA1300-35S-HA-Nluc-RBS vector. To construct the bait vector for the yeast two-hybrid assay, CDSs of StCBL4 and StCIPK2 were cloned into pGBKT7 (DNA-binding domain, BD) and

1 http://smart.embl-heidelberg.de/

pGADT7 (activation domain, AD) vectors, respectively. Meanwhile, pBWA(V)KS-StCBL4 and pBWA(V)KS-StCIPK2 constructs were generated and transformed into *A. tumefaciens* strain EHA105 using *Agrobacterium*-mediated transformation protocols for potato obtained from Wuhan Biorun Bio-Tech Co. Ltd. (Wuhan, China). Regenerated transgenic plants were transplanted in a standard MS medium (Murashige and Skoog, 1962) containing 50 mg/L kanamycin (Sangon Biotech Co., China). The primers used in this study are listed in Supporting Information Supplementary Table 2.

The images of subcellular localization of GFP- and RFP-tagged proteins were visualized through a Leica TCS SP8 confocal microscope (Leica Co., Germany) in *N. benthamiana* leaves expressing transiently p35S-CBL4-GFP and p35S-CIPK2-RFP constructs. Fluorescence signals were detected at 48 h after injection. GFP and RFP fluorescence was excited using argon lasers at 488 and 545 nm, and the emissions were collected within 495–545 and 580–620 nm, respectively. Relevant fluorescence data analysis and subsequent image processing of the indicated profile were conducted using Leica Application Suite X (LAS-X) software.

Yeast two-hybrid assay

For interaction analyses of StCBL4–StCIPK2, MatchMaker yeast two-hybrid assays were performed (Coolaber Co., China). After vector construction, paired pGADT7 (activation domain, AD) and pGBKT7 (DNA-binding domain, BD) plasmids were co-transformed into yeast strain AH109 *via* the lithium acetate method according to the Yeast Protocols Handbook. The positive control was the diploid hybrid yeast containing pGBKT7-53 and pGADT7-T. Yeast colonies were grown at 30°C for 2–4 days on selection medium before being photographed. After yeast cell numbers/ml were initially quantified using a hemocytometer, they were collected and diluted to 10^2 and 10^1 cells/ml in sterile ultrapure water for serial dilutions.

Luciferase complementation assay

The luciferase complementation assay was performed as described previously (Zhou et al., 2018) after Cluc and Nluc constructs were introduced into *N. benthamiana* leaves *via* the *Agrobacterium*-mediated transient expression-based method followed by co-expression of cloned genes in leaf cells for 2 days. Next, leaf disks in wells of a 96-well plate were incubated with 1 mM luciferin (Biovision Co., United States) then luminescence was measured using a microplate luminometer (Perkin Elmer Co., United States).

Co-immunoprecipitation assay

Two days after *Agrobacterium*-mediated transient injection of p35S-StCIPK2-HA constructs into *N. benthamiana*, leaves were collected for Co-IP experiments. Total proteins were extracted from agroinfiltrated leaves using protein immunoprecipitation (IP) buffer, which contains 50 mM HEPES (pH 7.5), 150 mM KCl, 5 mM EDTA, 0.5% Triton X-100, 1 mM DTT, and a proteinase inhibitor cocktail. Samples were centrifuged and the supernatant was transferred to another 1.5 ml centrifuge tube, and about 45 µl was taken for input analysis. The remaining extracts were then incubated with 10 µl agarose-conjugated anti-GFP antibody (Lablead Co., China) for 3 h at 4°C with shaking, followed by washing beads four times with IP buffer. Finally, about 50 µl elution buffer was added for output analysis. Immunoprecipitated proteins were separated *via* SDS-PAGE then proteins of interest were detected on immunoblots *via* probing membranes with anti-HA and anti-GFP antibodies.

Rhizoctonia infection assay

The *R. solani* AG-3 strain was used for plant infection and was cultured on a PDA medium at 25°C for 3 days. 5-mm-diameter mycelium plugs were incubated onto the abaxial side of detached leaves of intact *N. benthamiana* plants stored on moist tissue in sealed boxes for 24–48 h. Then inoculated leaves were photographed under UV light, and lesion areas were measured using ImageJ[2] software. For *S. tuberosum* experiments, mycelium inoculations were performed using *in vitro* cultured plantlets, as described previously (Yang et al., 2017).

Virus-induced gene silencing

To understand orthologous gene functions in *N. benthamiana*, phylogenetic relationships among CBLs and CIPKs from *S. tuberosum*, *N. benthamiana*, and *A. thaliana* were analyzed. Virus-induced gene silencing (VIGS) constructs were generated by cloning 300-bp PCR fragments of orthologous genes from *N. benthamiana* cDNA into the pBinary tobacco rattle virus (TRV) vector (Liu et al., 2002) between the *EcoR*I and *Kpn*I sites in the antisense orientation. A TRV construct expressing GFP, as described previously (McLellan et al., 2013), served as the negative control and a TRV construct expressing a cloned fragment of *N. benthamiana* phytoene desaturase (*NbPDS*) served as the positive control. Primer sequences are shown in Supplementary Table 2. Plants were either used in assays or to check gene silencing levels *via* quantitative RT-PCR 2–3 weeks later.

Oxidative burst measurement

Potato plants overexpressing the abovementioned genes were grown in a climate-controlled chamber under 16 h light/8 h dark

2 https://imagej.nih.gov/ij

conditions at 23°C. After 3–4 weeks of growth, detached leaves were assayed for H_2O_2 production. H_2O_2 was detected *via* staining of inoculated and uninoculated leaves with 1 mg/ml 3,3′-diaminobenzidine (DAB) for 8 h in the dark, and then the leaves were destained with ethanol prior to observation (Lu et al., 2021).

Quantitative RT-PCR analysis

Total RNA was isolated from *N. benthamiana* as described above. For *S. tuberosum* samples, RNA isolation was conducted after plants were inoculated with *R. solani* at 0, 6, 12, 24, 48, and 96 hpi (cv. Youjin-885) or 3 dpi (for different potato germplasm resources). Total RNA (5 μg) was reverse-transcribed using the GoScript™ Reverse Transcription System to generate a cDNA template. Next, cDNA was diluted tenfold for subsequent qRT-PCR analysis, using an ABI7500 Real-Time PCR System (Applied Biosystems, Carlsbad, CA) and TransStart Top Green qPCR SuperMix (TransGen, Beijing, China). Relative gene expression levels were calculated by normalization against internal controls *NbActin* (AY179605) and *StActin* (DQ252512) for *N. benthamiana* and *S. tuberosum*, respectively. All qRT-PCR experiments were performed at least three times. Relative quantification of expression levels was achieved using the $2^{-\Delta\Delta Ct}$ method.

Statistical analysis

Data were obtained from three replicates and analyzed by unpaired two-tailed Student's *t*-test with GraphPad Prism software (GraphPad Software, Inc., La Jolla, CA, United States). Values with $p < 0.05$ were considered statistically significant.

Results

StCBL4 and *StCIPK2* are rapidly induced following infection of potato with *Rhizoctonia solani*

In previous transcriptome analysis, preliminary screening of *StCBL4* and *StCIPK2* expression was conducted to determine whether infection of potato with *R. solani* could induce expression of these two genes. Then, relative levels of *StCBL4* and *StCIPK2* gene transcripts in cv. Youjin-885 plants were measured at 0, 6, 12, 24, 36, 48, and 96 hpi. The results revealed that the expression of *StCBL4* and *StCIPK2* was induced and upregulated significantly during the infection of *R. solani*. More specifically, the expression level of *StCBL4* was up-regulated and peaked at 24 hpi, 11.18-fold higher than the control level (Figure 1A). *StCIPK2* reached a peak level of expression 14.2-fold higher than the control level as early as 6 hpi (Figure 1B). Meanwhile, the lesion symptoms and relative levels of *StCBL4* and *StCIPK2* gene transcripts in various potato germplasm resources (with different levels of resistance to *R. solani*) at 7 dpi were measured. As shown in Figure 1C, 5 potato germplasm resources displayed the disease except the varieties of 133, 153, and 812. Compared with the mild symptom of cv. 827, the other four potato germplasm resources exhibited no less than a 5-fold disease level on stem of potato plantlet. Moreover, real-time PCR results revealed that expression levels of both *StCBL4* and *StCIPK2* were significantly up-regulated in asymptomatic potato plantlets compared with symptomatic plantlets. The latter exhibited no significant change in the expression of these genes except for *StCBL4* in potato *cv.* Z5 and *StCIPK2* in potato *cv.*106 (Figures 1D,E). Based on these observations, we speculated that *StCBL4* and *StCIPK2* might be involved in the host response to *R. solani* infection.

Sequence analysis of *StCBL4* and *StCIPK2*

Based on transcript sequences identified *via* RNA-seq, ORF sequences of *StCBL4* and *StCIPK2* were cloned and deposited into the GenBank database under accession numbers ON383960 and ON324205, respectively. The ORF of the *StCBL4* gene is 663 bp in length and contains 4 EF-hand conserved domains and an FPSF motif that interacts with CIPKs (Supplementary Figure 1A). The predicted StCBL4 ORF contains 220 aa, a polypeptide molecular mass of 25.32 kDa, and an isoelectric point (pI) of 4.77. Results of the phylogenetic analysis indicated that *StCBL4* is highly homologous to CBL4 from *Capsicum annuum* (Supplementary Figure 1B). *StCIPK2* is 1,413 bp in length and contains a NAF/FISL motif and a PPI motif (Supplementary Figure 2A). The predicted StCIPK2 ORF contains 470 aa, a polypeptide molecular mass of 53.01 kDa, and an isoelectric point (pI) of 8.66. Results obtained through homology analysis indicated that *StCIPK2* has high homology to *CIPK* of *Hordeum vulgare* (Supplementary Figure 2B).

Transient expression of *StCBL4* and *StCIPK2* enhances resistance to *Rhizoctonia solani* in *Nicotiana benthamiana*

To investigate whether *StCBL4* and *StCIPK2* enhanced host resistance against *R. solani* infection, we transiently expressed StCBL4-HA and StCIPK2-HA in *N. benthamiana* plants using *Agrobacterium*-mediated transient expression, with pCambia1300-35S-HA empty vector (EV) as control. The results showed that StCBL4-HA and StCIPK2-HA exhibited remarkably smaller lesion areas than the EV control (Figures 2A,C), and was about 51 and 50% lower than corresponding levels in control, respectively (Figures 2B,D). These findings indicated that *StCBL4* and *StCIPK2* could positively enhance *N. benthamiana* resistance to *R. solani* infection. Furthermore, western blotting elucidated the stability of

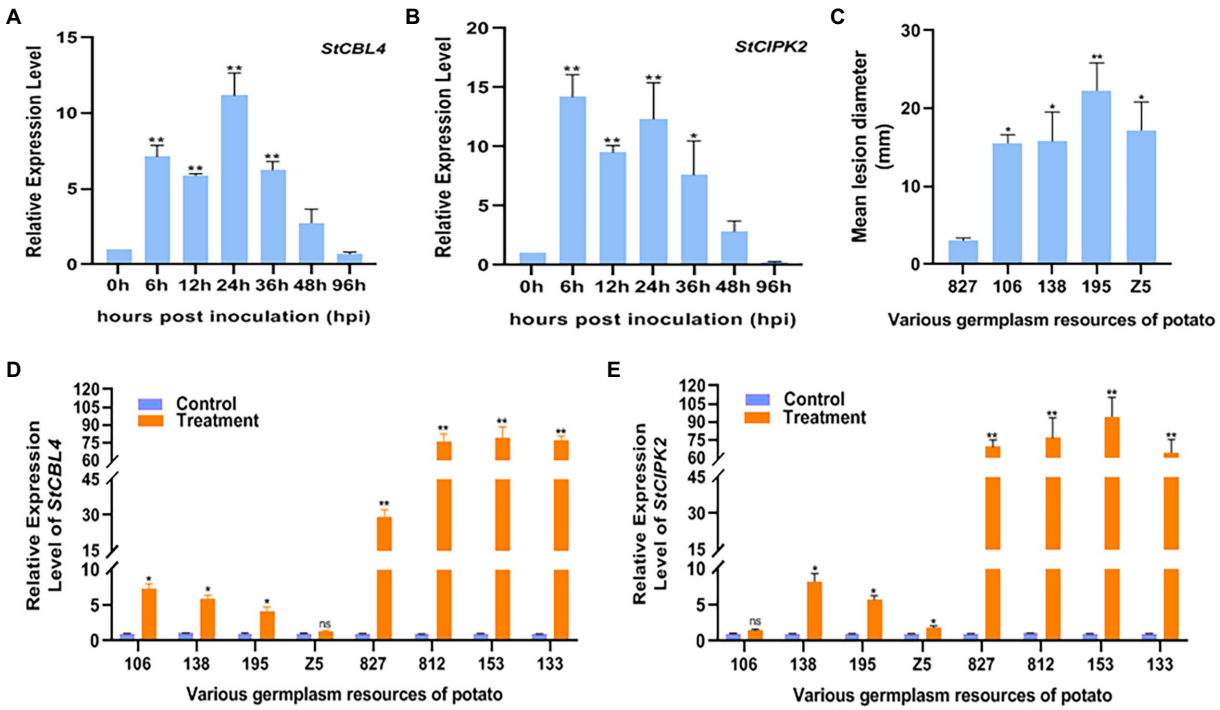

FIGURE 1
Expression profile of *StCBL4* and *StCIPK2* genes infected by *Rhizoctonia solani* in plantlet. **(A)** The relative expression level of the *StCBL4* gene at different hours post-inoculation. **(B)** The relative expression level of the *StCIPK2* gene at different hours post-inoculation. **(C)** Mean lesion diameter measured on various germplasm resources of potato after *R. solani* inoculation at 7 days post-inoculation. **(D)** The relative expression level of the *StCBL4* gene in treatment plantlets compared with control plantlets at 7 days post-inoculation. **(E)** The relative expression level of the *StCIPK2* gene in treatment plantlets compared with control plantlets at 7 days post-inoculation. The assay was performed by real-time RT-PCR. The relative mRNA levels were calculated with respect to the expression level of the WT plantlets without pathogen infection. All the experiments were repeated three times, and similar results were obtained. The data represent the means±SD of triplicate measurements. Asterisks above the columns represent significance based on an unpaired, two-tailed Student's *t*-test relative to the control. **p* <0.05; ***p* <0.01.

StCBL4-HA and StCIPK2-HA expressed in *N. benthamiana* (Figures 2B,D).

VIGS of *NbCBL* and *NbCIPK2* significantly enhance plant susceptibility to *Rhizoctonia solani*

In order to analyze the functions of *StCBL4* and *StCIPK2*, VIGS was conducted to silence the expression of orthologous genes *NbCBL* and *NbCIPK2* which was designed using the SGN VIGS Tool[3] in *N. benthamiana* (Supplementary Figures 3A,B, 4A,B). *NbPDS* VIGS plants began to show photobleaching after 10 days. Efficiencies of *NbCBL* and *NbCIPK2* silencing were confirmed by qRT-PCR of mRNA obtained from leaves that emerged 3 weeks after infiltration of plants with *Agrobacterium* transformed with TRV2:*NbCBL* and TRV2:*NbCIPK2* constructs. Results of qRT-PCR analysis confirmed that *NbCBL* and *NbCIPK2* were well silenced in VIGS plant leaves, with average expression levels in silenced plants found to be about 22 and 25%, respectively, lower than corresponding levels in negative control plants (TRV2:*GFP*; Figure 3B). Leaves of *NbCBL* and *NbCIPK2* VIGS plants exhibited visible disease symptoms at *R. solani* inoculation sites for 2 days. Lesion areas were measured at 60 hpi (Figure 3A). The results showed that *NbCBL* and *NbCIPK2* VIGS plants significantly increased disease lesions compared with GFP VIGS control plants (Figures 3C,D). Taken together, these results indicate that VIGS of *NbCBL* and *NbCIPK2* significantly enhance plant susceptibility to *R. solani*.

StCBL4 interacts with StCIPK2 *in vivo*

Yeast two-hybrid assays were performed to investigate the proposed interaction between identified proteins. Yeast growth on a minimal selective medium lacking histidine, leucine, tryptophan, and adenine (-His/−Leu/−Trp/−Ade) indicated a physical interaction between StCBL4 and StCIPK2 (Figure 4A). In addition, Co-IP assay and luciferase complementation assay in *N. benthamiana* by *Arobacterium*-mediated transient expression was conducted to validate the interaction further. Co-IP results confirmed the Y2H results using GFP beads with anti-HA

3 http://vigs.solgenomics.net/

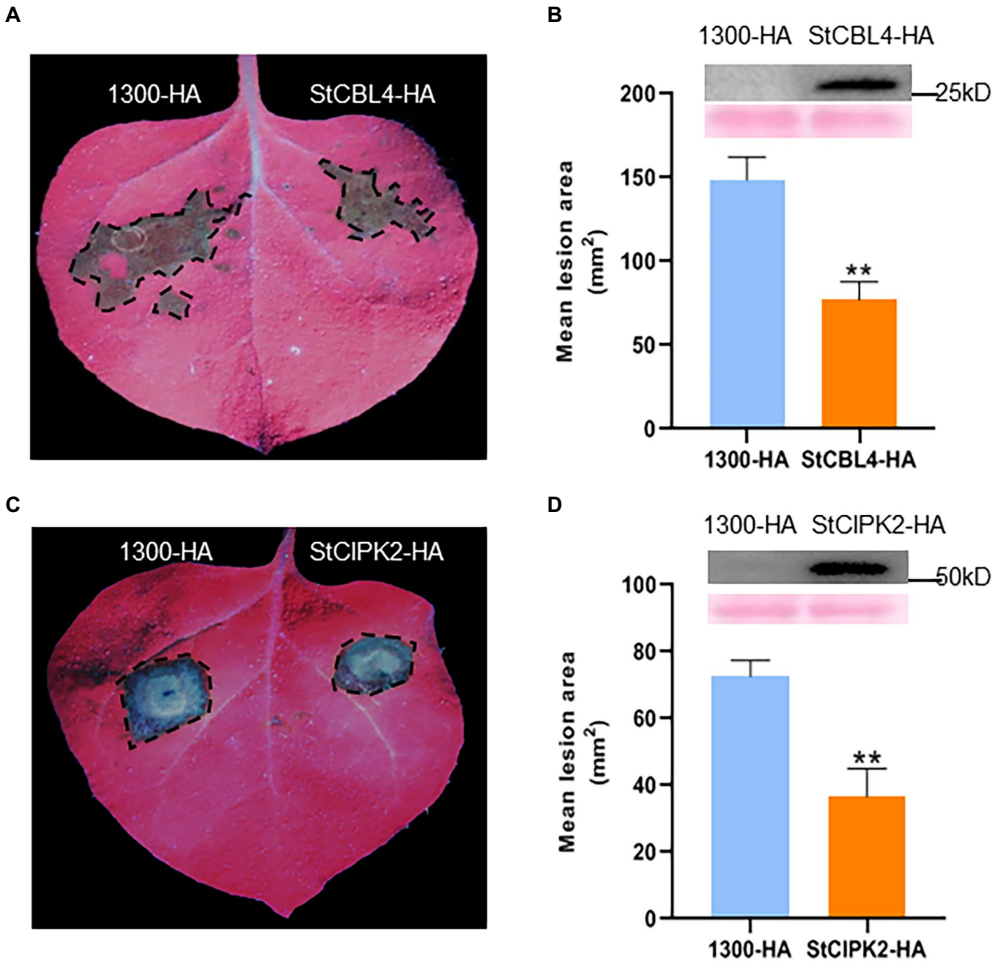

FIGURE 2
Transient expression of StCBL4 and StCIPK2 enhances the resistance to *Rhizoctonia solani* in *Nicotiana benthamiana*. StCBL4-HA, StCIPK2-HA, and 1,300-HA were expressed in *N. benthamiana* by *Agrobacterium*-mediated transient expression for 1 day. The leaves were inoculated by *R. solani* AG-3 and photographed under UV light 36 h later. **(A,C)** Representative leaf images (under UV light) by *StCBL4* and *StCIPK2* overexpression showing the extent of *R. solani* colonization on *N. benthamiana* leaves expressing each construct as indicated. **(B,D)** Immunoblotting showed the expression of StCBL4-HA and StCIPK2-HA. The lesion areas were measured and their sizes were calculated. The data represent the means±SD of measurements (n >8). The asterisks above the columns represent significance based on an unpaired, two-tailed Student's t-test relative to the EV. *p <0.05, **p <0.01.

antibody, StCIPK2-HA protein was successfuliy detected in output samples while GFP was used as a negative control (Figure 4B). In addition, the split luciferase complementation assay showed that StCBL4 interacted strongly with StCIPK2 and the immunoblot analysis showed that all proteins were normally expressed (Figure 4C). All things considered, these results demonstrated that StCBL4 and StCIPK2 interact *in vivo*.

Co-expression of *StCBL4* and *StCIPK2* significantly enhances *Rhizoctonia solani* resistance in *Nicotiana benthamiana*

To investigate the relationship between StCBL4 and StCIPK2 to *R. solani* resistance, StCBL4-GFP were co-expressed transiently with StCIPK2-HA in *N. benthamiana* for 24 h, then inoculated *R. solani* for 36 h. pCAMBIA1300-HA and pCAMBIA1300-GFP co-expression was performed as a control, and the lesion areas of leaves were photographed at 36 hpi by UV light. As shown results in Figure 5A, leaf lesion areas of co-expressing StCBL4-GFP and StCIPK2-HA exhibited significantly smaller and lower (about 20%) than corresponding levels of the control (Figure 5B). These results revealed a higher difference compared to the single-expression of two genes, and indicated that *StCBL4* plays a positive role in the function of StCIPK2 on *R. solani* resistance.

Meanwhile, to test the subcellular localization of StCBL4 and StCIPK2, we fused a GFP tag to the C-terminus of StCBL4 and an RFP tag to the C-terminus of StCIPK2, respectively, and viewed the Agrobacterium-mediated expression in *N. benthamiana* using confocal microscopy. Confocal images

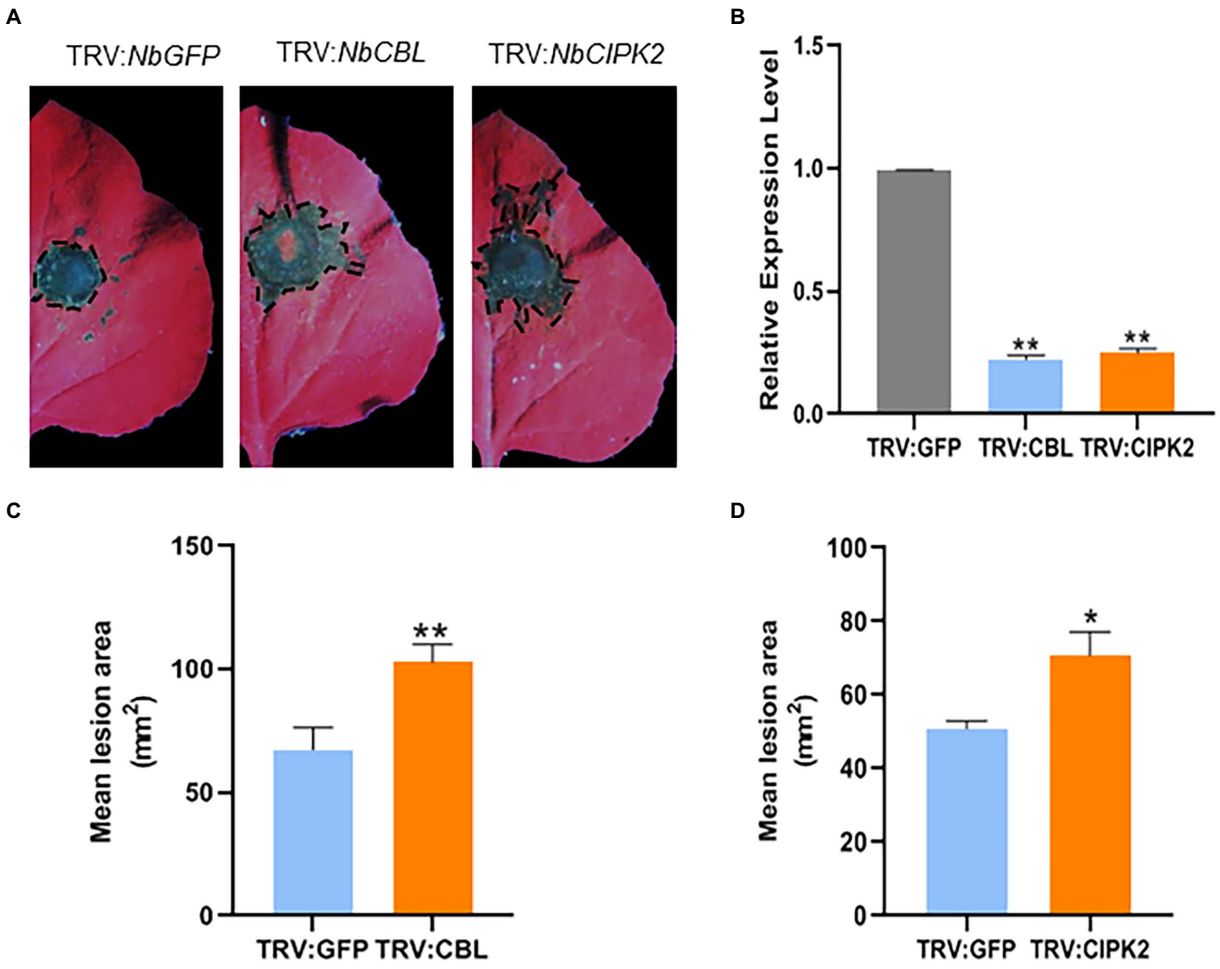

FIGURE 3
Virus-induced gene silencing (VIGS) of *NbCBL* and *NbCIPK2* significantly promotes *R. solani* colonization in *N. benthamiana*. **(A)** Representative leaf images (under UV light) showing the extent of *R. solani* colonization on *N. benthamiana* leaves expressing each construct as indicated. **(B)** TRV:NbCBL and TRV:NbCIPK2 constructs showed high silencing efficiency in *N. benthamiana* comparing with the TRV:GFP control vector. **(C,D)** Mean lesion area measured 60h after *R. solani* inoculation. Graph showing that silencing of TRV:NbCBL and TRV:NbCIPK2 constructs significantly increases *R. solani* lesion diameter compared with TRV:GFP control vector. The data represent the means±SD of measurements (n >20). The asterisks above the columns represent significance based on an unpaired, two-tailed Student's t-test relative to the V-GFP. *p <0.05, **p <0.01.

showed that the co-expression of StCBL4-GFP and StCIPK2-RFP displayed colocalization in the plasma membrane. Furthermore, the related intensity plots presented coincidence peaks between GFP and RFP fluorescence, indicating the co-localization of StCBL4 and StCIPK2 (Figure 5C).

Transgenic potato expressing *StCBL4* and *StCIPK2* enhances resistance to *Rhizoctonia solani*

Given that resistance to *R. solani* was enhanced in *N. benthamiana* that overexpressed *StCBL4* and *StCIPK2*, we next generated transgenic potato cultivar Désirée lines expressing *StCBL4* and *StCIPK2* to investigate the functions of these genes further. As shown process in Figure 6A, transgenic plants were obtained and confirmed *via* RT-PCR detection of *hygromycin* transcripts. Empty pBWA(V)KS vector-transformed plants served as wild-type (WT) controls.

The results of the qRT-PCR analysis revealed >30 and >20-fold upregulation of *StCBL4* and *StCIPK2* expression in overexpressing plants, respectively (Figures 6B,C). Subsequently, WT and overexpressing transgenic plantlets were incubated with 5-mm-diameter mycelium plugs. Then the plants were grown under identical conditions, and were observed for symptom development after 3 dpi. Compared with the visible symptom of WT plantlets, fewer transgenic plantlets showed canker symptoms at 10 dpi (Figure 6H). As shown in Figure 6J, lesion diameters were measured and showed to be about 16 and 20% lower than corresponding levels in WT. These findings indicated that overexpression of these genes in transgenic plantlets could potentially delay canker development to alter the course of the *R. solani* infection.

Accumulation of ROS, a significant plant regulatory factor, is an important indicator of plant resistance, especially during the

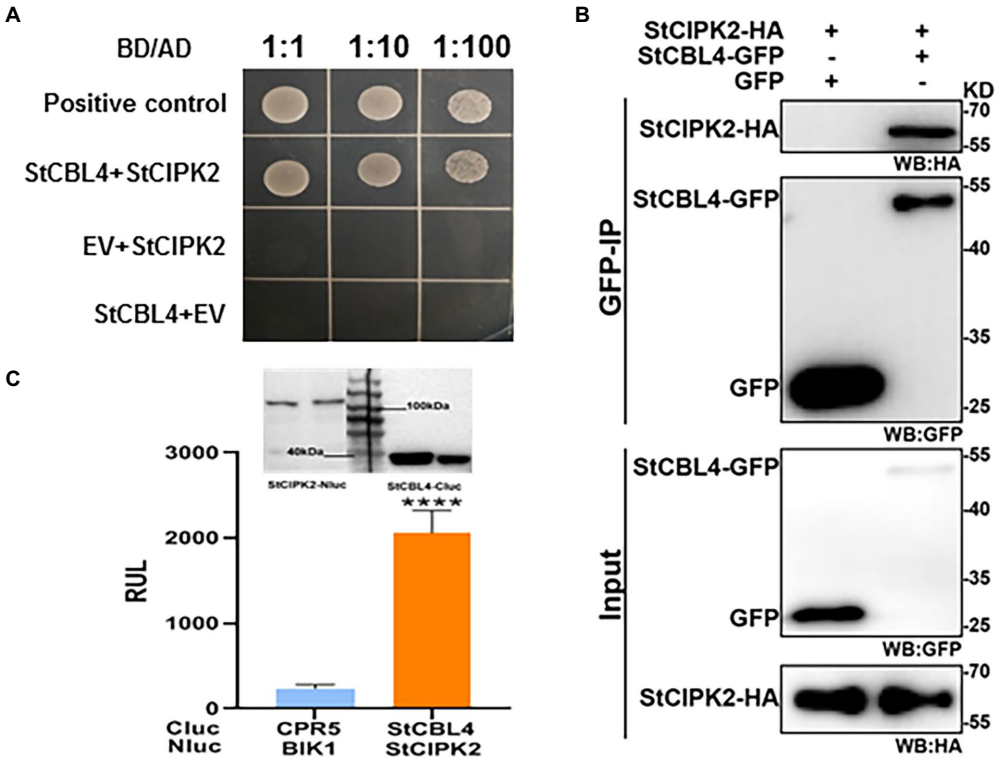

FIGURE 4
Validation of the protein interaction between StCBL4 and StCIPK2. **(A)** Yeast two-hybrid analysis of interactions between StCBL4 and StCIPK2. Yeast transformants co-expressing different bait and prey constructs were assayed on SD-Leu-Trp-His-Ade selective medium. BD-53 and AD-T were also co-transformed to serve as a positive control. **(B)** Co-IP assays were performed using an agarose-conjugated anti-GFP antibody. Input and bound proteins were detected *via* immunoblot using α-HA and α-GFP antibodies, respectively. **(C)** StCBL4 interacts with StCIPK2 by luciferase complementation assay and western blot. StCBL4-Cluc and StCIPK2-HA-Nluc constructs were transiently expressed in *N. benthamiana* plants, and the relative luminescence unit (RLU) was measured 2 days later. Cluc-CPR5 and BAK1-HA-Nluc were used as negative control (Liang et al., 2016). Immunoblotting showed the expression of StCBL4-Cluc and StCIPK2-HA-Nluc. The data represent the means±SD of measurements (n >20). The asterisks above the columns represent significance based on an unpaired, two-tailed Student's t-test relative to the V-GFP. ****p <0.0001.

early stage of infection. ROS plays important roles in early signaling events initiated by cellular metabolic perturbation and environmental stimuli (Lehmann et al., 2015). To verify whether StCBL4 and StCIPK2 are involved in H_2O_2 signaling, ROS bursts were induced in both *StCBL4*- and *StCIPK2*-overexpressing plants then H_2O_2 production was analyzed by analyzing images of DAB-stained leaves. As shown in Figure 6I, a ROS burst was observed by the dark yellow flecks in each overexpressing plants. The amount of H_2O_2 produced was measured to be about 4.84- and 3.74-fold higher than the corresponding levels in WT by calculating the DAB-stained area, respectively. The results revealed that both StCBL4 and StCIPK2 participate in H_2O_2 signaling.

Defense genes are upregulated in transgenic potato expressing *StCIPK2* and *StCBL4*

To understand molecular regulation underlying increased resistance to the *R. solani* pathogen, expression levels of plant defense genes were measured in infected *StCBL4*- and *StCIPK2*-overexpressing plants at 3 dpi. Defense genes that were studied included pathogenesis-related protein 1 (*StPR1*), Pto interaction protein 5 (*StPti5*), phenylalanine ammonia lyase (*StPAL*), pathogenesis-related protein 10 (*StPR10*), WRKY transcription factor 26 (*StWRKY26*), and their expression patterns were examined by qRT-PCR. The results revealed that expression levels of *StPR1* were upregulated by 2.67- and 18.9-fold in *StCBL4*- and *StCIPK2*-overexpressing plants compared with levels in WT plants. Meanwhile, expression levels of *StPti5*, *StWRKY26*, and *StPAL* were found to be 8.14- and 38.17-fold, 3.49- and 13.18-fold, and 54.46- and 20.14-fold higher in *StCBL4* and *StCIPK2*-overexpressing transgenic plants, respectively. Furthermore, compared with *StCBL4*-overexpressing plants, higher *PR* gene expression levels (except for that of *StPAL*) were observed in *StCIPK2*-overexpressing plants (Figures 6D–G).

Discussion

Rhizoctonia solani causes stem canker and black scurf, one of the most severe soil-borne fungal diseases of potato that

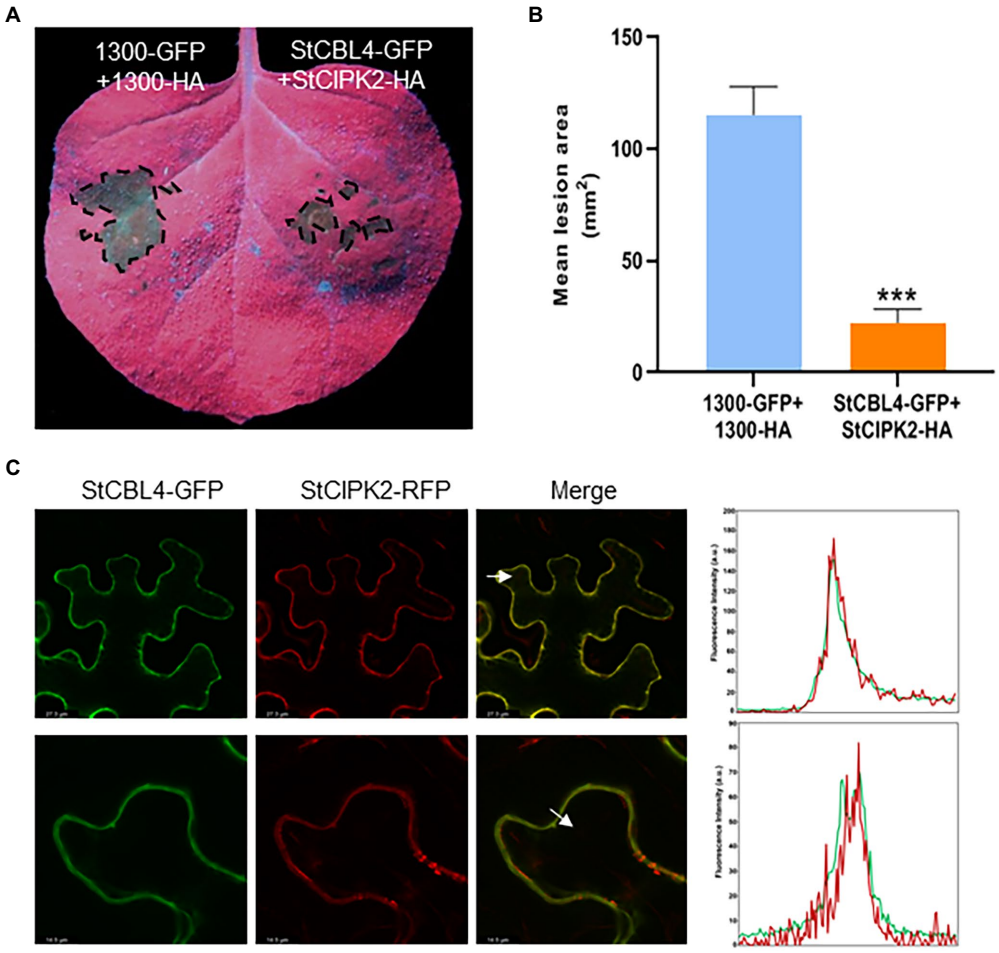

FIGURE 5
Analysis of transient co-expression and colocalization of StCBL4 and StCIPK2. **(A)** Transient co-expression of StCBL4 and StCIPK2 enhances the resistance to *R. solani* in *N. benthamiana*. Representative leaf images (under UV light) by *StCBL4* and *StCIPK2* co-overexpression showing the extent of *R. solani* colonization on *N. benthamiana* leaves expressing each construct as indicated. **(B)** The lesion areas were measured and their sizes were calculated by ImageJ software. The data represent the means±SD of measurements (n >8). The asterisks above the columns represent significance based on an unpaired, two-tailed Student's t-test relative to the control. ***p* <0.05. **(C)** Confocal laser scanning microscopy showing subcellular co-localization of StCBL4-GFP and StCIPK2-RFP fusion proteins expressed transiently in *N. benthamiana* leaves. The bottom row is the magnification of the top row. White arrowheads indicate the location of a profile across the membranes and the direction of the fluorescence intensity plot of the profile (right). *y* axis: Fluorescence intensity. *x* axis: Distance. Green line, GFP fluorescence. Red line, RFP fluorescence. ****p* <0.001.

dramatically reduce yield and quality. Breeding for disease-resistant varieties is viewed as the most effective and eco-friendly method for disease control, with potato disease resistance shown in a previously reported study to rely on *R. solani* infection-induced triggering of plant pathways that induce production of hormones jasmonic acid (JA) and salicylic acid (SA; Zrenner et al., 2021). However, as no endogenous resistance gene against *Rhizoctonia* disease has yet been identified in potato, the molecular response of potato to *R. solani* attack remains largely unknown. Our present study found that *StCBL4* and *StCIPK2* positively enhance potato anti-fungal responses for combating *Rhizoctonia* disease.

Although the role of the CBL-CIPK complex in regulating the response against abiotic stress is well documented, it remains unclear whether this complex also regulates responses against biotic stress. In a previous study, several CBL–CIPK interaction partners were hypothesized (based on limited evidence) to play roles in biotic and/or oxidative stress responses and developmental pathways (Pandey et al., 2014). For example, the interaction between OsCIPK14/15 and OsCBL4 plays a crucial role in enhancing rice resistance to *Trichoderma viride* ethylene-inducing xylanase (Kurusu et al., 2010). The TaCBL4-TaCIPK5 complex acts to promote ROS signaling to enhance the resistance of wheat to *Puccinia triiformis* f. sp. *tritici* (Liu et al., 2018). Since CBL4 has been reported to participate in biotic stress resistance functionally, we investigated whether StCBL4 may interact with StCIPK2 to perform similar functions in potato. In this study, transient overexpression of *StCBL4* and *StCIPK2* individually and synergistically increased the tolerance of potato plants to *R. solani* in *N. benthamiana*, meanwhile transgenic potato

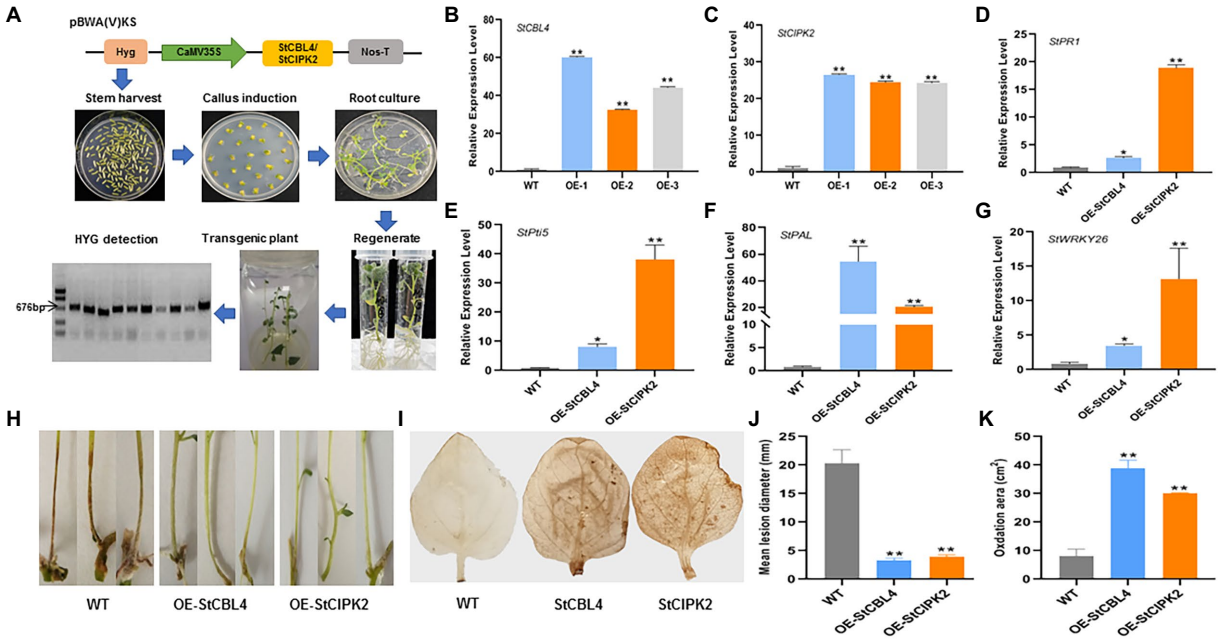

FIGURE 6
Generation and function analysis of Transgenic Plants on resistance to *R. solani*. **(A)** Generation of Transgenic Plants. Skeleton of pBWA(V)KS vectors was used for overexpressing *StCBL4* or *StCIPK2* gene. The schematic diagram shows the process of inducing plant. Target HYG was detected for the overexpressed positive plant. **(B,C)** Overexpression profile of *StCBL4* and *StCIPK2* gene in transgenic plant (OE-1, OE-2, and OE-3) by real-time RT-PCR. The relative mRNA levels were calculated with respect to the expression level of the corresponding gene in the WT plant. **(D)** The expression levels of *StPR1* were higher in StCBL4- and StCIPK2-overexpressing plants than WT plants after *R. solani* infection. **(E)** The expression levels of *StPti5* were higher in StCBL4- and StCIPK2-overexpressing plants than WT plants after *R. solani* infection. **(F)** The expression levels of *StPAL* were higher in StCBL4- and StCIPK2-overexpressing plants than WT plants after *R. solani* infection. **(G)** The expression levels of *StWRKY26* were higher in StCBL4- and StCIPK2-overexpressing plants than WT plants after *R. solani* infection. **(H)** Symptoms were observed on stems inoculated with *R. solani*. **(I)** DAB staining of H_2O_2 accumulation in leaves of a transgenic plant. **(J)** Mean lesion diameter measured after *R. solani* inoculation at 10days post-inoculation. **(K)** The amount of H_2O_2 produced was measured by calculating the DAB-stained area, in which the dark yellow flecks indicated the ROS burst sites. All the experiments were repeated three times, and similar results were obtained. The data represent the means±SD of triplicate measurements (n >10). Asterisks above the columns represent significance based on an unpaired, two-tailed Student's t-test relative to the control. *p <0.05; **p <0.01.

significantly enhanced resistance as well (Figures 2 and 5B,C,H,J); thus implying that these two genes play crucial roles in defensive responses and innate immunity in potato.

To further confirm that *StCBL4* and *StCIPK2* genes mediate the interaction between plant and *R. solani*, TRV-VIGS was used to successfully knock down the expression of *StCBL4* and *StCIPK2* orthologs *NbCBL* and *NbCIPK2*, respectively, that are found in *N. benthamiana* (Supplementary Figure 3). Notably, silencing of these genes in detached leaves followed by inoculation of leaves with *R. solani* led to larger lesions in plants with knocked down *NbCBL* and *NbCIPK2* expression compared to unsilenced controls. This result indicates that the knockdown of *NbCBL* and *NbCIPK2* expression increased sensitivity to *R. solani* infection (Figures 3C,D). Importantly, similar results were observed in wheat, where knockdown of TaCBL4 and TaCIPK5 expression led to a reduced wheat defense response against stripe rust fungus (Liu et al., 2018).

The abovementioned results notwithstanding, the mechanism responsible for the effects of these two proteins on plant resistance remains unknown. However, StCIPK2, an interaction partner of StCBL4, was identified based on results obtained *via* Y2H assays that were subsequently confirmed *via* LCA and Co-IP assays (Figure 4). Furthermore, previously reported results have shown that combinations of CBLs and CIPKs functions act as signaling nodes in response to environmental stimuli (Thoday-Kennedy et al., 2015). However, the CIPK protein sequence lacks localization motifs, subcellular localization of CBL-CIPK modules depends on myristoylation and acylation modifications of CBL sites (Mao et al., 2022). In this study, StCBL4 was found to interact with StCIPK2 to specifically recruit StCIPK2 to the plasma membrane in *N. benthamiana* cells, thus indicating that StCIPK2 interacted with a potentially myristoylated StCBL4 site as a necessary and sufficient condition for StCIPK2 anchoring to the plasma membrane to occur.

Production and accumulation of defense-related proteins in plants in response to biotic stresses are well-known crucial plant defense mechanisms (Wang et al., 2022). Salicylic acid (SA), a key signaling plant resistance molecule involved in resistance to biotrophs, induces the expression of pathogenesis-related (PR) proteins that induce systemic acquired resistance (SAR). As compared with their expression in WT plants, expression levels of PR protein-encoding genes (e.g., *PR1*, *Pti5*, and *WRKY26*)

were up-regulated significantly in both *StCBL4*- and *StCIPK2*-transgenic plants, thus indicating that *StCBL4* and *StCIPK2* participated in potato immune response to defend plants against the pathogen (Figures 6D,E,G). *PAL* is a critical gene in the phenylalanine metabolic pathway that effectively regulates the biosynthesis of corresponding secondary metabolites (Wang et al., 2021). In this study, high-level expression of *StPAL* revealed the role of an important downstream signaling node as a potential molecular mechanism underlying plant resistance to *R. solani* disease (Figure 6F).

The accumulation of reactive oxygen species (ROS) is a widespread defense mechanism in higher plants against pathogen attack and sometimes is the cause of cell death that facilitates attack by necrotrophic pathogens (Tian et al., 2021). As well known, necrotrophic fungi with a wide host range can kill host plant cells and use the contents to support their growth. However, despite their substantial role in crop losses, there is much less known about these pathogens and their ability to infect. As a necrotrophic fungus, *R. solani* could cause physical changes including stunted root growth of the host, transcriptional changes and ROS production (Foley et al., 2016). ROS has multiple functions in plant defense serving as a signaling molecule. It has been proved that H_2O_2, one of the important ROS productions, plays a role in plant defense as a messenger in signal transduction pathways linked to oxidative stress signaling (Huang et al., 2021). In our study, *StCBL4* and *StCIPK2* showed the highest induction in transgenic potato plants coinciding with the induction of H_2O_2 accumulation (Figures 6B,C,I,K). This observation agrees with previous studies that demonstrated that the function of many CBL-CIPK complexes in abiotic and biotic stress signaling is associated with the burst of ROS. Therefore, research focusing on the accumulation of ROS of fungal necrotrophs will also help to understand their pathogenic mechanisms on plants. Indeed, lots of previous research focusing on the RBOH family has confirmed the interaction with CIPKs (Sanyal et al., 2020). Thus, we also speculate that the ROS generation mediated by the StCBL4-StCIPK2 complex during potato resistance to *R. solani* potentially depends on RBOH proteins. Moreover, identifying which remember of RBOH family plays a role with StCIPK2 should be determined in further studies.

In conclusion, this studyhas illustrated that *StCBL4* and *StCIPK2* are involved in regulating the potato defensive immune response against *R. solani*. Furthermore, our results demonstrate that *StCBL4* functions in concert with *StCIPK2*, as positive regulators of immunity and contribute to combating stem canker disease in potato.

Data availability statement

The datasets presented in this study can be found in online repositories. The names of the repository/repositories and accession number(s) can be found in the article/Supplementary material.

Author contributions

SY and XW conceived and designed the experiments. SY, JLi, JLu, QW, WW, XD, and YM performed the experiments. SY, FM, MG, LH, and LW analyzed the data. SY, JLi, and XW wrote and revised the paper. All authors contributed to the article and approved the submitted version.

Funding

This work was supported by the Natural Science Foundation of Heilongjiang Province (YQ2019C022) and Key-Area Research and Development Program of Guangdong Province (2020B020219002).

Conflict of interest

The authors declare that the research was conducted in the absence of any commercial or financial relationships that could be construed as a potential conflict of interest.

Publisher's note

Supplementary material

The Supplementary material for this article can be found online at: https://www.frontiersin.org/articles/10.3389/fmicb.2022.1032900/full#supplementary-material

SUPPLEMENTARY FIGURE 1
Amino acid sequence alignment and phylogenetic tree analysis of potato StCBL4 with other crops CBL4. **(A)** Amino acid sequence alignment. **(B)** Phylogenetic tree analysis. StCBL4(ON383960): *Solanum tuberosum* CBL4; AtCBL4(AF192886): *Arabidopsis thaliana* CBL4; CaCBL4(XM_016694246): *Capsicum annuum* CBL4; CsCBL4(XM_004146172): *Cucumis sativus* CBL4; OsCBL4(DQ201198): *Oryza sativa* CBL4; TaCBL4(KU736850): *Triticum aestivum* CBL4; ZmCBL4(EU973091): Zea mays CBL4; VvCBL4(KT266265): *Vitis vinifera* CBL4; HvCBL4(HM175879): *Hordeum vulgare* CBL4.

SUPPLEMENTARY FIGURE 2
Amino acid sequence alignment and phylogenetic tree analysis of potato StCIPK2 with other crops CIPK2. **(A)** Amino acid sequence alignment. **(B)** Phylogenetic tree analysis. StCIPK2 (ON324205): *Solanum tuberosum* CIPK2; AtCIPK2 (AF192886): *Arabidopsis thaliana* CIPK2; OsCIPK2 (EU703793): *Oryza sativa* CIPK2; TaCIPK2 (KU736853): *Triticum aestivum*

CIPK2; HvCIPK2 (KP638475): *Hordeum vulgare* CIPK2; NtCIPK2 (XM_016647791): *Nicotiana tabacum* CIPK2.

SUPPLEMENTARY FIGURE 3
Phylogenetic relationship of CBLs and CIPKs from potato, *Arabidopsis* and tobacco. The Neighbor-joining (NJ) tree was constructed using MEGA 5.0 software. The black triangle and circle represent StCBL4 and StCIPK2 from potato, respectively. **(A)** Phylogenetic tree analysis of CBLs from potato, *Arabidopsis* and tobacco. **(B)** Phylogenetic tree analysis of CIPKs from potato, *Arabidopsis* and tobacco.

SUPPLEMENTARY FIGURE 4
Sequence alignment of StCBL4 with NbCBL and StCIPK2 with NbCIPK2. Sequence alignment was performed by DNAMAN 6.0 software. The red line represents the VIGS site searched by SGN VIGS Tool.

SUPPLEMENTARY TABLE 1
The list of various potato germplasm resources.

SUPPLEMENTARY TABLE 2
Primers used in this study.

References

Batistic, O., Waadt, R., Steinhorst, L., Held, K., and Kudla, J. (2010). CBL-mediated targeting of CIPKs facilitates the decoding of calcium signals emanating from distinct cellular stores. *Plant J.* 61, 211–222. doi: 10.1111/j.1365-313X.2009.04045.x

Cheong, Y. H., Pandey, G. K., Grant, J. J., Batistic, O., Li, L., Kim, B. G., et al. (2007). Two calcineurin B-like calcium sensors, interacting with protein kinase CIPK23, regulate leaf transpiration and root potassium uptake in Arabidopsis. *Plant J.* 52, 223–239. doi: 10.1111/j.1365-313x.2007.03236.x

Cui, X. Y., Du, Y. T., Fu, J. D., Yu, T. F., Wang, C. T., Ming, C., et al. (2018). Wheat CBL-interacting protein kinase 23 positively regulates drought stress and ABA responses. *BMC Plant Biol.* 18, 93–13. doi: 10.1186/s12870-018-1306-5

De la Torre, F., Gutierrez-Beltran, E., Pareja-Jaime, Y., Chakravarthy, S., Martin, G. B., and del Pozo, O. (2013). The tomato calcium sensor Cbl10 and its interacting protein kinase Cipk6 define a signaling pathway in plant immunity. *Plant Cell* 25, 2748–2764. doi: 10.1105/tpc.113.113530

Dong, Q. Y., Bai, B. W., Almutairi, B., and Kudla, J. (2021). Emerging roles of the CBL-CIPK calcium signaling network as key regulatory hub in plant nutrition. *J. Plant Physiol.* 257:153335. doi: 10.1016/j.jplph.2020.153335

Foley, R. C., Gleason, C. A., Anderson, J. P., Hamann, T., and Singh, K. B. (2013). Genetic and genomic analysis of *Rhizoctonia solani* interactions with Arabidopsis; evidence of resistance mediated through NADPH oxidases. *PLoS One* 8:e56814. doi: 10.1371/journal.pone.0056814

Foley, R. C., Kidd, B. N., Hane, J. K., Anderson, J. P., and Singh, K. B. (2016). Reactive oxygen species play a role in the infection of the necrotrophic fungi, *Rhizoctonia solani* in Wheat. *PLoS One* 11:e0152548. doi: 10.1371/journal.pone.0152548

Huang, Z. Q., Lu, J. J., Liu, R. W., Wang, P., Hu, Y. W., and Fang, A. F. (2021). SsCat2 encodes a catalase that is critical for the antioxidant response, QoI fungicide sensitivity, and pathogenicity of *Sclerotinia sclerotiorum*. *Fungal Genet. Biol.* 149:103530. doi: 10.1016/j.fgb.2021.103530

Ishitani, M., Liu, J., Halfter, U., Kim, C. S., Shi, W., and Zhu, J. K. (2000). SOS3 function in plant salt tolerance requires N-myristoylation and calcium binding. *Plant Cell* 12, 1667–1677. doi: 10.2307/3871181

Jung, H. J., Kayum, M. A., Thamilarasan, S. K., Nath, U. K., Park, J. I., Chung, M. Y., et al. (2017). Molecular characterisation and expression profiling of calcineurin B-like (CBL) genes in Chinese cabbage under abiotic stresses. *Funct. Plant Biol.* 44, 739–750. doi: 10.1071/FP16437

Kim, K. N., Lee, J. S., Han, H., Choi, S. A., Go, S. J., and Yoon, I. S. (2003). Isolation and characterization of a novel rice Ca2C-regulated protein kinase gene involved in responses to diverse signals including cold, light, cytokinins, sugars and salts. *Plant Mol. Biol.* 52, 1191–1202. doi: 10.1023/B:PLAN.0000004330.62660.a2

Kurusu, T., Hamada, J., Nokajima, H., Kitagawa, Y., Kiyoduka, M., Takahashi, A., et al. (2010). Regulation of microbe-associated molecular pattern-induced hypersensitive cell death, phytoalexin production, and defense gene expression by calcineurin B-like protein-interacting protein kinases, OsCIPK14/15, in rice cultured cells. *Plant Physiol.* 153, 678–692. doi: 10.1104/pp.109.151852

Lehmann, S., Serrano, M., L'Haridon, F., Tjamos, S. E., and Metraux, J. P. (2015). Reactive oxygen species and plant resistance to fungal pathogens. *Phytochemistry* 112, 54–62. doi: 10.1016/j.phytochem.2014.08.027

Liang, X., Ding, P., Lian, K., Wang, J., Ma, M., Li, L., et al. (2016). Arabidopsis heterotrimeric G proteins regulate immunity by directly coupling to the FLS2 receptor. *elife* 5:e13568. doi: 10.7554/eLife.13568

Liu, P., Duan, Y., Liu, C., Xue, Q., Guo, J., Qi, T., et al. (2018). The calcium sensor TaCBL4 and its interacting protein TaCIPK5 are required for wheat resistance to stripe rust fungus. *J. Exp. Bot.* 69, 4443–4457. doi: 10.1093/jxb/ery227

Liu, Z., Li, X., Sun, F., Zhou, T., and Zhou, Y. (2017). Overexpression of OsCIPK30 enhances plant tolerance to *Rice stripe virus*. *Front. Microbiol.* 8:2322. doi: 10.3389/fmicb.2017.02322

Liu, Y., Schiff, M., Marathe, R., and Dinesh-Kumar, S. P. (2002). Tobacco Rar1, EDS1 and NPR1/NIM1 like genes are required for N-mediated resistance to tobacco mosaic virus. *Plant J.* 30, 415–429. doi: 10.1046/j.1365-313x.2002.01297.x

Lu, J., Liu, T., Zhang, X., Li, J., Wang, X., Liang, X., et al. (2021). Comparison of the distinct, host-specific response of three solanaceae hosts induced by *Phytophthora infestans*. *Int. J. Mol. Sci.* 22:11000. doi: 10.3390/ijms222011000

Ma, X., Gai, W. X., Qiao, Y. M., Muhammad, A., Wei, A. M., Luo, D. X., et al. (2019). Identification of CBL and CIPK gene families and functional characterization of CaCIPK1 under *Phytophthora capsici* in pepper (*Capsicum annuum* L.). *BMC Genomics* 20:775. doi: 10.1186/s12864-019-6125-z

Ma, X., Li, Q. H., Yu, Y. N., Qiao, Y. M., and Gong, Z. H. (2020). The CBL–CIPK pathway in plant response to stress signals. *Int. J. Mol. Sci.* 21:5668. doi: 10.3390/ijms21165668

Ma, R., Liu, W., Li, S., Zhu, X., Yang, J., Zhang, N., et al. (2021). Genome-wide identification, characterization and expression analysis of the CIPK gene family in potato (*Solanum tuberosum* L.) and the role of StCIPK10 in response to drought and osmotic stress. *Int. J. Mol. Sci.* 22:13535. doi: 10.3390/ijms222413535

Mao, J. J., Mo, Z. J., Yuan, G., Xiang, H. Y., Visser, R. G. F., Bai, Y. L., et al. (2022). The CBL-CIPK network is involved in the physiological crosstalk between plant growth and stress adaptation. *Plant Cell Environ.* 1-11. doi: 10.1111/pce.14396

McLellan, H., Boevink, P. C., Armstrong, M. R., Pritchard, L., Gomez, S., Morales, J., et al. (2013). An RxLR effector from Phytophthora infestans prevents relocalisation of two plant NAC transcription factors from the endoplasmic reticulum to the nucleus. *PLoS Pathog.* 9:e1003670. doi: 10.1371/journal.ppat.1003670

Murashige, T., and Skoog, F. (1962). A revised medium for rapid growth and bioassay with tobacco tissue culture. *Physiol. Plant.* 15, 473–497. doi: 10.1111/j.1399-3054.1962.tb08052.x

Pandey, G. K., Kanwar, P., and Pandey, A. (2014). *Global Comparative Analysis of CBL-CIPK Gene Families in Plants*. Heidelberg: Springer

Sanyal, S. K., Mahiwal, S., Nambiar, D. M., and Pandey, G. K. (2020). CBL-CIPK module-mediated phosphoregulation: facts and hypothesis. *Biochem. J.* 477, 853–871. doi: 10.1042/BCJ20190339

Tang, R. J., Wang, C., Li, K., and Luan, S. (2020). The CBL–CIPK calcium signaling network: unified paradigm from 20 years of discoveries. *Trends Plant Sci.* 25, 604–617. doi: 10.1016/j.tplants.2020.01.009

Thoday-Kennedy, E. L., Jacobs, A. K., and Roy, S. J. (2015). The role of the CBL-CIPK calcium signalling network in regulating ion transport in response to abiotic stress. *Plant Growth Regul.* 76, 3–12. doi: 10.1007/s10725-015-0034-1

Tian, L., Li, J., Huang, C., Zhang, D., Xu, Y., Yang, X., et al. (2021). Cu/Zn superoxide dismutase (VdSOD1) mediates reactive oxygen species detoxification and modulates virulence in *Verticillium dahliae*. *Mol. Plant Pathol.* 22, 1092–1108. doi: 10.1111/mpp.13099

Verma, P., Sanyal, S. K., and Pandey, G. K. (2021). Ca2+–CBL–CIPK: a modulator system for efficient nutrient acquisition. *Plant Cell Rep.* 40, 2111–2122. doi: 10.1007/s00299-021-02772-8

Wang, M., Gu, D., Liu, T., Wang, Z., Guo, X., Hou, W., et al. (2007). Overexpression of a putative maize calcineurin B-like protein in Arabidopsis confers salt tolerance. *Plant Mol. Biol.* 65, 733–746. doi: 10.1007/s11103-007-9238-8

Wang, L., Lu, H., Zhan, J., Shang, Q., Wang, L., Yin, W., et al. (2022). Pathogenesis-related protein-4 (PR-4) gene family in Qingke (Hordeum vulgare L. var. nudum): genome-wide identification, structural analysis and expression profile under stresses. *Mol. Biol. Rep.* 49, 9397–9408. doi: 10.1007/s11033-022-07794-3

Wang, X. D., Zheng, K. K., Cheng, W. Y., Li, J., Liang, X. X., Shen, J., et al. (2021). Field application of star polymer-delivered chitosan to amplify plant defense against potato late blight. *Chem. Eng. J.* 417:129327. doi: 10.1016/j.cej.2021.129327

Weinl, S., and Kudla, J. (2009). The CBL–CIPK Ca^{2+}-decoding signaling network: function and perspectives. *New Phytol.* 184, 517–528. doi: 10.1111/j.1469-8137.2009.02938.x

Woodhall, J. W., Adams, I. P., Peters, J. C., Harper, G., and Boonham, N. (2013). A new quantitative real-time PCR assay for *Rhizoctonia solani* AG3-PT and the detection of AGs of *Rhizoctonia solani* associated with potato in soil and tuber samples in Great Britain. *Eur. J. Plant Pathol.* 136, 273–280. doi: 10.1007/s10658-012-0161-8

Xi, Y., Liu, J., Dong, C., and Cheng, Z. M. (2017). The CBL and CIPK gene family in grapevine (Vitis vinifera): genome-wide analysis and expression profiles in response to various abiotic stresses. *Front. Plant Sci.* 8:978. doi: 10.3389/fpls.2017.00978

Xiang, Y., Huang, Y., and Xiong, L. (2007). Characterization of stress-responsive CIPK genes in rice for stress tolerance improvement. *Plant Physiol.* 144, 1416–1428. doi: 10.1104/pp.107.101295

Xu, G. Y., Moeder, W., Yoshioka, K., and Shan, L. B. (2022). A tale of many families: calcium channels in plant. *Plant Cell* 34, 1551–1567. doi: 10.1093/plcell/koac033

Yang, S., Min, F. X., Wang, W. Z., Wei, Q., Dong, X. Z., Wang, X. D., et al. (2018). Transcriptome analysis of *Rhizoctonia solani* anastomosis group 5 early invasion in potato. *Int. J. Agric. Biol.* 20, 1751–1758. doi: 10.17957/IJAB/15.0684

Yang, S., Min, F. X., Wang, W. Z., Wei, Q., Guo, M., Gao, Y. F., et al. (2017). Anastomosis group and pathogenicity of *Rhizoctonia solani* associated with stem canker and black scurf of potato in Heilongjiang province of China. *Am. J. Potato Res.* 94, 95–104. doi: 10.1007/s12230-016-9535-3

Yin, X., Wang, Q. L., Chen, Q., Xiang, N., Yang, Y. Q., and Yang, Y. P. (2017). Genome-wide identification and functional analysis of the calcineurin B-like protein and calcineurin B-like protein-interacting protein kinase gene families in turnip (*Brassica rapa* var. *rapa*). *Front. Plant Sci.* 8:1191. doi: 10.3389/fpls.2017.01191

Zhou, Z., Bi, G., and Zhou, J. M. (2018). Luciferase complementation assay for protein-protein interactions in plants. *Curr. Protoc. Plant Biol.* 3, 42–50. doi: 10.1002/cppb.20066

Zrenner, R., Verwaaijen, B., Genzel, F., Flemer, B., and Grosch, R. (2021). Transcriptional changes in potato sprouts upon interaction with *Rhizoctonia solani* indicate pathogen-induced interference in the defence pathways of potato. *Int. J. Mol. Sci.* 22:3094. doi: 10.3390/ijms22063094

frontiers | Frontiers in Microbiology

TYPE Original Research
PUBLISHED 18 January 2023
DOI 10.3389/fmicb.2022.1019800

OPEN ACCESS

EDITED BY
Xiaodan Wang,
China Agricultural University, China

REVIEWED BY
Qiya Yang,
Jiangsu University, China
Tingli Liu,
Jiangsu Academy of Agricultural Sciences (JAAS), China

*CORRESPONDENCE
Shijiao Jiang
jiangshijiao@outlook.com

SPECIALTY SECTION
This article was submitted to Microbe and Virus Interactions with Plants, a section of the journal Frontiers in Microbiology

RECEIVED 15 August 2022
ACCEPTED 14 December 2022
PUBLISHED 18 January 2023

CITATION
Zhang T, Wen G, Song B, Chen Z and Jiang S (2023) Transcriptome profiling reveals the underlying mechanism of grape post-harvest pathogen *Penicillium olsonii* against the metabolites of *Bacillus velezensis*. *Front. Microbiol.* 13:1019800. doi: 10.3389/fmicb.2022.1019800

Transcriptome profiling reveals the underlying mechanism of grape post-harvest pathogen *Penicillium olsonii* against the metabolites of *Bacillus velezensis*

Tingfu Zhang, Guoqin Wen, Bo Song, Zhenyong Chen and Shijiao Jiang*

Key Laboratory of Southwest China Wildlife Resources Conservation, School of Life Sciences, China West Normal University, Nanchong, Sichuan, China

Introduction: Pathogen infection influences the post-harvest shelf life of grape berries. In a preliminary study, metabolites produced by *Bacillus velezensis* significantly inhibited the growth of the grape postharvest pathogen *Penicillium olsonii*.

Methods: To investigate the mechanism of interaction between *B. velezensis* and *P. olsonii*, a draft genome was generated for *P. olsonii* WHG5 using the Illumina NovaSeq platform, and the transcriptomic changes in WHG5 were analyzed in response to the exposure to *B. velezensis* metabolites (10% v/v).

Results: The expression levels of genes associated with sporulation, including *GCY1*, *brlA*, and *abaA*, were down-regulated compared with those of the control. In addition, spore deformation and abnormal swelling of the conidiophore were observed. The expression of crucial enzymes, including fructose 2,6-bisphosphate and mannitol-2-dehydrogenase, was down-regulated, indicating that the glycolytic pathway of WHG5 was adversely affected by *B. velezensis* metabolites. The KEGG pathway enrichment analysis revealed that glutathione metabolism and the antioxidant enzyme system were involved in the response to *B. velezensis* metabolites. The down-regulation of the pathogenesis-related genes, *PG1* and *POT1,* suggested that *B. velezensis* metabolites decreased the pathogenicity of *P. olsonii*. *B. velezensis* metabolites disrupted the homeostasis of reactive oxygen species in *P. olsonii* by affecting glucose metabolism, resulting in spore deformation and disruption of growth. In addition, the expression of key pathogenesis-related genes was down-regulated, thereby reducing the pathogenicity of *P. olsonii*.

Disscusion: This study provides insights into the responses of *P. olsonii* to *B. velezensis* metabolites and identifies potential target genes that may be

useful in biocontrol strategies for the suppression of post-harvest spoilage in grapes.

KEYWORDS

post-harvest pathogen, *penicillium olsonii*, *bacillus velezensis*, biocontrol, *vitis vinifera*

Introduction

Table grapes (*Vitis vinifera* L.) are among the most popular fresh fruit worldwide and have a relatively long post-harvest shelf life. However, pathogen infection strongly influences the post-harvest shelf life of grape berries (He et al., 2019). Pathogenic fungi, such as *Botrytis cinerea*, *Penicillium* spp., and *Aspergillus* spp., can severely shorten the storage longevity of table grapes and cause major post-harvest losses (Zhang et al., 2021b). In addition, *Penicillium* spp. can produce mycotoxins, of which many are classified as carcinogenic and can adversely affect human health, especially causing damage to the kidneys and the liver (Schmidtke et al., 2019). Controlling post-harvest infection of grape berries by pathogens is mainly dependent on the post-harvest application of synthetic chemical fungicides, which is considered the most economical and effective approach to suppress post-harvest spoilage. However, the use of synthetic chemical fungicides is increasingly prohibited owing to their toxicological risks to human health and the environment, as well as the increasing prevalence of resistance to antimicrobial agents among pathogenic strains (Romanazzi et al., 2012; Pertot et al., 2017; Zhang et al., 2020). The exploration of alternatives to synthetic chemical applications for post-harvest disease management has become an important research focus in recent years (Wang et al., 2019).

Biological control methods have shown great potential and are recognized as effective strategies for the control of post-harvest diseases, especially using antagonist microorganisms (biological control agents) and their metabolites (Jiang et al., 2018; Yu et al., 2020; Chaves-Gómez et al., 2021). Biological control agents have the ability to inhibit post-harvest deterioration and provide efficient eco-compatible biocontrol of post-harvest diseases, on account of their broad-spectrum antimicrobial activity and reduced risk of emergence of resistant fungal strains. *Bacillus* strains provide versatile biological control against plant pathogens owing to their diverse antagonistic mechanisms, which include competition for space and nutrients, antibiosis through secretion of compounds exhibiting antimicrobial activities, secretion of enzymes that degrade the plant pathogen cell wall, and stimulation of host resistance (Shafi et al., 2017; Fira et al., 2018; Dimkić et al., 2022).

Cyclic lipopeptides produced by *Bacillus* strains are the most prominent bioactive compounds for plant protection (Falardeau et al., 2013; Liu et al., 2014; Mora et al., 2015). Members of the surfactin family can induce resistance in diverse hosts against various diseases by stimulating plant immune responses (Hafeez et al., 2019; Park et al., 2019). Surfactins play an important role in the suppression of bacterial fruit blotch in grapes and show antiviral and antibacterial activities (Li et al., 2019). *Bacillus velezensis* KOF112 significantly up-regulates the expression of genes encoding class IV chitinases and β-1,3-glucanase in grape leaves (Hamaoka et al., 2021). *Bacillus cereus* NRKT stimulates an increase in the resveratrol content in the skin of grape berries, which is an important mechanism for the induction of disease resistance (Aoki et al., 2017). Thus, bioactive molecules produced by *Bacillus* spp. may act as elicitors of plant-induced systemic resistance. However, the defense responses tend to be specific to certain plant species or host–pathogen systems. For example, *Bacillus subtilis* BBG111 induces systemic resistance in rice (*Oryza sativa* L.) against *Rhizoctonia solani* but not in grapevine (Chandler et al., 2015). *Bacillus altitudinis* GLB194 and *Bacillus pumilus* GLB197 have strong inhibitory activities against grape downy mildew, and *Bacillus cereus* NRKT increases the resveratrol content in grape berries and reduces the incidence of grape anthracnose (Aoki et al., 2017). Thus, the antimicrobial activity of a strain may differ according to the plant–pathogen interaction.

Therefore, unraveling the mode of action in each plant pathosystem is necessary, and other mechanisms of *Bacillus* biocontrol, such as the strong and broad-spectrum antifungal and/or antibacterial activity, also deserve attention. For example, *Bacillus amyloliquefaciens* inhibits the growth of 13 fungal pathogens of grapes, including *Alternaria alternata*, *Penicillium verrucosum*, *Bacillus cinerea*, *Fomitiporia mediterranea*, *Fusarium oxysporum*, *Lasiodiplodia theobromae*, and *Phoma glomerata* (Alfonzo et al., 2012). The metabolites produced by *B. subtilis* in liquid culture inhibit spore germination and hyphal growth of certain pathogenic fungi (Jiang et al., 2014). *B. velezensis* secretes fungal cell wall-degrading enzymes, which is an important mechanism for inhibiting pathogens and it deserves further research (Ye et al., 2018). Overall, although *Bacillus* species exhibits well-defined antifungal activity and induces host-defense responses against plant pathogens, the mechanism by which *Bacillus* inhibits pathogen growth *in vitro* requires further study and may contribute to the biological control of plant diseases.

Our previous study provided the first report of the fungal pathogen *Penicillium olsonii* causing postharvest fruit rot of grapes (Zou et al., 2022). In a preliminary study, we observed that the growth of *P. olsonii* was significantly inhibited by metabolites produced by a biocontrol strain of *B. velezensis*. Our

aims in the present study were to (1) examine the response of *P. olsonii* to metabolites produced by *B. velezensis*, (2) generate a draft genome for *P. olsonii* WHG5 as a tool for further genetic analysis, and (3) elucidate the mechanisms of *B. velezensis* antifungal activity on *P. olsonii*. The results provide insight into the potential of metabolites produced by *B. velezensis* for effective biocontrol of post-harvest fruit rot to enhance the storage longevity of grape berries.

Materials and methods

Microbial stains

Penicillium olsonii WHG5 was isolated from rotting berries of grape (*V. vinifera* "Crimson") using the single spore isolation technique developed by Chomnunti et al. (2014). The identification and pathogenicity of WHG5 were reported previously (Zou et al., 2022). A WHG5 cell suspension was generated by washing the cultures grown for 72 h at 28°C on potato dextrose agar medium (PDA; 200 g fresh potato tuber, 20 g glucose, 15 g agar, 1 L distilled water) with sterile distilled water. *B. velezensis* isolate SB023 was obtained from the China General Microbiological Culture Collection Center, Beijing, China. An SB023 cell suspension was generated by culturing a single colony for 48 h at 32°C with shaking at 200 rpm in nutrient broth (NB; 20 g glucose, 5 g yeast extract, 10 g peptone, 5 g NaCl, 1 L distilled water, pH 6.5–6.7). All cell suspensions were mixed with 50% (v/v) glycerin solution (1:1, v/v) and stored at −80°C.

Metabolite exposure treatment

A sample (100 μl) of the preserved SB023 cell suspension was activated in 10 ml NB by incubation for 48 h at 32°C with shaking at 200 rpm and then adjusted to approximately 1×10^8 CFU/ml as measured with a hemocytometer. An aliquot (1 ml) of the cell suspension was inoculated into 100 ml NB, incubated under the same conditions, and then the culture was centrifuged at 10,000 *g* for 15 min. The cell-free supernatant was filtered through a Millex-HV filter (0.22 mm, 13 mm diameter; Millipore, Billerica, MA, USA) to obtain the sterile *B. velezensis* liquid-culture metabolites.

The WHG5 cell suspension was activated in 10 ml potato dextrose broth (PDB; PDA without agar) by incubation for 24 h at 28°C with shaking at 200 rpm, and then adjusted to approximately 1×10^8 CFU/ml, as measured with a hemocytometer. An aliquot (1 ml) of the culture was added to 100 ml PDB supplemented with 10% (v/v) *B. velezensis* metabolites. An identical volume of PDB supplemented with the equivalent volume of sterile distilled water served as the control. All liquid cultures were incubated for 5 days at 28°C with shaking at 200 rpm and then were used for DNA and RNA extraction. All experiments were repeated three times with three replicates.

Whole-genome sequencing analysis

Genomic DNA was extracted using a fungal DNA kit (Omega Bio-Tek Inc., Norcross, GA, USA) in accordance with the manufacturer's instructions. Strains were sequenced and the reads were assembled (by Nanjing Personal Gene Technology Co., Ltd., Nanjing, China) using the following procedure. The genomic DNA was sheared using a g-TUBE (Covaris, Inc., Woburn, MA, USA). A library of 400-bp paired-end reads was constructed in accordance with the standard Illumina TruSeq DNA sample preparation guide and sequenced using the Illumina NovaSeq platform (Illumina, Inc., San Diego, CA, USA) with a read length of 150 bp. The FastQC tool (Brown et al., 2017) was used for quality control on the high-throughput sequence data. High-quality sequence data were *de novo* assembled with A5-miseq v20150522 (Coil et al., 2015) and SPAdesv3.9.0 (Bankevich et al., 2012). The genome assembly was further proofread using Pilon v1.18 (Walker et al., 2014), and the integrity was assessed using BUSCO (Simão et al., 2015). Ultimately, a whole-genome assembly was obtained without redundancy.

Assembled scaffolds were processed using RepeatMasker v4.0.5 and RepeatModeler v1.0.4 software to predict genes (Tempel, 2012). Thereafter, tRNA and rRNA were predicted using rRNAscan-SE v1.3.1 (Lowe and Eddy, 1997) and RNAmmer v1.2 (Lagesen et al., 2007), respectively. Predictions of other non-coding RNAs were mainly obtained by comparison with the Rfam database (Griffiths-Jones, 2006). To improve the accuracy of gene prediction, Augustus v3.03, glimmerHMM v3.0.1, and SNAP software were used for the *de novo* prediction of genetic models in the WHG5 genome (Korf, 2004; Majoros et al., 2004; Stanke and Morgenstern, 2005). Exonerate v2.2.0 software[1] was used for the prediction of homology among related species. EVidenceModeler vr2012-06-25 software was used to integrate the *de novo* prediction results and the homology prediction results for related species (Haas et al., 2008).

The hmmscan (v3.1b2) and BLASTP (v2.5.0+) tools were used to predict the presence of CAZy enzyme and cytochrome P450 genes in the genome sequence, respectively (Finn et al., 2011). Predicted proteins were compared with the NCBI nr database (release 2017.10.10) using DIAMOND (v0.9.10.111) software (Buchfink et al., 2015) and then functionally annotated using the GO, eggNOG, KEGG, and Swiss-Prot databases. Completeness of genome annotation was estimated using the BUSCO Fungi datasets. Single-copy ortholog sequences were identified with OrthoFinder v2.0 (Emms and Kelly, 2019) and then aligned with the Operon Database v10.1 (Zaidi and

1 http://www.ebi.ac.uk/about/vertebrate-genomics/software

Zhang, 2016) using DIAMOND (v0.9.10.111) software. After the removal of identical sequences, the remaining sequences with an E value of $<10^{-5}$ and a coverage of $\geq$50% were used to construct a multiple sequence alignment using MAFFT software (Katoh and Toh, 2008). Finally, the aligned sequences were spliced according to species and a dendrogram was constructed using the neighbor-joining method with IQtree (Nguyen et al., 2015).

Transcriptome analysis

Total RNA was extracted using a fungal RNA kit (Omega Bio-Tek Inc., Norcross, GA, USA) following the manufacturer's instructions. The concentration and purity of the RNA were determined using a NanoDrop 2000 spectrophotometer (Thermo Fisher Scientific Inc., Waltham, MA, USA) and an Agilent 2100 Bioanalyzer (Agilent Technology Inc., Palo Alto, CA, USA), respectively. The cDNA libraries with an average insert size of 380 bp were prepared using the Illumina mRNA-seq sample preparation kit following the manufacturer's instructions and evaluated with an Agilent 2100 Bioanalyzer. The cDNA libraries were sequenced and analyzed (by Nanjing Personal Gene Technology Co., Ltd., Nanjing, China) in accordance with the Illumina standard protocol. The RNA-sequencing (RNA-seq) reads were aligned to the WHG5 genome sequence assembled in this research.

All read alignment positions of each paired-end read were mapped against the genome sequence and exon splicing junctions using HISAT2 software with the BWT algorithm (Sirén et al., 2014). Read counts per gene were determined from the primary read alignments using HTSeq and then normalized as fragments per kilobase per million mapped reads (FPKM). The read count files with FPKM $>$ 1 were analyzed with the "DESeq2" R package (Love et al., 2014) to identify differentially expressed genes (DEGs). Absolute $\log_2$ fold change $>$ 1 and statistical significance (P-value $<$ 0.05) were used as the criteria to identify the DEGs.

A gene ontology (GO) enrichment analysis was performed using the topGO Bioconductor package. All DEGs were mapped to corresponding GO terms and the number of genes in each term was calculated. The GO terms with significant enrichment of DEGs compared with the genomic background were defined using the hypergeometric test. The GO terms with a false discovery rate of (calculated P-value after correction) $\leq$ 0.05 were defined as significantly enriched DEG GO terms. This analysis determined the main biological functions of the DEGs (Mi et al., 2016).

A Kyoto Encyclopedia of Genes and Genomes (KEGG) pathway enrichment analysis was performed using the KEGG database.[2] The selected DEGs were categorized according to the protein function predicted by the KEGG database, and then the number of genes in each pathway was calculated. The KEGG pathways with significant enrichment of DEGs compared with the genomic background were defined using the hypergeometric test with the same conditions. This analysis predicted the cellular and metabolic functions associated with the observed changes in transcript levels.

Quantitative real-time PCR analysis

To validate the RNA-seq results, samples from the same treatment and RNA extraction for RNA-seq were also used for cDNA synthesis. The RNA was reverse-transcribed into cDNA using the PrimeScript RT Reagent Kit with gDNA Eraser (Takara, Shiga, Japan). A total of 20 DEGs that differed in their expression pattern were verified by quantitative real-time PCR (qRT-PCR). The selected DEGs were mostly associated with

TABLE 1 Genome assembly and annotation statistics of *Penicillium olsonii* WHG5.

Sample name	*Penicillium olsonii*	
Assembly statistics		
Scaffold total length (bp)	29,294,745	
Scaffold N50 length (bp)	1,105,645	
Scaffold N90 length (bp)	517,735	
GC content (%)	49.65	
Gene statistics		
Gene assembly (bp)	16,679,273	
Number of coding sequence genes	10,251	
Number of exons	31,134	
Total exons length (bp)	15,298,532	
Average length of coding sequence genes (bp)	1,627	
Average exons length (bp)	491.3	
Average introns length (bp)	66.1	
BUSCO statistics	**Numbers**	**Percent (%)**
Complete BUSCOs	3,928	97.1
Complete and single-copy BUSCOs	3,915	96.8
Complete and duplicated BUSCOs	13	0.3
Fragmented BUSCOss Missing BUSCOs	37	0.9
Missing BUSCOs	81	2.0
Total BUSCO groups searched	4,046	
Genome functional annotation	**Numbers**	**Percent (%)**
NR	10,003	97.58
GO	7,242	70.65
KEGG	4,003	39.05
KOG	9,544	93.10
SwissProt	7,589	74.03
CAZy	583	5.70

2 http://www.genome.jp/kegg/

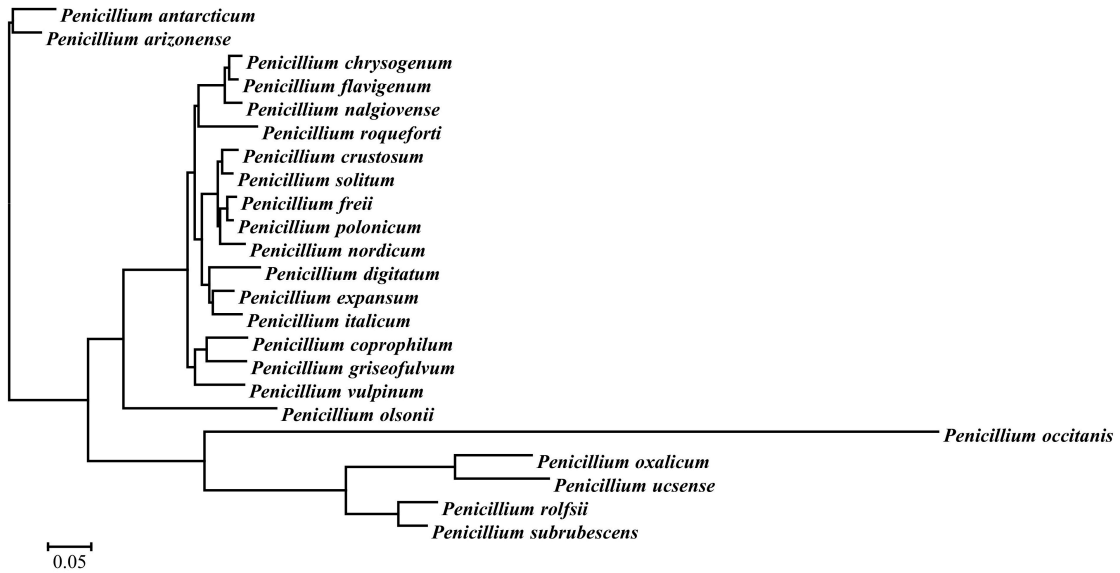

FIGURE 1
Phylogenetic tree for selected single-copy orthologous sequences in the genomes of *Penicillium olsonii* WGH5 and 23 other *Penicillium* species.

sugar metabolism, alternative carbon metabolism, glutathione metabolism, and plant–pathogen interactions. Primers for the selected DEGs were designed using Primer Premier v5.0 (Premier Biosoft, San Francisco, CA, USA). The *P. olsonii* β-*actin* (POLN_004133) gene was used as the internal control gene for each amplification. All primers used are listed in **Supplementary Table 1**. Each qRT-PCR analysis was performed using a Bio-Rad CFX-96 Real-Time PCR System (Bio-Rad Laboratories, Hercules, CA, USA). Reactions were conducted with a final volume of 10 μl, containing 1.0 μl of diluted cDNA template, 0.5 μl of each forward and reverse primer (1 μM), 5 μl of SYBR® Premix Ex Taq™ (Takara), and 3 μl of RNase-free water. The PCR protocol was as follows: initial denaturation at 96°C for 1 min, followed by 40 cycles at 96°C for 15 s, and primer extension at 62°C for 25 s. The relative expression level of each targeted gene was calculated using the $2^{-\Delta\Delta Ct}$ method. Three replicates of each qRT-PCR analysis were performed for each gene.

Observation of *P. olsonii* micromorphology after exposure to *B. velezensis* metabolites

Plates containing PDA medium were inoculated with 100 μl of WHG5 cell suspension and incubated at 28°C for 24 h. A small plug of the culture (diameter 5 mm) was inoculated onto plates containing PDA supplemented with either 10% *B. velezensis* metabolites or the equivalent volume of sterile distilled water (the control) and cultured at 28°C for 72 h. The micromorphology of *P. olsonii* conidia and mycelia was observed with a light microscope (DM500, Leica, Wetzlar, Germany).

Assay for the quantitative determination of reduced glutathione and trehalose contents and generation of intracellular reactive oxygen species

Reduced glutathione was quantified in accordance with the spectrophotometric assay method of Tietze (1969). GSH reacts with sulfhydryl reagent 5,5′-dithio-bis (2-nitrobenzoic acid) (DTNB) and forms a complex with a characteristic absorption peak at 412 nm. Trehalose content was determined using the modified method of Vandercammen et al. (1990). The amount of reducing sugar produced by the catalysis of trehalose by phenol was determined using the 3,5-dinitrosalicylic acid method in which brownish-red amino compounds are formed with a characteristic absorption peak at 620 nm. The generation of intracellular reactive oxygen species (ROS) was assessed using the ROS-sensitive fluorescence indicator 2′,7′-dichlorodihydrofluorescein diacetate following the modified method of Goto et al. (1993).

Statistical analysis

To ensure the validity of the experimental data and to reduce the variance, all tests were performed in triplicate. All statistical

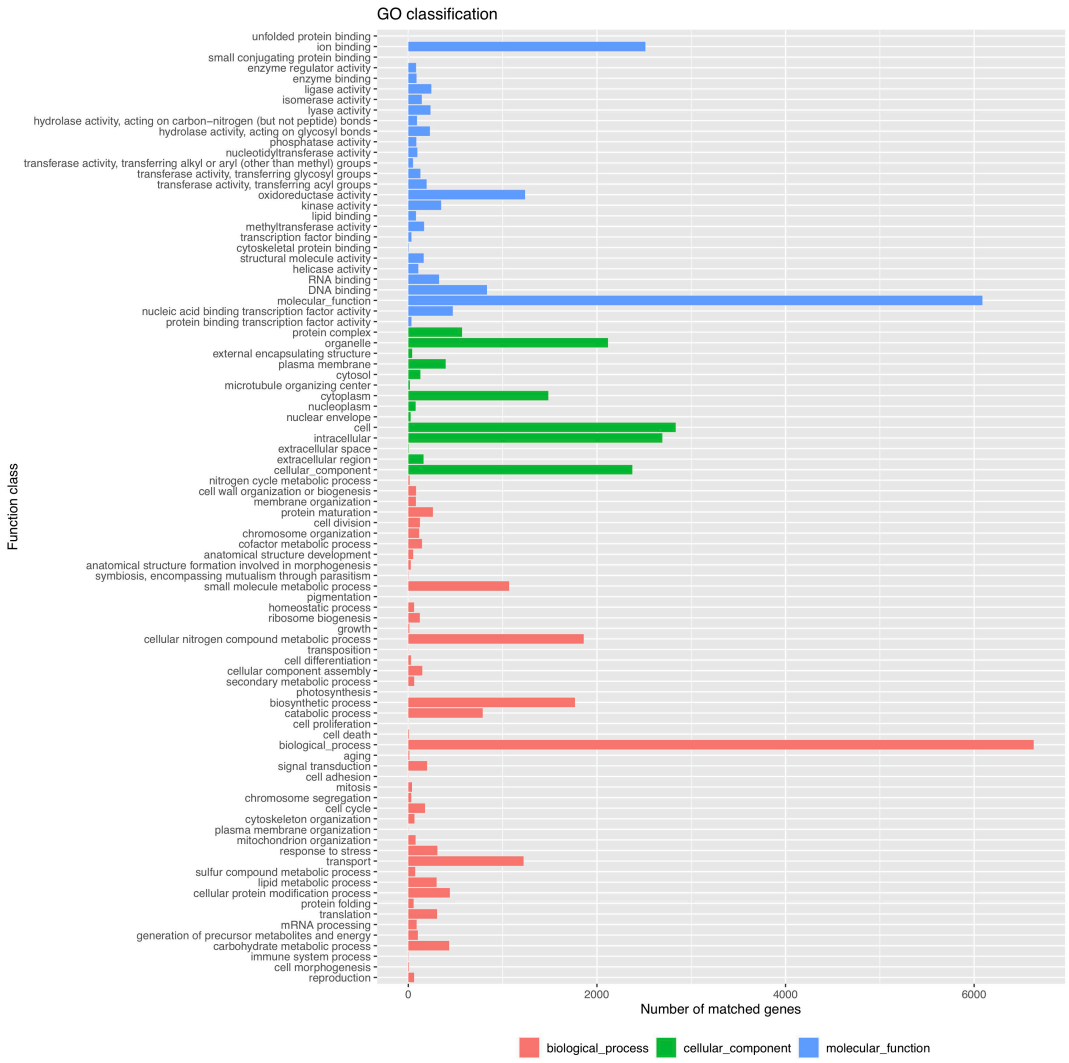

FIGURE 2
Gene ontology (GO) functional classification of the *Penicillium olsonii* WGH5 genome.

analyses were performed with GraphPad Prism v7.0 (GraphPad Software, San Diego, CA, USA). The significance of differences between the means of the treatments was analyzed with one-way ANOVA followed by paired-sample *t*-tests at the 5% significance level ($P < 0.05$).

Results

Sequencing and assembly of genomic data

A total of 4,972 Mb of sequence data were generated for *P. olsonii* WHG5 (Table 1). The estimated genome size was 29.96 Mb, which was revised to 29.95 Mb, with an N50 value of 1,105,645 bp. Through comparison with publicly available databases, 10,251 protein-coding genes were predicted in the *P. olsonii* genome. The length of non-coding RNA was 24,188 bp in total. The genome assembly is summarized in Table 1. The assembled *P. olsonii* genome comprised a total length of 16,679,273 bp. The integrity of the genome assembly was assessed with BUSCO using the hypocreales_odb10 dataset, which includes 4,494 single-copy genes from 50 species. The results showed that 97.1% of the total number of single-copy genes were fully aligned in the WHG5 genome sequence (Table 1). In general, a high percentage implies high quality of genome assembly integrity. In addition, genome protein sequences for 23 species of *Penicillium* were clustered with the selected single-copy ortholog sequences in the WHG5 genome and they yielded 2,462 single copies. After a BLAST search of the ortholog library, the remaining 419 single-copy genes

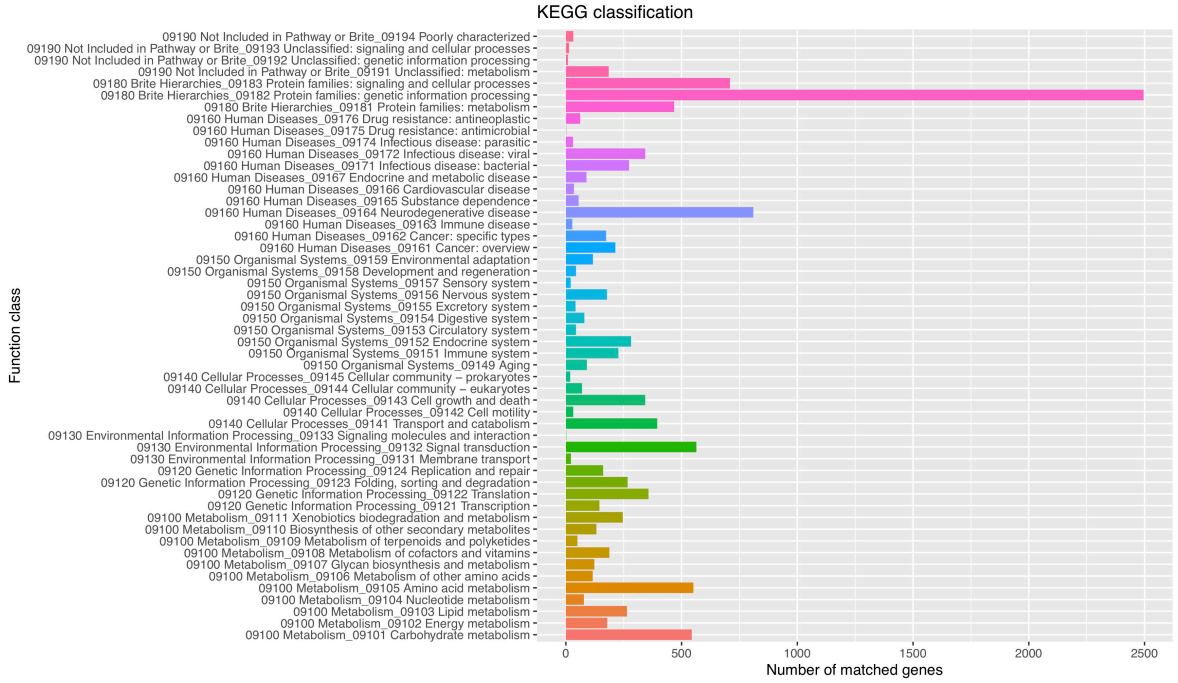

FIGURE 3
Kyoto encyclopedia of genes and genomes (KEGG) pathway functional classification of the *Penicillium olsonii* WGH5 genome.

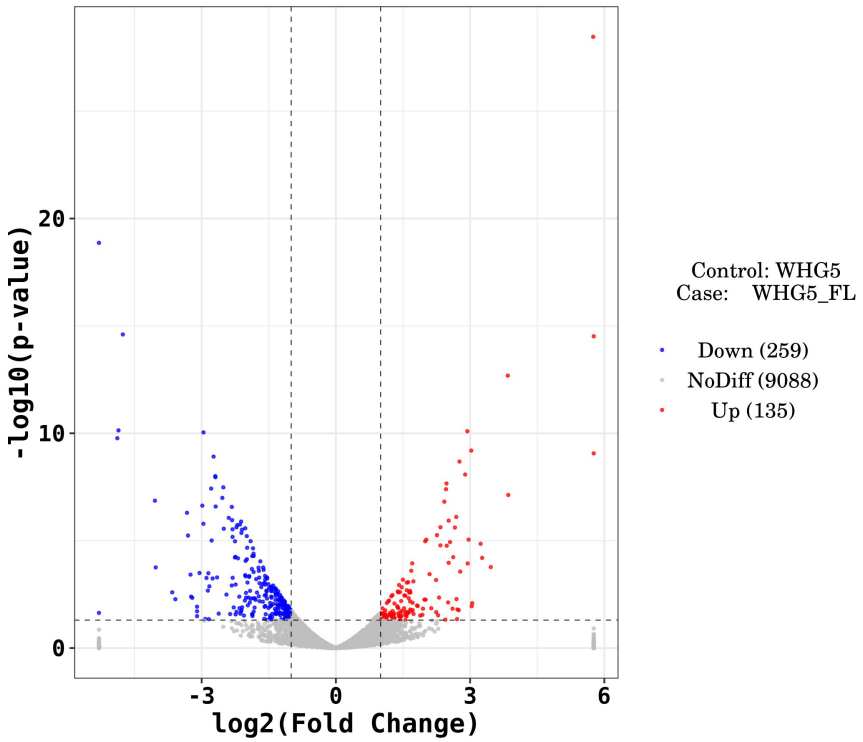

FIGURE 4
Differentially expressed genes (fold change > 1) between *Penicillium olsonii* WHG5 (control; WHG5 cultured without *Bacillus velezensis* metabolites) and WHG5_FL (treatment; WHG5 cultured with *B. velezensis* metabolites). Down-regulated genes are in blue, up-regulated genes are in red, and non-differentially expressed genes are in gray.

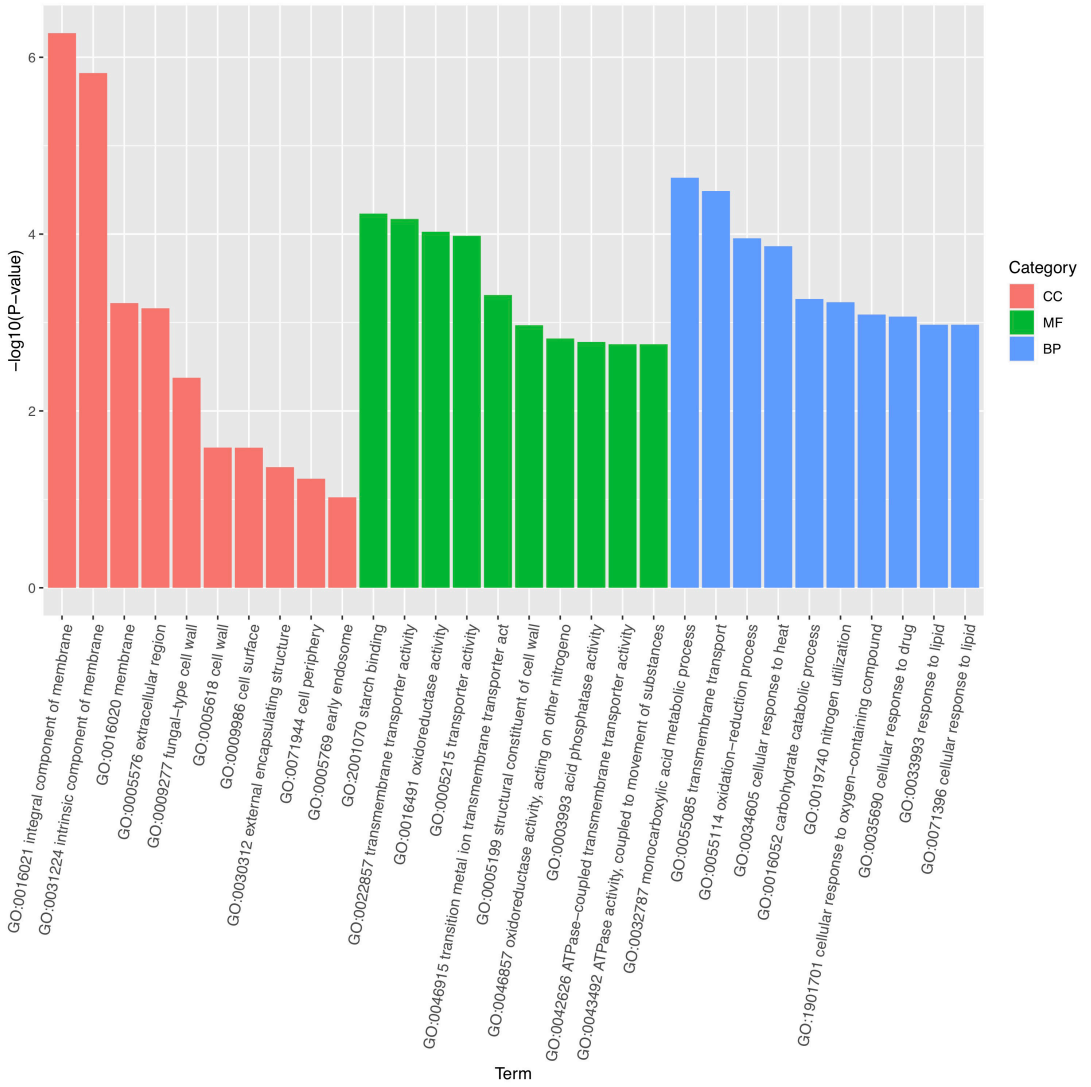

FIGURE 5
Gene ontology (GO) functional annotation and classification of expressed genes (fold change > 1) between *Penicillium olsonii* WHG5 (control; WHG5 cultured without *Bacillus velezensis* metabolites) and WHG5_FL (treatment; WHG5 cultured with *B. velezensis* metabolites).

were used for a neighbor-joining analysis. The dendrogram (Figure 1) indicated that the WHG5 genome was most similar to the genomes of other *Penicillium* species.

Functional analysis of the *P. olsonii* WHG5 genome was performed with the consideration of GO classification (Figure 2), KEGG pathways (Figure 3), and the eggNOG classification (Supplementary Figure 2). The GO-based classification revealed a total of 7,242 annotated genes in the WHG5 genome. Among genes classified in the biological process and molecular function categories, cell (2,893, 39.95%), ion binding (2,514, 34.71%), and cellular nitrogen compound metabolic process (1,860, 25.68%) were the most abundant. Among genes classified in the cellular component category, the greatest number of genes were assigned to the intracellular (2,694, 37.20%), organelle (2,118, 29.25%), and cytoplasm (1,485, 20.51%) terms. The KEGG database indicated that the most abundant genes were associated with genetic information (2,496, 62.35%), neurodegenerative disease (810, 20.23%), and signaling and cellular process (709, 17.71%) pathways. These findings suggested the presence of genes involved in a variety of protein metabolism, energy metabolism, and signal transduction processes in *P. olsonii*. Similarly, the most gene-rich KOG functional terms were carbohydrate transport and metabolism (817, 8.56%); amino acid transport and metabolism (530, 5.55%); and post-translational modification, protein turnover, and chaperones (490, 5.13%). In addition, carbohydrate-active enzymes (CAZymes) were important in the *P. olsonii* WHG5 genome (Supplementary Figure 3).

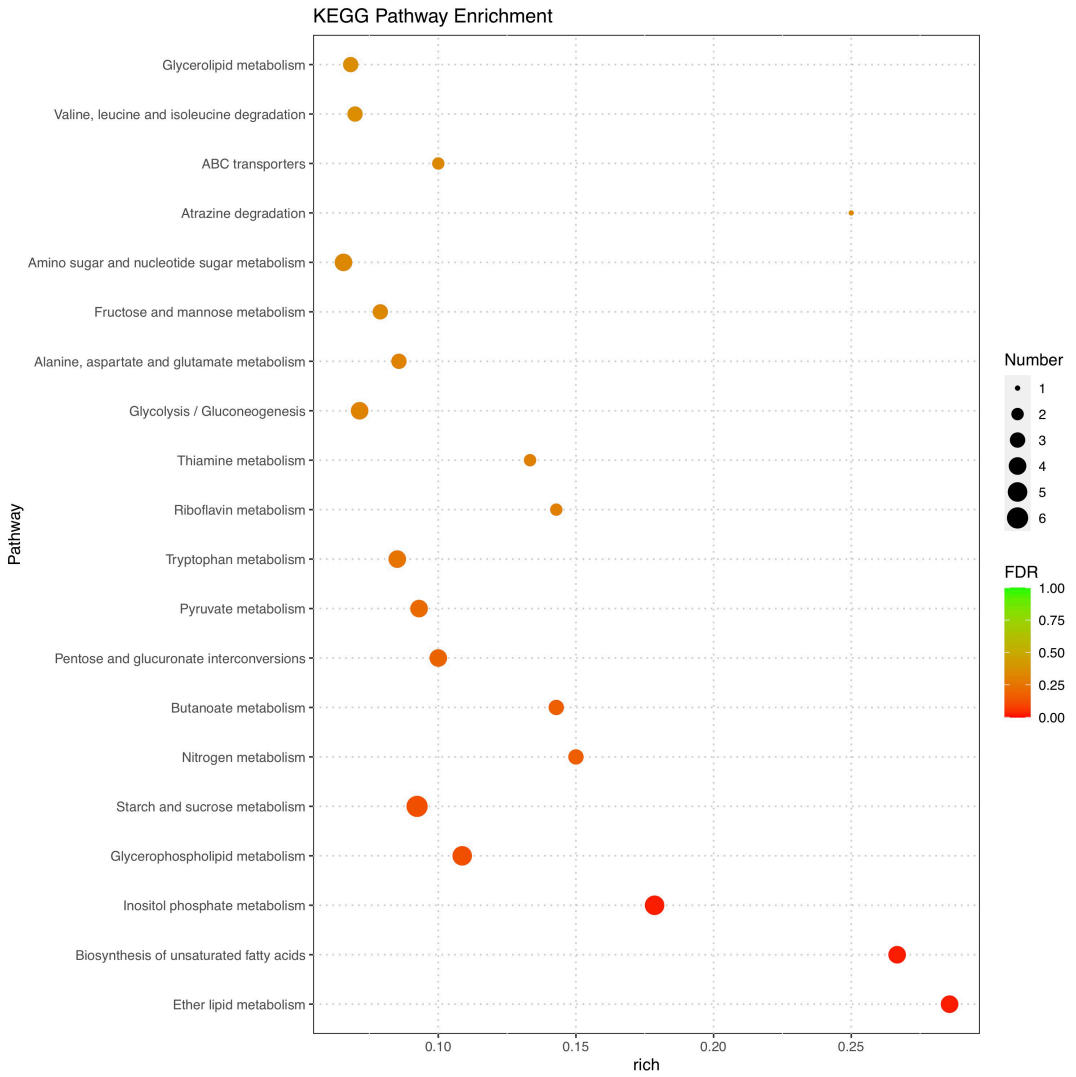

FIGURE 6
Kyoto encyclopedia of genes and genomes (KEGG) pathway functional annotation of differentially expressed genes (fold change > 1) between *Penicillium olsonii* WHG5 (control; WHG5 cultured without *Bacillus velezensis* metabolites) and WHG5_FL (treatment; WHG5 cultured with *B. velezensis* metabolites).

Evaluation of the transcriptome data

In our preliminary study, metabolites produced by *B. velezensis* SB023 significantly inhibited the growth of *P. olsonii* after culturing for 72 h. In the present study, *P. olsonii* cultured in the presence or absence of SB023 metabolites was subjected to RNA-seq to screen for potential candidate genes involved in the interaction between *B. velezensis* and *P. olsonii*. After the removal of low-quality reads, the number of clean reads ranged from 6.72 to 6.86 Gb. The bases with Q $\geq$ 30 comprised more than 95.50% of the total number and those with Q $\geq$ 20 comprised more than 98.43% (Supplementary Table 2). More than 91.79% of the clean RNA-seq data after quality control were mapped to the *P. olsonii* WHG5 reference genome, indicating that the quality of the transcriptome sequence data was reliable (Supplementary Table 2).

Marked differences in the transcriptome profiles were observed between *P. olsonii* WHG5 cultured in the presence or absence of *B. velezensis* metabolites. A total of 394 core DEGs were obtained. Compared with the control group (WHG5 cultured without *B. velezensis* metabolites), 135 and 259 DEGs were up-regulated and down-regulated, respectively, in WHG5 cultured with *B. velezensis* metabolites (Figure 4). To identify the biological processes, molecular functions, and cellular components of WHG5 growth influenced by *B. velezensis* metabolites, a GO term analysis was conducted on the selected DEGs (Figure 5). In the cellular process category, the most abundant GO terms were an integral

10.3389/fmicb.2022.1019800

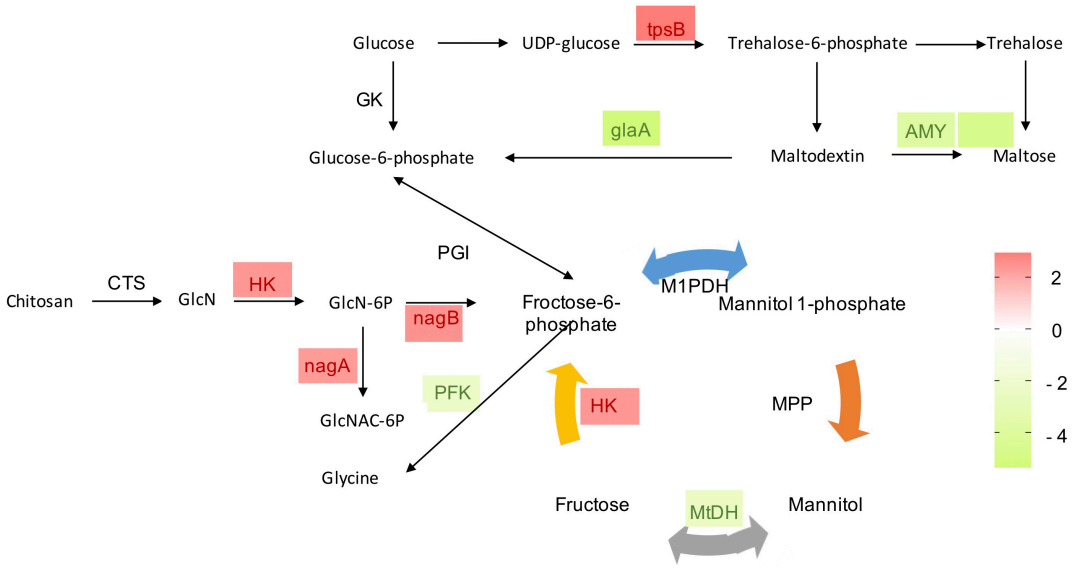

FIGURE 7
Heat maps of differentially expressed genes (DEGs) that may be involved in sugar metabolism. GK, glucokinase; PGI, phosphoglucose isomerase; MtDH, mannitol-2-dehydrogenase; HK, hexokinase; M1PDH, mannitol-1-phosphate dehydrogenase; MPP, mannitol-1-phosphate phosphatase; tpsB, trehalose 6-phosphate synthase; AMY, alpha-amylase A; gLaA, glucoamylase; CTS, chitosanase; GlcN, glucosamine; GlcN-6P, glucosamine 6-phosphate; GlcNAc-6P, 6-phosphate-*N*-acetylglucosamine; nagA, 6-phosphate-*N*-acetylglucosamine deacetylation; nagB, 6-phosphate glucosamine deaminase; PFK, phosphofructokinase. The expression image was generated using GraphPad Prism software: red, increase; green, decrease.

component of the membrane, an intrinsic component of the membrane, and the membrane. In the metabolic process category, the predominant GO terms comprised the starch binding, transmembrane transporter activity, and oxidoreductase activity. In the biological process category, the predominant GO terms comprised monocarboxylic acid transport, transmembrane transport, and oxidation–reduction process. The KEGG pathway analysis revealed that the DEGs mostly participated in lipid metabolism, biosynthesis of unsaturated fatty acids, inositol phosphate metabolism, glycerophospholipid metabolism, starch and sucrose metabolism, and nitrogen metabolism (Figure 6). The GO and KEGG analyses implied that *B. velezensis* metabolites influenced specific metabolic processes in *P. olsonii*. Notably, most of the genes in *P. olsonii* involved in starch and sucrose metabolism and oxidative phosphorylation were differentially expressed after exposure to *B. velezensis* metabolites.

Analyses of differentially expressed genes involved in sugar metabolism

Carbon utilization and metabolism are fundamental for cellular growth in every living organism. Therefore, glycolysis is vital for normal growth and metabolism. In the present study, mannitol metabolism starting with fructose-6-phosphate, and trehalose synthesis starting with glucose-6-phosphate of *P. olsonii* were affected by *B. velezensis* metabolites (Figure 7). Genes encoding key enzymes in these sugar metabolic pathways were differentially expressed in response to exposure to *B. velezensis* metabolites. Among these DEGs, a gene encoding mannitol-1-phosphate dehydrogenase (MtDH; POLN_001215), a crucial enzyme in the interconversion of mannitol and fructose, was down-regulated in the treatment group. Genes encoding alpha-amylase A (AMY; POLN_001517 and POLN_001645) and glucoamylase (glaA; POLN_001644) showed the same pattern. AMY1 is essential for the synthesis of a virulence factor and hence is associated with virulence. In addition, DEGs encoding other crucial enzymes were up-regulated in the treatment group, including 6-phosphate-*N*-acetylglucosamine deacetylation (nagA; POLN_005457), 6-phosphate glucosamine deaminase (nagB; POLN_005454), and hexokinase (HK; POLN_002794), which are key enzymes

TABLE 2 Contents of glutathione, trehalose, and reactive oxygen species in *Penicillium olsonii* WHG5.

	Control group	Treatment group
Glutathione (μmol/g fresh weight)	0.377 ± 0.017	0.875 ± 0.020
Trehalose (mg/g fresh weight)	5.750 ± 0.220	6.426 ± 0.218
Reaction oxygen species generation rate (u/s/g fresh weight)	3055.546 ± 89.418	1131.889 ± 63.653

10.3389/fmicb.2022.1019800

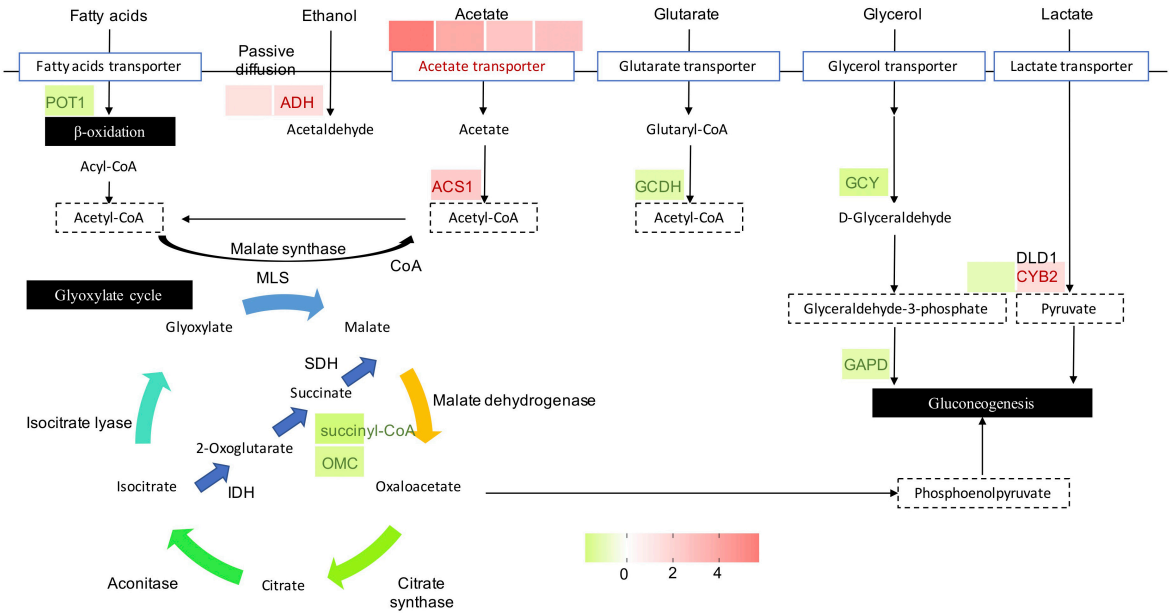

FIGURE 8
Heat maps of differentially expressed genes (DEGs) that may be involved in alternative carbon metabolism. POT, 3-ketoacyl-CoA thiolase; ADH, alcohol dehydrogenase; ACS, acetyl-CoA synthetase; GCDH, glutaryl-CoA dehydrogenase; GCY, glycerol 2-dehydrogenase; GAPD, glyceraldehyde-3-phosphate dehydrogenase; DLD, dihydrolipoamide dehydrogenase; CYB2, cytochrome b2; OMC, 2-oxoglutarate-malate carrier; SDH, succinate dehydrogenase; MLS, malate synthase; IDH, isocitrate dehydrogenase. The expression image was generated using GraphPad Prism software: red, increase; green, decrease.

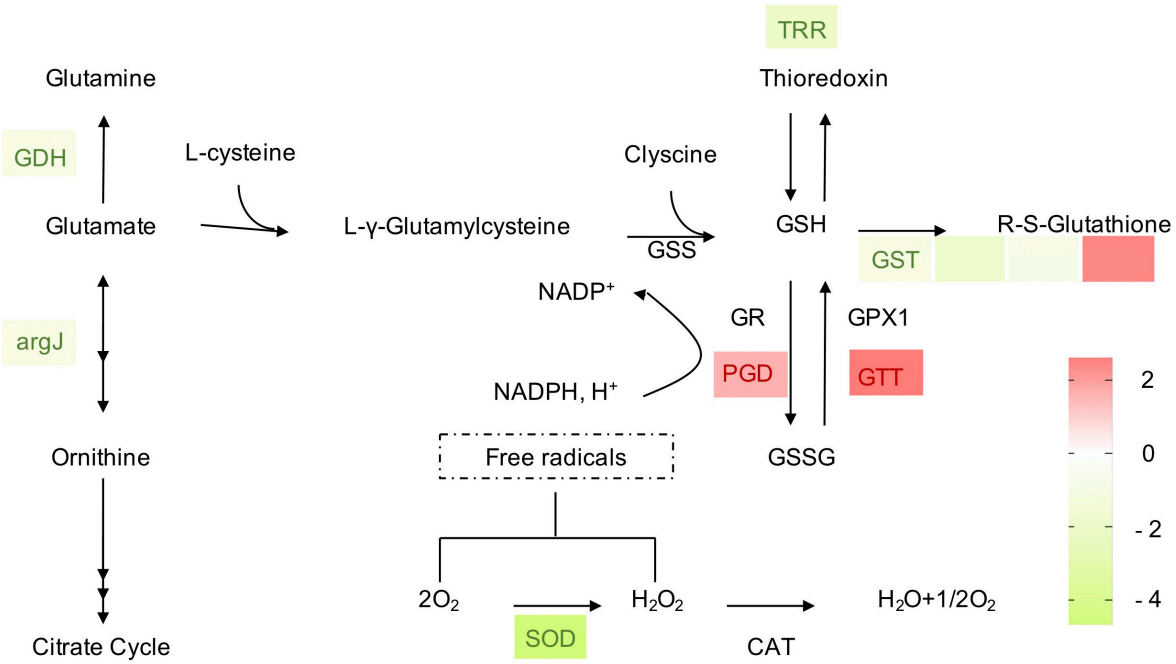

FIGURE 9
Heat maps of differentially expressed genes (DEGs) that may be involved in redox homeostasis. GDH, glutamate dehydrogenase; argJ, amino-acid acetyltransferase; GSS, glutathione synthase; GSH, glutathione; GR, glutathione reductase; PGD, 6-phosphogluconate dehydrogenase; GPX, glutathione peroxidase; GTT, glutathione transporter; GSSG, glutathione disulfide; GST, glutathione *S*-transferase; TRR, thioredoxin reductase; SOD, superoxide dismutase; CAT, catalase. The expression image was generated using GraphPad Prism software: red, increase; green, decrease.

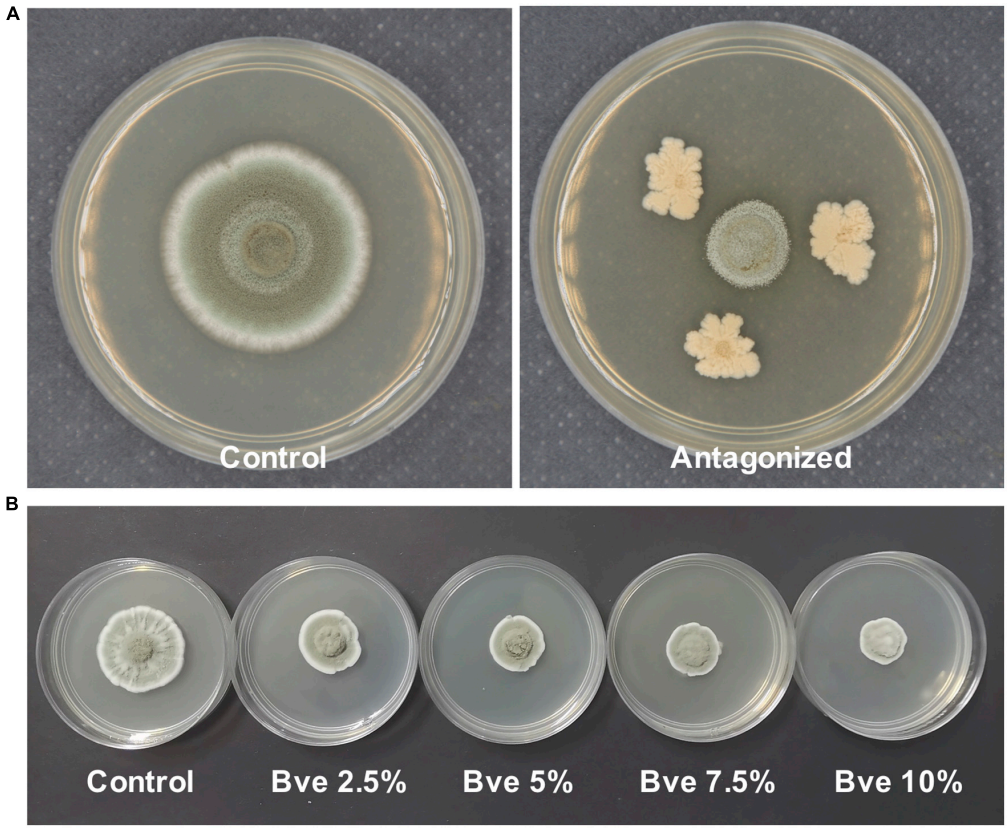

FIGURE 10
Morphology of *Penicillium olsonii* on potato dextrose broth (PDA) after exposure to *Bacillus velezensis* (5 days after inoculation). Antagonized by *B. velezensis* on PDA **(A)**, colony of *P. olsonii* after exposure to different concentrations of *B. velezensis* metabolites **(B)**.

involved in the breakdown of fructose and other sugars into fructose-6-phosphate for glycolysis. It was notable that the up-regulated enzymes also included trehalose 6-phosphate synthase (tpsB; POLN_002453), which is a critical enzyme in trehalose synthesis. In addition, the trehalose content was significantly increased ($P < 0.05$) in the treatment group (Table 2).

Analyses of differentially expressed genes involved in alternative carbon metabolism

As an important metabolic adaptation strategy, alternative carbon metabolism is utilized by a fungus to compensate for the deficiency of the preferred carbon source, glucose. In such a harsh microenvironment, the fungus converts other carbon sources to the central metabolite acetyl-CoA to fuel the glyoxylate cycle and gluconeogenesis for glucose and energy production. After exposure of *P. olsonii* to *B. velezensis* metabolites for 5 days, 15 DEGs encoded critical enzymes in the glyoxylate cycle and alternative carbon metabolism (Figure 8). Different sources of acetyl-CoA responded differently to *B. velezensis* metabolites. Among these DEGs, genes encoding 3-ketoacyl-CoA thiolase (POT1; POLN_005154) involved in β-oxidation of fatty acids, glutaryl-CoA dehydrogenase (GCDH; POLN_006747) involved in glutamate metabolism, glycerol 2-dehydrogenase (GCY1; POLN_008918) and glyceraldehyde-3-phosphate dehydrogenase (GAPD; POLN_006304) involved in glycerol metabolism, and cytochrome b2 (CYB; POLN_005941) involved in lactate metabolism were down-regulated in the treatment group. Conversely, key genes in other sources of acetyl-CoA were up-regulated in the treatment group, including DEGs encoding alcohol dehydrogenase (ADH; POLN_000033 and POLN_000551) involved in ethanol metabolism, and acetyl-CoA synthetase (ACS; POLN_000098) and related acetyltransferases (POLN_000095, POLN_006411, POLN_002030, and POLN_004443) involved in acetate metabolism. These results implied that *B. velezensis* metabolites influenced the β-oxidation of fatty acids, glutamate metabolism, glycerol metabolism, and lactate metabolism, and increased the metabolism of ethanol and acetate in *P. olsonii*. In the glyoxylate cycle, isocitrate is converted to malate through the glyoxylate process and utilizes acetyl-CoA. It is worth mentioning that two DEGs encoding key proteins in this process, succinyl-CoA

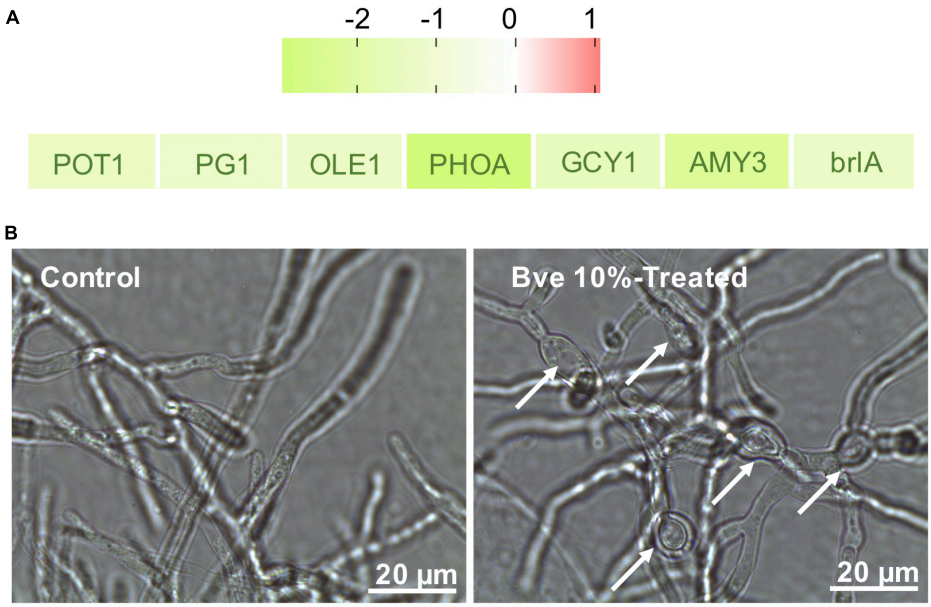

FIGURE 11
Identification of differentially expressed genes (fold change > 1) involved in plant–pathogen interactions by RNA sequencing **(A)**. Microscopic morphology of *Penicillium olsonii* after exposure to *Bacillus velezensis* (5 days after inoculation) metabolites. White arrows indicate mycelial swelling caused by 10% *B. velezensis* metabolites **(B)**.

(POLN_006914) and 2-oxoglutarate-malate carrier (OMC; POLN_009692), were down-regulated in the treatment group, which indicated that isocitrate conversion to malate through the succinate process was decreased by *B. velezensis* metabolites.

Analyses of differentially expressed genes involved in the maintenance of redox homeostasis

For fungal adaptation to an unfavorable environment, enzymatic [catalases, superoxide dismutases (SODs), and peroxidases] and non-enzymatic [glutathione (GSH)] mechanisms maintain the redox homeostasis within the cells. In these processes, the oxidation status is maintained and rapidly restored by the action of two redox-balancing systems: the GSH and thioredoxin pathways. In the present study, DEGs were enriched in the GSH pathway, indicating that *B. velezensis* metabolites affected GSH metabolism in *P. olsonii* (Figure 9). Four DEGs encoding glutathione *S*-transferases (GST; POLN_004024, POLN_001793, POLN_004336, and POLN_007150) were identified in the treatment group, of which one (POLN_004024) was up-regulated. As the main source of GSH, glutamate synthesis was affected in the treatment group by the down-regulation of the genes encoding glutamate dehydrogenase (GDH; POLN_000199) and amino-acid acetyltransferase (argJ; POLN_004328). GDH converts glutamate into glutamine, whereas argJ converts glutamate into ornithine and participates in the citrate cycle. Two DEGs encoding enzymes that participate in the interconversion of GSH and GSSH, namely 6-phosphogluconate dehydrogenase (PDG; POLN_008064) and glutathione transporter (GTT; POLN_002687), were up-regulated in the treatment group, indicating that interconversion between GSH and GSSH in *P. olsonii* was activated in response to exposure to *B. velezensis* metabolites. A gene encoding thioredoxin reductase (TRR; POLN_000490) was down-regulated in the treatment group, indicating that thioredoxin metabolism was decreased. In addition, the glutathione content was increased and intracellular ROS generation was reduced in the treatment group ($P < 0.05$) (Table 2). However, a gene encoding SOD (POLN_000741), a vital enzyme that maintains the redox homeostasis within the cell, was down-regulated in the treatment group, which indicated that *B. velezensis* metabolites depressed the growth of *P. olsonii*.

Analyses of differentially expressed genes involved in plant–pathogen interactions

Although we only observed the growth of *P. olsonii* on PDA plates supplemented with *B. velezensis* metabolites (Figure 10), the transcript data revealed that several DEGs were involved in plant–pathogen interactions (Figure 11A). In addition to *POT1* mentioned with regard to alternative

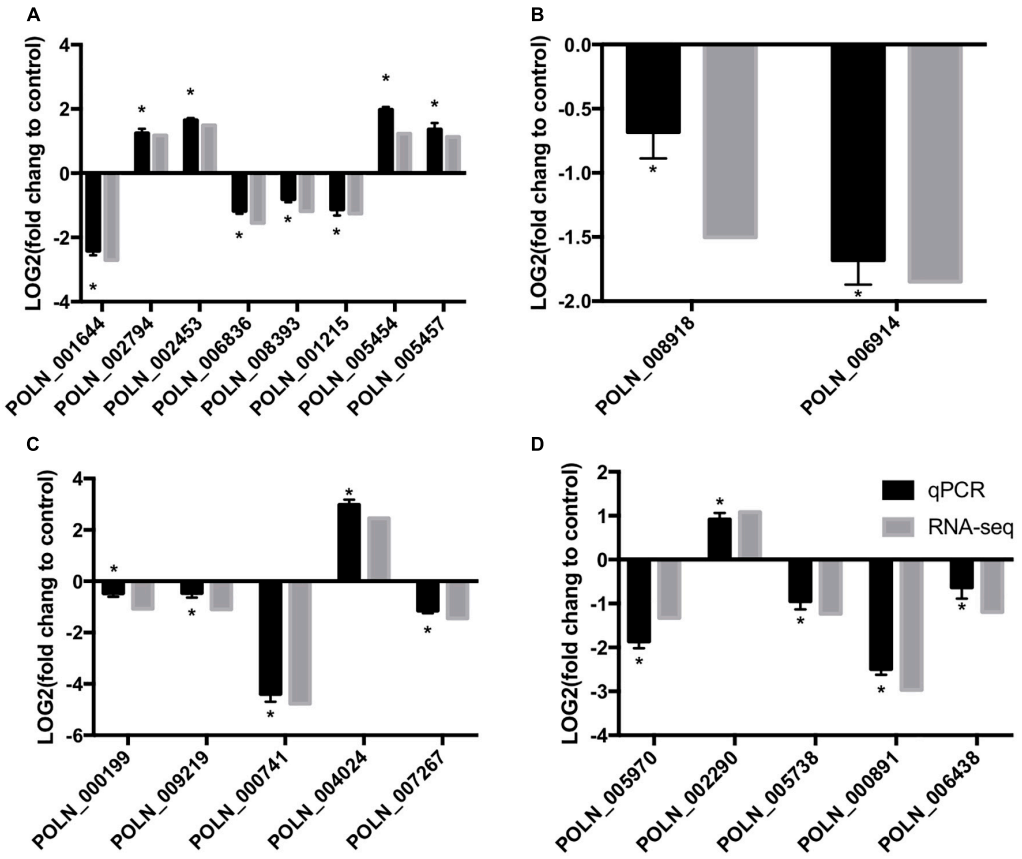

FIGURE 12
qRT-PCR verification of RNA-sequencing results with genes involved in sugar metabolism **(A)**, alternative carbon metabolism **(B)**, glutathione metabolism **(C)**, and plant–pathogen interactions **(D)**. Log_2(fold change) > 0 represents up-regulation of gene expression, Log_2(fold change) < 0 represents down-regulation of gene expression. An asterisk above an error bar indicates a significant difference between the treatment group and the control group ($P < 0.05$).

carbon metabolism, DEGs encoding polygalacturonase 1 (PG1; POLN_000891), stearoyl-coenzyme A desaturase 1 (OLE1; POLN_002255), and phosphate-repressible acid phosphatase (PHOA; POLN_005738) were down-regulated in the treatment group. PG1 is a key virulence protein of post-harvest pathogens, OLE1 is associated with fungal virulence, and PHOA is one of the main toxins of *Penicillium* species. Thus, *B. velezensis* metabolites may affect the pathogenicity of *P. olsonii*. In addition, given that spore formation requires the participation of mannitol, genes associated with sporulation were down-regulated in the treatment group, including *GCY1* and *AMY3* mentioned in relation to carbon metabolism, *PFK*, and *brlA* (regulatory protein, POLN_005970), a gene associated with conidia formation. These results indicated that *B. velezensis* metabolites may alter the normal sporulation of *P. olsonii*. To verify these results, the development of *P. olsonii* spores and mycelia was observed microscopically. The conidial spores were deformed and the swelling of the mycelia of *P. olsonii* was observed after exposure to *B. velezensis* metabolites (**Figure 11B**).

Validation of RNA-seq results by qRT-PCR analysis

To verify the changes in gene expression detected from the RNA-seq analysis, 20 DEGs that differed in expression pattern were quantified by qRT-PCR. The expression levels of almost all up- and down-regulated genes corresponded with the RNA-seq results (**Figure 12**). However, one DEG (POLN_000199) was down-regulated in the treatment group according to the RNA-seq analysis, but it showed a slight increase in expression in the treatment group according to the qRT-PCR analysis. These results verified the overall reliability of the RNA-seq data.

Discussion

The post-harvest storage life of fruit may be reduced as a result of infection by a variety of fungal pathogens. As a typical fresh fruit, the post-harvest shelf life of grape berries is greatly affected by pathogens. Considering the importance of food

safety, eco-friendly and effective measures are urgently needed to control post-harvest diseases of grapes. *B. velezensis* and its metabolites show potential as an eco-compatible alternative to the application of chemical fungicides (Rabbee et al., 2019; Fazle Rabbee and Baek, 2020). Our preliminary study indicated that metabolites of *B. velezensis* may control *P. olsonii* infection of grape berries by direct inhibition of *P. olsonii* growth (**Figure 10**). Research is increasingly focused on the indirect induction of disease resistance in grapes in response to pathogen infection, but how metabolites directly inhibit the growth of post-harvest pathogens is uncertain (Fan et al., 2018; Rabbee et al., 2019). Hence, we conducted an analysis of transcriptomic changes in *P. olsonii* isolate WHG5 after exposure to *B. velezensis* metabolites. The results confirmed that *B. velezensis* metabolites offer a promising strategy for the effective management of post-harvest *Penicillium* spp. to suppress post-harvest spoilage of grape berries.

The present results revealed that exposure to *B. velezensis* metabolites caused up-regulated expression of genes encoding the crucial enzymes (HK, nagB, and nagA) that generate fructose-6-phosphate, a central metabolite in sugar metabolism. This finding is consistent with previous research on fungi under stress (Ram, 2004; Arora et al., 2020). By affecting sugar metabolism in *P. olsonii*, treatment with *B. velezensis* metabolites might lead to energy deficiency in the pathogen. The decreased energy status would further accelerate the metabolism of energy-associated substances, and the disturbance of energy metabolism might ultimately accelerate cell death. Mannitol has generally been considered to function as a carbohydrate reserve, but more recently, it has been hypothesized to play a major role in fungal pathogenicity (Patel and Williamson, 2016). Double-knockout mutants (*Dmtdh Dm1pdh*) of *A. alternata* and *A. brassicicola*, which are deficient in mannitol synthesis, show greatly reduced virulence in tobacco and cabbage, respectively (Calmes et al., 2013). In the present research, the down-regulation of *MtDH* expression and up-regulation of *HK* expression may cause a decrease in mannitol content in *P. olsonii*. Moreover, an increase in *tasB* expression level and the down-regulation of *AMY* and *glaA* expression resulted in significantly higher contents of trehalose in the treatment group. Given that trehalose is a reserve carbohydrate (Li and Tian, 2007; Apaliya et al., 2018), the present results suggested that acceleration of sugar metabolism and increased activity of alternative carbon metabolism in *P. olsonii* were induced by *B. velezensis* metabolites. These conclusions were supported by the up-regulated expression of two genes (*ADH* and *ACS*) involved in alternative carbon metabolism, including ethanol metabolism and acetate metabolism (Fujino et al., 2001; Cobos et al., 2010). However, the activity of other alternative carbon metabolism pathways, such as β-oxidation of fatty acids, glutamate metabolism, glycerol metabolism, and lactate metabolism, was decreased by exposure to *B. velezensis* metabolites, as indicated by the down-regulated expression of genes encoding key enzymes involved in these pathways (POT1, GCDH, GCY, and GAPD) (Delgado et al., 2001; Ortiz et al., 2017; Weber et al., 2020; Zhang et al., 2021a). Hence, the present results showed that *B. velezensis* metabolites affected normal carbon metabolism in *P. olsonii* and may induce the pathogen to utilize alternative carbon metabolism through ethanol metabolism and acetate metabolism, which partly explained the antifungal activity of *B. velezensis* metabolites.

Glutathione metabolism in a fungus might play a pivotal role in amino acid transport, regulation of enzyme activity, and the maintenance of the tissue redox homeostasis, all of which contribute to the protection of the fungus against plant-derived toxic metabolites and the accumulation of ROS during infection at the host–pathogen interface (Gullner et al., 2018; Khullar and Reddy, 2018). The reduction of ROS is considered to follow the destruction of mitochondria, and ROS signals are required for apical dominance and development of the fungus (Hayashi et al., 2014; Sun et al., 2016). The decreased production of intracellular ROS in the treatment group indicated the destruction of *P. olsonii* caused by *B. velezensis* metabolites. In addition, multiple genes associated with the glutathione cycle (GST, GTT, PGD, and GDH) were differentially expressed in *P. olsonii* in response to exposure to *B. velezensis* metabolites. These changes were indicative of the damage to *P. olsonii* caused by *B. velezensis* metabolites and the compensatory responses of *P. olsonii* to this adverse stress. Treatment with *B. velezensis* metabolites decreased the expression levels of genes encoding GST, TRR, GDH, argJ, and SOD, and increased the content of reduced glutathione, which restricted the reduction and utilization of glutathione and the scavenging of free radicals, and thus may have disrupted the redox homeostasis in *P. olsonii*. *P. olsonii* responded to the stress caused by *B. velezensis* metabolites by up-regulating the expression of genes encoding PDG and fructose-bisphosphate aldolase, which are important enzymes in the pentose phosphate pathway (Rojas et al., 2014). This pathway provides NADPH without consuming ATP for the production of cellular fatty acids and reduced glutathione, thereby promoting the survival of the organism under stress (Rojas et al., 2014; Campbell et al., 2016). Notably, GST is also associated with pathogen virulence (Calmes et al., 2015; Gullner et al., 2018). Thus, the down-regulation of genes encoding GST in *P. olsonii* in the treatment group further demonstrated the potential for *B. velezensis* metabolites to suppress post-harvest spoilage in grapes.

Previous studies on biocontrol mechanisms have indicated that *B. velezensis* may suppress the growth and spore formation of pathogens by secreting certain secondary metabolites or releasing a number of volatile organic compounds (Calvo et al., 2020; Li et al., 2020). Scanning electron microscopic observation of *Penicillium roqueforti* conidiospores exposed to purified iturin A revealed the destruction and morphological changes in the spores, and the assessment of spore inactivation by fluorescence techniques indicated that iturin A may

permeabilize the spores and inhibit their germination (Calvo et al., 2020). In the current study, in addition to the observation that *B. velezensis* metabolites disrupted the mycelial growth of *P. olsonii*, the expression of genes associated with mycelial and spore growth was down-regulated (**Figure 11**). Among these genes, the down-regulation of *brlA* and *abaA* in *P. olsonii* in response to exposure to *B. velezensis* metabolites was noteworthy. Deletion of *PdbrlA* in *Penicillium digitatum* completely inhibited conidiophore development, whereas the deletion of *PdabaA* led to the formation of aberrant and non-functional phialides (Wang et al., 2015).

Several genes involved in plant–pathogen interactions were down-regulated in *P. olsonii* after exposure to *B. velezensis* metabolites. This response would enhance the reliability of *B. velezensis* metabolites as a potential biocontrol agent to suppress post-harvest spoilage in grapes. Given that the plant cell wall is a crucial physical barrier in plant–fungal pathogen interactions, the degradation of major components of the cell wall is vitally important for fungal infection (Underwood, 2012). In particular, pectinolytic enzymes are more important in the case of soft-rotting post-harvest pathogens than in other plant–fungus interactions (Reignault et al., 2007). Down-regulation of *PG1* in *P. olsonii* indicated the potential ability of *B. velezensis* metabolites to reduce the pathogenicity of *P. olsonii*. Moreover, the gene encoding the mycotoxin phomopsin A (*PHOA*) was down-regulated in *P. olsonii* after exposure to *B. velezensis* metabolites. PHOA is the primary toxin among the group of secondary metabolites formed by the fungus (Kunz et al., 2022). Therefore, the down-regulation of *PHOA* in *P. olsonii* caused by *B. velezensis* metabolites is an additional indication of the potential of *B. velezensis* metabolites as an eco-compatible alternative to harmful chemical fungicides.

Conclusion

Bacillus velezensis metabolites inhibit mycelial growth and cause the deformation of the conidia of the grape post-harvest pathogen *P. olsonii* WHG5. Genomic and transcriptomic analyses indicate that *B. velezensis* metabolites affect the expression of genes that influence the mycelial growth of *P. olsonii*. The inhibition of mycelial growth might be due to an initial impact on normal sugar metabolism and subsequent disturbance of alternative carbon metabolism and the stimulation of glutathione metabolism to maintain redox homeostasis. Although *P. olsonii* was grown on a PDA medium in this study, genes involved in plant–pathogen interactions were down-regulated by *B. velezensis* metabolites, which further verified the effect on the pathogenicity of *P. olsonii*. The results provide an overview of the main responses of *P. olsonii* to *B. velezensis* metabolites and highlight potential target genes for biocontrol agents to suppress post-harvest spoilage in grapes.

Data availability statement

The data presented in this study are deposited in the NCBI SRA repository, accession numbers SRX17100770 and SRX17100771.

Author contributions

TZ performed the experiments and wrote the original draft of the manuscript with the assistance of GW and SJ. BS and ZC carried out data curation and participated in the revision of the manuscript. SJ designed the research and provided financial support. All authors have read and approved the submitted version of the article.

Funding

This work was supported by the Natural Science Foundation of Sichuan Province in China (grant number: 2022NSFSC0098) and the Doctoral Start-up Funds of China West Normal University (grant numbers: 20E063 and 20E060).

Conflict of interest

The authors declare that the research was conducted in the absence of any commercial or financial relationships that could be construed as a potential conflict of interest.

Publisher's note

Supplementary material

The Supplementary Material for this article can be found online at: https://www.frontiersin.org/articles/10.3389/fmicb.2022.1019800/full#supplementary-material

References

Alfonzo, A., Lo Piccolo, S., Conigliaro, G., Ventorino, V., Burruano, S., and Moschetti, G. (2012). Antifungal peptides produced by *Bacillus amyloliquefaciens* AG1 active against grapevine fungal pathogens. *Ann. Microbiol.* 62, 1593–1599. doi: 10.1007/s13213-011-0415-2

Aoki, T., Aoki, Y., Ishiai, S., Otoguro, M., and Suzuki, S. (2017). Impact of *Bacillus cereus* NRKT on grape ripe rot disease through resveratrol synthesis in berry skin: Biocontrol of grape ripe rot by *Bacillus cereus* NRKT. *Pest. Manag. Sci.* 73, 174–180. doi: 10.1002/ps.4283

Apaliya, M. T., Zhang, H., Zheng, X., Yang, Q., Mahunu, G. K., and Kwaw, E. (2018). Exogenous trehalose enhanced the biocontrol efficacy of HANSENIASPORA UVARUM against grape berry rots caused by *Aspergillus tubingensis* and *Penicillium commune*. *J. Sci. Food Agric.* 98, 4665–4672. doi: 10.1002/jsfa.8998

Arora, N. K., Mishra, J., and Mishra, V. (2020). *Microbial Enzymes: Roles and Applications in Industries*. Singapore: Springer Singapore, doi: 10.1007/978-981-15-1710-5

Bankevich, A., Nurk, S., Antipov, D., Gurevich, A. A., Dvorkin, M., Kulikov, A. S., et al. (2012). SPAdes: A new genome assembly algorithm and its applications to single-cell sequencing. *J. Comput. Biol.* 19, 455–477. doi: 10.1089/cmb.2012.0021

Brown, J., Pirrung, M., and McCue, L. A. (2017). FQC Dashboard: Integrates FastQC results into a web-based, interactive, and extensible FASTQ quality control tool. *Bioinformatics* 33, 3137–3139. doi: 10.1093/bioinformatics/btx373

Buchfink, B., Xie, C., and Huson, D. H. (2015). Fast and sensitive protein alignment using DIAMOND. *Nat. Methods* 12, 59–60. doi: 10.1038/nmeth.3176

Calmes, B., Guillemette, T., Teyssier, L., Siegler, B., Pigné, S., Landreau, A., et al. (2013). Role of mannitol metabolism in the pathogenicity of the necrotrophic fungus *Alternaria brassicicola*. *Front. Plant Sci.* 4:131. doi: 10.3389/fpls.2013.00131

Calmes, B., Morel-Rouhier, M., Bataillé-Simoneau, N., Gelhaye, E., Guillemette, T., and Simoneau, P. (2015). Characterization of glutathione transferases involved in the pathogenicity of *Alternaria brassicicola*. *BMC Microbiol.* 15:123. doi: 10.1186/s12866-015-0462-0

Calvo, H., Mendiara, I., Arias, E., Gracia, A. P., Blanco, D., and Venturini, M. E. (2020). Antifungal activity of the volatile organic compounds produced by *Bacillus velezensis* strains against postharvest fungal pathogens. *Postharvest Biol. Technol.* 166:111208. doi: 10.1016/j.postharvbio.2020.111208

Campbell, K., Vowinckel, J., Keller, M. A., and Ralser, M. (2016). Methionine metabolism alters oxidative stress resistance *via* the pentose phosphate pathway. *Antioxid. Redox Signal.* 24, 543–547. doi: 10.1089/ars.2015.6516

Chandler, S., Van Hese, N., Coutte, F., Jacques, P., Höfte, M., and De Vleesschauwer, D. (2015). Role of cyclic lipopeptides produced by *Bacillus subtilis* in mounting induced immunity in rice (*Oryza sativa* L.). *Physiol. Mol. Plant Pathol.* 91, 20–30. doi: 10.1016/j.pmpp.2015.05.010

Chaves-Gómez, J. L., Chávez-Arias, C. C., Prado, A. M. C., Gómez-Caro, S., and Restrepo-Díaz, H. (2021). Mixtures of biological control agents and organic additives improve physiological behavior in cape gooseberry plants under vascular wilt disease. *Plants* 10:2059. doi: 10.3390/plants10102059

Chomnunti, P., Hongsanan, S., Aguirre-Hudson, B., Tian, Q., Peršoh, D., Dhami, M. K., et al. (2014). The sooty moulds. *Fungal Divers.* 66, 1–36. doi: 10.1007/s13225-014-0278-5

Cobos, R., Barreiro, C., Mateos, R. M., and Coque, J.-J. R. (2010). Cytoplasmic- and extracellular-proteome analysis of Diplodia seriata: a phytopathogenic fungus involved in grapevine decline. *Proteome Sci.* 8:46. doi: 10.1186/1477-5956-8-46

Coil, D., Jospin, G., and Darling, A. E. (2015). A5-miseq: an updated pipeline to assemble microbial genomes from Illumina MiSeq data. *Bioinformatics* 31, 587–589. doi: 10.1093/bioinformatics/btu661

Delgado, M. L., O'Connor, J. E., Azorín, I., Renau-Piqueras, J., Gil, M. L., and Gozalbo, D. (2001). The glyceraldehyde-3-phosphate dehydrogenase polypeptides encoded by the Saccharomyces cerevisiae TDH1, TDH2 and TDH3 genes are also cell wall proteins. *Microbiology* 147, 411–417. doi: 10.1099/00221287-147-2-411

Dimkić, I., Janakiev, T., Petrović, M., Degrassi, G., and Fira, D. (2022). Plant-associated Bacillus and *Pseudomonas* antimicrobial activities in plant disease suppression via biological control mechanisms – A review. *Physiol. Mol. Plant Pathol.* 117:101754. doi: 10.1016/j.pmpp.2021.101754

Emms, D. M., and Kelly, S. (2019). OrthoFinder: Phylogenetic orthology inference for comparative genomics. *Genome Biol.* 20:238. doi: 10.1186/s13059-019-1832-y

Falardeau, J., Wise, C., Novitsky, L., and Avis, T. J. (2013). Ecological and mechanistic insights into the direct and indirect antimicrobial properties of *Bacillus subtilis* lipopeptides on plant pathogens. *J. Chem. Ecol.* 39, 869–878. doi: 10.1007/s10886-013-0319-7

Fan, B., Wang, C., Song, X., Ding, X., Wu, L., Wu, H., et al. (2018). *Bacillus velezensis* FZB42 in 2018: The gram-positive model strain for plant growth promotion and biocontrol. *Front. Microbiol.* 9:2491. doi: 10.3389/fmicb.2018.02491

Fazle Rabbee, M., and Baek, K.-H. (2020). Antimicrobial activities of lipopeptides and polyketides *of Bacillus velezensis* for agricultural applications. *Molecules* 25:4973. doi: 10.3390/molecules25214973

Finn, R. D., Clements, J., and Eddy, S. R. (2011). HMMER web server: Interactive sequence similarity searching. *Nucleic Acids Res.* 39, W29–W37. doi: 10.1093/nar/gkr367

Fira, D., Dimkić, I., Berić, T., Lozo, J., and Stanković, S. (2018). Biological control of plant pathogens by *Bacillus* species. *J. Biotechnol.* 285, 44–55. doi: 10.1016/j.jbiotec.2018.07.044

Fujino, T., Kondo, J., Ishikawa, M., Morikawa, K., and Yamamoto, T. T. (2001). Acetyl-CoA Synthetase 2, a mitochondrial matrix enzyme involved in the oxidation of acetate. *J. Biol. Chem.* 276, 11420–11426. doi: 10.1074/jbc.M008782200

Goto, Y., Noda, Y., Mori, T., and Nakano, M. (1993). Increased generation of reactive oxygen species in embryos cultured in vitro. *Free Radic. Biol. Med.* 15, 69–75. doi: 10.1016/0891-5849(93)90126-F

Griffiths-Jones, S. (2006). miRBase: The MicroRNA Sequence Database. *Methods Mol. Biol.* 342, 129–138. doi: 10.1385/1-59745-123-1:129

Gullner, G., Komives, T., Király, L., and Schröder, P. (2018). Glutathione S-Transferase enzymes in plant-pathogen interactions. *Front. Plant Sci.* 9:1836. doi: 10.3389/fpls.2018.01836

Haas, B. J., Salzberg, S. L., Zhu, W., Pertea, M., Allen, J. E., Orvis, J., et al. (2008). Automated eukaryotic gene structure annotation using evidencemodeler and the program to assemble spliced alignments. *Genome Biol.* 9, R7. doi: 10.1186/gb-2008-9-1-r7

Hafeez, F. Y., Naureen, Z., and Sarwar, A. (2019). "Surfactin: An Emerging Biocontrol Tool for Agriculture Sustainability," in *Plant Growth Promoting Rhizobacteria for Agricultural Sustainability*, eds A. Kumar and V. S. Meena (Singapore: Springer Singapore), doi: 10.1007/978-981-13-7553-8_10

Hamaoka, K., Aoki, Y., and Suzuki, S. (2021). Isolation and characterization of endophyte *Bacillus velezensis* KOF112 from grapevine shoot xylem as biological control agent for fungal diseases. *Plants* 10:1815. doi: 10.3390/plants10091815

Hayashi, S., Yoshioka, M., Matsui, T., Kojima, K., Kato, M., Kanamaru, K., et al. (2014). Control of reactive oxygen species (ROS) production through histidine kinases in *Aspergillus nidulans* under different growth conditions. *FEBS Open Bio.* 4, 90–95. doi: 10.1016/j.fob.2014.01.003

He, C., Zhang, Z., Li, B., Xu, Y., and Tian, S. (2019). Effect of natamycin on *Botrytis cinerea* and Penicillium expansum—Postharvest pathogens of grape berries and jujube fruit. *Postharvest Biol. Technol.* 151, 134–141. doi: 10.1016/j.postharvbio.2019.02.009

Jiang, C., Shi, J., Liu, Y., and Zhu, C. (2014). Inhibition of *Aspergillus carbonarius* and fungal contamination in table grapes using *Bacillus subtilis*. *Food Control* 35, 41–48. doi: 10.1016/j.foodcont.2013.06.054

Jiang, C.-H., Liao, M.-J., Wang, H.-K., Zheng, M.-Z., Xu, J.-J., and Guo, J.-H. (2018). *Bacillus velezensis*, a potential and efficient biocontrol agent in control of pepper gray mold caused by Botrytis cinerea. *Biol. Control* 126, 147–157. doi: 10.1016/j.biocontrol.2018.07.017

Katoh, K., and Toh, H. (2008). Recent developments in the MAFFT multiple sequence alignment program. *Brief. Bioinform.* 9, 286–298. doi: 10.1093/bib/bbn013

Khullar, S., and Reddy, M. S. (2018). Ectomycorrhizal fungi and its role in metal homeostasis through metallothionein and glutathione mechanisms. *CBIOT* 7, 231–241. doi: 10.2174/2211550105666160531145544

Korf, I. (2004). Gene finding in novel genomes. *BMC Bioinformatics* 5:59. doi: 10.1186/1471-2105-5-59

Kunz, B. M., Pförtner, L., Weigel, S., Rohn, S., Lehmacher, A., and Maul, R. (2022). Growth and toxin production of phomopsin A and ochratoxin A forming fungi under different storage conditions in a pea (*Pisum sativum*) model system. *Mycotoxin Res.* 38, 37–50. doi: 10.1007/s12550-021-00446-8

Lagesen, K., Hallin, P., Rødland, E. A., Staerfeldt, H.-H., Rognes, T., and Ussery, D. W. (2007). RNAmmer: Consistent and rapid annotation of ribosomal RNA genes. *Nucleic Acids Res.* 35, 3100–3108. doi: 10.1093/nar/gkm160

Li, B. Q., and Tian, S. P. (2007). Effect of intracellular trehalose in *Cryptococcus laurentii* and exogenous lyoprotectants on its viability and biocontrol efficacy on *Penicillium expansum* in apple fruit. *Lett. Appl. Microbiol.* 44, 437–442. doi: 10.1111/j.1472-765X.2006.02080.x

Li, X., Wang, X., Shi, X., Wang, B., Li, M., Wang, Q., et al. (2020). Antifungal Effect of volatile organic compounds from *Bacillus velezensis* CT32 against *Verticillium dahliae* and *Fusarium oxysporum*. *Processes* 8:1674. doi: 10.3390/pr8121674

Li, Y., Héloir, M.-C., Zhang, X., Geissler, M., Trouvelot, S., Jacquens, L., et al. (2019). Surfactin and fengycin contribute to the protection of a *Bacillus subtilis* strain against grape downy mildew by both direct effect and defence stimulation. *Mol. Plant Pathol.* 20, 1037–1050. doi: 10.1111/mpp.12809

Liu, J., Hagberg, I., Novitsky, L., Hadj-Moussa, H., and Avis, T. J. (2014). Interaction of antimicrobial cyclic lipopeptides from *Bacillus subtilis* influences their effect on spore germination and membrane permeability in fungal plant pathogens. *Fungal Biol.* 118, 855–861. doi: 10.1016/j.funbio.2014.07.004

Love, M. I., Huber, W., and Anders, S. (2014). Moderated estimation of fold change and dispersion for RNA-seq data with DESeq2. *Genome Biol.* 15, 1–21. doi: 10.1186/s13059-014-0550-8

Lowe, T. M., and Eddy, S. R. (1997). tRNAscan-SE: A program for improved detection of transfer RNA Genes in genomic sequence. *Nucleic Acids Res.* 25, 955–964. doi: 10.1093/nar/25.5.955

Majoros, W. H., Pertea, M., and Salzberg, S. L. (2004). TigrScan and GlimmerHMM: two open source ab initio eukaryotic gene-finders. *Bioinformatics* 20, 2878–2879. doi: 10.1093/bioinformatics/bth315

Mi, H., Poudel, S., Muruganujan, A., Casagrande, J. T., and Thomas, P. D. (2016). PANTHER version 10: Expanded protein families and functions, and analysis tools. *Nucleic Acids Res.* 44, D336–D342. doi: 10.1093/nar/gkv1194

Mora, I., Cabrefiga, J., and Montesinos, E. (2015). Cyclic lipopeptide biosynthetic genes and products, and inhibitory activity of plant-associated *Bacillus* against phytopathogenic bacteria. *PLoS One* 10:e0127738. doi: 10.1371/journal.pone.0127738

Nguyen, L.-T., Schmidt, H. A., von Haeseler, A., and Minh, B. Q. (2015). IQ-TREE: A fast and effective stochastic algorithm for estimating maximum-likelihood phylogenies. *Mol. Biol. Evol.* 32, 268–274. doi: 10.1093/molbev/msu300

Ortiz, M. E., Bleckwedel, J., Fadda, S., Picariello, G., Hebert, E. M., Raya, R. R., et al. (2017). Global analysis of mannitol 2-dehydrogenase in *Lactobacillus reuteri* CRL 1101 during mannitol production through enzymatic, genetic and proteomic approaches. *PLoS One* 12, e0169441. doi: 10.1371/journal.pone.0169441

Park, G., Nam, J., Kim, J., Song, J., Kim, P. I., Min, H. J., et al. (2019). Structure and mechanism of surfactin Peptide from *Bacillus velezensis* Antagonistic to Fungi Plant Pathogens. *Bull. Korean Chem. Soc.* 40, 704–709. doi: 10.1002/bkcs.11757

Patel, T. K., and Williamson, J. D. (2016). Mannitol in plants, fungi, and plant–fungal interactions. *Trends Plant Sci.* 21, 486–497. doi: 10.1016/j.tplants.2016.01.006

Pertot, I., Giovannini, O., Benanchi, M., Caffi, T., Rossi, V., and Mugnai, L. (2017). Combining biocontrol agents with different mechanisms of action in a strategy to control Botrytis cinerea on grapevine. *Crop Protect.* 97, 85–93. doi: 10.1016/j.cropro.2017.01.010

Rabbee, M., Ali, M., Choi, J., Hwang, B., Jeong, S., and Baek, K. (2019). *Bacillus velezensis*: A valuable member of bioactive molecules within plant microbiomes. *Molecules* 24:1046. doi: 10.3390/molecules24061046

Ram, A. F. J. (2004). The cell wall stress response in *Aspergillus niger* involves increased expression of the glutamine: Fructose-6-phosphate amidotransferase-encoding gene (gfaA) and increased deposition of chitin in the cell wall. *Microbiology* 150, 3315–3326. doi: 10.1099/mic.0.27249-0

Reignault, P., Valette-Collet, O., and Boccara, M. (2007). The importance of fungal pectinolytic enzymes in plant invasion, host adaptability and symptom type. *Eur. J. Plant Pathol.* 120, 1–11. doi: 10.1007/s10658-007-9184-y

Rojas, C. M., Senthil-Kumar, M., Tzin, V., and Mysore, K. S. (2014). Regulation of primary plant metabolism during plant-pathogen interactions and its contribution to plant defense. *Front. Plant Sci.* 5:17. doi: 10.3389/fpls.2014.00017

Romanazzi, G., Lichter, A., Gabler, F. M., and Smilanick, J. L. (2012). Recent advances on the use of natural and safe alternatives to conventional methods to control postharvest gray mold of table grapes. *Postharvest Biol. Technol.* 63, 141–147. doi: 10.1016/j.postharvbio.2011.06.013

Schmidtke, L. M., Schwarz, L. J., Schueuermann, C., and Steel, C. C. (2019). Discrimination of *Aspergillus* spp., *Botrytis cinerea*, and *Penicillium expansum* in Grape Berries by ATR-FTIR Spectroscopy. *Am. J. Enol. Vitic.* 70, 68–76. doi: 10.5344/ajev.2018.18048

Shafi, J., Tian, H., and Ji, M. (2017). *Bacillus* species as versatile weapons for plant pathogens: a review. *Biotechnol. Biotechnol. Equip.* 31, 446–459. doi: 10.1080/13102818.2017.1286950

Simão, F. A., Waterhouse, R. M., Ioannidis, P., Kriventseva, E. V., and Zdobnov, E. M. (2015). BUSCO: Assessing genome assembly and annotation completeness with single-copy orthologs. *Bioinformatics* 31, 3210–3212. doi: 10.1093/bioinformatics/btv351

Sirén, J., Välimäki, N., and Mäkinen, V. (2014). Indexing graphs for path queries with applications in genome research. *IEEE/ACM Trans. Comput. Biol. Bioinform.* 11, 375–388. doi: 10.1109/TCBB.2013.2297101

Stanke, M., and Morgenstern, B. (2005). AUGUSTUS: A web server for gene prediction in eukaryotes that allows user-defined constraints. *Nucleic Acids Res.* 33, W465–W467. doi: 10.1093/nar/gki458

Sun, Q., Shang, B., Wang, L., Lu, Z., and Liu, Y. (2016). Cinnamaldehyde inhibits fungal growth and aflatoxin B1 biosynthesis by modulating the oxidative stress response of *Aspergillus flavus*. *Appl. Microbiol. Biotechnol.* 100, 1355–1364. doi: 10.1007/s00253-015-7159-z

Tempel, S. (2012). "Using and Understanding RepeatMasker," in *Mobile Genetic Elements Methods in Molecular Biology*, ed. Y. Bigot (Totowa, NJ: Humana Press), doi: 10.1007/978-1-61779-603-6_2

Tietze, F. (1969). Enzymic method for quantitative determination of nanogram amounts of total and oxidized glutathione: Applications to mammalian blood and other tissues. *Anal. Biochem.* 27, 502–522. doi: 10.1016/0003-2697(69)90064-5

Underwood, W. (2012). The plant cell wall: a dynamic barrier against pathogen invasion. *Front. Plant Sci.* 3:85. doi: 10.3389/fpls.2012.00085

Vandercammen, A., Francois, J. M., Torres, B. B., Maia, J. C. C., and Hers, H.-G. (1990). Fructose 2,6-bisphosphate and carbohydrate metabolism during the life cycle of the aquatic fungus *Blastocladiella emersonii*. *J. Gen. Microbiol.* 136, 137–146. doi: 10.1099/00221287-136-1-137

Walker, B. J., Abeel, T., Shea, T., Priest, M., Abouelliel, A., Sakthikumar, S., et al. (2014). Pilon: An integrated tool for comprehensive microbial variant detection and genome assembly improvement. *PLoS One* 9:e112963. doi: 10.1371/journal.pone.0112963

Wang, M., Sun, X., Zhu, C., Xu, Q., Ruan, R., Yu, D., et al. (2015). PdbrlA, PdabaA and PdwetA control distinct stages of conidiogenesis in *Penicillium digitatum*. *Res. Microbiol.* 166, 56–65. doi: 10.1016/j.resmic.2014.12.003

Wang, M., Zhao, L., Zhang, X., Dhanasekaran, S., Abdelhai, M. H., Yang, Q., et al. (2019). Study on biocontrol of postharvest decay of table grapes caused by *Penicillium rubens* and the possible resistance mechanisms by *Yarrowia lipolytica*. *Biol. Control* 130, 110–117. doi: 10.1016/j.biocontrol.2018.11.004

Weber, C. A., Sekar, K., Tang, J. H., Warmer, P., Sauer, U., and Weis, K. (2020). β-Oxidation and autophagy are critical energy providers during acute glucose depletion in S *accharomyces cerevisiae*. *Proc. Natl. Acad. Sci. U.S.A.* 117, 12239–12248. doi: 10.1073/pnas.1913370117

Ye, M., Tang, X., Yang, R., Zhang, H., Li, F., Tao, F., et al. (2018). Characteristics and application of a novel species of *Bacillus*: *Bacillus velezensis*. *ACS Chem. Biol.* 13, 500–505. doi: 10.1021/acschembio.7b00874

Yu, L., Qiao, N., Zhao, J., Zhang, H., Tian, F., Zhai, Q., et al. (2020). Postharvest control of *Penicillium expansum* in fruits: A review. *Food Biosci.* 36:100633. doi: 10.1016/j.fbio.2020.100633

Zaidi, S. S. A., and Zhang, X. (2016). Computational operon prediction in whole-genomes and metagenomes. *Brief. Funct. Genomics* 16:elw034. doi: 10.1093/bfgp/elw034

Zhang, H., Godana, E. A., Sui, Y., Yang, Q., Zhang, X., and Zhao, L. (2020). Biological control as an alternative to synthetic fungicides for the management of grey and blue mould diseases of table grapes: a review. *Crit. Rev. Microbiol.* 46, 450–462. doi: 10.1080/1040841X.2020.1794793

Zhang, Z.-Q., Chen, T., Li, B.-Q., Qin, G.-Z., and Tian, S.-P. (2021b). Molecular basis of pathogenesis of postharvest pathogenic Fungi and control strategy in fruits: Progress and prospect. *Mol. Hortic.* 1:2. doi: 10.1186/s43897-021-00004-x

Zhang, J., Hao, H., Liu, H., Wang, Q., Chen, M., Feng, Z., et al. (2021a). Genetic and functional analysis of the Zn(II)2Cys6 transcription factor HADA-1 in *Hypsizygus marmoreus*. *Appl. Microbiol. Biotechnol.* 105, 2815–2829. doi: 10.1007/s00253-021-11175-4

Zou, J., Zhang, T., Wen, G., Song, B., and Jiang, S. (2022). First Report of *Penicillium olsonii* causing postharvest fruit rot of grape (*Vitis vinifera*) in China. *Plant Dis.* 106, 1761. doi: 10.1094/PDIS-10-21-2354-PDN

Frontiers in Microbiology

Explores the habitable world and the potential of microbial life

The largest and most cited microbiology journal which advances our understanding of the role microbes play in addressing global challenges such as healthcare, food security, and climate change.

Discover the latest Research Topics

See more →

Frontiers

Avenue du Tribunal-Fédéral 34
1005 Lausanne, Switzerland
frontiersin.org

Contact us

+41 (0)21 510 17 00
frontiersin.org/about/contact